Synthesis and Characterization of New Diazocine Derivatives for Application in Photopharmacology and Material Science

Dissertation

zur Erlangung des Doktorgrades
der Mathematisch-Naturwissenschaftlichen Fakultät
der Christian-Albrechts-Universität zu Kiel

vorgelegt und bearbeitet
von

Thomas Brandt, geb. Griebenow

Otto-Diels-Institut für Organische Chemie

Kiel 2024

Erster Gutachter:	Prof. Dr. Rainer Herges
Zweiter Gutachter:	Prof. Dr. Christian Peifer
Tag der mündlichen Prüfung:	13.12.2024
Zum Druck genehmigt:	13.12.2024

Die vorliegende Arbeit wurde unter Anleitung von

Prof. Dr. Rainer Herges

in der Zeit von

Februar 2021 bis Oktober 2024

am Otto Diels-Institut für Organische Chemie

der Christian-Albrechts-Universität zu Kiel

angefertigt.

Teile dieser Arbeit wurden bereits veröffentlicht

Pascal Lentes, Jeremy Rudtke, Thomas Griebenow and Rainer Herges

Beilstein J. Org. Chem. **2021**, *17*, 1503-1508, DOI: 10.3762/bjoc.17.107.

Franziska Wages, Thomas Brandt, Hans-Jörg Martin, Rainer Herges and Edmund Maser

Chem. Biol. Interact. **2023**, *390*, 110872, DOI: 10.1016/j.cbi.2024.110872.

Eidesstattliche Erklärung

Hiermit erkläre ich, Thomas Brandt, geb. Griebenow, an Eides statt, dass ich die vorliegende Dissertation selbstständig und nur mit den angegebenen Quellen und Hilfsmitteln angefertigt habe. Die Arbeit ist nach Inhalt und Form, abgesehen von der Beratung durch meinen Betreuer Prof. Dr. Rainer Herges, durch mich eigenständig erarbeitet und verfasst worden. Die Arbeit ist unter Einhaltung der Regeln guter wissenschaftlicher Praxis der Deutschen Forschungsgemeinschaft entstanden und wurde weder in Auszügen noch in ganzer Form im Rahmen eines Prüfungsverfahrens vorgelegt. Dies ist mein erster Prüfungsversuch und mir wurde kein akademischer Grad entzogen.

Ort, Datum

Thomas Brandt

Danksagung

An dieser Stelle möchte ich mich bei allen Personen bedanken, die entweder maßgeblich an dieser Arbeit beteiligt waren oder mich beim während dieser Zeit unterstützt haben, denn ohne sie wäre die Arbeit in dieser Form nicht möglich.
Zunächst möchte ich mich bei Prof. Dr. Rainer Herges dafür bedanken, dass ich an diesem vielseitigen und spannenden Themenbereich arbeiten und stets meine eigenen Ideen einbringen konnte. Zudem wurde mir die Möglichkeit gegeben mich in nationalen und internationalen Kooperationen einzubringen, wodurch ich einen spannenden Einblick in Themen außerhalb meines eigenen Tellerrandes erhalten konnte und meine Forschung auf internationalen Konferenzen zu präsentieren.
Bei Prof. Dr. Christian Peifer möchte ich mich für die Übernahme des Zweitgutachtens bedanken.
Beim gesamten Arbeitskreis Herges möchte ich mich für die gemeinsam verbrachte Zeit voller angeregter Diskussionen über mal mehr, mal weniger fachbezogene Themen und die Hilfsbereitschaft und die angenehme Zusammenarbeit bedanken. Die gemeinsamen Unternehmungen und Konferenzteilnahmen waren immer sehr unterhaltsam. Vielen Dank auch für die Unterstützung, während ich verletzungsbedingt an die Couch gefesselt war. Ein großer Dank geht hier auch an meinen Laborpartner Mirco für die unterhaltsame und produktive Arbeitsatmosphäre bei immer ausgezeichneter Musik und die gemeinsam verbrachten Mittagspausen (Müsli, Müsli, Mjammjammjamm) bedanken.
Großer Dank geht auch an die spektroskopische Abteilung für das Messen der paar wenigen Substanzen, die über die Zeit zusammengekommen sind. Insbesondere geht der Dank an Marion, Gitta und Gaith, die mit mir unzählige Stunden bei PSS-Messungen am NMR-Spektrometer verbracht haben und Prof. Dr. Frank Sönnichsen, dass er immer ein offenes Ohr für Fragen und Sonderwünsche hatte und auch immer bereit war bei Problemen selbst Hand anzulegen. Danken möchte ich auch Prof. Dr. Christian Näther für die Durchführung der Einkristallstrukturanalysen, sowie allen Kooperationspartnern, insbesondere Franziska Wages und Prof. Dr. Edmund Maser aus der Toxikologie und der Finnlandfraktion Iussi Isokuortti und Nikita Durandin für die tolle und erfolgreiche Zusammenarbeit. Ebenso möchte ich mich bei meinen Bachelorstudenten Michael Hösgen, Jan Peter Mikosch und Lasse Cipriani und meinen Masterpraktikant*innen Ivonne Schweder, Tobias Schacht und (schon wieder) Jan Peter Mikosch für ihre fleißige Hilfe bei der Synthesearbeit bedanken.
Ich möchte mich auch bei meinen Kommiliton*innen Marvin, Jenny, Niklas[3] (Piet, Pipah und Ruser), Niels und Vivian dafür bedanken, dass sie mich seit Beginn des Studiums begleitet und unterstützt haben. Ich denke immer noch an die Lernrunden in der Mensa für eigentlich jede Klausur und PC-Übung sowie die gemeinsam absolvierten Praktika und gehaltenen Seminarvorträge. Teil der Runde ist natürlich auch Sascha Koller, der mich sogar seit Ausbildungsbeginn begleitet hat.
Ein großer Dank geht an die fleißigen Korrekturleser Daniel, Julia, Jan Simon, Jenny, Marvin, Mirco, Franzi und Marlene für jede Anmerkung und jeden Fehler den ihr gefunden habt.
Vielen Dank auch an Max für die seit der fünften Klasse bestehende Freundschaft und die gemeinsamen verbrachten Abende bei schlechten Filmen und Bier, den Angelausflügen und den gemeinsam besuchten Konzerten und Festivals.
Meiner Familie danke ich für die Hilfe, Unterstützung, Motivation und positive Prägung über die letzten Jahrzehnte.
Zuletzt möchte ich meiner Frau Marlene dafür danken, dass sie mich seit Beginn unserer Beziehung immer unterstützt hat, mich eingebremst hat, wenn ich mal wieder zu viel Zeit mit Chemie verbracht habe und sich liebevoll und fürsorglich um mich gekümmert hat, als mich mein Kreuzbandriss für mehrere Monate außer Gefecht gesetzt hat. Ich hoffe, dass ich dir nicht zu sehr auf die Nerven gegangen bin. Danke, dass du es seit nunmehr seit fast acht Jahren mit mir aushältst<3!

Kurzdarstellung

Die Inkorporation photoschaltbarer Moleküle in biologische oder technische Systeme ist ein vielversprechender Ansatz zur gezielten Beeinflussung derartiger Prozesse auf molekularer Ebene. Allerdings sind bisher viele bekannte molekulare Photoschalter aufgrund unzureichender photochemischer Eigenschaften in ihrer Anwendbarkeit eingeschränkt. Das Diazocin als Weiterentwicklung des am häufigsten verwendeten molekularen Photoschalters, dem Azobenzol, weist jedoch aufgrund erhöhter Rigidität eine hervorragende Schalteffizienz und sehr hohe Quantenausbeuten auf. Mittlerweile sind viele Methoden zur effektiven Darstellung und Derivatisierung auch asymmetrisch substituierter Diazocine bekannt, sodass ihr Anwendungsbereich und ihre Bedeutung bei der Entwicklung neuer lichtgesteuerter Moleküle stetig wachsen. Allerdings weist das Diazocin in Bezug auf die Unidirektionalität der Schaltbewegung, die Wellenlänge des für die Schaltung verwendeten Lichtes und die Wasserlöslichkeit noch einige Schwächen auf. Durch systematische Weiterentwicklung des ursprünglichen Diazocins konnten mit den Diindanodiazocinen (DIDs) und den *N*-Acetyl-Diazocinen (*N*-Ac Diazocin) eine vielversprechende „zweite Generation“ entwickelt werden, deren weitere Untersuchung und Derivatisierung im Fokus dieser Arbeit standen.

Durch systematische Eliminierung aller konformationellen und rotatorischen Freiheitsgrade konnten bei der Entwicklung der DIDs die Quantenausbeuten, sowie die Unidirektionalität der Schaltbewegung enorm verbessert werden. Darüber hinaus entstehen bei der Synthese zwei Diastereomere, von denen das Racemat chiral ist. Im Rahmen dieser Arbeit konnte das Racemat in seine beiden Enantiomere aufgetrennt und ihre photochemischen Eigenschaften untersucht werden. Hierbei standen insbesondere die chiroptischen Schalteigenschaften im Fokus, wobei enorme Unterschiede zwischen den Z- und E-Konfigurationen beider Enantiomere festgestellt wurden. Zusätzlich konnte durch Schaltung in die E-Konfiguration mit zirkular polarisiertem Licht das korrespondierende Enantiomer gezielt in dieser Konfiguration angereichert werden und der Enantiomerenüberschuss bestimmt werden. Um das DID-System für eine weitere Funktionalisierung zugänglich zu machen, wurden Synthesestrategien für die Darstellung di- und tetrahalogenierter DID-Diastereomere entwickelt. Auf diesem Wege konnten vier neue halogenierte DID-Diastereomere erhalten und im Anschluss photochemisch charakterisiert werden.

Im Gegensatz zum ursprünglichen Diazocin ist das *N*-Ac Diazocin intrinsisch wasserlöslich und die für die Schaltung adressierten n-π*-Absorptionsbanden sind stark bathochrom verschoben, sodass sie für einen Einsatz als Photopharmakophor in der wässrigen Umgebung biologischer Systeme prädestiniert sind. Unter Verwendung unterschiedlicher Varianten Übergangsmetall-katalysierter Kreuzkupplungen konnten ausgehend von den bereits bekannten monohalogenierten *N*-Ac Diazocinen zwölf neue Derivate synthetisiert und sowohl in organischen Lösungsmitteln als auch in wässriger Umgebung photochemisch charakterisiert werden. Im Rahmen einer Kooperation konnte für einige Derivate eine starke Inhibierung des die Testosteronbildung-katalysierenden, körpereigenen 17βHSD3-Enzyms festgestellt werden. Ein für den Einsatz in der Photopharmakologie notwendiger Wirkunterschied zwischen den Z- und E-Konfigurationen der Derivate konnte jedoch nicht beobachtet werden. Für eine Einbettung in größere und komplexere Systeme ist die beidseitige Funktionalisierung der *N*-Ac Diazocine notwendig. Als Ausgangspunkt hierfür konnte ein beidseitig bromiertes *N*-Ac Diazocin-Derivat synthetisiert und photochemisch charakterisiert werden. Aufgrund der sehr niedrigen Ausbeuten wurden verschiedene neue Synthesestrategien entwickelt und zunächst mit der Synthese des unsubstituierten *N*-Ac Diazocins getestet. Mit den vielversprechendsten Strategien wurden ebenfalls Versuche zur Darstellung beidseitig substituierter *N*-Ac Diazocin-Derivate unternommen, die jedoch allesamt nicht zum Zielmolekül führten.

Abstract

The incorporation of photoswitchable molecules into biological or technical systems is a promising approach for the selective control of such processes at the molecular level. However, many known molecular photoswitches are limited in their applicability due to insufficient photochemical properties. Due to its increased rigidity, diazocine, a further development of the most frequently used molecular photoswitch, azobenzene, exhibits excellent switching efficiency and very high quantum yields. Many methods for the effective synthesis and derivatization are known to date, so that their range of application and importance in the development of new light-controlled molecules is constantly growing. However, the initial diazocine still has some weaknesses with regard to the unidirectionality of the switching movement, the wavelength of the light used for switching and its solubility in water. By systematic improvement of the original diazocine, a promising "second generation" was developed with the diindanodiazocines (DIDs) and the *N*-acetyl diazocines (*N*-Ac diazocines), whose further investigation and derivatization were the focus of this work.

By systematically eliminating all conformational and rotational degrees of freedom, the quantum yields and the unidirectionality of the switching motion were improved enormously during the development of the DIDs. In addition, two diastereomers are formed during the synthesis, of which the racemate is chiral. In the course of this work, the racemate was separated into its two enantiomers and their photochemical properties were investigated. The focus here was particularly on the chiroptical switching properties, whereby enormous differences between the Z- and E-configurations of both enantiomers were observed. In addition, by switching to the E-configuration with circular polarized light, the corresponding enantiomer could be specifically enriched in this configuration and the enantiomeric excess could be determined. In order to make the DID-system accessible for further functionalization, synthesis strategies for the preparation of di- and tetrahalogenated DID-diastereomers were developed. This allowed four new halogenated DID diastereomers to be obtained and subsequently characterized photochemically.

In contrast to the original diazocine, the *N*-Ac diazocine is intrinsically water-soluble and the nπ*-absorptionbands addressed for switching are strongly bathochromically shifted. These properties make the *N*-Ac diazocines perfectly suitable for use as a photopharmacophore in the aqueous environment of biological systems. Using different variants of transition metal-catalyzed cross-couplings, twelve new derivatives were synthesized from the already known monohalogenated *N*-Ac diazocines. The new derivatives have been photochemically characterized both in organic solvents and in an aqueous environment. As part of a collaboration, a strong inhibition of the endogenous 17βHSD3 enzyme catalyzing testosterone formation was observed for some derivatives. However, a difference in efficacy between the Z- and E-configurations of the derivatives which would be necessary for use in photopharmacology could not be observed. For embedding in larger and more complex systems, the two-sided functionalization of the *N*-Ac diazocines is necessary. As a starting point, a two-side brominated *N*-Ac diazocine derivative was synthesized and photochemically characterized. As a result of the very low yields for the synthesis of two-side brominated *N*-Ac diazocine, various new synthesis strategies were developed and initially tested with the synthesis of the unsubstituted *N*-Ac diazocine. Using the most promising strategies, attempts were also made to synthesize *N*-Ac diazocine derivatives substituted on both sides, but none of these led to the target molecule.

.

Publications included in this thesis

The majority of the results obtained within this work are based on research described in the following publications.

Substituted nitrogen-bridged diazocines, P. Lentes, J. Rudtke, T. Griebenow, R. Herges, *Beilstein Journal of Organic Chemistry* **2021**, *17*, 1503-1508, DOI: 10.3762/bjoc.17.107.

Light-switchable diazocines as potential inhibitors of testosterone-synthesizing 17ß-hydroxysteroid dehydrogenase 3, F. Wages, T. Brandt, H.-J. Martin, R. Herges, E. Maser, *Chem. Biol. Interact.* **2023**, *390*, 110872, DOI: 10.1016/j.cbi.2024.110872.

N-Acetyl Diazocine Derivatives via Cross-Coupling, T. Brandt, P. Lentes, J. Rudtke, M. Hösgen, C. Näther, R. Herges, *The Journal of Organic Chemistry* **2024**, *submitted,* Manuscript ID: jo-2024-00398n.R2

The following manuscripts are prepared for submission.

Determination of Enantiomeric Excess via Photoswitching of Chiral Diindanodiazocine Racemic Mixture with Circular-Polarized Light, T. Brandt, W. Moormann, J. P. Mikosch, R. Herges, manuscript prepared for submission.

Synthesis and Characterization of New Diindanodiazocine Derivatives, T. Brandt, J. P. Mikosch, L. Cipriani, R. Herges, manuscript prepared for submission.

Studies not included within this thesis

During my time as doctoral candidate, I have contributed to collaborations which resulted in several peer-reviewed publications (listed below). These are not discussed in this thesis due to deviating topics. The proportionate contribution is briefly described in the individual publications.

Reduction of photoswitched, nitrogen bridged N-Acetyl diazocines limits inhibition of 17βHSD3 activity in transfected human embryonic kidney 293 cells, F. Wages, P. Lentes, T. Griebenow, R. Herges, C. Peifer, E. Maser, *Chemico-Biological Interactions* **2022**, *354*, 109822, DOI: 10.1016/j.cbi.2022.109822.

To Isomerize or not to Isomerize? E/Z Isomers of Cyclic Azobenzene Derivatives and Their Reactivity Upon One-Electron Reduction**,** G. Glotz, K. Knaipp, M. S. Maier, K. Hüll, A. Novak, A.-M. Kelterer, T. Griebenow, R. Herges, D. Trauner, G. Gescheidt, *Chemistry - A European Journal* **2023**, *29*, e202300146, DOI: 10.1002/chem.202300146.

Triplet Sensitization Enables Bidirectional Isomerization of Diazocine with 130 nm Redshift in Excitation Wavelengths**,** J. Isokurtti, T. Griebenow, J.-S. von Glasenapp, T. Raeker, M. A. Filatov, T. Laaksonen, R. Herges, N. A. Durandin, *Chemical Science* **2023**, *34*, 9161-9166, DOI: 10.1039/D3SC02681G.

Table of Contents

1. Introduction

Molecular switches play a key role in biology as a part of complex processes such as ion and proton transport or vision.[1-3] The process of switching generally takes place between at least two different states of a multistable system following the principle of bistability as a response to an external stimulus. Often the switching process results in a change of the molecules properties.[4-7] In contrast to a molecular motor, where the work performed upon stimulation drives a system as a function of trajectory, the work performed by a molecular switch affects a system as a function of the state of the switch itself. As a consequence, the work performed by the switch is reset to net zero after being switched back to its ground state.[8-10] Incorporated into more complex molecules or molecular assemblies, molecular switches are able to perform specific tasks in response to an external stimulus as part of a molecular machine.[6]

The photon-absorbing co-factor retinal is one of the best studied natural molecular switches. With the group of retinal-carrying retinylidene proteins, it performs a multitude of biological functions, though it is especially known for its role in mammalian eyesight.[3,11,12] In the process of vision retinal undergoes a very fast and high yielding Z- to E-isomerization upon irradiation with light when bound to the protein rhodopsin (**scheme 1.1**). This leads to the coupling of rhodopsin with G protein transducin followed by the activation of visual phototransduction.[13]

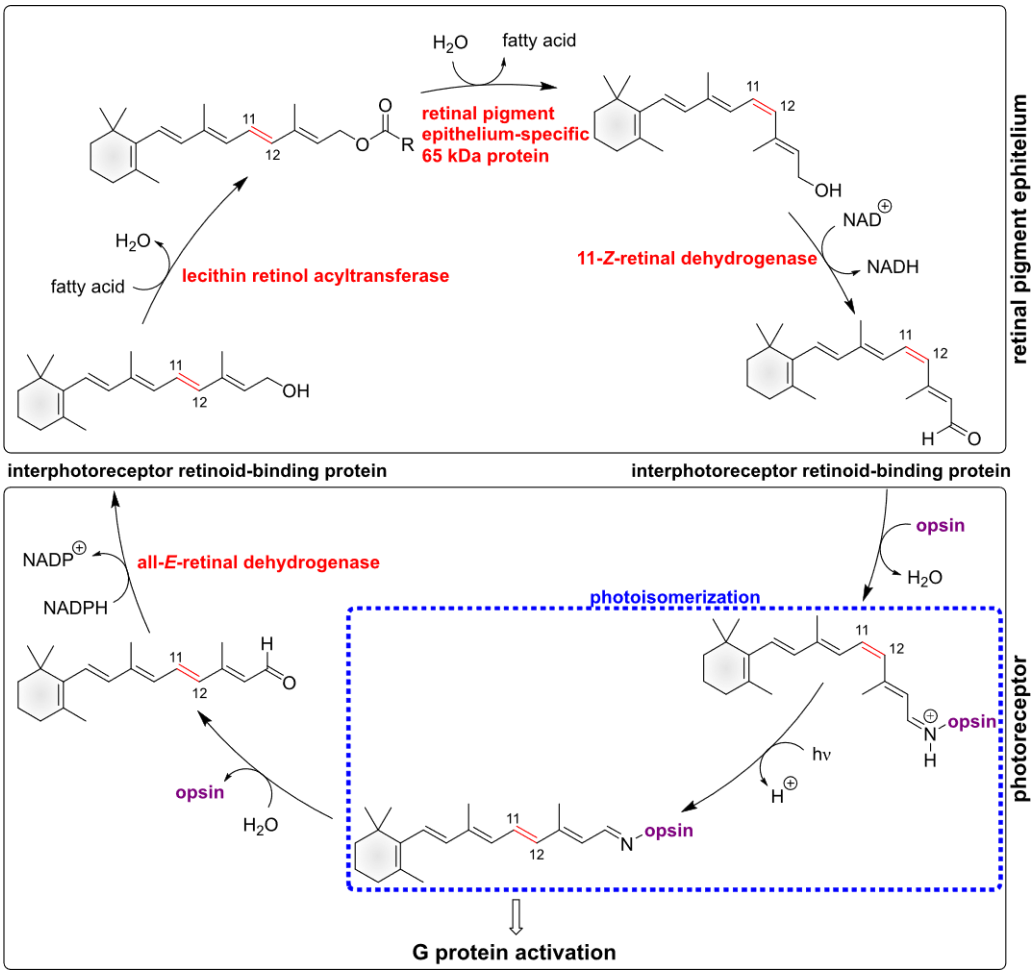

Scheme 1.1: Overview of the retinoid (visual) cycle including Z- to E-photoisomerization of retinal bound to the protein rhodopsin (blue box) leading to the signal transduction induced by G protein activation.[12,14] Afterwards regeneration of retinal takes place in both the photoreceptor and the retinal pigment epithelium mediated by various enzymes (red).[14]

Eyesight is one of many examples of light in the visible region of the electromagnetic spectrum regulating biological processes.[15] These have inspired many researchers for development of numerous artificial photosensitive systems among them low bandgap polymers for photovoltaic cells,[16] photochemical synthesis[17] or photopharmacology.[18-20] These systems exploit the properties of light as an external stimulus for molecular switches: it allows precise control over intensity, wavelength and polarization while also affording spatiotemporal and traceless application.[19,21-23]

1.1 Artificial Photoswitches

Just like their naturally occurring counterparts, artificial photoswitches undergo a reversible change in their molecular properties such as molecular geometry, rigidity, dielectric constant or refractive index.[24] By incorporation of artificial photoswitches into molecular systems or materials these changes on the molecular level can be used to reversibly affect and control targeted macroscopic properties.[24]

For the development and application of artificial photoswitches it is worth taking a look at their current or considered photochemical parameters: addressability, switching efficiency, thermal stability and reliability. The addressability describes the wavelength used for targeting the photoswitch and is defined by the absorption maxima (λ_{max}) and the separation of the absorption bands of the stable and the metastable form of the photoswitch.[23] Moreover, the band separation has an immense influence on the switching efficiency which is quantified by the photostationary state (PSS) (Γ). The PSS characterizes the maximum percentage accumulation of each isomer after irradiation and depends on the irradiation wavelength and quantum yield (Φ).[23,25] Thermal stability is quantified by the thermal half-life ($t_{1/2}$) of thermal back isomerization at constant temperature. The reliability of a photoswitch is based on the fatigue resistance which describes the amount of decomposition or side reactions taking place in competition with the photoisomerization over numerous switching cycles.[23] Artificial photoswitches are classified by the type of their light-induced isomerization reaction. Possible reactions are for example: bond dissociation, hydrogen transfer, cycloaddition, electrocyclization or E/Z-isomerization, with the last two categories mentioned being the most frequent (**scheme 1.2**).[23] Although most of the above photoswitches are still subject of current research they have successfully found their way into application. However, the most frequently used artificial molecular photoswitches are by far the azobenzene-based photoswitches, which are structurally similar to the stilbene.[26,27]

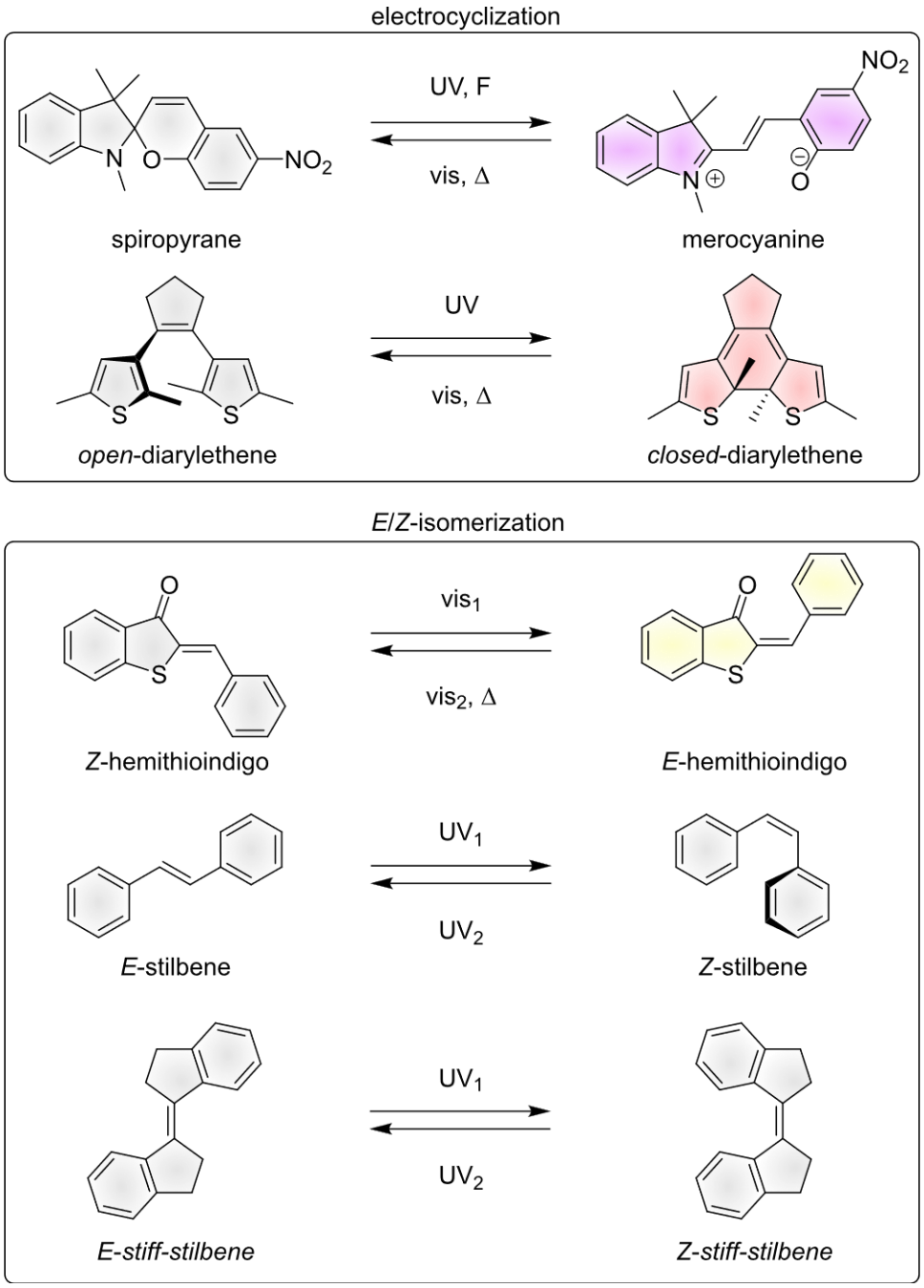

Scheme 1.2: Examples of molecular photoswitches with electrocyclization (top) and E/Z-isomerization (bottom) as underlying principle behind the switching mechanism.

1.2 Azobenzene-based Photoswitches

The core structure of initial azobenzene photoswitch consists of two phenyl rings connected via a diazene bridge, the so-called azo group. In its thermodynamically stable E-configuration, azobenzene exhibits a nearly planar structure with a barely existing dipole moment.[28] Upon irradiation with UV light (λ = 300-350 nm), the molecule undergoes a drastic structural change towards the metastable Z-configuration.[29] Here, the planes of the phenyl rings intersect with an angle of 56 ° due to a rotation of the phenyl rings around the C-N=N-C-dihedral angle. This is caused by both the reduction of distance between the *para*-carbon atoms from 9.0 Å to 5.5 Å and steric repulsion occurring after E- to Z-photoisomerization. This twisted structure leads to an increased dipole moment of $\mu \approx 3$ D.[30,31] Back-isomerization can be achieved either by irradiation with blue light (λ = 430-480 nm) or by thermal relaxation (**scheme 1.3**).[29]

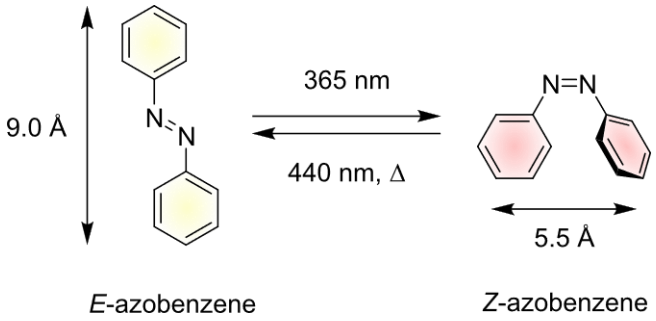

Scheme 1.3: The thermodynamically stable E-azobenzene can be converted into the metastable Z-configuration by irradiation with UV light. Back-isomerization can be achieved either by irradiation with blue light or thermally.

The E-configuration exhibits an intense π-π^*-transition at λ = 314 nm and a n-π^*-transition in the visible range at λ = 435 nm.[32] Due to the symmetry prohibition the n-π^*-transition shows a low intensity, so E-azobenzene is usually irradiated with UV light for photoisomerization.[29] In contrast to this, the n-π^*-transition of Z-azobenzene at λ = 440 nm is not forbidden for symmetrical reasons and thus, much more intense. Also, Z-azobenzene shows two π-π^*-absorption bands at λ = 280 nm and λ = 240 nm.[33] Because of this overlap in the absorption bands of both E- and Z-azobenzene, light-induced photoisomerization leads to PSS values of $\Gamma_{E\rightarrow Z}$ (317 nm) = 90% or $\Gamma_{Z\rightarrow E}$ (440 nm) = 79% without a complete formation of either configuration being possible.[29,32] Both transitions exhibit quantum yields of $\Phi_{E\rightarrow Z}$ = 0.14 and $\Phi_{Z\rightarrow E}$ = 0.47.[34] However, they vary and show a strong dependency from solvent and temperature.[35-39] Besides these relatively poor quantum yields azobenzene has many conformational degrees of freedom and therefore, exhibits a high flexibility. Thus, a switching process of azobenzene does not include directional movement.[40-42]

However, the lack of directional motion and the insufficient switching properties are compensated by a short synthesis path and good accessibility for derivatization since a wide range of synthesis procedures with a high tolerance for various functional groups are known in current literature (**scheme 1.4**).[43,44] The resulting wide range of derivatives enables a multitude of possible applications for example in photopharmacology,[18,20] material science[45,46] or energy-[25,47] and data storage systems.[48]

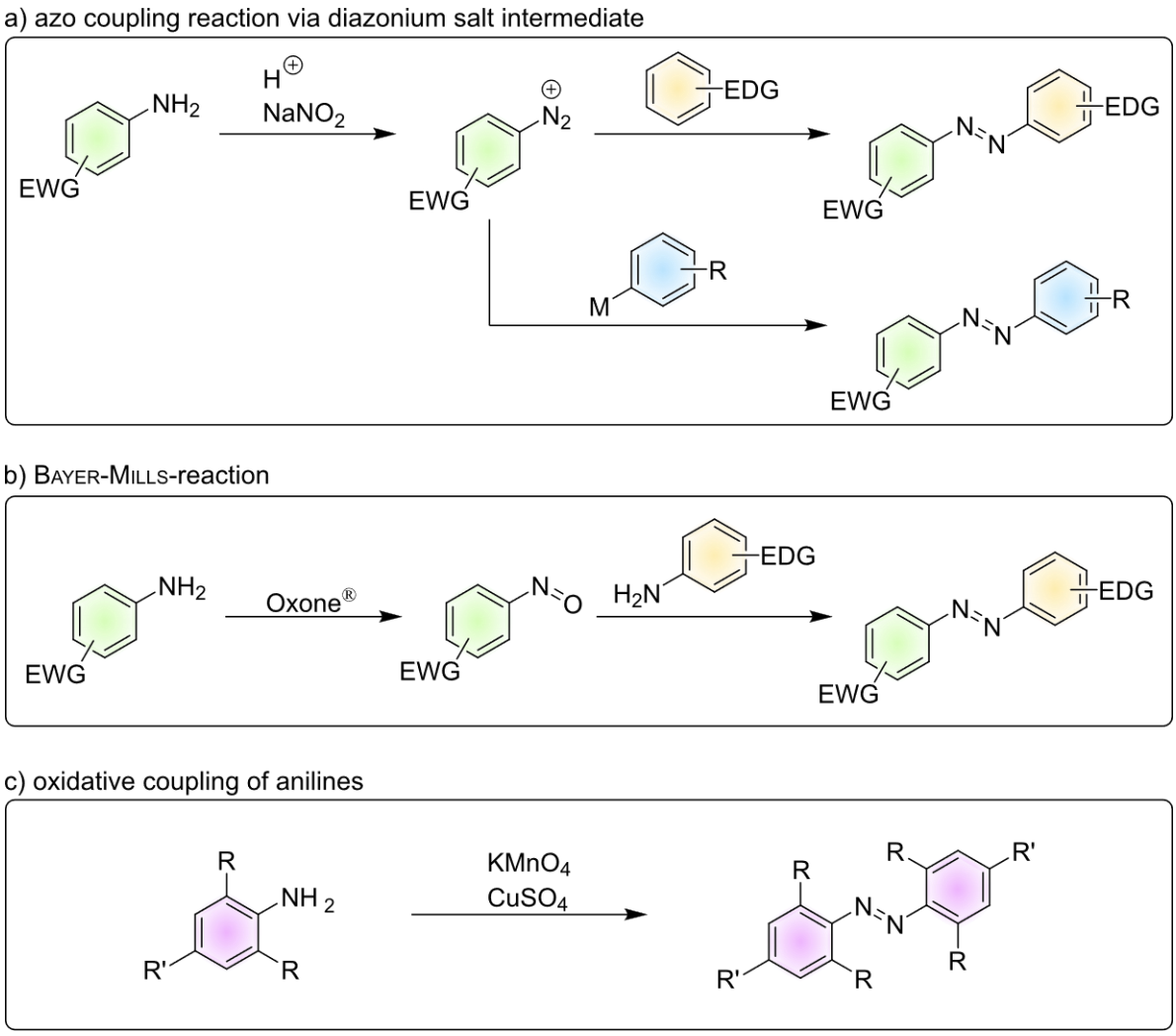

Scheme 1.4: Examples of the most frequently used reaction types for azobenzene synthesis: a) Initial azo-coupling reaction of an electron poor diazonium salt generated from an aniline which contains electron withdrawing substituents (EWG) and an arene which contains an electron donating substituent (EDG).[43,44] A more recent procedure describes the reaction of diazonium salts with metal-containing aromatic precursors.[49] b) BAYER-MILLS-reaction of electron poor anilines after oxidation to the corresponding nitroso compound, with an electron rich aniline.[43,44] c) Oxidation of anilines to the corresponding azo-bridged dimer.[43,44,50]

1.3 Modification of Azobenzenes

Several approaches for the improvement of photoswitching behavior are known in current literature, mainly targeting a significant bathochromic shift of absorption bands via reduction of the HOMO-LUMO energy difference. This, however, also affects the remaining switching parameters consequently.[15] By substitution with either electron donating (-OMe, -NR_2)[15,50-53] or electron withdrawing groups (-F, -Cl, -Br, -NO_2)[15,50,52,54,55] a significant bathochromic shift of n-π^*-transitions can be achieved with accompanying extension of the thermal half-life. A combination of electron donating and withdrawing substituents ("push-pull"-system) results in a significant bathochromic shift of π-π^*-absorption bands while the n-π^*-transitions are almost unaffected resulting in a higher overlap of absorption bands, though at the same time it causes an extremely shortened thermal half-life.[15,52,55] The same effect applies for the extension of π-systems leading to significant bathochromically shifted π-π^*-transition.[15] Also, the extension of π-systems is accompanied by accelerated thermal relaxation.[15,56]

In a different approach the photoswitching properties of azobenzene can be affected by either substitution of at least one benzene ring by five- or six-membered heteroarenes (azoheteroarenes) or by induction of geometric tension[15,57] and reduction of degrees of conformational freedom (diazocines, see chapter 1.4).[42] This so-called second generation of azobenzene-based photoswitches allows enhanced functionality compared to the initial azobenzene.[58]
Since a large number of heteroaromatics is known, a wide range of heteroaromatic azo photoswitches is accessible and therefore, a broader structural diversity combined with very different spectral properties is emerging. However, heteroarenes primarily containing nitrogen, or heteroarenes containing a different heteroatom (S, O) in addition to one nitrogen are most frequently used (**scheme 1.5**).[59] Compared to azobenzene, the introduction of heteroarenes leads to shifted transitions and therefore, to highly separated absorption bands, whereby different absorption bands are addressed depending on the used heteroarene. However, this allows good to nearly quantitative photoswitching in both directions. Moreover, superior quantum yields and extended half-lives compared to azobenzenes can be achieved easily.[58-62]

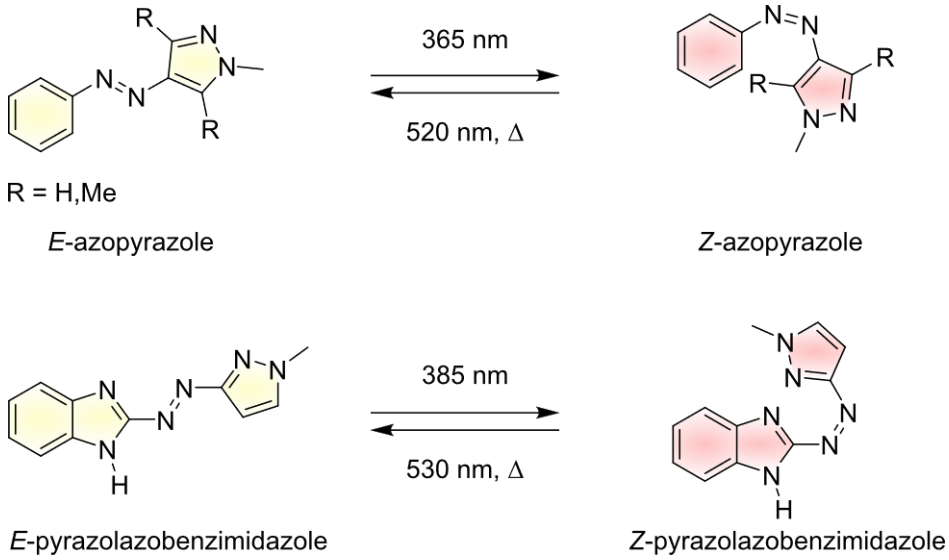

Scheme 1.5: Chemical structures of arylazopyrazole (top) and mixed heteroarene azo photoswitch containing a benzimidazole and a pyrazole moiety (bottom). Heteroarenes lead to shifted transitions and higher absorption band separation resulting in improved photochemical properties compared to parent azobenzene.

As an advantage of the use of five-membered heterocycles in *Z*-configuration, a new conformation is accessible that cannot be reached if six-membered aromatic rings are used. This conformation can be tuned sterically by substitution at the five-membered heterocycle with a drastic effect on the photochemical properties.[60-62] Furthermore, a higher water solubility and a high stability against glutathione are very good prerequisites for use in the field of photopharmacology.[58]

1.4 Diazocines

The *ortho*-ethylene bridging of azobenzene is another possible way to alter its photochemical properties by the introduction of geometric tension and reduction of degrees of conformational freedom.[15,42,57] The synthesis and structure of such a bridged azobenzene, also called diazocine, was already been published by DUVAL[63] in 1910, while its photochemical characterization only followed in 2009 in a publication by HERGES and TEMPS *et al*.[57] The additional ethylene bridge results in the formation of a strained eight-membered cycle in the center of the diazocine framework whose thermodynamically most favorable structure is the *boat*-conformation. This results in a *Z*-configuration

for the C-N=N-C bond, although usually E-configurations are preferred for azo compounds. This indicates an inverse thermodynamic stability of the diazocines' E- and Z-configurations with respect to azobenzene and azoheteroarenes (**scheme 1.6**). However, density-functional theory (DFT) calculations revealed two possible E-conformations, with the E-*twist*-configuration being more thermodynamically favorable than the E-*chair*-conformation.[57,64,65]

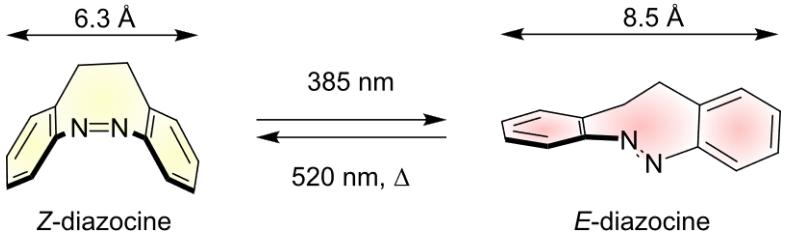

Scheme 1.6: Photoswitching of parent diazocine starting from thermodynamically stable Z-configuration with violet light to the metastable E-*twist*-configuration. Complete back isomerization can be achieved either with green light or thermal relaxation.

Due to geometric tension the n-π*-transitions are significantly shifted compared to azobenzene. The n-π*-transition of the Z-configuration undergoes a hypsochromic shift to λ = 404 nm while E-n-π*-transition is bathochromically shifted to λ = 490 nm, resulting in a high separation of absorption bands in the visible range of the electromagnetic spectrum.[57] Therefore, parent diazocine exhibits exceptionally high PSS values of $\Gamma_{Z\rightarrow E}$ (385 nm) = 92% for Z- to E- and $\Gamma_{E\rightarrow Z}$ (530 nm) = >99% for E- to Z-photoisomerization.[57] Furthermore, the rigidity introduced by the ethylene bridge allows a more defined and directional motion induced upon photoisomerization as the free rotation of the phenyl rings is prevented. This results in extraordinarily high quantum yields of $\Phi_{Z\rightarrow E}$ = 0.72 and $\Phi_{E\rightarrow Z}$ = 0.90.[57] These superior photochemical properties indicate that diazocines are promising candidates for application as molecular switches. Accordingly, diazocines have already been implemented in photoresponsive materials,[66], surface functionalization[67] or in biological applications such as photopharmacology.[68-74]

1.4.1 Synthesis of Diazocines

While the preparation of diazocines was initially associated with low reproducibility, low yields and low tolerance to functional groups, a number of methods have been developed in recent years that have largely overcome these problems, with the methods of MOORMANN *et al.*[75] (reductive coupling), MAIER *et al.*[76] (oxidative coupling) and LI *et al.*[77] (C-N-cascade-coupling) appearing to be the most promising as these methods are used in most publications on diazocine synthesis (**scheme 1.7**). There are other methods, including electrochemical cyclization,[78] BAYER-MILLS-reaction[64] or metal-catalyzed deoxygenation,[65,79-81], but these methods either resulted in insufficient yields, low reproducibility or an increased occurrence of overoxidation to the corresponding azoxy-compound. However, all of the above-mentioned synthesis procedures have in common that the phenyl rings are linked via the ethylene bridge in the first step followed by the formation of the azo group closing the eight membered cycle as second step.

The formation of the ethylene linkage itself already represents a crucial step as it is a limiting factor for the range of accessible substituents. The initial procedure via oxidative dimerization of *o*-nitrotoluenes (scheme 1.7) developed by CHAUDHARI *et al.*[82] and improved by MOORMANN *et al.*[75] provides very good yields for symmetrical target molecules, but is not very suitable for asymmetric target compounds. These are only accessible with low yields due to the low selectivity of the reaction giving a statistical distribution of different products if two different starting molecules are to be combined.[69] Furthermore, the oxidative dimerization reaction is causing problems for sensitive functional groups since a strong base and an oxidizing agent are required for successful coupling. A

well thought-out protecting group strategy or easily feasible late stage modification not affecting the azo group is therefore essential.[68,72,83]

The reductive dimerization developed by LI *et al.*[77] requires neither strong bases nor oxidizing agents and instead uses organolithium compounds, so that even in this case sensitive the introduction of functional groups is only accessible via protecting groups or late-stage modification. In addition, asymmetrically substituted diazocines have not yet been synthesized via this method.[77]

Using either a WITTIG-reaction according to LANGBEHN *et al.*[84] and SAMANTA *et al.*[50] or a SONOGASHIRA-coupling according to MAIER *et al.*[76], dimerizations are feasible under significantly milder conditions. These methods also allow a selective preparation of asymmetric diazocine precursors.[84,85] However, the preparation of the starting molecules is more difficult and functional groups must be resistant to reduction. Moreover, the double or triple bonds formed during the reaction still have to be reduced to the ethylene bridge.[86,87]

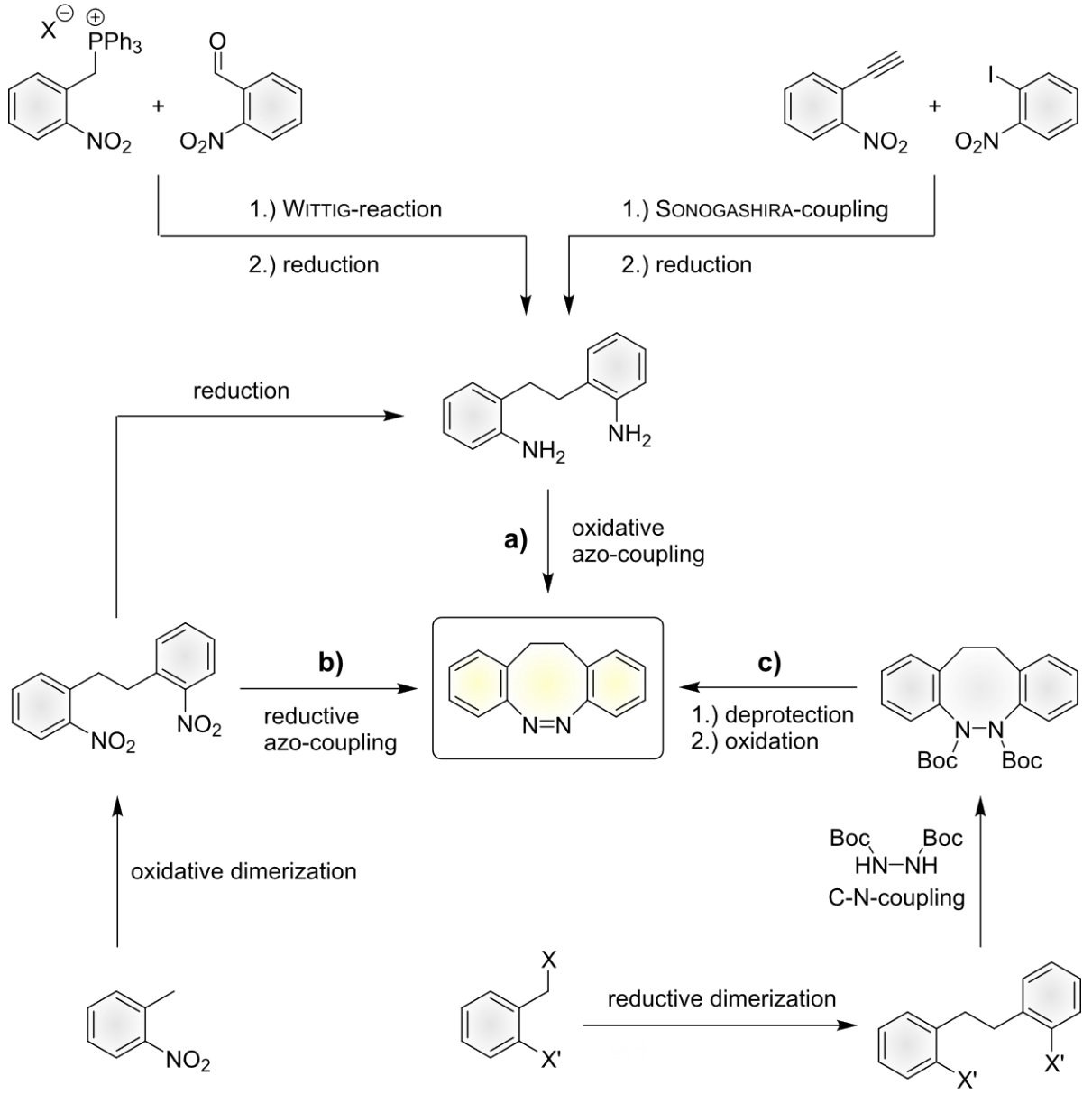

Scheme 1.7: Overview of the most common synthesis strategies for the formation of the diazocine framework: a) Oxidative azo condensation of dianiline precursors obtained by reduction of dinitro compounds which in turn can be prepared via WITTIG-reaction, SONOGASHIRA-coupling or oxidative dimerization. b) Reductive azo condensation of dinitro precursors usually synthesized via oxidative dimerization. c) Ring closure of aryl halogenide with protected hydrazine in a C-N-cascade-coupling reaction resulting in the formation of the diazocine after subsequent deprotection and oxidation. Aryl halogenides are prepared via reductive dimerization.

Reductive intramolecular azo condensation of *o*-ethylene bridged bis-nitrotoluenes has been performed with various reducing agents such as zinc[88] or glucose[89,90] under basic conditions in a one-step synthesis resulting yields that are both low and not reproducible. A two-step synthesis initially published by PAUDLER *et al.*[91], which includes a reductive step with zinc under basic conditions and an oxidative step with catalytic copper(II)chloride and oxygen, provides higher yields. Investigations of the reaction mechanism of the reduction step by MOORMANN *et al.*[75] showed that the corresponding azoxy-compound, initially formed in a BAYER-MILLS-like reaction from a nitroso and a hydroxylamine moiety reductively generated from the dinitro precursor, is subsequently reduced via diazocine intermediate giving a hydrazine derivative as main product. This is subsequently oxidized quantitatively in the second step to the corresponding diazocine. Due to this, the yield and the reproducibility of the reductive azo condensation could be significantly improved by tuning of the reaction parameters and elongation of reaction time.[75] However, the yields vary depending on the substituents and their positions. In addition, solubility problems occur in the polar solvent required for the reaction. To overcome these problems several procedures for the reductive reaction pathway have been developed. Examples include the preparation of the hydrazine derivative with lithium aluminum hydride,[92] the oxidation of the hydrazine derivative with mercury oxide,[93] synthesis of the azoxy-compound under ultrasonication with subsequent reduction to diazocine with phosphorous trichloride[79,81] or the solvent-free synthesis of diazocine with lead powder in a ball mill.[75] However, these methods play a subordinate role in diazocine synthesis.

In contrast to the reductive azo condensation the oxidative synthesis path is starting from a dianiline precursor. By addition of *meta*-chloroperbenzoic acid (*m*CPBA) one aniline moiety is oxidized to the corresponding nitroso group which subsequently undergoes an intramolecular BAYER-MILLS reaction with the remaining aniline moiety. However, the reaction remains sensitive to polymerization and formation of the overoxidized azoxy-side product. While polymerization can be suppressed by high dilution, the formation of azoxy-side product can be prevented by adding the oxidizing *m*CPBA not all at once but slowly over time, since the azoxy-compound is preferably formed by intramolecular coupling of overoxidized nitroso-hydroxylamine side product.[76]

Whereas the two previous synthesis strategies start from dianiline or dinitro compounds, the ring closing in the method presented by LI *et al*.[77] is based on intramolecular C-N-coupling of aryl iodides with *tert*-butoxycarbonyl (Boc) protected hydrazine via a diamine ligand-catalyzed ULLMANN-GOLDBERG-amidation cascade. The diazocine synthesis is then completed by LEWIS acid-induced cleavage of the Boc-protecting groups and subsequent oxidation resulting in the formation of the azo group. However, the practicability of the synthesis path is severely limited by both the high number of reaction steps and the optimization required for different substituents.[77]

1.5 Functionalization of Diazocines

For the incorporation of diazocines into functional materials or biological active compounds an additional functionalization of the diazocine framework is necessary. Unfortunately, a method for direct substitution at the aromatic system of the diazocine framework has not yet been explored due to the sensitivity of the azo group to many reaction conditions. Although one procedure describing an electrophilic substitution of the overoxidized azoxy-compound has been published, which, however, needs two additional reaction steps in the form of reduction of the azoxy to the hydrazine intermediate and subsequent oxidation forming the azo bond. While this procedure does result in the desired halogenated diazocine, the yields are insufficient.[79] Therefore, functional groups or halogens as starting points for subsequent derivatization have to be part of the building blocks for the dimerization reaction.[83] This requirement, though, limits the choice of functional groups, as the reaction conditions of the dimerization reactions are harsh and the oxidative or reductive conditions of the azo condensation require a suitable protecting group strategy. For this reason, a late-stage conversion of

functional groups into other functional groups is another possibility for diazocine framework functionalization. The limitation, in this case, is that the azo group is not inert under oxidative, reductive or basic conditions limiting the range of accessible functional groups as well.[76,83] But still, there are a few examples of different kinds of late-stage functionalization giving acetamides[89,94-96], ethers[95], amines[95] or activated carboxylic esters[72,95,97] which do not require functionalization by cross-coupling reaction.

For azobenzenes transition metal-catalyzed cross-coupling reactions have been a door opener for late-stage functionalization and derivatization. In these reactions azobenzenes have been used both as formal nucleophilic and formal electrophilic components.[98] For diazocines few examples are known in current literature, but the range of different cross-coupling reactions already proves the great potential for late-stage derivatization and functionalization (**scheme 1.8**). With diazocines as formal electrophilic components procedures for SUZUKI-[99], STILLE-[66,84,99,100], BUCHWALD-HARTWIG-[76,85], ULLMANN-[101], NEGISHI-[71], HECK-[68] and SONOGASHIRA-cross-coupling reactions[88,102] are known, while diazocines have been used as formal nucleophilic components only in SUZUKI- and STILLE-coupling reactions.[99] However, the cross-coupling of diazocines remains challenging since procedures using azobenzene components cannot be adapted without limitations. One reason for the problems in cross-coupling reactions of diazocines might be the electronic structure. More precisely, the problem might be rooted in the orientation of the lone electron pairs of both nitrogen atoms, which, in contrast to azobenzene, are not aligned with the π-system of the aromatic rings. Besides, sterical issues might also play an important role.[98]

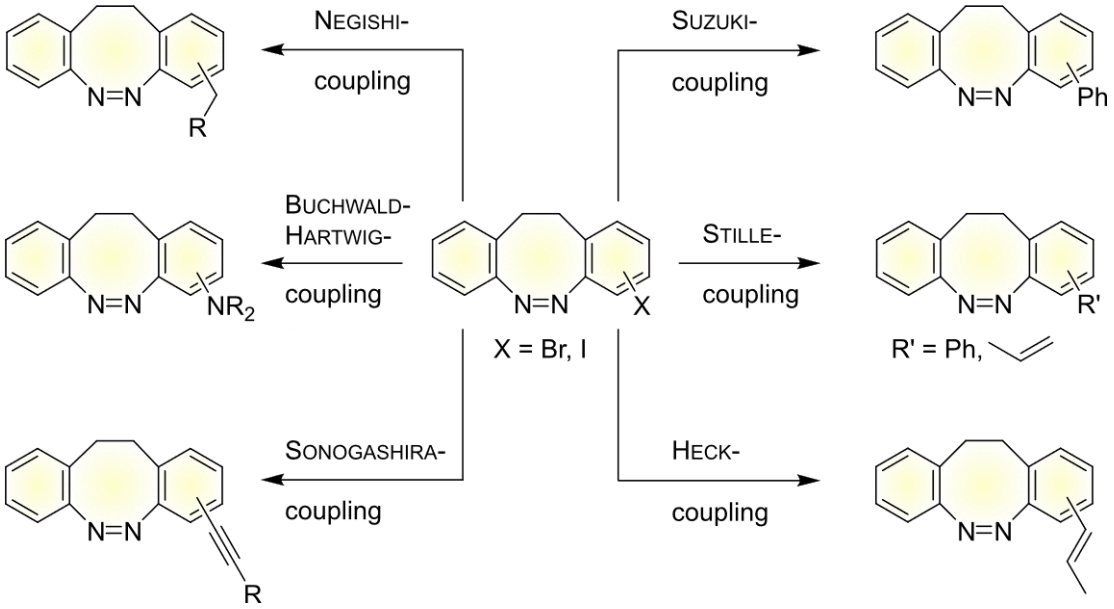

Scheme 1.8: Overview of cross-coupling procedures already known for parent diazocine starting from the corresponding halogenated compound. Except for SUZUKI- and STILLE-cross-coupling reactions, diazocines have only been used as formal electrophilic halogenated components in cross-coupling reactions.

The derivatization of diazocines, however, involves more than just the mere choice of substituents. Since targeted substitution of azobenzene is used to specifically affect its switching properties, a similar behavior can also be expected for diazocines.[15] Thus, if the switching behavior is not to be affected by the substituent(s), care must be taken to prevent the electronic influence on the azo group. The derivatization of azobenzene showed that the influence of substituents is at its maximum in *ortho*-[51,54] and *para*-positions,[50] which must therefore be avoided for a functionalization without influence on the switching behavior. An attenuation of the conjugation can be achieved by substitution in the *meta*-position, so that the influence on the switching behavior is reduced.[103,104] Another approach is the use of bridging methylene groups between the photoswitch and the substituent to disrupt the electronic

interactions between functional group and diazocine.[83,105] It is important to note, however, that the free rotation of bridging methylene groups introduces unwanted flexibility into the system.[103,104] By using bridging alkynes instead, rigidity can be maintained while at the same time interrupting the electronic coupling between the substituent and photoswitch.[102,106]

1.6 Limitations of Parent Diazocine

1.6.1 Undirectional Motion

Azobenzenes and diazocines are not unidirectional switches and therefore do not allow any unidirectional movement. In the case of azobenzenes two enantiomers are formed during photoisomerization, which interconvert rapidly at room temperature while in both Z- and E-configuration both phenyl rings rotate freely.[42] This rotation is suppressed in the diazocine framework by the ethylene linkage between both phenyl rings.[57] Despite the increased rigidity, conformational movements are still possible. However, these are limited to *twist*- and *twist-chair*-inversion in E- and *boat*-inversion in Z-configuration.[42,64] To overcome these degrees of conformational freedom the introduction of even more rigidity compared to parent diazocine seems a promising approach.[42] In addition to the directed motion achieved in this way, increased quantum yields of light-induced switching processes could be a side effect, since unproductive relaxation pathways are suppressed.[42,57]

1.6.2 Irradiation Wavelengths

Compared to most photoswitches parent diazocine exhibits bathochromically shifted n-π*-transitions suitable for induced isomerization with light in the visible range of the electromagnetic spectrum.[57,107] Nevertheless, parent diazocine is usually switched from Z- to E-configuration with light at 385 nm[57] which is still close to high energetic UV irradiation potentially damaging sensitive materials or biological tissue.[108] Additionally, light in the near infrared area between 680 nm and 900 nm has the largest penetration depth in aqueous and blood supported biological tissue compared to visible or UV light.[108,109] For this reason, further shift of n-π*-transitions is required to achieve light induced isomerization in the so called biooptical window.[64] For azobenzenes a bathochromic shift of absorption wavelengths has been achieved by *ortho*-/*para*-substitution with electron withdrawing substituents such as fluorine[54], push-pull systems[15] or by substitution of at least one phenyl ring with a heteroarene.[60-62] Due to the differences in the electronic structure of azobenzenes and diazocines this approach would likely prove unsuccessful.[98] However, DFT-calculations showed promising results concerning bathochromically shifted n-π*-transitions for diazocines in whose ethylene bridge a carbon atom has been substituted by a heteroatom (see 1.8 Heteroatom-bridged Diazocines).[64,65]

1.6.3 Water Solubility

Parent diazocine exhibits superior photochemical properties compared to azobenzene.[57] Yet, the application in aqueous media faces similar problems, since parent diazocine like azobenzene is mostly insoluble in pure water without the addition of highly polar organic solvent additives like dimethyl sulfoxide (DMSO) or acetonitrile (MeCN).[110] Concerning the applicability this is not a big obstacle, since it is common to utilize notable concentrations of MeCN[111] or DMSO[69,74,111,112] in stock solutions of nonpolar inhibitors or drugs which in turn are used in pharmacological testing via cell essays to prevent precipitation. However, even small quantities of organic solvents in water may alter the photochemical and even possibly the biological properties of the photoswitch, since it might be surrounded by a solvating shell of organic solvent instead of water.[110] Investigations of the photoconversion rates $\Gamma_{Z\rightarrow E}$ as a function of the water content in MeCN revealed a significant decrease

in the conversion rates from initially $\Gamma_{Z\rightarrow E}$ = 88% to $\Gamma_{Z\rightarrow E}$ =73% at 90% water content until precipitation at 100% water content.[110] Therefore, the addition of functional groups to increase the polarity and as a result also the solubility in water is required. This can be achieved by introduction of amino or carboxylic acid substituents that are separated from the diazocine framework by a bridging methylene group to prevent significant impact on the switching characteristics. This separation is necessary, because especially anilines are known to significantly deteriorate switching.[89,110] These derivatives are soluble in pure water, however, they have the disadvantage that they also show a significant decrease in photoconversion yields by about 30%.[110] Moreover, for a successful application both the solubilizing and the functional groups have to be present in the molecule at the same time, which makes the synthesis of water soluble and functionalized molecules even more difficult. In conclusion, it is required to achieve an intrinsic water solubility of the diazocine framework to make it suitable for application especially in aqueous media and a biological environment.

1.7 Heteroatom-bridged Diazocines

TD-DFT calculations revealed that if one carbon atom in the ethylene bridge of the diazocine framework is substituted by either an oxygen or sulfur atom, the n-π*-transitions of their respective E-configurations would bathochromically shift and an absorption band separation of about 100 nm could be expected. This assumption has been confirmed by UV-vis spectra showing maxima of the n-π*-transitions for Z-configurations at λ = 405 nm (*S*-diazocine) and λ = 385 nm (*O*-diazocine) and E-configurations at λ = 525 nm for both diazocines. Furthermore, the absorption bands of their E-configurations are significantly broadened up to 700 nm, allowing quantitative back isomerization with red light at 660 nm.[65] The photoconversion yields of both *S*- ($\Gamma_{Z\rightarrow E}$ (405 nm) = 70%) and *O*-diazocines' ($\Gamma_{Z\rightarrow E}$ (385 nm) = 80%) Z- to E-isomerization are lower than for parent diazocines. This significantly lower photoconversion yield of *S*-diazocine can be explained by an additional absorption band at 380 nm overlapping with the n-π*-transition of its Z-configuration.[65] In contrast to *O*- and parent diazocine, the relative energy difference between thermodynamically favored E-*twist*- and unfavored E-*chair*-conformation is only 1.6 kcal mol^{-1}, resulting in a significantly more frequent formation of unfavored E-*chair*-conformation due to fast interconversion (**scheme 1.9**). Therefore, the additional absorption band can be assigned to the E-*chair*-conformation.[64,65] Another difference between both heteroatom-bridged diazocines is their respective thermal half-live. The more strained *O*-diazocine exhibits a drastically shortened half-life of 89 s while the half-life of *S*-diazocine is elongated to 84 h.[65]

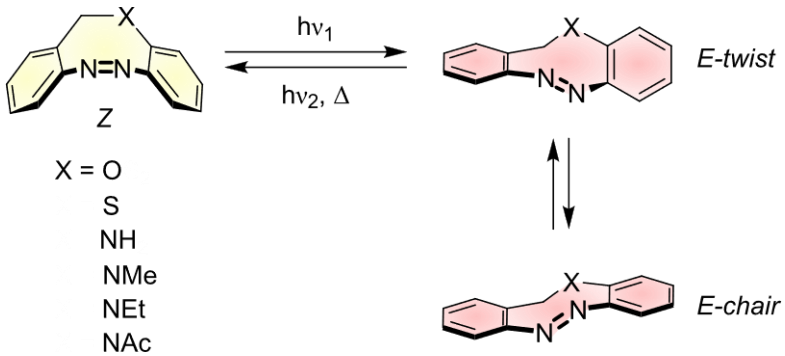

Scheme 1.9: Photoswitching of heteroatom-bridged diazocines. Z- to E-photoisomerization can be achieved with blue light at approximately 400 nm. Two conformations are accessible of which the E-*twist*-conformation is thermodynamically favored over the E-*chair*-conformation. Back switching can be achieved with light up to 740 nm or via thermal relaxation.

The substitution of one carbon atom of the ethylene bridge by a heteroatom leads to an advantage in the synthesis of diazocines since the bridge can now be linked by nucleophile substitution under mild conditions which in turn allows the introduction of sensitive substituents and asymmetric substitution patterns.[65] However, the final formation of the azo bond remains difficult, since the reductive reaction pathway following the procedure of MOORMANN *et al*.[75] resulted in no formation of corresponding heteroatom-bridged diazocine due to polymerization or (thio)ether cleavage under basic conditions.[65] Finally, following the reductive conditions of YAN *et al*.[79,81], the *S*- and *O*-diazocines were synthesized with lead powder under less basic conditions resulting, however, in insufficient yields.[65] This synthesis strategy, therefore, is rarely found in current literature.[74,113] Usage of C-N-cascade-coupling following the procedure of LI *et al*.[77] for ring closure led to little improvement of the obtained yields.[114] Besides oxygen- and sulfur-bridged diazocines, nitrogen-bridged diazocines have been taken into account. Here, TD-DFT calculations also predicted n-π*-absorption band separation of more than 100 nm between Z- and E-configurations for *N*-H diazocine as well as for alkyl or acyl derivatives since nitrogen-bridging opens the field of additional and easy bridge functionalization.[64] UV-vis spectra of all *N*-diazocine derivatives confirmed the very good band separation with maxima for the n-π*-transitions of the Z-configurations between 385 nm and 410 nm, while E-configurations exhibit absorption maxima around 520 nm for acyl derivatives and even around 560 nm for unsubstituted and alkylated derivatives. Additionally, the alkylated derivatives show broadened absorption bands for E-configurations, allowing quantitative light induced back isomerization with near-infrared light between 520 nm and 740 nm.[64] However, the photoconversion yields of Z- to E-photoisomerization are rather low with $\Gamma_{Z\rightarrow E}$ (405 nm) = 45-50% for alkylated and $\Gamma_{Z\rightarrow E}$ (405 nm) = 65% for unsubstituted *N*-diazocines, while acylated derivatives show significantly higher photoconversion yields of $\Gamma_{Z\rightarrow E}$ (405 nm) = 80-85%. The lower photoconversion yields of unsubstituted and alkylated derivatives are rooted in the higher overlap of the absorption bands due to their broadness.[64]

The preparation of unsubstituted *N*-H-diazocine is considerably more complex than the synthesis of parent diazocine, *S*- or *O*-diazocine since six reaction steps are required (**scheme 1.10**). The reason for this is the necessity of a well-thought-out orthogonal protecting group strategy due to the sensitivity of the bridging nitrogen atom towards side reactions. The key steps are the protection of the bridging secondary amine with a fluorenylmethoxycarbonyl (Fmoc) protecting group and the ring closing reaction under formation of the azo group. Therefore, an intramolecular BAYER-MILLS-reaction was used, though it suffered from low reproducibility and insufficient yields.[64]

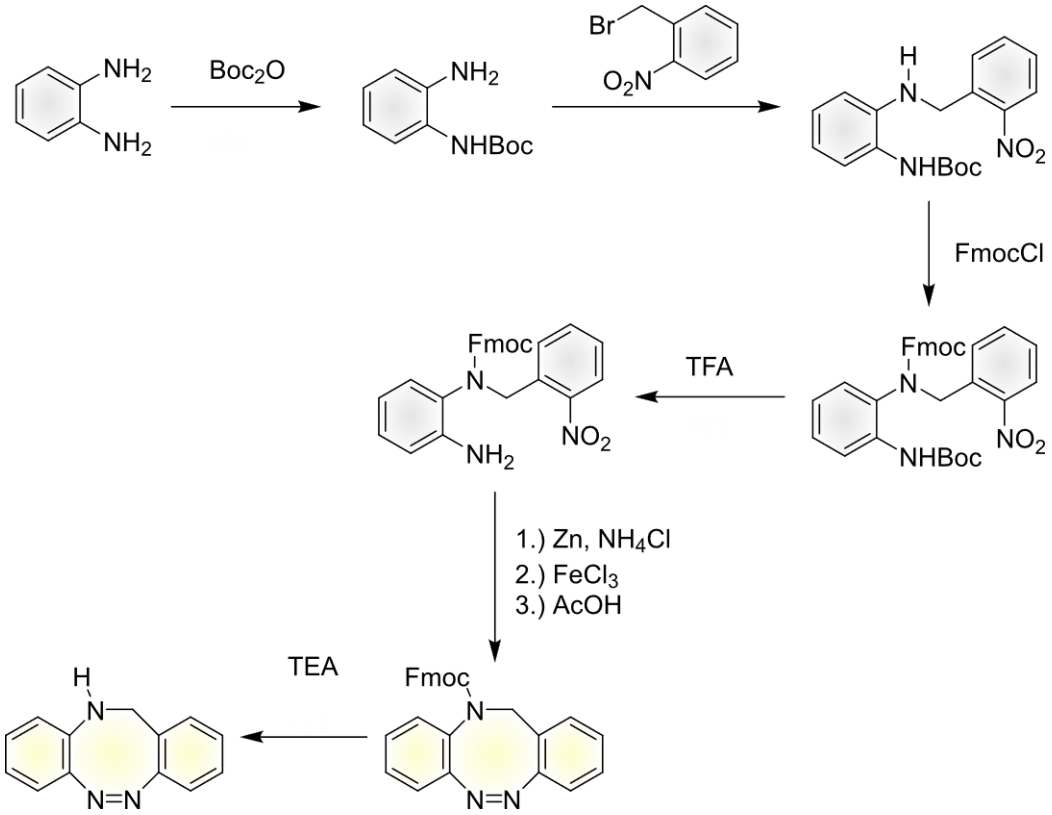

Scheme 1.10: Synthesis path for the preparation of the unsubstituted *N*-H-diazocine. Key steps are introduction of the Fmoc-protecting group and the azo group-forming ring closing reaction. This can either be carried out via intramolecular BAYER-MILLS-reaction.[64]

Functionalization of bridging nitrogen can only be achieved with strong reagents under mild conditions since the secondary amine is not as reactive due to the neighboring azo group and the azo group itself being sensitive for drastic reaction conditions (**scheme 1.11**). Strong alkylating agents like MEERWEIN-salts are necessary for alkylation of *N*-diazocine. Acetylation can be achieved with propanephosphonic acid anhydride (T3P) which activates the carboxylic acid for nucleophilic attack by the bridging nitrogen.[64]

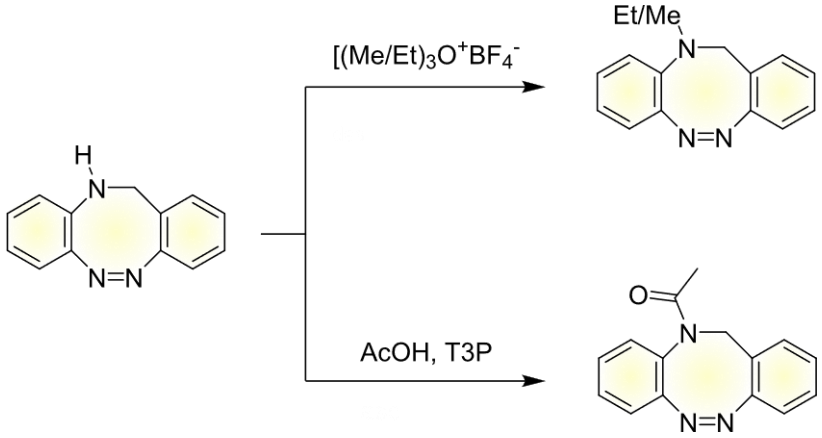

Scheme 1.9: Derivatization of *N*-H-diazocines. Alkylation can be achieved by methyl or ethyl MEERWEIN-salts while acetylation can be performed by T3P-mediated ester synthesis with acetic acid.[64]

The introduction of an acetyl group via substitution at the bridging nitrogen atom leads to a higher polarity of the whole molecule and leads to an intrinsic water solubility (∽1 mM) without any further functionalization.[64,110] UV-vis measurements in water revealed a slight hypsochromic shift of n-π*-transitions of both Z- and E-configurations and thermal half-life twice as long as in organic

solvents. At the same time the photoconversion yield of Z- to E-isomerization in water is just about 10% lower than in organic solvents while back isomerization can still be achieved quantitatively. Furthermore, quantum yields seem not to be affected by the change of solvent from organic to water.[64] This is a big advantage, since conversion rates, quantum yields and thermal half-lives are often observed to be significantly lower in water.[111,115] Thus, acetylated nitrogen bridged diazocines are a powerful tool and promising candidate for application in aqueous and biological environments for example as photoswitches in light activatable drugs.

1.7 Diindanodiazocines

Since rotational degrees of freedom have been eliminated in the development stage from azobenzene to parent diazocine, only elimination of conformational degrees of freedom remains in the way of turning azobenzene into directional photoswitches.[42,57] The introduction of two additional ethylene bridges between positions 1 and 12 and positions 10 and 11 significantly increases the rigidity already present in the parent diazocine framework and ensures that the last conformational degrees of freedom are eliminated as intended. The resulting diindanodiazocine (DID) no longer shows any inversion between different *boat*- or *twist*-conformations, since both Z- and E-configurations are limited to only one conformation due to the increased rigidity.[42] Moreover, the two additional ethylene bridges cause the formation of two stereocenters, resulting in a *meso*-compound and a racemic mixture (*rac*) (**scheme 1.12a**). The photochemical properties of both diastereomers can be investigated separately, as conversion is not possible because an inversion on a sp^3-carbon would be necessary.[42] Surprisingly, the two diastereomers show distinct differences in their switching properties, particularly with regard to their thermal relaxation. While the thermal half-life of *rac*-DID (117 h) is about four times as long as of parent diazocine (27.6 h), thermal relaxation of *meso*-DID (3 s) is four orders of magnitude faster. This may be caused by the differences in the relative energies of Z- and E-configurations of both diastereomers. The Z-configuration of *meso*-DID is thermodynamically more favored over the highly strained E-*meso*-configuration by a relative energy difference of approximately 18.5 kcal mol^{-1}. In contrast, the difference in relative energies between Z-*rac*-DID and E-*rac*-DID is much smaller (3.5 kcal mol^{-1}) resulting in a significantly longer half-life.[42] The UV spectra of *meso* -DID is quite similar to those of parent diazocine with absorption maxima at λ = 411 nm (Z-configuration) and λ = 468 nm (E-configuration) indicating almost completely separated n-π*-transitions. This leads to a photoconversion of $\Gamma_{Z\rightarrow E}$ (385 nm) = 84% and almost quantitative back isomerization ($\Gamma_{E\rightarrow Z}$ (530 nm) = >99%). Since the n-π*-transition of the Z-configuration of *rac*-DID (λ = 431 nm) is shifted significantly to higher wavelengths, it overlaps with transition of the E-configuration (λ = 478 nm). This leads to lower photoconversion yields for Z- to E-photoisomerization $\Gamma_{Z\rightarrow E}$ (385 nm) = 76% and complete back isomerization is only accessible via thermal relaxation, as a PSS of merely $\Gamma_{E\rightarrow Z}$ (530 nm) = 94% can be achieved by irradiation (**scheme 1.12b**).[42]

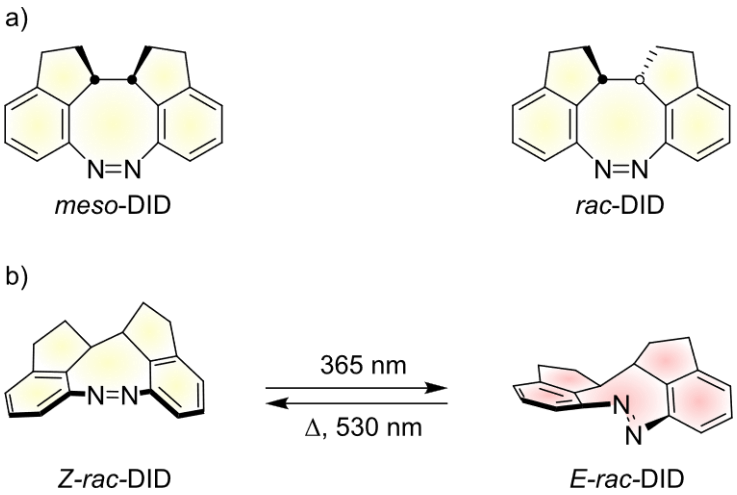

Scheme 1.12: Structures of *rac*- and *meso*-DID diastereomers (top) and photoisomerization of *rac*-DID (bottom). Light induced Z- to E-isomerization can be achieved with blue light, while back isomerization can be performed either by green light up to the PSS or completely by thermal relaxation.

Due to the elimination of all unproductive rotational and conformational degrees of freedom the photoconversion yields of both diazocine diastereomers are exceptionally high. With photoconversion yields of $\Phi_{Z\rightarrow E}$ = 0.7 and $\Phi_{E\rightarrow Z}$ = 0.9 for the *meso*-compound and $\Phi_{Z\rightarrow E}$ = 0.8 and $\Phi_{E\rightarrow Z}$ = 0.9 for the racemic mixture, both diastereomers exceed all known artificial and naturally occurring photoswitches.[42] In addition, the racemic diastereomer consists of two chiral enantiomers and therefore exhibits intrinsic chirality, which makes it the smallest chiral photoswitch known to date.[42] Because of the significant differences in their photochemical properties, the two diastereomers are suitable for very different applications. The very short half-life and excellent photoconversion yields make the *meso*-diastereomer an ideal candidate as actuator for driving molecular machines, while *rac*-DID as a chiral photoswitch is ideally suited for chiroptical switching and controlling of chirality for example in liquid crystals.[42,116-119]

2. Scope

Parent diazocines exhibit superior photochemical properties and have therefore generated a high level of interest in the field of photopharmacology[68,74] and the development of mechano- and photoresponsive materials.[66,67] However, with regard to the usable wavelength range, solubility and switching properties in aqueous media and the non-directional motion during the switching process, they still have some weaknesses. These have been addressed by further development either by systematic elimination of conformational degrees of freedom resulting in the DID[42] or by substitution of one carbon atom in the ethylene bridge by a nitrogen and subsequent introduction of a polar acetyl substituent resulting in the water soluble *N*-Ac diazocine.[64] These two further developments of parent diazocine can therefore be described as second-generation diazocines.

During the formation of the DID framework two diastereomers are formed of which the racemic form is a chiral photoswitch.[42] The chiroptical properties of both racemate-forming enantiomers could not yet be investigated. Thus, separation of both enantiomers should be achieved via *high performance liquid chromatography* (HPLC) for determination of their absolute configuration via single crystal structure analysis and subsequent characterization of their chiroptical properties. Furthermore, it should be investigated whether an enantiomeric excess could be achieved within the DID-racemate by Z- to E-photoisomerization with circular polarized light (CPL). In order to make the chiroptical properties of *rac*-DID accessible for further applications, synthesis strategies should be developed for halogen functionalization.

Nitrogen-bridged diazocines offer great potential for application in photopharmacology since they offer red-shifted n-π^*-absorption bands and intrinsic water solubility.[64] For intended application derivatization and incorporation into bigger molecules is required. Therefore, bromine and iodine substituents should be introduced as starting points for further derivatization. Additionally, reaction conditions for further derivatization of functionalized *N*-Ac diazocines should be identified. For this purpose, reaction conditions for a wide range of cross-coupling reactions should be screened. Of the derivatives obtained in this way, the influence of the new substituents on the switching behavior was to be investigated in organic and aqueous solvents.

Since the synthesis of *N*-Ac diazocines via the initial synthesis path developed by LENTES *et al*.[64,120] is quite complex with at least seven synthesis steps, new synthesis strategies should be developed and tested, which are characterized by higher overall yields with a simultaneous reduction in the number of synthesis steps. After successful preparation of the unsubstituted *N*-Ac diazocine via the new developed synthesis route, the suitability for different functional groups should be investigated.

3. Chiroptical Switching, Enrichment of Enantiomeric Excess and Derivatization of Diindanodiazocines

In structural chemistry chirality is defined by the symmetry of the corresponding molecules or supramolecular assemblies. Systems that either have no symmetry or only rotational axes (C_n) are chiral. Therefore, the absence of mirror planes, inversion centers and rotational reflection axes is a basic requirement for the presence of chirality in a molecule. At the molecular level, this means that there are two isomeric compounds of a chiral molecule, the so-called enantiomers, which cannot be superimposed with the aid of symmetry operations.[121,122] In organic chemistry, a distinction is made between chirality based on stereogenic centers, axial or planar chirality and helicity.[121] In nature a countless amount of molecules is chiral and therefore they often only occur as enantiomerically pure compounds[122] such as L-amino acids, D-saccharides or L-phospholipids.[123] Thus, interactions between chiral compounds or assemblies and their biosynthesis in biological systems hold a key position in nature.[124,125] Therefore, the control over stereochemical information under the influence of external stimuli like heat, solvent, redox reaction, pH or light has generated a great deal of interest aiming for the development of new functional materials.[123] Especially light-induced isomerization has proven to be a versatile tool since it is a non-destructive and traceless stimulus with a high spatiotemporal resolution and precisely adjustable wavelength.[126] Molecules that show a significant change in their chiral properties induced by stimuli mentioned above are called chiroptical switches.[5] Upon switching there are three conceivable effects: First, selective on-off switching of molecular chirality can be achieved. Second, the already existing chirality can be amplified upon stimuli induced switching and third an inversion of chirality can occur (**figure 3.1**).[125]

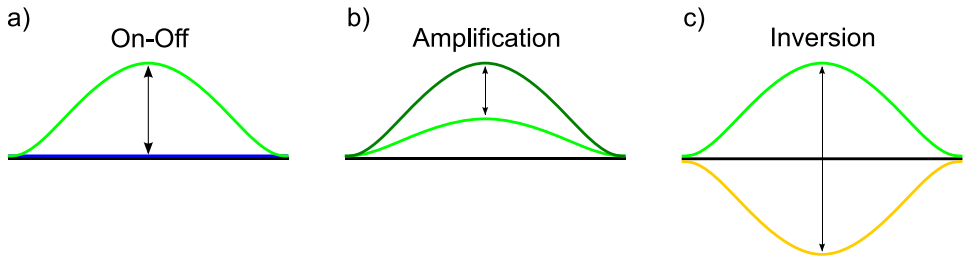

Figure 3.1: Possibilities of influencing optical activity upon switching: a) turning on and off of optical activity by switching. b) signal of optical activity is amplified or weakened due to stimuli induced switching. c) inversion of optical activity by switching. The change in optical activity is detectable via measurement of specific rotation or circular dichroism.[125]

Helical structures are a dominant structural element in biological systems and therefore dynamic control over helical chirality is a key process making numerous biological functions even accessible.[127,128] For this reason, control over helicity by chiroptical switching has generated a great deal of interest in the fields of medicine, biochemistry and polymer chemistry.[123] Especially overcrowded alkene photoswitches and motors with an intrinsic helical chirality induced by sterical hinderance initially developed by FERINGA *et al.* outgoing from the *stiff-stilbene* system have proven to be powerful tools.[129-132] Incorporated into helical structures helical chirality could be inverted reversibly during photoisomerization.[129-132] Besides controlling intermolecular interactions between helicates by chiroptical switching these molecules have been used to differentiate between several catalytic reactions.[133] Moreover, azobenzenes have been attached to helical polymer backbones as side chains. Irradiation of these helical polymers also resulted in an inversion of helical chirality due to light-induced azobenzene isomerization leading to a change in non-covalent interactions between polymer strings.[134,135] Furthermore, a three state switch consisting of two azobenzene moieties connecting two imidazole-containing clamps has been developed.[136] Starting from E,E-ground state in a first photoisomerization to Z,Z-state M-helicity can be induced which subsequently is turned into P-helicity in a second photoisomerization where the E,Z-isomer is formed.[136] Of other types of

chirality like planar chirality, axial chirality or chirality induced by stereogenic centers, there are significantly fewer examples in current literature relating to chiroptical switching induced by unpolarized light.[123]

At the same time the idea of using circular polarized light (CPL) as stimulus for chiroptical switches emerged (**figure 3.2**). This approach is based on the property of CPL to interact differently with the enantiomers depending on the direction of rotation of the electric field vector and therefore, being used for enantioselective photodecomposition of chiral molecules in a racemic mixture.[137-140] Also CPL has been observed in regions of the universe were young stars are formed and for this reason might be the origin of molecular asymmetry in nature.[141-143]

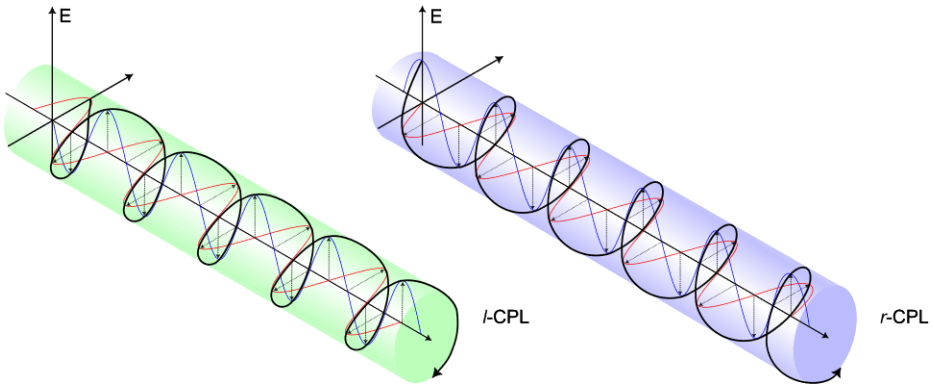

Figure 3.2: Schematic illustration of left-handed (green, l-CPL) and right-handed circular polarized light (blue, r-CPL). CPL is a superposition of two different waves polarized in orthogonal planes (blue and red curves) with a relative shift of a quarter of the corresponding wavelength resulting in an electric field vector (black) rotating around the axis of light propagation. Clockwise rotation of the electric field vector results in right-handed CPL (r-CPL) while anticlockwise rotation gives left-handed CPL (l-CPL).[144,145]

Starting from a racemic mixture of a molecule with axial or helical chirality both enantiomers can reversibly interconvert into its mirror image enantiomer in the process of photoresolution under irradiation with CPL. Thereby, the irradiation of a racemic mixture with CPL selectively excites the corresponding enantiomer leading to subsequent racemization under formation of an excess of the respective mirror image enantiomer and vice versa.[140,146,147] The selectivity to be expected during photoresolution can be estimated by Kuhn anisotropy factor g which can also be used to calculate a theoretical enantiomeric excess (**equation 1**) using the molar circular dichroism $\Delta\varepsilon$ and molar extinction coefficient ε_λ.[148] However, it must be noted that ee achieved by photoresolution rarely exceeds 0.5%, as values of less than 0.01 are usually achieved for the molecular anisotropy factor.[146,149]

$$ee = \frac{g}{2} = \frac{\Delta\varepsilon}{2\varepsilon_\lambda} \tag{1}$$

Photoresolution can also be achieved by switching between two interconvertable enantiomers of chiroptical photoswitches with CPL from a racemic mixture. The possibility to interconvert selectively between both enantiomers without photodegradation, a high g factor, thermally stable enantiomers and an efficient photoracemization with high quantum yields are therefore necessary requirements for a successful CPL switch.[146] This type of dynamic photoresolution has been achieved for overcrowded alkenes[138] and bicyclic ketones,[140,150] whereby these molecules are brought to an excited state via CPL in which racemization of the enantiomer corresponding to the handedness of the used CPL occurs.[146] Another example are mono-[151] and bicyclic azobenzene derivatives[152] as chiroptical switches for photoresolution although this takes place via a different reaction pathway. Outgoing from the thermodynamically stable E-configuration cyclic azobenzenes are excited to Z-ground state where fast racemization of the enantiomer corresponding to the CPL used for excitation takes place.[151,152]

CPL can also be used for asymmetric synthesis aiming for the introduction of chirality into an achiral precursor resulting in an enantiomeric imbalance. However, the conversion of achiral diarylolefines into their chiral helicene derivatives is the only example in current literature for this type of irreversible chirality induction.[153-157] The only example of dynamic asymmetric synthesis resulting in an enantiomeric imbalance starting from an achiral photoswitchable compound was provided by the TAMAOKI group and is based on an E,E-azobenzene dimer.[158] Irradiation of the E,E-dimer with CPL results in formation of a racemic mixture of two E,Z-enantiomers whereby an *ee* of the enantiomer corresponding to the handedness of the used CPL could be achieved. The chirality can be removed by either switching to the Z,Z-configuration or thermal or respectively light-induced relaxation to the initial E,E-configuration. Basic requirement is that both enantiomers cannot be interconverted into each other.[158]

In terms of their use, a wide range of applications for light-controlled chiroptical switches are conceivable. For example, enormous potential is offered in the field of asymmetric synthesis, where chiroptical switches could be incorporated into catalysts with switchable chirality. For targeting a specific enantiomer, the corresponding chiral catalyst is required. If the opposite enantiomer is targeted the same catalyst could be used with inverted chirality adjusted by external CPL-stimulus.[123,133,159] Besides, light-driven chiroptical switches have been incorporates into helical foldamers for inversion and affection of their chirality for application in molecular recognition[134,135] or host-guest chemistry.[136] Furthermore, great potential is offered in the field of tunable liquid crystals. There are already examples in current literature, where light-induced chiroptical switching of chiral liquid crystalline polymers has affected their macromolecular organization and therefore an interconversion between various liquid crystal phases could be induced.[116,160]

Although azobenzenes as direct predecessors of diazocines have been applied in a variety of ways in the field of light-driven chiroptical switching the parent diazocine itself has not been used as a chiroptical photoswitch so far. The *rac*-DID recently reported from the HERGES group[42] could bring bridged azobenzenes into the focus of chemists working on chiroptical photoswitches due to its superior photochemical properties and its intrinsic chirality. Therefore, the intention of this project was to investigate the chiroptical properties of *rac*-DID in detail and to make the molecule accessible for subsequent application by derivatization.

3.1 Summary of Determination of Enantiomeric Excess by Photoswitching of Chiral Diindanodiazocine Racemic Mixture with Circular Polarized Light

Previously our group reported the successful synthesis of *rac*- and *meso*-DID diastereomers.[42] Both are photoswitches in which unproductive conformational and rotational degrees of freedom have been eliminated in favor of improved switching characteristics. The synthesis results in two diastereomers of which the racemate consists of two non-convertible chiral enantiomers whereby chirality is induced by the presence of two stereogenic centers in the molecule.[42] Within the scope of this work we developed a method to separate both enantiomers via chiral HPLC. Single crystal structures of both enantiomers could be obtained and with the help of specific rotation measurements as well as quantum-mechanical calculations absolute configuration could be determined. Measurements of specific rotation before and after photoisomerization showed a huge difference of optical activity between Z- and E-configuration in form of massive amplification of optical activity. This is supported by spectra of circular dichroism (CD) showing significantly different spectra for both Z- and E-configuration as well.

Since TAMAOKI *et al.* showed that enantiomeric excess (ee) could be obtained after irradiation of a prochiral azobenzene dimer with CPL, we aimed for selective photoresolution of one *rac*-DID enantiomer after irradiation of the racemic mixture with the corresponding CPL.[151,158] For this purpose, the ee to be expected was calculated with help of molecular dissymmetry (g-factor) using molar extinction coefficient (ε) and molar circular dichroism ($\Delta\varepsilon$) of *rac*-DID at irradiation wavelength giving theoretical ee values of about 0.32%. In the following a solution of *rac*-DID was irradiated with CPL and from the ellipticity measured at defined wavelength in the CD spectrometer under assumption of the PSS as quasistationary state the ee could be calculated with values of about 0.35% being slightly higher than the theoretical value but still in very good agreement (**scheme 3.1**).

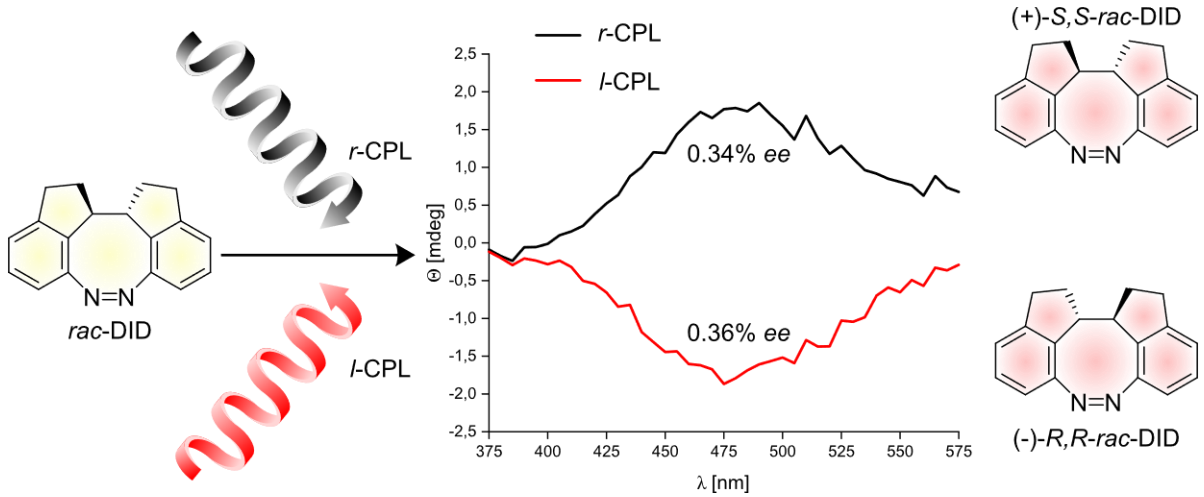

Scheme 3.1: Photoisomerization of Z-*rac*-DID (yellow) after irradiation with r-CPL or l-CPL respectively of 405 nm wavelength. By this way of photoresolution ee values of 0.34% for r-CPL and 0.36% for l-CPL could be achieved for the corresponding E-enantiomers (red).

Besides being the smallest chiral photoswitch known to date superior switching characteristics and chiroptical switching properties presented in this article make *rac*-DID a promising candidate for application in chiral smart materials or liquid crystals.

3.2 Determination of Enantiomeric Excess by Photoswitching of Chiral Diindanodiazocine Racemic Mixture with Circular Polarized Light

Thomas Brandt, Widukind Moormann, Jan-Simon von Glasenapp, Jan Peter Mikosch, Christian Näther and Rainer Herges

Manuscript prepared for submission.

Scientific contribution to this paper: UV-vis (spectra, determination of extinction coefficents) and NMR measurements (determination of PSS), single crystal growth, measurement of optical rotation, calculation of theoretical *ee*, determination of *ee* from switching experiments with CPL, writing of the manuscript and supporting information.

WILEY-VCH

RESEARCH ARTICLE

Determination of Enantiomeric Excess by Photoswitching of Chiral Diindanodiazocine Racemic Mixture with Circular Polarized Light

Thomas Brandt[a], Widukind Moormann[a], Jan Simon von Glasenapp[a], Jan Peter Mikosch[a], Christian Näther[b], Rainer Herges[a]*

[a] T. Brandt, Dr. W. Moormann, J. S. von Glasenapp, J. P. Mikosch, Prof. Dr. R. Herges
Otto-Diels-Institut für Organische Chemie
Christian-Albrechts-Universität zu Kiel
Otto-Hahn-Platz 4, 24118 Kiel (Germany)
E-mail: rherges@oc.uni-kiel.de

[b] Prof. Dr. C. Näther
Institut für Anorganische Chemie
Christian-Albrechts-Universität zu Kiel
Max-Eyth-Str. 2, 24118 Kiel (Germany)

Supporting information for this article is given via a link at the end of the document.((Please delete this text if not appropriate.))

Abstract: Insert abstract text here. ((Maximum 200 words in length. Please ensure your abstract is written so that it can be understood on its own (for example, in an abstracting service such as PubMed), with all abbreviations defined.))

Introduction

The interactions between chiral compounds or assemblies in biological systems are a key factor of molecular processes in nature.[1,2] Thus, control of stereochemical information on a molecular level by external stimuli has gained a lot interest concerning the development of new functional materials in the broad field of supramolecular chemistry.[3] Molecules that undergo a significant change in their optical behavior (dynamic chirality) under the influence of an external stimulus like redox reactions, heat, solvent, pH or light are called chiroptical switches.[4] Especially light-induced photoisomerization is a versatile tool as a traceless and non-destructive stimulus.[5] The best investigated chiral irradiation is circular polarized light (CPL),[6,7] which is also assumed to be the root of molecular asymmetry.[6-11] Therefore, the interaction of CPL with chiral molecules or assemblies to affect the enantiomeric balance remains an area of high interest.[12-19] The enrichment of an enantiomer from a racemic mixture via CPL are either performed by photodestruction, photoresolution or asymmetric synthesis.[6] While photodestruction with l -CPL selectively decomposes the corresponding (*S*)-enantiomer the opposing (*R*)-enantiomer is enriched without interconversion in the racemic mixture and vice versa photoresolution enables nondestructive enrichment. For this the irradiation of a racemic mixture with *l*-CPL causes the formation and consequently accumulation of a *R*-enantiomer due to selective excitation and racemization of *S*-enantiomer up to an equilibrium. Enrichment of *S*-enantiomer works the same way with r -CPL. In contrast to these two methods asymmetric synthesis starts from an achiral precursor, whereby irradiation with l-CPL gives the *R*- and irradiation with r-CPL gives the *S*-enantiomer.[6] There are a few examples in literature for dynamic photoresolution initiated by CPL irradiation like overcrowded alkenes,[13] bicyclic ketones[20,21] or mono-[14] and bicyclic[18] azobenzene derivatives. Also, a dynamic CPL-induced asymmetric synthesis of an unbalanced racemic mixture of an azobenzene dimer obtained from a prochiral precursor was reported,[19] showing that azobenzenes which are the most commonly used photoswitches are a factor in the field of dynamic chirality.[2] Although they are superior to azobenzenes in almost all aspects[22,23] bridged azobenzenes, so called diazocines, to the best of our knowledge have not been taken to account for chiroptical switching so far while finding application in the fields of material science[24-26] or photopharmacology[27-30] and great achievements have been made in their further development.[31-36]

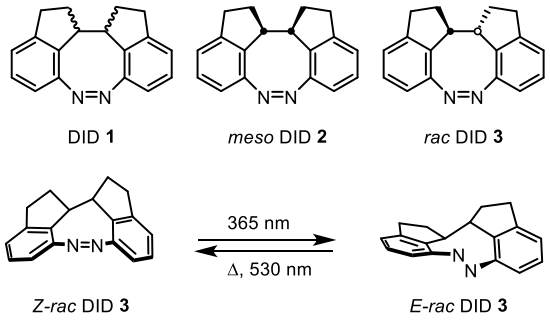

Figure 1. General structure of diindanodiazocine **1** and of *meso*- **2** and *rac*-diastereomers **3** (top). Light-induced switching between *Z*- and *E*-configurations of *rac*-DID **3**.

Our group recently reported the development of diindanodiazocines (DID) **1** which are showing superior quantum

yields outnumbering even the highest yields known from natural (rhodopsin) and artificial photoswitches. Furthermore, the elimination of conformational degrees of freedom by introduction of further ethylene bridges compared to diazocine parent system leads to an outstandingly high efficiency converting light to chemical energy and directional motion upon photoisomerization which can be achieved with light in the visible range. Besides, the additional ethylene bridges lead to a diastereomeric mixture containing the achiral *meso*-DID **2** and the chiral *rac*-DID **3**, the latter being the smallest chiral photoswitch known to date. Both diastereomers can easily be obtained on a multigram scale in a two-step synthesis path.[35]

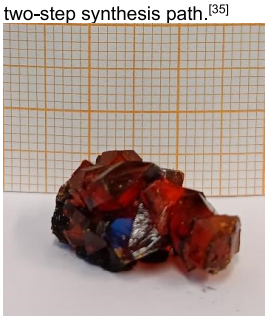

Figure 2: Grown crystal of *rac*-diindanodiazocine **3**.

In this work we explored the chiroptical properties of our recently presented *rac*-diindanodiazocine **3** and its' enantiomers in thermodynamically stable *Z*-configuration and in the PSS after irradiation with light. In addition, we studied the effect the enantiomeric ratio of *rac*-DID **3** in the PSS after excitation from ground state after excitation with CPL of a specific wavelength. Furthermore, the kinetic resolution from PSS to the ground state was performed with CPL. The determinations of enantiomeric excess were performed via CD-spectroscopy and compared to calculated values. To the best of our knowledge this is the first example of dynamic photoresolution of a chiroptical switch only by CPL-induced *Z*-to *E*-isomerization without racemization.

Results and Discussion

Synthesis and structural characterization

The *rac*-DID **3** has been synthesized according to our previously published two-step synthesis path where the diastereomeric mixture of dinitroprecursor **4** could be separated via column chromatography.[35] The chiroptical properties of *rac*-DID **3** should be examined subsequently. Therefore, *rac*-DID **3** has been separated into the enantiomers via *high performance liquid chromatography* (HPLC) on Daicel Chiracel® OD-H chiral column with *n*-heptane/isopropanol 98:2 as eluent (figure 3).

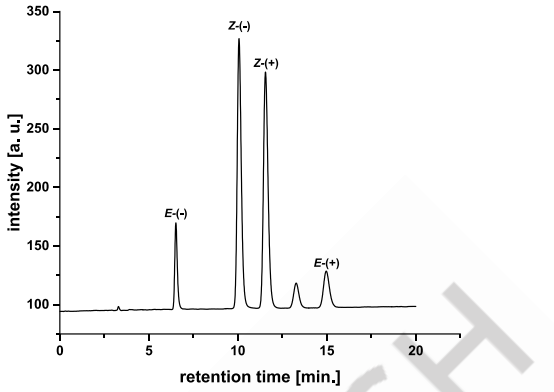

Figure 3: Chromatogram of enantiopurification of *rac*-DID **3** via chiral HPLC.

The specific rotation of both enantiomers was determined for identification of the left- and the right-handed enantiomer. The unirradiated (-)-DID **5** shows a specific rotation of -370 ° while the unirradiated (+)-DID **6** shows a specific rotation of 390 °.

For assignment of (-)- **5** and (+)-DID **6** to the absolute configuration single crystals were grown and the single crystal structure was determined (figure 4). The (-)-DID **5** could be assigned to the *R*,*R*-enantiomer and the (+)-DID **6** the *S*,*S*-enantiomer.

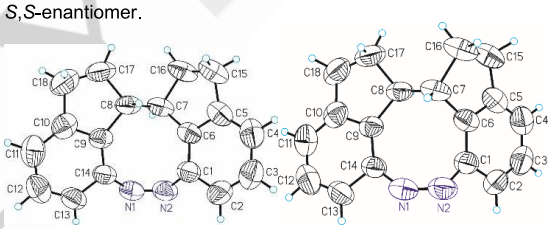

Figure 4: Single crystal structures of (-)-DID **5** (left) and (+)-DID **6** (right). The *R*,*R*-configuration could be assigned to the (-)-DID **5** and the *S*,*S*-configuration to the (+)-DID **6**.

Chiroptical characterization

Since the conformational changes and the differences of the photochemical properties of *rac*-DID **3** upon photoisomerization are quite big, this should also be visible in the specific rotation values and the CD-spectra of the *Z*- and *E*-configurations. To assign the specific rotation TD-DFT calculations were performed. The obtained theoretical CD-Spectra assign positive Molar circular dichroism values to the (+)-*S*,*S*-enantiomer **6** (See SI "Quantum Chemical Calculations" for details).[37-46] We were subsequently able to obtain enantiomeric pure compounds **5** and **6**. For switching of the specific rotation the unirradiated (-)-*R*,*R*-enantiomer **5** was measured at first giving a specific rotation of -370 °. Then the sample was irradiated with blue light of 385 nm and measured again giving a seven times higher specific rotation of -1358 ° before being switched back to -196 ° with green light at 530 nm. Irradiation of (+)-*S*,*S*-enantiomer **6** with a specific rotation of 390 ° gave a value of 1524 ° after irradiation with blue light (385 nm) which also about seven times higher as the value of 216 ° after irradiation with green light (530 nm). For both enantiomers the switching between specific

rotation of *E*- and *Z*-configuration could be performed repeatedly for several times without fatigue (figure 5).

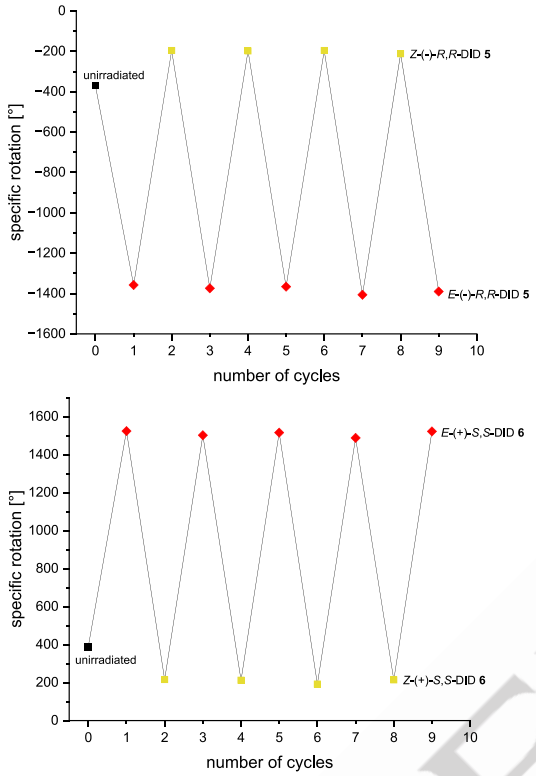

Figure 5: Repeated switching of specific rotation at 589 nm of (-)-*R*,*R*-DID **5** (top) and (+)-*S*,*S*-DID **6** (bottom) upon irradiation with 385 nm (*Z* to *E*) or 530 nm (*E* to *Z*) in acetone at 20 °C with a concentration of 50 mg/100 mL.

This enormous change is also visible in the CD-spectra of unirradiated and irradiated DID enantiomers **5** and **6** (figure 6). The CD-spectra of pure *trans*-configurations of both enantiomers were extrapolated from the CD-spectra measured at PSS in THF at 25 °C after irradiation with blue light (385 nm). The determination of the PSS in THF-d_8 at 25 ° resulted in a value of 77%.

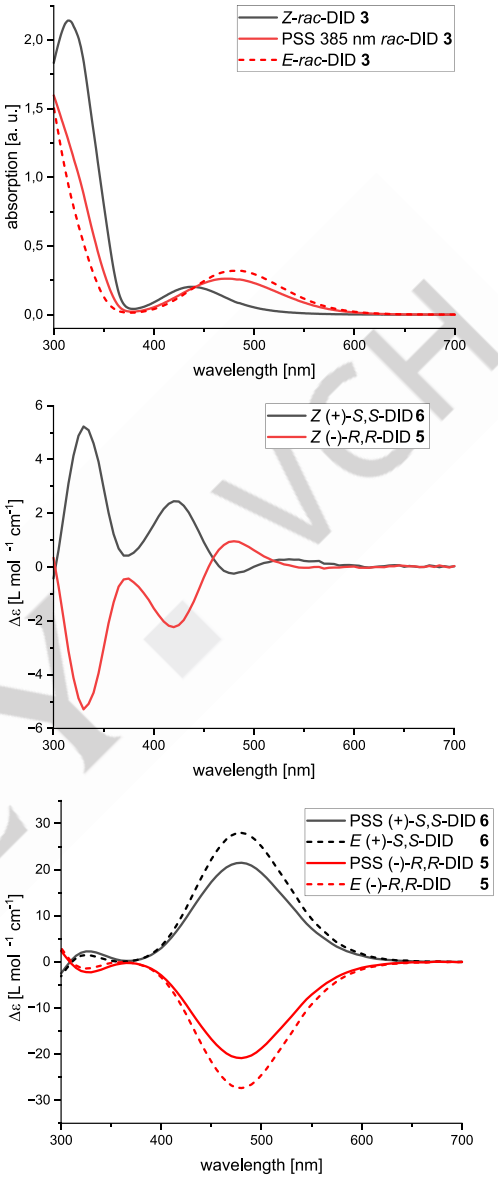

Figure 6: a) UV-spectra of *rac*-DID **3** (1 mM) in THF at 25 °C. Spectra of pure *E*-configuration were extrapolated from PSS at 385 nm.
b) Molar circular dichroism $\Delta\varepsilon$ of (-)-*R*,*R*-DID **5** (1.04 mM) and (+)-*S*,*S*-DID **6** (1.34 mM) before (center) and at PSS after irradiation with blue light at 385 nm (bottom) in THF at 25°C. The spectra of pure trans-configuration were extrapolated from PSS values and spectra.

Enrichment of the enantiomers via CPL

In this work we aimed for the induction of enantiomeric imbalance by irradiation with CPL from a racemic mixture of chiral diindanodiazocine **3** as a new type of photoresolution without racemization. Therefore, a 0.86 mM solution of *Z*-*rac*-DID **3** was irradiated with *r*/*l*-CPL at 405 nm to achieve a high concentration

of E-configuration and a high value of $\Delta\varepsilon$ for both enantiomers. Irradiation with r -CPL at 405 nm resulted in a positive CD spectrum after an irradiation time of 27 min. The opposing CD signals with the same intensity could be achieved by irradiating the sample with l-CPL at 405 nm for the same time (figure 7) while irradiation with unpolarized light lead to an inactive CD spectrum.

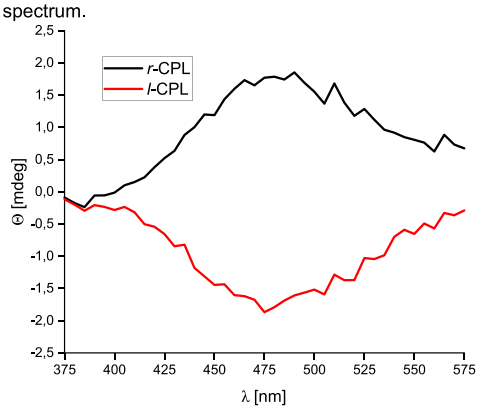

Figure 7: Induced CD spectra of *rac*-DID **3** 0.86 mM in THF at PSS after 27 min. of irradiation with r-CPL (black) or l-CPL (red) at 405 nm.

The ability of chiral molecules is defined by its absorption selectivity of CPL light which is quantified by the dissymmetry or g -factor[47-49] which can be calculated from the molar circular dichroism $\Delta\varepsilon$ of the pure enantiomer and the molar extinction coefficient ε for the excitation wavelength (eqn 1).[19,48] Inserting the experimental values of $\Delta\varepsilon_{405\,nm}$ (1.88353 L mol^{-1} cm^{-1}) and $\varepsilon_{405\,nm}$ (286.93 L mol^{-1} cm^{-1}) for the irradiation of *Z*-*S*,*S*-DID **6** with r-CPL at 405 nm results in a g-factor of 6.56 × 10^{-3} while for irradiation of *Z*-*R*,*R*-DID **5** with l-CPL a g-factor of 6.23 × 10^{-3} is achieved with $\Delta\varepsilon_{405\,nm}$ = -1.78884 L mol^{-1} cm^{-1}.

$$g = \frac{|\Delta\varepsilon|}{\varepsilon} \quad (1)$$

The *g*-factor also allows the calculation a the theoretical *ee* (eqn 3) for the photoresolution with CPL if the values of $\Delta\varepsilon$ and ε for the excitation wavelengths are used.[19]

$$ee_{PSS} = \frac{\Delta\varepsilon}{2\varepsilon} \times 100\% = \frac{g}{2} \times 100\% \quad (2)$$

This gave a theoretical *ee* of 0.328% for *E*-*S*,*S*-DID **6** (r-CPL at 405 nm) and 0.312% for *E*-*R*,*R*-DID **5** (l-CPL at 405 nm) after irradiation with CPL.

For experimental determination of the enantiomeric excess (*ee*) of *E*-*rac*-DID **3** after irradiation with r / l -CPL at 405 nm we performed several measurements at 480 nm with increasing irradiation times up to 31 min. to ensure the achievement of the PSS (figure 8). We calculated the photoinduced *ee* using eqn 3 following the method of TAMAOKI and coworkers[19] from the molar circular dichroism $\Delta\varepsilon_{480\,nm}$ of the pure *E*-enantiomer and the induced CD value $\theta_{480\,nm}$ for a 0.86 mM solution of *rac*-DID **3** in THF (table 1). For the calculations the PSS of *rac*-DID **3** was determined via ^{1}H-NMR at 298 K with 67% after irradiation with blue light at 405 nm.

$$ee_{PSS\,405\,nm} = \frac{[S]-[R]}{[S]+[R]} \times 100\% \quad (3)$$

where

$$[S] - [R] = \frac{\theta_{480\,nm}}{32980 \times \Delta\varepsilon_{480\,nm} \times 1cm}$$

$$[S] + [R] = [E\text{-}rac\text{-DID } \mathbf{3}] \text{ at } PSS_{405\,nm}$$

These calculations gave an *ee* of 0.344% for *E*-*S*,*S*-DID **6** after irradiation with r-CPL at 405 nm while irradiation with l-CPL at the same wavelength resulted in an *ee* of 0.357% of *E*-*R*,*R*-DID **5**. These values are in very good agreement with the theoretical values calculated from the enantiomers g-factors.

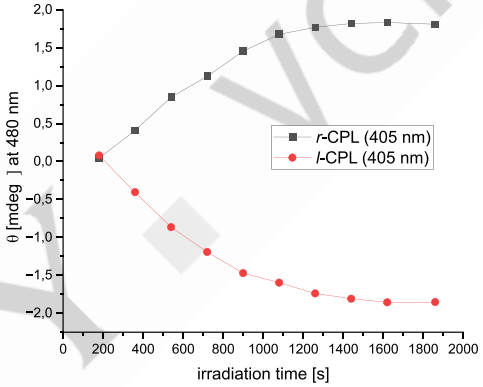

Figure 8: Induced ellipticity Θ at 480 nm of *E*-*rac*-DID **3** (0.86 mM) after irradiation with r-CPL (black) and l-CPL (red) at 405 nm depending on the irradiation time.

Table 1: Values used for the calculation of the enantiomeric excess of *E*-*rac*-DID **3** (0.86 mM) after irradiation with *r*/*l*-CPL at 405 nm.

CPL nm	$\Delta\varepsilon_{480\,nm}$ L mol^{-1} cm^{-1}	θ_{480nm}	$ee_{PSS\,405\,nm}$
r-405	27.97355	1.83124	0.344%
l-405	-27.36345	-1.85721	0.357%

Conclusion

Racemic mixture of diindanodiazocine **3** has been synthesized according to previously published literature[35] and separated into its enantiomers **5** and **6** via HPLC. Absolute configuration of both enantiomers could be assigned via specific rotation, single crystal structure determination and quantum mechanical calculations. It could be shown that *Z*- and *E*-configuration of both enantiomers show different interactions with linear polarized light. Specific rotation can therefore be influenced via switching between *Z*- and *E*-configurations with light by a factor of seven. Measurements of circular dichroism of both enantiomers also showed a significant change of the interaction of *Z*- and *E*-configurations with circular polarized light. Thus, the ratio of both enantiomers being isomerized upon irradiation should be assessable via photoisomerization with CPL. This could be shown with CD spectra of the racemic mixture after irradiation with l- or r-CPL

respectively. The accessible *ee* of the *Z* to *E* photoisomerization with l- and r-CPL at 405 nm has been calculated from the molecules g-factor and was in very good agreement with the results from CD measurements. These promising results of the smallest chiral photoswitch known so far are proof of its potential for application in liquid crystals or chiral smart materials.

Supporting Information ((optional))

The authors have cited additional references within the Supporting Information.[30, 31] ((Please include SI references with consecutive numbering directly after the last manuscript reference: 1, 2, 3,…30, 31))

Acknowledgements ((optional))

Acknowledgements Text. ((Data Availability and Conflicts of Interest statements are generated automatically from information in Editorial Manager!))

Keywords: ((Use American English; keywords should be concise, 5 maximum!)) keyword 1 • keyword 2 • keyword 3 • keyword 4 • keyword 5

References

[1] J. J. D. de Jong, L. N. Lucas, R. M. Kellogg, J. H. van Esch, B. L. Feringa, *Science* **2004**, *304*, 278-281.
[2] L. Zhang, H.-X. Wang, S. Li, M. Liu, *Chem. Soc. Rev.* **2020**, *49*, 9095-9120.
[3] D. Sahoo, R. Benny, N. K. Ks, S. De, *ChemPlusChem* **2022**, *87*, e202100322.
[4] B. L. Feringa, R. A. van Delden, N. Koumura, E. M. Geertsema, *Chem. Rev.* **2000**, *100*, 1789-1816.
[5] H. K. Bisoyi, Q. Li, *Angew. Chem. Int. Ed.* **2016**, *55*, 2994-3010.
[6] B. L. Feringa, R. A. van Delden, *Angew. Chem. Int.l Ed.* **1999**, *38*, 3418-3438.
[7] M. Avalos, R. Babiano, P. Cintas, J. L. Jiménez, J. C. Palacios, L. D. Barron, *Chem. Rev.* **1998**, *98*, 2391-2404.
[8] J. A. Le Bel, *Bull. Soc. Chim. Fr.* **1874**, *22*, 337-347.
[9] J. A. Le Bel, *Bull. Soc. Chim. Fr.* **1874**, *22*, 337-347.
[10] J. H. Hoff, *Voorstel tot uitbreiding der tegenwoordig in de scheikunde gebruikte structuur-formules in de ruimte: Benevents een daarmeê samenhangende opmerking omtrent het verband tusschen optisch actief vermogen en chemische constitutie van organische verbindingen*, J. Greven, Utrecht, **1874**.
[11] J. H. Hoff, *Die Lagerung der Atome im Raume*, Friedrich Vieweg und Sohn, Braunschweig, 2nd edn, **1894**.
[12] J. Hou, J. Liao, Y. Feng, B. L. Feringa, J. Chen, H. Li, G. Zhou, *ChemPlusChem* **2020**, *85*, 1104-1110.
[13] N. P. M. Huck, W. F. Jager, B. de Lange, B. L. Feringa, *Science* **1996**, *273*, 1686-1688.
[14] P. K. Hashim, R. Thomas, N. Tamaoki, *Chem. Eur. J.* **2011**, *17*, 7304-7312.
[15] A. Adam, G. Haberhauer, *J. Am. Chem. Soc.* **2017**, *139*, 9708-9713.
[16] H. Nishino, M. Hosaka, M. Katoh, Y. Inoue, *Chem. Eur. J.* **2013**, *19*, 13929-13936.
[17] H. Nishino, A. Kosaka, G. A. Hembury, F. Aoki, K. Miyauchi, H. Shitomi, H. Onuki, Y. Inoue, *J. Am. Chem. Soc.* **2002**, *124*, 11618-11627.
[18] N. Tamaoki, M. Wada, *J. Am. Chem. Soc.* **2006**, *128*, 6284-6285.
[19] K. Rijeesh, P. K. Hashim, S.-I. Noro, N. Tamaoki, *Chem. Sci.* **2015**, *6*, 973-980.
[20] Y. Zhang, G. B. Schuster, *J. Org. Chem.* **1995**, *60*, 7192-7197.
[21] M. Suarez, G. B. Schuster, *J. Am. Chem. Soc.* **1995**, *117*, 6732-6738.
[22] R. Siewertsen, H. Neumann, B. Buchheim-Stehn, R. Herges, C. Näther, F. Renth, F. Temps, *J. Am. Chem. Soc.* **2009**, *131*, 15594-15595.
[23] R. Siewertsen, J. B. Schönborn, B. Hartke, F. Renth, F. Temps, *Phys. Chem. Chem. Phys.* **2011**, *13*, 1054-1063.
[24] M. H. Burk, D. Langbehn, G. Hernández Rodríguez, W. Reichstein, J. Drewes, S. Schröder, S. Rehders, T. Strunskus, R. Herges, F. Faupel, *ACS Appl. Polym. Mater.* **2021**, *3*, 1445-1456.
[25] D. Hugenbusch, M. Lehr, J.-S. von Glasenapp, A. J. McConnell, R. Herges, *Angew. Chem. Int. Ed.* **2023**, *62*, e202212571.
[26] W. Moormann, D. Langbehn, R. Herges, *Beilstein J. Org. Chem.* **2019**, *15*, 727-732.
[27] G. Cabré, A. Garrido-Charles, À. González-Lafont, W. Moormann, D. Langbehn, D. Egea, J. M. Lluch, R. Herges, R. Alibés, F. Busquéet al., *Org. Lett.* **2019**, *21*, 3780-3784.
[28] J. Ewert, L. Heintze, M. Jordà-Redondo, J.-S. von Glasenapp, S. Nonell, G. Bucher, C. Peifer, R. Herges, *J. Am. Chem. Soc.* **2022**, *144*, 15059-15071.
[29] L. Heintze, D. Schmidt, T. Rodat, L. Witt, J. Ewert, M. Kriegs, R. Herges, C. Peifer, *Int. J Mol. Sci.s* **2020**, *21*, *8961*.
[30] F. Wages, P. Lentes, T. Griebenow, R. Herges, C. Peifer, E. Maser, *Chem.-Biol. Interact.* **2022**, *354*, 109822.
[31] M. Hammerich, C. Schütt, C. Stähler, P. Lentes, F. Röhricht, R. Höppner, R. Herges, *J. Am. Chem. Soc.* **2016**, *138*, 13111-13114.
[32] J. Isokuortti, T. Griebenow, J.-S. von Glasenapp, T. Raeker, M. A. Filatov, T. Laaksonen, R. Herges, N. A. Durandin, *Chem. Sci.* **2023**, *14*, 9161-9166.
[33] P. Lentes, P. Frühwirt, H. Freißmuth, W. Moormann, F. Kruse, G. Gescheidt, R. Herges, *J. Org. Chem.* **2021**, *86*, 4355-4360.
[34] P. Lentes, E. Stadler, F. Röhricht, A. Brahms, J. Gröbner, F. D. Sönnichsen, G. Gescheidt, R. Herges, *J. Am. Chem. Soc.* **2019**, *141*, 13592-13600.
[35] W. Moormann, T. Tellkamp, E. Stadler, F. Röhricht, C. Näther, R. Puttreddy, K. Rissanen, G. Gescheidt, R. Herges, *Angew. Chem. Int. Ed.* **2020**, *59*, 15081-15086.
[36] M. S. Maier, K. Hüll, M. Reynders, B. S. Matsuura, P. Leippe, T. Ko, L. Schäffer, D. Trauner, *J. Am. Chem. Soc.* **2019**, *141*, 17295-17304.
[37] T. Lu, F. Chen, *J. Comput. Chem.* **2012**, *33*, 580-592.
[38] F. Weigend, *Physical chemistry chemical physics PCCP* **2006**, *8*, 1057-1065.
[39] F. Weigend, R. Ahlrichs, *Phys. Chem. Chem. Phys.* **2005**, *7*, 3297-3305.
[40] J. P. Perdew, K. Burke, M. Ernzerhof, *Phys. Rev. Lett.* **1996**, *77*, 3865-3868.
[41] J.-D. Chai, M. Head-Gordon, *J. Chem. Phys.* **2008**, *128*, 84106.
[42] S. J. Strickler, R. A. Berg, *J. Chem. Phys.* **1962**, *37*, 814-822.
[43] E. Caldeweyher, C. Bannwarth, S. Grimme, *J. Chem. Phys.* **2017**, *147*, 34112.
[44] E. Caldeweyher, S. Ehlert, A. Hansen, H. Neugebauer, S. Spicher, C. Bannwarth, S. Grimme, *J. Chem. Phys.* **2019**, *150*, 154122.
[45] S. Grimme, *J. Chem. Phys.* **2013**, *138*, 244104.
[46] B. de Souza, F. Neese, R. Izsák, *J. Chem. Phys.* **2018**, *148*, 34104.
[47] J. L. Greenfield, J. Wade, J. R. Brandt, X. Shi, T. J. Penfold, M. J. Fuchter, *Chem. Sci.* **2021**, *12*, 8589-8602.
[48] W. Kuhn, *Trans. Faraday Soc.* **1930**, *26*, 293.
[49] R. M. Pagni, J. Bartmess, *Chirality* **2006**, *18*, 419-425.

3.3 Summary of Synthesis and Characterization of New Diindanodiazocine Derivatives

Diindanodiazocines have shown to be superior photoswitches compared to known naturally occurring and artificial switches due to the elimination of rotational and conformational degrees of freedom.[42] Further investigations on the chiral *rac*-diastereomer and the consisting enantiomers also showed significant change in chiroptical properties upon light induced Z- to E-isomerization and also accumulation of one favored enantiomer could be achieved by irradiation with corresponding CPL.[161] For further derivatization and functionalization di- and tetrahalogenated DID derivatives should be synthesized and characterized (scheme 3.2).

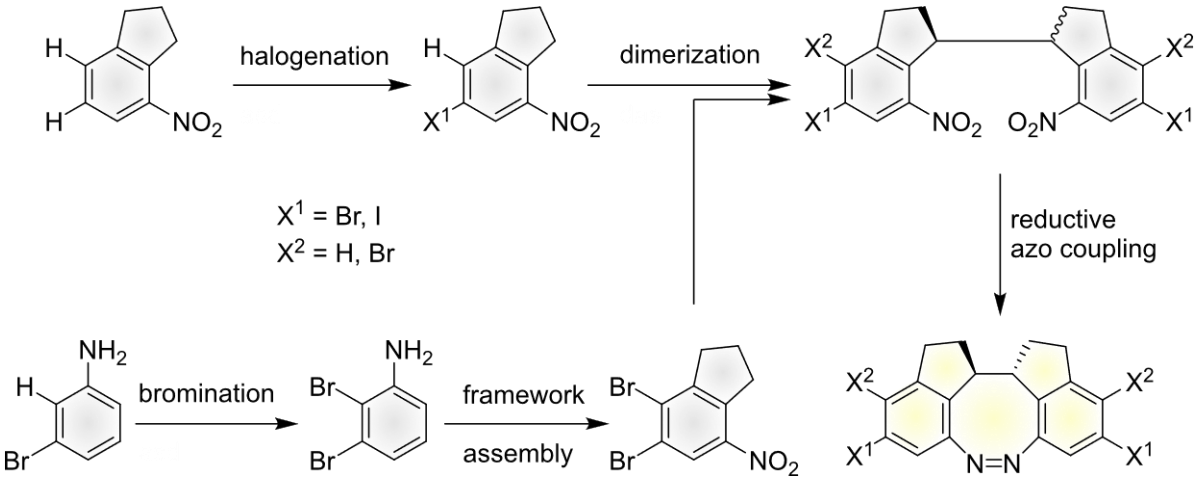

Scheme 3.2: Schematic synthesis of given halogenated DID derivatives following the procedure of MOORMANN *et al*. for unsubstituted DID framework.[42] Dihalogenated building blocks could be obtained by electrophilic aromatic substitution of nitroindane while for tetrasubstituted DID halogen substituents had to be introduced before setting up the indane framework.

Halogenated derivatives could be synthesized according to the known procedure established by MOORMANN *et al*.[42] after the halogenated nitroindane building blocks had been prepared. For dihalogenated derivatives the corresponding nitroindane building blocks could easily be obtained by electrophilic aromatic substitution of nitroindane with corresponding halogen succinimide. While *meso*- and *rac*-diastereomers of dibrominated DID could be synthesized without complications, only the *rac*-diiodo DID could be obtained. As the reason for this reduction of the iodine substituent occurring during the reductive azo condensation. Therefore, *meso*-diodo DID was reduced to the unsubstituted DID in its entirety. For tetrabrominated DID the second bromo substituent had to be introduced before synthesizing the indane framework resulting in low yields of the corresponding building block due to side reactions. Additionally, only the racemate of tetrabrominated DID could be synthesized due to the unfavored formation of the *meso*-diastereomer. Photochemical characterization revealed only minor deviation from the corresponding unsubstituted diastereomers concerning absorption wavelengths and photoconversion yields while at the same time thermal half-lives of all derivatives synthesized within this project are significantly shortened after introduction of halogen substituents.

3.4 Synthesis and Characterization of New Diindanodiazocine Derivatives

Thomas Brandt, Jan Peter Mikosch, Lasse Cipriani and Rainer Herges

Manuscript prepared for submission.

Scientific contribution to this paper: Conceptual Design, Development of the Synthesis pathway, Synthesis and Characterization of compounds with help of Jan Peter Mikosch and Lasse Cipriani, UV (spectra and half-lives) and NMR measurements (spectra and PSS measurements), writing of the manuscript and Supporting Information.

Synthesis and Characterization of New Diindanodiazocine Derivatives

Thomas Brandt[1], Jan Peter Mikosch[1], Lasse Cipriani[1], Rainer Herges*[1]

Address: [1]Otto-Diels-Institut für Organische Chemie
Christian-Albrechts-Universität zu Kiel
Otto-Hahn-Platz 4, 24118 Kiel (Germany)

Email: Rainer Herges - E-mail: rherges@oc.uni-kiel.de

* Corresponding author

‡ Equal contributors

Abstract

Abstract text

Keywords

keyword; keyword; keyword; keyword; keyword

Introduction

Bridged azobenzenes, so called diazocines, exhibit exceptional photophysical properties [1,2] and are therefore frequently used photoswitches with a broad field of application such as material science [3-6] or photopharmycology [7-11]. Especially the

well separated $n - \pi^*$ transition in the visible range of the electromagnetic spectrum allowing excellent photoconversion between *Z* and *E* configurations ($\Gamma_{Z\rightarrow E,\ 385\,nm} = 92\%$, $\Gamma_{Z\rightarrow E,\ 525\,nm} > 99\%$ in n-hexane) and high quantum yields ($\Phi_{Z\rightarrow E} = 0.72$, $\Phi_{Z\rightarrow E} = 0.9$) of these transitions are noteworthy. [2] The reason for these improved photochemical properties compared to parent azobenzene is the additional ethylene bridge in *ortho*-position to the azo group between both phenyl rings reducing the conformational flexibility of the molecule. Moreover, this strained eight-membered framework leads to a higher light-to-chemical-energy conversion efficiency. [12]

A systematical improvement of the diazocine parent system by even more reduction of the conformational flexibility in form of two additional ethylene bridges between the parent systems benzyl position and the neighboring aromatic carbon lead to the previously reported diindanodiazocine (DID). In addition to its photochemical properties, this molecule is characterized by the fact that two diastereomers, a *meso*-form **1** and a racemic mixture (*rac*) **2**, of DID are formed during synthesis. To the best of our knowledge the unsubstituted *rac*-DID **2** is the smallest chiral photoswitch known so far. Both diastereomers **1** and **2** show the highest quantum yields of an artificial photoswitch known to date and also outperform the best naturally occurring photoswitch rhodopsin. [12]

Additionally, the reduction of conformational movement leads to a directional motion during the switching process in contrast to azobenzene and parent diazocine which are in fact no directional photoswitches. Furthermore, the DID by far more efficient concerning the efficiency of conversion of light into chemical energy than parent diazocine or azobenzene. Besides, both diastereomers show quite different behavior concerning thermal half-life. While *rac*-DID **2** shows a very long half-life in the range of

a few days while *meso*-DID **1** only needs a few seconds to relax at room temperature which makes both diastereomers suitable for different applications. [12]

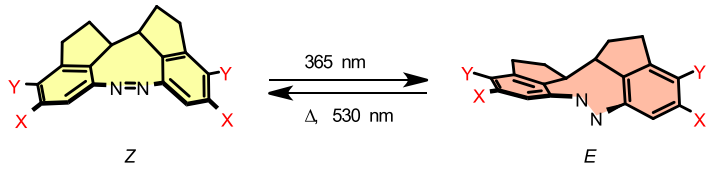

X	Y	*meso*	*rac*
H	H	**1**	**2**
Br	H	**3**	**4**
I	H	-	**5**
Br	Br	-	**6**

Figure 1: Diindanodiazocines synthesized and characterized in this work.

To make this new class of azobenzene based photoswitch accessible for further derivatization and application we focused on the symmetrical derivatization of DID with bromo- or iodo-substituents. Therefore, we synthesized the *meso*- **3** and *rac*-diastereomers **4** of dibromosubstituted DID, the *rac*-diastereomer **5** of diiodosubstituted DID and *rac*-diastereomer **6** of tetrabromosubstituted DID (figure 1) and characterized their photochemical properties.

Results and Discussion

Synthesis

The synthesis of unsubstituted DID's **1** and **2** is straightforward by dimerizing unsubstituted nitroindane **7** to the corresponding diastereomers followed by reductive azo coupling. [12] Since there is no example in current literature of electrophilic

aromatic substitution of diazocines the halogenic substitution targeted in this work has to be performed before the dimerization step (Scheme 1). The halogenation has been performed by adding NXS to a solution of the nitroindane **7** in sulfuric acid following a procedure of RAJU *et al.* [13] and the corresponding product could be obtained quantitatively (bromide **8**) and a rather low yield for the iodide **9**. Subsequent dimerization yields for the dimerization products (*meso*-dibromodimer **10**, *rac*-dibromodimer **11**, *meso*-diiododimer **12** and *rac*-diiododimer **13**) are not significantly influenced by halogen substitution of the building blocks compared to the unsubstituted system. This also fits the reductive azo coupling of the dibromodimers **10** and **11** to the corresponding DID's **3** and **4**. In contrast to this the diiodocompounds are affected during the reductive azo coupling by reduction of the iodo-substituents to the corresponding unsubstituted DID, so that the *rac*-diiodo-DID **5** can be obtained in a ratio of 3:1 together with the unsubstituted *rac*-DID **2** while the *meso*-compound **14** could not be obtained due to reduction to the unsubstituted *meso*-DID **1** in its entirety. A similar reduction of the bromo derivatives to the unsubstituted system could not be observed.

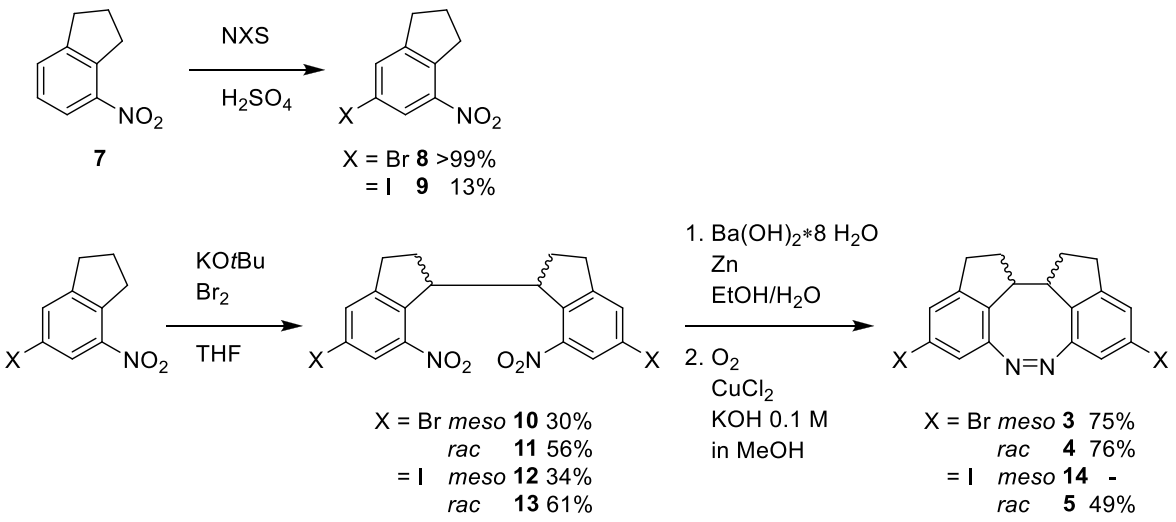

Scheme 1: Synthesis of *meta*-substituted DID's **3,4** and **5**.

For the synthesis of tetrabromo-DID the same strategy was used as for the synthesis of the disubstituted DID's: At first synthesis of the halogenated nitroindane building block **15** followed by the established dimerization and reductive azo coupling. Since the second bromine substitutent cannot be introduced directly to the already synthesized bromnitroindane building block **8** the electrophilic aromatic substitution has to take place before the indane framework is formed and the nitro group is introduced (Scheme 2). For that reason the synthesis path starts with an electrophilic aromatic bromination of 3-bromaniline (**16**) following the procedure of BARTOLI *el al*. [14] giving the desired dibromaniline **17** in a quantitative yield. The formation of the indanone framework was performed according to the procedure of TIRFOIN *et al*. [15] with a nucleophilic aromatic substitution to establish a propanoic acid side chain in the dibromo intermediate **18** followed by FRIEDEL-CRAFTS-Acylation to close the indanone ring system **19**. However, following the procedure of TIRFOIN *et al.* [15] resulted in no product formation, so that the reaction was carried out in pure trifluoromethane sulfonic acid giving the desired indanone **19** in a yield of 20% along with the side product 5,6-dibromo-indan-1-one (80%). The undesired side product is favoured in the ring-closing reaction due to less sterical hinderance during the electrophilic attack. The subsequent reduction to the dibromoindane **20** could be achieved in a quantitative yield while the nitration giving the dibromonitroindane building block **15** in a yield of 32% also affected by the formation of an unwanted side product.

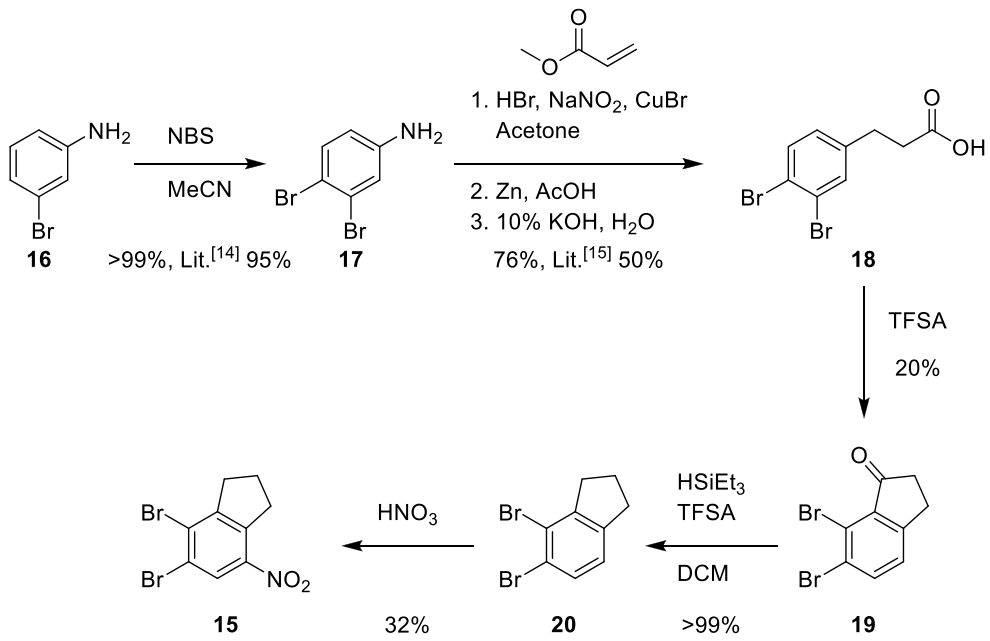

Scheme 2: Synthesis of the dibromonitroindane building block **15** starting from 3-bromaniline (**16**).

Starting with dibromonitroindane building block **15** the synthesis of the corresponding *rac*-DID **6** can be obtained following the established procedure (Scheme 3). The corresponding *meso*-tetrabromodiindanodiazocine **21** however, could not be obtained, since the *meso*-precursor **22** was formed in an amount of only 5% compared to the *rac*-precursor **23** and therefore could not be separated from the *rac*-diastereomer. Additionally, the yields of both dimerization and reductive azo-coupling are by far worse than for di- or unsubstituted systems.

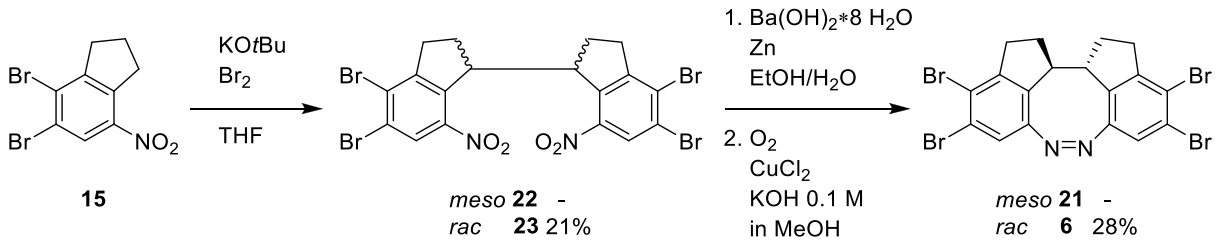

Scheme 3: Synthesis of *rac* tetrabromo-DID **6** from dibromonitroindane **15** building block.

Photochemical Characterization

The UV-vis spectra of DID's **2,4-6** were recorded at 298 K and of **1** and **3** at 233 K and acetone was used as solvent for all measurements. PSS values (Γ) were determined via NMR spectroscopy in acetone. Thermal half-lives of *rac*-diastereomers **4-6** were investigated via UV-vis measurements at 298 K while *meso*-diastereomer **3** was examined via UV-vis measurements at 233 K, 238 K, 243 K and NMR spectroscopy at 238 K (For details, see Supporting Information File 1, section SIII and SIV). As well as the unsubstituted *meso*-DID **1** the dihalogenated *meso*-DID **3** shows a high separation of n – π* transitions of *Z* and *E* configuration with absorption maxima at 405 nm (*Z* configuration) and 464 nm (*E* configuration) (Figure 2). Likewise, the photoconversion yield (Γ) shows no significant difference to the unsubstituted system for *Z* to *E* photoisomerization at 385 nm (Table 1). Complete reisomerization can be achieved by light with a wavelength of 530 nm. In contrast to the unsubstituted *meso* diastereomer **1** the *rac* diastereomer **2** exhibits a significant bathochromic shift of the *Z* n – π* transition about 20 nm to 431 nm and a less strong bathochromic shift of the *E* n – π* transition to 478 nm. This leads to significantly lower photoconversion yields for *Z* to *E* and *E* to *Z* isomerization due to a high overlap of these transition bands. Both disubstituted *rac* DIDs **4** and **5** show an even higher bathochromic shifts for *Z* to *E* n – π* transitions to 435 nm leading to significantly lower photoconversion yields with 68% with 385 nm while *E* to *Z* isomerization with light at 530 nm exhibits a slight decrease to 92%. In contrast the tetrabromosubstituted DID **6** exhibits a more bathochromically shifted *E* n – π* transition at 483 nm resulting in a slightly higher PSS of 78% for *Z* to *E* photoisomerization with light at 385 nm compared to unsubstituted *rac* DID **2**.

When considering thermal relaxation ($t_{1/2}$), an influence of the halogen substituents is also evident. The already very short half-life of *meso*-DID **1** is significantly shortened

about the factor of twelve to 0.25 s for the brominated *meso*-DID **3** at 298 K. A similar effect of halogen substitution is also visible for *rac*-DID's **4-6**. Compared to the unsubstituted *rac*-DID **2** with an half-life of 117 h the thermal relaxation of dihalogenated DID's **4,5** is reduced by more than half to about 50 h. Even stronger is the effect of tetrahalogenation leading to half-life to 29.2 h. So, in general halogenation of DID-system leads to a significant decrease of thermal relaxation.

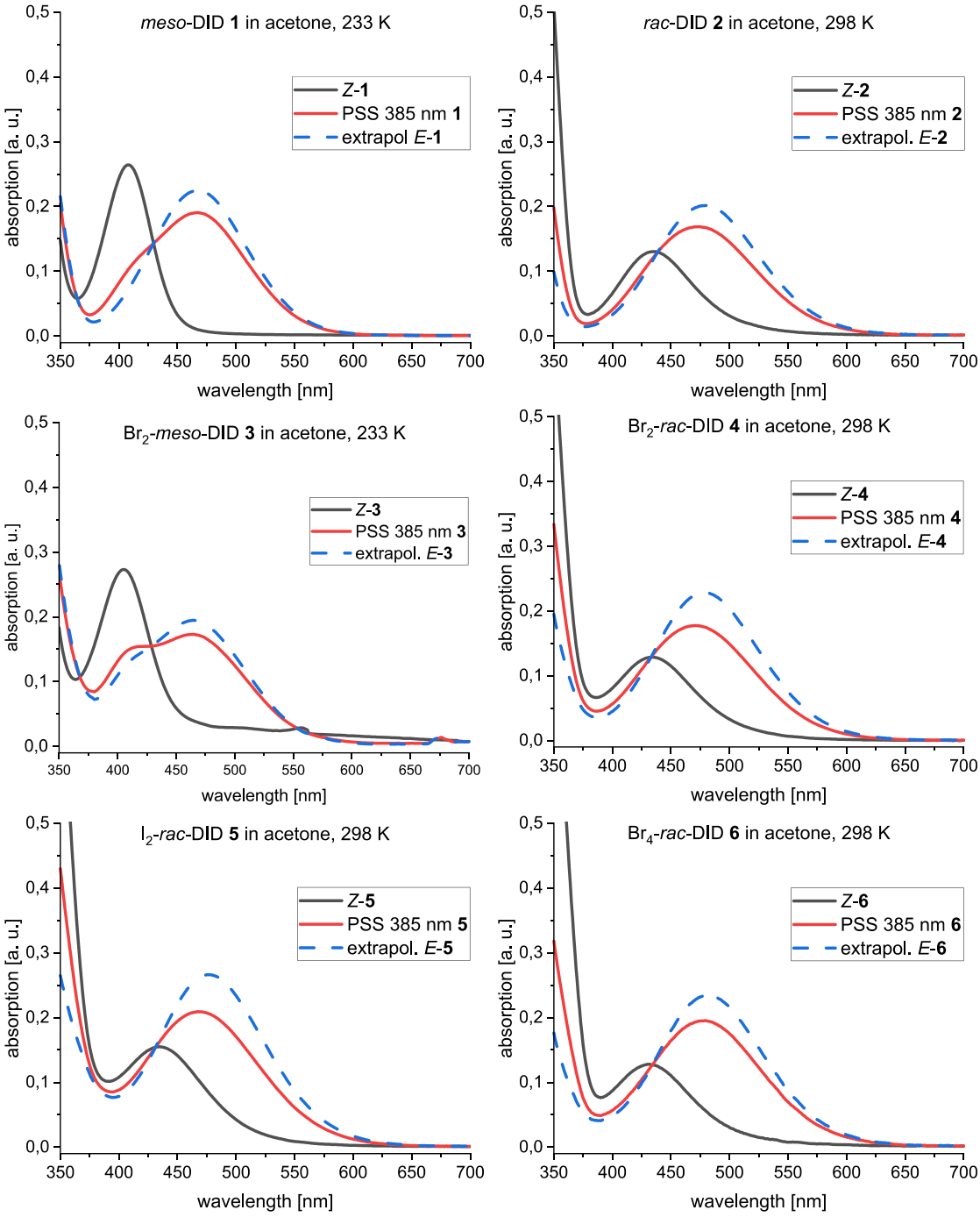

Figure 2: UV-vis spectra of unsubstituted (**1**,**2**), dibromo (**3**,**4**), diiodo (**5**) and tetrabromo (**6**) DID's. All spectra were recorded in acetone. The spectra of *Z*-configurations are given in black, the spectra of the PSS at 385 nm are represented in red and the extrapolated spectra of pure *E*-configurations are presented as dashed blue lines.

Table 1: Photophysical properties of DID's (**1-6**) in acetone.

	$\lambda_{\max\,(Z)}$	$\lambda_{\max\,(E)}$	$t_{1/2}$ (25 °C)	$\Gamma_{Z\rightarrow E}$ (385 nm)	$\Gamma_{E\rightarrow Z}$ (530 nm)
	nm		h	%	
1[12]	411	468[a]	8.8*10^{-4} [b]	84[a]	>99[a]
2[12]	431	478	117	76	94
3	405	464[a]	7.0*10^{-5} [b]	86[c]	>99[d]
4	435	479	51.5	68	92
5	435	476	50.8	67	92
6	431	483	29.2	78	93

[a]measured at 233 K; [b]measured at four temperatures (233 K, 238 K, 243 K, 248 K) and then extrapolated to 298 K (For details, see Supporting Information File 1, section SIV.); [c]measured at 238 K and extrapolated (for details, see Supporting Information File 1, section SIII; [d]measured at 238 K.

Conclusion

In context of this work four new additionally bridged diazocines (diindanodiazocines) have been synthesized and characterized. For this purpose, bromo- (**3** and **4**) and iodo-substituents (**5**) have been introduced in *meta*-position related to the azo-bridge by substitution of nitroindane building block **7.** Furthermore, the indane framework has been built up around a dibromo substitution pattern resulting in the successful synthesis of tetrabromosubsituted *rac*-diindianodiazocine **6.** The meso-diastereomers of diodo- or tetrabromo-DID's could not be obtained due to either reduction of the halogen substituent or insufficient yield.

The new DID derivatives have been investigated with regard to their photochemical

properties. It could be shown that *meta*-halogenation of *rac*-diindanodiazocine framework leads to drop in their PSS due to a higher $n - \pi^*$ transition overlap for the synthesized *rac*-DID derivatives **4** and **5** while the PSS stays at the same level for *meta*- and *para*-brominated DID **6** compared to the unsubstituted system **2.** The *meta*-bromination of *meso*-DID framework **3** also showed no significant influence on the PSS. However, all new DID-derivatives share a drastic shortening of thermal relaxation as common property.

Since both *meso*- and *rac*-diindanodiazocine frameworks offer quite different photochemical properties different fields of application can be targeted. Due to their very short thermal half-life, excellent switching behavior and the directed motion upon photoisomerization *meso*-diindanodiazocines are predestined for application as actuators in molecular machines. *Rac*-diindanodiazocines also exhibit superior photochemical properties and long thermal half-lives while being the smallest chiral photoswitches known to date and are consequently ideal candidates for controlling of chirality in liquid crystals or chiroptical switching. The functionalization presented in this work makes these excellent photoswitches now accessible for application in these fields.

Supporting Information

Analytical equipment, experimental procedures, NMR and UV-vis spectra

Supporting Information File 1:

File Name: Text

File Format: Text

Title: Synthesis and Characterization of New Diindanodiazocine Derivatives_SI

Acknowledgements (optional)

The authors thank the analytics department of the Otto-Diels-Institute for their help and support collecting NMR and MS data.

Funding (optional)

Funding text

References

[1] R. Siewertsen, J. B. Schönborn, B. Hartke, F. Renth, F. Temps, *Phys. Chem. Chem Phys* **2011**, *13*, 1054-1063.

[2] R. Siewertsen, H. Neumann, B. Buchheim-Stehn, R. Herges, C. Näther, F. Renth, F. Temps, *J. Am. Chem. Soc.* **2009**, *131*, 15594-15595.

[3] Y. Wang, M. Li, C. Yan, N. Ma, Y. Chen, *CCS Chem* **2022**, *4*, 704-712.

[4] S. Li, R. Colaco, A. Staubitz, *ACS Appl. Polym. Mater.* **2022**, *4*, 6825-6833.

[5] D. Hugenbusch, M. Lehr, J.-S. von Glasenapp, A. J. McConnell, R. Herges, *Angew. Chem. Int. Ed.* **2023**, *62*, e202212571.

[6] M. H. Burk, D. Langbehn, G. Hernández Rodríguez, W. Reichstein, J. Drewes, S. Schröder, S. Rehders, T. Strunskus, R. Herges, F. Faupel, *ACS Appl. Polym. Mater.* **2021**, *3*, 1445-1456.

[7] J. Ewert, L. Heintze, M. Jordà-Redondo, J.-S. von Glasenapp, S. Nonell, G. Bucher, C. Peifer, R. Herges, *J. Am. Chem. Soc.* **2022**, *144*, 15059-15071.

[8] G. Cabré, A. Garrido-Charles, À. González-Lafont, W. Moormann, D. Langbehn, D. Egea, J. M. Lluch, R. Herges, R. Alibés, F. Busquéet al., *Org. Lett.* **2019**, *21*, 3780-3784.

[9] T. Ko, M. M. Oliveira, J. M. Alapin, J. Morstein, E. Klann, D. Trauner, *J. Am. Chem. Soc.* **2022**, *144*, 21494-21501.

[10] N. Preußke, W. Moormann, K. Bamberg, M. Lipfert, R. Herges, F. D. Sönnichsen, *Org. Biomol. Chem.* **2020**, *18*, 2650-2660.

[11] J. B. Trads, K. Hüll, B. S. Matsuura, L. Laprell, T. Fehrentz, N. Görldt, K. A. Kozek, C. D. Weaver, N. Klöcker, D. M. Barberet al., *Angew. Chem. Int. Ed.* **2019**, *58*, 15421-15428.

[12] W. Moormann, T. Tellkamp, E. Stadler, F. Röhricht, C. Näther, R. Puttreddy, K. Rissanen, G. Gescheidt, R. Herges, *Angew. Chem. Inter. Ed.* **2020**, *59*, 15081-15086.

[13] P. Raju, G. Gobi Rajeshwaran, M. Nandakumar, A. K. Mohanakrishnan, *Eur J Org Chem* **2015**, *2015*, 3513-3523.

[14] S. Bartoli, A. Cipollone, A. Squarcia, A. Madami, D. Fattori, *Synthesis* **2009**, *2009*, 1305-1308.

[15] R. Tirfoin, J. A. B. Abdalla, S. Aldridge, *Chem. Eur. J.* **2015**, *21*, 11813-11824.

4. Synthesis and Characterization of New *N*-Acetyl Diazocines for Application in Photopharmacology

The basic concept of photopharmacology is the control of biological or pharmacological activity of a drug by light for activation and deactivation. The use of light as an external stimulus is particularly suitable since it does not interfere with most biological and chemical systems and is therefore a traceless and biorthogonal stimulus. Furthermore, light can be used with high spatiotemporal resolution and can be tuned precisely in intensity and wavelength as a highly selective stimulus (**figure 4.1**).[19,115,162]

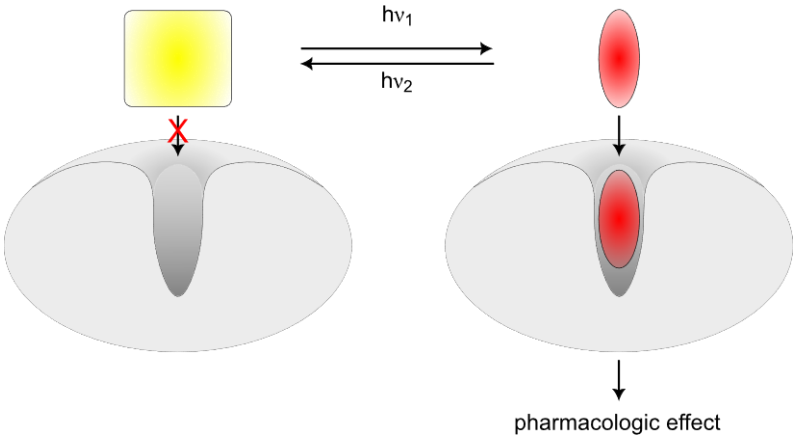

Figure 4.1: Schematic illustration of the basic principle of photopharmacology. The photoresponsive drug (yellow) cannot bind to the targeted receptor binding pocket due to sterical hindrance and is therefore biologically inactive. By irradiation with a certain wavelength ($h\nu_1$) a photoisomerization is induced. This leads to a structural change and allows binding of the now biologically active photopharmacophore to the receptor inducing the desired pharmacologic effect. Irradiation with light of a different wavelength ($h\nu_2$) converts the photoresponsive drug back into its biologically inactive initial form.[18-20,162,163]

Basic requirement for a reversibly light-controllable pharmacophore is the presence of a photosensitive chromophore as part of the molecule. By irradiation of the photopharmacophore a photoisomerization reaction is induced accompanied by a geometrical change of the molecule allowing the formation of a receptor-ligand complex followed by the pharmacologic effect.[18-20] Usually, photoswitchable molecules are used as chromophoric units, which are subject to high demands. The photopharmacophore should offer high photoconversion yields, ideally quantitative switching between both active and inactive form in aqueous media, especially under physiological conditions. Thus, the absorption bands used for induction of the photoisomerization reactions must be well separated and offer high quantum yields.[164] The wavelengths used for isomerization should be chosen in order to avoid interference with the biological environment and, importantly, to prevent damage to surrounding tissue. Therefore, UV light should be avoided and light of the visible region or near infrared irradiation (NIR) be used instead. Especially, NIR is preferable due to high penetrating depth in aqueous media and biological tissue (biooptical window).[108,109,164] The light-induced structural change upon isomerization of the chromophore should cause a significant difference in pharmacological activity of the whole photopharmacophore for switching between completely activated or deactivated configurations.[164,165] Besides, the stability of the chromophore against influences causing decomposition is a key aspect. The presence of naturally occurring intracellular reducing agents like glutathione or certain enzymes have shown that they are able to reduce photoswitches containing an azo group.[74,164,166] The choice of the right chromophore must therefore be carefully considered, as every known photoswitch has its advantages and disadvantages concerning switching properties and applicability in biological environment.

The basic principle of a pharmacophore that can be activated and at a designated point of impact deactivated later on aims to provide an effective alternative to conventional drugs and

prodrugs (**figure 4.2**). For conventional drugs, liberation and resorption already take place in the active form and are likewise distributed throughout the body by the circulatory system, which means that the effect is not limited to the designated site of action, but also extends across the entire body. This leads to adverse drug reactions and resistances or even collateral damage if more aggressive drugs are used. Furthermore, the active drug is excreted in the active form and is released in to the environment.[19,163] Especially synthetic hormones and other endocrine disruptors are very problematic as they damage human and animal organs and endocrine systems even in low concentrations.[167,168] Prodrugs are introduced into the body in their inactive form and are then converted into their active form within the metabolism after resorption. The activation of a prodrug is irreversible and ensures that they are also distributed and excreted from the body in their active form. Therefore, they share the disadvantages of conventional drugs.[19,163]
Photopharmacophores instead, can selectively be activated with high spatiotemporal resolution at the designated point of action after being resorbed by the metabolism leading to a lower concentration of active pharmacophore being distributed across the body and therefore inducing less adverse drug reactions and resistances. Furthermore, the activation of the photopharmacophore is reversible and therefore deactivation can be achieved by irradiation of a different wavelength or thermal relaxation. Therefore, the photopharmacophores are excreted in their inactive form so that environmental contamination is significantly reduced.[19,163]

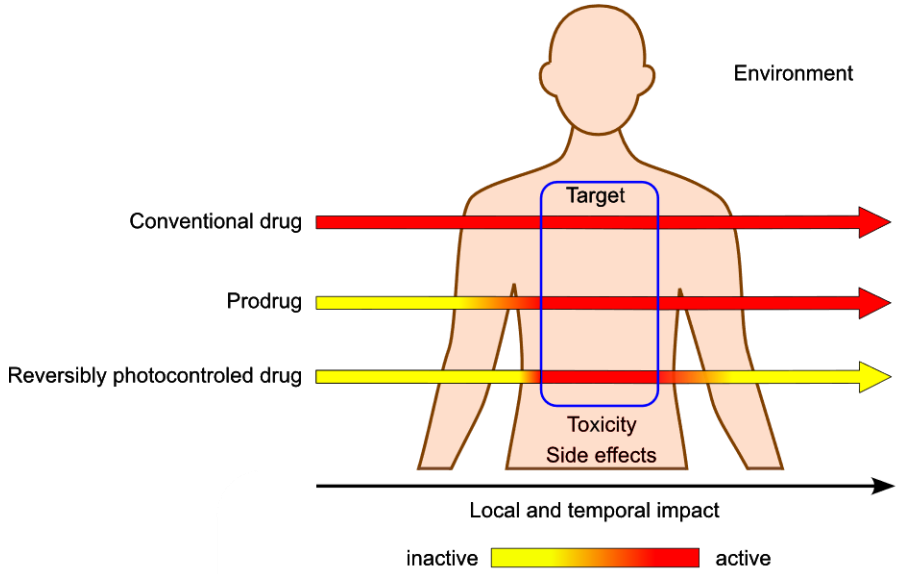

Figure 4.2: Schematic comparison of the local and temporal impact of conventional drugs, prodrugs and reversibly photocontroled drugs before medication, in the metabolism before and after the designated place of impact and after excretion.[19,163]

A variety of photoswitches are conceivable for use as chromophores within a photopharmacophore. For example diazocines, spiropyranes and azobenzenes or respectively azoheteroarenes have already been used as chromophores, with the latter being most frequently used to date.[18-20,163] Azobenzenes and azoheteroarenes are particularly suitable since the structural motif of two aromatic or heteroaromatic rings separated by diatomic linker (e.g. -CH_2-CH_2-, -CH=CH-, -CH_2-NH-, -CONH-, -CH_2-O-, -SO_2-NH-, and others) can frequently be found in pharmacophores and easily be replaced by an azo group. The high amount of candidates for this azologization shows the great potential of this approach developing photopharmacophores.[169] Also for diazocines structural analogs can be found in the field of pharmacophores since a wide range of tricyclic antidepressants,[170,171] calcium antagonists,[172] antihistamines[173] and other enzyme inhibitors[174] are known and are therefore predestined for azologization giving a diazocine-based photopharmacophore.
Compared to azobenzenes diazocine offer superior photoconversion yields, higher quantum yields and

switching in the visible range of the electromagnetic spectrum. But most importantly the thermodynamical stability of E- and Z-configurations are inversed compared to azobenzenes with the latter being favored.[57] This indicates that for diazocines the bend sterically more hindered and thermodynamically stable Z-configuration does not fit into the enzyme binding pocket resulting in the formation of a receptor ligand complex being prevented. If irradiated the diazocine isomerizes to the more flat E-configuration which is able to slip into the enzymatic binding pocket of the receptor easily. By irradiation or thermal relaxation the diazocine is switched back to the bulky Z-configuration and the receptor ligand complex is resolved (figure 4.3).[69,85] This is a great advantage over azobenzenes and azoheteroarenes since they are thermodynamically stable in their flat E-configuration which is also biologically active and therefore can only be turned off for a short time by being switched into the more hindered and biologically active Z-configuration.[85,169]

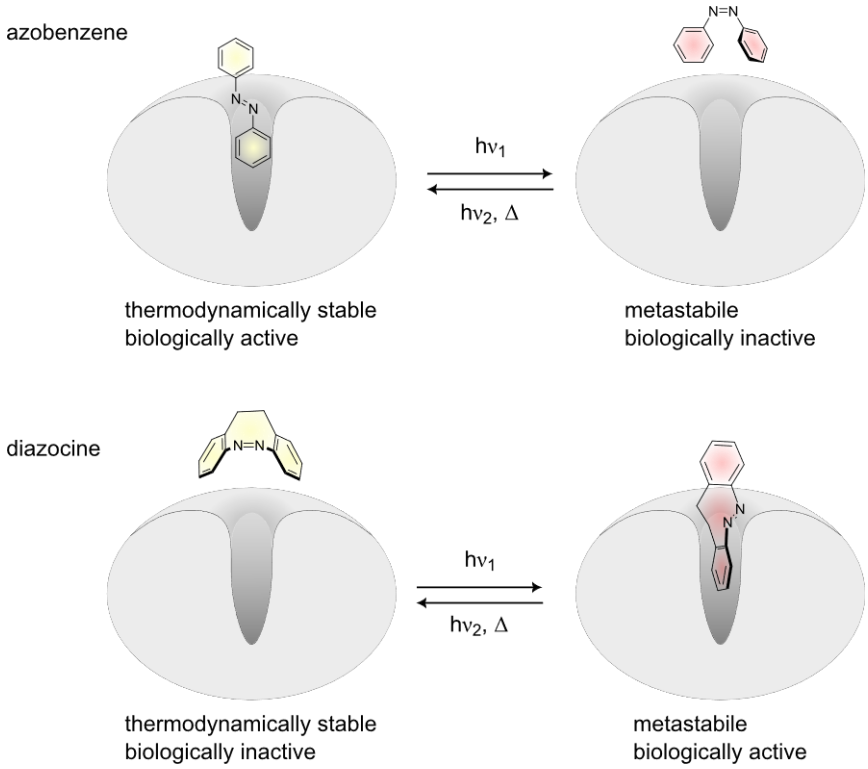

Figure 4.3: Schematic view of the binding of azobenzene and diazocine binding to a receptor. The planar and thermodynamically stable E-azobenzene fits into the binding pocket while the azobenzene in its metastable Z-configuration obtained by irradiation cannot bind due to sterical hinderance. In contrast the bend and sterical hindered thermodynamically stable Z-diazocine does not fit into the binding pocket whereas the stretched and less hindered metastable E-diazocine can bind to the receptor.[69,85,169]

So diazocines are predestined to be applied as chromophores in light-controllable pharmacophores since the drug can be introduced into the organism in its biologically inactive form and subsequently be activated at the designated target. After leaving the target region the pharmacophore can be selectively switched to inactivity either by light or thermal relaxation. This leads to prevention of drug adverse side effects while being transferred throughout the body and environmental toxicity after excretion.

However, as the parent diazocine lacks the property of sufficient water solubility a functionalization is needed which, unfortunately, is accompanied by a deterioration of switching properties in aqueous media.[110] The *N*-Ac diazocine offers more than satisfactory water solubility up to 1 mM without significantly influencing the switching properties.[64,110,120] This is a most recent finding by the HERGES group and therefore no work has been put in the late-stage functionalization for application of *N*-Ac diazocines so far. For this reason, the derivatization and functionalization of water-soluble *N*-Ac diazocine was the target within this project. Additionally, the complex synthesis path of the

unsubstituted *N*-Ac diazocine used so far should be revised and improved to less reaction steps and a higher total yield. Afterwards the insights of this work should be applied on substituted systems.

4.1 Summary of Substituted Nitrogen-Bridged Diazocines

In contrast to parent diazocine the improved *N*-Ac diazocine offers intrinsic water solubility without significant reduction of the switching properties in aqueous media.[64,110] Furthermore, the n-π*-transitions targeted for Z- to E- and vice versa-photoisomerization offer a significant bathochromic shift.[64,110] These properties indicate that *N*-Ac diazocines could be a promising candidate for application in aqueous biological environments. For accessibility of more *N*-Ac diazocine derivatives further functionalization is required. For this purpose, halogen substituents can be used as linking points. Since late-stage functionalization of N-Ac diazocines turned out to be very difficult, the targeted halogen functionalization had to be included in the starting material. The synthesis of the new *N*-Ac diazocine derivatives followed the initial synthesis path except the azo condensation, which followed the oxidative approach of MAIER *et al*.[76] with mCPBA after previous reduction to the corresponding dianiline intermediate (**scheme 4.1**).[64,76] This improvement lead to higher and more reproducible yields.

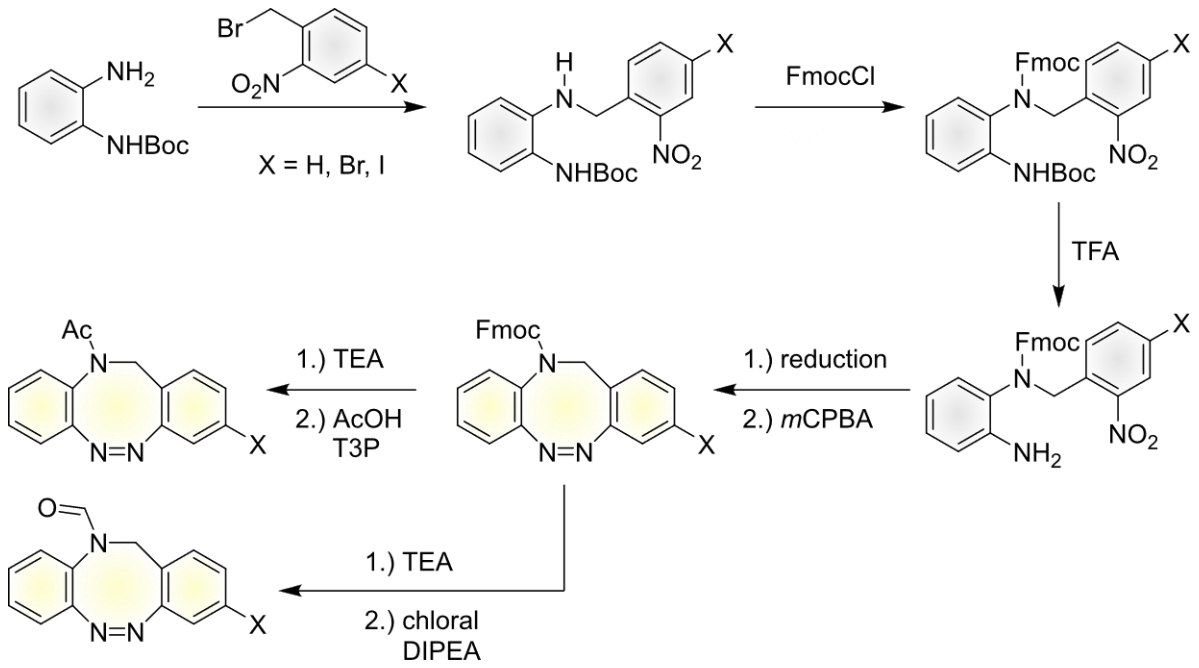

Scheme 4.1: Synthesis procedure for preparation of halogenated *N*-Ac and *N*-formyl diazocine derivatives. The initial synthesis path developed by LENTES *et al*.[64] was improved by performing the oxidative azo cyclization by MAIER *et al*.[76] resulting in higher and reproducible yields.

For investigations on the influence of other polar substituents at the bridging nitrogen atom also formyl substituents were introduced, so that in total five new *N*-diazocine derivatives could be synthesized. All new derivatives offered excellent PSS between 80% and 85% for the Z- to E-photoisomerization and quantitative E- to Z-isomerization. Thermal half-lives of the halogenated *N*-Ac diazocines derivatives does not significantly differ from unsubstituted *N*-Ac diazocine, while thermal relaxation of the formyl derivatives was significantly slowed down. Additionally, the photochemical characteristics of the monobrominated *N*-Ac diazocine and the unsubstituted *N*-formyl diazocine were investigated in water. The PSS values in aqueous media of both derivatives do not significantly differ from the unsubstituted *N*-Ac diazocine while the thermal relaxation of *N*-formyl diazocine is considerably extended.

4.2 Substituted Nitrogen-Bridged Diazocines

Pascal Lentes, Jeremy Rudtke, Thomas Griebenow and Rainer Herges

Beilstein Journal of Organic Chemistry **2021**, *17*, 1503-1508.

DOI: 10.3762/bjoc.17.107.

Scientific contribution to this paper: UV-vis (spectra and half-lives) (partially) and NMR measurements (spectra and PSS measurements) (partially), writing of the manuscript and supporting information (partially).

BEILSTEIN JOURNAL OF ORGANIC CHEMISTRY

Substituted nitrogen-bridged diazocines

Pascal Lentes, Jeremy Rudtke, Thomas Griebenow and Rainer Herges*

Full Research Paper

Open Access

Address:
Otto Diels-Institute of Organic Chemistry, Christian Albrechts University Kiel, Otto-Hahn-Platz 4, 24118 Kiel, Germany

Email:
Rainer Herges* - rherges@oc.uni-kiel.de

* Corresponding author

Keywords:
bridged azobenzene; diazocine; photopharmacology; photoswitch; triazocine; visible light switch; water-soluble switch

Beilstein J. Org. Chem. **2021,** *17,* 1503–1508.
https://doi.org/10.3762/bjoc.17.107

Received: 05 March 2021
Accepted: 11 June 2021
Published: 25 June 2021

Associate Editor: C. Stephenson

Abstract

Novel nitrogen-bridged diazocines (triazocines) were synthesized that carry a formyl or an acetyl group at the CH_2NR-bridge and bromo- or iodo-substituents at the distant phenyl ring. The photophysical properties were investigated in acetonitrile and water. As compared to previous approaches the yields of the intramolecular azo cyclizations were increased (from ≈40 to 60%) using an oxidative approach starting from the corresponding aniline precursors. The $Z \rightarrow E$ photoconversion yields in acetonitrile are 80–85% and the thermal half-lives of the metastable E configurations are 31–74 min. Particularly, the high photoconversion yields (≈70%) of the water-soluble diazocines are noteworthy, which makes them promising candidates for applications in photopharmacology. The halogen substituents allow further functionalization via cross-coupling reactions.

Introduction

Diazocines (bridged azobenzenes) are frequently used photoswitches with outstanding photophysical properties. Parent diazocine (CH_2–CH_2-bridged) exhibits well-separated n–π^* transitions, which allow excellent photoconversion between the Z and E configurations ($(Z \rightarrow E)_{385\ nm}$ = 92%, $(E \rightarrow Z)_{525\ nm}$ > 99% in n-hexane) with light in the visible region [1]. Moreover, the Z-boat configuration is the thermodynamically stable isomer [2-9]. The latter property (i.e., the inverted stability compared to azobenzenes) makes them promising candidates for applications in photopharmacology. In the majority of azobenzene-based photopharmacophores, the bent Z configuration is biologically inactive [10-12]. Hence, (and in contrast to azobenzenes) the thermodynamically stable and biologically inactive Z-isomer can be administered and switched on with light at the site of interest with spatiotemporal resolution. Moreover, the photoconversion yield for the $E \rightarrow Z$ isomerization is quantitative (within the detection limit of UV and NMR spectroscopy). A high efficiency in switching the biological activity off is important to avoid side effects of residual concentrations of the active form [13].

Water solubility and high $Z \rightarrow E$ switching efficiencies in water are additional important criteria for applications in biological environments [14]. Our previously published NAc-bridged diazocine **10c** (Scheme 1, Table 1) exhibits both properties [15]. This is in stark contrast to the CH_2–CH_2 and S–CH_2-bridged diazocines and the majority of azobenzenes [9,16-20]. Spurred by the promising properties of CH_2–NR-bridged diazocines

Beilstein J. Org. Chem. **2021,** *17,* 1503–1508.

(triazocines), we now explored this class of photoswitches and developed synthetic access to these photochromes (Figure 1).

Results and Discussion

Synthesis

The first three stages of the synthesis of CH_2–NR-bridged diazocines are analogous to the previously described synthesis of CH_2–NH-bridged diazocine [15]. The single Boc-protected 1,2-phenylenediamine (**2**, Scheme 1) is reacted with halogen-substituted 2-nitrobenzyl bromides **3** [21] forming *N*-benzylanilines **4**, which were protected with Fmoc chloride to accomplish an orthogonal protective group strategy. The removal of the Boc groups from compounds **5** with TFA gave the mixed aniline and nitro precursors **6**.

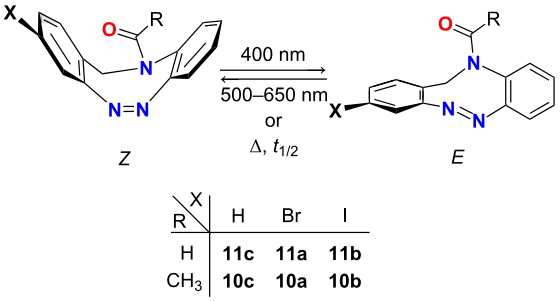

Figure 1: Bridged diazocines synthesized and investigated in this work.

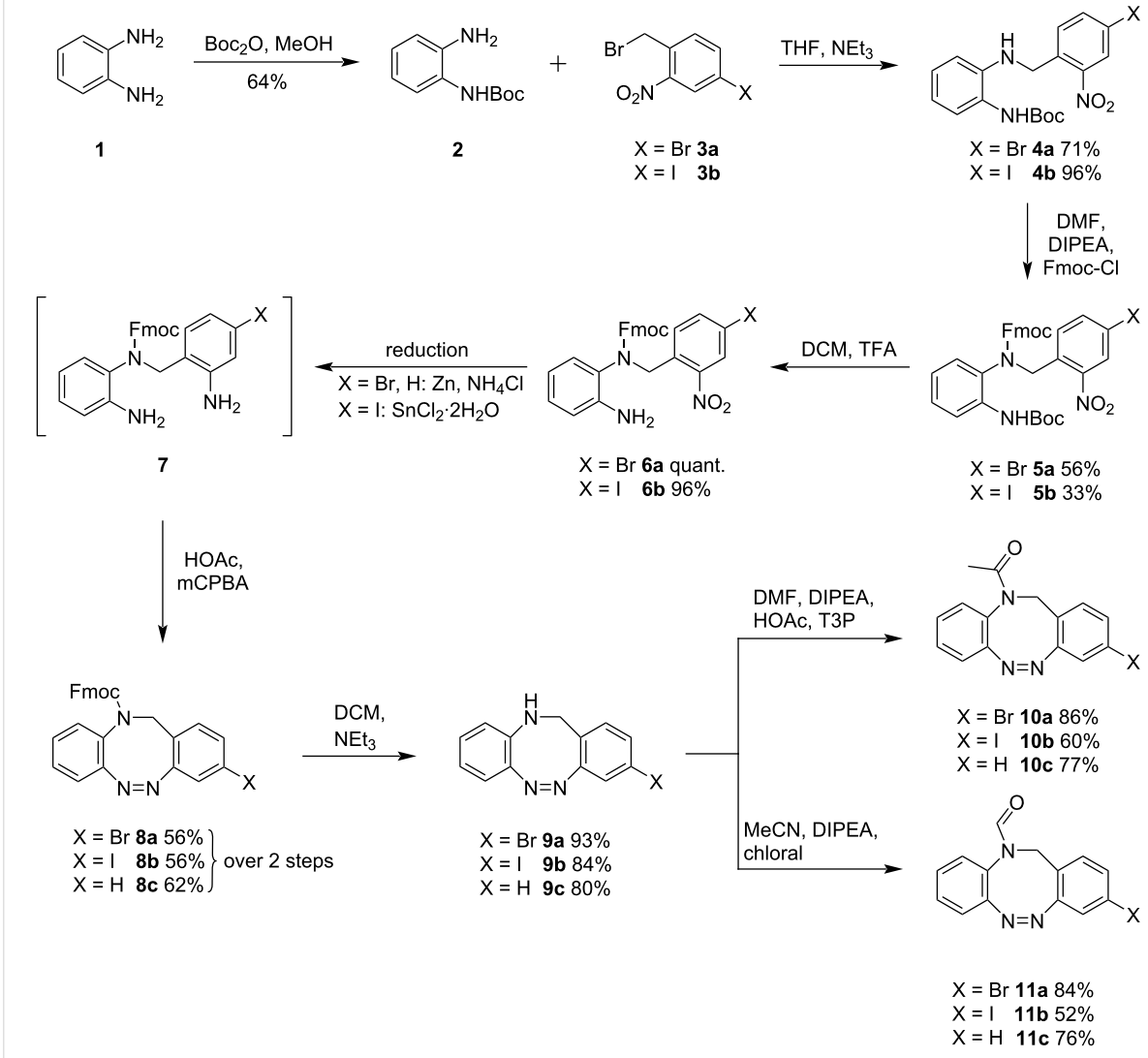

Scheme 1: Synthesis of 3-bromo- and 3-iodo-acetylated CH_2NR diazocines **10** (R = Ac) and formylated diazocines **11** (R = CHO).

Beilstein J. Org. Chem. **2021,** *17,* 1503–1508.

In previous approaches, the nitro groups were reduced to hydroxylamines with zinc and oxidized to the corresponding nitroso compounds with iron(III) to perform an intramolecular Baeyer–Mills reaction [15,21]. We found that a complete reduction of the nitro group to aniline **7** and oxidation with mCPBA is increasing the yield of the intramolecular cyclization from 39% to 62% (over two steps) for the unsubstituted diazocine **8c** as compared to the pathway via the hydroxylamine. The 3-bromo **8a** and 3-iodo **8b** compounds were obtained in 56% yield using the oxidative method of Trauner [22] with mCPBA. The Fmoc groups were removed with NEt_3 to yield the NH-diazocines **9**. The acetylated diazocines **10a–c** were synthesized using a mixed anhydride of acetic acid and T3P (propanephosphonic acid anhydride). The formylation of NH-diazocines **9a–c** was accomplished with chloral [23] under non-acidic conditions.

Investigation of the photophysical properties

The UV–vis spectra of diazocines **10a–c**, and **11a–c** were recorded in acetonitrile at 25 °C. All compounds exhibit an *n*–π* transition at about 400 nm (*Z*→*E* conversion) and an *n*–π* transition at about 520 nm (*E*→*Z* conversion, Figure 2, Table 1).

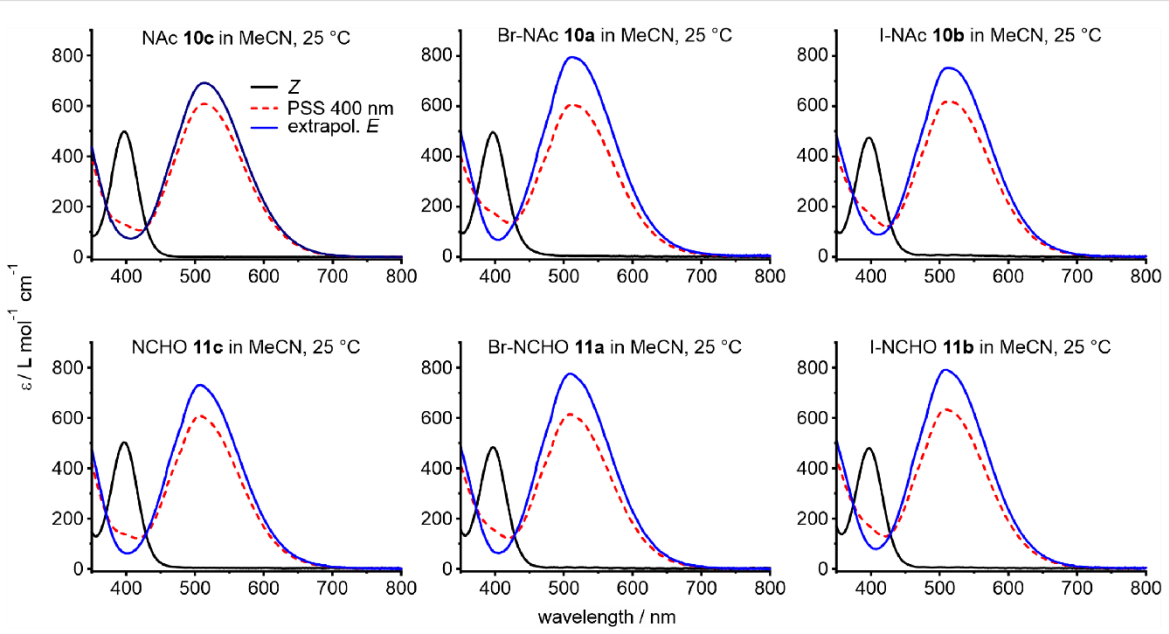

Figure 2: UV–vis spectra of 3-bromo and 3-iodo, and unsubstituted CH_2NAc-bridged (**10a–c**) and CH_2NCHO-bridged (**11a–c**) diazocines. The spectra of *Z*-isomers are given in black, the photostationary states at 400 nm are represented as dashed red lines and the extrapolated spectra of the pure *E*-isomers are in blue.

Table 1: Photophysical properties of *N*-diazocines **10a–c** and **11a–c** in acetonitrile.

	acetonitrile							
	$\lambda_{max(Z)}$	$\lambda_{max(E)}$	$\varepsilon_{\lambda max(Z)}$	$\varepsilon_{\lambda max(E)}$	$\Gamma_{Z\rightarrow E}$[a]	$t_{1/2}$ (25 °C)	E_A	ln(A)
	nm		L mol^{-1} cm^{-1}		%	min	kJ mol^{-1}	
Br-NAc **10a**	397	515	495	791	81	30.9	93.4	29.8
I-NAc **10b**	397	517	480	778	82	28.6	87.0	27.3
NCHO **11c**	397	509	502	760	85	74.0	88.4	26.9
Br-NCHO **11a**	397	509	469	784	82	49.9	93.9	29.5
I-NCHO **11b**	398	511	483	798	80	48.1	90.9	28.3
NAc **10c**	397	513	495	759	88	29.5	87.6	27.5

[a]Extrapolated values (for details, see Supporting Information File 1, section IV).

Beilstein J. Org. Chem. **2021,** *17,* 1503–1508.

Irradiation with 400 nm gives the metastable *E*-isomers of the acetylated and formylated derivatives **10** and **11** with good photoconversion yields (Γ) of 80–85% (Table 1) in acetonitrile. A complete $E \rightarrow Z$ conversion (>99%) can be achieved with light between 520 and 600 nm. The unsubstituted acetylated and formylated diazocines **10c** and **11c** exhibit similar conversion yields (88% and 85%) and halogenation as well does not have a significant influence. However, thermal half-lives ($t_{1/2}$) of the metastable *E*-isomers of the 3-bromo and 3-iodo *N*-acetyl diazocines **10a** and **10b** (≈30 min) are significantly smaller than the half-lives of the corresponding bromo and iodo *N*-formyl derivatives **11a** and **11b** (≈50 min). In general, halogenation decreases the half-lives compared to unsubstituted diazocines **10c** and **11c**. The activation barrier (E_A) of the $E \rightarrow Z$ isomerization (obtained by an Arrhenius plot) is higher in formylated compounds **11** compared to acetylated compounds **10** and is further increased by halogenation.

The unsubstituted *N*-formyl diazocine **11c** and brominated *N*Ac-diazocine **10a** were also investigated in pure water since they are water-soluble (**11c**: ≈250 µM, **10a**: ≈150 µM). The highest $Z \rightarrow E$ conversion yields are observed by irradiation with 400 nm in water and the back-isomerization $E \rightarrow Z$ can be accomplished by irradiation with light in the range of 525 and 600 nm (Figure 3, Table 2).

The photoconversion yields ($Z \rightarrow E$) of *N*-formyl diazocine **11c** in water and bromo-*N*Ac diazocine **10a** are about 70%, which do not differ significantly from unsubstituted NAc diazocine **10c** (72%) [15]. It is interesting to note that the half-lives and activation barriers ($E \rightarrow Z$) are increasing ($t_{1/2} \approx$ 2–2.5-fold) in water as compared to the less polar acetonitrile.

Conclusion

Five nitrogen-bridged diazocines (triazocines) were synthesized and characterized. Formyl (R = CHO) and acetyl groups (R = Ac) were introduced at the CH_2NR bridge and the distant phenyl rings are Br and I substituted. In contrast to previous approaches, the azo cyclization (ring closure) was achieved via the oxidation of the bis-anilines **7** with *m*CPBA (≈60% yield). Among the nitrogen-bridged diazocines compounds **10a** and **11c** are water soluble and retained their high switching efficiency (≈70%) also in water. The half-lives of the metastable *E*-isomers are larger for the *N*-formyl diazocines **11a–c** compared to the acetylated compounds **10a–c** and generally, the half-lives are larger in water than in acetonitrile. Halogen atoms

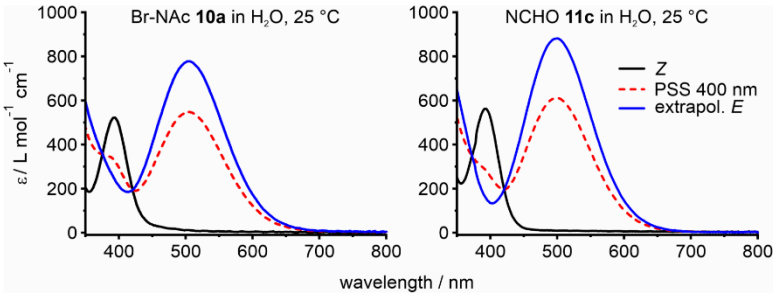

Figure 3: UV–vis spectra of 3-bromo-*N*Ac-diazocine **10a** and *N*-formyl-diazocine **11c** in water. Spectra of *Z*-isomers (black curve), the photostationary states at 400 nm (dashed red line), and the extrapolated spectra of the pure *E*-isomers (blue).

Table 2: Photophysical properties of water-soluble *N*-diazocines **10a**, **10c**, and **11c** in H_2O.

	H_2O							
	$\lambda_{max(Z)}$	$\lambda_{max(E)}$	$\varepsilon_{\lambda max(Z)}$	$\varepsilon_{\lambda max(E)}$	$\Gamma_{Z \rightarrow E}$[a]	$t_{1/2}$ (25 °C)	E_A	ln(A)
	nm		L mol^{-1} cm^{-1}		%	min	kJ mol^{-1}	
Br-NAc **10a**	394	502	534	975	70	69.6	99.9	31.6
NCHO **11c**	393	500	567	871	69	198	97.8	29.7
NAc **10c**	393	502	564	850	72	72.8	90.4	27.7

[a]Extrapolated values (for details, see Supporting Information File 1, section IV).

Br and I at the phenyl rings in 3-position as in **10a**,**b**, and **11a**,**b** are a good starting point for further functionalization [17,20,24]. We conclude that CH_2NAc and CH_2NCHO bridged diazocines (triazocines) are promising candidates for applications in biological environments and particularly as photoswitches in light-activatable drugs.

Supporting Information

Supporting Information File 1

Analytical equipment, experimental procedures, NMR and UV–vis spectra.
[https://www.beilstein-journals.org/bjoc/content/supplementary/1860-5397-17-107-S1.pdf]

Acknowledgments

The authors thank Malte Wellmann for his assistance in synthesis.

Funding

The authors gratefully acknowledge financial support by the Deutsche Forschungsgesellschaft (DFG) within the Sonderforschungsbereich 677, “Function by Switching”.

ORCID® iDs

Jeremy Rudtke - https://orcid.org/0000-0001-8079-7715
Rainer Herges - https://orcid.org/0000-0002-6396-6991

Preprint

A non-peer-reviewed version of this article has been previously published as a preprint: https://doi.org/10.3762/bxiv.2021.16.v1

References

1. Siewertsen, R.; Neumann, H.; Buchheim-Stehn, B.; Herges, R.; Näther, C.; Renth, F.; Temps, F. *J. Am. Chem. Soc.* **2009,** *131,* 15594–15595. doi:10.1021/ja906547d
2. Siewertsen, R.; Schönborn, J. B.; Hartke, B.; Renth, F.; Temps, F. *Phys. Chem. Chem. Phys.* **2011,** *13,* 1054–1063. doi:10.1039/c0cp01148g
3. Moormann, W.; Langbehn, D.; Herges, R. *Synthesis* **2017,** *49,* 3471–3475. doi:10.1055/s-0036-1590685
4. Moormann, W.; Langbehn, D.; Herges, R. *Beilstein J. Org. Chem.* **2019,** *15,* 727–732. doi:10.3762/bjoc.15.68
5. Samanta, S.; Qin, C.; Lough, A. J.; Woolley, G. A. *Angew. Chem., Int. Ed.* **2012,** *51,* 6452–6455. doi:10.1002/anie.201202383
6. Sell, H.; Näther, C.; Herges, R. *Beilstein J. Org. Chem.* **2013,** *9,* 1–7. doi:10.3762/bjoc.9.1
7. Li, S.; Eleya, N.; Staubitz, A. *Org. Lett.* **2020,** *22,* 1624–1627. doi:10.1021/acs.orglett.0c00122
8. Hammerich, M.; Schütt, C.; Stähler, C.; Lentes, P.; Röhricht, F.; Höppner, R.; Herges, R. *J. Am. Chem. Soc.* **2016,** *138,* 13111–13114. doi:10.1021/jacs.6b05846
9. Heintze, L.; Schmidt, D.; Rodat, T.; Witt, L.; Ewert, J.; Kriegs, M.; Herges, R.; Peifer, C. *Int. J. Mol. Sci.* **2020,** *21,* 8961–8981. doi:10.3390/ijms21238961
10. Beharry, A. A.; Woolley, G. A. *Chem. Soc. Rev.* **2011,** *40,* 4422–4437. doi:10.1039/c1cs15023e
11. Szymański, W.; Beierle, J. M.; Kistemaker, H. A. V.; Velema, W. A.; Feringa, B. L. *Chem. Rev.* **2013,** *113,* 6114–6178. doi:10.1021/cr300179f
12. Hüll, K.; Morstein, J.; Trauner, D. *Chem. Rev.* **2018,** *118,* 10710–10747. doi:10.1021/acs.chemrev.8b00037
13. Fuchter, M. J. *J. Med. Chem.* **2020,** *63,* 11436–11447. doi:10.1021/acs.jmedchem.0c00629
14. Lubbe, A. S.; Szymanski, W.; Feringa, B. L. *Chem. Soc. Rev.* **2017,** *46,* 1052–1079. doi:10.1039/c6cs00461j
15. Lentes, P.; Stadler, E.; Röhricht, F.; Brahms, A.; Gröbner, J.; Sönnichsen, F. D.; Gescheidt, G.; Herges, R. *J. Am. Chem. Soc.* **2019,** *141,* 13592–13600. doi:10.1021/jacs.9b06104
16. Lentes, P.; Frühwirt, P.; Freißmuth, H.; Moormann, W.; Kruse, F.; Gescheidt, G.; Herges, R. *J. Org. Chem.* **2021,** *86,* 4355–4360. doi:10.1021/acs.joc.1c00065
17. Cabré, G.; Garrido-Charles, A.; González-Lafont, À.; Moormann, W.; Langbehn, D.; Egea, D.; Lluch, J. M.; Herges, R.; Alibés, R.; Busqué, F.; Gorostiza, P.; Hernando, J. *Org. Lett.* **2019,** *21,* 3780–3784. doi:10.1021/acs.orglett.9b01222
18. Trads, J. B.; Hüll, K.; Matsuura, B. S.; Laprell, L.; Fehrentz, T.; Görldt, N.; Kozek, K. A.; Weaver, C. D.; Klöcker, N.; Barber, D. M.; Trauner, D. *Angew. Chem., Int. Ed.* **2019,** *58,* 15421–15428. doi:10.1002/anie.201905790
19. Preußke, N.; Moormann, W.; Bamberg, K.; Lipfert, M.; Herges, R.; Sönnichsen, F. D. *Org. Biomol. Chem.* **2020,** *18,* 2650–2660. doi:10.1039/c9ob02442e
20. Thapaliya, E. R.; Zhao, J.; Ellis-Davies, G. C. R. *ACS Chem. Neurosci.* **2019,** *10,* 2481–2488. doi:10.1021/acschemneuro.8b00734
21. Schehr, M.; Hugenbusch, D.; Moje, T.; Näther, C.; Herges, R. *Beilstein J. Org. Chem.* **2018,** *14,* 2799–2804. doi:10.3762/bjoc.14.257
22. Maier, M. S.; Hüll, K.; Reynders, M.; Matsuura, B. S.; Leippe, P.; Ko, T.; Schäffer, L.; Trauner, D. *J. Am. Chem. Soc.* **2019,** *141,* 17295–17304. doi:10.1021/jacs.9b08794
23. Liebig, J. *Ann. Pharm. (Lemgo, Ger.)* **1832,** *1,* 182–230. doi:10.1002/jlac.18320010203
24. Biffis, A.; Centomo, P.; Del Zotto, A.; Zecca, M. *Chem. Rev.* **2018,** *118,* 2249–2295. doi:10.1021/acs.chemrev.7b00443

Beilstein J. Org. Chem. **2021,** *17,* 1503–1508.

4.3 Summary of Cross-Coupling of *N*-Acetyl Diazocines

A big advantage of *N*-Ac diazocines is the intrinsic water solubility without a significant deterioration of its switching properties.[64,110,120] However, for application further derivatization is required which unfortunately cannot be achieved by late-stage aromatic substitution.[175] Therefore, either functionalization or connection point for late-stage derivatization via cross-coupling reaction have to be introduced in the initial building blocks. In previous work monohalogenated *N*-Ac diazocines have already been synthesized and characterized.[120] The missing dibrominated *N*-Ac diazocine should be synthesized within this project and the range of cross-coupling reactions accessible for *N*-Ac diazocines should be elaborated for synthesis of potential new photopharmacophores.
The targeted dibrominated *N*-Ac diazocine could be synthesized following the synthesis path established by LENTES *et al*.[120], albeit only very low yields could be achieved especially caused by problematic Fmoc-protecting step. In contrast, the cross-coupling of monohalogenated *N*-Ac diazocines could be successfully achieved with fifteen new *N*-Ac diazocine derivatives now accessible via SUZUKI-, STILLE-, IQBAL- or BUCHWALD-HARTWIG-coupling reactions (**scheme 4.1**). STILLE-coupling proved to be an effective method for vinylation while arylation could only be achieved with poor yields. For this, SUZUKI-coupling proved to be an efficient method for arylation especially for phenyl derivatives while heteroaromatics seemed to be problematic. Boc-protected anilines could be synthesized in good yields and arylated anilines in insufficient yields via BUCHWALD-HARTWIG coupling.

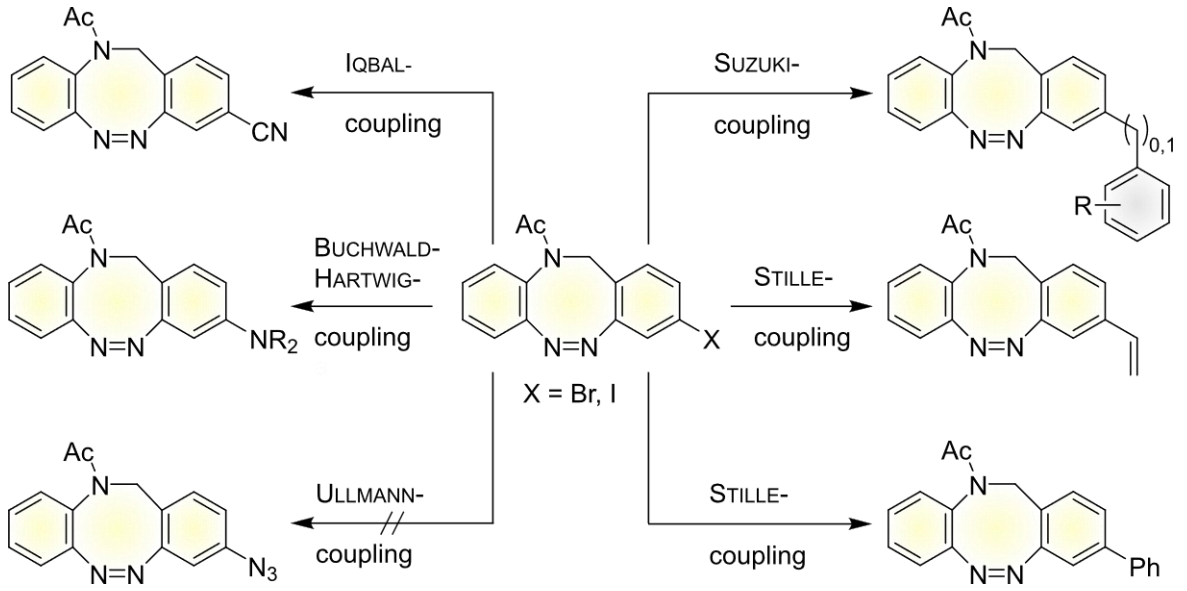

Scheme 4.2: Overview of cross-coupling reactions performed within this work. SUZUKI-coupling with phenylboronic acids could be achieved in yields from 46% to 88%, with heteroarene boronic acids gave only low yields. Vinylation via STILLE-coupling gave good yield between 65% and 78% whereas phenylation resulted in yields of 10%. BUCHWALD-HARTWIG-coupling products could be obtained in yields between 25% and 72%. Nitrile derivative could be obtained via IQBAL-coupling in yields up to 81%.

All new *N*-Ac diazocine derivatives have been photochemically characterized in organic solvent and showed excellent photoconversion yields of $\Gamma_{Z\rightarrow E}$ (405 nm) = 76%—85% for arylated and vinylated compounds while aniline derivatives showed lower values of $\Gamma_{Z\rightarrow E}$ (405 nm) = 41%—50%. Thermal relaxation of all new compounds was quite similar to the unsubstituted *N*-Ac diazocine in a range between 28 and 40 minutes. Quantitative back isomerization could be achieved for all new *N*-Ac diazocines. Furthermore, the switching of chosen derivatizes was performed in aqueous media at different pH values. Compared to unsubstituted *N*-Ac diazocine photoconversion yields of selected benzoic acid and aniline derivative were significantly lower ($\Gamma_{Z\rightarrow E}$ (405 nm) = 37%—62%). However, it is worth noting that photoconversion yield of aniline derivative for Z- to E-photoisomerization in aqueous media in slightly acidic pH is improved compared to organic solvent.

4.4 Cross-Coupling of *N*-Acetyl Diazocines

Thomas Brandt, Pascal Lentes, Jeremy Rudtke, Michael Hösgen, Christian Näther and Rainer Herges

J. Org. Chem **2024***, submitted,* Manuscript ID: jo-2024-00398n.R2

Scientific contribution to this paper: Concept Design, Development of the Synthesis pathway, Synthesis and characterization of compounds with help of Jeremy Rudtke and Michael Hösgen, UV-vis (spectra and half-lives) and NMR measurements (spectra and PSS measurements), writing of the manuscript and supporting information.

N-Acetyl Diazocine Derivatives via Cross-Coupling

Thomas Brandt[a], Pascal Lentes[a], Jeremy Rudtke[a], Michael Hösgen[a], Christian Näther[b], Rainer Herges[a]*

[a] T. Brandt, P. Lentes, J. Rudtke, M. Hösgen, Prof. Dr. R. Herges
Otto Diels Institute for Organic Chemistry
Kiel University, Otto-Hahn-Platz 4, 24118 Kiel, Germany
E-Mail: rherges@oc.uni-kiel.de

[b] C. Naether, Institute for Inorganic Chemistry, Max-Eyth-Straße 2, 24118 Kiel, Germany

KEYWORDS: photoswitch, • diazocine • cross coupling • photoisomerization • N-acetyl diazocine • thermal relaxation

ABSTRACT: Diazocines are photoswitches derived from azobenzenes by bridging the two phenyl rings in *ortho* position with a CH_2CH_2 group forming an eight membered (diazocine) ring. Diazocine is superior to most azobenzenes in almost all photophysical properties (switching efficiency, quantum yield, wavelengths etc.). The biggest advantage, especially in photopharmacology and when used in photoswitchable materials, is the inverted thermodynamic stability of the two switching states (isomers). The *Z* isomer is more stable than the *E* form. However, one disadvantage that it shares with the frequently used azobenzene is that the switching efficiency decreases sharply with increasing water content in the solvent. In a recently published paper, we reported that replacing one CH_2 group in the bridge with $NCOCH_3$ not only confers intrinsic water solubility, but also largely eliminates the problem of reduced switching efficiency in aqueous solutions. In order to investigate the chemistry of this promising photoswitch and to unlock further applications, we now investigate strategies for the synthesis of derivatives, which are based on cross-coupling reactions. 20 vinyl-, aryl-, cyano-, and amino-substituted diazocines were prepared via Stille, Suzuki, and Buchwald-Hartwig reactions. X-ray structures are presented for derivatives **1**, **2** and **7**.

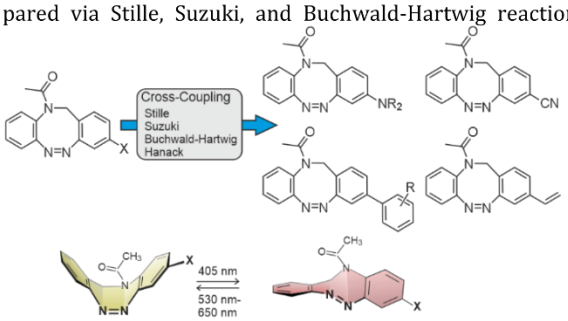

Introduction

Diazocines are frequently used photoswitches with superior photophysical properties. The parent ethylene bridged diazocine shows excellent switching photoconversion between the *Z* and the *E* configurations ($\Gamma(Z \rightarrow E)_{385nm}$ = 92% and $\Gamma(E \rightarrow Z)_{520nm}$ > 99 % in *n*-hexane) due to well-separated *n*-π*-transitions in the visible part of the electromagnetic spectra.[1] Moreover the ethylene bridge creates a cyclic 8-membered core, inverting the thermodynamically stability in favor of the *Z* boat conformation compared to parent azobenzene, which has a stable *E* configuration.[1-4] Preceding studies including azobenzene-based photopharmacophores showed that, in most cases, the sterically demanding *Z* configuration is biologically inactive, while the stretched *E* configuration is biologically active.[5-7] Because of the inverted thermodynamic stability compared to azobenzene, the stable *Z* configuration of the diazocine can be administered and subsequently activated with light at the site of illness with high spatiotemporal resolution. Thus, collateral damage in the surrounding healthy tissue can be avoided. In addition, the quantitative thermal back-isomerization from the active *E* to the inactive *Z* configuration prevents contamination and accumulation in the environment after excretion.[1,6,7] These superior properties of diazocines have been exploited in several applications such as the control of protein folding by implementation as cross-linkers between protein side chains[8] or in peptide backbones[9], as photoswitchable neurotransmitters[10,11] or as switching units for potential dependent potassium channels.[12] Compared to the $Z \rightarrow E$ conversion rate of 92% (in *n*-hexane) of the parent diazocine the conversion water/DMSO mixtures is decreasing with increasing water concentration (73% in water/DMSO 9:1).[8-12] Moreover, the parent diazocine is in-

soluble in water (precipitation in water/DMSO > 9:1). Substitution with polar substituents such as CH_2NH_2 provides water solubility, however, it does not restore the high $Z \rightarrow E$ conversion rates of the parent system in organic solvents, which is a disadvantage, since biochemical reactions usually take place in aqueous environments.[13] The substitution of one CH_2 group in the CH_2CH_2 bridge by N-CO-CH_3 leads to an intrinsic water solubility of the *N*-acetyl diazocine **1** (Figure 1).[3] Furthermore the photoconversion of **1** shows no significant drop in pure water in contrast to the solubilized parent diazocine. These superior properties make the *N*-acetyl diazocine **1** an ideal candidate for application in the field of photopharmacology especially in aqueous environments.[13]

There are two strategies of applying diazocines in photopharmacology. The first one exploits the structural similarity of the tricyclic diazocine framework to the tricyclic structure of e. g. tetrahydrodibenzazocines[14,15] and tetracyclic steroid scaffolds such as 17β-estradiol[16] where the diazocine core mimics the framework of the bioactive compound. The other option is to attach the diazocine photoswitch as a substituent (appendix) to the biologically active molecule.[6,10,17-19] The art of designing a photoswitchable drug is to place the switch at a position in the pharmacophore that allows switching of the biological effect by irradiation with light without greatly reducing the overall activity by unselective interference with the inhibitor-receptor interaction. This is a difficult task because the design of a photoswitchable agent usually starts with a known, non-switchable drug or a known biological molecule, which is already carefully "optimized" either by pharmaceutical industry or by nature. Hence, there is a high risk that any change in structure will also lead to a reduction in efficiency. In any case the light-induced geometry change via isomerization should selectively control the interaction between the inhibitor and the receptor.[19]

Currently there is only one example reported in the literature for the incorporation of *N*-acetyl diazocines into biologically active molecules.[15] As a starting point for further derivatization, the synthesis and characterization of monohalogenated *N*-acetyl diazocines **2** and **3** (Figure 1) have been performed.[20] Unfortunately, diazocines in general, and *N*-acetyl diazocines in particular cannot be derivatized by electrophilic aromatic substitution. Substituents such as halogen atoms must be introduced into the *N*-acetyl diazocine structure during the synthesis of the building blocks. In the present work we start from mono- and dihalogenated *N*-acetyl diazocine **2-4** (Figure 1) and focus on the further derivatization via cross-coupling reactions and the synthesis of a new dihalogenated *N*-acetyl diazocine **4** (Figure 1).

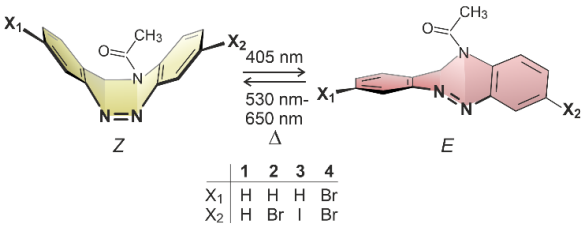

	1	2	3	4
X_1	H	H	H	Br
X_2	H	Br	I	Br

Figure 1. The halogen substituted *N*-acetyl diazocines **2-4** were used as the starting compounds for further derivatization via Pd-catalyzed cross-coupling reactions. Solutions of the *Z* isomers are yellow. The *E* isomers are red.

Results and discussion

The monosubstituted *N*-acetyl diazocines **2** and **3** were synthesized according to the procedure published by our group recently.[20] The synthesis of disubstituted compound **4** followed the same procedure except the preparation of the dianiline building block **5**, which was prepared by boc-protection of the *o*-nitroaniline starting material **6** and subsequent reduction of the nitro group (See supporting information chapter II.1).

Crosscoupling reactions

Stille cross-coupling reactions were performed by an organic halide reacting with an organotin compound. A great advantage of the used organostannanes is the easy accessibility, and their high air and moisture stability, so that usually a wide range of functional groups can be introduced under mild conditions.[21] Nevertheless the arylation of monohalogenated *N*-acetyl diazocines via Stille coupling in our case gave unsatisfying results (Table 1). Reactions with tetrakis(triphenylphosphine)-palladium(0) as catalyst resulted in no product (**7**) formation. Bis(tri-*tert*-butylphosphin)-palladium(0) as catalyst gave rise to the product in very low yields independent from the used halogenated diazocine. In contrast to other cross coupling reactions described in this work, most of the starting material decomposed during the reaction and could not be re-isolated.

Table 1. Reaction conditions of arylation of halogenated *N*-acetyl diazocines via Stille coupling reaction.

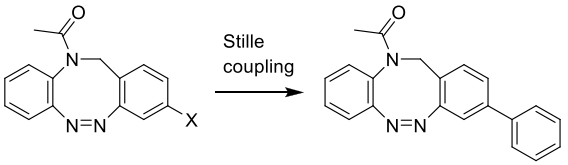

2,3 **7**

cat. system	Organotin compound	conditions	yield
$Pd(OAc)_2$ PPh_3	Ph_3SnCl	abs. DMF N_2, 100 °C, 16 h	-
$Pd(tBu_3P)_2$	Ph_3SnCl	abs. THF N_2, 65 °C, 16 h	X = Br 10% X = I 10%

In contrast, the vinylation of diazocines **2** and **3** provides good yields of 65% resp. 71% for the vinyl *N*-acetyl diazocine **8** (Table 2). An alternative way of vinylating *N*-acetyl diazocines is the Pd-catalyzed vinylation with polyvinylsiloxanes and TBAF as activating agent following the method by DENMARK et al. giving rise to even higher yields (74% and 78% Table 2).[22]

Table 2. Vinylation of halogenated *N*-acetyl diazocines via Pd-catalyzed coupling reactions.

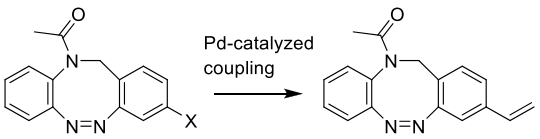

2,3 **8**

cat. system	reaction partner or additive	conditions	yield
$Pd(OAc)_2$ PPh_3	tributylvinyltin	abs. DMF, N_2, 100 °C, 16 h	X = Br 65% X = I 71%
$PdBr_2$ JohnPhos	D_4^V [a] TBAF	abs. THF, N_2, 50 °C, 16 h	X = Br 74% X = I 78%

[a] D_4^V: 1,3,5,7-tetramethyl-1,3,5,7-tetravinylcyclotetrasiloxane

To overcome the problems of poor yields in the arylation of *N*-acetyl diazocines via Stille-coupling we used Suzuki-Miyaura reactions of the diazocines **2** and **3** with different arylboronic acids.[23,24] There are several examples of last-step-modifications of azobenzenes via Suzuki-Miyaura reactions in the current literature, which indicate that the reaction conditions are compatible with azo groups.[25,26] Suzuki-Miyaura-reaction of **2** and **3** with different phenylboronic acids resulted in the formation of the corresponding arylated *N*-acetyl diazocines **7**, **9-13** in yields from 68 to 88% (Table 3). The yields increased slightly if boronic acids with electron withdrawing groups were used. An influence of bulky substituents like carboxyl groups in *ortho*-position of the phenyl boronic acids on the reaction was not observed. The synthesis of *N*-acetyl diazocines connected to heteroaromatic aromatic systems **14-16** was less successful. The pyridine substituted *N*-acetyl diazocine **14** was formed in yields of 7% or 19% while furan **15** and thiophene substituted *N*-acetyl diazocine **16** could not be obtained. The reaction with benzylboronic acid gave the corresponding *N*-acetyl diazocine **17** (46%, Table 3). Interestingly this reaction only took place if brominated *N*-acetyl diazocine **2** was used as starting material although iodo aryl compounds are in general more reactive.[23] The reaction of halogenated *N*-acetyl diazocines **2** and **3** with bis(pinacolato)diboron did not lead to the formation of the pinacolborane substituted N-acetyl diazocine **18**. Accordingly, the Suzuki-Miyaura reaction with inversed roles between *N*-acetyl diazocine boronic acid pinacol ester and aryl or alkyl halides could not be investigated.

Table 3. Derivatization of halogen-substituted *N*-acetyl diazocines via Suzuki-Miyaura reaction.

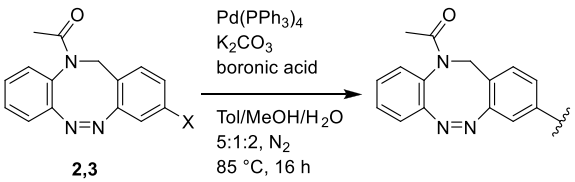

2,3

boronic acid	product	Yield
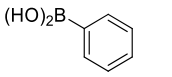	**7** 	X = Br 74% X = I 83%
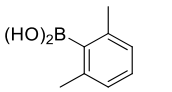	**9** 	X = Br 68% X = I 74%
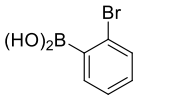	**10** 	X = I 82%
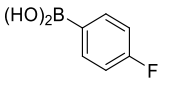	**11** 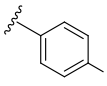	X = Br 81% X = I 88%
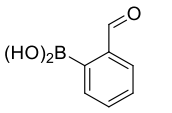	**12** 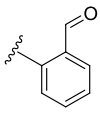	X = Br 70% X = I 77%
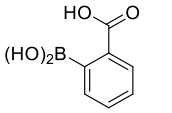	**13** 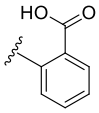	X = Br 76%[a] X = I 79%[a]
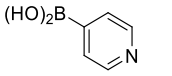	**14** 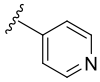	X = Br 7% X = I 19%
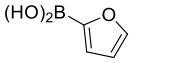	**15** 	X = Br - X = I -
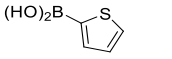	**16** 	X = Br - X = I -
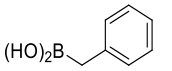	**17** 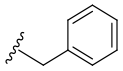	X = Br 46% X = I -
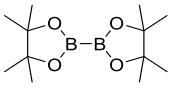	**18** 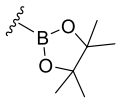	X = Br - X = I -

[a]Reaction was carried out in abs. DMF at 100 °C because no reaction took place if the Suzuki-Miyaura standard procedure was applied.

The Buchwald-Hartwig amination is a versatile and powerful tool for C-N bond formation and applied widely in the synthesis of new pharmaceutical substances.[27-29] Furthermore azobenzenes[30,31] as well as diazocines[32,33] have been derivatized via Buchwald-Hartwig amination.

The Buchwald-Hartwig amination of halogenated *N*-acetyl diazocines according to the procedure of MAIER et. al.[32] with *tert*-butyl carbamate resulted in the formation of boc-protected aniline-substituted *N*-acetyl diazocine **19** in a yield of 72%. However, the reaction only took place if the iodo *N*-acetyl diazocine **3** was used as starting material. Using diphenylamine as a more electron rich amine resulted in the formation of diphenylaniline-substituted *N*-acetyl diazocine **20** in a significantly lower yield of 25% starting from the bromide **2** and 47% starting from the iodo precursor **3** (Table 5).

Table 4. Derivatization of halogenated *N*-acetyl diazocines **2** and **3** via Buchwald-Hartwig amination.

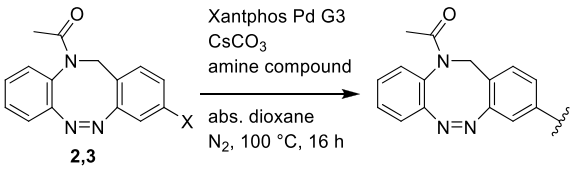

amine compound	product	yield
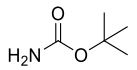	19 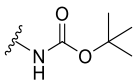	X = Br - X = I 72%
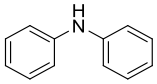	20 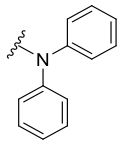	X = Br 25% X = I 47%

Deprotection of the carbamate **19** with trifluoroacetic acid provided the corresponding aniline-substituted *N*-acetyl diazocine **21** (Scheme 1).

Scheme 1. Synthesis of aniline *N*-acetyl diazocine by deprotection of the carbamate.

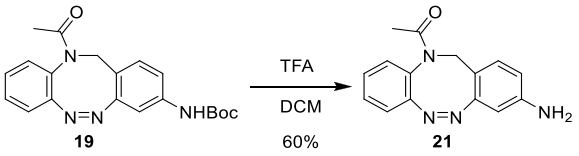

Another option for carbon-heteroatom bond formation reactions are copper catalyzed Ullmann type reactions, which have already been applied to the parent diazocine.[34,35] The attempted synthesis of azide functionalized *N*-acetyl diazocine **22** under the conditions described by HUGENBUSCH et al.[35] showed no product formation and only starting material could be obtained (Scheme 2).

Scheme 2. Reaction conditions for the attempted Ullmann-type reaction with sodium azide

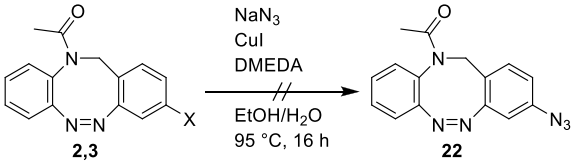

The palladium catalyzed introduction of cyano groups under mild conditions in analogy to IQBAL et al.[36] gave the cyano-substituted N-acetyl diazocine **23** in yields of 61% from bromide **2** and 81% from iodide **3** (Scheme 3).

Scheme 3. Reaction conditions for the palladium catalyzed synthesis introduction of nitrile functionality

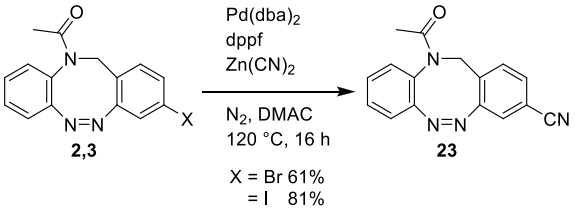

Nitriles are a good starting point for further functional group interconversions.[37]

Crystal structures have been obtained for the *Z* isomers of the *N*-acetyl diazocine derivatives **1**, **2** and **7**. It should be noted that the carbonyl group in all three molecules is oriented towards the CH_2 group as drawn in all structural representations. For details see Supporting Information Chapter V.

Photochemical characterization

With these new *N*-acetyl diazocine derivatives at hand we turned towards the photochemical characterization, in particular to gain insight into the effects of different substituents on UV-spectra and switching behavior. For determination of the nπ*-absorption maxima of the *E* and *Z* isomers 250 μM solutions of each compound in acetonitrile were prepared and measured at 25 °C. All compounds (**4**, **7-14**, **17**, **19-21**, **23**) exhibit an $n\pi^*$-transition at approximately 400 nm, matching the $n\pi^*$-transition of unsubstituted *N*-acetyl diazocine **1** (Table 5). Irradiation with 405 nm gives the metastable *E* isomers with photoconversion yields of 76-85% due to a very good separation of the $n\pi^*$-transitions. The nitrogen-substituted derivatives **19-21** show significantly lower conversion rates of 41-61%. This behavior has already been observed in other amino-substituted diazocines as well and is probably due to the overlap of $n\pi^*$-transitions of the *E* and *Z* isomers.[38] An almost complete $E \rightarrow Z$ conversion (>99%) can be achieved by irradiation with light between 520 and 600 nm for all synthesized compounds.

Table 5. Photophysical properties of *N*-acetyl diazocines **1-4, 7-14, 17, 19-21, 23** in acetonitrile.

	λ_{max} (Z)	λ_{max} (E)	$t_{1/2}$ (25 °C)	k (25 °C)	$\Gamma_{Z\rightarrow E}$ (405 nm)[a]	$\Gamma_{E\rightarrow Z}$ (530 nm)
	nm		min.	10^{-4} s^{-1}		
1[20]	397	513	29.5	3.916	88%	>99%
2[20]	397	515	30.9	3.744	81%	>99%
3[20]	397	517	28.6	4.036	82%	>99%
4	396	519	16.9	6.820	85%	>99%
7	399	516	29.3	3.944	79%	>99%
8	398	515	29.6	3.897	76%	>99%
9	394	515	34.2	3.374	77%	>99%
10	396	516	34.2	3.382	82%	>99%
11	397	515	33.8	3.418	78%	>99%
12	396	517	29.8	3.877	80%	>99%

13	399	517	31.2	3.688	77%	>99%
14[b]	396	515	39.9	2.897	79%	>99%
17	398	515	29.3	3.944	82%	>99%
19	397	514	30.6	3.779	61%	>99%
20	389	510	31.5	3.670	49%	>99%
21	396	511	38.9	2.973	41%	>99%
23	396	518	39.8	2.906	83%	>99%

[a]Extrapolated values (for details, see Supporting Information Sektion IV) in deuterated acetonitrile 5 mM.

[b]UV spectra measured with a concentration of 128 µM in acetonitrile and NMR spectra with a concentration of 2.55 mM.

Thermal half-lives ($t_{1/2}$) were determined by monitoring the thermal relaxation of the synthesized diazocines at 25 °C in the UV spectrometer (see Supporting Information IV). The dihalogenated *N*-acetyl diazocine **4** shows a significantly reduced half-life compared to the mono- **2** and **3** and the unsubstituted system **1**. The substitution with a phenyl group does not show a significant influence on the thermal half-life whereby it makes no difference if there is a bridging methylene group between diazocine and the substituent or not. The half-lives of molecules **7** and **17** are nearly identical compared to the parent system **1**. If electron withdrawing substituents are added in *ortho*-position of the additional phenyl ring (**12** and **13**) the half-life is not affected significantly as well. An increase of about 10% of the half-lives has been observed for weak +M-substituents bromine (**10**) and fluorine (**11**) or methyl groups (**9**) in *ortho*- and *para*-positions. The increase is even stronger if pyridine- (**14**), cyano- (**23**) or aniline-substituents (**21**) are attached to the *N*-acetyl diazocine in *meta*-position. In contrast to the extended half-life of the aniline **21** the Boc-protected **19** and the diphenyl-substituted aniline **20** show half-lives not significantly longer than the parent *N*-acetyl diazocine **1**.

Given the water solubility and the excellent switching behavior of parent **1** in aqueous media[3,13,20], the photochemical properties of water-soluble substituted *N*-acetyl-diazocines **13** and **21**were also investigated in aqueous solution (**13** and **21** in aqueous PBS buffer solution at pH 7.4 250 µM, **23** at pH 3.5 250 µM, **13** at pH 9 250 µM). The pH values were chosen tome make sure that the aniline **21** is completely protonated and the carboxylic acid **13** is completely deprotonated. UV measurements revealed that the absorption maxima of the $n\pi^*$ transitions of the *Z* isomers of **13** and **21** are almost independent of solvent and pH (392-398 nm), while the $n\pi^*$ transitions of the *E* isomers at ∽515 nm are significantly shifted to shorter wavelengths ($\Delta\lambda_{max}$=10 - 20 nm) in water (Table 7). At the same time the $n\pi^*$ transition of the azobenzene substructure of the *E* isomer which is usually hidden under the $\pi\pi^*$ transition in organic solvents is shifted to higher wavelengths (see Figure SIII.15-SIII.20). For diazocine **13** this leads to a drop in the PSS ($\Gamma_{Z\rightarrow E}$) from 77% in acetonitrile to 53% in water at pH 7.4 and 48% at pH 9 due to a higher overlap of both isomers $n\pi^*$ transitions. For the aniline type substituted diazocine **21** the PSS ($\Gamma_{Z\rightarrow E}$) decreases slightly from 41% in acetonitrile to 37% in water at pH 7.4 and increases again to 62% at pH 3.5. This drastic increase in the PSS is probably rooted in a lower $n\pi^*$ transition gap caused a by protonated aniline **21** at pH 3.5 as well as a higher band separation compared to the unprotonated form at pH 7.4. The thermal half-lives of **13** and **21** increase by a factor 2.5 and 4.2 when changing the solvent from acetonitrile to water at pH 7.4which is consistent with the current literature for thermal half-lives of substituted parent diazocines in aqueous media.[16,37]

Table 6. Photophysical properties of *N*-acetyl diazocines **1**, **13**, **21** in water at various pH values.

	λ_{max} (Z)	λ_{max} (E)	$t_{1/2}$ (25 °C)	k (25 °C)	$\Gamma_{Z\rightarrow E}$ (405 nm)[a]	$\Gamma_{E\rightarrow Z}$ (530 nm)
	nm		min.	10^{-4} s^{-1}		
1[20]	393	502	72.8	1.587	72%	>99%
13 at pH 9	392	502	106.4	1.086	48%	>99%
13 at pH 7.4	392	505	78.2	1.477	53%	>99%
21 at pH 3.5	392	495	118.0	0.975	62%	>99%
21 at pH 7.4	392	489	162.5	0.711	37%	>99%

[a]Extrapolated values (for details, see Supporting Information IV) in deuterated water 5 mM.

Conclusion

Thirteen mono-*meta*-substituted (**7**-**14**, **17**, **19**-**21**, **23**) and one di-*meta*-substituted (**4**) *N*-acetyl diazocines have been synthesized and characterized. The synthesis has been performed from halogenated precursors and cross-coupling reactions for further functionalization. The reaction conditions of various cross-coupling reactions have been correspondingly adjusted. The arylation of the *N*-acetyl diazocine system could be achieved via Suzuki coupling reactions in high yields (**7**, **9**-**14**, **17**) as well as the vinylation via Stille-coupling (**8**). These compounds also exhibit excellent switching properties. Electron withdrawing substituents at the aryl substituents have no significant influence on the

switching behavior while weak +M-substituents like bromine and fluorine as well as electron poor heteroaromatic systems lead to increased thermal half-lives. An amino-substituted (aniline type) derivative (**21**) was obtained via Buchwald-Hartwig coupling with Boc-carbamate and subsequent deprotection. Amino-substituted *N*-acetyl diazocines (**19-21**) exhibit lower photostationary states (PSS) in analogy to aminosubstituted azobenzenes and previously synthesized diazocines. We also investigated the switching properties of the water-soluble derivatives **13** and **21** in water at different pH. The half-lives of the metastable *E* isomers are significantly longer in water than in less polar solvents like acetonitrile. For carboxylic acid substituted **13**, the *Z*→*E* conversion upon irradiation with 405 nm drops from 77% to 53% upon changing the solvent from acetonitrile to water (pH 7.4). The reverse effect was observed with amino substituted **21**.

The photophysical properties of photoswitchable drugs in photopharmacology are usually determined in organic solvents. Their natural environment, however, is the aqueous phase. There is a risk of overestimating the performance of photochromic drugs because photoconversion to the active state usually drops considerably in water, and also half-lives are different. Light-activatable drugs based on *N*-acetyldiazocines are more hydrophilic than those derived from the parent system diazocine and corresponding azobenzenes. They retain their switching properties even in an aqueous environment and are therefore promising switches in photopharmacological applications.

ASSOCIATED CONTENT

Data availability statement. The data underlying this study are available in the published article and its Supporting Snformation

Supporting Information. "This material is available free of charge via the Internet at http://pubs.acs.org. "
Synthetic procedures, UV-vis and NMR switching experiments, copies of UV-vis and NMR spectra, X-ray crystallographic data

CCDC-2329263 (1), CCDC-2329261 (2), and CCDC- 2329262 (7) contain the supplementary crystallographic data for this paper. These data can be obtained free charge from the Cambridge Crystallographic Data Centre via http://www.ccdc.cam.ac.uk/data_request/cif. Cambridge CB2 1EZ, UK; fax: +44 1223 336033"

The data underlying this study are available in the published article and its Supporting Information.

AUTHOR INFORMATION

Corresponding Author

Prof. Dr. Rainer Herges
rherges@oc.uni-kiel.de

https://orcid.org/0000-0002-6396-6991

Present Addresses

Author Contributions

The manuscript was written through contributions of all authors. / All authors have given approval to the final version of the manuscript.

Funding Sources

None

Notes

The authors declare no competing financial interest.

ACKNOWLEDGMENT

ABBREVIATIONS

CCR2, CC chemokine receptor 2; CCL2, CC chemokine ligand 2; CCR5, CC chemokine receptor 5; TLC, thin layer chromatography.

REFERENCES

(Word Style "TF_References_Section"). References are placed at the end of the manuscript. Authors are responsible for the accuracy and completeness of all references. Examples of the recommended formats for the various reference types can be found at http://pubs.acs.org/page/4authors/index.html. Detailed information on reference style can be found in The ACS Style Guide, available from Oxford Press.

References

[1] Siewertsen, R.; Neumann, H.; Buchheim-Stehn, B.; Herges, R.; Näther, C.; Renth, F.; Temps, F. Highly Efficient Reversible Z E Photoisomerization of a Bridged Azobenzene with Visible Light through Resolved S1(nπ*) Absorption Bands. *J. Am. Chem. Soc.* **2009**, *131*, 15594-15595.

[2] Hammerich, M.; Schütt, C.; Stähler, C.; Lentes, P.; Röhricht, F.; Höppner, R.; Herges, R. Heterodiazocines: Synthesis and Photochromic Properties, *Trans* to *Cis* Switching within the Bio-optical Window. *J. Am. Chem. Soc.* **2016**, *138*, 13111-13114.

[3] Lentes, P.; Stadler, E.; Röhricht, F.; Brahms, A.; Gröbner, J.; Sönnichsen, F. D.; Gescheidt, G.; Herges, R. Nitrogen Bridged Diazocines: Photochromes Switching within the Near-Infrared Region with High Quantum Yields in Organic Solvents and Water. *J. Am. Chem. Soc.* **2019**, *141*, 13592-13600.

[4] Siewertsen, R.; Schönborn, J. B.; Hartke, B.; Renth, F.; Temps, F. Superior Z → E and E → Z photoswitching of dihydrodibenzodiazocine, a bridged azobenzene, by S1(nπ*) excitation at λ = 387 and 490 nm. *Phys. Chem. Chem. Phys.* **2011**, *13*, 1054-1063.

[5] Beharry, A. A.; Woolley, G. A. Azobenzene photoswitches for biomolecules. *Chem. Soc. Rev*. **2011**, *40*, 4422-4437.

[6] Hüll, K.; Morstein, J.; Trauner, D. In Vivo Photopharmacology. *Chem. Rev*. **2018**, *118*, 10710-10747.

[7] Szymański, W.; Beierle, J. M.; Kistemaker, H. A. V.; Velema, W. A.; Feringa, B. L. Reversible Photocontrol of Biological Systems by the Incorporation of Molecular Photoswitches. *Chem. Rev*. **2013**, *113*, 6114-6178.

[8] Preußke, N.; Moormann, W.; Bamberg, K.; Lipfert, M.; Herges, R.; Sönnichsen, F. D. Visible-light-driven photocontrol of the Trp-cage protein fold by a diazocine cross-linker. *Org. Biomol. Chem*. **2020**, *18*, 2650-2660.

[9] Albert, L.; Peñalver, A.; Djokovic, N.; Werel, L.; Hoffarth, M.; Ruzic, D.; Xu, J.; Essen, L.-O.; Nikolic, K.; Douet, Y.; Vázquez, O. Modulating Protein-Protein Interactions with Visible-Light-Responsive Peptide Backbone Photoswitches. *ChemBioChem* **2019**, *20*, 1417-1429.

[10] Cabré, G.; Garrido-Charles, A.; González-Lafont, À.; Moormann, W.; Langbehn, D.; Egea, D.; Lluch, J. M.; Herges, R.; Alibés, R.; Busqué, F.; Gorostiza, P.; Hernando, J. Synthetic Photoswitchable Neurotransmitters Based on Bridged Azobenzenes. *Org. Lett*. **2019**, *21*, 3780-3784.

[11] Thapaliya, E. R.; Zhao, J.; Ellis-Davies, G. C. R. Locked-Azobenzene: Testing the Scope of a Unique Photoswitchable Scaffold for Cell Physiology. *ACS Chem. Neurosci*. **2019**, *10*, 2481-2488.

[12] Trads, J. B.; Hüll, K.; Matsuura, B. S.; Laprell, L.; Fehrentz, T.; Görldt, N.; Kozek, K. A.; Weaver, C. D.; Klöcker, N.; Barber, D. M.; Trauner, D. Sign Inversion in Photopharmacology: Incorporation of Cyclic Azobenzenes in Photoswitchable Potassium Channel Blockers and Openers. *Angew. Chem. Int. Ed*. **2019**, *58*, 15421-15428.

[13] Lentes, P.; Frühwirt, P.; Freißmuth, H.; Moormann, W.; Kruse, F.; Gescheidt, G.; Herges, R. Photoswitching of Diazocines in Aqueous Media. *J. Org. Chem*. **2021**, *86*, 4355-4360.

[14] Fink, B. E.; Gavai, A. V.; Tokarski, J. S.; Goyal, B.; Misra, R.; Xiao, H.-Y.; Kimball, S. D.; Han, W.-C.; Norris, D.; Spires, T. E.; You, D.; Gottardis, M. M.; Lorenzi, M. V.; Vite, G. D. Identification of a novel series of tetrahydrodibenzazocines as inhibitors of 17β hydroxysteroid dehydrogenase type 3. *Bioorg. Med. Chem. Lett*. **2006**, *16*, 1532-1536.

[15] Wages, F.; Lentes, P.; Griebenow, T.; Herges, R.; Peifer, C.; Maser, E. Reduction of Photoswitched, nitrogen bridged *N*-acetyl diazocines limits inhibition of 17βHSD3 activity in transfected human embryonic kidney 293 cells. *Chem. Biol. Interact*. **2022**, *354*, 109822.

[16] Ewert, J.; Heintze, L.; Jordà-Redondo, M.; von Glasenapp, J.-S.; Nonell, S.; Bucher, G.; Peifer, C.; Herges, R. Photoswitchable Diazocine-Based Estrogen Receptor Agonists: Stabilization of the Active Form inside the Receptor. *J. Am. Chem. Soc.* **2022**, *144*, 15059-15071.

[17] Schoenberger, M.; Damijonaitis, A.; Zhang, Z.; Nagel, D.; Trauner, D.; Development of a New Photochromic Ion Channel Blocker via Azologization of Fomocaine. *ACS Chem. Neurosci*. **2014**, *5*, 514-518.

[18] Gorostiza, P.; Isacoff, E. Y. Optical Switches for Remote and Noninvasive Control of Cell Signaling. *Science* **2008**, *322,* 395-399.

[19] Velema, W. A.; Szymanski, W.; Feringa, B. L. Photopharmacology: Beyond Proof of Principle. *J. Am. Chem. Soc.* **2014**, *136*, 2178-2191.

[20] Lentes, P.; Rudtke, J.; Griebenow, T.; Herges, R. Substituted nitrogen-bridged diazocines. *Beilstein J. Org. Chem*. **2021**, *17*, 1503-1508.

[21] Stille, J. K. The Palladium-Catalyzed Cross-Coupling Reactions of Organotin Reagents with Organic Electrophiles. *Angew. Chem. Int. Ed*. **1986**, *25*, 508-524.

[22] Denmark, S. E.; Butler, C. R. Vinylation of Aryl Bromides Using an Inexpensive Vinylpolysiloxane. *Org. Lett*. **2006**, *8*, 63-66.

[23] Miyaura, N.; Suzuki, A. Palladium-Catalyzed Cross-Coupling Reactions of Organoboron Compounds. *Chem. Rev*. **1995**, *95*, 2457-2483.

[24] Suzuki, A. Recent Advances in the cross-coupling reactions of organoboron derivatives with organic electrophiles, 1995-1998. *J. Organomet. Chem*. **1999**, *576*, 147-168.

[25] Walther, M.; Kipke, W.; Schultzke, S.; Ghosh, S.; Staubitz, A. Modifications of Azobenzenes by Cross-Coupling Reactions. *Synthesis* **2021**, *53*, 1213-1228.

[26] Walther, M.; Kipke, W.; Renken, R.; Staubitz, A. Stille vs. Suzuki - cross-coupling for the functionalization of diazocines. *RSC Adv*. **2023**, *13*, 15805-15809.

[27] Guram, A. S.; Rennels, R. A.; Buchwald, S. L. A Simple Catalytic Method for the Conversion of Aryl Bromides to Arylamines. *Angew. Chem. Int. Ed*. **1995**, *34*, 1348-1350.

[28] Louie, J.; Hartwig, J. F. Palladium-Catalyzed Synthesis of Arylamines from Aryl Halides. Mechanistic Studies Lead to Coupling in the Absence of Tin Reagents. *Tetrahedron Lett*. **1995**, *36*, 3609-3612.

[29] Brown, D. G.; Boström, J.; An analysis of past and present synthetic methodologies on medicinal chemistry: Where have all the new reactions gone?. *J. Med. Chem*. **2016**, *59*, 4443-4458.

[30] Kanbara, T.; Oshima, M.; Imayasu, T.; Hasegawa, K. Preparation of New Polymers Containing an Azobenzene Group in the Side Chain by Palladium-Catalyzed Polymer Reaction and Polycondensation and Characterization of the Polymers. *Macromolecules* **1998**, *31*, 8725-8730.

[31] Heindl, A. H.; Wegner, H. A. Starazo triple switches - synthesis of unsymmetrical 1,3,5-tris(arylazo)benzenes. *Beilstein J. Org. Chem*. **2020**, *16*, 22-31.

[32] Maier, M. S.; Hüll, K.; Reynders, M.; Matsuura, B. S.; Leippe, P.; Ko, T.; Schäffer, L.; Trauner, D. Oxidative Approach Enables Efficient Access to Cyclic Azobenzenes. *J. Am. Chem. Soc*. **2019**, *141*, 17295-17304.

[33] Zhu, Q.; Wang, S.; Chen, P. Diazocine Derivatives: A Family of Azobenzenes for Photochromism with Highly Enhanced Turn-On Fluorescence. *Org. Lett*. **2019**, *21*, 4025-4029.

[34] Sambiagio, C.; Marsden, S. P.; Blacker, A. J.; McGowan, P. C. Copper catalysed Ullmann type chemistry: from mechanistic aspects to modern development. *Chem. Soc. Rev*. **2014**, *43*, 3525-3550.

[35] Hugenbusch, D.; Lehr, M.; von Glasenapp, J.-S.; McConnell, A. J.; Herges, R. Light-Controlled Destruction and Assembly: Switching between Two Differently Composed Cage-Type Complexes. *Angew. Chem. Int. Ed*. **2023**, *62*, e202212571.

[36] Iqbal, Z.; Lyubimtsev, A.; Hanack, M. Synthesis of Phtalonitriles Using a Palladium Catalyst. *Synlett* **2008**, *2008*, 2287-2290.

[37] Xia, Y.; Jiang, H.; Wu, W. Recent Advances in Chemical Modifications of Nitriles. Eur. *J. Org. Chem.* **2021**, *2021*, 6658-6669.

[38] Sell, H.; Näther, C.; Herges, R. Amino-substituted diazocines as pincer-type photochromic switches. *Beilstein J. Org. Chem.* **2013**, *9*, 1-7.

4.5 Summary of Light-Switchable Diazocines as Potential Inhibitors of Testosterone-Synthesizing 17ß-Hydroxysteroid Dehydrogenase 3

Please note: The abbreviations used herein are used only to give context to the publication discussed in this section and therefore apply only here.

The hormone testosterone occurring in almost all vertebrates is a key molecule in metabolism and predominantly formed in the testicular LEYDIG-cells. In the final step, the carbonyl function of the precursor androstenedione at C17 is reduced to the secondary alcohol catalyzed by 17β-hydroxysteroid dehydrogenase type 3 (17βHSD3).[176-179] It is known to have a growth-stimulating effect in tissues with androgen receptors and is also found in greater concentrations in certain growing cancer cells, where an increased formation of 17βHSD3 can also be observed in parallel as self-reinforcing effect.[177,180,181] In this context, the influence of testosterone on the growth of human prostate cancer cells has been particularly well researched.[180,181] Therefore, the reduction of testosterone level and 17βHSD3 activity are possible therapeutic approaches.[182]
For the inhibition of 17βHSD3 catalyzed reduction of androstenedione to testosterone several inhibitors are known, but for this project tricyclic tetrahydrodibenzazocine (THB) was of special interest since it offers a high structural similarity to the previously reported *N*-Ac diazocine photoswitch.[166] Therefore, azologized THB analog *N*-Ac diazocine and its functionalized derivatives should be investigated as photopharmacophore in the inhibition 17βHSD3 catalyzed testosterone biosynthesis in transfected human embryonic kidney cells (HEK-293). In previous work already unsubstituted *N*-Ac diazocine (DA) and brominated *N*-Ac diazocine (bDA) were examined with the result of no significant inhibition of testosterone biosynthesis whereby it made no difference whether the diazocines were in Z- or E-configuration. Additionally, further analysis revealed partial decomposition of *N*-Ac diazocines to the corresponding dianiline.[166]
By late-stage modification via various cross-coupling reactions the range of accessible *N*-Ac diazocine derivatives has been growing considerably opening the path for the development of new light-switchable pharmacophores.[183] Due to their tricyclic core structurally similar to the THB inhibitor structure the influence of various functional groups and additional phenyl substituents containing various functional groups at different positions should be investigated on their inhibitory effect on 17βHSD3-catalyzed testosterone biosynthesis and their stability against intracellular reduction (**figure 4.4**). It was intended, that the substituents would allow the photopharmacophore to fill the enzymatic binding pocket more effectively resulting in the desired inactivity of the enzyme.

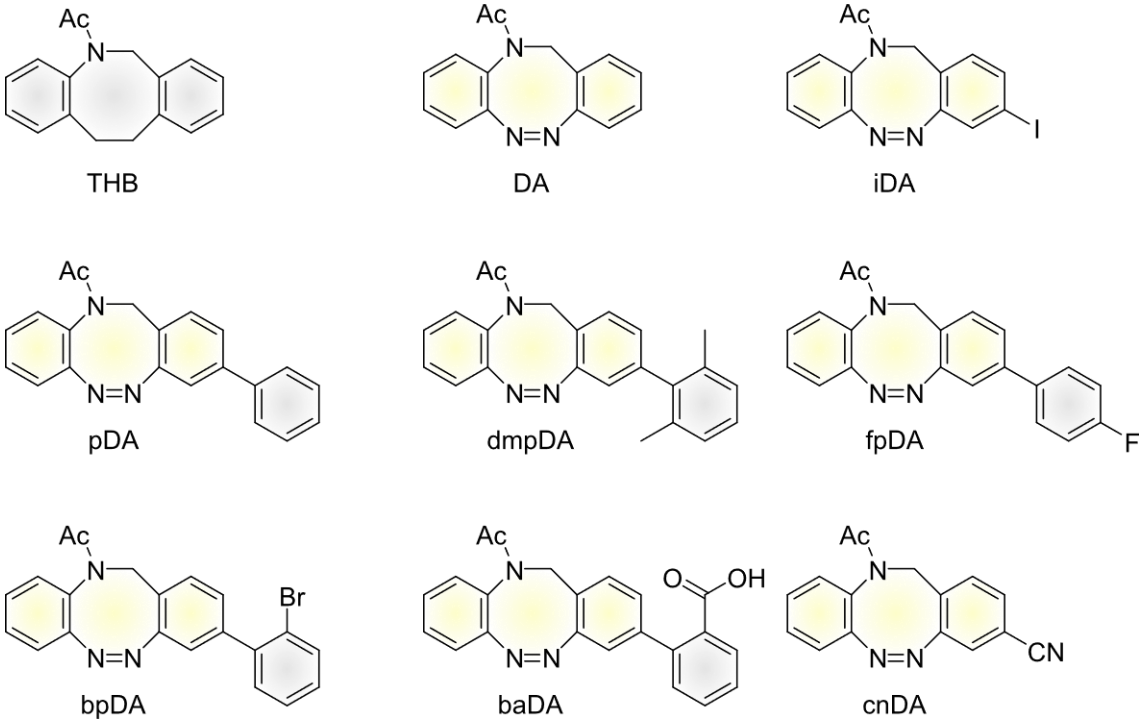

Figure 4.4: Overview of known 17βHSD3 inhibitor THB and the structurally related *N*-Ac diazocine derivatives used in inhibition assays with 17βHSD3-transfected HEK-293 cells. Please note: The abbreviations used herein are used only to give context to the publication discussed in this section and therefore apply only here.

Biological testing was performed via inhibition assays with HEK-293 cells and microsome assays with microsomes also received from HEK-293 cells. In both assays cells or respectively microsomes were incubated with androstenedione and reference inhibitors or *N*-Ac diazocine derivatives. Both methods showed excellent inhibition of 17βHSD3-catalyzed testosterone biosynthesis for dmpDA, fpDA and bpDA to the same extent as the reference inhibitor THB. The other *N*-Ac diazocine compounds used within this work showed only partial inhibition. However, all measurements showed that the extent of inhibition was independent from whether the samples were irradiated or not. Therefore, the *N*-Ac diazocines, which are part of this publication, showed no difference in their biological activity of their Z- or E-configurations. Furthermore, partial reduction of the used *N*-Ac diazocines to the corresponding dianiline could be observed.

Nevertheless, this work shows great potential of substituted *N*-Ac diazocines as potential photopharmacophores, although it should be noted that problems such as configuration-independent inhibition and intracellular or intramicrosomal reduction, which have already been observed in previous work[166], have not yet been solved.

4.6 Light-Switchable Diazocines as Potential Inhibitors of Testosterone-Synthesizing 17ß-Hydroxysteroid Dehydrogenase 3

Franziska Wages, Thomas Brandt, Hans-Jörg Martin, Rainer Herges and Edmund Maser

Chem. Biol. Interact. **2023**, *390*, 110872.

DOI: 10.1016/j.cbi.2024.110872

Scientific contribution to this paper: Synthesis and characterization of compounds, UV-vis (spectra and half-lives) in aqueous media, writing of the manuscript (proportionate participation) and supporting information (proportionate participation).

Chemico-Biological Interactions 390 (2024) 110872

Contents lists available at ScienceDirect

Chemico-Biological Interactions

journal homepage: www.elsevier.com/locate/chembioint

Light-switchable diazocines as potential inhibitors of testosterone-synthesizing 17β-hydroxysteroid dehydrogenase 3

F. Wages [a], T. Brandt [b], H.-J. Martin [a], R. Herges [b], E. Maser [a,*]

[a] Institute of Toxicology and Pharmacology for Natural Scientists, University Medical School Schleswig-Holstein, Campus Kiel, Brunswiker Str. 10, 24105 Kiel, Germany
[b] Otto Diels Institute of Organic Chemistry, Christian-Albrecht University of Kiel, Otto Hahn Platz 4, 24118 Kiel, Germany

ARTICLE INFO

Keywords:
17β-hydroxysteroid dehydrogenase 3
Enzyme inhibition
N-acetyl diazocine
Prostate cancer
Photopharmacology
Irradiation
Photoswitch

ABSTRACT

In patients with prostate carcinoma as well as in some other cancer types, the reduction of testosterone levels is desired because the hormone stimulates cancer cell growth. One molecular target for this goal is the inhibition of 17β-hydroxysteroid dehydrogenase type 3 (17βHSD3), which produces testosterone from its direct precursor androstenedione. Recent research in this field is trying to harness photopharmacological properties of certain compounds so that the inhibitory effect could be turned on and off by irradiation.

Seven new light-switchable diazocines were investigated with regard to their inhibition of 17βHSD3. For this purpose, transfected HEK-293 cells and isolated microsomes were treated with the substrate and the potential inhibitors with and without irradiation for an incubation period of 3 or 5 h. The amount of generated testosterone was measured by UHPLC and compared between samples and control as well as between irradiated and non-irradiated samples. There was no significant difference between samples with and without irradiation. However, four of the seven diazocines led to a significantly lower testosterone production both in cell and in microsome assays. In some of the irradiated samples, a partial destruction of the diazocines was observed, indicated by an additional UHPLC peak. However, the influence on the inhibition is negligible, because the majority of the substance remained intact. In conclusion, new inhibitors of 17βHSD3 have been found, but so far without the feature of a light switch, since the configurational alteration of the diazocines by irradiation did not lead to a change in bioactivity. Further modification might help to find a light-switching molecule that inhibits only in one configuration.

1. Introduction

Cancer is one of the leading causes of death worldwide [1]. Among men prostate cancer is the second most frequently occurring cancer and the fifth common cause of cancer-related mortality [2]. Moreover, the incidence is expected to rise as the society grows older. Between 2014 and 2019 the incidence of prostate cancer in the United States increased 3 % annually - the number of newly diagnosed cases is estimated to exceed 288.000 this year [3]. Globally, more than 1.4 million prostate cancer cases were reported for 2020 [4].

As a male sex hormone, testosterone exhibits androgenic effects and therefore is important for virilization. Since testosterone is involved in the metabolism of all macronutrients, has an anabolic function and is crucial for protein and nucleic acid build-up, it has been discussed for some time whether it also enhances malignant cell growth and could be a pharmacological target in case of cancer [5–7].

All naturally occurring androgens in the body are C_{19}-steroids and are built from cholesterol in several steps. In men testosterone is endogenously synthesized in the testicular Leydig cells and to a very small degree in the adrenal glands [6,8,9]. The synthesis is induced by luteinizing hormone (LH) which binds on the surface of the Leydig cells [10,11]. Physiologically, prostate cells do not produce testosterone. Under pathological conditions, on the other hand, degenerated prostate cells partially acquire the ability of testosterone synthesis [12,13].

Testosterone is produced from the weak androgen androstenedione by the NADPH-dependent enzyme 17β-hydroxysteroid dehydrogenase 3 (17βHSD3). In most peripheral tissues and effector regions, like the prostate, it is converted into the more active derivative 5α-dihydrotestosterone (5α-DHT) by 5α-reductase. To exert its various effects, the androgen binds to an intracellular receptor.

In tissues with androgen receptors, testosterone can have a growth-promoting effect [14]. This also applies to prostate cancer cells, which, in addition, may show altered expression levels of steroidogenic

* Corresponding author.
E-mail address: maser@toxi.uni-kiel.de (E. Maser).

https://doi.org/10.1016/j.cbi.2024.110872
Received 15 October 2023; Received in revised form 24 December 2023; Accepted 12 January 2024
Available online 18 January 2024

Abbreviations

17βHSD3 17β-Hydroxysteroid Dehydrogenase Type 3
baDA(Z)-2-(11-acetyl-11,12-dihydrodibenzo[c,g] [1,2,5] triazocin-3-yl)benzoic acid (Z)-2-(11-acetyl-11,12-dihydrodibenzo[c,g] [1,2,5] triazocin-3-yl)benzoic acid(benzoic acid N-acetyl diazocine)
bDA(Z)-1-(3-bromodibenzo[c,g] [1,2,5]triazocin-11(12H)-yl) ethan-1-one (Z)-1-(3-bromodibenzo[c,g] [1,2,5]triazocin-11(12H)-yl)ethan-1-one(brominated N-acetyl diazocine)
BP-12,4-dihydroxy-benzophenone 2,4-dihydroxy-benzophenone(benzophenone-1)
bpDA(Z)-1-(3-(2-bromophenyl)dibenzo[c,g] [1,2,5]triazocin-11 (12H)-yl)ethan-1-one (Z)-1-(3-(2-bromophenyl)dibenzo[c,g] [1,2,5] triazocin-11(12H)-yl)ethan-1-one(bromophenyl N-acetyl diazocine)
cnDA(Z)-11-acetyl-11,12-dihydrodibenzo[c,g] [1,2,5]triazocine-3-carbonitrile (Z)-11-acetyl-11,12-dihydrodibenzo[c,g] [1,2,5] triazocine-3-carbonitrile(cyano N-acetyl diazocine)
DA(Z)-11-acetyl-11,12-dihydrodibenzo[c,g] [1,2,5]triazocine (Z)-11-acetyl-11,12-dihydrodibenzo[c,g] [1,2,5] triazocine(N-acetyl diazocine)
Dianiline *N*-(2-aminobenzyl)-*N*-(2-aminophenyl)acetamide
dmpDA(Z)-1-(3-(2,6-dimethylphenyl)dibenzo[c,g] [1,2,5] triazocin-11(12H)-yl)ethan-1-one (Z)-1-(3-(2,6-dimethylphenyl)dibenzo[c,g] [1,2,5] triazocin-11(12H)-yl)ethan-1-one(dimethylphenyl N-acetyl diazocine)
DTT 1,4-Dithiothreitol
fpDA(Z)-1-(3-(4-fluorophenyl)dibenzo[c,g] [1,2,5]triazocin-11 (12H)-yl)ethan-1-one (Z)-1-(3-(4-fluorophenyl)dibenzo[c,g] [1,2,5]triazocin-11(12H)-yl)ethan-1-one(fluorophenyl N-acetyl diazocine)
iDA(Z)-1-(3-iododibenzo[c,g] [1,2,5]triazocin-11(12H)-yl)-ethan-1-one (Z)-1-(3-iododibenzo[c,g] [1,2,5]triazocin-11(12H)-yl)-ethan-1-one(iodinated N-acetyl diazocine)
LH Luteinizing hormone
MTT 3-(4,5-dimethylthiazol-2-yl)-2,5-diphenyltetrazolium bromide
NADPH Nicotinamide adenine dinucleotide phosphate (reduced form)
pDA(Z)-1-(3-phenyldibenzo[c,g] [1,2,5]triazocin-11(12H)-yl) ethan-1-one (Z)-1-(3-phenyldibenzo[c,g] [1,2,5]triazocin-11(12H)-yl)ethan-1-one(phenyl N-acetyl diazocine)
THB Tetrahydrodibenzazocine

enzymes, like 17βHSD3. Thus, circulating androgens, which are taken up by the tumor, are readily transformed into more potent ones and can activate the receptor even stronger [12,13,15]. On top of that, an overexpression of the androgen receptor is not uncommon in prostate carcinomas [16,17].

Whereas in the past it was assumed that high testosterone levels also increase the risk of developing prostate cancer, for instance, because it is very rare in eunuchs and men who have had a testicle removal during adolescence or as young adults [18–20], data now indicate that testosterone only influences the progression and outcome of prostate cancer negatively [21,22]. Nevertheless, men with low levels of free testosterone might have a lower risk of developing prostate cancer [23,24] and newer studies show that the combination of high unbound testosterone with high levels of insulin-like growth factor-I may be a risk factor for the disease [25,26].

Currently, there are different antiandrogenic drugs available and androgen deprivation therapy is an important option in the treatment of (certain types of) prostate carcinoma [27]. As described before, various factors modulate testosterone effectiveness. Consequently, there are also several molecular targets to either lower testosterone levels or its activity. Among them are luteinizing hormone-releasing hormone (LHRH) antagonists and agonists, which both interfere with the LHRH receptor and to this end lead to a decreased testosterone production - the first by blocking the receptor and thereby inhibiting the release of LH; the second by a perpetual overstimulation of the receptor, ultimately resulting in a downregulated receptor expression and thus lower LH availability [28–30]. Inhibitors of 5α-reductase attenuate the transformation of testosterone into 5α-DHT and therefore decrease the androgenic effect. It is also possible to diminish testosterone precursors by inhibition of 17α-hydroxylase, which is expressed in the testes, the adrenal glands and the tumorous prostate tissue [6]. Another target is the androgen receptor [31–33]: Androgen receptor antagonists counteract the effects of testosterone or 5α-DHT by interrupting the receptor-androgen-interaction and therefore suppress the transcriptional cascade, which otherwise would follow receptor activation [6]. Lastly, there is the possibility of surgical castration (orchiectomy), which can drastically reduce testosterone levels, but does not always help, because as mentioned above, the tumor might build its own testosterone ("castration resistant prostate cancer") [17,34].

This work focuses on the inhibition of 17βHSD3 as a point of attack. Albeit some inhibitors already exist [35–39], recent research not only looks for new substances but also searches for compounds with improved properties in terms of stability, susceptibility to resistance or light-switchability [40,41]. In the field of photopharmacology, drugs are activated or inactivated by irradiation with light. This is advantageous because the effect can be limited both temporally and locally. In addition, the intermittence might slow down the "drug" (= the emergence of resistance). In order to be suitable for a photopharmacological approach, the molecules need to have photochromic characteristics [42–44].

Here, we present nitrogen bridged diazocines [45,46], which have been designed based on the structure of the known 17βHSD3 inhibitor tetrahydrodibenzazocine (THB, Fig. 1a) [37]. They differ by the exchange of the $-CH_2CH_2-$ group by an azo group (-N═N-) within the central 8-ring, which accounts for the photoswitchable properties. Diazocine (DA) is thermodynamically stable in its bent *Z*-configuration. Upon irradiation with blue light the stretched *E*-isomer is formed (Fig. 1b), which resembles the almost planar original inhibitor THB. Hence, only the *E*-isomer should exert an inhibitory effect. In our previous studies, we investigated two different diazocines (DA and brominated DA). So far, these diazocines did not show the desired effect: We observed only a slight inhibition, which was independent of the irradiation treatment. Furthermore, the inhibition was partially limited by reduction of the diazocines to their corresponding dianilines when irradiated [40]. The insertion of new substituents to the tricyclic molecule was aimed to augment the inhibitory potency and stability. Thus, seven new light-switchable *N*-acetyl diazocines were synthesized (Fig. 1c) [47] and tested as potential 17βHSD3 inhibitors.

2. Material and methods

2.1. Chemicals

All diazocines (as well as the control substance THB for test validation) were synthesized as previously described [45–48]. Androst-4-ene-3,17-dione (androstenedione), testosterone and 2,

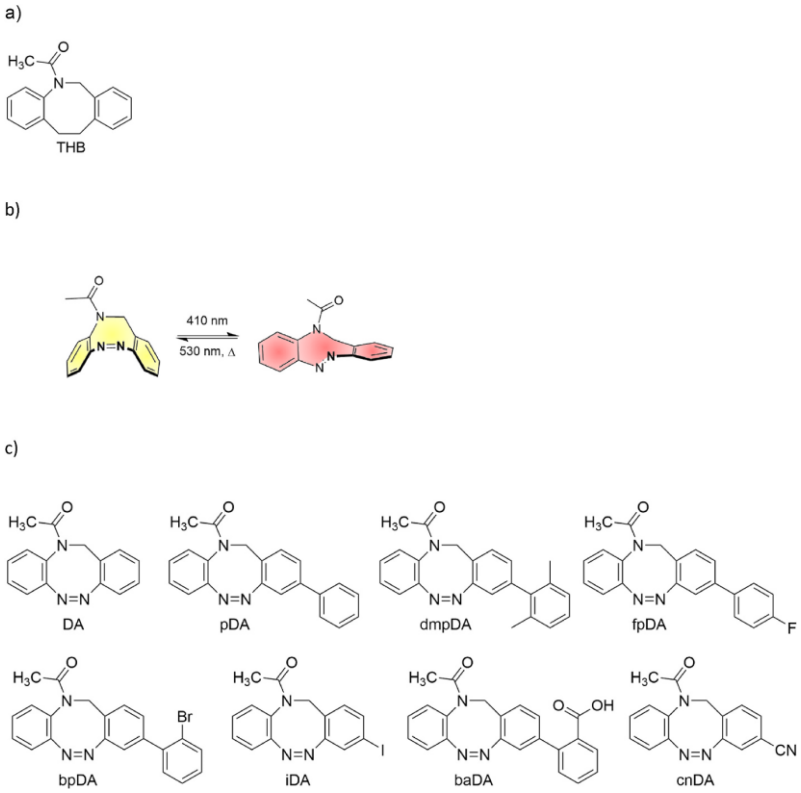

Fig. 1. a) Structure of tetrahydrodibenzazocine (THB). b) Photoswitching of diazocine. The bent *Z*-isomer is thermodynamically stable (resting state). c) Chemical structures of the initial *N*-acetyl diazocine (DA) and the seven new diazocines: phenyl *N*-acetyl diazocine (pDA), dimethylphenyl *N*-acetyl diazocine (dmpDA), fluorophenyl *N*-acetyl diazocine (fpDA), bromophenyl *N*-acetyl diazocine (bpDA), iodinated *N*-acetyl diazocine (iDA), benzoic acid *N*-acetyl diazocine (baDA) and cyano *N*-acetyl diazocine (cnDA).

4-dihydroxy-benzophenone (benzophenone-1, BP-1) were purchased from Sigma-Aldrich, Steinheim, Germany. The plasmid expression vector pcDNA3 with the gene HSD17B3 was generously provided by professor Odermatt and his research group of the Department of Pharmaceutical Sciences, University of Basel, Switzerland [49].

2.2. Cell culture, transfection and microsome isolation

HEK-293 cells (human embryonic kidney cells, CLS, Eppelheim, Germany) were cultured in Dulbecco's Modified Eagle's Medium (DMEM, PAN-Biotech, Aidenbach, Germany) as described before [40]; when a passage number of 25–30 was reached, they were discarded. Prior to each experiment, cells were transfected transiently with the gene sequence of 17βHSD3. For this purpose, cells were detached from 75 cm^2 tissue culture flasks with trypsin and seeded in 3.5 cm dishes (8.55 cm^2) at a cell count of 0.7×10^6 and with a total volume of 2 ml. After 24 h the cells were transfected with 1.2 μg plasmid DNA/dish. For microsome preparation 10.2×10^6 cells were grown in at least eight 175 cm^2 tissue culture flasks and transfected with 25 μg plasmid DNA/flask. Invitrogen's lipofectamine 3000 transfection kit was used for the transfection procedure as described before [40]. The protocol of Legeza et al. (2013) was applied for the microsome isolation [49] and adjusted to the higher cell count. The microsomal protein concentration was determined by Qubit Fluorometer 2.0.

2.3. Test of cytotoxicity

All substances, which were tested as inhibitors, were examined for cytotoxicity using standard MTT assay [50,51] (Fig. S1).

2.4. Plasmid DNA amplification and isolation

The Plasmid DNA was amplified as described before [40]. Afterwards, the DNA concentration was determined using the Qubit Fluorometer 2.0.

2.5. Irradiation

Light-switching by irradiation of the diazocines was done at a wavelength of 400 nm. For this purpose, a custom-built lamp with five LEDs was used at full (100 %) or dimmed (20 %) intensity and placed in a distance of 6 cm to the cell culture dishes or 96-well plate (Fig. S2). All seven diazocines and the two known inhibitors were dissolved in DMSO. To investigate the photoswitched diazocines a stock solution in DMEM (cell assay) or sodium phosphate buffer (microsome assay) was prepared and pre-irradiated for 7 min at full lamp intensity. Samples were treated with the stock solution so that the desired inhibitor concentration was reached (cell assays: 10 μM; microsome assays: 10 and 50 μM); solvent content did not exceed 0.2 % and was constant throughout the whole experiment. Then, the samples were further irradiated at a lower lamp intensity of 20 % during the whole incubation period (3 h). In case of the microsome assays, the lamp intensity was either lowered to 20 % or kept

at 100 % during incubation (5 h/3 h). In both assays non-irradiated and irradiated controls without test compound were run along. For the latter, irradiation was done exactly as for the irradiated samples.

2.6. Inhibition assays with cells

A diazocine concentration of 10 μM was selected for the cell assays, so that a cytotoxic effect could be ruled out (see 2.3 and Fig. S1). 24 h after transfection, the cell inhibition assay was started: the cells in the 3.5 cm dishes were treated either only with 20 μM substrate (controls) or with 20 μM substrate and 10 μM test compound. Samples with pre-irradiated diazocines and some of the controls were irradiated during the 3-h incubation period as described above (section 2.5). An untransfected control was included in each cell experiment to see the transfection success in the transfected controls in comparison and to proof that no other testosterone-synthesizing system was active. As positive control for the inhibition the two known 17βHSD3 inhibitors BP-1 and THB were used.

2.7. Inhibition assays with microsomes

The microsome inhibition assays were performed in two different modes: the first series of experiments was done with a reduced lamp intensity of 20 %, comparable to the cell assays, and an incubation period of 5 h; the second experimental series was done for 3 h at full lamp intensity to see if stronger irradiation leads to greater differences between the non-irradiated and corresponding irradiated diazocine treatment group.

150 μg microsomal protein was used for each sample in the microsome inhibition assays. Since NADPH is the natural cofactor of testosterone-synthesizing 17βHSD3, a NADPH-generating system with the final concentrations of 2 mM $NADP^+$, 7 mM glucose-6-phosphate, 0.002 mg/100 μl glucose-6-phosphate dehydrogenase, 5 mM $MgCl_2$ and 73 mM Na_xPO_4-buffer was used. Each sample was prepared in a 1.5 ml tube containing 10 μl of NADPH-generating system, 2 μl of androstenedione (5 mM in methanol:buffer, 50:50 (v/v)), 50 μl of test compound (20 μM and 100 μM in phosphate buffer) and was filled up at 100 μl with sodium phosphate buffer, pH 7.4, so that androstenedione concentration was 100 μM, final inhibitor concentration was either 10 or 50 μM and DMSO concentration was 0.2 %. For the purpose of irradiation, the samples were pipetted into a 96-well plate, the plate was partly covered with aluminum foil (non-irradiated samples) and the lamp was positioned on top of it (Fig. S2). Incubation was performed in an incubator with 37 °C. As in the cell experiments, the known 17βHSD3 inhibitors BP-1 and THB were used to assess test validity.

2.8. Sample preparation and UHPLC analysis

After incubation the cells and the medium were transferred into a glass tube and extracted three times with 2 ml diethyl ether. The microsome samples were transferred from the 96-well plate into 1.5 ml Eppendorf tubes and extracted twice with 200 μl diethyl ether. All samples were shaken vigorously on a vortex mixer (1 min/30 s) and centrifuged (5 min at 3200 rpm/1 min at 13,000 rpm) to ease phase separation. The upper solvent phases were pooled in new glass tubes. The diethyl ether was evaporated with a gentle flow of nitrogen gas and the dry residue was either stored at −80 °C for later usage or dissolved in 100 μl methanol for direct analysis. The androgens were separated by UHPLC: Samples were filtered (0.22 μm pore size), 2 μl in case of cell assay or 5 μl in case of microsomal assay were injected in the Nexera X2 UHPLC system (Shimadzu, Duisburg, Germany) with a Shim-pack GIST C18 column (2 μm pore size, 15 cm length, Shimadzu) and the measurement was run with conditions as described before [40].

3. Statistical analysis and data evaluation

UHPLC chromatograms were used for the evaluation. To identify a potential inhibitory effect, the peak area (mAU x s) of testosterone was compared between the different treatment groups. The mean testosterone in the control group was set 100 % and the mean testosterone of the given treatment group was calculated in relation to that.

Data are reported as mean ± standard deviation (SD) from $n \geq 4$ biological replicates of two independent cell experiments and $n \geq 3$ biological replicates in case of microsome assays. Differences among means were determined using Kruskal-Wallis one way ANOVA for non-parametric data.

The mean rank of the irradiated sample groups was compared with the mean rank of the irradiated control group; non-irradiated samples were compared to the non-irradiated control group. Additionally, for each test compound, a comparison of the mean rank with and without irradiation was performed to see if there were differences in the inhibitory potency due to photoswitching. All data were analyzed using GraphPad Prism 9.4.1 (GraphPad Software, San Diego, CA, USA). Group differences were considered statistically significant if $p \leq 0.05$.

4. Results

4.1. Inhibition of 17βHSD3 in cells

During the 3-h incubation testosterone was readily formed both in non-irradiated and irradiated controls as shown by the detected testosterone peak (Fig. S3). Testosterone production did not vary between non-irradiated (mean peak area 1,083,258 mAU x s ± 171,288 mAU x s) and irradiated controls (mean peak area 1,093,875 mAU x s ± 153,256 mAU x s) (Fig. S4).

Fig. 2 shows the results of the 3-h cell assay with 20 μM androstenedione and 10 μM test compound. Four of the seven new diazocines (pDA, dmpDA, fpDA, bpDA) led to a significant inhibition of testosterone formation compared to either non-irradiated or irradiated control. The strongest inhibition by 83.9 % ± 5.4 % (without irradiation) and 85.5 % ± 4.2 % (with irradiation) was observed in samples treated with the dimethylphenyl substituted diazocine (dmpDA). Nevertheless, no significant difference was found in either of the non-irradiated diazocines when compared to their corresponding irradiated group. Samples treated with the known inhibitors BP-1 and THB showed a highly significant decrease of built testosterone by 91.6 % ± 3.6 % and 75.1 % ± 6.7 %, respectively, compared to the control (Fig. 2).

4.2. Inhibition of 17βHSD3 in microsomes

Similar to the cell assays, in the microsome assays the enzyme activity in the controls was satisfactory as testosterone was readily formed from its precursor androstenedione (Fig. S5). The testosterone production in the non-irradiated and irradiated control did not differ significantly (5 h incubation without irradiation: mean peak area 611,508 mAU x s ± 106,701 mAU x s and with 20 % lamp intensity: 622,679 mAU x s ± 89,541 mAU x s; 3 h incubation without irradiation: mean peak area 703,067 mAU x s ± 301,962 mAU x s and with 100 % lamp intensity 583,946 mAU x s ± 202,926 mAU x s), though the mean value was slightly smaller in the irradiated control when light exposure was done at full lamp intensity.

Figs. 3 and 4 show the results of the two different experimental series with microsomes (5 h incubation and 20 % lamp intensity vs. 3 h incubation and 100 % lamp intensity) isolated from 17βHSD3-transfected HEK-293 cells and treated with potential inhibitors in two different concentrations (10 and 50 μM).

In both series four of the seven new diazocines (dmpDA, fpDA, bpDA, iDA) resulted in a significant lower testosterone production compared to the corresponding control. In contrast to the cell assays, pDA did not lead to a significant testosterone decrease, but in the higher

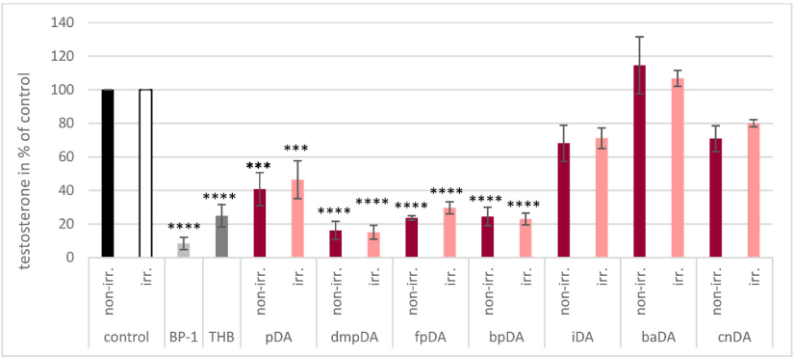

Fig. 2. Produced testosterone in 17βHSD3-transfected HEK-293 cells after 3-h incubation with 20 μM androstenedione without (=controls) and with 10 μM known (BP-1, THB) or potential (pDA, dmpDA, fpDA, bpDA, iDA, baDA, cnDA) inhibitor. Lighter bars indicate irradiation at a lamp intensity of 20 % during the whole incubation and for 7 min at full (100 %) lamp intensity prior to incubation (=irr.). Darker bars indicate no sample irradiation (=non-irr.). Data are expressed as percentage of determined testosterone compared to the control. Values are given as means ± SD of n ≥ 4 biological replicates. Significance levels are set as follows: *p ≤ 0.05; **p ≤ 0.01; ***p ≤ 0.001; ****p ≤ 0.0001.

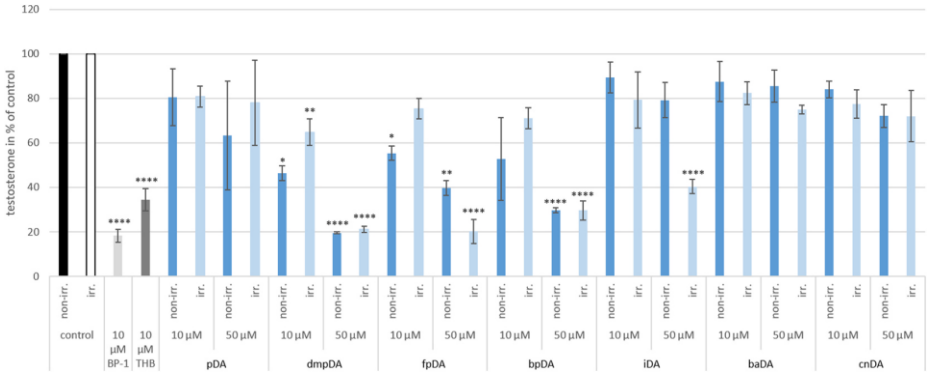

Fig. 3. Produced testosterone in microsomes from 17βHSD3-transfected HEK-293 cells after 5-h incubation with 100 μM androstenedione (=control) or 100 μM androstenedione plus 10 or 50 μM, respectively, (potential) inhibitors, without irradiation (=non-irr.) or with irradiation (diazocine stock solution for 7 min at 100 % lamp intensity and further irradiation of samples and control at 20 % lamp intensity during 5-h incubation = irradiated). Data are expressed as testosterone in percent of control, in case of irradiated samples in percent of irradiated control. Values are given as means ± SD of n ≥ 3 biological replicates. Significance levels were set as follows: *p ≤ 0.05; **p ≤ 0.01; ***p ≤ 0.001; ****p ≤ 0.0001.

concentration iDA did: in the 5-h assay the testosterone decline compared to the control was only significant in the irradiated iDA group (40,3 % ± 3.2 % of control; Fig. 3); there was no statistical significance when 50 μM non-irradiated iDA was compared to the associated non-irradiated control group (79.3 % ± 7.8 % of control). In the 3-h assay significant lower testosterone levels were found in both the irradiated and non-irradiated iDA group at 50 μM (39.8 % ± 4.6 % and 30.8 % ± 4.5 % of control; Fig. 4).

Generally, in the microsome assays the inhibitory effect of the same diazocines in the same concentration (10 μM) was not as strong as in the cell assays (Figs. 2–4). Higher concentrations of the test compounds (50 μM) were needed in the microsome assays to accomplish comparable inhibition.

Higher lamp intensity throughout the incubation (Fig. 4) did not result in a better inhibition nor a significant difference between the irradiated and non-irradiated form.

10 μM of BP-1 and THB lowered testosterone in the microsome assays significantly (BP-1: 18.2 % ± 3.0 % of control (5 h, 20 %) and 25.9 % ± 3.8 % of control (3 h, 100 %); THB: 34.5 % ± 5.0 % of control (5 h, 20 %) and 32.2 % ± 10.4 % of control (3 h, 100 %)), but not as strong as in the cell assays (BP-1: 8.4 % ± 3.6 % of control; THB: 24.9 ± 6.7 % of control).

5. Discussion

Huggins and Hodges (1941) [20,52] were the first who saw an association between androgen levels and prostate carcinoma. Since then, considerable research in this field was done and androgen deprivation therapy became an essential part in the treatment of prostate cancer [27, 53].

The goal of the present research was to find light-activatable 17βHSD3 inhibitors to lower endogenous testosterone synthesis and thereby disrupt the self-reinforcing loop of prostate cancer proliferation. Unfortunately, the goal was not fully achieved: Some of the new diazocines led to a significant decrease in testosterone, but there was no significant difference in terms of the inhibitory potency with or without irradiation. One of the reasons for this finding could be that some of the diazocines appear to decompose to some extend when treated with light. This is indicated by an additional substance peak seen in the chromatograms of the irradiated samples and a smaller original substance peak compared to the non-irradiated sample (Fig. S6.1 and S6.2).

These results are consistent with those from our previous research with two other diazocines [40], where it was shown that it is most likely that the diazocines become susceptible to reduction after irradiation, thus in the *E* configuration. Reducing substances or enzymes in the

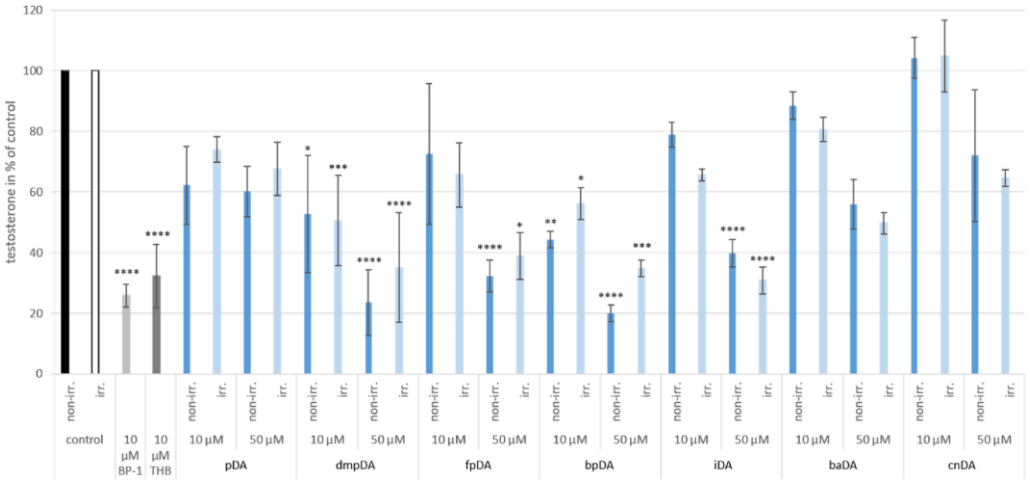

Fig. 4. Produced testosterone in microsomes from 17βHSD3-transfected HEK-293 cells after 3-h incubation with 100 µM androstenedione (=control) or 100 µM androstenedione plus 10 or 50 µM, respectively, (potential) inhibitors, without irradiation (=non-irr.) or with irradiation (diazocine stock solution for 7 min at 100 % lamp intensity and further irradiation of samples and control at 100 % lamp intensity during 24-h incubation = irradiated). Data are expressed as testosterone in percent of control, in case of irradiated samples in percent of irradiated control. Values are given as means ± SD of n ≥ 3 biological replicates. Significance levels were set as follows: *p ≤ 0.05; **p ≤ 0.01; ***p ≤ 0.001; ****p ≤ 0.0001.

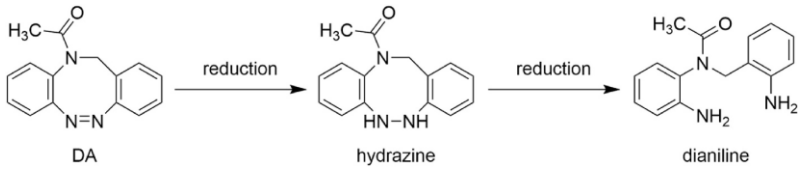

Fig. 5. Scheme of possible diazocine breakdown by azo-bridge reduction to the corresponding hydrazine or dianiline.

microsomal and cell environment appear to catalyze an azo-bridge reduction, possibly followed by a ring opening of the diazocines at the central 8-ring, resulting in the formation of the corresponding hydrazines or dianilines (Fig. 5). Mass spectrometry could help to identify the newly emerging substances as it was done before for DA and bDA [40].

Similar observations were formerly made in studies with photoswitchable diarylazo compounds as potential protein kinase inhibitors: Here, irreversible reduction of the diarylazo unit to the corresponding hydrazine by typical reducing agents like dithiothreitol (DTT) and glutathione was observed which made the photoswitching of the biological activity impossible [54]. Kolarski et al. (2021) [41] also report the problem of instability and consequent lack of activity of light-switchable azo compounds due to reduction.

Despite their relatively bulky spatial shape, some of the diazocines studied are also biologically active in the Z configuration. This was surprising, because the Z-isomers are quite bent and should not fit easily into the active site of the 17βHSD3. Alternatively, the products of diazocine decomposition (reduction), e. g. the corresponding hydrazine (Fig. 5), could be biochemically active. The hydrazine is structurally even more similar to the lead compound THB than the diazocines. Here, compared to THB, the CH_2CH_2-group is replaced by NH–NH. This means that the hydrazine is just as conformationally flexible as THB and can thus adapt to the active site in the enzyme. Hydrazines do not switch, which would explain why we do not see any change in activity upon irradiation. Nevertheless, the reductive destruction of the diazocines probably affected the inhibition only marginally, because there still was a bigger part of the intact test compound as indicated by the large substance peak with the same retention time as the associated standard (Fig. S6.1 and S6.2).

Despite the lacking change of activity with and without light exposure, some of the modified diazocines decreased testosterone production much stronger than the initial diazocines DA and bDA. This effect is most likely caused by an inhibition of 17βHSD3 activity, because no cytotoxic effect was observed at the concentration used and no other testosterone-synthesizing system was enabled in the HEK-293 cells or microsome assays as proofed by an untransfected control (Fig. S3) or a microsome-free control (Fig. S5). Although photoswitchability did not play a major role here, the finding of new diazocine structures as potential inhibitors of 17βHSD3 activity is promising, since it is always favorable to have a range of drugs with different modes of action available in order to prevent the development of cancer treatment resistance [17,55].

The cell assays allow to study the enzymatic activity and the identification of activity modulators within the enzyme's natural milieu, which is of course advantageous and might deliver more transferable data than the microsome assays with regard to a whole organism. On the other hand, there should be fewer interfering factors in the microsomes than in cells, so theoretically a potential inhibition might in this case be determined more easily. However, our present study shows a different outcome: The inhibition of the diazocines was weaker in the microsome assays than in the cell assays and these results matched the ones of the known 17βHSD3 inhibitors BP-1 and THB.

One reason could be that in the vesicle-like microsomes the potential inhibitors were not able to reach the enzyme or its active site. However, Legeza et al. (2013) state that the method used for the isolation of the subcellular fractions generates to a vast majority inside-out microsomal vesicles, in which the enzyme-containing cytoplasmic side is exposed to the outside [49]. Hence, it should be possible for the test compound to access the enzyme.

In the last step of the preparation of the microsomes a solution containing 0.5 mM DTT was used to resuspend the microsomal pellet, which possibly could have reduced the diazocines partially, but does not explain the weaker inhibition, knowing that there are also intracellular reducing agents, like glutathione [56,57]. Furthermore, the reducing agents of the cytosol should be present in notably lower concentrations in the microsomal fraction.

The results of the microsome assays seemed to have a high variation, which might be explained by the resuspension step possibly leading to an inhomogeneous microsomal suspension, which could cause difficulties when working with the fractions. It has also been shown in other studies that the activity of commercially purchased microsomes can vary significantly [58,59]. The transient transfection of the cells prior to each microsome preparation may also have led to a higher variability in the microsomal activity due to differences in the transfection yield.

In both assay types, four of the studied diazocines led to a significant inhibition of 17βHSD3 activity, however, one of the four differed: in the cell assays pDA, dmpDA, fpDA and bpDA inhibited significantly, whereas in the microsome assays iDA, dmpDA, fpDA and bpDA did.

Our results show that the known inhibitor THB, on which the diazocines are based, does lead to a weaker inhibition than the known inhibitor BP-1. On the other hand, some of the new diazocines resulted in a better inhibition compared to the model molecule THB, regardless of whether they were irradiated or non-irradiated.

A possible explanation for the failure of our photoswitchability approach could be that the half-life of the *E*-isomers is not sufficient to have a stronger effect, i. e. that the *E*-isomers thermally react back to the Z-isomers too quickly. However, this is unlikely, because measurements of the diazocines in aqueous solution showed a prolonged half-life compared to the results of the same measurements in organic solvents (Tab. S7 and Fig. S8 - S15.2) [45,47,60]. Another reason could be variations in the switching efficiency, yet this was not possible to investigate due to poor solubility and thus insufficient substance concentration for NMR spectroscopy to determine the photostationary states. Nevertheless, previous studies of the initial DA in aqueous media showed satisfactory photoconversion yields [60]. On the other hand, the irradiation in the cell experiments has not been carried out at full lamp intensity, as this would have had a negative effect on cell viability.

In any case, we have identified new 17βHSD3 inhibitors by the modification of the original DA. Now, further research in this field should focus on a light switch which activates or inactivates the molecule in terms of the inhibition, so that it would be possible to control the location and duration of the effect. For the future development of new light-switchable molecules a strong inhibitor should be used as starting point.

Credit authorship statement

Wages F.: Data curation, Investigation, Methodology, Writing – original draft. Brandt T.: Data curation, Formal analysis, Methodology, Visualization. Matin H.-J.: Methodology, Writing - review & editing. Herges R.: Conceptualization, Investigation, Resources, Validation, Writing – review & editing. Maser E.: Conceptualization, Funding acquisition, Investigation, Project administration, Resources, Writing – review & editing.

Declaration of competing interest

The authors declare that they have no known competing financial interests or personal relationships that could have appeared to influence the work reported in this paper.

Data availability

Data will be made available on request.

Acknowledgement

We thank Prof. Alex Odermatt for providing the plasmid expression vector pcDNA3 and Dr. Claus Bier for providing the lamp for the irradiation assays.

Appendix A. Supplementary data

Supplementary data to this article can be found online at https://doi.org/10.1016/j.cbi.2024.110872.

References

[1] F. Bray, M. Laversanne, E. Weiderpass, I. Soerjomataram, The ever-increasing importance of cancer as a leading cause of premature death worldwide, Cancer 127 (2021) 3029–3030, https://doi.org/10.1002/cncr.33587.
[2] H. Sung, J. Ferlay, R.L. Siegel, M. Laversanne, I. Soerjomataram, A. Jemal, F. Bray, Global cancer statistics 2020: GLOBOCAN Estimates of incidence and mortality worldwide for 36 cancers in 185 countries, CA, Cancer J. Clin. 71 (2021) 209–249, https://doi.org/10.3322/caac.21660.
[3] R.L. Siegel, K.D. Miller, N.S. Wagle, A. Jemal, Cancer statistics, 2023, CA, Cancer J. Clin. 73 (2023) 17–48, https://doi.org/10.3322/caac.21763.
[4] L. Wang, B. Lu, M. He, Y. Wang, Z. Wang, L. Du, Prostate cancer incidence and mortality: global status and temporal trends in 89 countries from 2000 to 2019, Front. Public Health 10 (2022) 811044, https://doi.org/10.3389/fpubh.2022.811044.
[5] D.M. Kelly, T.H. Jones, Testosterone: a metabolic hormone in health and disease, J. Endocrinol. 217 (2013), https://doi.org/10.1530/JOE-12-0455. R25–R45.
[6] E. Mutschler, G. Geisslinger, H.K. Kroemer, S. Menzel, P. Ruth, Mutschler Arzneimittelwirkungen: Lehrbuch der Pharmakologie, der klinischen Pharmakologie und Toxikologie: mit einführenden Kapiteln in die Anatomie, Physiologie und Pathophysiologie, 10., vollständig überarbeitete und erweiterte Auflage, WVG, Wissenschaftliche Verlagsgesellschaft, Stuttgart, 2013.
[7] M. Sheffield-Moore, Androgens and the control of skeletal muscle protein synthesis, Ann. Med. 32 (2000) 181–186, https://doi.org/10.3109/07853890008998825.
[8] A.H. Payne, D.B. Hales, Overview of steroidogenic enzymes in the pathway from cholesterol to active steroid hormones, Endocr. Rev. 25 (2004) 947–970, https://doi.org/10.1210/er.2003-0030.
[9] W. Arlt, P.M. Stewart, Adrenal corticosteroid biosynthesis, metabolism, and action, Endocrinol Metab. Clin. N. Am. 34 (2005) 293–313, https://doi.org/10.1016/j.ecl.2005.01.002.
[10] A.H. Payne, G.L. Youngblood, Regulation of expression of steroidogenic enzymes in Leydig Cells 1, Biol. Reprod. 52 (1995) 217–225, https://doi.org/10.1095/biolreprod52.2.217.
[11] H.V. Stroomberg, A. Jørgensen, K. Brasso, J.E. Nielsen, A. Juul, H. Frederiksen, M. Blomberg Jensen, M.A. Røder, Novel functions of the luteinizing hormone/chorionic gonadotropin receptor in prostate cancer cells and patients, PLoS One 15 (2020) e0238814, https://doi.org/10.1371/journal.pone.0238814.
[12] P.R. Dillard, M.-F. Lin, S.A. Khan, Androgen-independent prostate cancer cells acquire the complete steroidogenic potential of synthesizing testosterone from cholesterol, Mol. Cell. Endocrinol. 295 (2008) 115–120, https://doi.org/10.1016/j.mce.2008.08.013.
[13] M. Barnard, E.A. Mostaghel, R.J. Auchus, K.-H. Storbeck, The role of adrenal derived androgens in castration resistant prostate cancer, J. Steroid Biochem. Mol. Biol. 197 (2020) 105506, https://doi.org/10.1016/j.jsbmb.2019.105506.
[14] K. Fujita, N. Nonomura, Role of androgen receptor in prostate cancer: a review, World J. Mens Health 37 (2019) 288, https://doi.org/10.5534/wjmh.180040.
[15] E. Koh, T. Noda, J. Kanaya, M. Namiki, Differential expression of 17?-hydroxysteroid dehydrogenase isozyme genes in prostate cancer and noncancer tissues, Prostate 53 (2002) 154–159, https://doi.org/10.1002/pros.10139.
[16] T. Visakorpi, E. Hyytinen, P. Koivisto, M. Tanner, R. Keinänen, C. Palmberg, A. Palotie, T. Tammela, J. Isola, O.-P. Kallioniemi, In vivo amplification of the androgen receptor gene and progression of human prostate cancer, Nat. Genet. 9 (1995) 401–406, https://doi.org/10.1038/ng0495-401.
[17] T. Chandrasekar, J.C. Yang, A.C. Gao, C.P. Evans, Mechanisms of resistance in castration-resistant prostate cancer (CRPC), Transl. Androl. Urol. 4 (2015) 365–380, https://doi.org/10.3978/j.issn.2223-4683.2015.05.02.
[18] J.J. Stocking, M.V. Fiandalo, E.A. Pop, J.H. Wilton, G. Azabdaftari, J.L. Mohler, Characterization of prostate cancer in a functional eunuch, J. Natl. Compr. Cancer Netw. 14 (2016) 1054–1060, https://doi.org/10.6004/jnccn.2016.0116.
[19] S. Slater, R.T.D. Oliver, Testosterone: its role in development of prostate cancer and potential risk from use as hormone replacement therapy, Drugs Aging 17 (2000) 431–439, https://doi.org/10.2165/00002512-200017060-00001.
[20] C. Huggins, C.V. Hodges, Studies on prostatic cancer: I. The effect of castration, of estrogen and of androgen injection on serum phosphatases in metastatic carcinoma of the prostate, J. Urol. 168 (2002) 9–12, https://doi.org/10.1016/S0022-5347(05)64820-3.
[21] A. Yassin, K. AlRumaihi, R. Alzubaidi, S. Alkadhi, A. Al Ansari, Testosterone, testosterone therapy and prostate cancer, Aging Male 22 (2019) 219–227, https://doi.org/10.1080/13685538.2018.1524456.

[22] C.C. Schulman, J. Irani, J. Morote, J.A. Schalken, F. Montorsi, P.L. Chlosta, A. Heidenreich, Testosterone measurement in patients with prostate cancer, Eur. Urol. 58 (2010) 65–74, https://doi.org/10.1016/j.eururo.2010.04.001.
[23] E.L. Watts, R. Goldacre, T.J. Key, N.E. Allen, R.C. Travis, A. Perez-Cornago, Hormone-related diseases and prostate cancer: an English national record linkage study, Int. J. Cancer 147 (2020) 803–810, https://doi.org/10.1002/ijc.32808.
[24] E.L. Watts, P.N. Appleby, A. Perez-Cornago, H.B. Bueno-de-Mesquita, J.M. Chan, C. Chen, B.A. Cohn, M.B. Cook, L. Flicker, N.D. Freedman, G.G. Giles, E. Giovannucci, R.E. Gislefoss, G.J. Hankey, R. Kaaks, P. Knekt, L.N. Kolonel, T. Kubo, L. Le Marchand, R.N. Luben, T. Luostarinen, S. Männistö, E.J. Metter, K. Mikami, R.L. Milne, K. Ozasa, E.A. Platz, J.R. Quirós, H. Rissanen, N. Sawada, M. Stampfer, F.Z. Stanczyk, P. Stattin, A. Tamakoshi, C.M. Tangen, I.M. Thompson, K.K. Tsilidis, S. Tsugane, G. Ursin, L. Vatten, N.S. Weiss, B.B. Yeap, N.E. Allen, T. J. Key, R.C. Travis, Low free testosterone and prostate cancer risk: a collaborative analysis of 20 prospective studies, Eur. Urol. 74 (2018) 585–594, https://doi.org/10.1016/j.eururo.2018.07.024.
[25] E.L. Watts, G.K. Fensom, K. Smith Byrne, A. Perez-Cornago, N.E. Allen, A. Knuppel, M.J. Gunter, M.V. Holmes, R.M. Martin, N. Murphy, K.K. Tsilidis, B.B. Yeap, T. J. Key, R.C. Travis, Circulating insulin-like growth factor-I, total and free testosterone concentrations and prostate cancer risk in 200 000 men in UK Biobank, Int. J. Cancer 148 (2021) 2274–2288, https://doi.org/10.1002/ijc.33416.
[26] C. Mantzoros, A. Tzonou, L. Signorello, M. Stampfer, D. Trichopoulos, H.-O. Adami, Insulin-like growth factor 1 in relation to prostate cancer and benign prostatic hyperplasia, Br. J. Cancer 76 (1997) 1115–1118, https://doi.org/10.1038/bjc.1997.520.
[27] K. Desai, J.M. McManus, N. Sharifi, Hormonal therapy for prostate cancer, Endocr. Rev. 42 (2021) 354–373, https://doi.org/10.1210/endrev/bnab002.
[28] H.J. Stricker, Luteinizing hormone–releasing hormone antagonists in prostate cancer, Urology 58 (2001) 24–27, https://doi.org/10.1016/S0090-4295(01)01238-9.
[29] Y. Tolkach, S. Joniau, H. Van Poppel, Luteinizing hormone-releasing hormone (LHRH) receptor agonists vs antagonists: a matter of the receptors?: LHCRH-R agonists vs antagonists, BJU Int. 111 (2013) 1021–1030, https://doi.org/10.1111/j.1464-410X.2013.11796.x.
[30] A.V. Schally, Luteinizing hormone-releasing hormone analogs: their impact on the control of tumorigenesis☆, Peptides 20 (1999) 1247–1262, https://doi.org/10.1016/S0196-9781(99)00130-8.
[31] C. Helsen, T. Van Den Broeck, A. Voet, S. Prekovic, H. Van Poppel, S. Joniau, F. Claessens, Androgen receptor antagonists for prostate cancer therapy, Endocr. Relat. Cancer 21 (2014) T105–T118, https://doi.org/10.1530/ERC-13-0545.
[32] S. Singh, S. Gauthier, F. Labrie, Androgen receptor antagonists (antiandrogens) structure-activity relationships, Curr. Med. Chem. 7 (2000) 211–247, https://doi.org/10.2174/0929867003375371.
[33] M.E. Tan, J. Li, H.E. Xu, K. Melcher, E. Yong, Androgen receptor: structure, role in prostate cancer and drug discovery, Acta Pharmacol. Sin. 36 (2015) 3–23, https://doi.org/10.1038/aps.2014.18.
[34] E. Mostaghel A, Steroid hormone synthetic pathways in prostate cancer, Transl. Androl. Urol. 2 (2013) 212–227, https://doi.org/10.3978/j.issn.2223-4683.2013.09.16.
[35] D. Poirier, 17β-Hydroxysteroid dehydrogenase inhibitors: a patent review, Expert Opin. Ther. Pat. 20 (2010) 1123–1145, https://doi.org/10.1517/13543776.2010.505604.
[36] D. Poirier, Inhibitors of 17β-hydroxysteroid dehydrogenases, Curr. Med. Chem. 10 (2003) 453–477, https://doi.org/10.2174/0929867033368222.
[37] B.E. Fink, A.V. Gavai, J.S. Tokarski, B. Goyal, R. Misra, H.-Y. Xiao, S.D. Kimball, W.-C. Han, D. Norris, T.E. Spires, D. You, M.M. Gottardis, M.V. Lorenzi, G.D. Vite, Identification of a novel series of tetrahydrodibenzazocines as inhibitors of 17β-hydroxysteroid dehydrogenase type 3, Bioorg, Med. Chem. Lett. 16 (2006) 1532–1536, https://doi.org/10.1016/j.bmcl.2005.12.039.
[38] T.E. Spires, B.E. Fink, E.K. Kick, D. You, C.A. Rizzo, I. Takenaka, R.M. Lawrence, Z. Ruan, M.E. Salvati, G.D. Vite, R. Weinmann, R.M. Attar, M.M. Gottardis, M. V. Lorenzi, Identification of novel functional inhibitors of 17β-hydroxysteroid dehydrogenase type III (17β-HSD3), Prostate 65 (2005) 159–170, https://doi.org/10.1002/pros.20279.
[39] L.G. Nashev, D. Schuster, C. Laggner, S. Sodha, T. Langer, G. Wolber, A. Odermatt, The UV-filter benzophenone-1 inhibits 17β-hydroxysteroid dehydrogenase type 3: virtual screening as a strategy to identify potential endocrine disrupting chemicals, Biochem. Pharmacol. 79 (2010) 1189–1199, https://doi.org/10.1016/j.bcp.2009.12.005.
[40] F. Wages, P. Lentes, T. Griebenow, R. Herges, C. Peifer, E. Maser, Reduction of photoswitched, nitrogen bridged N-acetyl diazocines limits inhibition of 17βHSD3 activity in transfected human embryonic kidney 293 cells, Chem. Biol. Interact. 354 (2022) 109822, https://doi.org/10.1016/j.cbi.2022.109822.
[41] D. Kolarski, A. Sugiyama, T. Rodat, A. Schulte, C. Peifer, K. Itami, T. Hirota, B. L. Feringa, W. Szymanski, Reductive stability evaluation of 6-azopurine photoswitches for the regulation of CKIα activity and circadian rhythms, Org. Biomol. Chem. 19 (2021) 2312–2321, https://doi.org/10.1039/D1OB00014D.
[42] W.A. Velema, W. Szymanski, B.L. Feringa, Photopharmacology: beyond proof of principle, J. Am. Chem. Soc. 136 (2014) 2178–2191, https://doi.org/10.1021/ja413063e.
[43] M.W.H. Hoorens, W. Szymanski, Reversible, spatial and temporal control over protein activity using light, Trends Biochem. Sci. 43 (2018) 567–575, https://doi.org/10.1016/j.tibs.2018.05.004.
[44] J. Broichhagen, J.A. Frank, D. Trauner, A roadmap to success in photopharmacology, Acc. Chem. Res. 48 (2015) 1947–1960, https://doi.org/10.1021/acs.accounts.5b00129.
[45] P. Lentes, E. Stadler, F. Röhricht, A. Brahms, J. Gröbner, F.D. Sönnichsen, G. Gescheidt, R. Herges, Nitrogen bridged diazocines: photochromes switching within the near-infrared region with high quantum yields in organic solvents and in water, J. Am. Chem. Soc. 141 (2019) 13592–13600, https://doi.org/10.1021/jacs.9b06104.
[46] P. Lentes, J. Rudtke, T. Griebenow, R. Herges, Substituted nitrogen-bridged diazocines, Beilstein J. Org. Chem. 17 (2021) 1503–1508, https://doi.org/10.3762/bjoc.17.107.
[47] T. Brandt, P. Lentes, J. Rudtke, M. Hösgen, C. Näther, R. Herges, N-acetyl Diazocines via Cross-Coupling, Draft Unpubl. (n.d.)..
[48] W. Moormann, D. Langbehn, R. Herges, Solvent-free synthesis of diazocine, Synthesis 49 (2017) 3471–3475, https://doi.org/10.1055/s-0036-1590685.
[49] B. Legeza, Z. Balázs, L.G. Nashev, A. Odermatt, The microsomal enzyme 17β-hydroxysteroid dehydrogenase 3 faces the cytoplasm and uses NADPH generated by glucose-6-phosphate dehydrogenase, Endocrinology 154 (2013) 205–213, https://doi.org/10.1210/en.2012-1778.
[50] T. Mosmann, Rapid colorimetric assay for cellular growth and survival: application to proliferation and cytotoxicity assays, J. Immunol. Methods 65 (1983) 55–63, https://doi.org/10.1016/0022-1759(83)90303-4.
[51] P.W. Sylvester, Optimization of the tetrazolium dye (MTT) colorimetric assay for cellular growth and viability, in: S.D. Satyanarayanajois (Ed.), Drug Des. Discov., Humana Press, Totowa, NJ, 2011, pp. 157–168, https://doi.org/10.1007/978-1-61779-012-6_9.
[52] C. Huggins, C.V. Hodges, Studies on Prostatic Cancer: I. The effect of castration, of estrogen, and of androgen injection on serum phosphatases in metastatic carcinoma of the prostate, Cancer Res. (1941) 293–297.
[53] M.B. Garnick, Hormonal therapy in the management of prostate cancer: from Huggins to the present, Urology 49 (1997) 5–15, https://doi.org/10.1016/S0090-4295(97)00163-5.
[54] M. Schehr, C. Lanes, J. Weisner, L. Heintze, M.P. Müller, C. Pichlo, J. Charl, E. Brunstein, J. Ewert, M. Lehr, U. Baumann, D. Rauh, U. Knippschild, C. Peifer, R. Herges, 2-Azo-, 2-diazocine-thiazols and 2-azo-imidazoles as photoswitchable kinase inhibitors: limitations and pitfalls of the photoswitchable inhibitor approach, Photochem. Photobiol. Sci. 18 (2019) 1398–1407, https://doi.org/10.1039/c9pp00010k.
[55] K.M. Wadosky, S. Koochekpour, Molecular mechanisms underlying resistance to androgen deprivation therapy in prostate cancer, Oncotarget 7 (2016) 64447–64470, https://doi.org/10.18632/oncotarget.10901.
[56] J.L. Gilge, M. Fisher, Y.-C. Chai, The effect of oxidant and the non-oxidant alteration of cellular thiol concentration on the formation of protein mixed-disulfides in HEK 293 cells, PLoS One 3 (2008) e4015, https://doi.org/10.1371/journal.pone.0004015.
[57] F.G. Hopkins, On an autoxidisable constituent of the cell, Biochem. J. 15 (1921) 286–305, https://doi.org/10.1042/bj0150286.
[58] L. Di, E.H. Kerns, Y. Hong, T.A. Kleintop, O.J. Mc Connell, D.M. Huryn, Optimization of a higher throughput microsomal stability screening assay for profiling drug discovery candidates, SLAS Discov 8 (2003) 453–462, https://doi.org/10.1177/1087057103255988.
[59] L. Jia, X. Liu, The conduct of drug metabolism studies considered good practice (II): in vitro experiments, Curr. Drug Metabol. 8 (2007) 822–829, https://doi.org/10.2174/138920007782798207.
[60] P. Lentes, P. Frühwirt, H. Freißmuth, W. Moormann, F. Kruse, G. Gescheidt, R. Herges, Photoswitching of diazocines in aqueous media, J. Org. Chem. 86 (2021) 4355–4360, https://doi.org/10.1021/acs.joc.1c00065.

4.7 Simplification of *N*-Acetyl Diazocine Synthesis

4.7.1 Initial Synthesis Path

The *N*-Ac diazocines synthesized within this and previous work could only be obtained via a long synthesis route containing at least seven reaction steps, which is based on an orthogonal protecting group strategy including Fmoc- and Boc-protecting groups (**scheme 4.2**).[64,120,183] Boc-protection of aniline is required for selective monosubstitution of dianiline building block with *o*-nitrobenzylbromide derivatives and selective introduction of Fmoc-protecting group at the bridging nitrogen atom. The Fmoc-protecting group is necessary to prevent side reaction during the oxidative ring closing azo condensation in particular to avoid oxidation to the *N*-oxide by *m*CPBA. This strategy has proven to deliver sufficient total yields between 15% and 20% for unsubstituted and monohalogenated *N*-Ac diazocines.[64,120] The introduction of Fmoc-protecting group turned out to be the crucial step, as the yields were lower than in the other reaction steps and the purification proved to be very complex and time-consuming due to the formation of many by-products. Variation of reaction time and temperature did not bring any improvement.[175]

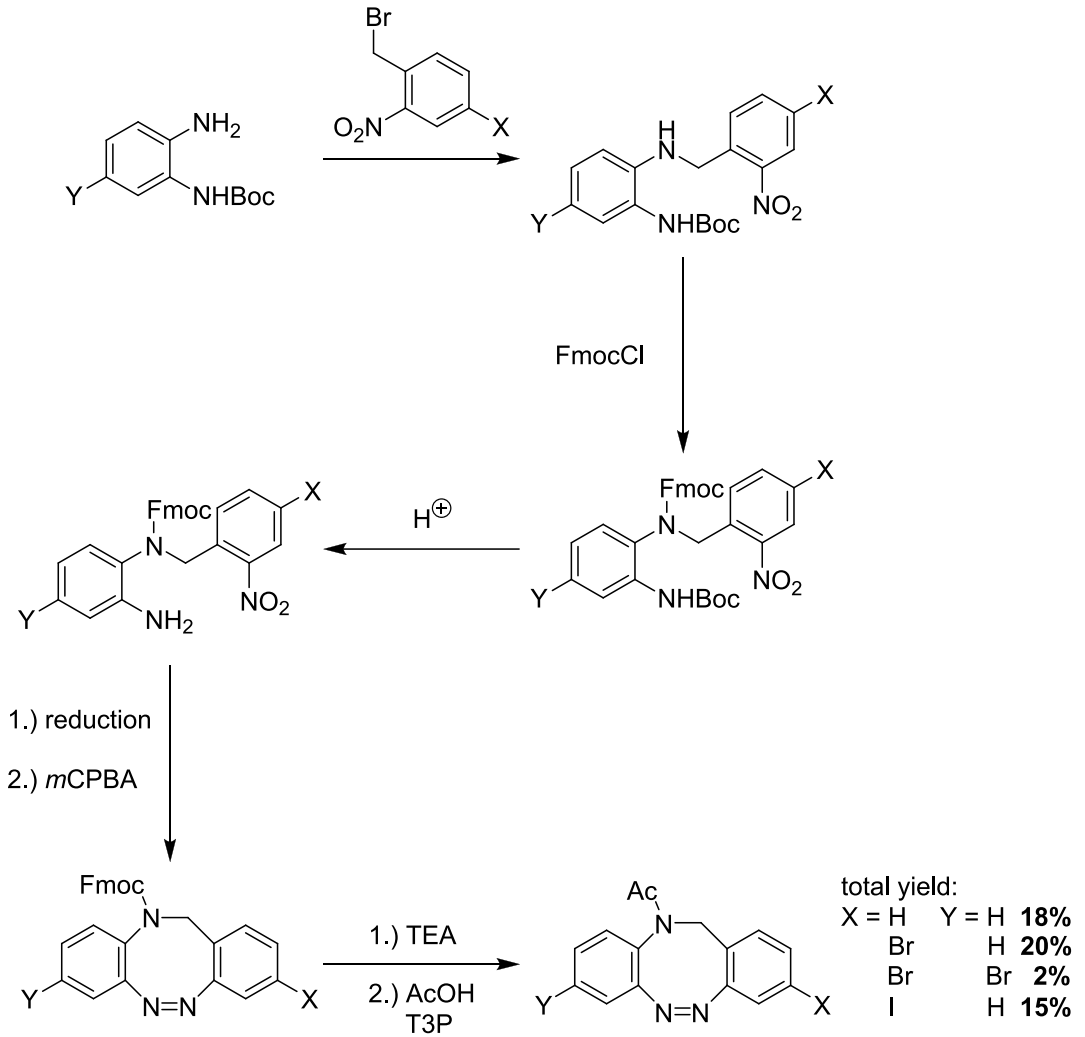

Scheme 4.2: Schematic view of the initial *N*-Ac diazocine synthesis path by LENTES *et al*.[64,120,183] starting from Boc-protected dianiline. After nucleophilic substitution with *o*-nitrobenzylbromide the bridging nitrogen is protected by introduction of Fmoc-protecting group. After acidic cleaving of the Boc-protecting group the nitro group is also reduced to aniline and both anilines are subsequently condensed to the corresponding azo group via oxidative azo condensation. Finally, after cleaving of the Fmoc-protecting group the acetyl group is introduced via mixed anhydride mediated nucleophilic substitution.

While the yields for the introduction of the Fmoc protecting group were still sufficient with unsubstituted and monosubstituted intermediates, the yields collapsed to a maximum of 13% when dibrominated starting material was used (**scheme 4.3**).[183] This drastic change in reactivity cannot be attributed to the sterical hinderance of the used Fmoc-Cl or the secondary amine starting material, since no change has taken place concerning these factors compared to mono- and unsubstituted compounds. Therefore, the introduction of bromine substituent at the dianiline building block might reduce the reactivity from the actually highly reactive secondary amine by lowering its electron density and consequently its nucleophilicity.

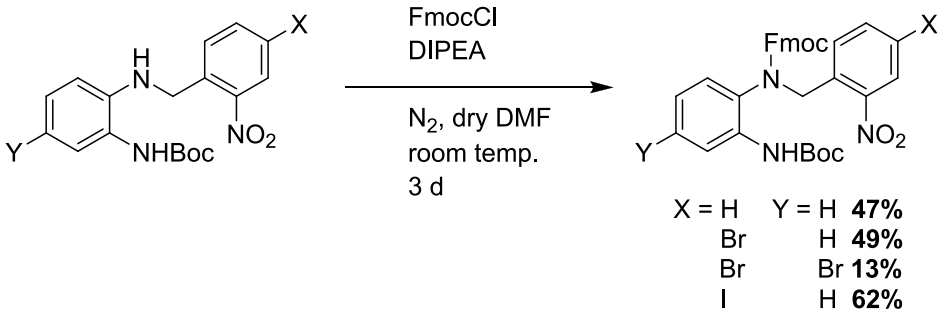

Scheme 4.3: Detailed view on the limiting Fmoc-protection step of the initial *N*-Ac diazocine synthesis pathway. Due to the low to sufficient yields this reaction step is the limiting factor especially for the synthesis of double-side brominated *N*-Ac diazocine.

In addition to the variations in the reaction conditions already mentioned for mono- and unsubstituted *N*-Ac diazocines, several approaches were made to increase the nucleophilicity of the dibrominated secondary amine. For this purpose, an attempt was made to convert the secondary amine into the corresponding amide by deprotonation in order to increase the nucleophilicity (**scheme 4.4**). Therefore, different deprotonating agents like sodium carbonate, sodium hydroxide and sodium hydride were used but the formation of the desired Fmoc-protected product could not be observed. Instead, the more acidic proton of the Boc-protected aniline was presumably deprotonated, resulting in either no product formation or unintended side reactions.[175] Due to this limitation, the initial synthesis procedure is not suitable for a large scale production of dihalogenated *N*-Ac diazocines aiming for subsequent late-stage functionalization.

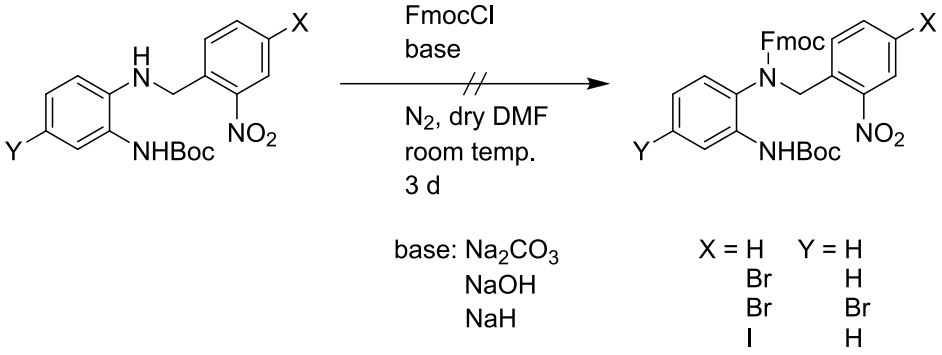

Scheme 4.4: Attempts to improve the nucleophilicity of secondary amine intermediate for Fmoc-protection by adding different bases did not result in the successful formation of the desired product.

Therefore, the first approach is to find a suitable replacement for the Fmoc-protecting group that is orthogonal to the Boc-protecting group and compatible with the synthesis pathway. Reductively cleavable protecting groups are not suitable for the bridging amine, as the nitro group of the *o*-nitrobenzylbromide building block has to be reduced during the initial synthesis path. It would be conceivable to introduce the acetyl group in the second reaction step already, which would also save two reaction steps. However, the use of an acetyl group together with an acid-cleavable Boc-protecting

group is an inappropriate combination, since catalyzed by the excess addition of deprotecting acid, a proton catalyzed imine condensation between deprotected aniline and the acetyl-protecting group could occur as side reaction. Consequently, a nitroaniline instead of a Boc-protected dianiline building block should be used to prevent this side reaction. Then, the acetyl group could be introduced. The acetyl-protected dinitro intermediate offers the possibility of either going the way of reductive azo condensation or after prior reduction to the dianiline the oxidative pathway is followed. However, the nucleophilicity of nitroaniline for a nucleophilic attack on *o*-nitrobenzylbromide is reduced by the nitro group, so that the corresponding *o*-nitrobenzaldehyde should serve as electrophile instead. This new approach is examined in detail in the following section.

4.7.2 Imine Condensation Approach

Condensation reactions of a carbonyl compounds with amines or anilines are a powerful tool in quick and efficient synthesis for formation of imine bonds which also often occur in biological systems and have also proven to be a valuable method in organic synthesis.[184-186] Therefore, this reaction between *o*-nitroaniline (**1**) and *o*-nitrobenzaldehyde (**2**) should form the starting point of the new synthetic strategy for the preparation of *N*-Ac diazocine **3** (**scheme 4.5**). The imine intermediate is subsequently reduced to secondary amine **4**. Here, the choice of a suitable reducing agent is of great importance, as a reduction of both nitro groups must be avoided since selective protection of the bridging nitrogen is therefore no longer feasible. Hence, transition metal catalyzed addition of hydrogen is not suitable since they reduce both imine and nitro groups. Instead, boranes or borohydrides can be used for selective imine reduction.[185] For subsequent acetylation highly reactive acetyl chloride shall be used as electrophile for nucleophilic substitution. For final ring closing reaction two methods are suitable resulting in the formation of *N*-Ac diazocine **3**. Reductive reaction pathway following the procedure by MOORMANN *et al*.[75] for parent diazocine can be performed directly from acetylated dinitro precursor **5**. For oxidative pathway following the procedure by MAIER *et al*.[76] established for synthesis of parent diazocine and *N*-Ac diazocines prior reduction of both nitro groups to the corresponding dianiline intermediate is required.

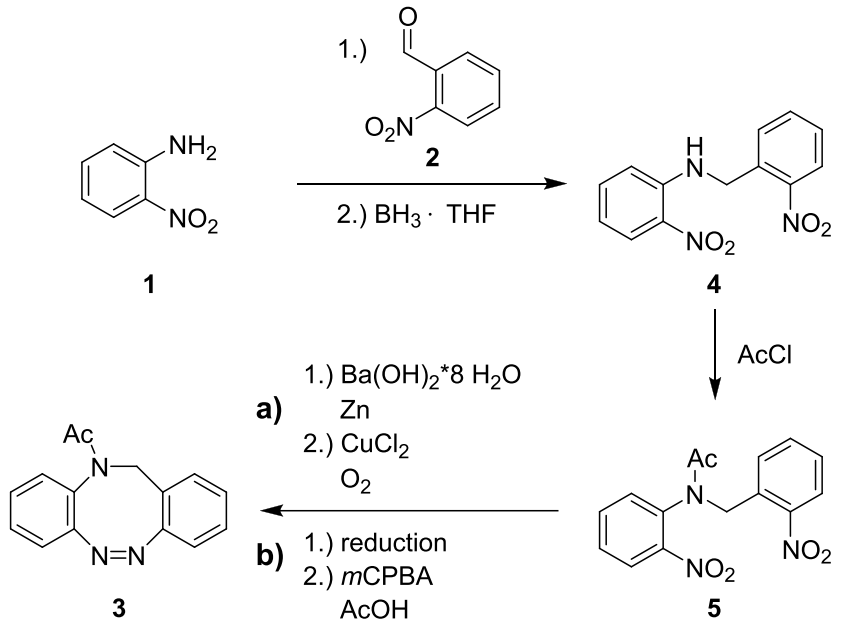

Scheme 4.5: Schematic view of the new approach for *N*-Ac diazocine synthesis avoiding the Fmoc protecting group. After imine condensation of *o*-nitroaniline (**1**) and *o*-nitrobenzaldehyde (**2**) and subsequent reduction to the secondary amine **4**, acetyl group is introduced giving the acetylated dinitro precursor **5**. Finally, the ring closing azo condensation can be performed via reductive MOORMANN *et al*.[75] (a) or oxidative MAIER *et al*.[76] procedure (b) for formation of unsubstituted *N*-Ac diazocine **3**, the letter after prior reduction to corresponding dianiline intermediate.

Imine condensation of *o*-nitroaniline (**1**) with *o*-nitrobenzaldehyde (**2**) was carried out based on the method by TOUBI *et al*.[187] in methanol catalyzed by sulfuric acid. However, first syntheses lead to insufficient imine formation and variation of reaction time led to no significant increase. Since imine condensations are reversible reactions its dynamic equilibrium can be shifted towards increased product formation by removal of water side product by addition of water binding agents like magnesium sulfate.[185,186] With this improvement the yield of imine condensation was significantly increased. Subsequent reduction to secondary amine **4** was carried out with borane tetrahydrofuran complex under nitrogen atmosphere without affection of both nitro groups. Via this two-step reaction sequence secondary amine **4** could be obtained with a 60% yield (**scheme 4.6**). The treatment of secondary amine **4** with acetylchloride (AcCl) resulted in the formation of acetylated dinitro compound **5** in a yield of 38%. The reason for this is rooted in the reduced nucleophilicity of the secondary amine induced by the neighboring electron withdrawing nitro group. Finally, two different routes were used to achieve final azo cyclization to *N*-Ac diazocine **3**. At first the reductive azo condensation pathway following the procedure by MOORMANN *et al*.[75] was carried out but resulted in no formation of the desired product **3**. The starting material was already consumed in the first reaction step indicating that side reactions are favored over closing of the eight membered ring. The oxidative reaction pathway following the procedure of MAIER *et al*.[76] over two reaction steps containing reduction of dinitro compound **5** to corresponding dianiline intermediate followed by *m*CPBA induced BAYER-MILLS-like azo condensation lead to formation of *N*-Ac diazocine **3** in a yield of 55%. The reduction was carried out via palladium-catalyzed reduction under hydrogen atmosphere, where *thin layer chromatography* (TLC) and a crude product NMR showed a complete conversion of dinitro compound **5** to the aniline intermediate. In the following oxidative azocyclization was achieved with *m*CPBA in acetic acid. In addition to the desired *N*-Ac diazocine **3**, however, the formation of a significant amount of 23% a by-product **6** was observed. The reason for this is an intramolecular imine condensation between the acetyl protecting group and the neighboring aniline which is probably catalyzed by the solvent acetic acid. The side product is stabilized by formation of an aromatic benzimidazole system and therefore it is unlikely to cleave the actually reversible imine bond to reobtain the starting material. Due to this problem and the difficult introduction of the acetyl group the *N*-Ac diazocine **3** can be obtained in a total yield of 13% over five synthesis steps which is no improvement to the initial synthesis path.

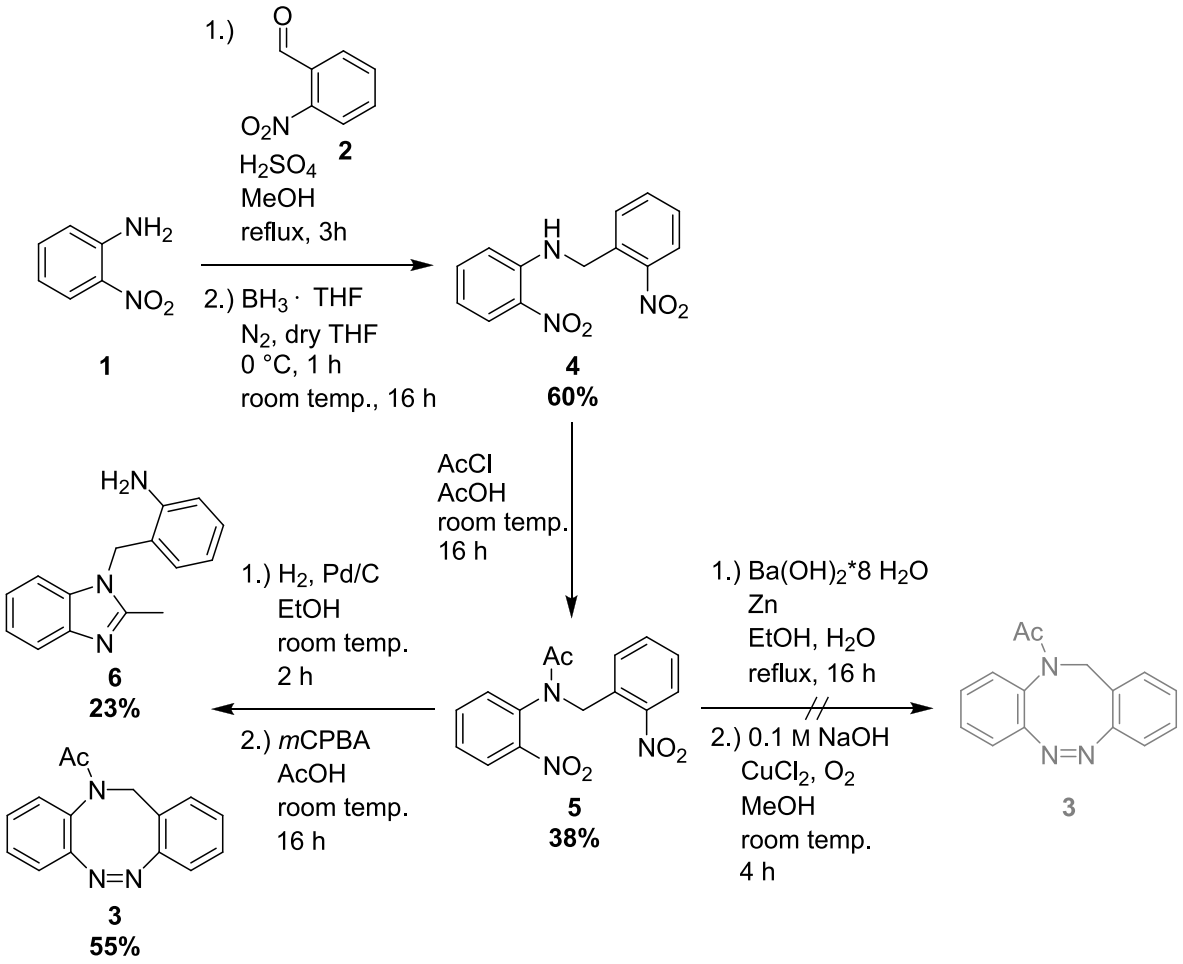

Scheme 4.6: Synthesis path for formation of unsubstituted *N*-Ac diazocine (**3**) starting with imine condensation of *o*-nitroaniline (**1**) with *o*-nitrobenzaldehyde **2** and subsequent reduction to the secondary amine **4** in a yield of 60%. The introduction of acetyl protecting group turned out to be the limiting step with an insufficient yield of 38%. After prior reduction to dianiline intermediate the target compound **3** could be obtained in yield of 55% and an overall yield of 13%. Additionally, the formation of side product **6** via intramolecular imine condensation has been observed.

To prevent the undesired side reaction in form of an intramolecular imine condensation between acetyl protecting group and neighboring aniline other protecting groups shall be used. The initial synthesis path by LENTES *et al.*[64,120] includes the use of carbamate type-protecting group in form of Fmoc-protecting group. Since the carbamate does not interfere with the deprotected free neighboring aniline, carbamate type-protecting groups shall be introduced instead of an acetyl group. Both Boc- or Fmoc-protecting group should be used for this (**scheme 4.7**). Unfortunately, this would lead to two more reaction steps of deprotection and introduction of acetyl group after oxidative ring closing azo condensation. In case of a higher overall yield compared to the initial synthesis procedure, this would be justifiable.

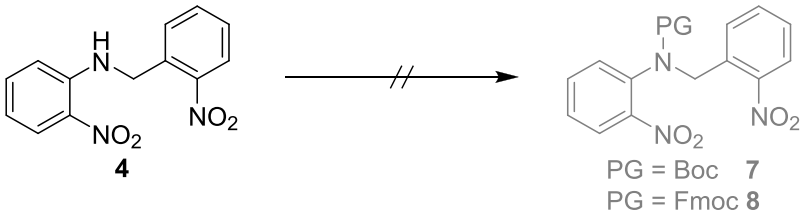

Scheme 4.7: The introduction of both Fmoc- or Boc-protecting groups could not be achieved. Reagents and conditions are shown in **table 4.1**.

However, the introduction of both protecting groups to Fmoc- **7** or respectively Boc-protected dinitroamine **8** turned out to be very difficult since although various conditions in form of solvent, temperature and reaction time were used no product formation could be observed (**table 4.1**). The reason for this is most likely the reduced nucleophilicity of the otherwise very reactive secondary amine due to the neighboring nitro group. Furthermore, the steric requirements of the reagents used to introduce the protecting groups and of the starting material are also likely to play a significant role. To overcome the problem of weakened nucleophilicity stronger bases were used to deprotonate the secondary amine and therefore increase its nucleophilicity. Yet the use of sodium carbonate or sodium hydride as bases was also unsuccessful.

Table 4.1: Reaction conditions used for the introduction of Fmoc- or Boc-protecting groups. A successful introduction of the given protecting groups could not be achieved.

protecting group precursor	base	solvent	temperature	reaction time
FmocCl	DIPEA	DMF	room temp.	24 h
FmocCl	DIPEA	DMF	60 °C	24 h
FmocCl	Na_2CO_3	DMF	room temp.	24 h
FmocCl	NaH	DMF	room temp.	24 h
FmocCl	NaH	DMF	room temp.	72 h
Boc_2O	Na_2CO_3	THF	room temp.	24 h
Boc_2O	Na_2CO_3	THF	65 °C	24 h
Boc_2O	NaH	THF	room temp	24 h
Boc_2O	NaH	DMF	room temp.	24 h
Boc_2O	NaH	DMF	room temp.	72 h

Despite the problems encountered, it should be investigated whether the imine condensation approach does not provide higher yields for dibrominated *N*-Ac diazocine **9** than the initial synthesis path (**scheme 4.8**). This was investigated in a supervised work by MIKOSCH.[188] For this purpose, 4-bromo-2-nitroaniline (**10**) and 4-bromo-2-nitrobenzaldehyde (**11**) were, in analogy to the new synthesis route for unsubstituted *N*-Ac diazocine **3**, converted to the corresponding imine via imine condensation and then reduced to the secondary imine **12** with a yield of 24% over two reaction steps.

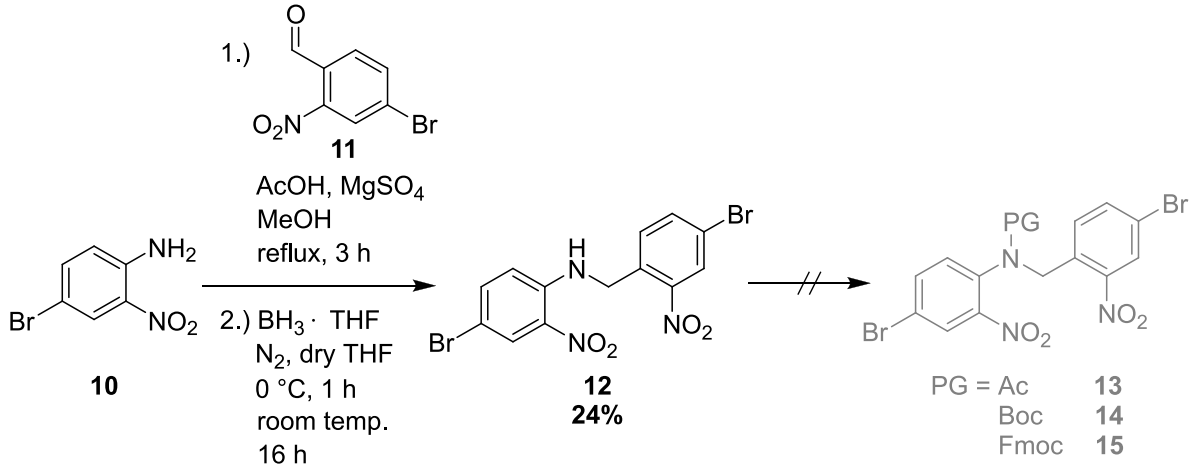

Scheme 4.8: Attempted synthesis of dibrominated *N*-Ac diazocine **9** starting from brominated nitroaniline **10** and nitrobenzaldehyde **11** giving the corresponding secondary amine **12** after subsequent reduction with borane THF complex in a yield of 24% over two steps. The consecutive introduction of three different protecting groups under varying reaction conditions was not successful (**table 4.2**).

In the following, acetyl- **13**, Boc- **14** and Fmoc-protected dinitroamines **15** should be synthesized, but none of the compounds mentioned could be obtained although reaction conditions were varied (**table 4.2**). The fact that not even the acetyl group could be introduced is probably due to the further reduced nucleophilicity of the starting material **12** compared to the unsubstituted dinitroamine **4** caused by the additional bromine substituent in *para*-position.

Table 4.2: Reaction conditions of attempted protecting group introduction to obtained protected dinitro compounds **13-15** starting from **12**.

protecting group precursor	base	solvent	temperature	reaction time
AcCl	TEA	CH_2Cl_2	room temp.	24 h
Boc_2O	Na_2CO_3	THF	room temp.	24 h
Boc_2O	Na_2CO_3	DMF	room temp.	24 h
Boc_2O	NaH	THF	room temp.	24 h
Boc_2O	NaH	DMF	room temp.	72 h
FmocCl	Na_2CO_3	DMF	room temp.	24 h
FmocCl	NaH	THF	room temp	24 h
FmocCl	NaH	DMF	room temp.	24 h

Although the imine condensation approach leads to the formation of *N*-Ac diazocine **3** the overall yield remains insufficient. Furthermore, application of this approach on halogenated starting materials was not successful at all since introduction of protecting groups at the bridging nitrogen atom in the second reaction step could not be achieved. Therefore, a new approach has to be developed for the synthesis of *N*-Ac diazocine framework **3**.

As the protecting group must necessarily be present during the azo condensation in order to prevent side reactions, it cannot be omitted. However, due to the problem in the previous approach, the protecting group cannot be introduced after the heteroatom bridge is formed. It must therefore be present in the aniline building block prior to the nucleophilic substitution. Due to its stability and low steric requirement, the acetyl group is suitable for this purpose. Moreover, deprotonated primary amides are known to be good nucleophiles and since the acetyl group is present in the target molecule **3** it no longer needs to be exchanged in the further course of a synthesis pathway.[189]

4.7.3 Amidate Anion Approach

Nucleophilic substitutions of primary amides with alkyl halogenides have often been used for synthesis of secondary amides since deprotonated amides (amidate anions) are good nucleophiles.[189-192] This requires the deprotonation of the acetanilide to the corresponding amidate anion to increase the nucleophilicity. Such reactions have already been performed with *o*-nitroacetanilide nucleophiles and alkyl halide electrophiles.[193-195] Therefore, nucleophilic substitution of *o*-nitroacetanilide **16** with *o*-nitrobenzyl bromide **17** to the acetylated dinitro compound **5** shall be the key reaction step of a new synthesis path leading to *N*-Ac diazocine **3** (**scheme 4.9**). As final ring closing step oxidative azo condensation procedure developed by MAIER *et al*.[76] was carried out after prior reduction to the corresponding dianiline intermediate.

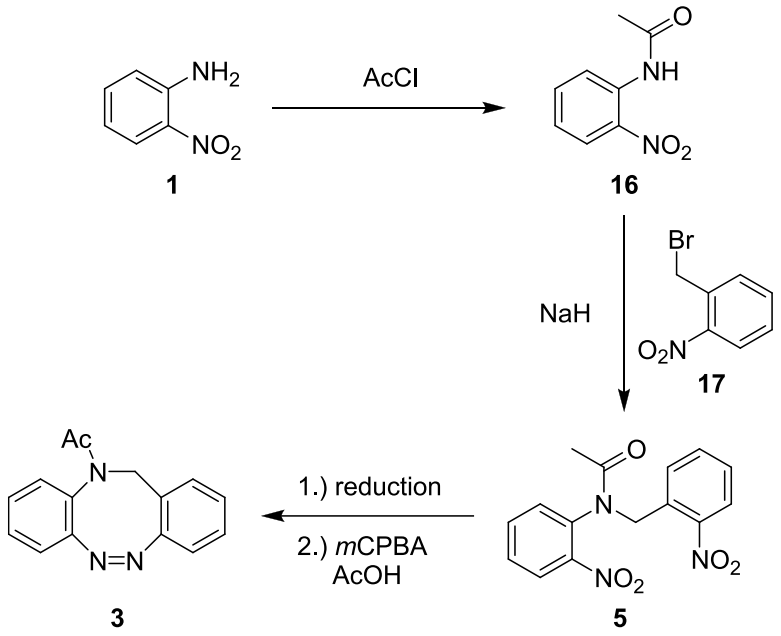

Scheme 4.9: Overview of new synthesis path for formation of *N*-Ac diazocine **3** starting from *o*-nitroaniline (**1**) which is protected with an acetyl group in the first step. The resulting acetanilid **16** can be deprotonated to react with *o*-nitrobenzyl bromide (**17**) in a nucleophilic substitution giving the acetylated dinitro precursor **5**. The final ring closing shall be achieved via oxidative azo condensation leading to the desired *N*-Ac diazocine **3**.

As in the previous imine condensation approach, this synthesis path uses *o*-nitroaniline (**1**) as starting material which is this case protected with an acetyl group in the first reaction step (**scheme 4.10**). For this purpose, the aniline **1** was treated with triethylamine (TEA) and acetyl chloride (AcCl) following a synthesis procedure of LI *et al*.[196] giving the desired acetanilid **16** in a yield of 92%. For the following nucleophilic substitution, the nitroacetanilide **16** was deprotonated at first with sodium hydride as a strong base. The amidate anion generated in this way serves as a nucleophile in the reaction and is stabilized by the polar aprotic solvent dimethylformamide (DMF). In the following the *o*-nitrobenzyl bromide electrophile **17** is added which leads to the formation of the desired acetylated dinitro compound **5** in an excellent yield of 98%. To complete the preparation of the diazocine, the dinitro precursor **5** was first reduced to the corresponding dianiline intermediate under a hydrogen atmosphere using a palladium catalyst and then converted to the desired *N*-Ac diazocine **3** in an oxidative azo condensation according to MAIER *et al*.[76] in a yield of 49% over two steps. However, like in the previous imine condensation approach (see previous chapter 4.3.2) the formation of an undesired side product **6** was observed in a significant amount of 21%. Nevertheless, the desired *N*-Ac diazocine **3** could be obtained in a very good overall yield of 45% over four reaction steps making the amide anion approach a promising synthesis path for preparation of unsubstituted *N*-Ac diazocine **3**.

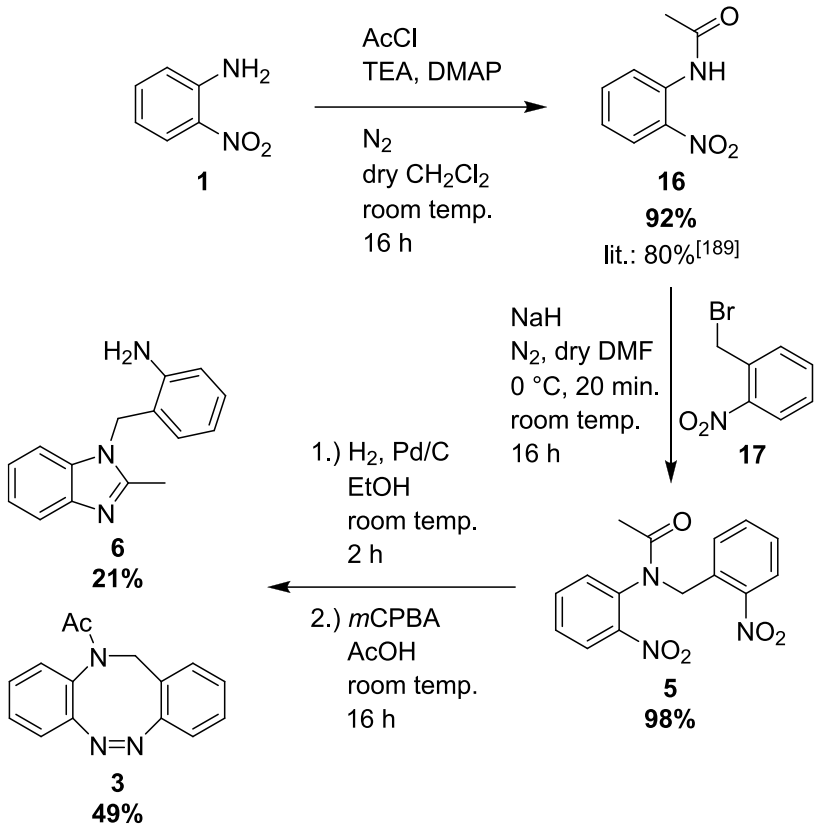

Scheme 4.10: Synthesis path for preparation of unsubstituted *N*-Ac diazocine **3** starting with an acetyl protection of *o*-nitroaniline (**1**) in a yield of 92%. The synthesis of acetylated dinitro compound **5** has been achieved via nucleophile substitution of acetanilide **16** with *o*-nitrobenzylbromide (**17**) in a yield of 98% which then was converted to the desired *N*-Ac diazocine **3** in a yield of 49% via oxidative azo condensation after prior reduction. The overall yield of this synthesis path was 45% over four reaction steps. However, similar to prior imine condensation approach (see **chapter 4.3.2**) formation of undesired side product **6** was observed.

Despite the problem with the undesirable side reaction in the final azo condensation step, this synthesis route is suitable for derivatization due to the excellent yield in the first two synthesis steps. For this purpose, the substituents to be introduced must already be present in the acetanilide and nitrobenzyl bromide building blocks. Initially, the symmetrically halogenated *N*-Ac diazocines were to be prepared via this synthesis path in a supervised work by HÖSGEN[197] (**scheme 4.11**) For this purpose, the brominated **18** or iodinated nitroanilines **19** were used as starting materials. The synthesis of corresponding acetanilides **20** and **21** was performed following the procedure of REUTER *et al.*[198] using acetic acid and acetic acid anhydride as acetylating agents resulting in yields of 55% for the bromonitroacetanilide **20** and 83% for the iodonitroacetanilide **21**. The differences in the yields of acetylation are likely caused by differences in their nucleophilicity since the brominated nitroaniline **18** is less electron rich than the corresponding iodinated nitroaniline **19** and therefore less reactive against the acetic acid anhydride electrophile. Both acetanilides **20** and **21** should be reacted with the corresponding halogenated nitrobenzyl bromides **22** and **23** in a nucleophilic substitution reaction giving the brominated **24** and iodinated dinitro compound **25** in analogy to the unsubstituted model system **3** using sodium hydride as a base. In contrast to the unsubstituted system with almost complete conversion the yields for the halogenated dinitro compounds are very low with 13% for the brominated **24** and 8% for the iodinated dinitro compound **25**. Additionally, the compounds could only be obtained in an impure form. Analysis of all fractions obtained during purification revealed a complete consumption of both nitrobenzyl bromide building blocks **22** and **23** while the unconverted acetanilides **20** and **21** could be obtained completely indicating the formation of undesired side products. Variation of solvent, reaction temperature and ratio of used starting materials showed no

positive effect on the product yields and starting material consumption. As the two compounds could only be obtained in impure form and in small quantities, the synthesis path was not continued.[197]

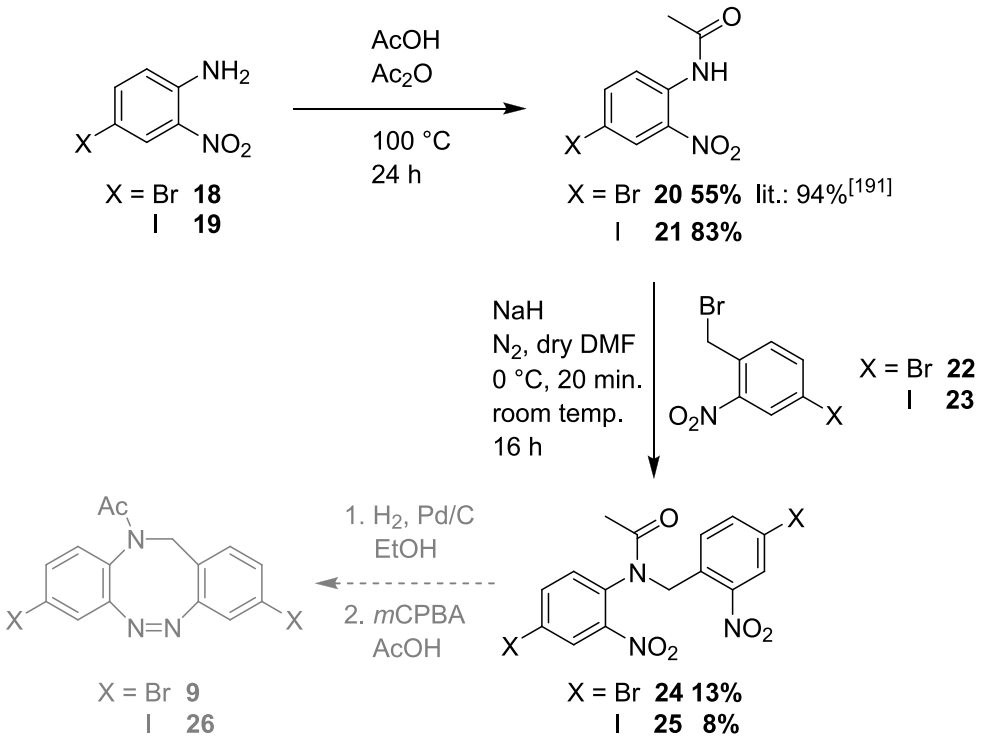

Scheme 4.11: Synthesis path for preparation of brominated **9** and iodinated *N*-Ac diazocine **26** following the amidate anion approach. Halogenated acetanilides **20** and **21** could be obtained with yields of 55% or respectively 83%. The following nucleophilic substitution resulted in poor yields of 13% for the brominated **24** and 8% for the iodinated dinitro compound **25**.[197]

Given the low conversion rates, it should be investigated which building block has the greater influence on the result of the substitution reaction since both exhibit a bromine substituent in *para*-position. For this purpose, the unsubstituted acetanilide **16** was first reacted with the brominated nitrobenzyl bromide **22** (**scheme 4.12**). Analysis of the reaction products showed complete consumption of nitrobenzyl bromide building block **22** while the acetanilide could be recovered quantitatively. This indicates that an increased nucleophilicity has no influence on the substitution reaction and the side reaction is preferred.[197]

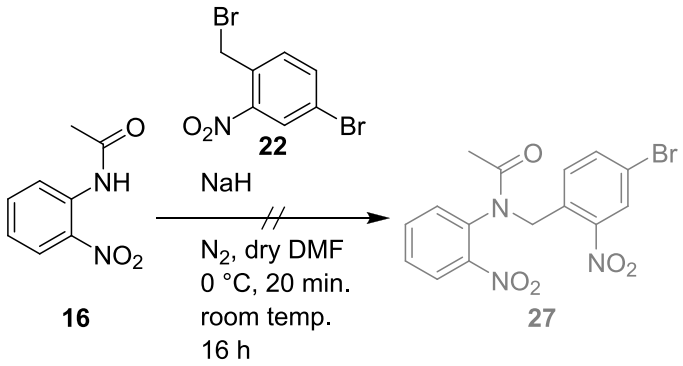

Scheme 4.12: Synthesis of monobrominated dinitro compound **27** from nitroacetanilide **16** with bromonitrobenzyl bromide **22** resulting in no product formation. Instead, nitrobenzyl bromide **22** was consumed completely while acetanilide could be recovered quantitatively.[197]

For the same reason brominated acetanilide **20** was deprotonated with sodium hydride and unsubstituted *o*-nitrobenzyl bromide **17** was added resulting in the formation of monobrominated dinitro compound **28** in a yield of 8% (**scheme 4.13**).[197] The unreacted acetanilide **20** could be

obtained completely while the nitrobenzyl bromide building block **17** could only be recovered in parts since a huge amount was still consumed in a side reaction.[197] This indicates a concurrence between the desired nucleophilic substitution reaction and an undesired side reaction consuming the nitrobenzyl bromide building blocks. As the test reactions with different substitution patterns show, the extend of the side reaction depends on whether other substituents are present on the nitrobenzyl bromide component. However, it was shown that the side reaction also occurs in the case of an unsubstituted nitrobenzyl bromide **17**, albeit to a much lesser extent. This was not noticeable, though, due to the desired dinitro compound being formed almost quantitatively when the significantly more nucleophilic unsubstituted *o*-nitroacetanilide **16** was used as reaction partner.

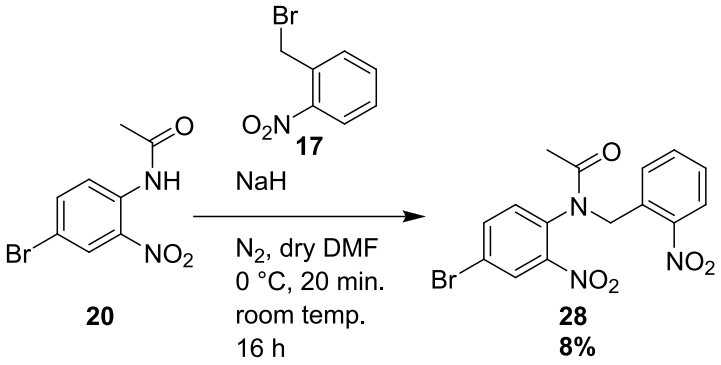

Scheme 4.13: Synthesis of monobrominated dinitro compound **28** from brominated acetanilide **20** and *o*-nitrobenzyl bromide (**17**) could be achieved in a yield of 8%.[197]

A possible explanation for this consumption of used *o*-nitrobenzyl bromide derivatives **17**, **22** and **23** during the nucleophilic substitution reaction may be the lability of *o*-nitrobenzyl derivatives upon irradiation. Due to this circumstance, *o*-nitrobenzyl compounds are commonly used as photolabile protecting groups.[199-201] The cleavage of the *o*-nitrobenzyl protecting group **29** is carried out by exposure to light in the wavelength range from near UV to 420 nm, depending on the substitution pattern.[201,202] The mechanism of *o*-nitrobenzyl protecting group cleavage is well studied and initially proceeds via proton transfer from the alkyl side chain to the nitro group after prior photoexcitation (**scheme 4.14**). The rate constant for the decay of the protonated nitro group depends on substitution pattern, solvent and pH of the surrounding media and takes place via the irreversible formation of a five membered intermediate. The subsequent ring-opening leads to a hemiacetal intermediate releasing the leaving group under formation of an *o*-nitrosobenzaldehyde byproduct **30**.[201,203-205] However, the NMR spectra of the byproduct fraction of the performed nucleophilic substitution reactions with halogenated building blocks **20-23** showed not only *o*-nitrosobenzaldehyde but also the formation of numerous other side products. This can be explained on the one hand by the high reactivity and on the other hand by further light-induced side reactions of *o*-nitrosobenzaldehyde derivatives.[201] This indicates that a decomposition of the *o*-nitrobenzyl bromide building blocks has taken place. The occurrence of a small amount of the desired substitution products implies that the intended substitution reaction has indeed taken place. However, the bromine or iodine substituents in *para*-position appear to enhance the degree of light-induced degradation by either lowering the energy barrier required for cleavage and thus shifting the required wavelength bathochromically and/or increasing the quantum yield of the photoexcitation. Since the cleavage of the halogenated *o*-nitrobenzyl building blocks already took place in daylight without further irradiation in the substitution reactions carried out, this approach for the preparation of symmetrically halogenated *N*-Ac diazocines causes major problems in the synthesis and workup, making it unsuitable for further application.

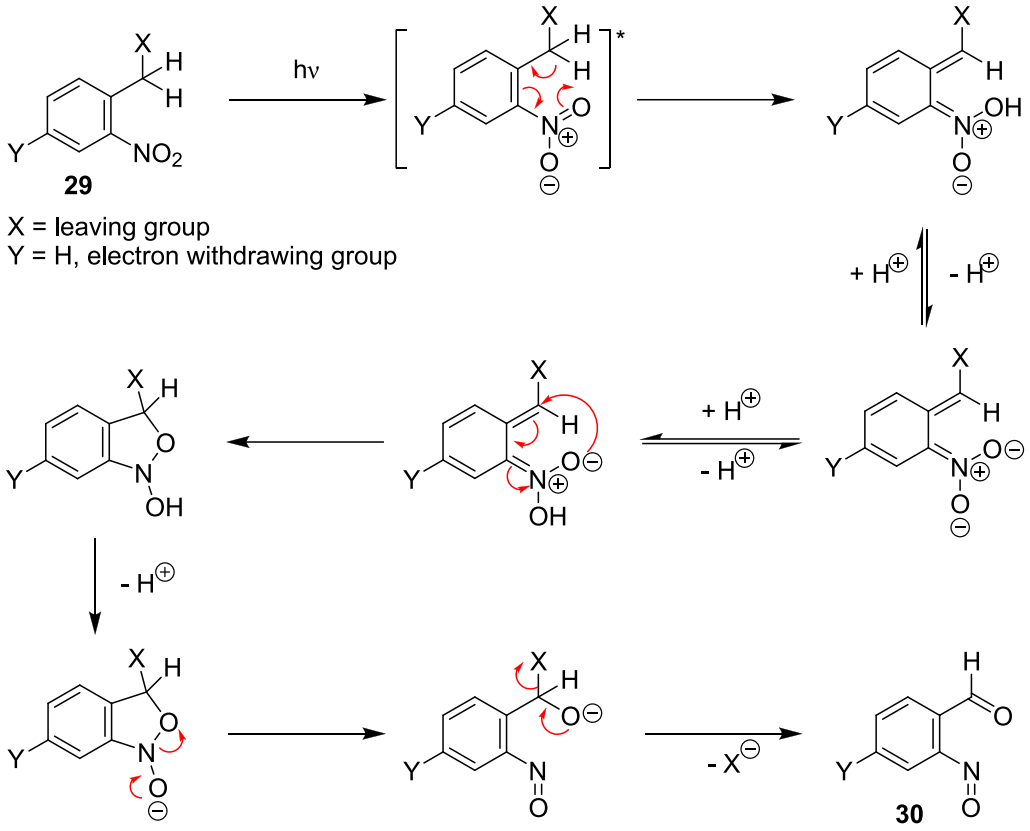

Scheme 4.14: Mechanism of photodegradation of *o*-nitrobenzyl derivatives **29** to *o*-nitrosobenzaldehydes **30**. 2-Nitrobenzyl derivatives are used as photolabile protecting groups for numerous functional groups.[201,203-205]

5. Conclusion

Photoswitches, especially azobenzenes, offer great potential for selective control of molecular properties and are therefore used in a wide field of applications like material science or photopharmacology. Bridged azobenzenes, so-called diazocines, represent the next development step of azobenzene photoswitches. Their superior switching properties have been discovered by HERGES and TEMPS[57] in 2009 and have been brought to application ever since. However, the parent diazocine framework still offers some disadvantages in form of the required switching wavelengths, the lack of solubility in aqueous media and the still insufficient directional movement. These weaknesses have been systematically addressed during the development of the so-called second generation of diazocines. On the one hand, these are the very rigid and therefore highly efficient switching diindanodiazocines which allow directional motion since all forms of unproductive degrees of motional freedom have been eliminated and a very high conversion rate of light to chemical energy. With two diastereomers, these offer two forms that differ greatly in their switching properties. In addition, the racemic diastereomer is the smallest chiral photoswitch known to date.[42] On the other hand, nitrogen-bridged diazocines were developed, which allow switching in the near IR range due to a strong bathochromic shift of the absorption wavelengths. Substitution at the bridging nitrogen atom with an acetyl group ensures high intrinsic water solubility. Furthermore, in contrast to the parent system, the switching properties do not deteriorate in aqueous media.[64,110]
The tasks addressed in this work include the characterization of the chiral properties of diindanodiazocines, as well as their derivatization with the aim of their application in smart materials and liquid crystals. In addition, the *N*-acetyl diazocines were to be further derivatized and new potential inhibitors were to be developed for use in the field of photopharmacology.

5.1 Chiroptical Switching, Enrichment of Enantiomeric Excess and Derivatization of Diindanodiazocines

Superior switching properties of DID diastereomers **31** and **32** have been examined and published in previous work.[42] However, the chiroptical properties of the racemic mixture have not been investigated so far. Therefore, the racemate **32** was separated into both enantiomers via chiral HPLC. As a result, the absolute configuration of both enantiomers could be assigned with help of qualitative optical rotation measurements and single crystal structure analysis. In addition, the quantitative measurements of the specific rotation showed that switching from thermodynamically stable Z- to metastable E-configuration increases the extent of the specific rotation by a factor of seven. Light-induced back-switching from E- to Z-configuration reduced the level of specific rotation back to the initial value. This could be repeated over a large number of cycles without any signs of fatigue for both enantiomers. Measurements of molar circular dichroism of Z-and E-configurations of both enantiomers showed a huge difference between both forms. In addition, the maxima of the spectra of the E-configurations of both enantiomers exhibited a significantly higher value for the molar circular dichroism. This shows that the racemic DID **32** is a chiroptical switch whose chirality is amplified by the switching process from Z-to E-configuration (**scheme 5.1**).

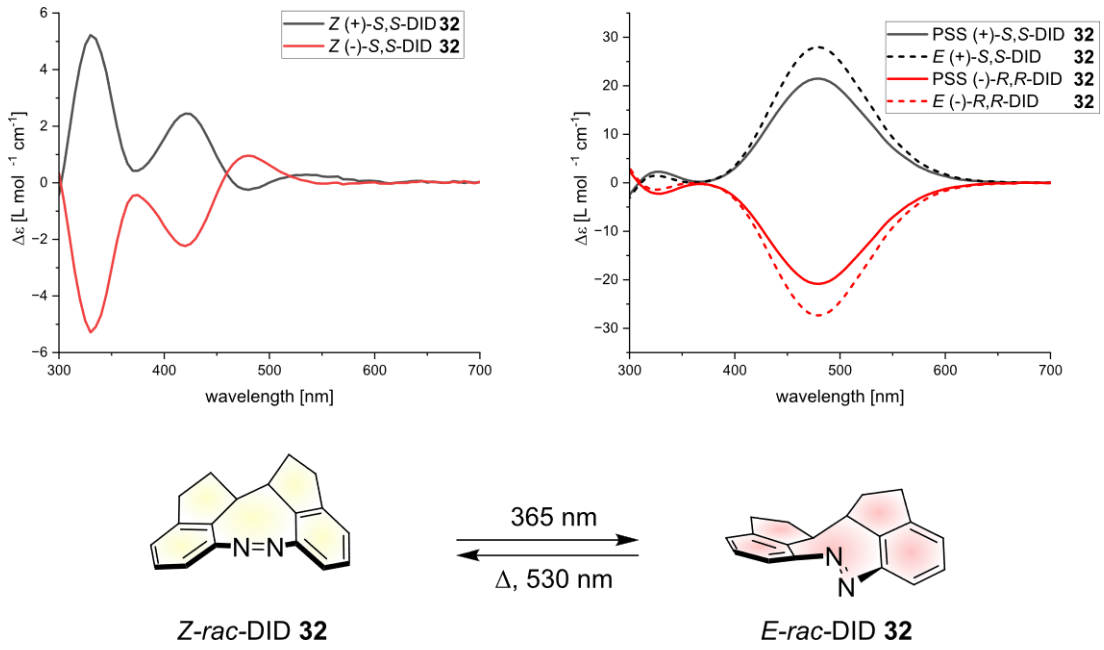

Scheme 5.1: Amplification of molar circular dichroism of *rac*-DID **32** enantiomers upon photoisomerization.

Enantiomeric imbalance in a racemic mixture can be achieved via dynamic photoresolution with circular polarized light. This concept should be applied to the Z- to E-photoisomerization of racemic DID **32** to selectively enrich one of the two enantiomers from the racemic mixture in the metastable state with corresponding circular polarized light. For this purpose, the enantiomeric excess to be expected was at first calculated from the molecular dissymmetry factor g. For determination of enantiomeric excess, a solution of racemic mixture was irradiated with r- or respectively l-CPL until the PSS was reached and spectra of molecular circular dichroism were measured immediately. For the calculation of enantiomeric excess from molar circular dichroism the method established by TAMAOKI *et al*.[158] was used. The enantiomeric excesses calculated via this method were in good agreement with the theoretical values calculated from molecular dissymmetry factor g (**table 5.1**).

Table 5.1: Overview over enantiomeric excess calculated from molecular dissymmetry factor g and calculated from experimental data obtained from measurements of molecular circular dichroism after irradiation to the PSS with CPL 405 nm of a racemic mixture of *rac*-DID **32** in THF.

CPL	$ee_{theoretical}$	$ee_{PSS\ 405\ nm}$
r-405 nm	0.328%	0.344%
l-405 nm	0.312%	0.357%

The chiroptical properties of racemic DID **32** examined within this project show great potential for the world's smallest chiroptical switch known so far for application in smart chiral materials or liquid crystals. To make the DID more suitable for further derivatization and applications mentioned above, the framework should be equipped with connecting points in form of bromine or iodine substituents giving the symmetrically di- and tetrahalogenated DIDs **33-37**. The preparation should be carried out according to the proven principle that the substituents should already be present in the nitroindane building blocks before the DID is finally synthesized according to the established method. Halogenated building blocks **38** and **39** of disubstituted DIDs could be easily obtained by electrophilic aromatic substitution of 2-nitroindane (**40**) (**scheme 5.2**). Preparation of dibrominated DID diastereomers **33** and **34** could be achieved via standard procedure in good yields while corresponding diiodinated compounds caused problems in the final ring closing steps since iodine substituents were partially (*rac*-diastereomer **36**) or totally reduced (*meso*-diastereomer **35**) by the used reductive agents.

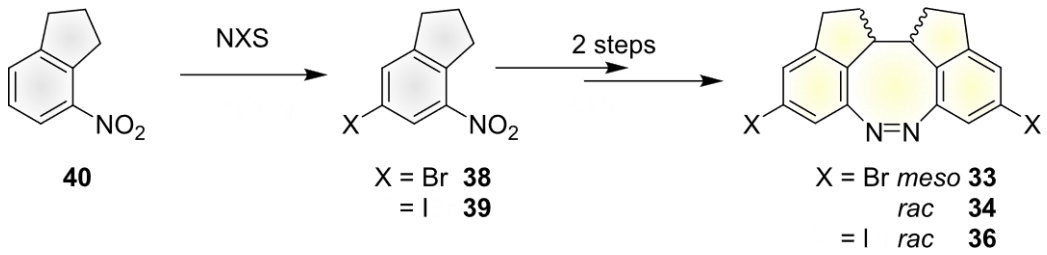

Scheme 5.2: Synthesis path for preparation of the disubstituted DIDs **33**, **34** and **36** and the building blocks **38** and **39** were prepared via electrophilic aromatic substitution. The diiodinated *meso*-DID **35** could not be obtained due to reduction of the iodine substituents during reductive azo condensation.

Synthesis of dibrominated 2-nitroindane **41** could not be achieved via direct electrophilic aromatic substitution of 2-nitroindane (**40**). Consequently, the preparation of the building block had to start with the introduction of the second bromine substituent before the indane framework is formed (**scheme 5.3**). Due to the formation of undesired side products the desired building block could be obtained only in very low yields. Furthermore, the final diazocine synthesis remained challenging and only *rac*-diastereomer of tetrabrominated DID **37** could be obtained.

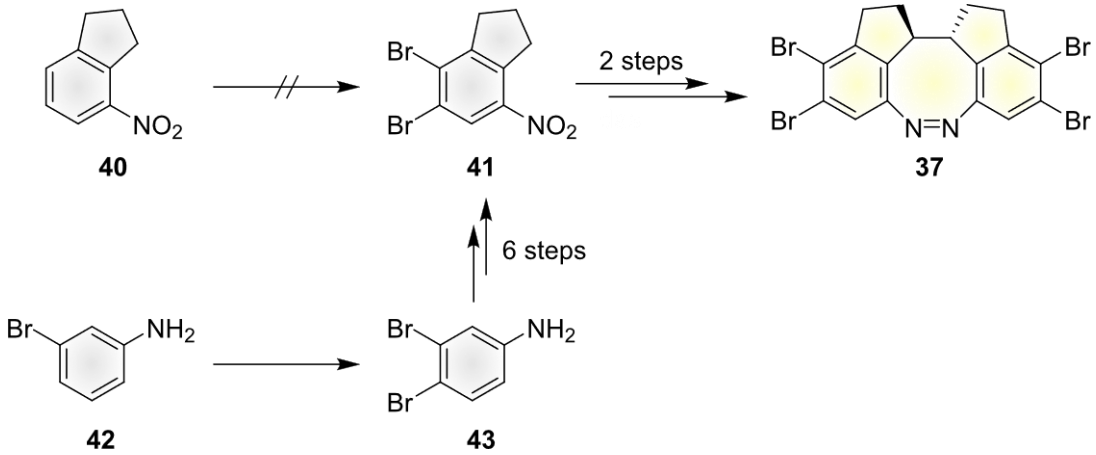

Scheme 5.3: Synthesis path for preparation of tetrabrominated *rac* DID **37** starting with bromination of 3-bromoaniline **42** to 3,4-bromoaniline **43** followed by formation of the indane framework.

The introduced halogen substituents showed only a slight reduction in the PSS for racemic mixtures of dihalogenated DIDs **34** and **36**, while tetrasubstitution **37** showed no significant influence as well as for the dibrominated *meso*-diastereomer **33**. However, thermal relaxation for all new DID derivatives after irradiation is significantly accelerated (**table 5.2**).

Table 5.2: Overview of photochemical properties of new DID derivatives **33, 34, 36, 37** compared to the unsubstituted diastereomers **31** and **32** determined via UV-vis and NMR spectroscopy. All compounds were measured in acetone.

	$\lambda_{max}(Z)$	$\lambda_{max}(E)$	$t_{1/2}$ (25 °C)	$\Gamma_{Z\rightarrow E}$ (385 nm)	$\Gamma_{Z\rightarrow E}$ (530 nm)
	nm		h	%	
31[42]	411	468[a]	8.8*10^{-4} [b]	84[a]	>99[a]
32[42]	431	478	117	76	94
33	405	464[a]	7.0*10^{-5} [b]	86[c]	>99[d]
34	435	479	51.5	68	92
36	435	476	50.8	67	92
37	431	483	29.2	78	93

[a]measured at 233 K; [b]measured at lower temperatures (233 K, 238 K, 243 K, 248 K) and then extrapolated to room temperature; [c]measured at 238 K and extrapolated; [d]measured at 238 K.

Within the scope of this work chiroptical properties of the *rac*-DID enantiomers could be examined. Furthermore, by introduction of halogen substituents the DID system has been prepared for future derivatization via cross-coupling reactions and is therefore available for application.

5.2 Synthesis and Characterization of new *N*-Acetyl Diazocines for Application in Photopharmacology

The *N*-Ac diazocine system shows promising photophysical properties in organic and aqueous media but no further derivatization has been carried out so far.[64,110,120] Within this work the monosubstituted brominated **44** and iodinated *N*-Ac **45** and *N* formyl -diazocines **46-48** as well as double-side brominated *N*-Ac diazocine **9** could be synthesized via established *N*-Ac diazocine synthesis path, which was improved by usage of oxidative azo condensation by Maier et al. [76]. Additionally, monohalogenated *N*-Ac diazocines **44** and **45** could be derivatized via various cross-coupling reactions in high yields. In this way, a wide range of aryl derivatives and various other functional groups have been introduced (**figure 5.1**).

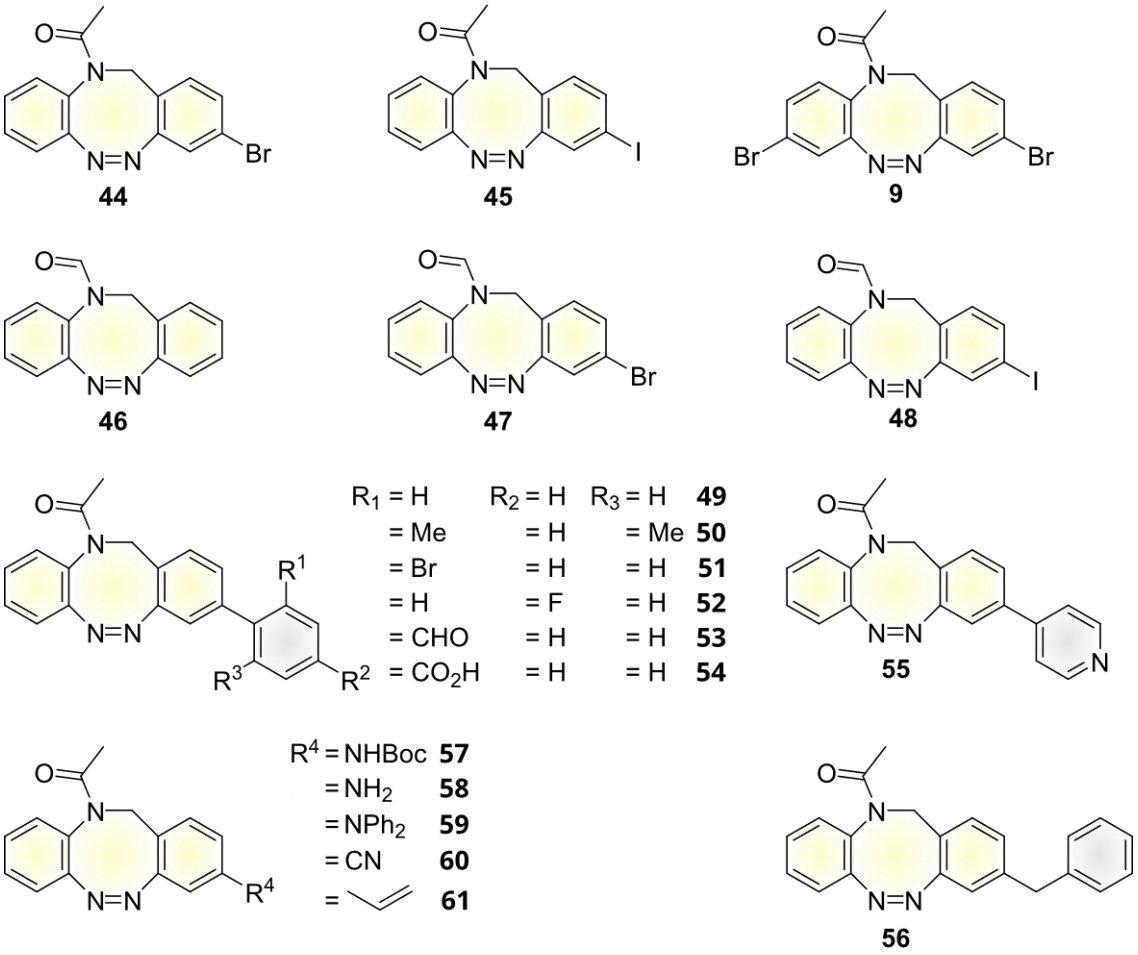

Figure 5.1: Overview showing new *N*-Ac diazocine derivatives **9, 44-61** synthesized within this work and the monohalogenated *N*-Ac diazocines **44** and **45** used as starting material for performed cross-coupling reactions.

Photochemical properties of all new *N*-Ac diazocines were examined in organic solvent and apart from the aniline derivatives **57-59** all compounds showed high PSS values just below the unsubstituted *N*-Ac diazocine **3** (**table 5.3**). With 29.3 min. to 39.8 min. thermal half-lives are also within the range of the unsubstituted *N*-Ac diazocine **3**. Only dibrominated *N*-Ac diazocine **9** exhibits a significantly accelerated thermal relaxation of 16.9 min. Formylated *N*-diazocines exhibit increased thermal half-lives at about 49 min for the halogenated and 74 min. for the unsubstituted derivatives.

Table 5.3: Photochemical properties of the unsubstituted *N*-Ac diazocine **3**, the new *N*-Ac **9, 44, 45, 49-61** and *N*-formyl diazocine derivatives **46-48** in acetonitrile determined via UV-vis and NMR spectroscopy.

	$\lambda_{max}(Z)$	$\lambda_{max}(E)$	$t_{1/2}$ (25 °C)	$\Gamma_{Z\rightarrow E}$ (405 nm)	$\Gamma_{Z\rightarrow E}$ (530 nm)
	nm		min.	%	
3	397	513	29.5	88	>99
9	396	519	16.9	85	>99
44	397	515	30.9	81	>99
45	397	517	28.6	82	>99
46	397	509	74.0	85	>99
47	397	509	49.9	82	>99
48	398	511	48.1	80	>99
49	399	516	29.3	79	>99
50	394	515	34.2	77	>99
51	396	516	34.2	82	>99
52	397	515	33.8	78	>99
53	396	517	29.8	80	>99
54	399	517	31.2	77	>99
55	396	515	39.9	79	>99
56	398	515	29.3	82	>99
57	397	514	30.6	61	>99
58	396	511	38.9	41	>99
59	389	510	31.5	49	>99
60	396	518	39.8	83	>99
61	398	515	29.6	76	>99

Since unsubstituted *N*-Ac diazocine **3** offers intrinsic water solubility, the new *N*-Ac diazocine derivatives **44**, **54** and **58** as well as *N*-formyl diazocine **46** were examined on their water solubility and their switching properties (**table 5.4**). Since the derivatives **54** and **58** exhibit functional groups potentially affected by the pH, this influence was investigated for this specific compounds as well. PSS values of new derivatives **54** and **58** in water at various pH are significantly lower than for the unsubstituted system **3** while brominated derivative **44** and *N*-formyl diazocine **46** exhibit only a minor deviation. Nevertheless, it is worth noting that aniline derivative **58** shows improved PSS values at pH 3.5 compared to organic solvent. Thermal half-lives of all analyzed compounds are elongated compared to organic solvent, whereas the values of the unsubstituted *N*-Ac diazocine **3** and the derivatives **44** and **54** are all in the range of 70 min. to 80 min at neutral pH while the values of the aniline derivative **58** and the *N*-formyl diazocine **46** are significantly higher. The deprotonated benzoic acid derivative **54** exhibits increased thermal half-life at pH 3.5 compared to neutral pH. Meanwhile, at pH 3.5 the protonated aniline derivative **58** exhibits an accelerated thermal relaxation compared to neutral pH.

Table 5.4: Photochemical properties of unsubstituted *N*-Ac diazocine **3** and new *N*-Ac diazocine derivatives **44** and **54** at neutral pH and **58** and *N*-formyl diazocine **46** in aqueous media at different pH. Data were determined via UV-vis and NMR spectroscopy.

	$\lambda_{max}(Z)$	$\lambda_{max}(E)$	$t_{1/2}$ (25 °C)	$\Gamma_{Z\rightarrow E}$ (405 nm)	$\Gamma_{Z\rightarrow E}$ (530 nm)
	nm		min	%	
3	393	502	72.8	72	>99
44	394	502	69.6	70	>99
46	393	500	198	69	>99
54 at pH 9	392	502	106.4	48	>99
54 at pH 7.4	392	505	78.2	53	>99
58 at pH 3.5	392	495	118.0	62	>99
58 at pH 7.4	392	489	162.5	37	>99

Since *N*-Ac diazocines are structurally similar to known inhibitor THB for testosterone synthesizing enzyme 17ßHSD3 the unsubstituted system has been examined as potential inhibitor for intracellular testosterone synthesis but unfortunately showed no significant effect.[166] Nevertheless, new *N*-Ac diazocine derivatives **45, 49-52, 54** and **60** were used as potential inhibitors for 17ßHSD3 inhibition. While most of the examined *N*-Ac diazocine derivatives showed no significant inhibiting effect on intracellular testosterone production, the two derivatives **50** and **52** showed promising inhibiting behavior in the range of known inhibitor THB (**figure 5.2**). However, inhibition was independent from the switching of used *N*-Ac diazocines between actually considered biologically inactive Z- and considered biologically active E-configurations. A possible reason for this could be insufficient steric hinderance of the use inhibitors or excessive flexibility of the addressed enzymatic binding pocket. Both reasons would ensure, that inhibition takes place regardless of the configuration present.

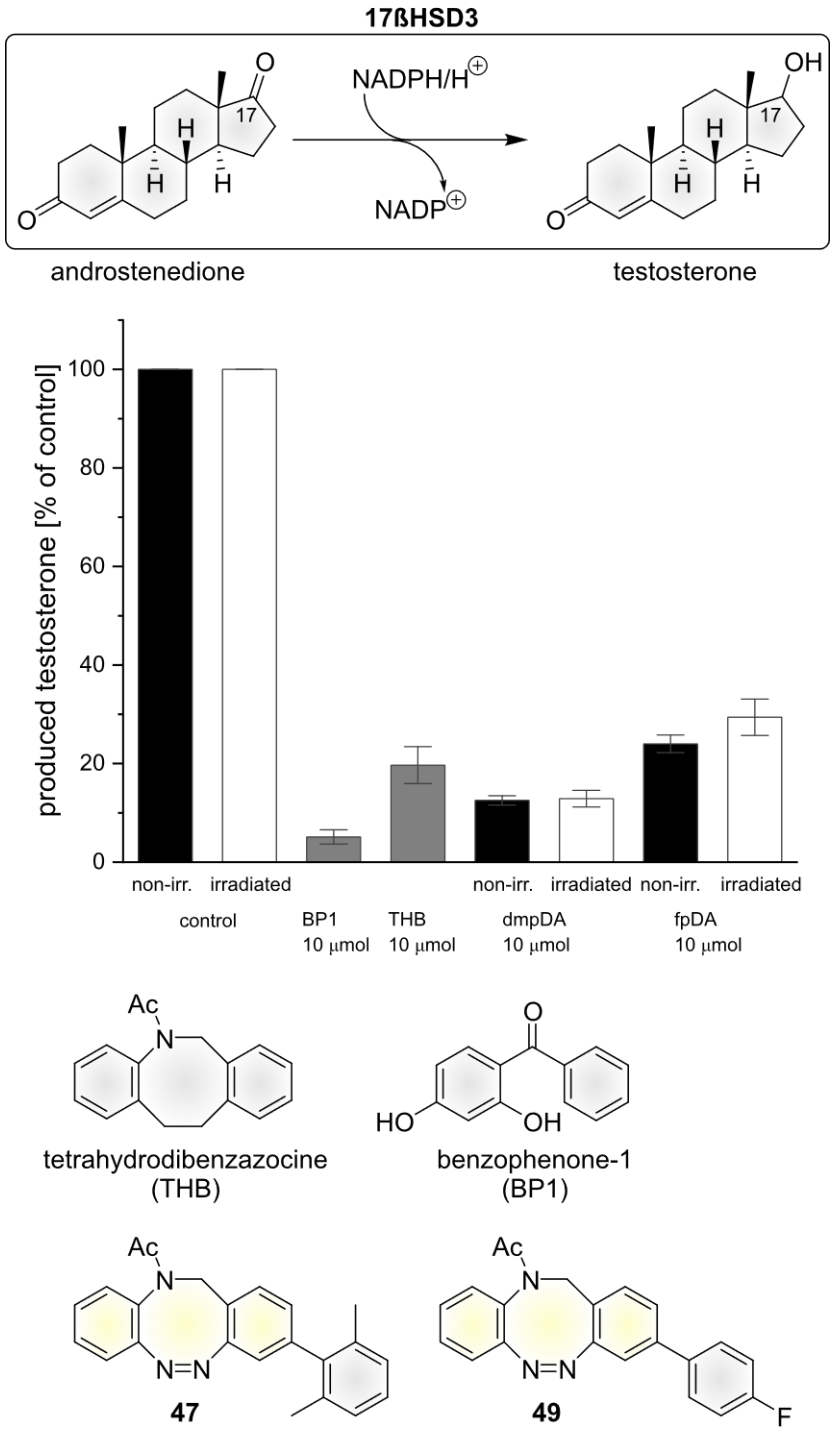

Figure 5.2: New *N*-Ac diazocine derivatives **50** and **52** show great inhibition of 17ßHSD3 enzyme activity in the range of known inhibitors THB and BP1.

6. Outlook

In this work the chiroptical properties of racemic DID diastereomer were investigated. Furthermore, new substituted DID derivatives have been synthesized as precursors for further functionalization. Based on the results included in this work, new conceivable follow-up projects will arise. Due to their very different switching properties, the DID diastereomers can be considered for numerous applications. The *meso*-DID offers incredibly short thermal half-lives in the range of milliseconds to seconds and could therefore be suitable as actuator for artificial molecular machines where high frequency switching is required. One conceivable application here is as a drive unit for light-driven molecular pumps.

In contrast, *rac*-DID offers thermal relaxation half-lives over a span of days depending on the substituents. One possibility of application is the incorporation into mechanoresponsive materials, which serve to indicate mechanical stress within a material by color changes for the human eye.[206] Therefore, the targeted materials have to be coated with a thin polymer film containing the polymerized DID moiety. Vinylated derivatives of parent diazocine have already been incorporated in similar materials via solvent-free initiated chemical vapor deposition (iCVD).[66,67,207,208] Vinylated DIDs, which would be accessible via STILLE-coupling or active ester functionalization, would be suitable materials for this purpose (**scheme 6.1a**). In order to utilize the intrinsic chirality of *rac*-DIDs, they could be incorporated into liquid crystalline structures to selectively induce or influence liquid crystalline phases in smart materials as has already been done with azobenzenes.[45] Furthermore, *rac*-DID could be incorporated into chiral helical structures to affect extent of their chirality to be applied as selective chiral catalysts for asymmetric synthesis (**scheme 6.1b**).

Enlargement of the delocalized π-electron system of a photoswitch leads to a bathochromic shift of n-π^*-absorptions bands required for photoisomerization.[15,56] In previous work the π-electron system of parent diazocine has already been extended via STILLE-coupling of tetrahalogenated diazocines with stannafluorenes leading to an extended switching motion improved power transmission.[100,105] The tetrabrominated DID could also be used as building block for π-electron system enlargement since systematic elimination of conformational and rotational degrees of freedom lead to unidirectional motion and improved light to chemical energy conversion (**scheme 6.1c**). In combination with increased switching motion would lead to powerful directional power transmission. This system could be applied either as molecular pincer or incorporated in polymers after being functionalized with polymerizable substituents.

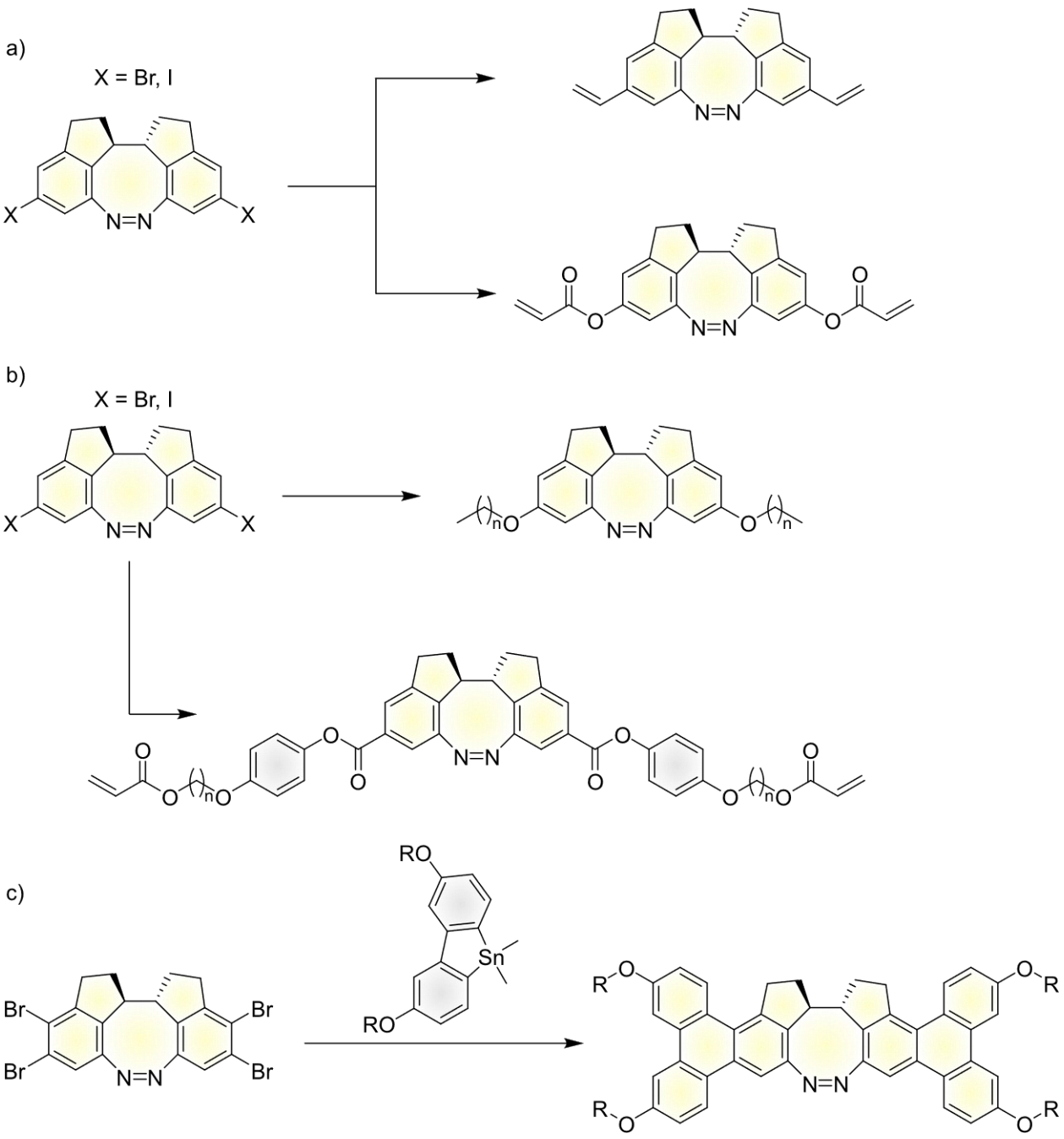

Scheme 6.1: a) Vinylation of DIDs as preparation for incorporation into polymer films. b) Functionalization of DIDs for application in light controllable liquid crystals or chiroptical helical switches. c) Enlargement of π-electron system via STILLE-coupling with stannafluorenes for application as molecular pincer or photoswitch with increased power transmission in smart materials.

Nitrogen-bridged diazocines have shown to be promising candidates for application in photopharmacology. To bring these new photoswitches into application one possible approach is the azologization of already known biologically active compounds. Here, functional groups in the core of the drug are replaced by an azo group to transform the molecule into a light-controllable active ingredient.[169] Since there are many examples of drugs containing tricyclic core units with a side chain attached to the core via either amine or amide bond the replacement of the tricyclic core unit by a nitrogen-bridged diazocine is a promising approach in the design and development of new photopharmacophores (**scheme 6.2**).

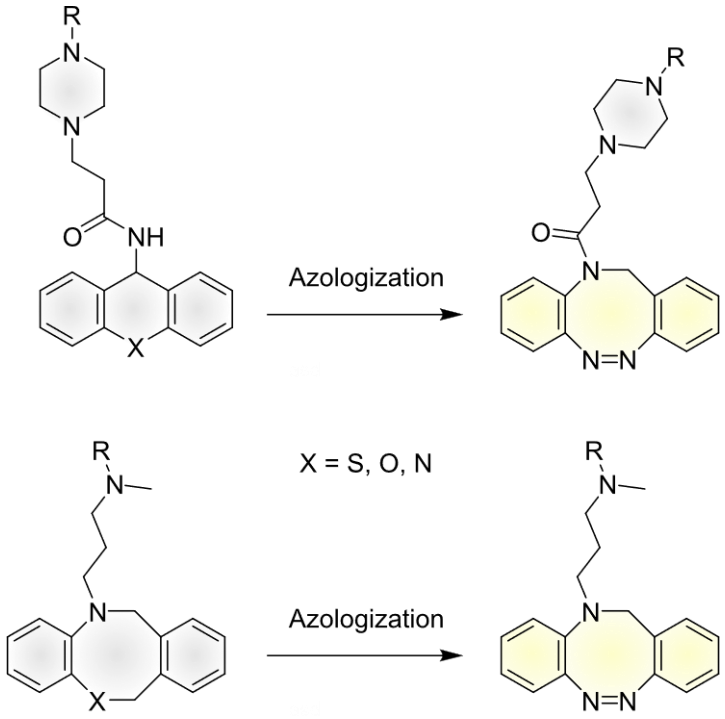

Scheme 6.2: Azologization of known biologically active compounds by replacement of the tricyclic core by a nitrogen-bridged diazocine moiety to turn them into photopharmacophores.

However, the development of new *N*-Ac diazocine based photoswitchable molecules is limited to either substitution at the bridging nitrogen or monofunctionalization since until now only monosubstituted *N*-Ac diazocines are accessible in sufficient amounts. Therefore, for double-sided substitution of *N*-Ac diazocines a new improved synthesis procedure is required. In this work *o*-nitrotoulene-based building blocks were used. These turned out to be suitable for established synthesis path if amine bond was not weakened by electron withdrawing substituents at both building blocks as *o*-nitrotoluenes are known as photolabile protecting groups. Probably for this reason, after introduction of Fmoc-protecting group in the initial synthesis path, the photolabile *o*-nitrotoluene moiety was cleaved leaving only small amounts of desired Fmoc-protected intermediate. To overcome this problematic *o*-toluidine based building blocks could be used instead of *o*-nitrotoluenes (**scheme 6.3**). After bromination of benzylic position of *o*-toluidine building block Boc-protection of the amino function is required to ensure selective formation of nitrogen-bridge. The Fmoc-protecting group can then be used again to protect the bridging nitrogen atom since the low yields in the initial procedure are probably not caused due to low nucleophilicity of the nitrogen during the reaction but rather by the lability of the *o*-nitrotoluene to irradiation and subsequent cleaving. The use of two Boc-protected aniline building blocks offers the advantage that after acid induced deprotection no subsequent reduction is required since nitro-groups are not present in this synthesis path. Additionally, this opens the door for the use of substituents sensitive to reduction. From this point the established procedure containing oxidative azo condensation and subsequent exchange of

Fmoc-protecting group to the desired acetyl group can be applied. Although this proposed synthesis path is significantly longer than the previous approaches carried out within this work, the yields should improve significantly and allow double-sided derivatization of *N*-Ac diazocines.

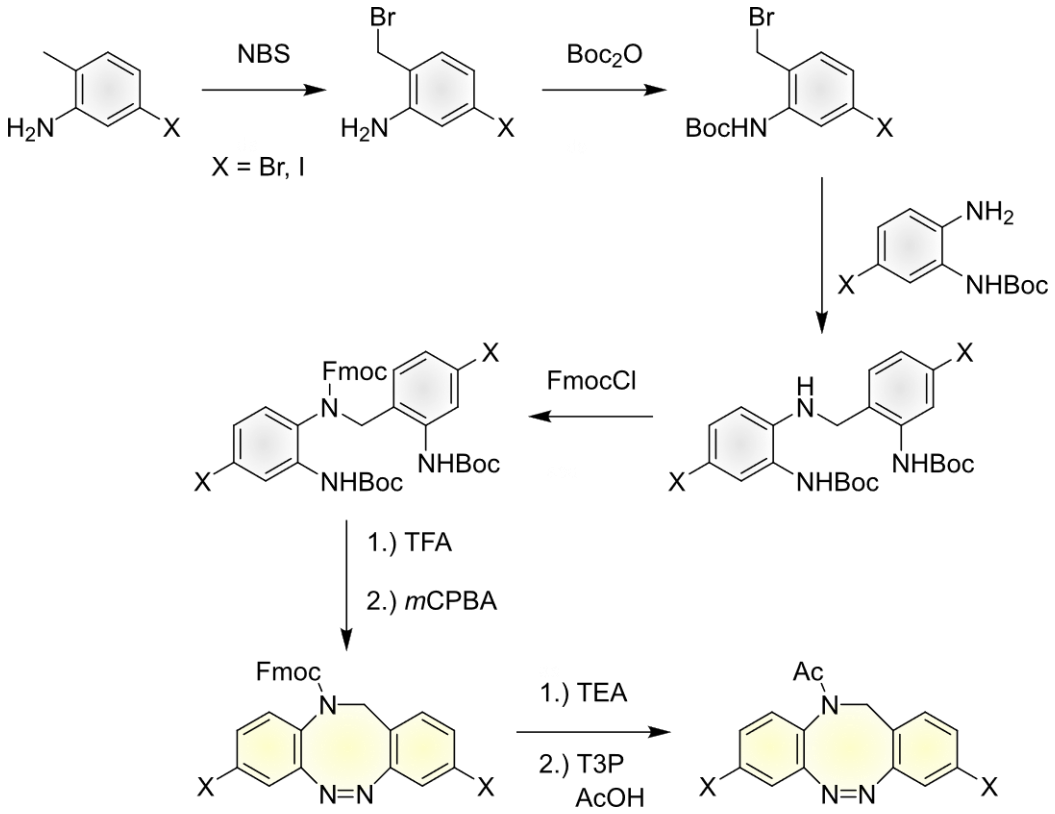

Scheme 6.3: New synthesis strategy for the preparation of double-side halogenated *N*-Ac diazocines based on the use *o*-toluidine derivatives instead of photolabile *o*-nitrotoluenes. For this approach Fmoc protecting group is again considered as suitable since it is most likely not responsible for the very low yields of dibrominated *N*-Ac diazocine via the initial pathway. Furthermore, reduction step limiting the range of accessible substituents is not required anymore.

If the disubstituted *N*-Ac diazocine is accessible in acceptable yields and can therefore be prepared to a higher extend, further double-side functionalizations via cross-coupling reactions are possible making *N*-Ac diazocines accessible for a far wider range of applications in the field of photopharmacology. One potential approach in this field is the linkage to biologically active compounds or incorporation into biologically active substructures. A relatively new field of interest is the targeted degradation of targeted proteins via the proteolysis targeting chimeras (PROTACs) concept. In recent studies photoswitches have been used to synthesize light-controllable compounds applied in this field. *N*-Ac diazocines are predestined for application as photochemically targeting chimeras (PHOTACs) due to their superior switching behavior in aqueous media compared to azobenzenes and parent diazocine (**scheme 6.4**).[209]

Further derivatization of *N*-Ac diazocine could also lead to the synthesis of an “amino acid *N*-Ac diazocine” for incorporation into the peptide backbone targeting for control over protein folding and protein tertiary structure. This is an important field of current medical science since defective protein folding and protein aggregation are connected to the development of diseases like Creuzfeldt-Jakob disease or Alzheimer’s disease.[210,211]

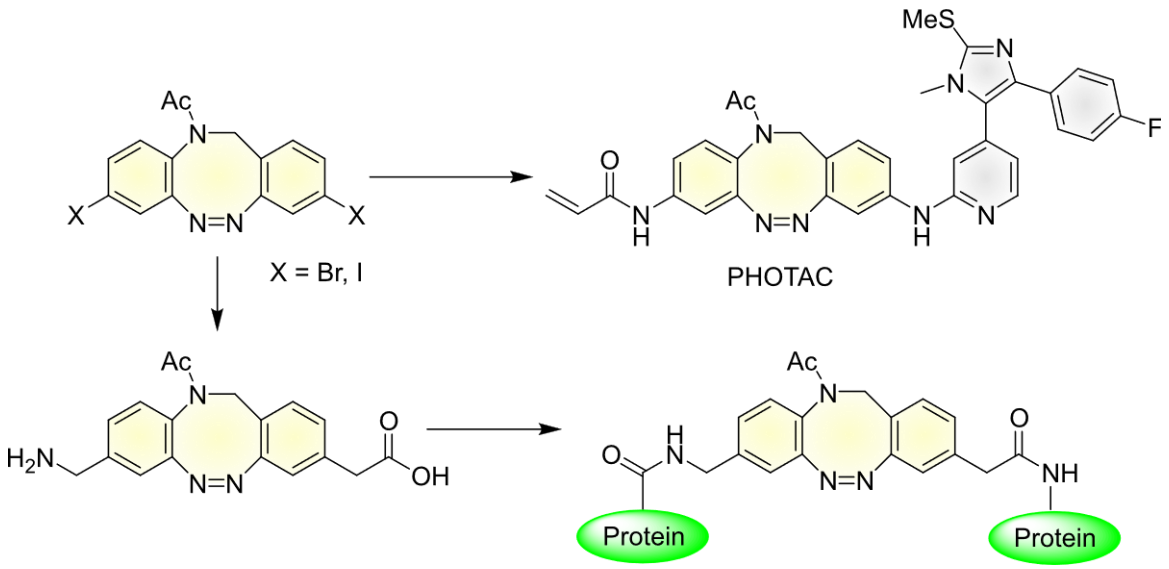

Scheme 6.4: Possible applications of disubstituted *N*-Ac diazocines after further derivatization as PHOTAC for disease treatment via targeted protein degradation or incorporated into peptide backbone for targeted studies of protein folding and control over protein activity.

7. Experimental Section

7.1 Chemicals

The chemicals used were purchased commercially and used without further processing.

Table 7.1: Overview of the chemicals used in this work.

Chemical (purity)	Supplier
(2-Bromophenyl)boronic acid	BLDpharm
(2-Formylphenyl)boronic acid	BLDpharm
(4-Fluorophenyl)boronic acid	TCI
1,1'-Bis(diphenylphosphino)ferrocene	TCI
1,3,5,7-Tetramethyl-1,3,5,7-tetravinylcyclotetrasiloxane	Manchester Organics
1,4 Dioxane	laboratory stock
1,4-Dioxane, dry	Acros Organics
2,6-Dimethylphenylboronic acid	Alfa Aesar
2-Benzyl-4,4,5,5-tetramethyl-1,3,2-dioxoborolane	BLDpharm
2-Boronobenzoic acid	BLDpharm
2-Nitroaniline	VWR
2-Nitrobenzaldehyde (>99%)	Acros Organics
2-Nitrobenzylbromide	TCI
3-Bromoaniline	Alfa Aesar
4-Bromo-1-methyl-2-nitrobenzene (98%)	Apollo Scientific
4-Bromo-2-nitroaniline (98%)	TCI
4-Bromo-2-nitrobenzaldehyde	BLDpharm
4-Iodo-1-methyl-2-nitrobenzene (99.7%)	Apollo Scientific
4-Iodo-2-nitroaniline (95%)	abcr
4-Nitroindane	Sigma Aldrich
5-Bromo-2-nitroaniline	Fluorochem
9-Fluorenylmethoxycarbonyl chloride (99%)	abcr
Acedic anhydride (99.5%)	Grüssing
Acetic Acid (99.5%)	Grüssing
Acetone	laboratory stock
Acetone (ACS grade)	Sigma Aldrich
Acetonitrile	laboratory stock
Acetonitrile, dry	Acros Organics
Acetyl chloride (98%)	Merck
Barium hydroxide octahydrate (97%	abcr
Benzoyl peroxide (75%)	Merck

Bis(triphenylphosphine)palladium chloride	Matrix Scientific
Bis(tri-*tert*-butylphosphine)palladium(0)	BLDpharm
Borane tetrahydrofurane complex (1M)	Sigma Aldrich
Bromine (99%)	Sigma Aldrich
Caesium carbonate (99.9%)	Fisher Scientific
Carbon tetrachloride	VWR
Celite® 545	VWR
Chloroform	laboratory stock
Copper(I)bromide	Alfa Aesar
Copper(I)iodide (>99%)	Merck
Copper(II)chloride (99.9%)	Acros Organics
Cyclohexane	laboratory stock
Dichloromethane	laboratory stock
Dichloromethane, abs.	laboratory stock
Dimethylacetamide (99.5%)	Acros Organics
Diethyl ether	laboratory stock
Dimethylformamide, dry	Acros Organics
Diphenylamine	Sigma-Aldrich
Di-*tert*-butyl dicarbonate (95%)	Fluka
Ethanol	laboratory stock
Ethyl acetate	laboratory stock
Hydrobromic acid (48%)	Alfa Aesar
Hydrochloric Acid (37%)	Grüssing
Hydrogen	laboratory stock
JohnPhos	Sigma Aldrich
Magnesium sulfate (99%)	Grüssing
m-Chloroperbenzoic acid	Sigma Aldrich
Methanol	laboratory stock
Methyl acrylate	TCI
N,N-Diisopropylamine (95%)	abcr
N-Bromosuccinimide (95%)	Merck
N-Iodosuccinimide	laboratory stock
Nitric acid (100%)	Merck
Nitrogen	laboratory stock
n-Pentane	laboratory stock
Palladium on activated charcoal (10% Pd)	Sigma Aldrich
Palladium(II) acetate (47% Pd)	Fluka
Palladium(II) bromide	Sigma Aldrich
Phenylacetylene (98%)	Sigma Aldrich

Phenylboronic acid	Acros
Potassium butoxide (>97%)	TCI
Potassium carbonate	Grüssing
Potassium hydroxide	Grüssing
Pyridine-4-boronic acid	BLDpharm
Sodium bicarbonate (99%)	Grüssing
Sodium chloride (99%)	Grüssing
Sodium dithionite	VWR
Sodium hydride (60%)	Acros
Sodium hydroxide (99%)	Grüssing
Sodium nitrite (>99%)	Merck
Sodium sulfate (99%)	Grüssing
Sodium thiosulfate	Grüssing
Sulfuric acid (99%)	laboratory stock
T3P	abcr
tert-Butyl carbamate (>98%)	TCI
Tetrahydrofurane (>99.9%)	Riedel-de-Haen
Tetrahydrofurane, dry	laboratory stock
Tetrakis(triphenylphosphine)palladium(0)	Matrix Scientific
Tetra-*n*-butylammonium fluoride	TCI
Tin dichloride	Sigma Aldrich
Toluene	laboratory stock
Triethylamine (99%)	laboratory stock
Triethylsilane	TCI
Trifluoroacetic acid (99%)	Sigma Aldrich
Trifluoromethanesulfonic acid	TCI
Triphenylphosphine (98.5%)	TCI
Triphenyltin chloride	Alfa Aesar
Tris(dibenzylideneacetone)dipalladium(0)	TCI
Vinyltributyltin (97%)	Sigma Aldrich
Xantphos Pd G3	Sigma Aldrich
Zinc cyanide (98%)	Alfa Aesar
Zinc powder	Merck

7.2 Analytical Equipment

7.2.1 Melting Point

Melting points were measured with a Melting Point B-560 (Büchi) in melting point tubes without further correction.

7.2.2 NMR Spectroscopy

NMR spectra were measured in deuterated solvents (Deutero). The spectra were referenced to the following solvent residual signals:

solvent	degree of deuteration	^{1}H signal ppm	^{13}C signal ppm
acetone-d_6	99.8%	2.05 (quintet)	29.84 (septet)
chloroform-d_1	99.8%	7.26 (singlet)	77.16 (triplet)
acetonitrile-d_3	99.8%	1.94 (singlet)	1.32 (septet), 118.26 (multiplet)
water-d_2	99.9%	4.79 (singlet)	
tetrahydrofurane-d_8	99.8	3.58 (singlet), 1.73 (singlet)	25.37 (quintet), 67.57 (quintet),

The spectra were recorded with a Bruker DRX 500 (^{1}H-NMR: 500 MHz, ^{13}C-NMR: 125 MHz) and a Bruker AV 600 (^{1}H-NMR: 600 MHz, ^{13}C-NMR: 150 MHz). The multiplicities of the signals were abbreviated with a s (singlet), d (doublet), t (triplet), q (quartet), quint. (quintet), m (multiplet) and br. (broad) in addition for broad signals.

7.2.3 Mass Spectrometry

Mass spectra (EI) and high-resolution mass spectra (HR-EI) were measured with an AccuTOF-GCv 4G (Joel) time of flight mass spectrometer with an ionization energy of 70 eV. HR-ESI mass spectra were measured with a Q Exactive Plus Hybrid Quadrupole Orbitrap (Thermo Scientific) ESI mass spectrometer.

7.2.4 High Performance Liquid Chromatography

The separation of enantiomers was performed with an Agilent HPLC System from the 1100 series with autosampler and fraction collector. As column a Daicel Chiracel OD-H column was used with a tris(dimethylphenylcarbamate) cellulose stationary phase and *n*-heptane/isopropanol (98:2) as eluent.

7.2.5 IR Spectroscopy

Infrared spectra were measured with a Perkin-Elmer 1600 FT-IR spectrometer with an A531-G Golden-Gate-Diamond ATR unit. Signals were abbreviated with w (weak), m (medium) or s (strong) for its intensity.

7.2.6 UV-vis Spectroscopy

UV-vis spectra were measured with a Shimadzu UV 2600 I UV-vis spectrometer and a Perkin Elmer Lambda 14 UV-vis spectrometer. Quartz cuvettes of 10 mm optical path length were used.

7.2.7 Thin layer Chromatography and Column Chromatography

Silica gel (Merck, particle size 0.040-0.063 mm) was used for column chromatography purifications. R_f values were determined via thin layer chromatography on Polygram® SilG/UV254 (Macherey Nagel, 0.2 mm particle size). For detection of the different fractions a CAMAG UV light source with a wavelength of 254 nm was used.

7.2.8 Light sources

For irradiation different custom-built light sources with a wavelength of 385 nm, 405 nm, 420 nm, 530 nm and 590 nm (Sahlmann Photochemistry Solutions & in-house built) were used.

7.2.9 CD Spectroscopy

The CD data were recorded with a Jasco J-720 spectropolarimeter. Quartz cuvettes of 1 mm and 10 mm optical path length were used.

7.2.10 Optical Rotation

Optical rotations and specific rotations were measured with an Anton Paar MCP5100 modular polarimeter (sodium D-line: 589 nm, cell length 100 mm).

7.2.11 X-ray Crystallography

Data collection was performed with a XtaLAB Synergy, Dualflex, HyPix diffractometer. The structure was solved with SHELXT[212] and refined with SHELXL[213] refinement package using Least Squares minimization.

7.3 Syntheses

7.3.1 Synthesis of 2-nitro-*N*-(2-nitrobenzyl)aniline (4)

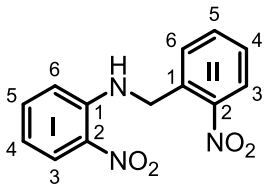

2-Nitroaniline (**1**, 4.57 g, 33.1 mmol) and 2-nitrobenzaldehyde (**2**, 5.00 g, 33.1 mmol) were dissolved in methanol and a catalytic amount of conc. sulfuric acid was added. The reaction mixture was stirred under reflux for 3 h and after cooling filtered under reduced pressure. The residue was washed with ethanol to obtain the imine intermediate as yellow solid. This was dissolved in dry THF under a nitrogen atmosphere and cooled to 0°C. Borane-tetrahydrofuran complex (8.00 mL, 8.00 mmol) was added dropwise and the reaction mixture was stirred at 0 °C for 1 h and for 16 h at room temperature. The reaction mixture was poured on ice and the formed precipitate was filtered off. The precipitate was dried under reduced pressure to obtain the impure product as yellow solid (5.43 g, 19.9 mmol, 60% over two steps). Impurities could not be separated from the desired product as it decomposes during the purification.

melting point: 131.0 °C

^{1}H-NMR (500 MHz, $CDCl_3$, 298 K): δ = 8.52 (s, 1 H, N*H*), 8.22 (d, ^{3}J = 8.5 Hz, 1 H, Ar^{I}-*H*-3), 8.16 (d, ^{3}J = 7.5 Hz, 1 H, Ar^{II}-*H*-3), 7.60 (d, ^{3}J = 7.0 Hz, 1 H, Ar^{II}-*H*-4), 7.57 (d, ^{3}J = 7.0 Hz, 1 H, Ar^{II}-*H*-6), 7.53-7.32 (m, 2 H, Ar^{I}-*H*-5, Ar^{II}-*H*-5), 6.76-6.68 (m, 1 H, Ar^{I}-*H*-4), 6.65 (d, ^{3}J = 8.5 Hz, 1 H, Ar^{I}-*H*-6), 4.99 (d, ^{3}J = 5.5 Hz, 2 H, CH_2) ppm.

^{13}C{^{1}H}-NMR (125 MHz, $CDCl_3$, 298 K): δ = 148.0 (Ar^{II}-*C*-2), 144.8 (Ar^{II}-*C*-1), 136.4 (Ar^{II}-*C*-5), 134.1 (Ar^{II}-*C*-4), 133.6 (Ar^{I}-*C*-1), 132.7 (Ar^{I}-*C*-2), 128.8 (Ar^{II}-*C*-6), 128.6 (Ar^{I}-*C*-5), 127.0 (Ar^{I}-*C*-3), 125.6 (Ar^{II}-*C*-3), 116.4 (Ar^{I}-*C*-4), 113.9 (Ar^{I}-*C*-6), 44.5 (-*C*H_2) ppm.

IR (ATR): $\tilde{\nu}$ = 3389 (m), 3093 (w), 2849 (w), 1611 (m), 1574 (m), 1505 (s), 1444 (w), 1426 (w), 1334 (s), 1288 (m), 1242 (s), 1153 (s), 1041 (m), 988 (w), 950 (w), 898 (w), 864 (s), 777 (m), 727 (s), 696 (m), 666 (m), 586 (w), 543 (m), 524 (s) cm^{-1}.

HR-MS (ESI, DCM): *m/z* $[M+H]^+$ calculated for $C_{13}H_{11}O_4N_3+H^+$: 274.08201; found: 274.08223 ± 0.83 ppm.

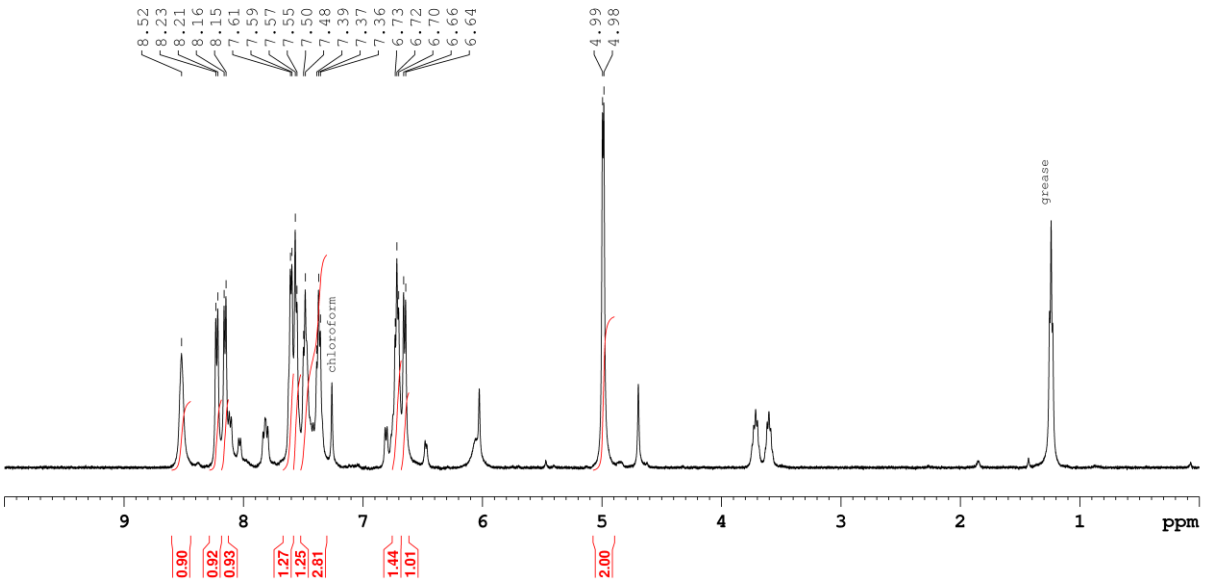

Figure 7.1: 500 MHz ^{1}H-NMR spectrum of 2-nitro-*N*-(2-nitrobenzyl)aniline (**4**) in $CDCl_3$. Unlabeled signals represent impurities that could not be separated since the target molecule decomposes during purification.

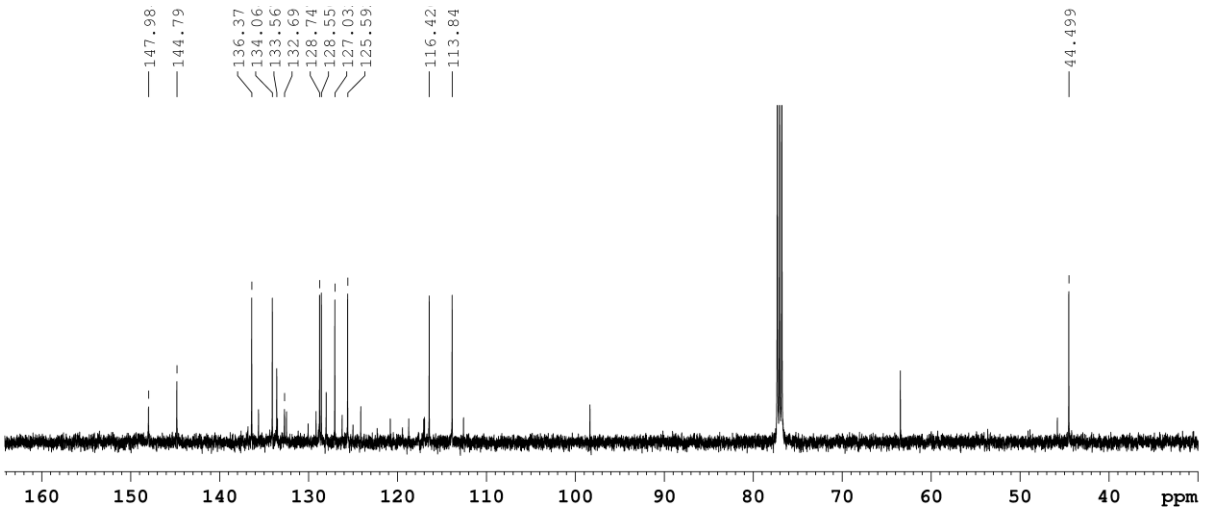

Figure 7.2: 125 MHz ^{13}C-NMR spectrum of 2-nitro-*N*-(2-nitrobenzyl)aniline (**4**) in $CDCl_3$. Unlabeled signals represent impurities that could not be separated since the target molecule decomposes during purification.

7.3.2 Synthesis of *N*-(2-nitrobenzyl)-*N*-(2-nitrophenyl)acetamide (5)

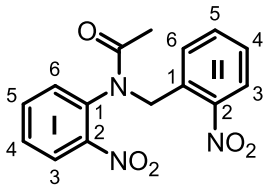

Method A: Imine condensation approach

2-Nitro-*N*-(2-nitrobenzyl)aniline (**4**, 500 mg, 1.83 mmol) was dissolved in acetic anhydride (24 mL) and acetyl chloride (4.73 g, 4.3 mL, 60.3 mmol) was added. The reaction mixture was stirred over 16 h at room temperature and poured on ice. The formed precipitate was filtered off under reduced pressure. The filtered off solid was washed with dem. water and dried under reduced pressure to give the product as yellow solid (217 mg, 689 µmol, 38%).

Method B: Amidate anion approach

Sodium hydride (88.0 mg, 2.20 mmol) was dispersed in dry DMF (2 mL) under a nitrogen atmosphere at 0 °C. *N*-(2-nitrophenyl)acetamide (**16**, 200 mg, 1.10 mmol) dissolved in dry DMF (5 mL) was added dropwise and the mixture was stirred for 20 min. at room temperature, then 2-nitrobenzyl bromide (**17**, 475 mg, 2.20 mmol) dissolved in dry DMF (5 mL) was added dropwise and the reaction mixture was stirred for 16 h. The reaction mixture was quenched with saturated ammonium chloride solution and extracted twice with 50 mL diethyl ether. The combined organic layers were washed with brine, dried over magnesium sulfate and the solvent was evaporated under reduced pressure. The product could be obtained via column chromatography on silica (cyclohexane/ethyl acetate 5:1, R_f = 0.12) as yellow solid (344 mg, 1.08 mmol, 98%).

melting point: 134.0 °C

^{1}H-NMR (600 MHz, $CDCl_3$, 298 K): δ = 7.98 (d, ^3J = 7.9 Hz, 1 H, Ar^I-*H*-3), 7.84 (d, ^3J = 8.2 Hz, 1 H, Ar^{II}-*H*-3), 7.69 (d, ^3J = 7.5 Hz, 1 H, Ar^{II}-*H*-6), 7.62-7.56 (m, 2 H, Ar^I-*H*-5, Ar^{II}-*H*-5), 7.54 (t, ^3J = 7.5 Hz, 1 H, Ar^I-*H*-4), 7.43 (t, ^3J = 7.7 Hz, 1 H, Ar^I-*H*-4), 7.12 (d, ^3J = 7.7 Hz, 1 H, Ar^I-*H*-6), 5.48 (d, ^2J = 15.5 Hz, 1 H, C*H*$_2$), 4.93 (d, ^2J = 15.6 Hz, 1 H, C*H*$_2$'), 1.92 (s, 3 H, C*H*$_3$) ppm.

^{13}C{^{1}H}-NMR (150 MHz, $CDCl_3$, 298 K): δ = 170.6 (*C*=O), 150.0 (Ar^{II}-*C*-1), 148.9 (Ar^{II}-*C*-2), 146.8 (Ar^I-*C*-2), 135.8 (Ar^I-*C*-1), 134.4 (Ar^I-*C*-5), 133.5 (Ar^{II}-*C*-5), 132.1 (Ar^{II}-*C*-6), 131.5 (Ar^I-*C*-6), 131.3 (Ar^{II}-*C*-1), 129.9 (Ar^I-*C*-4), 128.8 (Ar^{II}-*C*-4), 125.9 (Ar^I-*C*-3), 124.6 (Ar^{II} *C*-3), 48.7 (-*C*H$_2$), 22.5 (-*C*H$_3$) ppm.

IR (ATR): $\tilde{\nu}$ = 3073 (w), 2162 (w), 1978 (w), 1735 (w), 1668 (s), 1602 (m), 1580 (w), 1515 (s), 1482 (w), 1446 (w), 1420 (w), 1393 (m), 1345 (s), 1298 (s), 1271 (m), 1146 (w), 1018 (w), 979 (w), 896 (w), 854 (m), 796 (s), 785 (s), 748 (w), 732 (s), 706 (m), 679 (w), 639 (w), 614 (w), 575 (m) cm^{-1}.

HR-MS (ESI, EtOAc/MeOH): *m/z* $[M+H]^+$ calculated for $C_{15}H_{13}O_5N_3+H^+$: 316.09280; found: 316.09273 ± 0.23 ppm.

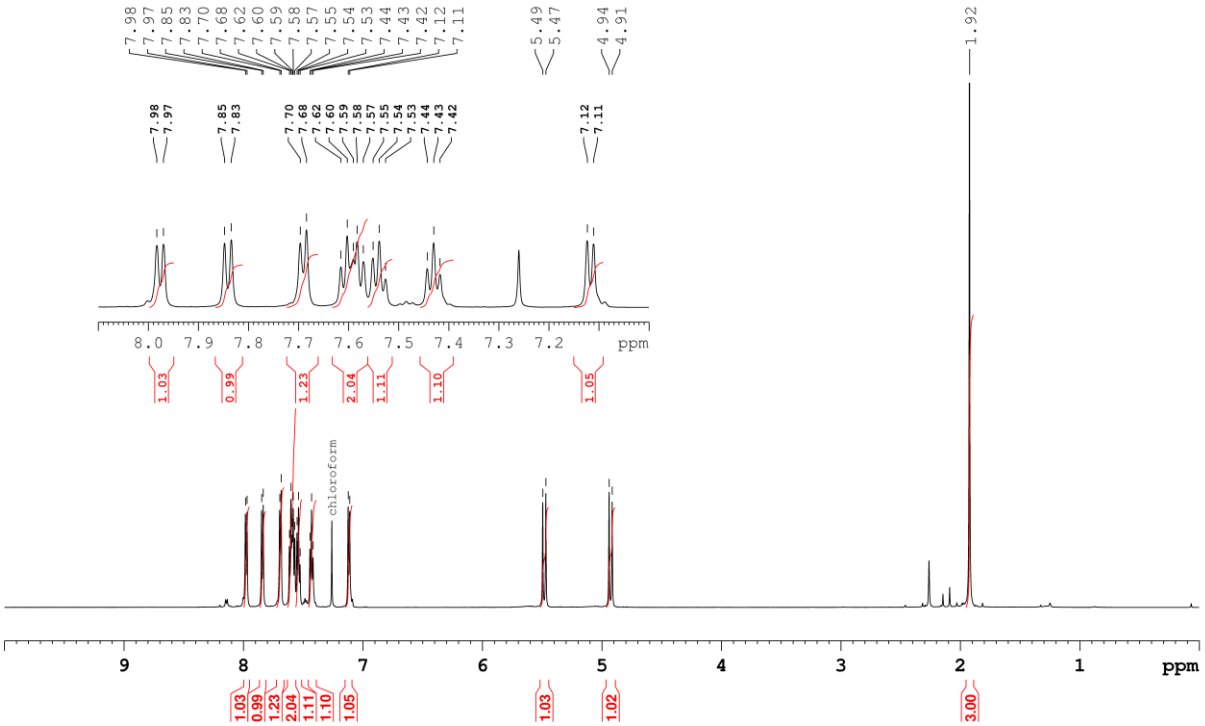

Figure 7.3: 600 MHz ^{1}H-NMR spectrum of *N*-(2-nitrobenzyl)-*N*-(2-nitrophenyl)acetamide (**5**) in $CDCl_3$.

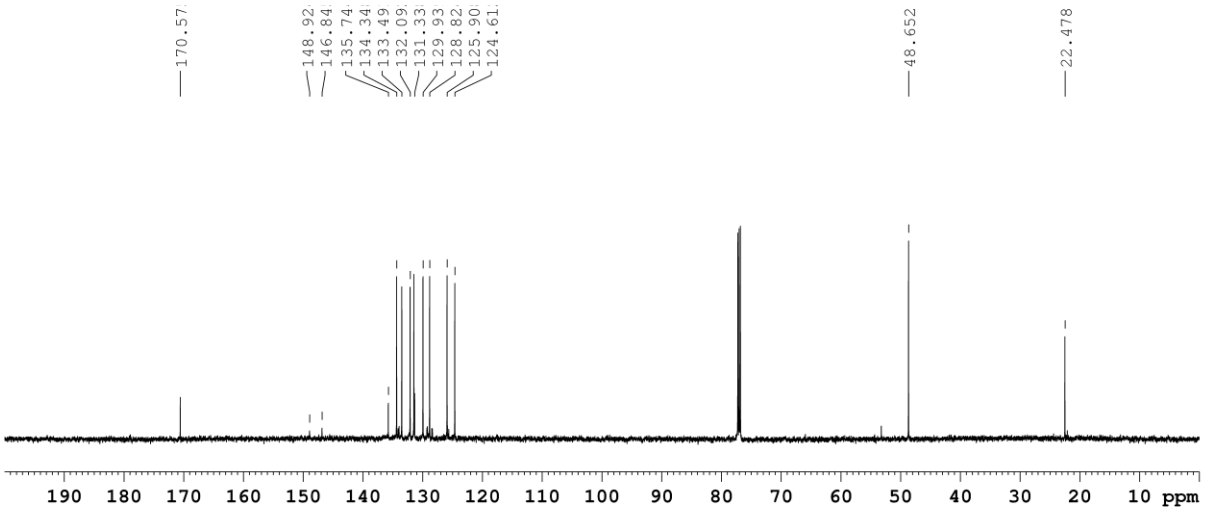

Figure 7.4: 150 MHz ^{13}C-NMR spectrum of *N*-(2-nitrobenzyl)-*N*-(2-nitrophenyl)acetamide (**5**) in $CDCl_3$.

7.3.3 Synthesis of (*Z*)-1-(dibenzo[*c,g*][1,2,5]triazocin-11(12*H*)-yl)ethan-1-one (3)

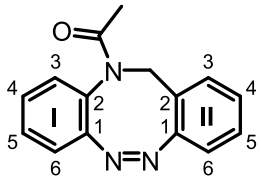

N-(2-nitrobenzyl)-*N*-(2-nitrophenyl)acetamide (**5**, 160 mg, 627 µmol) was dissolved in ethanol and a catalytic amount of palladium on charcoal was added. The reaction mixture was stirred under a hydrogen atmosphere at room temperature for 2 h. The reaction mixture was filtered through Celite® and the solvent was evaporated under reduced pressure giving the desired dianiline intermediate. The solid was dissolved in acetic acid (15 mL) and *m*CPBA (280 mg, 1.25 mmol) dissolved in acetic acid (15 mL) was added dropwise within 2 h. The reaction mixture was stirred for 16 h and the solvent was evaporated under reduced pressure. 100 mL dichloromethane and 100 mL half concentrated sodium bicarbonate solution were added to the residue. The organic layer was separated and the aqueous layer was extracted with 50 mL dichloromethane twice. The combined organic layers were dried over magnesium sulfate and the solvent was evaporated under reduced pressure. After column chromatography on silica (cyclohexane/ethyl acetate 2:1, R_f = 0.17) the product could be obtained as yellow solid (86.7 mg, 345 µmol, 55%.)

melting point: 134.0 °C

^{1}H-NMR (600 MHz, acetone-d_6, 298 K): δ = 7.35 (td, ^3J = 7.3 Hz, ^4J = 1.4 Hz, 1 H, Ar^I-*H*-5), 7.33-7.22 (m, 3 H, Ar^{II}-*H*-5, Ar^I-*H*-6, Ar^I-*H*-4), 7.20 (d, ^3J = 7.6 Hz, 1 H, Ar^{II}-*H*-3), 7.12 (td, ^3J = 7.6 Hz, ^4J = 0.9 Hz, 1 H, Ar^{II}-*H*-4), 6.99 (dd, ^3J = 7.9 Hz, ^4J = 1.1 Hz, 1 H, Ar^I-*H*-3), 6.89 (d, ^3J = 7.8 Hz, 1 H, Ar^{II}-*H*-6), 5.03 (d, ^2J = 14.5 Hz, 1 H, CH_2), 4.30 (d, ^2J = 14.5 Hz, 1 H, CH_2'), 1.80 (s, 3 H, CH_3) ppm.

^{13}C{^{1}H}-NMR (150 MHz, acetone-d_6, 298 K): δ = 169.5 (*C*=O), 156.4 (Ar^{II}-*C*-1), 154.3 (Ar^I-*C*-1), 130.8 (Ar^{II}-*C*-3), 130.09 (Ar^I-*C*-6), 130.01 (Ar^{II}-*C*-5), 129.5 (Ar^{II}-*C*-2), 129.21 (Ar^I-*C*-2), 129.17 (Ar^I-*C*-4), 128.4 (Ar^{II}-*C*-4), 119.91 (Ar^I-*C*-3), 119.79 (Ar^{II}-*C*-6), 52.1 (-*C*H$_2$), 23.1 (-*C*H$_3$) ppm.

IR (ATR): $\tilde{\nu}$ = 2920 (w), 2870 (w), 1651 (s), 1591 (w), 1512 (w), 1475 (m), 1439 (m), 1348 (s), 1372 (m), 1341 (s), 1289 (m), 1242 (m), 1155 (w), 1100 (w), 1078 (w), 1043 (m), 975 (m), 952 (m), 909 (w), 834 (w), 782 (m), 768 (s), 755 (s), 741 (s), 685 (m), 624 (m), 558 (s), 533 (w), 431 (s) cm^{-1}.

HR-MS (ESI, DCM): *m/z* [M+H]$^+$ calculated for $C_{15}H_{13}ON_3$+H$^+$: 252.11314; found: 252.11281 ± 1.31 ppm.

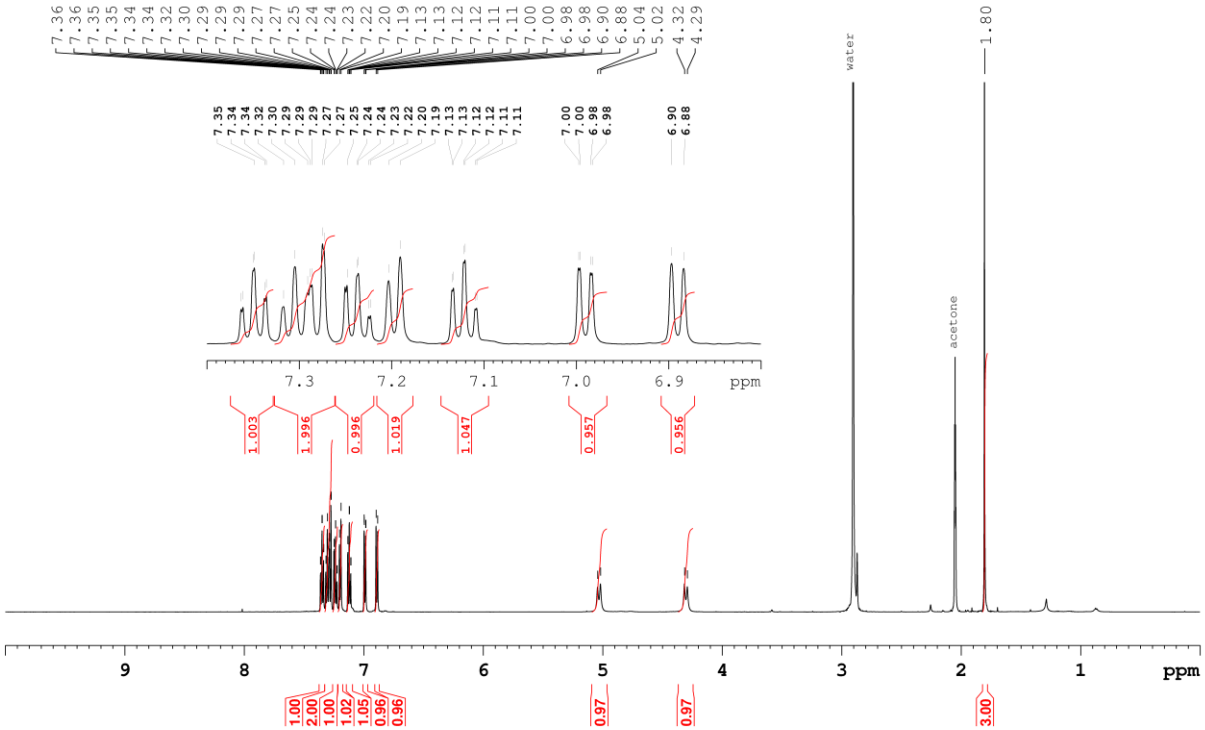

Figure 7.5: 600 MHz ^{1}H-NMR spectrum of *(Z)*-1-(dibenzo[*c,g*][1,2,5]triazocin-11(12*H*)-yl)ethan-1-one (**3**) in acetone-d_6.

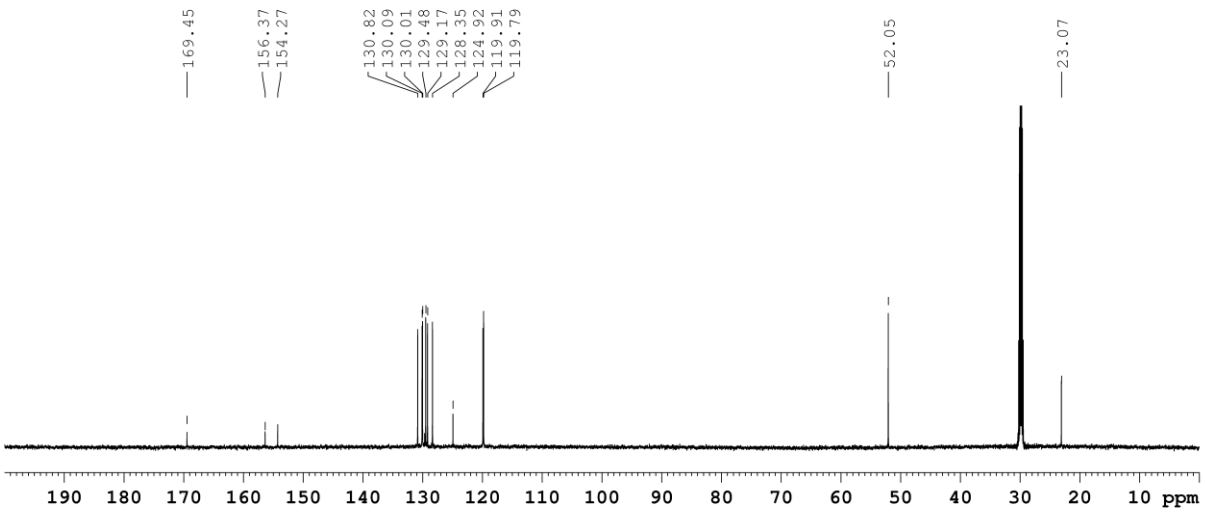

Figure 7.6: 150 MHz ^{13}C-NMR spectrum of *(Z)*-1-(dibenzo[*c,g*][1,2,5]triazocin-11(12*H*)-yl)ethan-1-one (**3**) in acetone-d_6.

7.3.4 Synthesis of 4-bromo-*N*-(4-bromo-2-nitrobenzyl)-2-nitroaniline (12) (prepared in supervised work by J. P. MIKOSCH)[188]

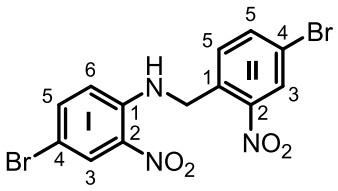

To a solution of 4-bromo-2-nitroaniline (**10**, 5.00 g, 23.0 mmol) and 4-bromo-nitrobanzaldehyde (**11**, 5.30 g, 23.0 mmol) in ethanol (50 mL) a few drops of acetic acid and magnesium sulfate were added and stirred under reflux for 3 h. The reaction mixture was filtrated under reduced pressure while still hot and the solvent was evaporated. The imine intermediate could be obtained as orange solid after purification via column chromatography on silica (ethyl acetate/cyclohexane 1:9, R_f = 0.40) which was dissolved in dry THF (10 mL) under a nitrogen atmosphere and cooled to 0 °C. Borane-tetrahydrofuran complex (0.80 mL, 0.80 mmol) was added dropwise and the reaction mixture was stirred at room temperature for 16 h. The reaction mixture was poured on ice and the formed precipitate was filtered off. The filtrate was dried over magnesium sulfate and the solvent was evaporated under reduced pressure. Column chromatography on silica (cyclohexane/ethyl acetate 9:1, R_f = 0.32) gave the impure solid as yellow solid (0.25 g, 0.58 mmol. 24% over two steps). Impurities could not be separated from the desired product as it decomposes during the purification.

melting point: 163.5 °C

^{1}H-NMR (500 MHz, acetone-d_6, 298 K): δ = 8.73 (br. s, 1 H, N*H*), 8.31 (d, ^4J = 2.1 Hz, 1 H, Ar^{II}-*H*-3), 8.27 (d, ^4J = 2.5 Hz, 1 H, Ar^{I}-*H*-3), 7.87 (dd, ^3J = 8.4 Hz, ^4J = 2.1 Hz, 1 H, Ar^{II}-*H*-5), 7.65 (d, ^3J = 8.3 Hz, 1 H, Ar^{II}-*H*-6), 7.53 (dd, ^3J = 9.2 Hz, ^4J = 2.7 Hz, 1 H, Ar^{I}-*H*-5), 6.94 (d, ^3J = 9.2 Hz, 1 H, Ar^{I}-*H*-6), 5.11 (d, ^3J = 6.9 Hz, 2 H, C*H*$_2$) ppm.

^{13}C{^{1}H}-NMR (125 MHz, acetone-d_6, 298 K): δ = 149.7 (Ar^{II}-*C*-2), 144.8 (Ar^{I}-*C*-1), 139.6 (Ar^{I}-*C*-5), 137.7 (Ar^{II}-*C*-5), 134.3 (Ar^{II}-*C*-1), 131.7 (Ar^{II}-*C*-6), 129.3 (Ar^{I}-*C*-3), 128.9 (Ar^{II}-*C*-3), 121.6 (Ar^{II}-*C*-4), 117.8 (Ar^{I}-*C*-6), 107.3 (Ar^{I}-*C*-4), 54.8 (-*C*H$_2$) ppm.

IR (ATR): $\tilde{\nu}$ = 3388 (w), 3097 (w), 2923 (w), 2854 (w), 1613 (m), 1561 (m), 1521 (s), 1498 (s), 1342 (m), 1291 (m), 1225 (s), 880 (s), 802 (s), 753 (s), 573 (m), 523 (s), 485 (w) cm^{-1}.

HR-MS (ESI, DCM): *m/z* [M+H]$^+$ calculated for $C_{13}H_9O_4N_3{}^{79}Br_2$+H$^+$: 428.89598; found: 429.09326 ± 0.11 ppm.

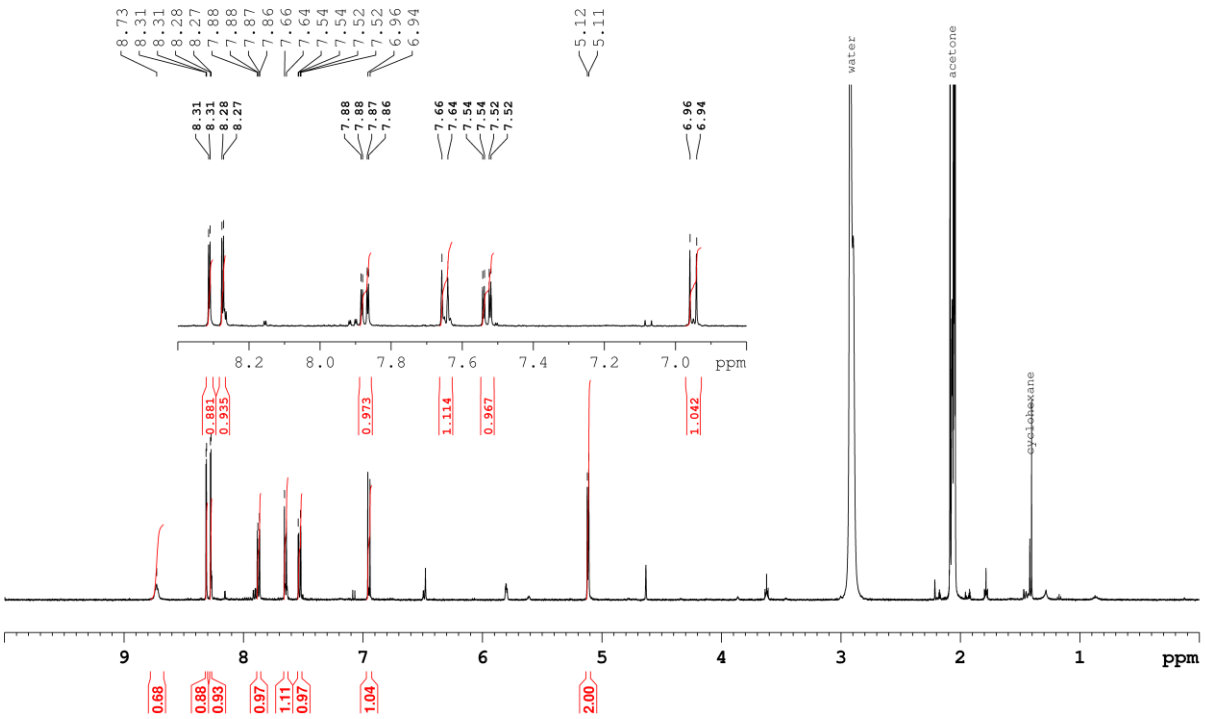

Figure 7.7: 500 MHz ^{1}H-NMR spectrum of 4-bromo-*N*-(4-bromo-2-nitrobenzyl)-2-nitroaniline (**12**) in acetone-d_6. Unlabeled signals represent impurities that could not be separated since the target molecule decomposes during purification.

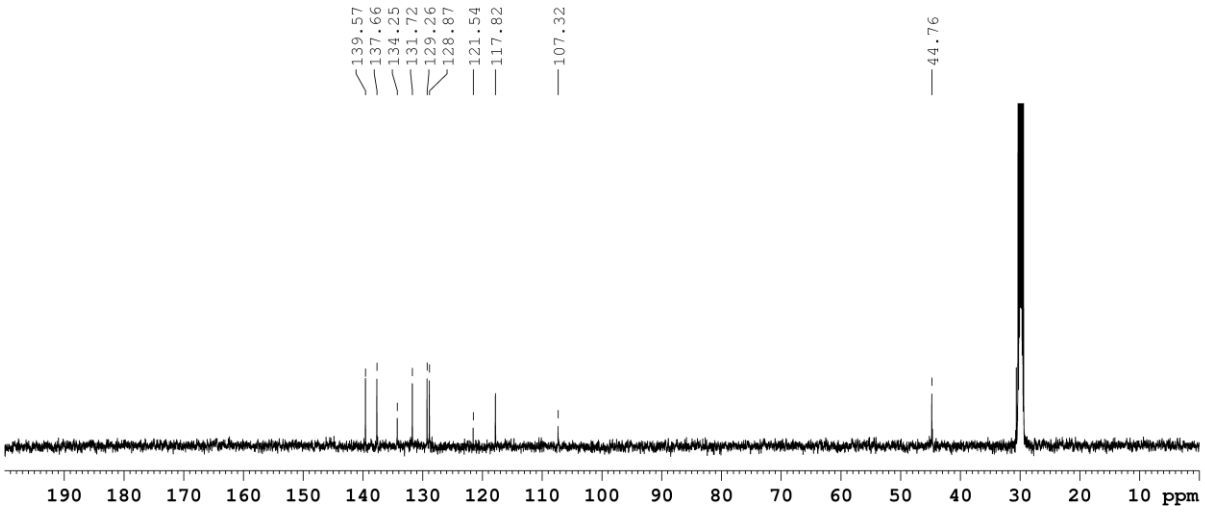

Figure 7.8: 125 MHz ^{13}C-NMR spectrum of 4-bromo-*N*-(4-bromo-2-nitrobenzyl)-2-nitroaniline (**12**) in acetone-d_6. Unlabeled signals represent impurities that could not be separated since the target molecule decomposes during purification.

7.3.5 Synthesis of *N*-(2-nitrophenyl)acetamide (16)[196]

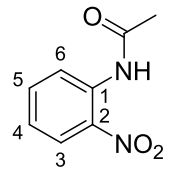

2-Nitroaniline (**1**, 1.00 g, 7.20 mmol), 4-dimethylaminopyridine (20.0 mg, 164 µmol) and triethylamine (161 mg, 220 µL, 1.60 mmol) were dissolved in dry dichloromethane (20 mL) under a nitrogen atmosphere. Acetyl chloride (1.13 g, 1.03 mL, 14.4 mL) dissolved in dichloromethane (10 mL) was added dropwise and the reaction mixture was stirred at room temperature for 16 h. Saturated sodium bicarbonate solution was added and the organic layer was separated. The aqueous layer was extracted three times with dichloromethane and the combined organic layers were washed with brine, dried over magnesium sulfate and the solvent was evaporated under reduced pressure. Column chromatography on silica gel (cyclohexane/ethyl acetate 5:1, R_f = 0.29) gave the product as yellow solid (1.20 g, 6.63 mmol, 92%, lit. 80%[196]).

melting point: 89.9 °C

^{1}H-NMR (600 MHz, $CDCl_3$, 298 K): δ = 10.32 (s, 1 H, N*H*), 8.76 (dd, ^3J = 8.5 Hz, ^4J = 1.3 Hz, 1 H, *H*-6), 8.20 (dd, ^3J = 8.5 Hz, ^4J = 1.5 Hz, 1 H, *H*-3), 7.64 (td, ^3J = 8.7 Hz, ^4J = 1.4 Hz, 1 H, *H*-5), 7.17 (td, ^3J = 8.5 Hz, ^4J = 1.3 Hz, 1 H, *H*-4), 3.29 (s, 3 H, CH_3) ppm.

^{13}C{^{1}H}-NMR (150 MHz, $CDCl_3$, 298 K): δ = 169.0 (*C*=O), 136.4 (*C*-2), 136.0 (*C*-5), 134.9 (*C*-1), 125.7 (*C*-3), 123.2 (*C*-4), 122.2 (*C*-6), 25.6 (*C*H_3) ppm.

IR (ATR): $\tilde{\nu}$ = 3368 (m), 3090 (m), 1698 (s), 1607 (m), 1583 (m), 1540 (w), 1496 (s), 1367 (m), 1339 (s), 1272 (m), 1225 (m), 1161 (m), 1145 (m), 1084 (w), 1037 (m), 1000 (w), 968 (w), 872 (w), 858 (m), 835 (w), 748 (s), 705 (s), 688 (w), 660 (s), 650 (s), 593 (m), 523 (s) cm^{-1}.

HR-MS (ESI, DCM): *m/z* $[M]^+$ calculated for $C_8H_8O_3N_2^+$: 180.05349; found: 180.05333 ± 0.16 ppm.

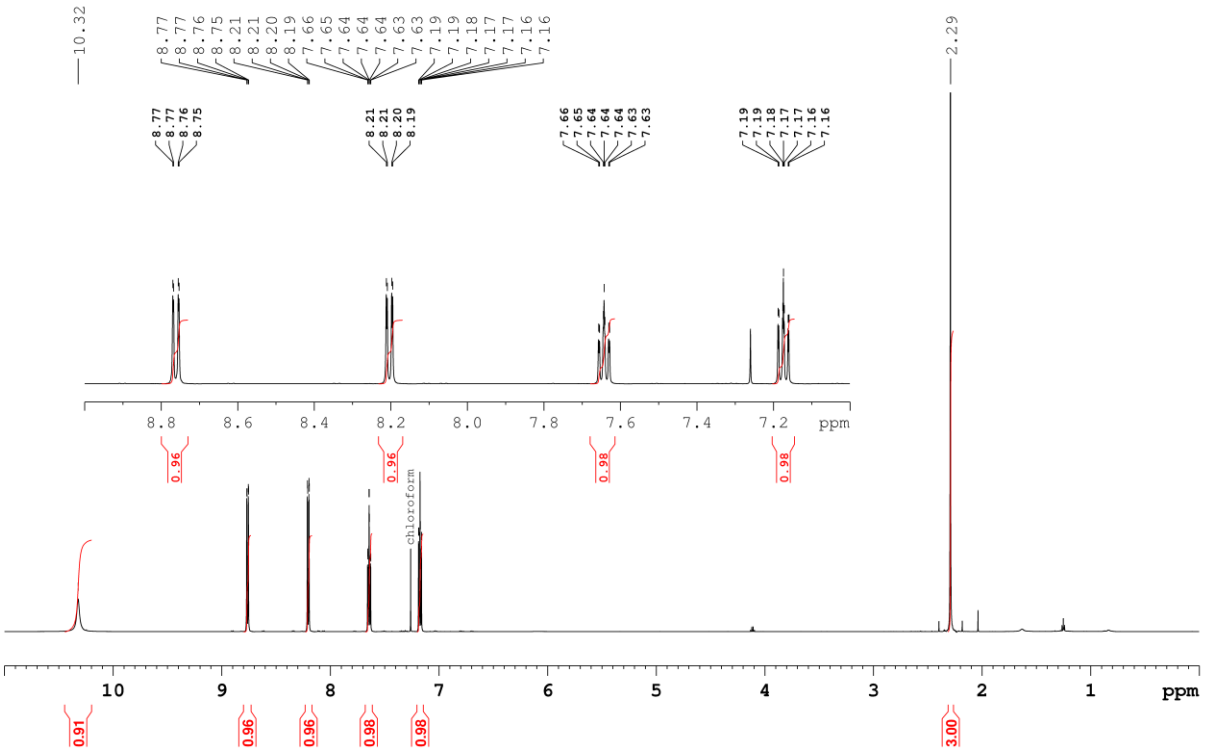

Figure 7.9: 600 MHz ^{1}H-NMR spectrum of *N*-(2-nitrophenyl)acetamide (**16**) in $CDCl_3$.

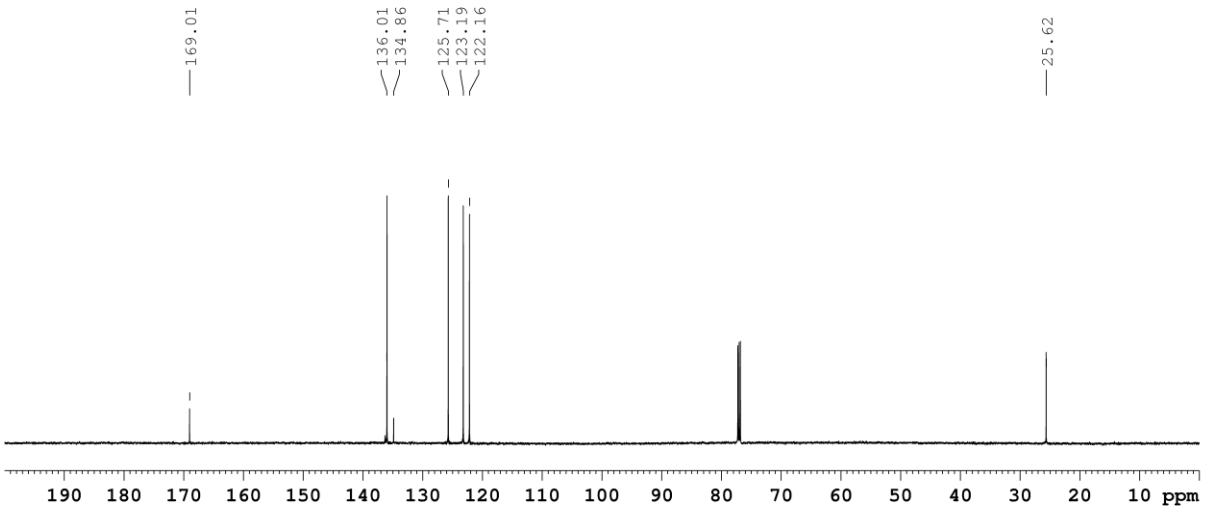

Figure 7.10: 150 MHz ^{13}C-NMR spectrum of *N*-(2-nitrophenyl)acetamide (**16**) in $CDCl_3$.

7.3.6 Synthesis of *N*-(4-bromo-2-nitrophenyl)acetamide (20)[198] (prepared in supervised work by M. HÖSGEN)[197]

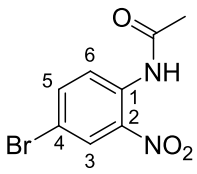

4-bromo-nitroaniline (**18**, 2.02 g, 9.34 mmol) was dissolved in acetic acid (15.0 mL) and acetic anhydride (1.08 g, 1.00 mL, 10.6 mmol) was added and the reaction mixture was stirred at 100 °C for 24 h. The reaction mixture was poured on ice and the formed precipitate was filtered off and washed with dem. water. The precipitate was dissolved in dichloromethane (50 mL) and dried over magnesium sulfate. Evaporation of the solvent under reduced pressure gave the product as yellow solid (1.33 g, 5.14 mmol, 55%, lit. 94%[198]).

melting point: 101.8 °C

^{1}H-NMR (600 MHz, $CDCl_3$, 298 K): δ = 10.25 (s, 1 H, N*H*), 8.71 (d, ^3J = 9.1 Hz, 1 H, *H*-6), 8.34 (d, ^4J = 2.2 Hz, 1 H, *H*-3), 7.73 (dd, ^3J = 9.1 Hz, ^4J = 2.2 Hz, 1 H, *H*-5), 2.29 (s, 3 H, -CH_3) ppm.

^{13}C{^{1}H}-NMR (150 MHz, $CDCl_3$, 298 K): δ = 168.9 (*C*=O), 138.7 (*C*-4), 133.9 (*C*-1), 128.2 (*C*-5), 123.6 (*C*-6), 115.2 (*C*-2), 25.6 (-*C*H_3) ppm.

IR (ATR): $\tilde{\nu}$ = 3363 (m), 3124 (m), 2169 (w), 1954 (w), 1710 (s), 1602 (m), 1571 (s), 1537 (m), 1480 (w), 1435 (w), 1362 (w), 1334 (m), 1256 (m), 1218 (m), 1141 (m), 1074 (m), 997 (w), 898 (w), 872 (m), 759 (s), 720 (m), 658 (m), 587 (m), 526 (s) cm^{-1}.

HR-MS (EI, 70 eV, DCM): *m/z* $[M]^+$ calculated for $C_8H_7O_3N_2{}^{79}Br^+$: 257.96383; found: 257.96400 ± 0.17 ppm.

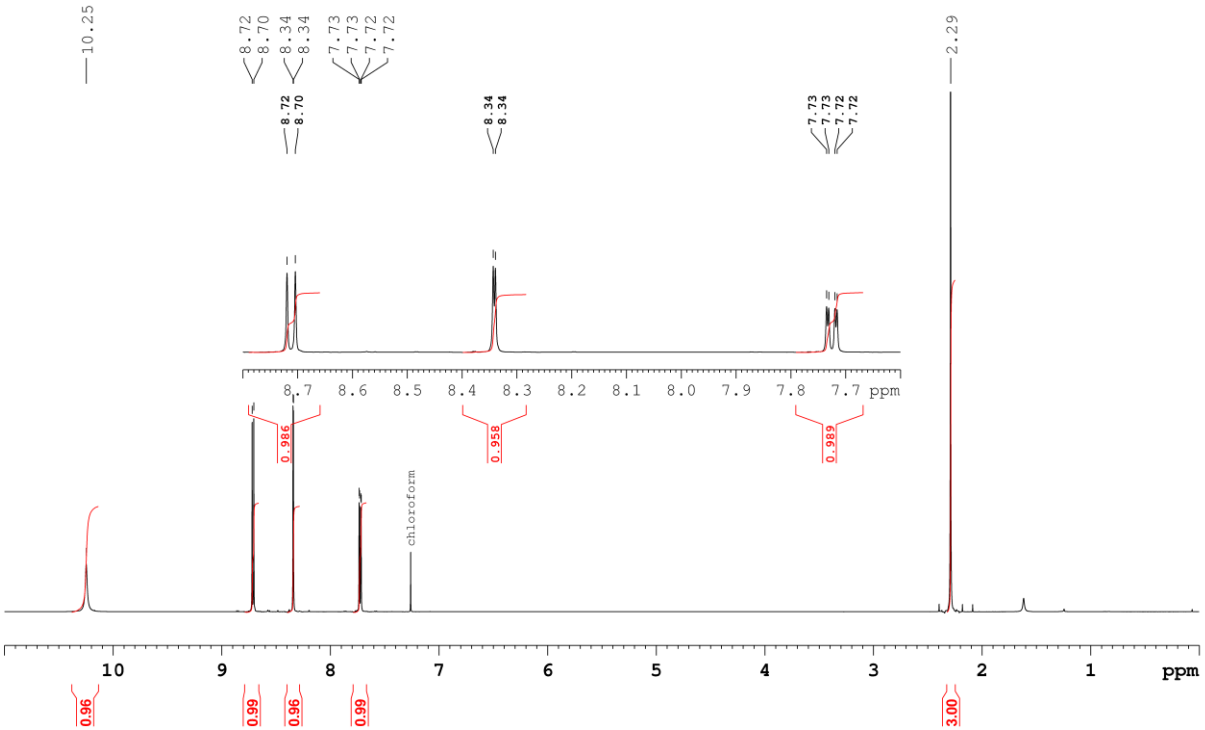

Figure 7.11: 600 MHz ^{1}H-NMR spectrum of *N*-(4-bromo-2-nitrophenyl)acetamide (**20**) in $CDCl_3$.

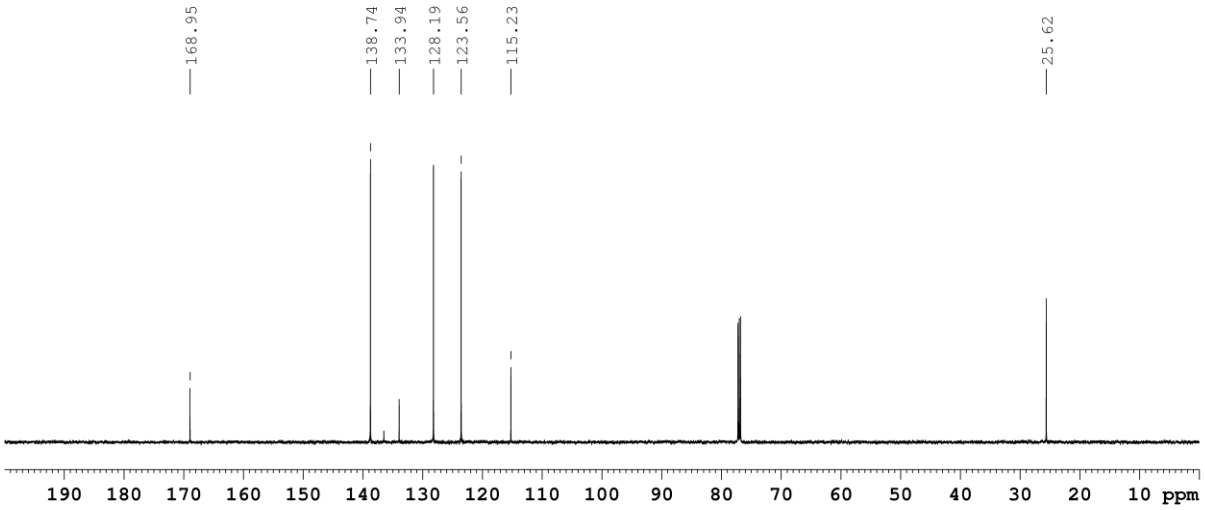

Figure 7.12: 150 MHz ^{13}C-NMR spectrum of *N*-(4-bromo-2-nitrophenyl)acetamide (**20**) in $CDCl_3$.

7.3.7 Synthesis of *N*-(4-iodo-2-nitrophenyl)acetamide (21) (prepared in supervised work by M. HÖSGEN)[197]

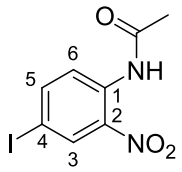

4-iodo-nitroaniline (**19**, 1.01 g, 3.82 mmol) was dissolved in acetic acid (7.5 mL) and acetic anhydride (756 mg, 0.70 mL, 7.41 mmol) was added and the reaction mixture was stirred at 100 °C for 24 h. The reaction mixture was poured on ice and the formed precipitate was filtered off and washed with dem. water. The precipitate was dissolved in dichloromethane (50 mL) and dried over magnesium sulfate. Evaporation of the solvent under reduced pressure gave the product as yellow solid (0.97 g, 3.17 mmol, 83%).

melting point: 109.7 °C

^{1}H-NMR (500 MHz, $CDCl_3$, 298 K): δ = 10.25 (s, 1 H, N*H*), 8.57 (d, ^3J = 9.3 Hz, 1 H, *H*-6), 8.51 (d, ^4J = 2.0 Hz, 1 H, *H*-3), 7.90 (dd, ^3J = 9.3 Hz, ^4J = 2.0 Hz, 1 H, *H*-5), 2.29 (s, 3 H, -CH_3) ppm.

^{13}C{^{1}H}-NMR (125 MHz, $CDCl_3$, 298 K): δ = 169.0 (*C*=O), 144.5 (*C*-2), 136.6 (*C*-1), 134.6 (*C*-3), 134.0 (*C*-6), 123.8 (*C*-5), 84.8 (*C*-4), 25.7 (-*C*H_3) ppm.

IR (ATR): $\tilde{\nu}$ = 3356 (m), 3084 (w), 2240 (w), 1689 (s), 1603 (s), 1571 (s), 1487 (s), 1448 (w), 1365 (m), 1332 (s), 1262 (s), 1230 (w), 1156 (s), 1078 (m), 1032 (w), 1002 (w), 959 (w), 888 (m), 869 (m), 841 (s), 758 (s), 715 (s), 688 (w), 666 (w), 624 (m), 585 (m), 529 (s) cm^{-1}.

HR-MS (EI, 70 eV, DCM): *m/z* $[M]^+$ calculated for $C_8H_7O_3N_2{}^{127}I^+$: 305.95000; found: 305.95013 ± 0.14 ppm.

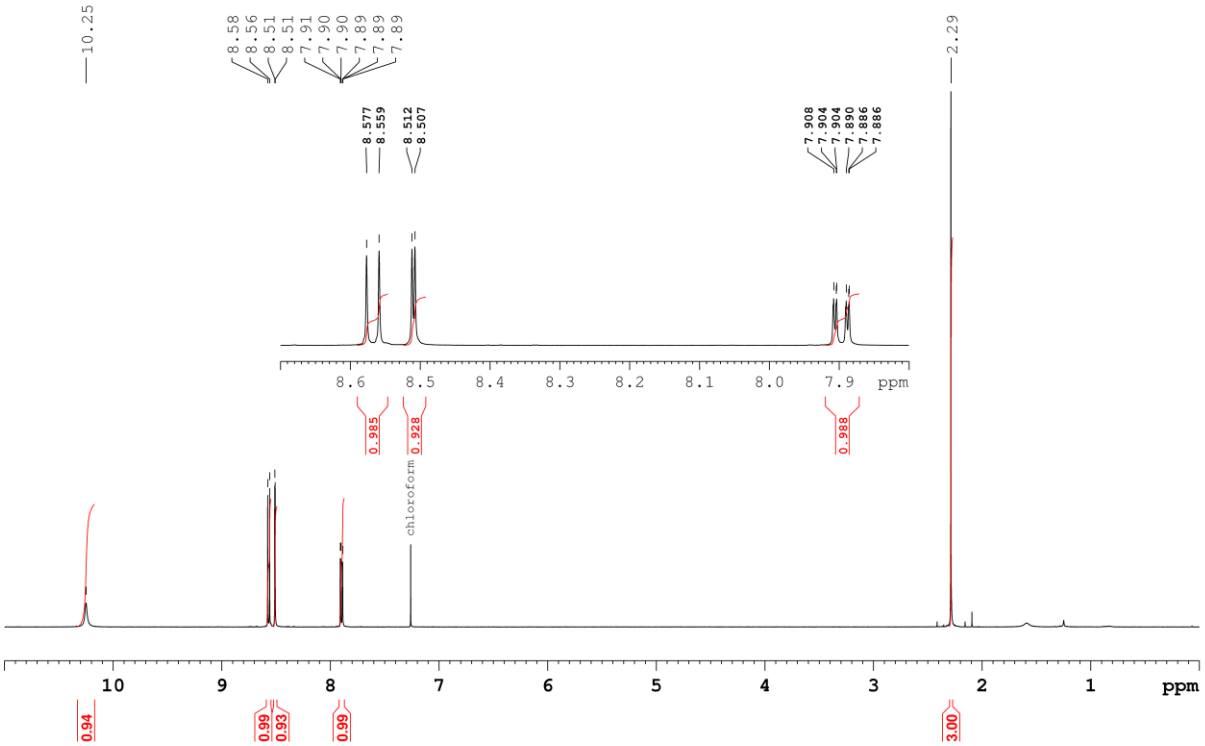

Figure 7.13: 500 MHz ^{1}H-NMR spectrum of *N*-(4-iodo-2-nitrophenyl)acetamide (**21** in $CDCl_3$.

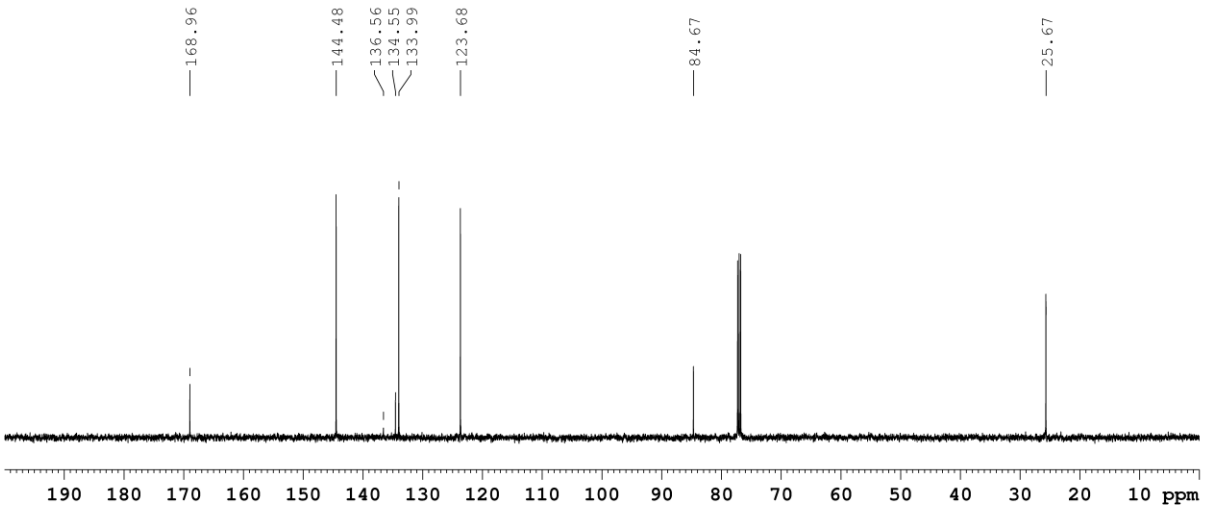

Figure 7.14: 125 MHz ^{13}C-NMR spectrum of *N*-(4-iodo-2-nitrophenyl)acetamide (**21** in $CDCl_3$.

7.3.8 Synthesis of *N*-(4-bromo-2-nitrobenzyl)-*N*-(4-bromo-2-nitrophenyl)acetamide (24) (prepared in supervised work by M. HÖSGEN)[197]

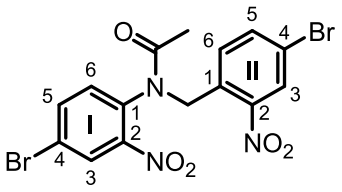

Sodium hydride (231 mg, 9.63 mmol) was dispersed in dry DMF (2 mL) under a nitrogen atmosphere at 0 °C. *N*-(4-bromo-2-nitrophenyl)acetamide (**20**, 754 mg, 2.92 mmol) dissolved in dry DMF (5 mL) was added dropwise and the mixture was stirred for 20 min. at room temperature, then 4-bromo-1-(bromomethyl)-nitrobenzene (**22**, 1.71 g, 5.83 mmol) dissolved in dry DMF (5 mL) was added dropwise and the reaction mixture was stirred for 16 h. The reaction mixture was quenched with saturated ammonium chloride solution and extracted twice with 50 mL diethyl ether. The combined organic layers were washed with brine, dried over magnesium sulfate and the solvent was evaporated under reduced pressure. The impure product could be obtained via column chromatography on silica (cyclohexane/ethyl acetate 3:1, R_f = 0.24) as yellow solid (180 mg, 380 µmol, 13%). Due to the high extent of impurities no high-resolution mass spectrum could be obtained

melting point: 176.5 °C

^{1}H-NMR (600 MHz, $CDCl_3$, 298 K): δ = 8.13 (d, ^4J = 1.9 Hz, 1 H, Ar^{I}-*H*-3), 7.99 (d, ^4J = 1.3 Hz, 1 H, Ar^{II}-*H*-3), 7.75-7.70 (m, 2 H, Ar^{I}-*H*-5, Ar^{II}-*H*-5), 7.59 (d, ^3J = 8.2 Hz, 1 H, Ar^{II}-*H*-6), 7.00 (d, ^3J = 8.2 Hz, 1 H, Ar^{I}-*H*-6), 5.33 (d, ^2J = 15.8 Hz, 1 H, C*H*$_2$), 4.86 (d, ^2J = 15.4 Hz, 1 H, C*H*$_2$'), 1.91 (s, 3 H, -C*H*$_3$) ppm.

^{13}C{^{1}H}-NMR (150 MHz, $CDCl_3$, 298 K): δ = 170.4 (*C*=O), 149.2 (Ar^{II}-*C*-2), 147.2 (Ar^{I}-*C*-2), 137.5 (Ar^{I}-*C*-5), 136.6 (Ar^{II}-*C*-5), 134.6 (Ar^{I}-*C*-1), 133.8 (Ar^{II}-*C*-6), 132.7 (Ar^{II}-*C*-6), 130.1 (Ar^{II}-*C*-1), 129.0 (Ar^{I}-*C*-3), 127.6 (Ar^{II}-*C*-3), 123.4 (Ar^{II}-*C*-4), 122.3 (Ar^{II}-*C*-4), 48.2 (*C*H$_2$), 29.7 (-*C*H$_3$) ppm.

IR (ATR): $\tilde{\nu}$ = 3076 (w), 2212 (w), 2084 (w), 1978 (w), 1611 (w), 1529 (s), 1461 (w), 1443 (w), 1408 (m), 1345 (s), 1278 (w), 1157 (m), 1095 (m), 1045 (m), 959 (w), 915 (m), 891 (w), 875 (m), 840 (m), 806 (m), 745 (m), 680 (w), 659 (w), 610 (w) cm^{-1}.

MS (EI, 70 eV, DCM): *m/z* (%) 347.04 $[C_{15}H_{11}{}^{81}BrN_2O_3]^+$ (40), 259.99 $[C_8H_9BrN_2O_3]^+$ (39), 217.97 $[C_7H_9BrNO_2]^+$ (68), 134.03 $[C_7H_4BrNO_2]^+$ (100).

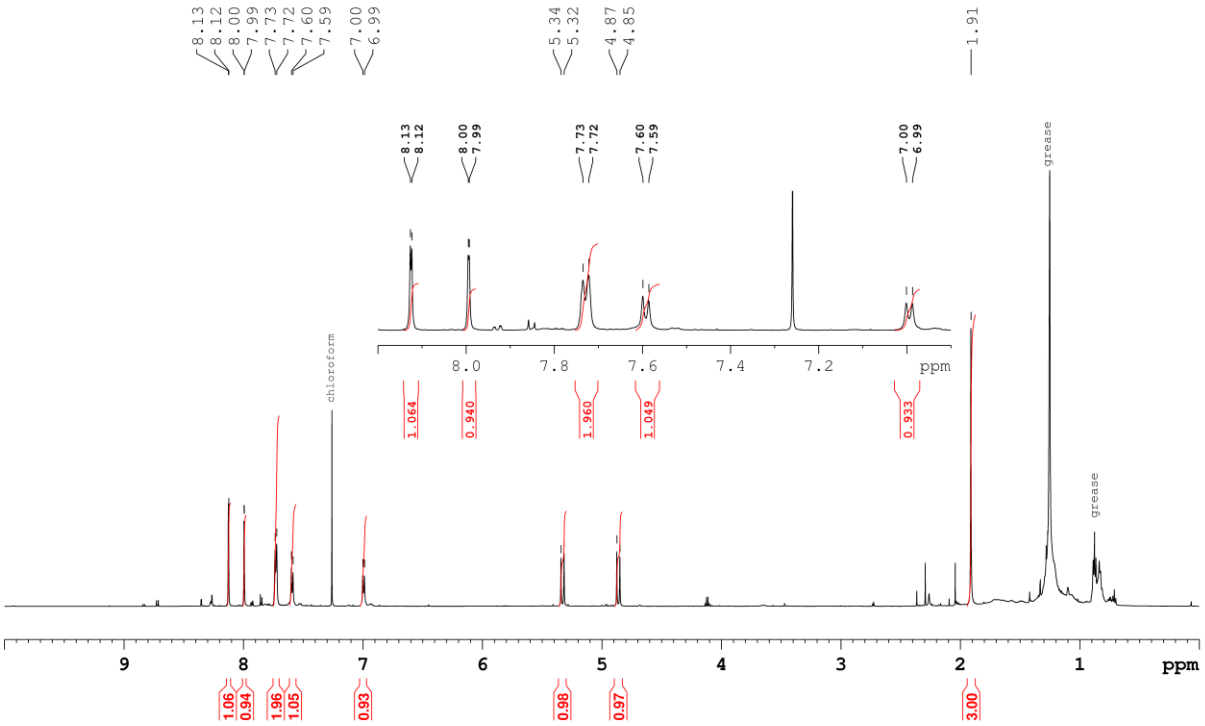

Figure 7.15: 600 MHz ^{1}H-NMR spectrum of *N*-(4-bromo-2-nitrobenzyl)-*N*-(4-bromo-2-nitrophenyl)acetamide (**24**) in $CDCl_3$. Unlabeled signals represent impurities that could not be separated since the target molecule decomposes during purification.

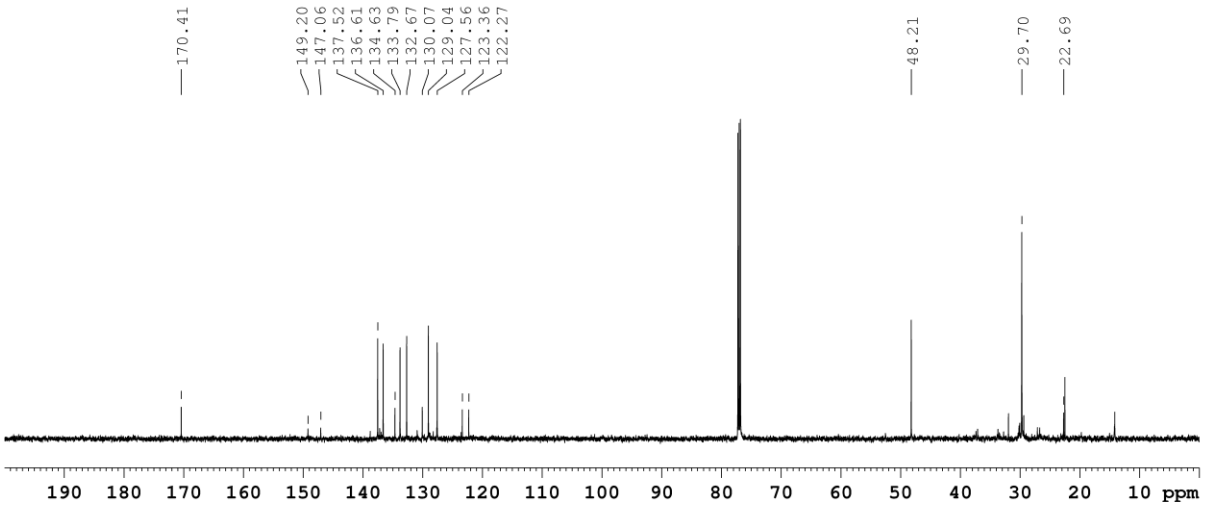

Figure 7.16: 150 MHz ^{13}C-NMR spectrum of *N*-(4-bromo-2-nitrobenzyl)-*N*-(4-bromo-2-nitrophenyl)acetamide (**24**) in $CDCl_3$. Unlabeled signals represent impurities that could not be separated since the target molecule decomposes during purification.

7.3.9 Synthesis of *N*-(4-iodo-2-nitrobenzyl)-*N*-(4-iodo-2-nitrophenyl)acetamide (25) (prepared in supervised work by M. HÖSGEN)[197]

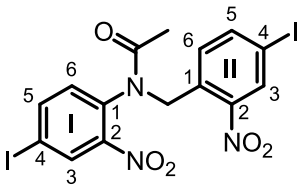

Sodium hydride (117 mg, 4.86 mmol) was dispersed in dry DMF (2 mL) under a nitrogen atmosphere at 0 °C. *N*-(4-iodo-2-nitrophenyl)acetamide (**21**, 598 mg, 1.95 mmol) dissolved in dry DMF (5 mL) was added dropwise and the mixture was stirred for 20 min. at room temperature, then 4-iodo-1-(bromomethyl)-nitrobenzene (**23**, 1.00 g, 2.93 mmol) dissolved in dry DMF (5 mL) was added dropwise and the reaction mixture was stirred for 16 h. The reaction mixture was quenched with saturated ammonium chloride solution and extracted twice with 50 mL diethyl ether. The combined organic layers were washed with brine, dried over magnesium sulfate and the solvent was evaporated under reduced pressure. The impure product could be obtained via column chromatography on silica (cyclohexane/ethyl acetate 4:1, R_f = 0.21) as yellow solid (88.5 mg, 156 µmol, 8%).

melting point: 176.5 °C

^{1}H-NMR (500 MHz, $CDCl_3$, 298 K): δ = 8.28 (d, ^4J = 1.9 Hz, 1 H, Ar^I-*H*-3), 8.16 (d, ^4J = 1.6 Hz, 1 H, Ar^{II}-*H*-3), 7.93-7.88 (m, 2 H, Ar^I-*H*-5, Ar^{II}-*H*-5), 7.42 (d, ^3J = 8.2 Hz, 1 H, Ar^{II}-*H*-6), 6.83 (d, ^3J = 8.3 Hz, 1 H, Ar^I-*H*-6), 5.32 (d, ^2J = 15.5 Hz, 1 H, CH_2), 4.82 (d, ^2J = 15.5 Hz, 1 H, CH_2'), 1.91 (s, 3 H, -CH_3) ppm.

^{13}C{^{1}H}-NMR (125 MHz, $CDCl_3$, 298 K): δ = 170.4 (*C*=O), 149.1 (Ar^{II}-*C*-2), 146.9 (Ar^I-*C*-2), 143.5 (Ar^I-*C*-5), 142.4 (Ar^{II}-*C*-5), 135.3 (Ar^I-*C*-1), 134.7 (Ar^I-*C*-3), 133.7 (Ar^{II}-*C*-6), 133.2 (Ar^{II}-*C*-3), 132.7 (Ar^I-*C*-6), 130.8 (Ar^{II}-*C*-1), 93.9 (Ar^{II}-*C*-4), 92.8 (Ar^I-*C*-4), 48.3 (*C*H_2), 22.5 (-*C*H_3) ppm.

IR (ATR): $\tilde{\nu}$ = 2929 (w), 2166 (w), 2021 (w), 1667 (s), 1588 (w), 1520 (s), 1479 (m), 1414 (w), 1398 (w), 1378 (w), 1339 (s), 1294 (s), 1224 (m), 1164 (w), 1078 (w), 1016 (m), 976 (m), 870 (m), 842 (m), 798 (m), 769 (w), 749 (s), 716 (w), 692 (w), 597 (w), 557 (s) cm^{-1}.

HR-MS (EI, 70 eV, DCM): *m/z* $[M]^+$ calculated for $C_{15}H_{11}O_5N_3{}^{127}I_2{}^+$: 566.87881; found: 566.49815 ± 0.38 ppm.

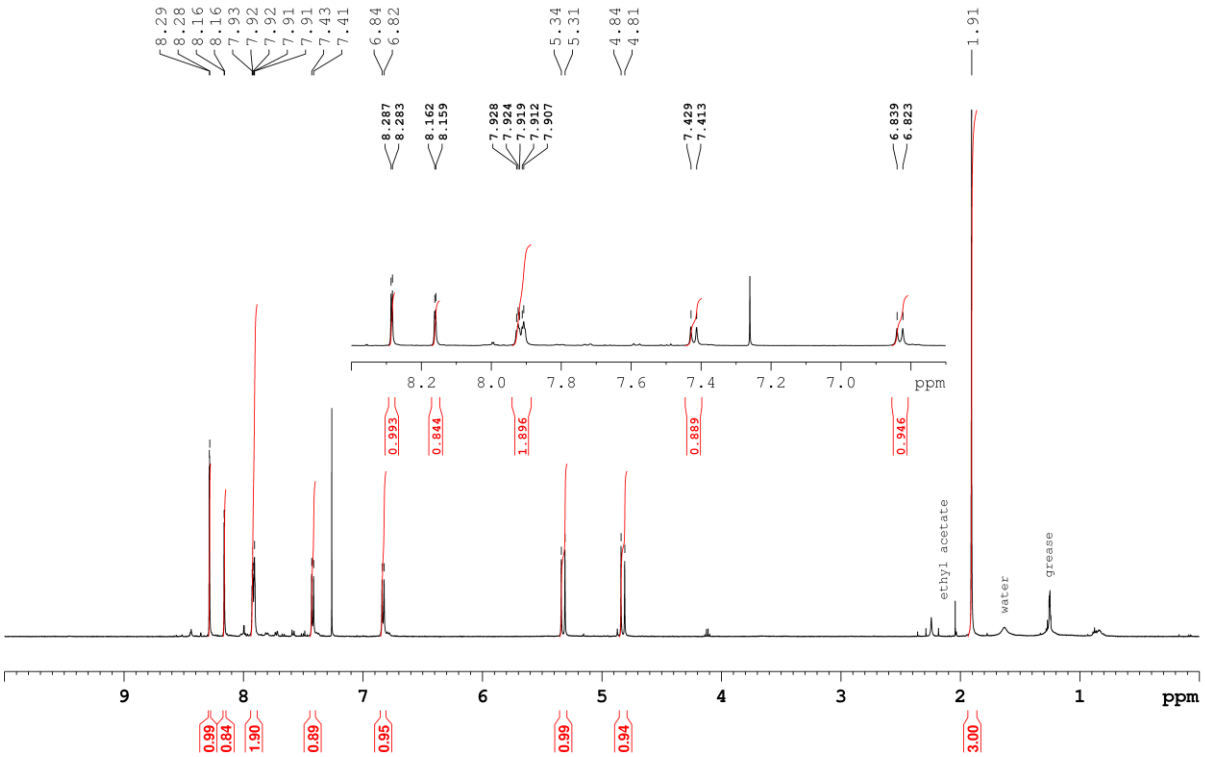

Figure 7.17: 500 MHz ^{1}H-NMR spectrum of *N*-(4-iodo-2-nitrobenzyl)-*N*-(4-iodo-2-nitrophenyl)acetamide (**25**) in $CDCl_3$. Unlabeled signals represent impurities that could not be separated since the target molecule decomposes during purification.

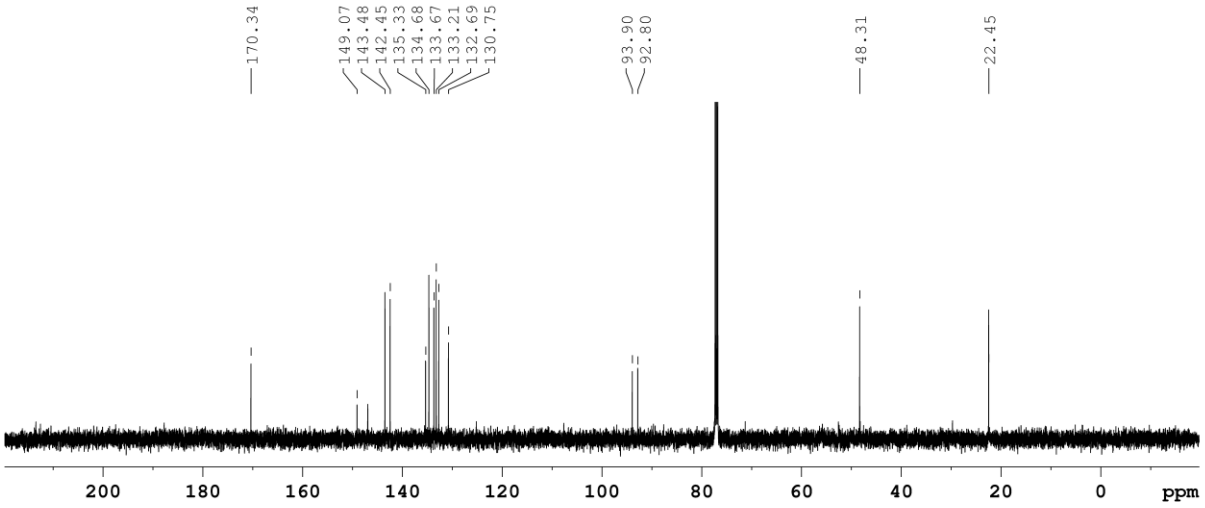

Figure 7.18: 125 MHz ^{13}C-NMR spectrum of *N*-(4-iodo-2-nitrobenzyl)-*N*-(4-iodo-2-nitrophenyl)acetamide (**25**) in $CDCl_3$. Unlabeled signals represent impurities that could not be separated since the target molecule decomposes during purification.

7.3.10 Synthesis of *N*-(4-bromo-2-nitrobenzyl)-*N*-(2-nitrobenzyl)acetamide (28) (prepared in supervised work by M. HÖSGEN)[197]

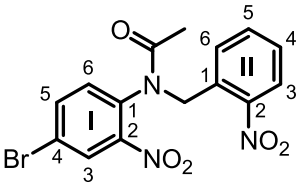

Sodium hydride (93.0 mg, 4.88 mmol) was dispersed in dry DMF (2 mL) under a nitrogen atmosphere at 0 °C. *N*-(4-bromo-2-nitrophenyl)acetamide (**21**, 500 mg, 1.94 mmol) dissolved in dry DMF (5 mL) was added dropwise and the mixture was stirred for 20 min. at room temperature, then 2-nitrobenzylbromide (**17**, 635 mg, 2.94 mmol) dissolved in dry DMF (5 mL) was added dropwise and the reaction mixture was stirred for 16 h. The reaction mixture was quenched with saturated ammonium chloride solution and extracted twice with 50 mL diethyl ether. The combined organic layers were washed with brine, dried over magnesium sulfate and the solvent was evaporated under reduced pressure. The impure product could be obtained via column chromatography on silica (cyclohexane/ethyl acetate 5:1, R_f = 0.11) as yellow solid (61.2 mg, 155 µmol, 8%). Due to the high extent of impurities no high-resolution mass spectrum or IR spectrum could be obtained.

melting point: 172.3 °C

^{1}H-NMR (600 MHz, $CDCl_3$, 298 K): δ = 8.10 (d, ^4J = 2.2 Hz, 1 H, Ar^I-*H*-3), 7.84 (dd, ^3J = 8.2 Hz, ^4J = 1.0 Hz, 1 H, Ar^{II}-*H*-3), 7.69 (dd, ^3J = 8.2 Hz, ^4J = 2.3 Hz, 1 H, Ar^I-*H*-5), 7.66 (dd, ^3J = 7.8 Hz, ^3J = 1.3 Hz, 1 H, Ar^{II}-*H*-6), 7.60 (td, ^3J = 7.6 Hz, ^4J = 1.0 Hz, 1 H, Ar^{II}-*H*-5), 7.44 (td, ^3J = 7.7 Hz, ^4J = 1.4 Hz, 1 H, Ar^{II}-*H*-4), 6.99 (d, ^3J = 8.4 Hz, 1 H, Ar^I-*H*-6), 5.43 (d, ^2J = 15.5 Hz, 1 H, CH_2), 4.89 (d, ^2J = 15.5 Hz, 1 H, CH_2'), 1.92 (s, 3 H, -CH_3) ppm.

^{13}C{^{1}H}-NMR (150 MHz, $CDCl_3$, 298 K): δ = 170.3 (*C*=O), 148.9 (Ar^{II}-*C*-2), 147.2 (Ar^I-*C*-2), 137.4 (Ar^I-*C*-5), 134.7 (Ar^I-*C*-1), 133.6 (Ar^{II}-*C*-5), 132.8 (Ar^I-*C*-6), 132.2 (Ar^{II}-*C*-6), 131.0 (Ar^{II}-*C*-1), 129.02 (Ar^{II}-*C*-4), 128.92 (Ar^I-*C*-3), 124.6 (Ar^{II}-*C*-3), 123.1 (Ar^I-*C*-4), 48.4 (*C*H_2), 22.5 (-*C*H_3) ppm.

MS (EI, 70 eV, DCM): *m/z* (%) 396.02 [$C_{15}H_{12}{}^{81}BrN_3O_5$]$^+$ (1), 394.06 [$C_{15}H_{12}{}^{79}BrN_3O_5$]$^+$ (1), 347.02 [$C_{15}H_{12}BrN_2O_3$]$^+$ (34), 259.98 [$C_8H_9BrN_2O_3$]$^+$ (36), 217.96 [$C_{11}H_9N_2O_3$]$^+$ (65), 134.03 [$C_7H_4BrNO_2$]$^+$ (100).

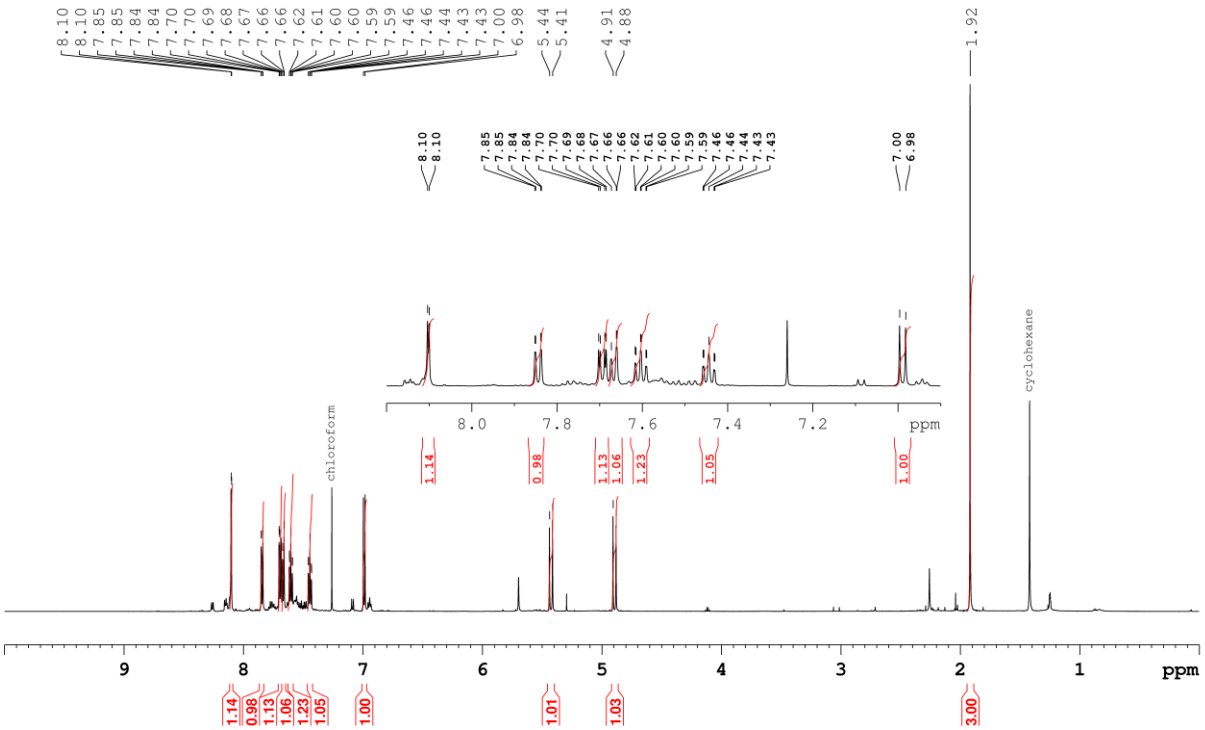

Figure 7.19: 600 MHz ^{1}H-NMR spectrum of *N*-(4-bromo-2-nitrobenzyl)-*N*-(2-nitrobenzyl)acetamide (**28**) in $CDCl_3$. Unlabeled signals represent impurities that could not be separated since the target molecule decomposes during purification.

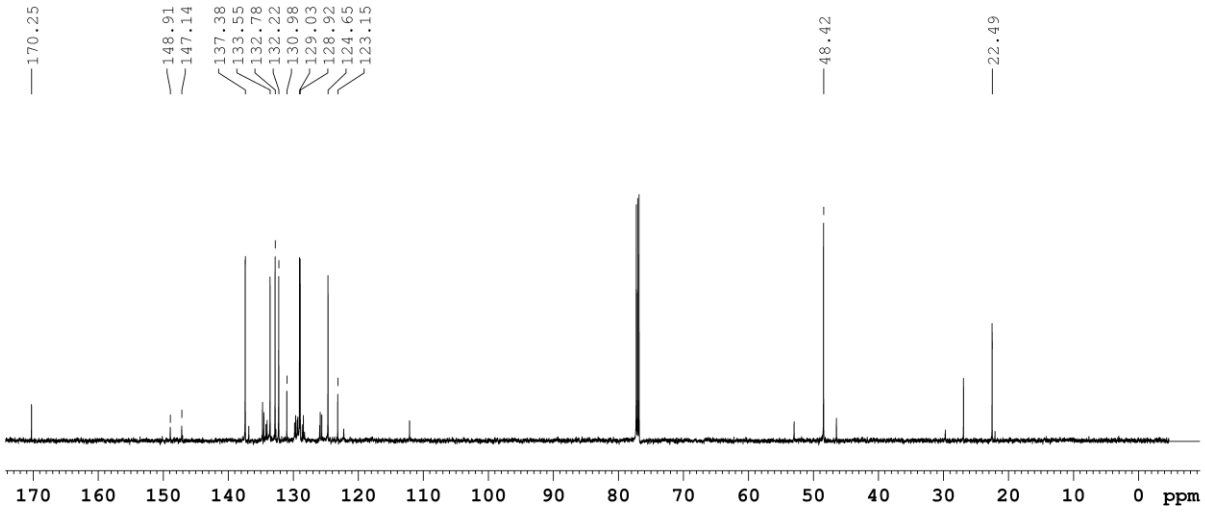

Figure 7.20: 150 MHz ^{1}H-NMR spectrum of *N*-(4-bromo-2-nitrobenzyl)-*N*-(2-nitrobenzyl)acetamide (**28**) in $CDCl_3$. Unlabeled signals represent impurities that could not be separated since the target molecule decomposes during purification.

8. Appendix

8.1 Index of Abbreviations

abbreviation	meaning
17βHSD3	17β-hydroxysteroid dehydrogenase type 3
A	absorption
abs.	absolute
Ac	acetyl group
AcCl	acetyl chloride
Ac_2O	acetic anhydride
AcOH	acetic acid
ATR	Attenuated Total Reflection
baDA	benzoic acid *N*-Ac diazocine
bDA	brominated *N*-Ac diazocine
Boc	*tert*-butoxycarbonyl
Boc_2O	di-*tert*-butyldicarbonate
bpDA	bromophenyl *N*-Ac diazocine
brine	saturated sodium chloride solution
calc.	calculated
CD	circular dichroism
$CDCl_3$	deuterated chloroform
cnDA	nitrile *N*-Ac diazocine
conc.	concentrated
CPL	cirularly polarized light
d	day(s)
DA	*N*-Ac diazocine
DBPO	benzoyl peroxide
DCM	dichloromethane
dem.	demineralized
DID	diindanodiazocine
DIPEA	*N,N*-diisopropylamine
DMAP	4-dimethylaminopyridine
DMF	dimethylformamide
dmpDA	dimethylphenyl *N*-Ac diazocine
DMSO	dimethylsulfoxide
E	extinction
EDG	electron donating group
EE	ethyl acetate
ee	enantiomeric excess

EI	electron ionization
eq	equivalent(s)
ESI	electrospray ionization
Et	ethyl
EtOH	ethanol
EWG	electron withdrawing group
extrapol.	extrapolated
Fmoc	fluorenylmethoxycarbonyl
FmocCl	fluorenylmethoxycarbonyl chloride
fpDA	fluorophenyl *N*-Ac diazocine
FT	Fourier Transformation
h	hour(s)
HEK-293	human embryonic kidney cells
HMBC	heteronuclear multiple bond correlation
HOMO	highest occupied molecule orbitale
HPLC	high performance liquid chromatography
HR	high resolution
HSQC	heteronuclear single quantum coherence
Hz	Hertz
iCVD	initiated chemical vapour deposition
iDA	iodinated *N*-Ac diazocine
IR	infrared
l-CPL	left-handed circular polarized light
LED	light-emitting diode
LUMO	lowest unoccupied molecule orbitale
m	medium
*m*CPBA	*meta*-chloroperbenzoic acid
Me	methyl
MeCN	acetonitrile
MeOH	methanol
min.	minute(s)
MS	mass spectrometry
N-Ac	*N*-acetyl
NBS	*N*-bromosuccinimide
NIR	near infrared irradiation
NIS	*N*-iodosuccinimide
NMR	nuclear magnetic resonance
org.	organic
ox	oxidative

[Ox]	oxidation
pDA	phenyl *N*-Ac diazocine
PG	protecting group
Ph	phenyl
PHOTAC	photochemically targeting chimeras
ppm	parts per million
PROTAC	targeted degradation of targeted proteins via the proteolysis targeting chimeras
PSS	photostationary state
quant.	quantitative
R	organic rest
rac	racemic
r-CPL	right-handed circular polarized light
R_f	retention factor
rt	room temperature
s	second(s)
s	strong
T3P	propylphosponic anhydride
TBAF	tetrabutylammonium fluoride
*t*BuOK	potassium *tert*-butoxide
TD-DFT	time-dependent density functional theory
TEA	triethylamine
TFA	trifluoroacetic acid
TFSA	trifluoromethanesulfonic acid
THB	tetrahydrodibenzazocine
THF	tetrahydrofurane
TLC	thin layer chromatography
TOF	time of flight
UV	ultraviolet region of the electromagnetic spectrum
vis	visible range of the electromagnetic spectrum
w	weak

8.2 Supporting Information of the Publications and Manuscripts

8.2.1 Determination of Enantiomeric Excess by Photoswitching of Chiral Diindanodiazocine Racemic Mixture with Circular Polarized Light

Supporting Information

Determination of Enantiomeric Excess by Photoswitching of Chiral Diindanodiazocine Racemic Mixture with Circular Polarized Light

Thomas Brandt, Widukind Moormann, Jan Simon von Glasenapp, Jan Peter Mikosch, Christian Näther, Rainer Herges*

Table of contents

I. Analytical Equipment

NMR spectroscopy

NMR spectra were measured in deuterated solvents (Deutero). The spectra were referenced to the following solvent residual signals:

solvent	degree of deuteration	^{1}H signal ppm	^{13}C-signal ppm
acetone-d_6	99.8%	2.05 (quintet)	29.84 (septet)
chloroform-d_1	99.8%	7.26 (singlet)	77.16 (triplet)
THF-d_8	99.8%	3.58 (singlet), 1.73 (singlet)	67.57 (quintet), 25.37 (quintet)

The spectra were recorded with a Bruker DRX 500 (^{1}H-NMR: 500 MHz, ^{13}C-NMR: 125 MHz) and a Bruker AV 600 (^{1}H-NMR: 600 MHz, ^{13}C-NMR: 150 MHz). The Multiplicities of the signals were abbreviated with s (singlet), d (doublet), t (triplet), q (quartet), quint. (quintet), m (multiplet), and br. (broad) in addition for broad signals.

Melting Point

Melting Points were measured with a Melting Point B-560 (Büchi) in melting point tubes without further correction.

Mass spectrometry

Mass spectra (EI) and high-resolution mass spectra (HR-EI) were measured with an AccuTOF GCv 4G (Joel) with an ionization energy of 70 eV. HR-ESI mass spectra were measured with a Q Exactive Plus (Thermo Scientific).

High Performance Liquid Chromatography

The separation of the enantiomers was performed with an Agilent HPLC System from the 1100 series with autosampler and fraction collector. As column a Daicel Chiracel OD-H column was used with a tris(dimethylphenylcarbamate) cellulose stationary phase and *n*-heptane/isopropanol (98:2) as eluent.

IR spectroscopy

Infrared spectra were measured with a Perkin-Elmer 1600 FT-IR spectrometer with an A531-G Golden-Gate-Diamond-ATR-unit. Signals were abbreviated with w (weak), m (medium) or s (strong) for its intensity.

UV-vis spectroscopy

UV-vis spectra were measured with a Perkin-Elmer Lambda 14 UV-vis spectrometer. Quartz cuvettes of 10 mm optical path length were used.

CD spectroscopy

The CD-data were recorded with a Jasco J-720 spectropolarimeter. Quartz cuvettes of 1 mm and 10 mm optical path length were used.

Optical Rotations

Optical rotations and specific rotations were measured with an Anton Paar MCP5100 modular polarimeter (sodium D-line: 589 nm, cell length 100 mm).

X-ray cristallography

Data collection was performed with a XtaLAB Synergy, Dualflex, HyPix diffractometer. The structure was solved with SHELXT[1] and refined with the SHELXL[1] refinement package using Least Squares minimisation.

Chromatography

Silica gel (Merck, particle size 0.040-0.063 mm) was used for column chromatography purifications. R_f values were determined via thin layer chromatography on Polygram® SilG/UV254 (Macherey Nagel, 0.2 mm particle size).

Chemicals

All commercially available chemicals were used without further purification.

Light sources

For irradiation different custom-built light sources with a wavelength of 385 nm, 405 nm, 530 nm and 590 nm were used (Sahlmann Photochemistry Solutions & in-house built). Irradiation wavelengths for all (385 nm, 405 nm, 530 nm and 590 nm) LED units were measured via a mobile UV-vis spectrometer (USB4000-UV-VIS, Ocean Optics, Largo, FL, USA). All emission spectra were normalized. Figure SI1 shows the normalized emission spectra of all LED units used.

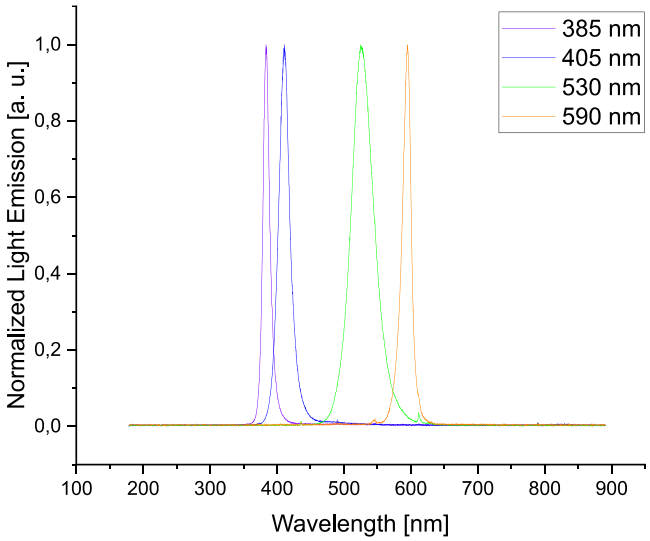

Figure SI.1: Emission spectra of all LED units used. For better comparison all datasets were normalized to its maximum.

The full width at half maximum (FWHM) amounts to 13 nm (378-390 nm, maximum at 384 nm) for the 385 nm LED unit, 19 nm (401-420 nm, maximum at 410 nm) for the 405 nm LED unit, to 38 nm (509-547 nm, maximum at 525 nm) for the 530 nm LED unit and to 14 nm (586-600 nm, maximum at 595 nm) for the 590 nm LED unit.

II. Syntheses

II.1.1 Synthesis of (1R,1'R/1S,1'S)-7,7'-dinitro-2,2',3,3'-tetrahydro-1H,1'H-1,1'-diindene and (1R,1'S)-7,7'-dinitro-2,2',3,3'-tetrahydro-1H,1'H-1,1'-diindene[2]

4-Nitroindane (1.00 g, 6.13 mmol) was dissolved in dry THF under nitrogen atmosphere, cooled to 0 °C and potassium butoxide (1.03 g, 9.18 mmol) was added. The reaction was stirred for 30 s before bromine (1.17 g, 0.37 mL, 7.34 mmol) was added rapidly. The reaction was stirred for further 10 min. and 150 g of ice were added. The aqueous solution was extracted with DCM (3 × 40 mL) and the combined organic layers were wash with saturated sodium thiosulfate solution, dried with over $MgSO_4$ and the solvent was removed under reduced pressure. The crude product was purified by column chromatography (silica gel, *n*-pentane/DCM, 5:2) to afford the diastereomers as colorless solids.

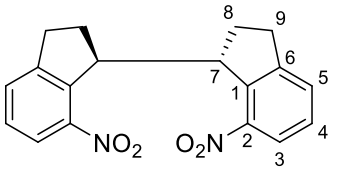

yield: 520 mg (1.60 mmol, 52%)

mp.: 178 °C

R_f = 0.15 (*n*-pentane/DCM, 2:1)

^{1}H-NMR (500.1 MHz, $CDCl_3$, 300 K): δ = 7.66 (d, ^3J = 8.1 Hz, 2 H, *H*-3), 7.49 (d, ^3J = 6.5 Hz, 2 H, *H*-5), 7.30 (d, ^3J = 8.1 Hz, 2 H, *H*-4), 4.28 (m, 2 H, *H*-7), 3.31 (m, 2 H, *H*-9a), 2.93 (dd, ^2J = 16.2 Hz, ^3J = 8.6 Hz, 2 H, *H*-9b), 2.32 (m, 2 H, *H*-8a), 2.09 (dd, ^2J = 12.6 Hz, ^3J = 7.0 Hz, 2 H, *H*-8b) ppm.

^{13}C-NMR (125.8 MHz, $CDCl_3$, 300 K): δ = 149.20 (C-6), 146.21 (C-2), 140.16 (C-1), 130.15 (C-5), 128.40 (C-4), 122.34 (C-3), 47.09 (C-7), 32.33 (C-8), 30.73 (C-9) ppm.

MS (HR): m/z $(C_{18}H_{17}O_4N_2)^+$: calc.: 325.11828, found: 325.11787 ± 1.26 ppm.

IR (ATR): $\tilde{\nu}$ = 3084 (w), 2929 (m), 2850 (w), 1730 (w), 1609 (w), 1574 (w), 1520 (s), 1455 (m), 1352 (s), 1339 (s), 1323 (s), 1228 (w), 1175 (w), 1132 (w), 1070 (w), 982 (w), 939 (w), 864 (w), 838 (w), 813 (s), 793 (s), 755 (m), 733 (s), 677 (w), 615 (w) cm^{-1}.

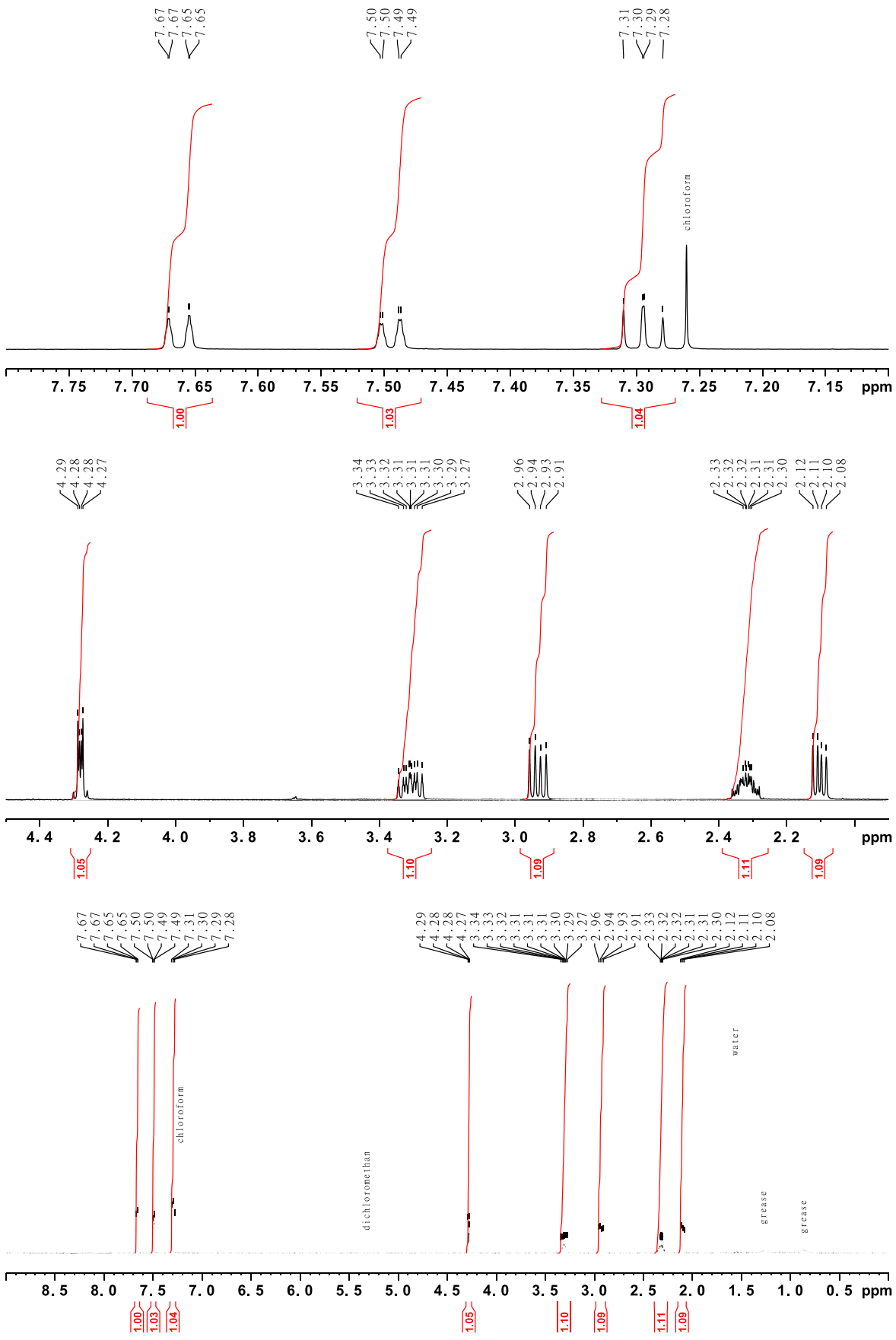

Figure SII.1: ^{1}H-NMR spectrum of (1R,1'R/1S,1'S)-7,7'-dinitro-2,2',3,3'-tetrahydro-1H,1'H-1,1'-diindene.

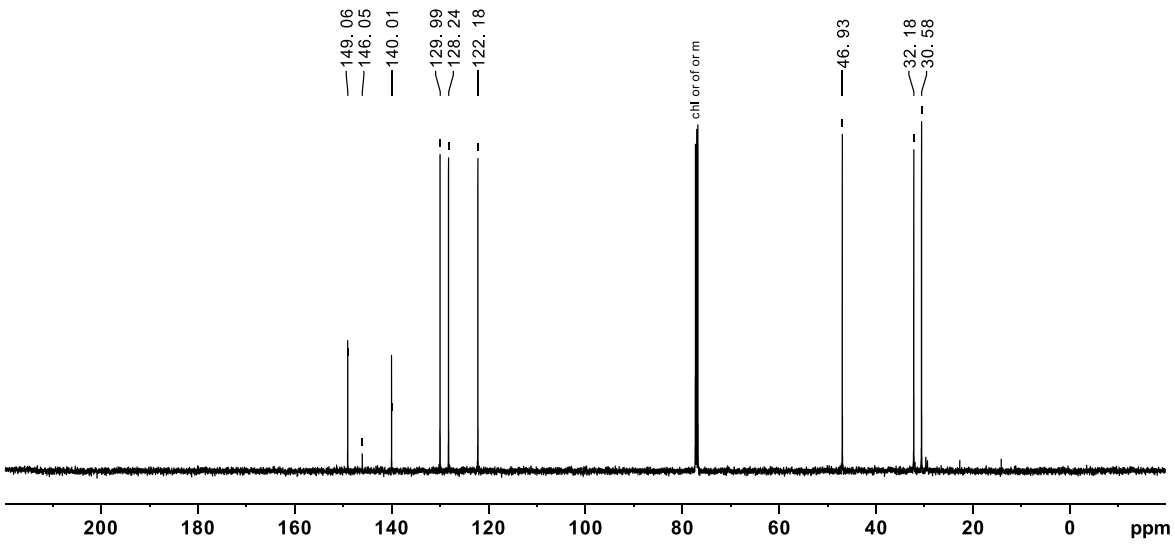

Figure SII.2: ^{13}C-NMR spectrum of (1R,1'R/1S,1'S)-7,7'-dinitro-2,2',3,3'-tetrahydro-1H,1'H-1,1'-diindene.

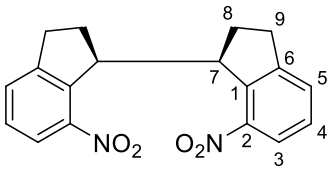

yield: 340 mg (1.05 mmol, 34%)

mp.: 168 °C

R_f = 0.11 (*n*-pentane/DCM, 2:1)

^{1}H-NMR (500.1 MHz, $CDCl_3$), 300 K): δ = 7.82 (d, ^3J = 7.1 Hz, 2 H, *H*-3), 7.38 (d, ^3J = 6.1 Hz, 2 H, *H*-5), 7.32 (d, ^3J = 7.6 Hz, 2 H, *H*-4), 4.55 (d, ^3J = 8.4 Hz, 2 H, *H*-7), 2,74 (dd, ^2J = 16.4 Hz, ^3J = 9.8 Hz, 2 H, *H*-9a), 2.49 (m, 2 H, *H*-9b), 2.35 (m, 2 H, *H*-8a), 2.02 (dd, ^2J = 13.4 Hz, ^3J = 8.0 Hz, 2 H, *H*-8b) ppm.

^{13}C-NMR (125.8 MHz, $CDCl^3$, 300 K): δ = 148.57 (C-6), 147.25 (C-2), 140.02 (C-1), 130.39 (C-5), 128.47 (C-4), 122.83 (C-3), 49.27 (C-7), 32.34 (C-9), 30.02 (C-8) ppm.

MS (HR): m/z $(C_{18}H_{17}O_4N_2)^+$ = calc.: 325.11828, found: 325.11780 ±1.48 ppm.

IR (ATR): $\tilde{\nu}$ = 3084 (w), 2929 (m), 2850 (w), 1730 (w), 1609 (w), 1574 (w), 1520 (s), 1455 (m), 1352 (s), 1339 (s), 1323 (s), 1228 (w), 1175 (w), 1132 (w), 1070 (w), 982 (w), 939 (w), 864 (w), 838 (w), 813 (s), 793 (s), 755 (m), 733 (s), 677 (w), 615 (w) cm^{-1}.

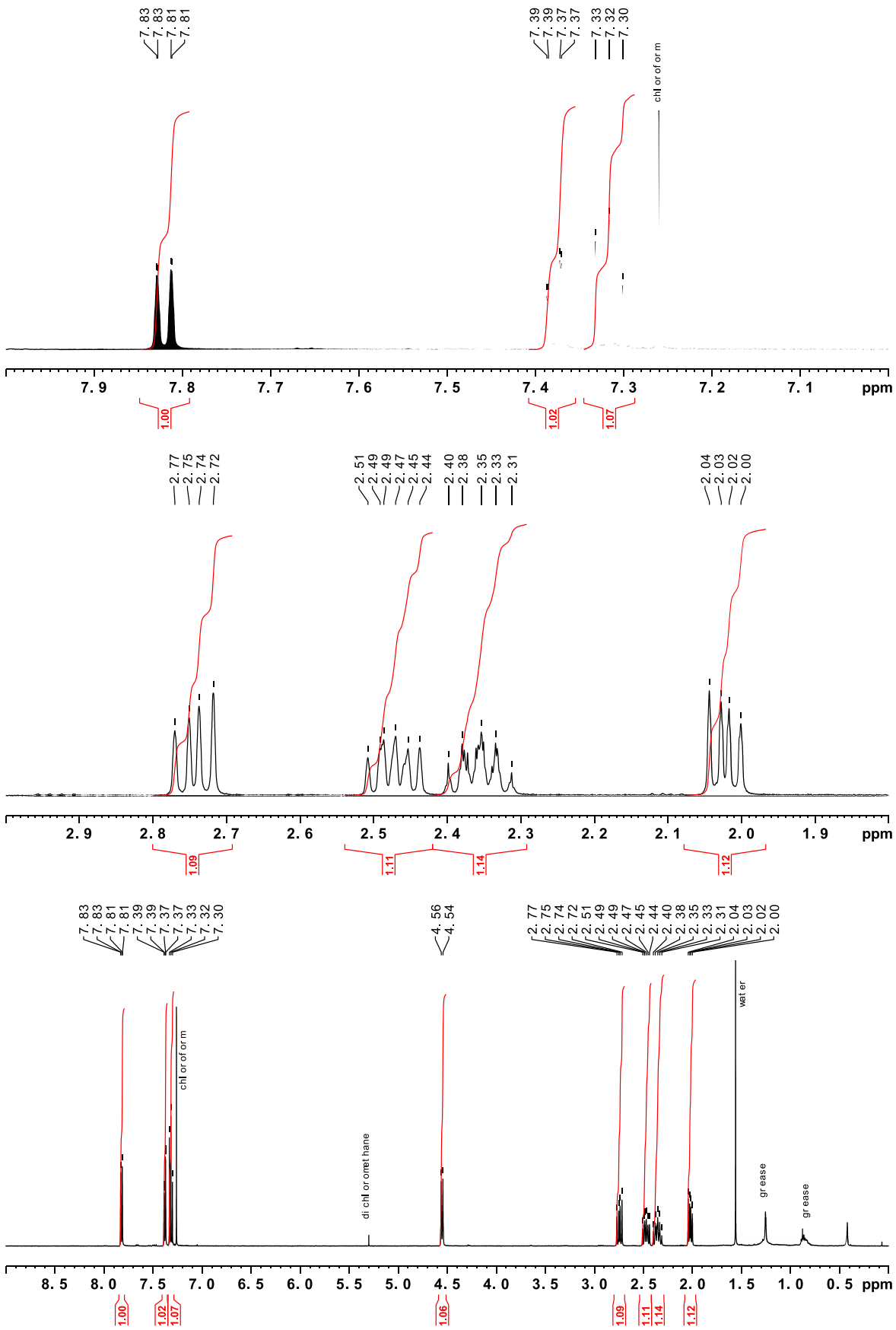

Figure SII.3: ^{1}H-NMR spectrum of (1R,1'S)-7,7'-dinitro-2,2',3,3'-tetrahydro-1H,1'H-1,1'-diindene.

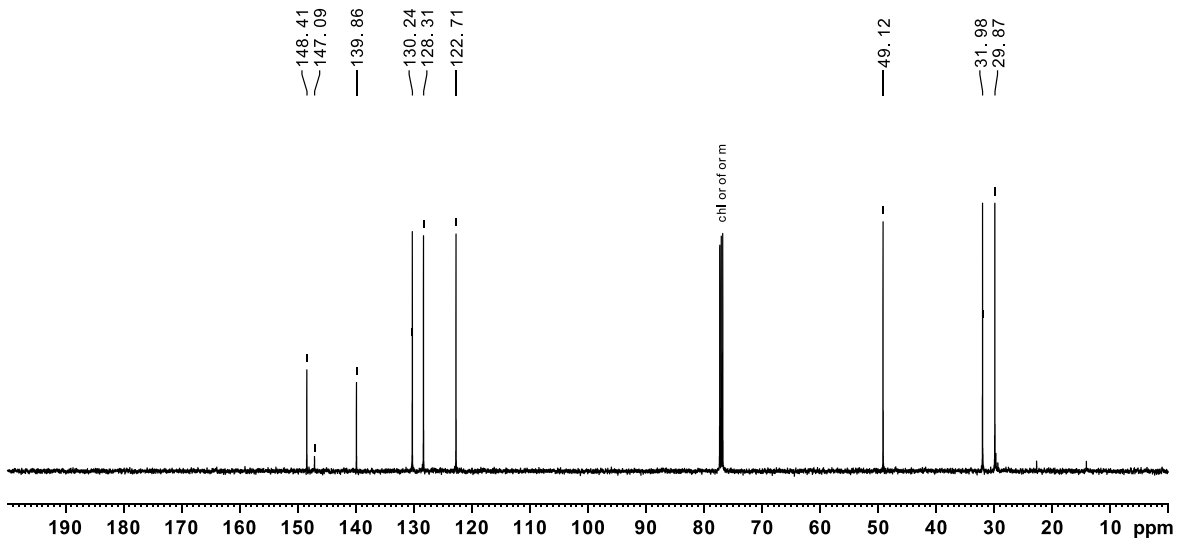

Figure SII.4: ^{13}C-NMR spectrum of (1R,1'S)-7,7'-dinitro-2,2',3,3'-tetrahydro-1H,1'H-1,1'-diindene.

II.1.1 Synthesis of (12aR,12bR/12aS,12bS/Z)-1,2,11,12,12a,12b-hexahydrodiindeno[7,1-cd:1',7'-fg][1,2]-diazocine (3)[2]

To a solution of (1R,1'R/1S,1'S)-7,7'-dinitro-2,2',3,3'-tetrahydro-1H,1'H-1,1'-diindene (500 mg, 1.54 mmol) in EtOH an aqueous solution of barium hydroxide [$Ba(OH)_2 \cdot 8\ H_2O$] (1.70 g, 5.39 mmol) in H^2O (48 mL) and zinc powder (1.90 g, 29.06 mmol) and the mixture was stirred for 16 h under reflux. The reaction mixture was filtered through Celite, and the solvent was removed under reduced pressure. The crude product was dissolved in 0.1 M methanolic NaOH solution (130 mL), $CuCl_2$ (10 mg, 0.07 mmol) was added and the reaction mixture was stirred at room temperature until completion while air was bubbled through the solution. The reaction was neutralized with 6 M HCl solution. Saturated sodium bicarbonate solution (60 mL) was added and the aqueous layer was extracted with DCM (3 × 40 mL). The combined organic layers were dried over $MgSO_4$ and the solvent was removed under reduced pressure. The crude product was purified by column chromatography (silica gel, cyclohexane/EE, 20:1) to afford a yellow solid.

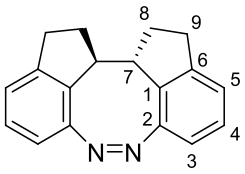

yield: 295 mg (1.13 mmol, 73%)

mp.: 169 °C

R_f = 0.3 (cyclohexane/EE, 20:1)

^{1}H-NMR (500.1 MHz, $CDCl_3$, 300 K): δ = 7.43 (d, ^3J = 7.89 Hz, 2 H, *H*-3), 7.31 (t, ^3J = 7.3 Hz, 2 H, *H*-4), 7.15 (d, ^3J = 7.2 Hz, 2 H, *H*-5), 3.13-2.80 (m, 6 H, *H*-7, *H*-9a, *H*-9b), 2.21 (m, 2 H, *H*-8a), 1.98 (m, 2 H, *H*-8b) ppm.

^{13}C-NMR (125.8 MHz, $CDCl_3$, 300 K): δ = 148.79 (C-2), 144.54 (C-6), 132.94 (C-1), 127.06 (C-4), 125.78 (C-3), 124.56 (C-5), 49.38 (C-7), 31.53 (C-8), 31.49 (C-9) ppm.

MS (HR): m/z = $[C_{18}H_{17}N_2]^+$ calc.: 261.13863, found: 261.13846 ± 0.62 ppm.

IR (ATR): $\tilde{\nu}$ = 3786 (w), 2970 (w), 2914 (w), 2839 (w), 1585 (w), 1530 (w), 1460 (w), 1446 (w), 1423 (w), 1288 (w), 1248 (w), 1227 (w), 1193 (w), 1157 (w), 1122 (w), 1043 (w), 965 (w), 903 (w), 870 (w), 825 (w), 818 (w), 786 (s), 757 (s), 739 (m), 717 (m), 691 (w), 665 (w), 628 (w) cm^{-1}.

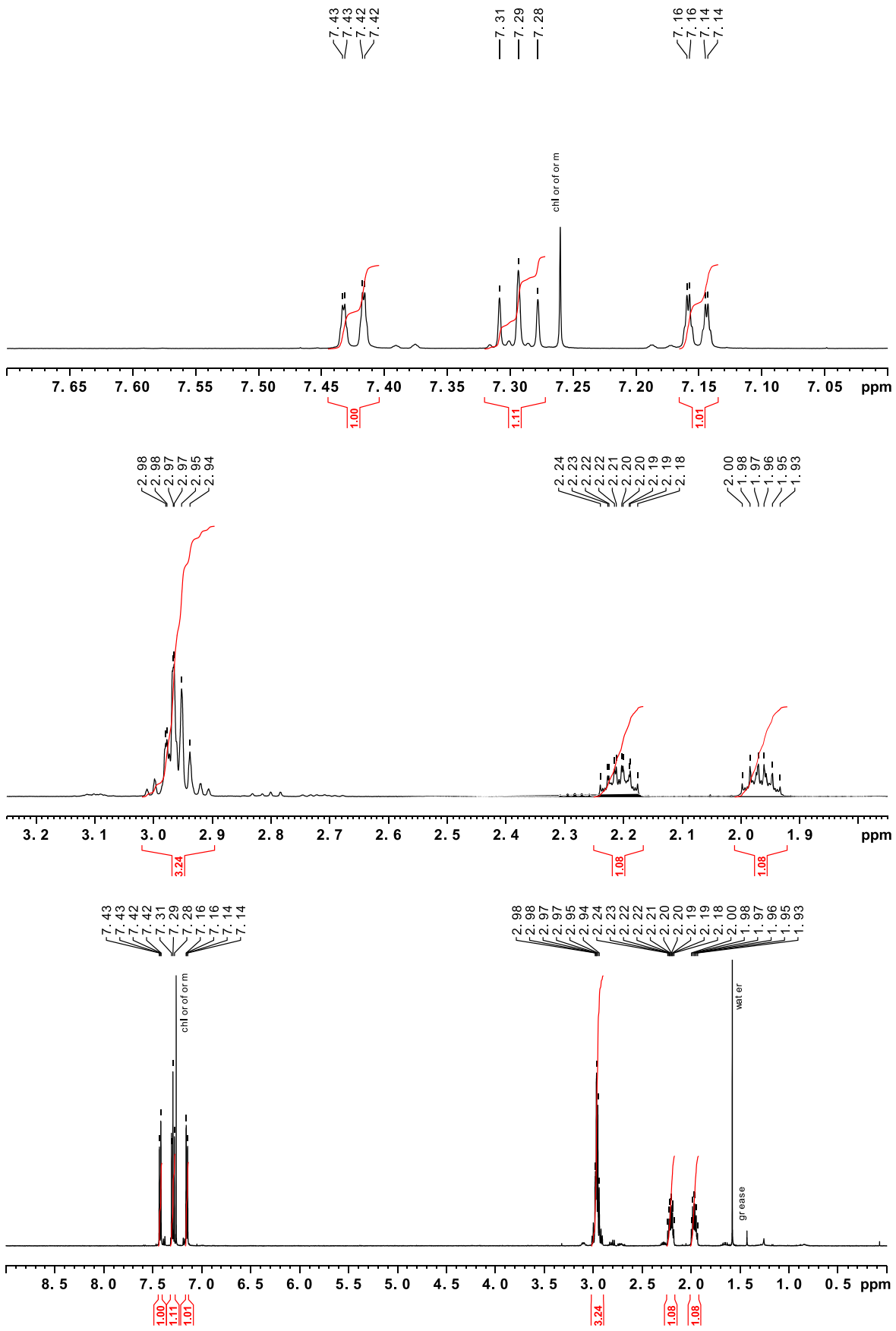

Figure SII.5: ^{1}H-NMR spectrum of (12aR,12bR/12aS,12bS/Z)-1,2,11,12,12a,12b-hexahydrodiindeno[7,1-cd:1',7'-fg][1,2]-diazocine (**3**).

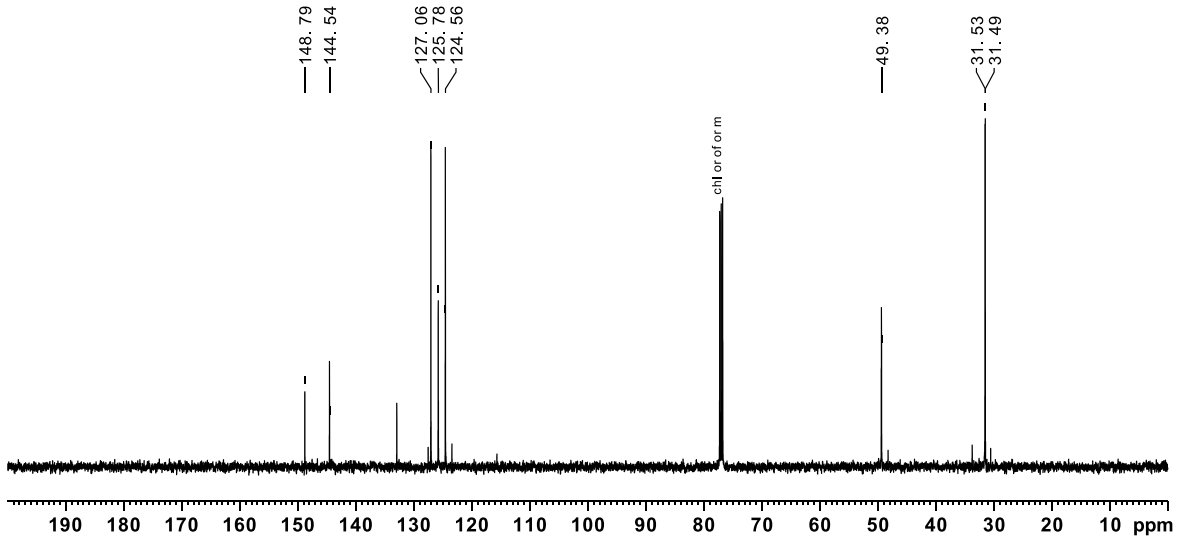

Figure SII.6: ^{13}C-NMR spectrum of (12aR,12bR/12aS,12bS/Z)-1,2,11,12,12a,12b-hexahydrodiindeno[7,1-cd:1',7'-fg][1,2]-diazocine (**3**).

III. Single Crystal Structure Determinations

Preparation of crystal samples

For crystal growth 10 mg of the given compound were dissolved in 0.2 ml acetone in a small glass vial and a drop of water was added. The vial was closed with a perforated cap and was stored in the dark for 3 weeks for slow evaporation of the solvent. Suitable crystals were selected subsequently.

III.1 (12aR,12bR/Z)-1,2,11,12,12a,12b-hexahydrodiindeno[7,1-cd:1',7'-fg][1,2]-diazocine 5

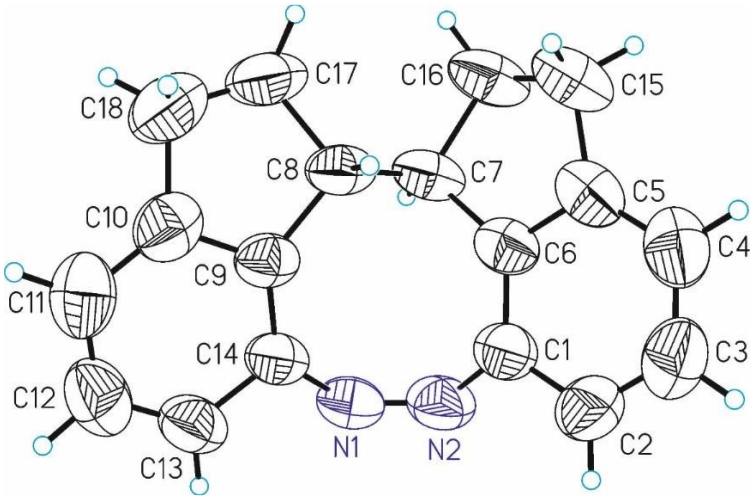

Figure SIII.1: Crystal structure of (12aR,12bR/Z)-1,2,11,12,12a,12b-hexahydrodiindeno[7,1-cd:1',7'-fg][1,2]-diazocine **5.**

Table S.III.1: Selected crystal data and details of the structure refinement for **5.**

Empirical formula	$C_{18}H_{16}N_2$
Formula weight	260.33
Temperature/K	293(2)
Crystal system	orthorhombic
Space group	$P2_12_12_1$
a/Å	8.86340(10)
b/Å	10.3545(2)
c/Å	15.0879(2)
α/°	90
β/°	90
γ/°	90
Volume/Å^3	1384.71(4)
Z	4
ρ_{calc}g/cm^3	1.249
μ/mm^{-1}	0.570

F(000)	552.0
Crystal size/mm^3	0.16 × 0.14 × 0.08
Radiation	Cu Kα (λ = 1.54184)
2Θ range for data collection/°	10.362 to 159.386
Index ranges	-10 ≤ h ≤ 11, -13 ≤ k ≤ 13, -18 ≤ l ≤ 18
Reflections collected	8657
Independent reflections	2944 [R_{int} = 0.0155, R_{sigma} = 0.0158]
Reflections with [I>=2σ (I)]	2806
Data/restraints/parameters	2944/0/181
Goodness-of-fit on F^2	1.067
Final R indexes [I>=2σ (I)]	R_1 = 0.0375, wR_2 = 0.1157
Final R indexes [all data]	R_1 = 0.0386, wR_2 = 0.1170
Largest diff. peak/hole / e Å^{-3}	0.15/-0.12

III.2 (12aS,12bS/Z)-1,2,11,12,12a,12b-hexahydrodiindeno[7,1-cd:1',7'-fg][1,2]-diazocine 6

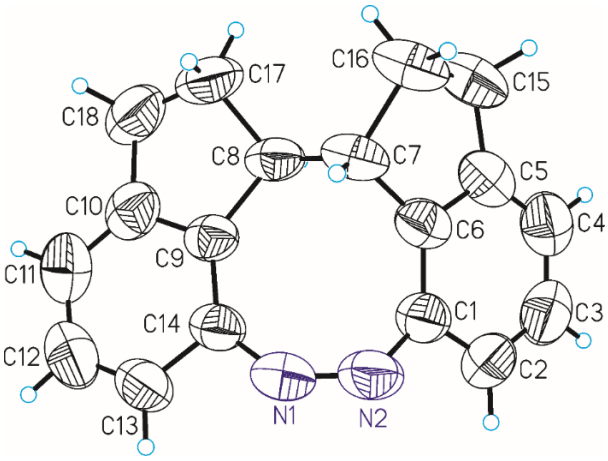

Figure SIII.1: Crystal structure of (12aS,12bS/Z)-1,2,11,12,12a,12b-hexahydrodiindeno[7,1-cd:1',7'-fg][1,2]-diazocine **6.**

Table S.III.1: Selected crystal data and details of the structure refinement for **6.**

Empirical formula	$C_{18}H_{16}N_2$
Formula weight	260.33
Temperature/K	293(2)
Crystal system	orthorhombic
Space group	$P2_12_12_1$
a/Å	8.86321(10)
b/Å	10.35512(15)
c/Å	15.09001(18)

α/°	90
β/°	90
γ/°	90
Volume/Å^3	1384.95(3)
Z	4
ρ_{calc}g/cm^3	1.249
μ/mm^{-1}	0.570
F(000)	552.0
Crystal size/mm^3	0.2 × 0.18 × 0.05
Radiation	Cu Kα (λ = 1.54184)
2Θ range for data collection/°	10.36 to 159.376
Index ranges	-9 ≤ h ≤ 11, -13 ≤ k ≤ 13, -19 ≤ l ≤ 18
Reflections collected	14816
Independent reflections	2968 [R_{int} = 0.0179, R_{sigma} = 0.0095]
Reflections with [I>=2σ (I)]	2891
Data/restraints/parameters	2968/0/181
Goodness-of-fit on F^2	1.046
Final R indexes [I>=2σ (I)]	R_1 = 0.0367, wR_2 = 0.1120
Final R indexes [all data]	R_1 = 0.0372, wR_2 = 0.1126
Largest diff. peak/hole / e Å^{-3}	0.15/-0.14

IV. Photostationary states (PSS)

Photostationary states (PSS) of *rac*-DID **3** were measured via ^{1}H-NMR by integration of the different species after irradiation with different wavelengths (3 min. irradiation time). The values of the integrals are given in Table SIV.1. ^{1}H-NMR spectra were measured at 7.68 mM concentrations at 298 K. All spectra were measured at a Bruker AV600 spectrometer.

Table SIV.1: Measured photostationary states of *rac*-DID **3** in THF-d_8.

wavelength	measured PSS	
nm	% *Z*-**3**	% *E*-**3**
unirradiated	94	6
385	23	77
405	33	67
530	89	11
590	>99%	<1%

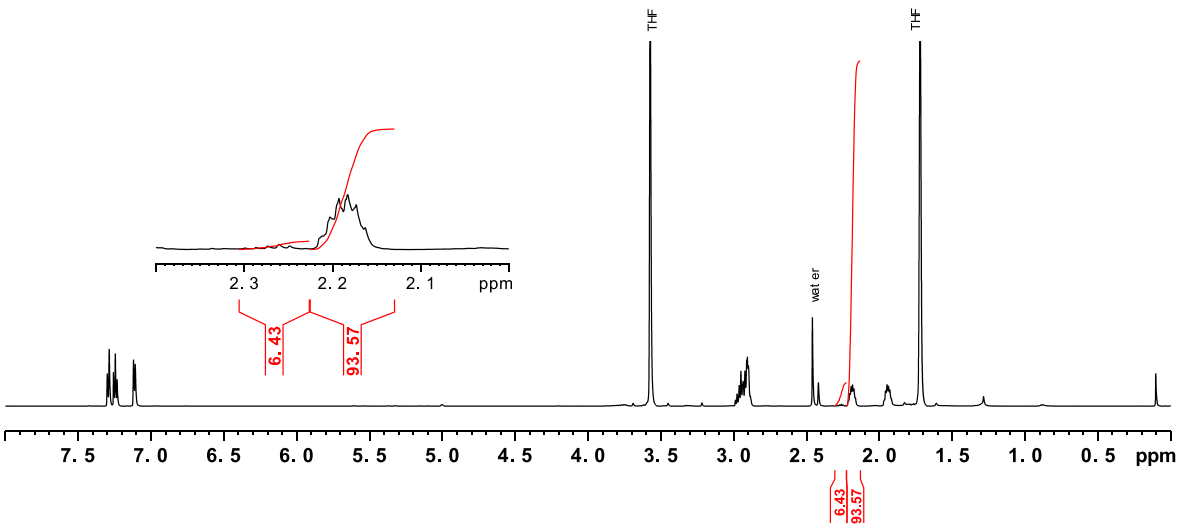

Figure SIV.1: ^{1}H-NMR spectra of unirradiated *rac*-DID **3** in THF-d_8 at 298 K.

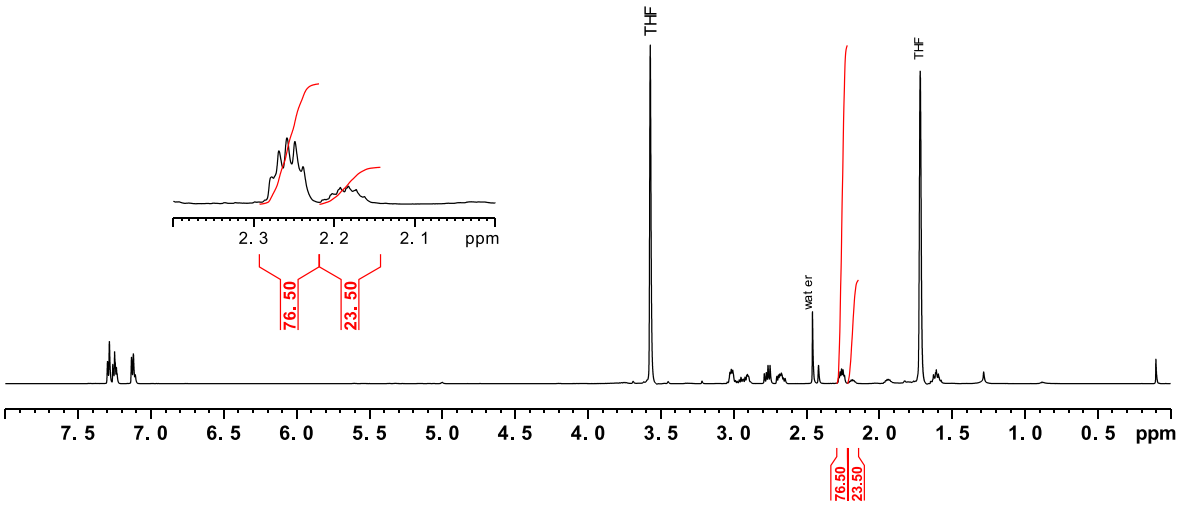

Figure SIV.2: ^{1}H-NMR spectra of *rac*-DID **3** in THF-d_8 at 298 K after irradiation with 385 nm.

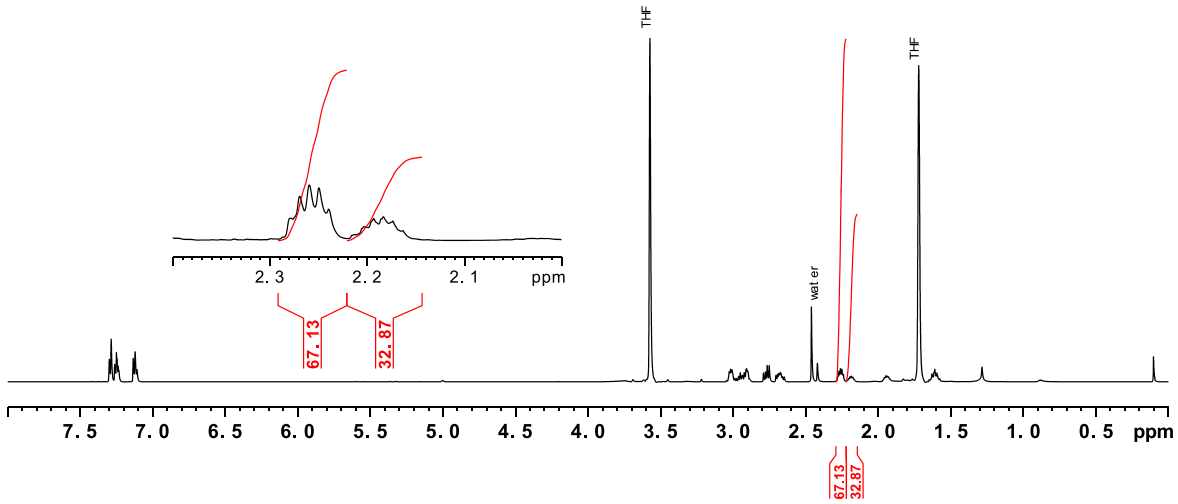

Figure SIV.3: ^{1}H-NMR spectra of *rac*-DID **3** in THF-d_8 at 298 K after irradiation with 405 nm.

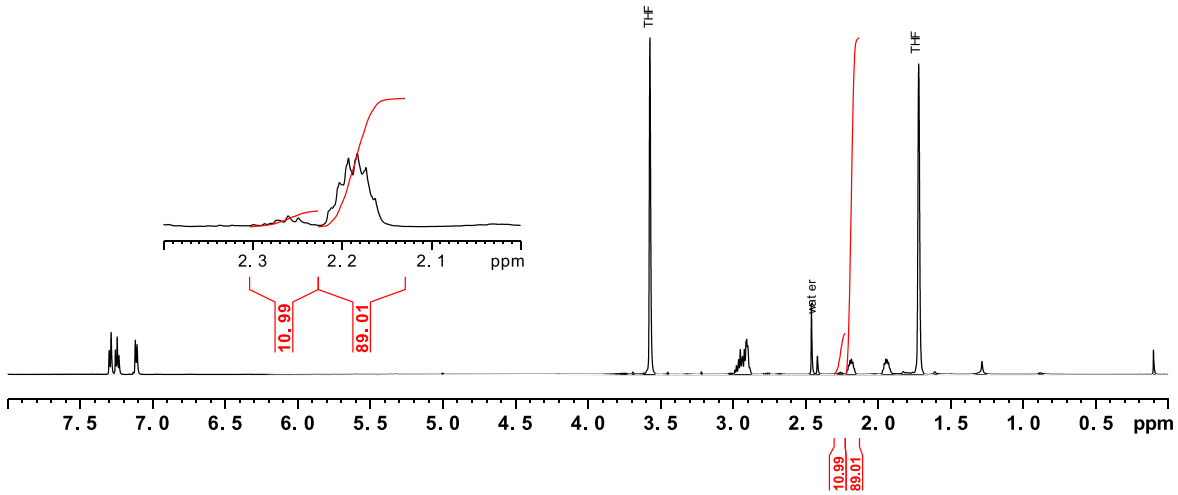

Figure SIV.4: ^{1}H-NMR spectra of *rac*-DID **3** in THF-d_8 at 298 K after irradiation with 530 nm.

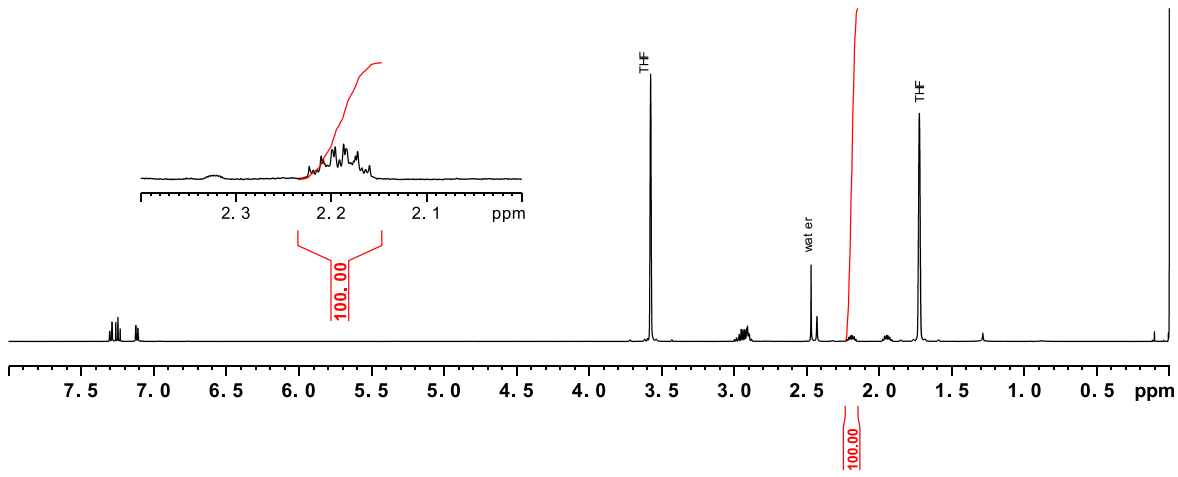

Figure SIV.5: ^{1}H-NMR spectra of *rac*-DID **3** in THF-d_8 at 298 K after irradiation with 590 nm.

V. Optical rotation

The values for optical rotation are given in table SV.1. Optical rotations α were measured at c = 50 mg/100 mL concentrations in acetone at 298 K with a cell length of l = 1 dm. For switching experiments 10 mL solution in acetone were prepared. For each measurement 0.8 mL of measuring solution were used. After measuring the unirradiated sample the whole 10 mL flask was irradiated as exposure in the cuvette was not possible and another 0.8 mL were taken for the measurement. This process was repeated for several measurements and irradiation at different wavelengths.

Table SV.1: Values for optical rotation α of enantiomers **5** and **6** before and after repeated irradiation at 385 nm and 530 nm.

wavelength nm	(-)-*R*,*R*-DID **5** °	(+)-*S*,*S*-DID **6** °
unirradiated	-0.185	0.195
385	-0.679	0.762
530	-0.098	0.108
385	-0.687	0.751
530	-0.099	0.106
385	-0.683	0.758
530	-0.098	0.096
385	-0.703	0.744
530	-0.106	0.107
385	-0.695	0.761

Specific rotations $[\alpha]_\lambda^T$ for both enantiomers were calculated following equation 1 and are shown in Table SV.2.

$$[\alpha]_D^{298\,K} = \frac{100 \times \alpha}{l \times c} \quad (1)$$

Table SV.2: Values for specific rotation $[\alpha]_\lambda^T$ before and after repeated irradiation at 385 nm and 530 nm.

wavelength nm	(-)-*R*,*R*-DID **5** °	(+)-*S*,*S*-DID **6** °
unirradiated	-370	390
385	-1358	1524
530	-196	216
385	-1374	1502
530	-198	212
385	-1366	1516
530	-196	192
385	-1406	1488
530	-212	214
385	-1390	1522

VI. Circular dichroism

The CD spectrometer was purged with N_2 for 10 min. Spectra were measured between 300 nm and 700 nm with a standard sensitivity of 100 mdeg, a data pitch of 5 nm, a scanning speed of 20 nm min^{-1} and a response time of 2 s, using a quartz cuvette (path length d = 0.1 cm). The solutions were prepared in THF and measured at 20 °C. A blank was measured before and after every recorded spectrum.

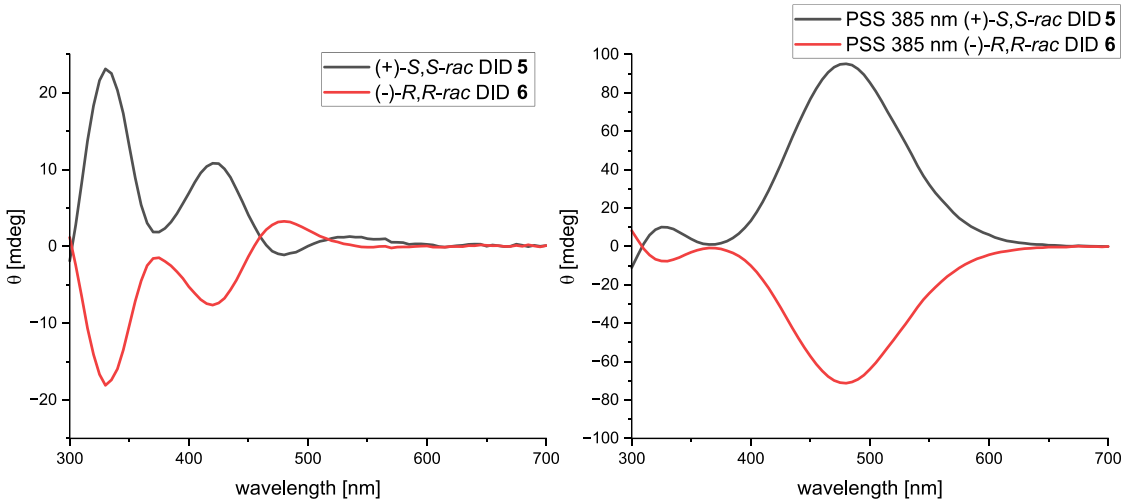

Figure SVI.1: CD spectra showing the ellipticity Θ of *Z*- (left) and *E*-configurations (right) of (+)-*S*,*S*-*rac*-DID **6** (c = 1.34 mM) and (-)-*R*,*R*-*rac*-DID **5** (c = 1.04 mM) in THF at 25 °C.

Molar circular dichroism $\Delta\varepsilon$ was calculated from the ellipticity ε following equation 2 which can be obtained by converting Beer-Lambert law.

$$\Delta\varepsilon = \varepsilon_{LH} - \varepsilon_{RH} = \frac{\Delta A}{c \cdot d} = \frac{\Theta}{32980 \cdot c \cdot l} \tag{2}$$

with

$$\Delta A = \frac{\Theta}{32980}$$

$$c = \%PSS \cdot [enantiomer]$$

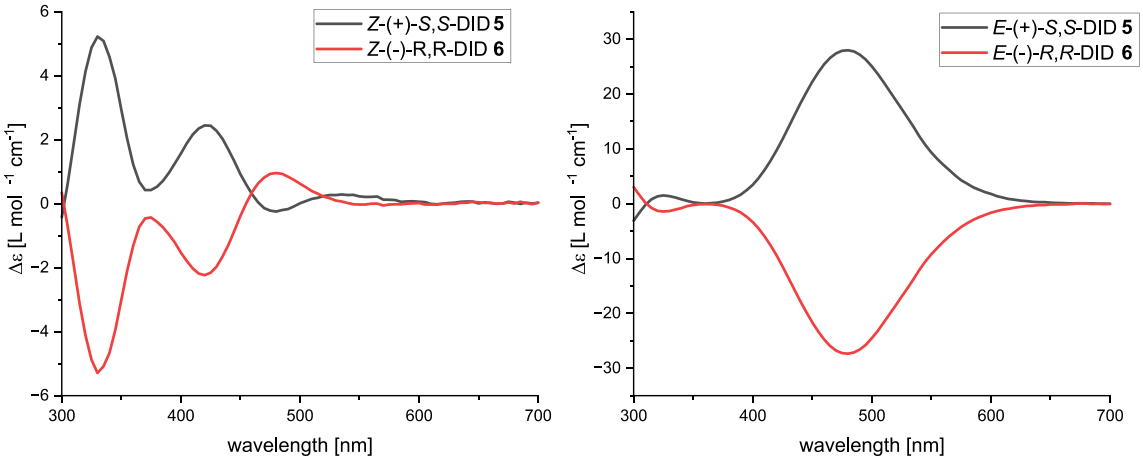

Figure SVI.2: Molar circular dichroism $\Delta\varepsilon$ of (-)-*R*,*R*-*rac*-DID **5** (1.04 mM) and (+)-*S*,*S*-*rac*-DID **6** (1.34 mM) before (left) and at PSS after irradiation with blue light at 385 nm (right) in THF at 25°C.

The molar circular dichroism $\Delta\varepsilon$ of pure *E*-configurations of both enantiomers **5** and **6** was calculated via equation 3 from the molar circular dichroism $\Delta\varepsilon$ at PSS, the PSS values determined from ^{1}H-NMR in THF-d_8 at 298 K after irradiation at 385 nm and molar circular dichroism $\Delta\varepsilon$ of pure *Z*-configurations.

$$\Delta\varepsilon_{E,extrapol.} = \frac{\Delta\varepsilon_{PSS} - [\Delta\varepsilon_Z \cdot (1 - PSS)]}{PSS} \tag{4}$$

VII. UV-vis experiments

All samples were irradiated to the photostationary state (PSS) with 385 nm in THF. The extrapolated UV-vis spectra of the *E*-configurations were calculated from the UV-vis spectra of the PSS, the pure *Z*-configuration and the percentage of *E*-configuration measured by ^{1}H-NMR (for details see SIV) by the following equation (4):

$$A_{E,extrapol.} = \frac{A_{PSS} - [A_Z \cdot (1 - PSS)]}{PSS} \quad (4)$$

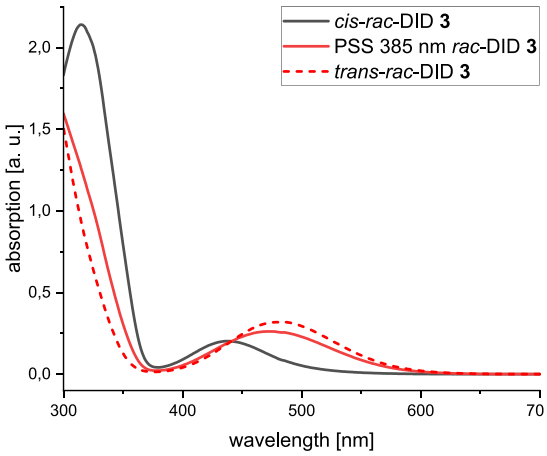

Figure SVII.1: UV-vis spectra of *rac*-DID 3 (1 mM) in THF at 25 °C before (black) and after irradiation with 385 nm (red). The extrapolated *E*-spectrum is shown as dashed red line.

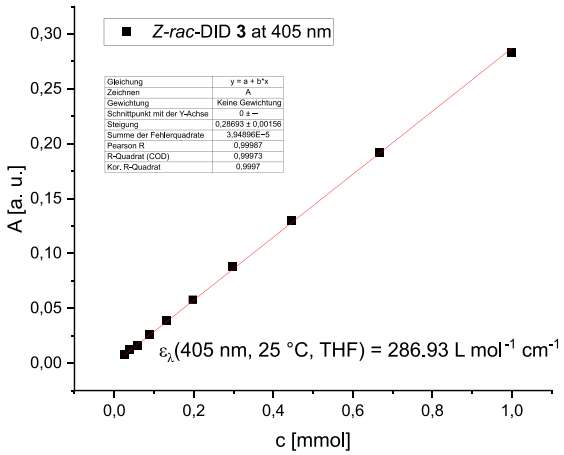

Figure SVII.2: Determination of molar extinction coefficient ε in THF at 25°C at 405 nm.

VIII. Determination of enantiomeric excess (ee) at PSS405 nm

The sample cell holder was removed from the CD spectrometer and a 1×1 cm magnetic stirrer was installed for homogenous irradiation. To ensure that only CPL reaches the sample an irradiation box was printed in a 3D-printer, in which the LED and the CPL filter were installed. The irradiation box was positioned next to the magnetic stirrer in a way that the sample could be irradiated without opening the spectrometer. The distance between LED and CPL-filter was 2 cm and between CPL-filter and sample 1 cm. A fan was also installed to prevent the sample from heating.

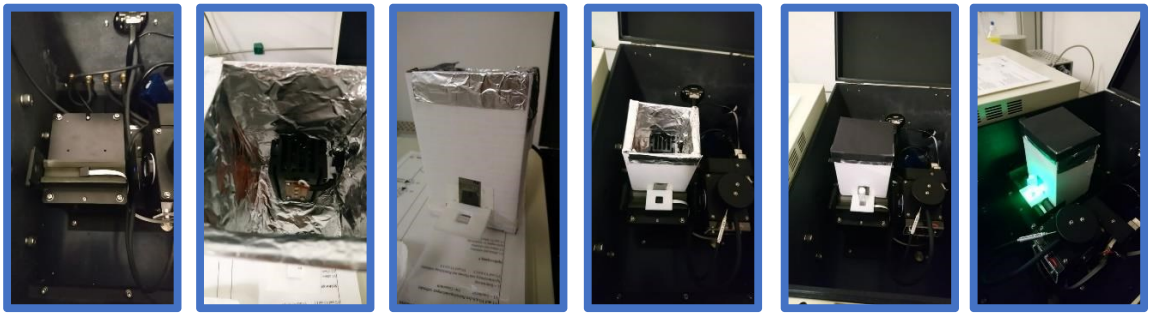

Figure SVIII.1: Setup for irradiation with CPL inside the CD spectrometer for determination of ellipticity Θ depending from the irradiation time.

A solution of *rac*-DID **3** (c = 0.86 mM) was stirred (600 rpm) in a quartz cuvette (d = 1 cm) while irradiated with r/l-CPL at 405 nm and measured directly after irradiation at 480 nm with a measuring time of 1 min. Before each irradiation with CPL the sample was irradiated with 590 nm to start from pure *Z*-configuration.

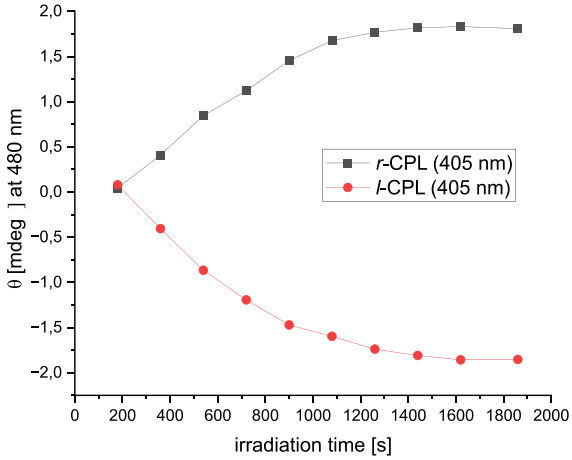

Figure 8: Induced ellipticity Θ at 480 nm of *E*-*rac*-DID **3** (0.86 mM) after irradiation with r-CPL (black) and l-CPL (red) at 405 nm depending on the irradiation time.

The ee values were calculated from the induced ellipticity Θ after irradiation with r/l-CPL (405 nm) at 480 nm of the sample solution and the molar circular dichroism $\Delta\varepsilon_{480\,nm}$ of the pure enantiomers at the following equation 5 according to RIJESH et al.[3] The concentration of *E*-*rac*-DID **3** was calculated from the analyte concentration and the PSS value in THF after irradiation with 405 nm (see SIV).

$$\%ee = \frac{[S]-[R]}{[S]+[R]} \cdot 100\% = \frac{\Theta_{480\,nm}}{32980 \cdot \Delta\varepsilon_{480\,nm} \cdot d \cdot PSS \cdot c} \cdot 100\% \quad (5)$$

With

$$[S]-[R] = \frac{\Theta_{480\,nm}}{32980 \cdot \Delta\varepsilon_{480nm} \cdot d}$$

$$[S]+[R] = [rac] = PSS \cdot c$$

Experimental ee values for *rac*-DID **3** after irradiation with r/l-CPL (405 nm):

$$\%ee_{(+)-405\,nm} = \frac{1.83124}{32980 \cdot 27.97355 \frac{L}{mol \cdot cm} \cdot 1\,cm \cdot 0.67 \cdot 0.00086 \frac{mol}{l}} \cdot 100\% = 0.344\% \quad (6)$$

$$\%ee_{(-)-405\ nm} = \frac{-1.85721}{32980 \cdot (-27.36345 \frac{L}{mol \cdot cm}) \cdot 1\ cm \cdot 0.67 \cdot 0.00086 \frac{mol}{l}} \cdot 100\% = 0.357\% \quad (7)$$

Calculation of the theoretical ee following equation 7:[3]

$$\%ee = \frac{g}{2} \cdot 100\% = \frac{\Delta\varepsilon_{405\ nm}}{2 \cdot \varepsilon_{405\ nm}} \cdot 100\% \quad (8)$$

with

$$g = \frac{\Delta\varepsilon_{405\ nm}}{\varepsilon_{405\ nm}}$$

Theoretical ee values for the irradiation of *rac*-DID **3** with r/l-CPL (405 nm):

$$\%ee_{(+)-405\ nm} = \frac{1.88353 \frac{L}{mol \cdot cm}}{2 \cdot 286.93 \frac{L}{mol \cdot cm}} \cdot 100\% = 0.32822\% \quad (9)$$

$$\%ee_{(-)-405\ nm} = \frac{\left|-1.78884 \frac{L}{mol \cdot cm}\right|}{2 \cdot 286.93 \frac{L}{mol \cdot cm}} \cdot 100\% = 0.31172\% \quad (10)$$

IX. Quantum Chemical Calculations

All calculations were performed using ORCA[4] the data was extracted using Multwfn 3.8.[5] Geometries the for (+)-*S*,*S*-enantiomer **1** were optimized on a pbe/def2-SVP[6-8] level of theory. ECD calculations were performed on a ωB97X/def2-QZVP[6,7,9] level of theory employing a conductor-like polarizable continuum model (CPCM)[10] for tetrahydrofuran as well as Grimmes D4 dispersion correction.[11,12] All obtained spectra were shifted in energy to match the local maximum in molar circular dichroism. The molar circular dichroism itself was normalized to match experimentally obtained values for said maximum. The width at half maximum (FWHM) was set to 0.25 eV for the *Z* and 0.666eV for the *E*-configuration.

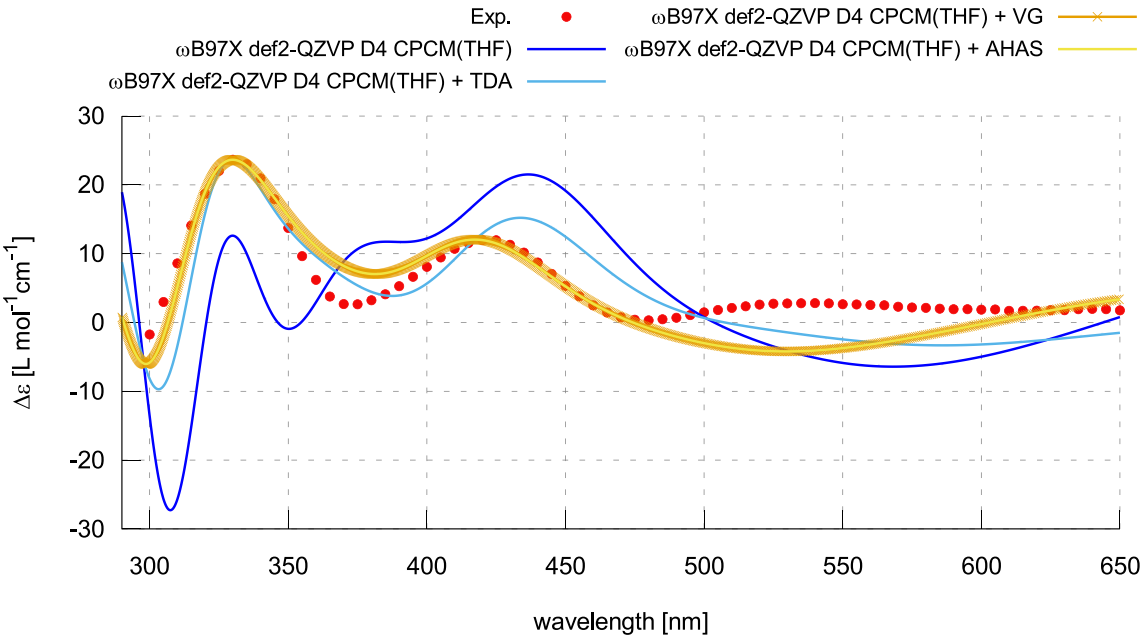

Figure 9: CD-Spectrum of the (+)-*S*,*S*-enantiomer **6.** Calculated spectra plotted against the experimentally obtained CD-spectrum of the Z-configuration (red). The structure was fully optimized on a pbe/def2-SVP level of theory. The CD-Spectra were calculated on a ωB97X/def2-QZVP level of theory employing a conductor-like polarizable continuum model (CPCM) for tetrahydrofuran as well as Grimmes D4 dispersion correction. We tested a simple TD-DFT calculation with and without the simplified Tamm-Dancoff approach (TDA). The simplified simplified Tamm-Dancoff approach matches the experimentally obtained data a lot closer. We further applied two methods without TDA to include excited state dynamics the Vertical Gradient (VG) and Adiabatic Hessian after Step (AHAS) approximations. Both methods produce the same CD-Spectrum which is reasonably close to the experimentally observed. All obtained spectra were shifted in energy. The molar circular dichroism was normalized to match experimentally obtained values.

We tested a simple TD-DFT calculation with and without the simplified Tamm-Dancoff approach (TDA).[13] It is easily evident that the TD-calculation with the simplified simplified Tamm-Dancoff approach matches the experimentally obtained data for the *Z*-configuration a lot closer. We further employed two methods without TDA to include excited state dynamics the Vertical Gradient (VG) and Adiabatic Hessian after Step (AHAS) approximations.[14] Both methods perform equally well for the prediction of the CD-Spectrum for the *Z*-configuration. After normalization and shift the obtained spectrum is reasonably close to the experimentally obtained. For the *E*-configuration all applied methods yield the same result for the observed range in wavelength which is reasonably close to the experimental CD-Spectrum.

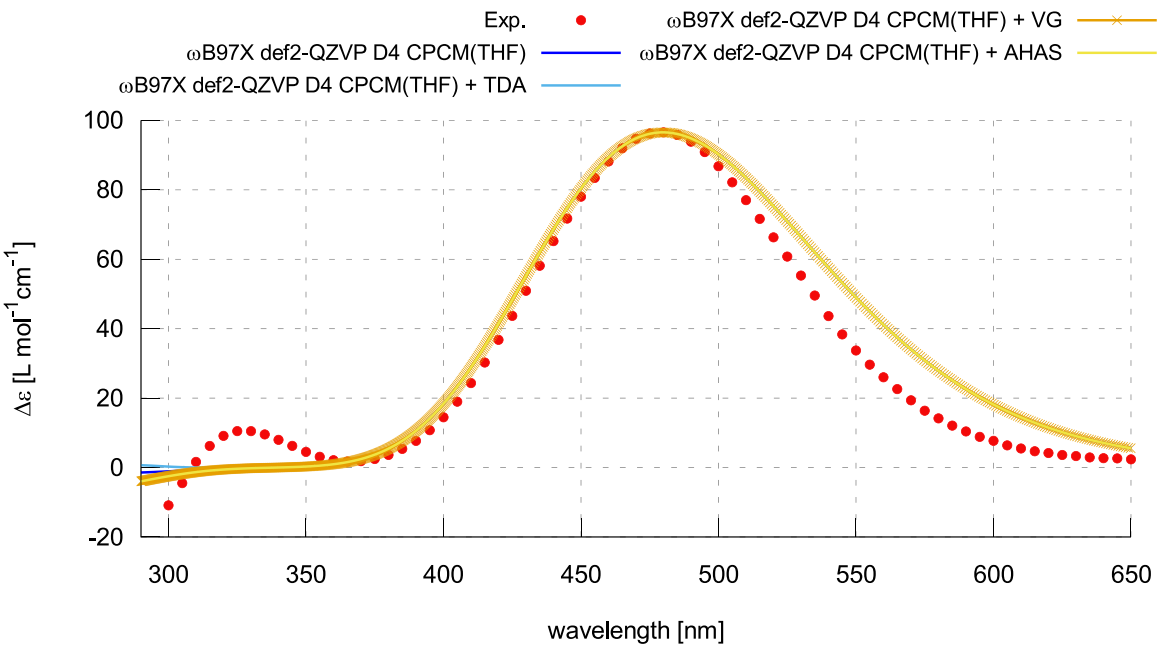

Figure 10: CD-Spectrum of the (+)-*S*,*S*-enantiomer **6**. Calculated spectra plotted against the experimentally obtained CD-spectrum of the *E*-configuration (red). The structure was fully optimized on a pbe/def2-SVP level of theory. The CD-Spectra were calculated on a ωB97X/def2-QZVP level of theory employing a conductor-like polarizable continuum model (CPCM) for tetrahydrofuran as well as Grimmes D4 dispersion correction. We tested a simple TD-DFT calculation with and without the simplified Tamm-Dancoff approach (TDA). We further employed two methods without TDA to include excited state dynamics the Vertical Gradient (VG) and Adiabatic Hessian after Step (AHAS) approximations. All methods produce the same CD-Spectrum which is reasonably close to the experimentally observed. All obtained spectra were shifted in energy. The molar circular dichroism was normalized to match experimentally obtained values.

X. References

[1] G. M. Sheldrick, *Acta Cryst. Section* **2015**, *71*, 3-8.

[2] W. Moormann, T. Tellkamp, E. Stadler, F. Röhricht, C. Näther, R. Puttreddy, K. Rissanen, G. Gescheidt, R. Herges, *Angew. Chem. Int. Ed.* **2020**, *59*, 15081-15086.

[3] K. Rijeesh, P. K. Hashim, S.-I. Noro, N. Tamaoki, *Chem. Science* **2015**, *6*, 973-980.

[4] F. Neese, *J. Chem. Phys.* **2020**, *152*, 224108.

[5] T. Lu, *J. Comput. Chem.* **2012 ,***33*, 580-592. DOI: 10.1002/jcc.22885

[6] J. Perdew, Phys. Phys. Rev. Lett. **1997**, *78*, 1396.

[7] F. Weigend, *Phys. Chem. Chem. Phys*. **2005**, *7*, 3297.

[8] F. Weigend, *Phys. Chem. Chem. Phys.* **2006**, *8*, 1057.

[9] J.-D. Chai, *J. Chem. Phys.* **2008**, *128*, 084106.

[10] S. J. Strickler, *J. Chem. Phys*. **1962**, *37*, 814.

[11] E. Caldeweyher, *J.Chem.Phys*. **2017**, *147*, 034112.

[12] E.Caldeweyher, *J. Chem. Phys.* **2019**, *150*, 154122.

[13] S. Grimme, *J. Chem. Phys.* **2013**, *138*, 244104.

[14] B. de Souza, *J. Chem. Phys.* **2018**; *148* ,034104.

8.2.2 Synthesis and Characterization of New Diindanodiazocine Derivatives

Supporting Information

Synthesis and Characterization of New Diindanodiazocine Derivatives

Thomas Brandt, Jan Peter Mikosch, Lasse Cipriani, Rainer Herges*

Table of contents

SI. Analytical Equipment

NMR spectroscopy

NMR spectra were measured in deuterated solvents (Deutero). The spectra were referenced to the following solvent residual signals:

solvent	degree of deuteration	^{1}H signal ppm	^{13}C-signal ppm
acetone-d_6	99.8%	2.05 (quintet)	29.84 (septet)
chloroform-d_1	99.8%	7.26 (singlet)	77.16 (triplet)

The spectra were recorded with a Bruker DRX 500 (^{1}H-NMR: 500 MHz, ^{13}C-NMR: 125 MHz) and a Bruker AV 600 (^{1}H-NMR: 600 MHz, ^{13}C-NMR: 150 MHz). The Multiplicities of the signals were abbreviated with s (singlet), d (doublet), t (triplet), q (quartet), quint. (quintet), m (multiplet), and br. (broad) in addition for broad signals.

Melting Point

Melting Points were measured with a Melting Point B-560 (Büchi) in melting point tubes without further correction.

Mass spectrometry

Mass spectra (EI) and high-resolution mass spectra (HR-EI) were measured with an AccuTOF GCv 4G EI-time of flight mass spectrometer from the company Joel. An ionization energy of 70 eV was used. HR-ESI mass spectra were measured with a Q Exactive Plus Hybrid Quadrupole-Orbitrap ESI-mass spectrometer of the company Thermo Scientific.

IR spectroscopy

Infrared spectra were measured with a Perkin-Elmer 1600 FT-IR spectrometer with an A531-G Golden-Gate-Diamond-ATR-unit. Signals were abbreviated with w (weak), m (medium) or s (strong) for its intensity.

UV-vis spectroscopy

UV-vis spectra were measured with a Perkin-Elmer Lambda 14 UV-vis spectrometer. Quartz cuvettes of 10 mm optical path length were used.

Chromatography

Silica gel (Merck, particle size 0.040-0.063 mm) was used for column chromatography purifications. R_f values were determined via thin layer chromatography on Polygram® SilG/UV254 (Macherey Nagel, 0.2 mm particle size).

Chemicals

All commercially available chemicals were used without further purification.

Light sources

For irradiation different custom-built light sources with a wavelength of 385 nm and 530 nm were used (Sahlmann Photochemistry Solutions & in-house built). Irradiation wavelengths for all (385 nm and 530 nm) LED units were measured via a mobile UV-vis spectrometer (USB4000-UV-VIS, Ocean Optics, Largo, FL, USA). All emission spectra were normalized. Figure SI1 shows the normalized emission spectra of all LED units used.

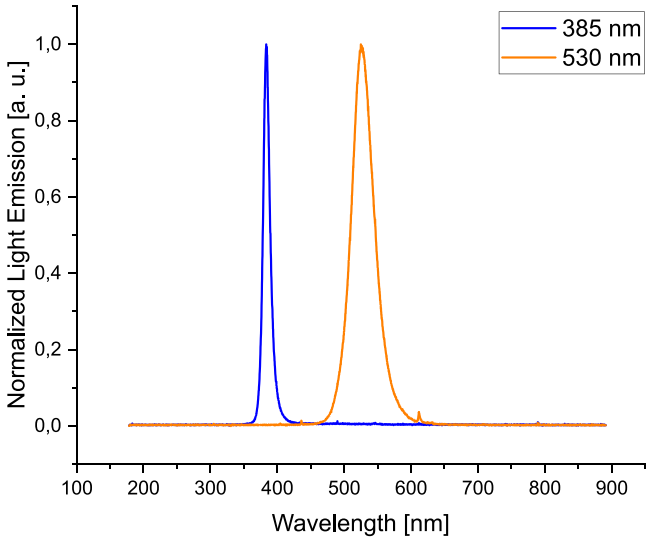

Figure SI.1: Emission spectra of all LED units used. For better comparison all datasets were normalized to its maximum.

The full width at half maximum (FWHM) amounts to 13 nm (378-390 nm, maximum at 384 nm) for the 385 nm LED unit, and to 38 nm (509-547 nm, maximum at 525 nm) for the 530 nm LED unit.

SII. Syntheses

SII.1.1 Synthesis of 2-bromo-4-nitroindane (8)

4-Nitroindane (**7**) (3.02 g, 18.5 mmol) was dissolved in 15 mL conc. sulfuric acid at 0 °C and *N*-bromosuccinimide (3.60 g, 20.2 mmol) was added. After removing the ice bath, the reaction mixture was stirred at room temperature for 3 h and poured on ice subsequently. The reaction mixture was extracted with DCM and the combined organic phases were washed with sat. sodium thiosulfate solution. After drying over magnesium sulfate the solvent was removed under reduced pressure and the product could be obtained as brown solid which was used without further purification.

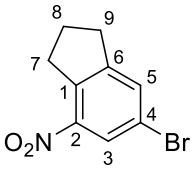

8

yield: 4.59 g (18.5 mmol, >99%)

mp.: 82 °C

^{1}H-NMR (500.1 MHz, $CDCl_3$, 300 K): δ = 8.13-8.12 (m, 1 H, *H*-3), 7.64-7.62 (m, 1 H, *H*-5), 3.35 (t, ^3J = 7.6 Hz, 2 H, *H*-7), 3.01 (t, ^3J = 7.6 Hz, 2 H, *H*-9), 2.16 (q, ^3J = 7.6 Hz, 2 H, *H*-8) ppm.

^{13}C-NMR (125.8 MHz, $CDCl_3$, 300 K): δ = 150.33 (C-6), 145.91 (C-2), 139.99 (C-1), 133.16 (C-5), 124.96 (C-3), 120.13 (C-4), 33.81 (C-7), 32.89 (C-9), 24.92 (C-8) ppm.

HR-MS (EI, 70 eV, DCM): m/z $[M]^+$ calculated for $C_9H_8{}^{79}Br_1NO_2^+$: 240.97384; found: 240.97391 ± 0.27 ppm.

IR (ATR): $\tilde{\nu}$ = 3085 (m), 2956 (m), 1739 (w), 1583 (w), 1525 (s), 1432 (m), 1401 (m), 1349 (s), 1310 (s), 1269 (m), 1195 (m), 1148 (m), 1050 (w), 952 (m), 914 (w), 850 (s), 754 (s), 689 (m) cm^{-1}.

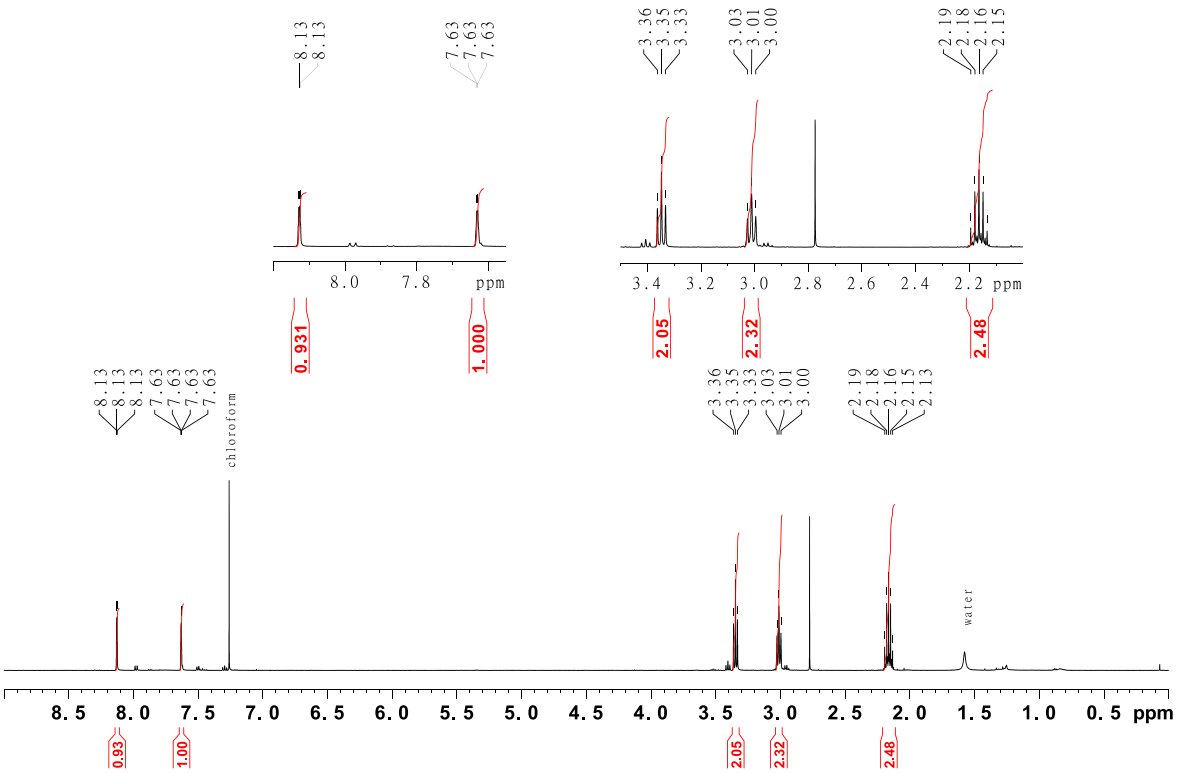

Figure SII.1: 500 MHz ^{1}H-NMR spectrum of 2-bromo-4-nitroindane (**8**).

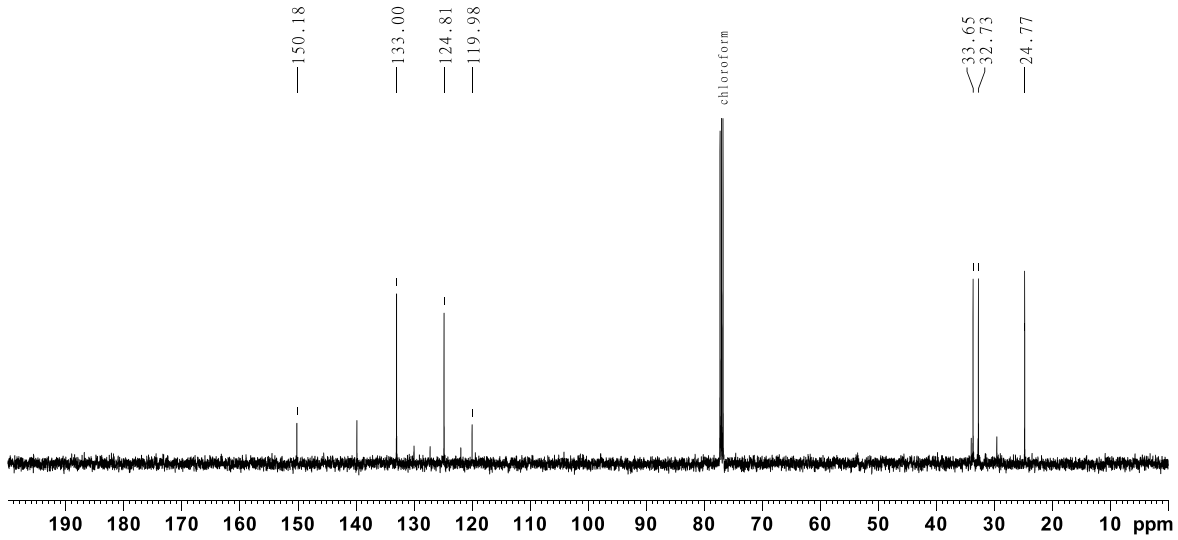

Figure SII.2: 125 MHz ^{13}C-NMR spectrum of 2-bromo-4-nitroindane (**8**).

SII.1.2 Synthesis of (1*R*,1'*S*)-5,5'-dibromo-7,7'-dinitro-2,2',3,3'-tetrahydro-1*H*,1'*H*-1,1'-diindene (10) and (1*R*,1'*R*/1*S*,1'*S*)-5,5'-dibromo-7,7'-dinitro-2,2',3,3'-tetrahydro-1*H*,1'*H*-1,1'-diindene (11)

2-Bromo-4-nitroindane (**8**, 2.00 g, 8.26 mmol) was dissolved in dry THF under nitrogen atmosphere, cooled to 0 °C and potassium butoxide (1.40 g, 12.4 mmol) was added. The reaction was stirred for 30 s before bromine (1.66 g, 0.52 mL, 10.4 mmol) was added rapidly. The reaction was stirred for further 10 min. and 150 g of ice were added. The aqueous solution was extracted with DCM (3 × 40 mL) and the combined organic layers were wash with saturated sodium thiosulfate solution, dried with over $MgSO_4$ and the solvent was removed under reduced pressure. The crude product was purified by column chromatography (silica gel, *n*-pentane/DCM, 3:1) to afford the diastereomers as colorless solids.

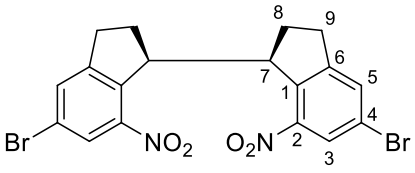

10

yield: 587 mg (1.40 mmol, 34%)

mp.: 217 °C

R_f = 0.09 (*n*-pentane/DCM, 4:1)

^{1}H-NMR (600 MHz, $CDCl_3$), 300 K): δ = 7.98 (s, 2 H, *H*-3), 7.53 (a, 2 H, *H*-5), 4.47 (d, ^3J = 9.0 Hz, 2 H, *H*-7), 2,77 (dd, ^2J = 16.7 Hz, ^3J = 8.9 Hz, 2 H, *H*-9a), 2.55-2.46 (m, 2 H, *H*-9b), 2.42-2.32 (m, 2 H, *H*-8a), 2.01 (dd, ^2J = 13.5 Hz, ^3J = 7.9 Hz, 2 H, *H*-8b) ppm.

^{13}C-NMR (150 MHz, $CDCl^3$, 300 K): δ = 150.26 (C-6), 147.17 (C-2), 138.70 (C-1), 133.29 (C-5), 125.73 (C-3), 121.46 (C-4), 48.70 (C-7), 31.97 (C-9), 29.78 (C-8) ppm.

HR-MS (EI, 70 eV, DCM): m/z $[M]^+$ calculated for $C_{18}H_{14}{}^{79}Br_2N_2O_4^+$: 479.93203; found: 479.93187 ± 0.33 ppm.

IR (ATR): $\tilde{\nu}$ = 3091 (w), 2986 (m), 2921 (m), 2851 (m), 1763 (w), 1604 (w), 1561 (w), 1515 (s), 1456 (m), 1430 (w), 1402 (w), 1347 (s), 1305 (s), 1283 (m), 1231 (m), 1196 (m), 1168 (w), 1136 (m), 994 (w), 948 (w), 918 (w), 898 (w), 878 (s), 852 (s), 785 (m), 758 (s), 721 (w), 693 (s), 619 (w) cm^{-1}.

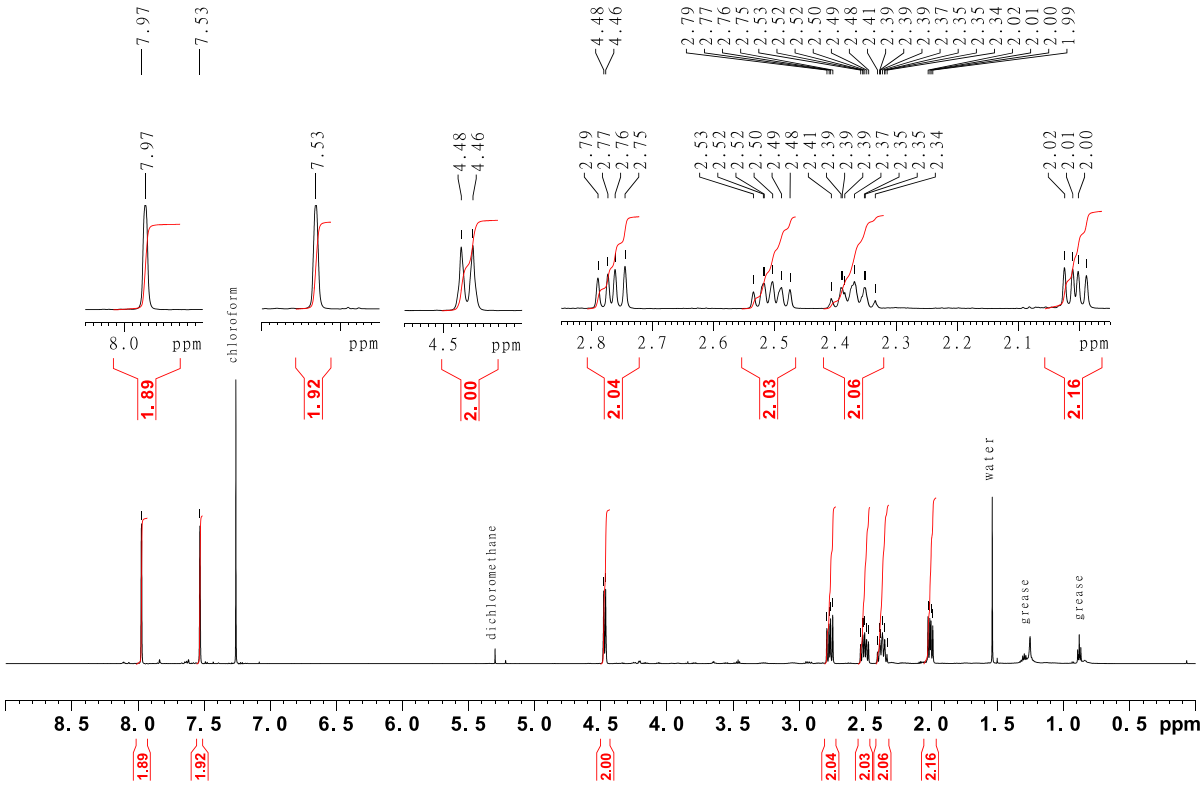

Figure SII.3: 600 MHz ^{1}H-NMR spectrum of (1*R*,1'*S*)-5,5'-dibromo-7,7'-dinitro-2,2',3,3'-tetrahydro-1*H*,1'*H*-1,1'-diindene (**10**).

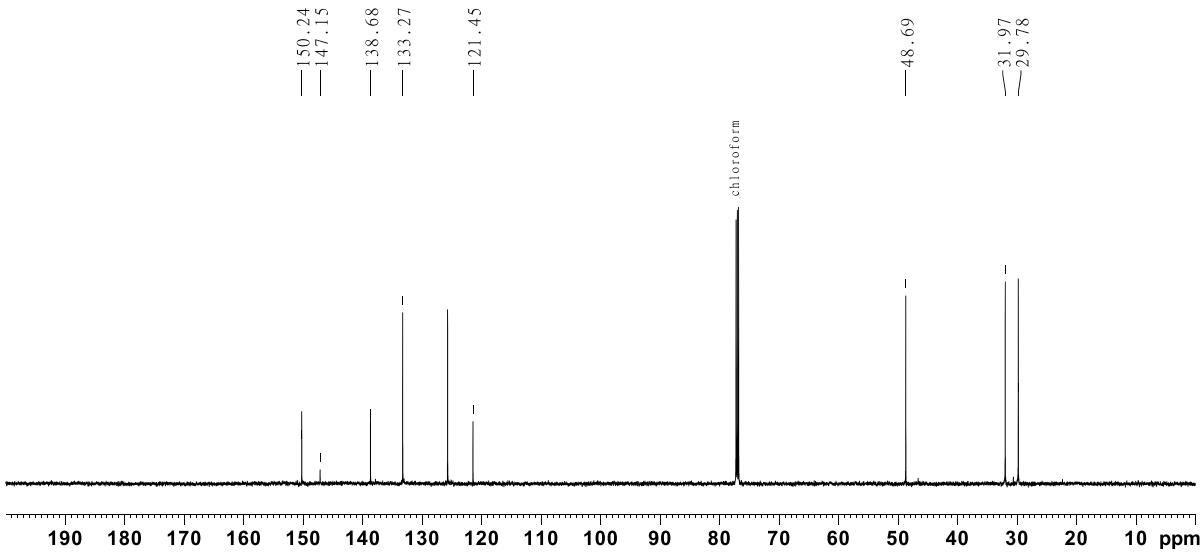

Figure SII.4: 150 MHz ^{13}C-NMR spectrum of (1*R*,1'*S*)-5,5'-dibromo-7,7'-dinitro-2,2',3,3'-tetrahydro-1*H*,1'*H*-1,1'-diindene (**10**).

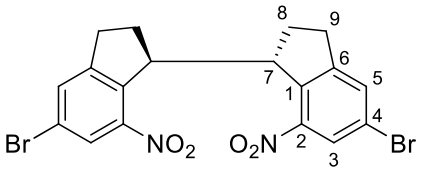

11

yield: 1.12 g (2.31 mmol, 56%)

mp.: 182 °C

R_f = 0.17 (*n*-pentane/DCM, 4:1)

^{1}H-NMR (500 MHz, $CDCl_3$, 300 K): δ = 7.84 (m, 2 H, *H*-3), 7.62 (m, 2 H, *H*-5), 4.23-4.18 (m, 2 H, *H*-7), 3.32-3.22 (m, 2 H, *H*-9a), 2.93 (dd, ^2J = 16.5 Hz, ^3J = 8.6 Hz, 2 H, *H*-9b), 2.35-2.26 (m, 2 H, *H*-8a), 2.05 (dd, ^2J = 12.8 Hz, ^3J = 7.2 Hz, 2 H, *H*-8b) ppm.

^{13}C-NMR (125 MHz, $CDCl_3$, 300 K): δ = 150.93 (C-6), 146.15 (C-2), 138.85 (C-1), 133.01 (C-5), 125.12 (C-3), 121.36 (C-4), 46.60 (C-7), 31.87 (C-8), 30.63 (C-9) ppm.

HR-MS (EI, 70 eV, DCM): m/z $[M]^+$ calculated for $C_{18}H_{14}{}^{79}Br_2N_2O_4^+$: 479.93203; found: 479.93187 ± 0.33 ppm.

IR (ATR): $\tilde{\nu}$ = 3090 (m), 2923 (m), 2852 (w), 1751 (w), 1560 (w), 1520 (s), 1454 (m), 1430 (m), 1401 (m), 1347 (s), 1305 (s), 1243 (m), 1231 (m), 1195 (m), 1152 (m), 1050 (w), 1029 (w), 993 (w), 948 (m), 903 (w), 877 (m), 804 (w), 784 (w), 757 (s), 723 (w), 694 (m), 640 (w), 619 (w) cm^{-1}.

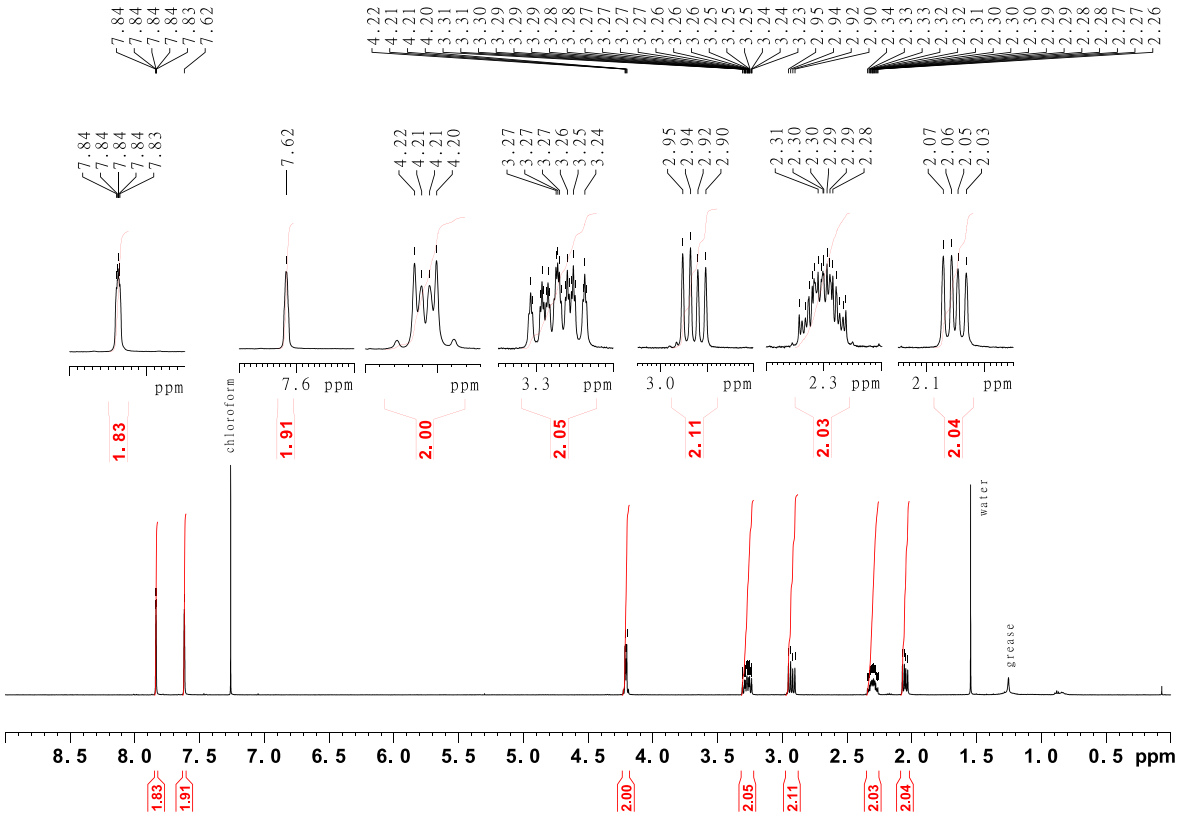

Figure SII.5: 500 MHz ^{1}H-NMR spectrum of (1*R*,1'*R*/1*S*,1'*S*)-5,5'-dibromo-7,7'-dinitro-2,2',3,3'-tetrahydro-1*H*,1'*H*-1,1'-diindene (**11**).

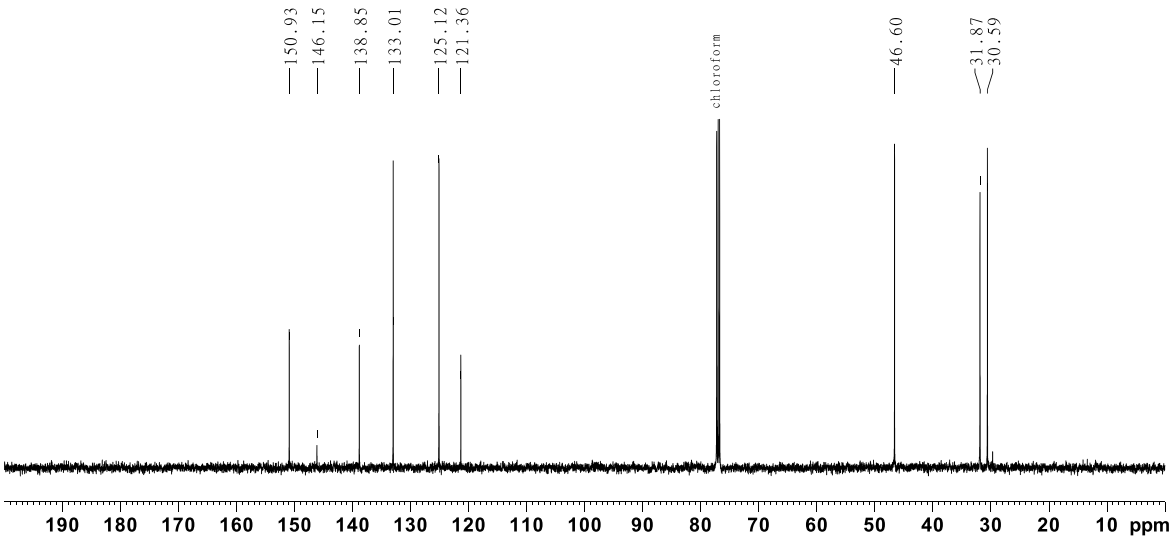

Figure SII.6: 125 MHz ^{13}C-NMR spectrum of (1*R*,1'*R*/1*S*,1'*S*)-5,5'-dibromo-7,7'-dinitro-2,2',3,3'-tetrahydro-1*H*,1'*H*-1,1'-diindene (**11**).

SII.1.3 Synthesis of (12a*R*,12b*S*,*Z*)-4,9-dibromo-1,2,11,12,12a,12b-hexahydrodiindeno[7,1-*cd*:1',7'-*fg*][1,2]-diazocine (3)

To a solution of (1R,1'S)-5,5'-dinitro-2,2',3,3'-tetrahydro-1H,1'H-1,1'-diindene (**10**, 431 mg, 893 µmol) in 54 mL EtOH and an aqueous solution of barium hydroxide [$Ba(OH)_2 \cdot 8\ H_2O$] (910 mg, 2.88 mmol) in 24 mL H_2O and zinc powder (1.00 g, 15.4 mmol) were added and the mixture was stirred for 16 h under reflux. The reaction mixture was filtered through Celite and the solvent was removed under reduced pressure. The residue was dissolved in DCM and filtered through Celite and the solvent was removed under reduced pressure. The crude product was dissolved in 60 mL of 0.1 M methanolic NaOH solution, $CuCl_2$ (8 mg, 55.9 µmol) was added and the reaction mixture was stirred at room temperature until completion while air was bubbled through the solution. The reaction was neutralized with 6 M HCl solution. Saturated sodium bicarbonate solution (60 mL) was added and the aqueous layer was extracted with DCM (3 × 40 mL). The combined organic layers were dried over $MgSO_4$ and the solvent was removed under reduced pressure. The crude product was purified by column chromatography (silica gel, cyclohexane/EE, 20:1) to afford a yellow solid.

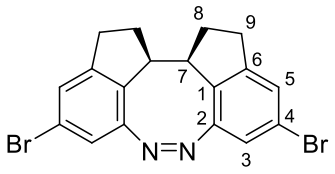

3

yield: 282 mg (674 µmol, 75%)

mp.: 149 °C

R_f = 0.34 (cyclohexane/EE, 20:1)

^{1}H-NMR (600 MHz, $CDCl_3$, 300 K): δ = 7.17 (s, 2 H, *H*-5), 7.03 (s, 2 H, *H*-3), 3.51-3.48 (m, 2 H, *H*-7), 2.90-2.77 (m, 4 H, *H*-9a, *H*-9b), 2.29-2.22 (m, 2 H, *H*-8a), 1.86-1.78 (m, 2 H, *H*-8b) ppm.

^{13}C-NMR (150 MHz, $CDCl_3$, 300 K): δ = 152.58 (C-2), 147.46 (C-6), 132.08 (C-1), 126.82 (C-3), 121.12 (C-5), 120.79 (C-4), 46.90 (C-7), 32.55 (C-9), 29.78 (C-8) ppm.

HR-MS (ESI, DCM): m/z $[M+H]^+$ calculated for $C_{18}H_{14}{}^{79}Br_2N_2+H^+$: 416.95965; found: 416.95893 ± 1.74 ppm.

IR (ATR): $\tilde{\nu}$ = 3061 (w), 2937 (m), 2846 (m), 1721 (w), 1579 (2), 1524 (m), 1448 (s), 1431 (m), 1393 (m), 1346 (m), 1305 (m), 1257 (w), 1199 (w), 1179 (w), 1157 (m), 1082 (w), 1036 (w), 1016 (w), 961 (w), 855 (s), 832 (w), 800m (s), 774 (w), 738 (s), 708 (m), 640 (m), 613 (m), 571 (m) cm^{-1}.

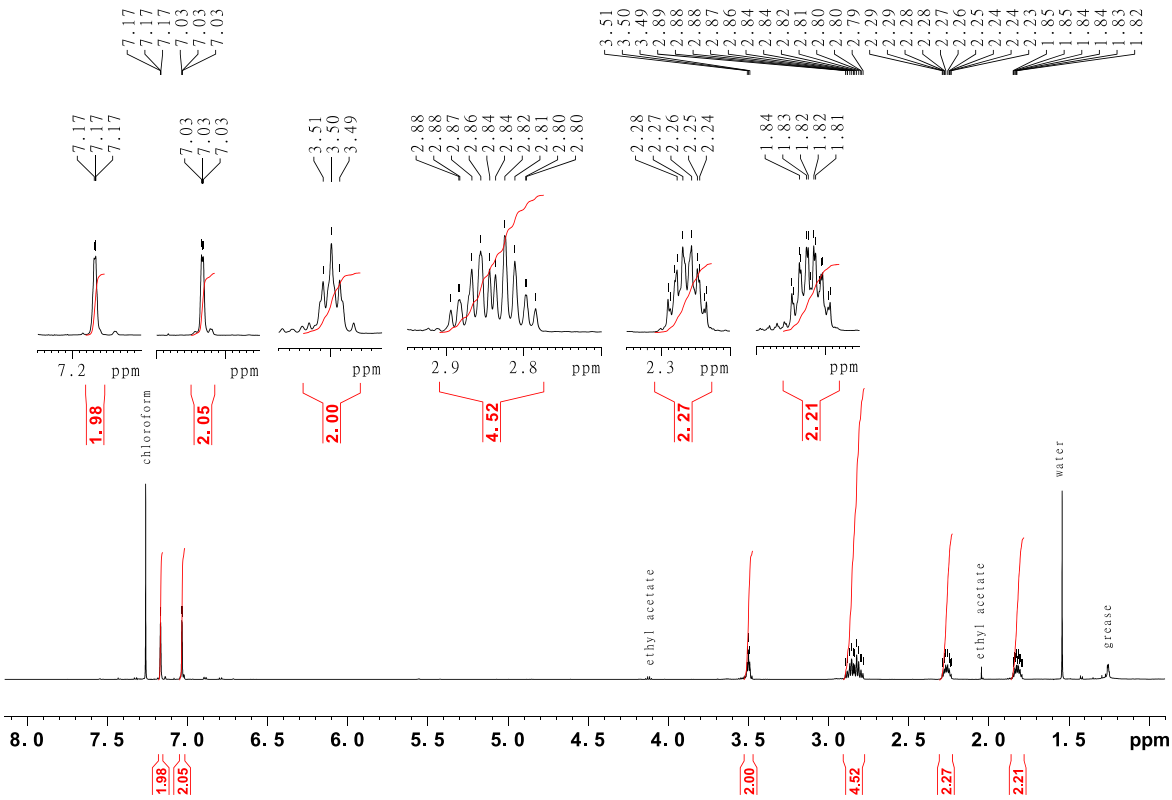

Figure SII.7: 600 MHz ^{1}H-NMR spectrum of (12a*R*,12b*S*,*Z*)-4,9-dibromo-1,2,11,12,12a,12b-hexahydrodiindeno[7,1-*cd*:1',7'-*fg*][1,2]-diazocine (**3**).

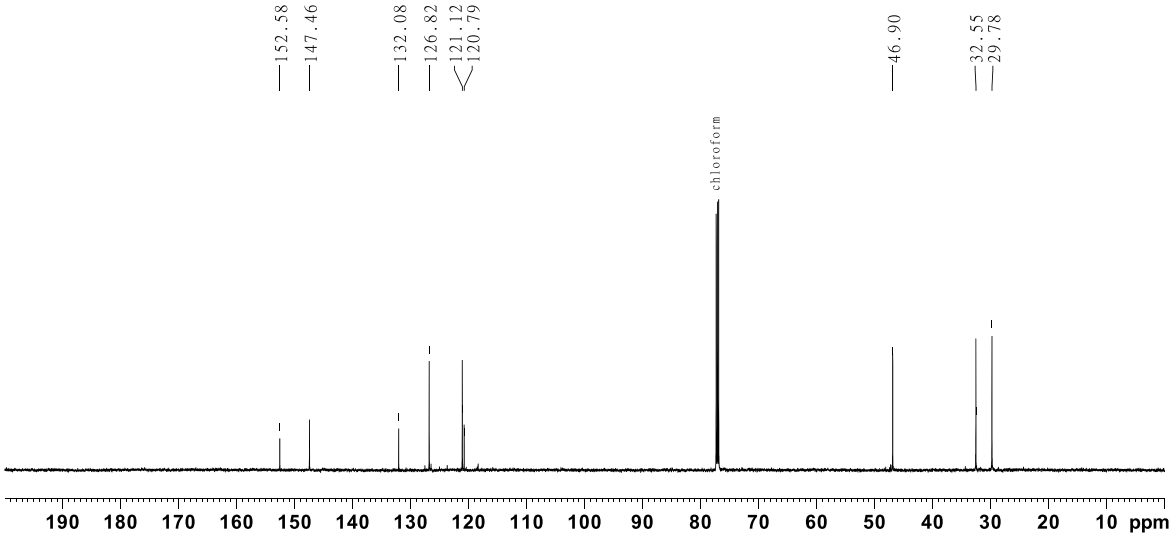

Figure SII.8: 150 MHz ^{13}C-NMR spectrum of (12a*R*,12b*S*,*Z*)-4,9-dibromo-1,2,11,12,12a,12b-hexahydrodiindeno[7,1-*cd*:1',7'-*fg*][1,2]-diazocine (**3**).

SII.1.4 Synthesis of (12a*R*,12b*R*/12a*S*,12b*S*,*Z*)-4,9-dibromo-1,2,11,12,12a,12b-hexahydrodiindeno[7,1-*cd*:1',7'-*fg*][1,2]-diazocine (4)

To a solution of (1R,1'R/1S,1'S)-7,7'-dinitro-2,2',3,3'-tetrahydro-1H,1'H-1,1'-diindene (**11**, 1.07 g, 2.23 mmol) in 134 mL EtOH an aqueous solution of barium hydroxide [$Ba(OH)_2 \cdot 8\ H_2O$] (2.28 g, 7.21 mmol) in 61 mL H_2O and zinc powder (2.51 g, 38.4 mmol) were added and the mixture was stirred for 16 h under reflux. The reaction mixture was filtered through Celite and the solvent was removed under reduced pressure. The residue was dissolved in DCM and filtered through Celite and the solvent was removed under reduced pressure. The crude product was dissolved in 150 mL 0.1 M methanolic NaOH solution, $CuCl_2$ (20 mg, 140 µmol) was added and the reaction mixture was stirred at room temperature until completion while air was bubbled through the solution. The reaction was neutralized with 6 M HCl solution. Saturated sodium bicarbonate solution (60 mL) was added and the aqueous layer was extracted with DCM (3 × 40 mL). The combined organic layers were dried over $MgSO_4$ and the solvent was removed under reduced pressure. The crude product was purified by column chromatography (silica gel, cyclohexane/EE, 20:1) to afford an orange solid.

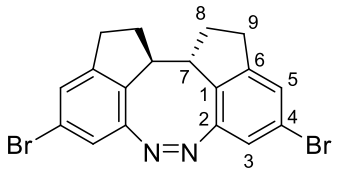

4

yield: 708 mg (1.69 mmol, 76%)

mp.: 150 °C

R_f = 0.39 (cyclohexane/EE, 20:1)

^{1}H-NMR (500 MHz, $CDCl_3$, 300 K): δ = 7.55-7.53 (m, 2 H, *H*-3), 7.29-7.27 (m, 2 H, *H*-5), 2.99-2.89 (m, 4 H, *H*-9a, *H*-9b), 2.89-2.85 (m, 2 H, *H*-7), 2.24-2.16 (m, 2 H, *H*-8a), 1.99-1.91 (m, 2 H, *H*-8b) ppm.

^{13}C-NMR (125 MHz, $CDCl_3$, 300 K): δ = 149.28 (C-6), 146.85 (C-2), 131.73 (C-1), 128.04 (C-3), 127.90 (C-5), 120.35 (C-4), 48.99 (C-7), 31.46 (C-8), 31.42 (C-9) ppm.

HR-MS (ESI, DCM): m/z $[M+H]^+$ calculated for $C_{18}H_{14}{}^{79}Br_2N_2+H^+$: 416.95965; found: 416.95893 ± 1.74 ppm.

IR (ATR): $\tilde{\nu}$ = 3786 (w), 2970 (w), 2914 (w), 2839 (w), 1585 (w), 1530 (w), 1460 (w), 1446 (w), 1423 (w), 1288 (w), 1248 (w), 1227 (w), 1193 (w), 1157 (w), 1122 (w), 1043 (w), 965 (w), 903 (w), 870 (w), 825 (w), 818 (w), 786 (s), 757 (s), 739 (m), 717 (m), 691 (w), 665 (w), 628 (w) cm^{-1}.

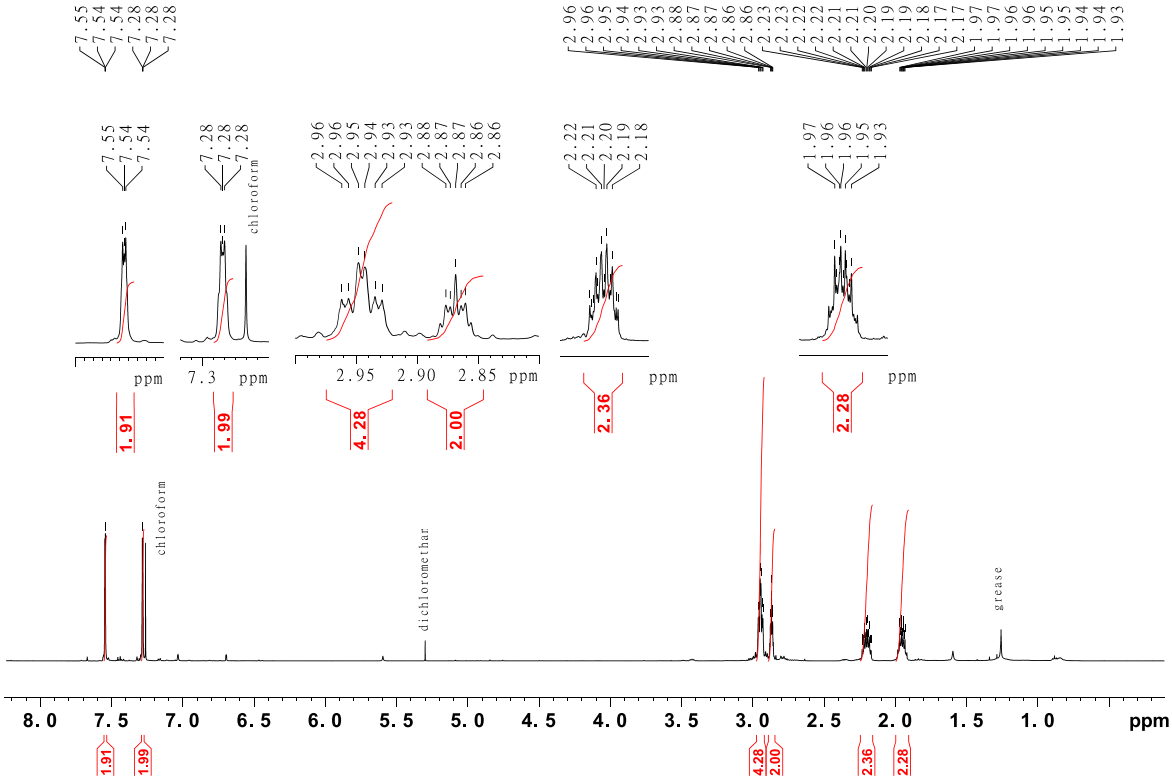

Figure SII.9: 500 MHz ^{1}H-NMR spectrum of (12a*R*,12b*R*/12a*S*,12b*S*,*Z*)-4,9-dibromo-1,2,11,12,12a,12b-hexahydrodiindeno[7,1-*cd*:1',7'-*fg*][1,2]-diazocine (**4**).

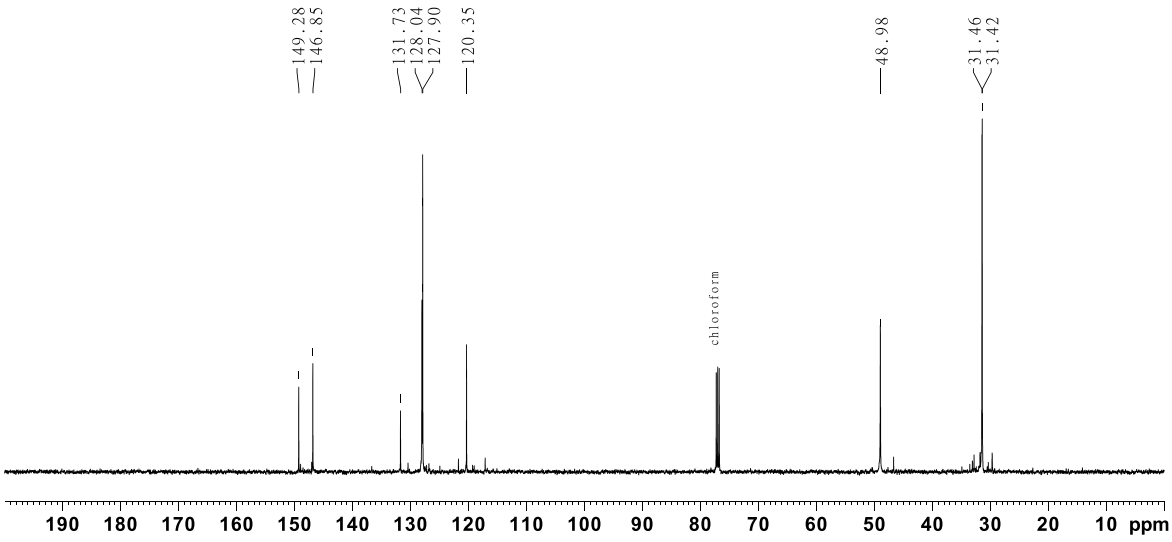

Figure SII.10: 125 MHz ^{13}C-NMR spectrum of (12a*R*,12b*R*/12a*S*,12b*S*,*Z*)-4,9-dibromo-1,2,11,12,12a,12b-hexahydrodiindeno[7,1-*cd*:1',7'-*fg*][1,2]-diazocine (**4**).

SII.1.5 Synthesis of 2-iodo-4-nitroindane (9)

4-Nitroindane (**7**, 1.00 g, 6.10 mmol) was dissolved in 5 mL conc. sulfuric acid and *N*-iodosuccinimide (2.50 g, 6.66 mmol) was added. After removing the ice bath, the reaction mixture was stirred at room temperature for 3 h and poured on ice subsequently. The reaction mixture was extracted with dichloromethane and the combined organic phases were washed with sat. sodium thiosulfate solution. After drying over magnesium sulfate the solvent was removed under reduced pressure. The crude product was purified by column chromatography (silica gel, cyclohexane/EE, 20:1) to afford a slight yellow solid

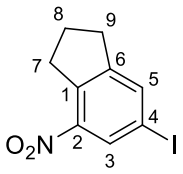

9

yield: 230 mg (793 µmol, 13%)

mp.: 79 °C

***R*f =** 0.60 (cyclohexane/EE, 20:1)

^{1}H-NMR (500 MHz, $CDCl_3$, 300 K): δ = 8.29 (s, 1 H, *H*-3), 7.83 (m, 1 H, *H*-5), 3.34 (t, ^{3}J = 7.7 Hz, 2 H, *H*-7), 3.00 (t, ^{3}J = 7.7 Hz, 2 H, *H*-9), 2.14 (q, ^{3}J = 7.6 Hz, 2 H, *H*-8) ppm.

^{13}C-NMR (125 MHz, $CDCl_3$, 300 K): δ = 150.35 (C-6), 145.98 (C-2), 140.61 (C-1), 138.82 (C-5), 130.53 (C-3), 90.29 (C-4), 33.75 (C-7), 32.56 (C-9), 24.66 (C-8) ppm.

HR-MS (ESI, DCM): m/z $[M+H]^+$ calculated for $C_9H_9{}^{127}I_1NO_2+H^+$: 289.967725; found: 289.96687 ± 1.30 ppm.

IR (ATR): $\tilde{\nu}$ = 3077 (m), 2951 (m), 2901 (w), 2840 (w), 1521 (s), 1456 (m), 1422 (m), 1395 (m), 1345 (s), 1307 (m), 1267 (m), 1194 (m), 1167 (w), 1145 (w), 948 (m), 914 (w), 882 (m), 837 (m), 800 (w), 773 (w), 752 (s), 678 (m), 523 (m) cm^{-1}.

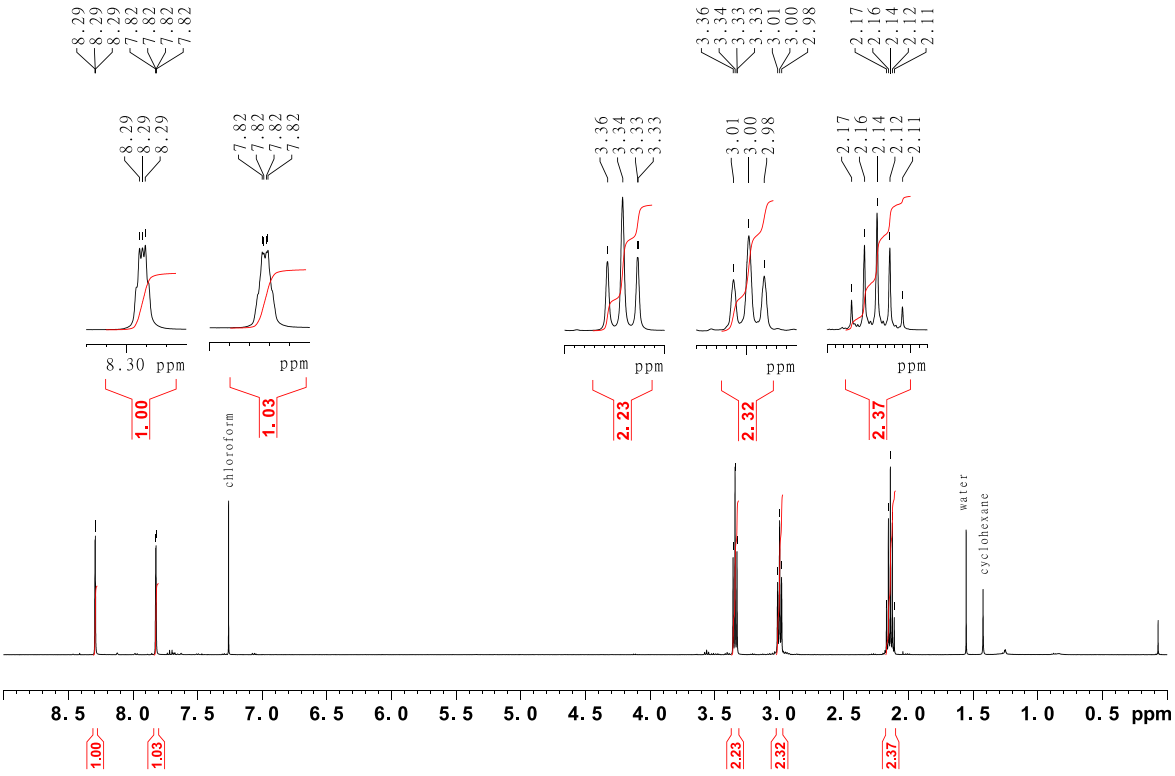

Figure SII.11: 500 MHz ^{1}H-NMR spectrum of 2-iodo-4-nitroindane (**9**).

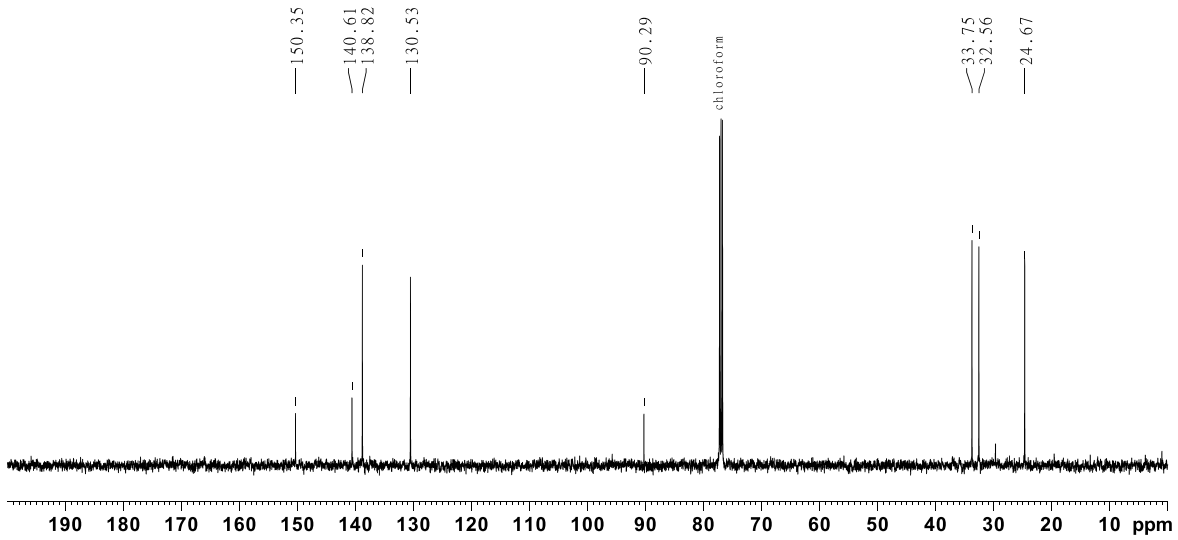

Figure SII.12: 125 MHz ^{13}C-NMR spectrum of 2-iodo-4-nitroindane (**9**).

SII.1.6 Synthesis of (1*R*,1'*S*)-5,5'-diiodo-7,7'-dinitro-2,2',3,3'-tetrahydro-1*H*,1'*H*-1,1'-diindene (12) and (1*R*,1'*R*/1*S*,1'*S*)-5,5'-diiodo-7,7'-dinitro-2,2',3,3'-tetrahydro-1*H*,1'*H*-1,1'-diindene (13)

2-Iodo-4-nitroindane (**9**, 795 mg, 2.75 mmol) was dissolved in dry THF under nitrogen atmosphere, cooled to 0 °C and potassium butoxide (462 mg, 4.13 mmol) was added. The reaction was stirred for 30 s before bromine (548 mg, 0.20 mL, 3.43 mmol) was added rapidly. The reaction was stirred for further 10 min. and 150 g of ice were added. The aqueous solution was extracted with DCM (3 × 40 mL) and the combined organic layers were wash with saturated sodium thiosulfate solution, dried with over $MgSO_4$ and the solvent was removed under reduced pressure. The crude product was purified by column chromatography (silica gel, *n*-pentane/DCM, 3:1) to afford the diastereomers as colorless solids.

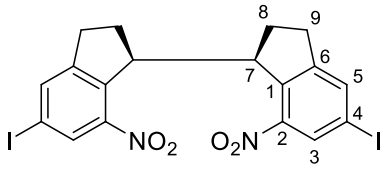

12

yield: 272 mg (472 µmol, 34%)

mp.: 185 °C

R_f = 0.10 (*n*-pentane/DCM, 4:1)

^{1}H-NMR (500 MHz, $CDCl_3$, 300 K): δ = 8.14 (s, 2 H, *H*-3), 7.30 (s, 2 H, *H*-5), 4.46 (d, ^3J = 8.7 Hz, 2 H, *H*-7), 2.75 (dd, ^2J = 17.1 Hz, ^3J = 9.8 Hz, 2 H, *H*-9a), 2.53-2.43 (m, 2 H, *H*-9b), 2.40-2.30 (m, 2 H, *H*-8a), 1.98 (dd, ^2J = 13.7 Hz, ^3J = 8.0 Hz, 2 H, *H*-8b) ppm.

^{13}C-NMR (125 MHz, $CDCl_3$, 300 K): δ = 150.36 (C-6), 147.18 (C-2), 139.42 (C-1), 139.17 (C-5), 131.34 (C-3), 91.89 (C-4), 48.74 (C-7), 31.76 (C-9), 29.64 (C-8) ppm.

HR-MS (ESI, DCM): m/z $[M+H]^+$ calculated for $C_{18}H_{14}{}^{127}I_2N_2O_4+H^+$: 576.91157; found: 576.91176 ± 0.32 ppm.

IR (ATR): $\tilde{\nu}$ = 3079 (w), 2944 (w), 1598 (w), 1520 (s), 1454 (m), 1432 (w), 1398 (w), 1345 (s), 1303 (w), 1233 (m), 1196 (w), 1137 (m), 949 (m), 903 (w), 873 (m), 843 (m), 784 (w), 756 (m), 747 (m), 726 (w), 686 (m), 555 (m) cm^{-1}.

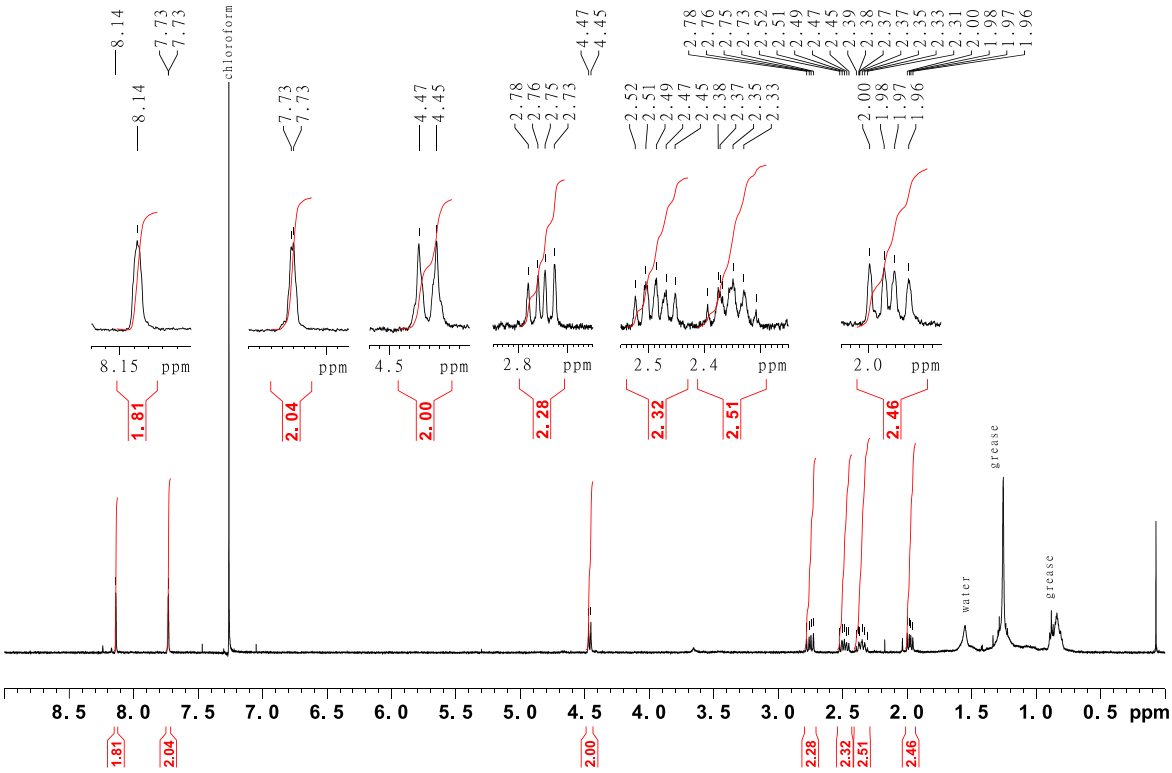

Figure SII.13: 500 MHz ^{1}H-NMR spectrum of (1*R*,1'*S*)-5,5'-diiodo-7,7'-dinitro-2,2',3,3'-tetrahydro-1*H*,1'*H*-1,1'-diindene (**12**).

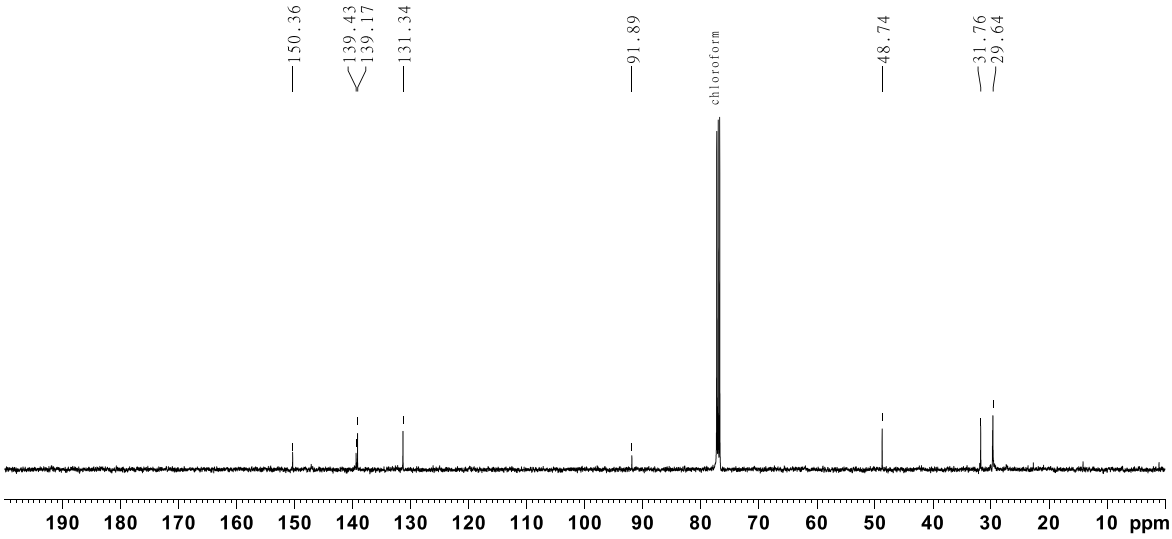

Figure SII.14: 125 MHz ^{13}C-NMR spectrum of (1*R*,1'*S*)-5,5'-diiodo-7,7'-dinitro-2,2',3,3'-tetrahydro-1*H*,1'*H*-1,1'-diindene (**12**).

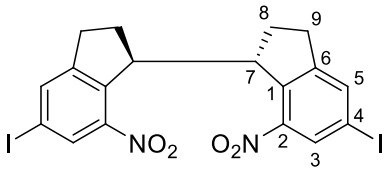

13

yield: 480 mg (834 µmol, 61%)

mp.: 200 °C

R_f = 0.14 (*n*-pentane/DCM, 4:1)

^{1}H-NMR (500 MHz, $CDCl_3$), 300 K): δ = 8.01 (m, 2 H, *H*-3), 7.81 (m, 2 H, *H*-5), 4.22-4.18 (m, 2 H, *H*-7), 3.29-3.20 (m, 2 H, *H*-9a), 2.91 (dd, ^2J = 16.5 Hz, ^3J = 8.5 Hz, 2 H, *H*-9b), 2.32-2.24 (m, 2 H, *H*-8a), 2.01 (dd, ^2J = 12.7 Hz, ^3J = 7.1 Hz, 2 H, *H*-8b) ppm.

^{13}C-NMR (125 MHz, $CDCl^3$, 300 K): δ = 150.98 (C-6), 146.20 (C-2), 139.58 (C-1), 138.83 (C-5), 130.82 (C-3), 91.82 (C-4), 46.65 (C-7), 31.69 (C-8), 30.43 (C-9) ppm.

HR-MS (ESI, DCM): m/z $[M+H]^+$ calculated for $C_{18}H_{14}{}^{127}I_2N_2O_4+H^+$: 576.91157; found: 576.91120 ± 0.64 ppm.

IR (ATR): $\tilde{\nu}$ = 3080 (w), 2925 (m), 2851 (m), 1597 (w), 1521 (s), 1455 (m), 1427 (w), 1396 (m), 1334 (s), 1306 (w), 1283 (w), 1240 (m), 1193 (w), 1141 (m), 1124 (w), 1028 (w), 949 (m), 929 (w), 902 (w), 874 (s), 843 (s), 799 (m), 755 (s), 721 (m), 690 (m), 634 (w), 565 (s) cm^{-1}.

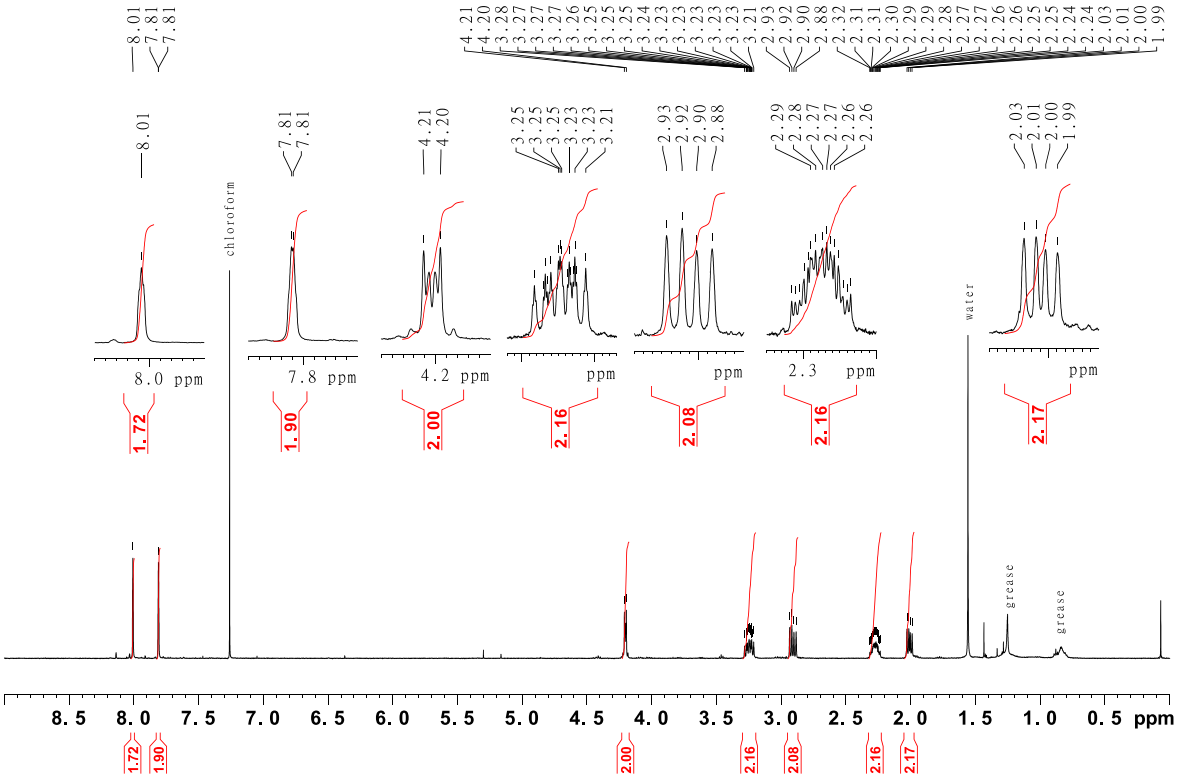

Figure SII.15: 500 MHz ^{1}H-NMR spectrum of (1*R*,1'*R*/1*S*,1'*S*)-5,5'-diiodo-7,7'-dinitro-2,2',3,3'-tetrahydro-1*H*,1'*H*-1,1'-diindene (**13**).

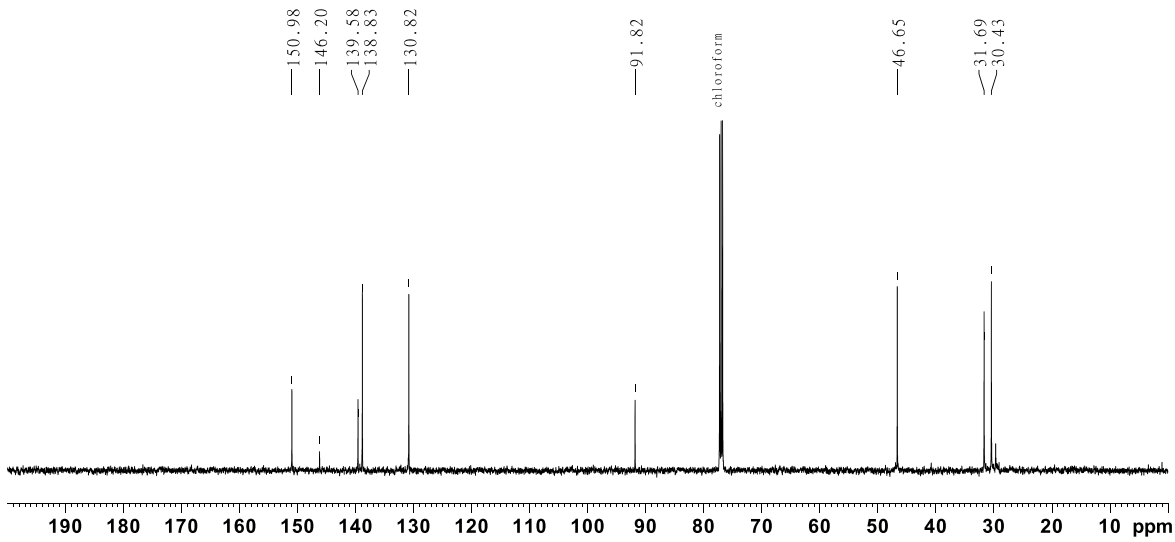

Figure SII.16: 125 MHz ^{13}C-NMR spectrum of (1*R*,1'*R*/1*S*,1'*S*)-5,5'-diiodo-7,7'-dinitro-2,2',3,3'-tetrahydro-1*H*,1'*H*-1,1'-diindene (**13**).

SII.1.7 Synthesis of (12a*R*,12b*R*/12a*S*,12b*S*,*Z*)-4,9-diiodo-1,2,11,12,12a,12b-hexahydrodiindeno[7,1-*cd*:1',7'-*fg*][1,2]-diazocine (5)

To a solution of (1R,1'R/1S,1'S)-7,7'-dinitro-2,2',3,3'-tetrahydro-1H,1'H-1,1'-diindene (**13**, 325 mg, 635 µmol) in 94 mL EtOH an aqueous solution of barium hydroxide [$Ba(OH)_2$·8 H_2O] (646 mg, 2.05 mmol) in 43 mL H_2O and zinc powder (713 mg, 10.8 mmol) were added and the mixture was stirred for 16 h under reflux. The reaction mixture was filtered through Celite and the solvent was removed under reduced pressure. The residue was dissolved in DCM and filtered through Celite and the solvent was removed under reduced pressure. The crude product was dissolved in 43 mL 0.1 M methanolic NaOH solution, $CuCl_2$ (5.70 mg, 39.7 µmol) was added and the reaction mixture was stirred at room temperature until completion while air was bubbled through the solution. The reaction was neutralized with 6 M HCl solution. Saturated sodium bicarbonate solution (60 mL) was added and the aqueous layer was extracted with DCM (3 × 40 mL). The combined organic layers were dried over $MgSO_4$ and the solvent was removed under reduced pressure. The crude product was purified by column chromatography (silica gel, cyclohexane/EE, 20:1) to afford an orange solid. The target molecule **5** was separated from the unsubstituted reduction product **2** by column chromatography (silica gel, *n*-pentane/DCM, 2:1) to afford a yellow solid.

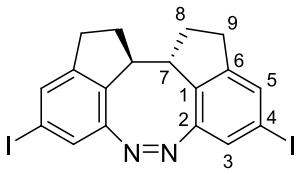

5

yield: 234 mg (457 µmol, 72%)

mp.: 175 °C

R_f = 0.26 (*n*-pentane/DCM, 2:1)

^{1}H-NMR (500 MHz, $CDCl_3$, 300 K): δ = 7.75-7.72 (m, 2 H, *H*-3), 7.49-7.46 (m, 2 H, *H*-5), 2.96-2.91 (m, 2 H, *H*-9a, *H*-9b), 2.89-2.86 (m, *H*-7), 2.23-2.14 (m, 2 H, *H*-8a), 1.97-1.90 (m, 2 H, *H*-8b) ppm.

^{13}C-NMR (125 MHz, $CDCl_3$, 300 K): δ = 149.49 (C-6), 146.93 (C-2), 133.91 (C-3), 133.67 (C-5), 132.51 (C-1), 91.31 (C-4), 49.07 (C-7), 31.34 (C-8), 31.21 (C-9) ppm.

HR-MS (ESI, DCM): m/z $[M+H]^+$ calculated for $C_{18}H_{14}{}^{127}I_2N_2+H^+$: 512.93191; found: 512.93199 ± 0.16 ppm.

IR (ATR): $\tilde{\nu}$ = 3073 (w), 2920 (m), 2850 (m), 2252 (w), 1737 (w), 1575 (m), 1520 (m), 1446 (m), 1429 (w), 1383 (w), 1347 (w), 1308 (w), 1260 (m), 1245 (w), 1192 (w), 1157 (w), 1019 (m), 905 (w), 854 (s), 825 (s), 800 (s), 753 (m), 734 (s), 715 (m), 675 (w), 652 (w), 628 (w), 554 (m) cm^{-1}.

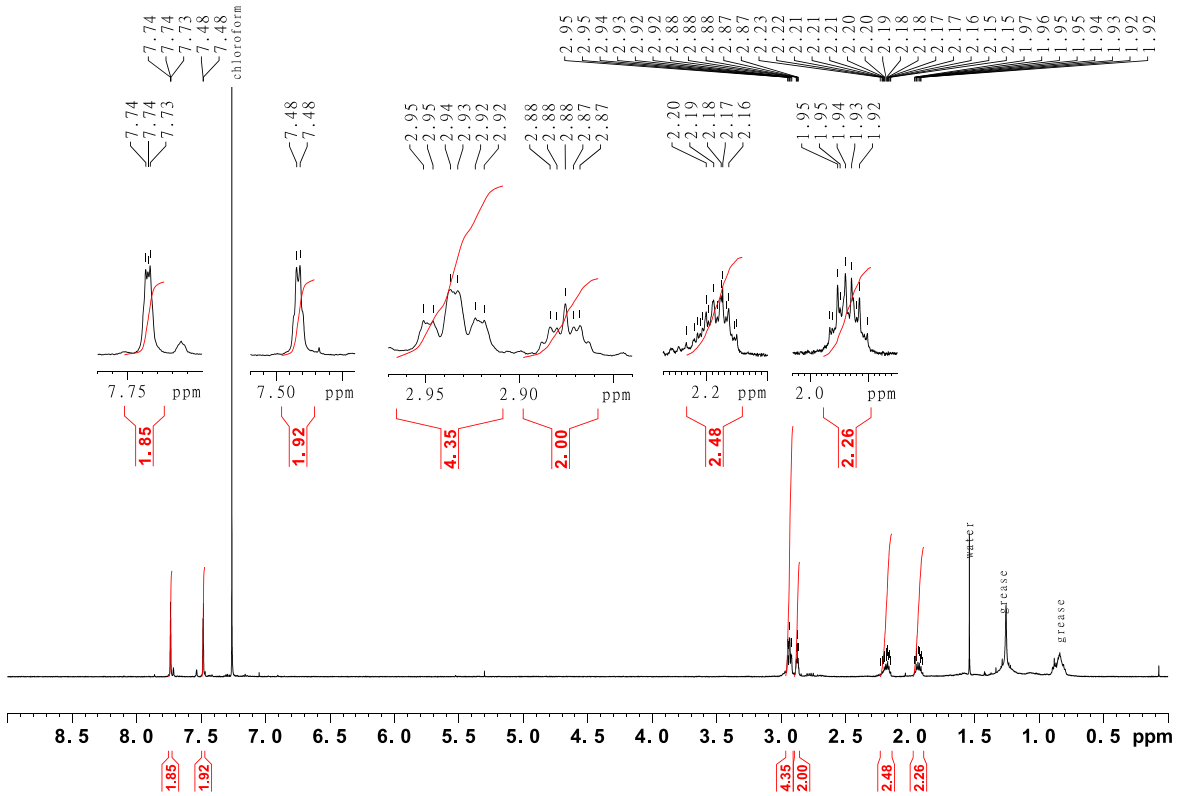

Figure SII.17: 500 MHz ^{1}H-NMR spectrum of (12a*R*,12b*R*/12a*S*,12b*S*,*Z*)-4,9-diiodo-1,2,11,12,12a,12b-hexahydrodiindeno[7,1-*cd*:1',7'-*fg*][1,2]-diazocine (**5**).

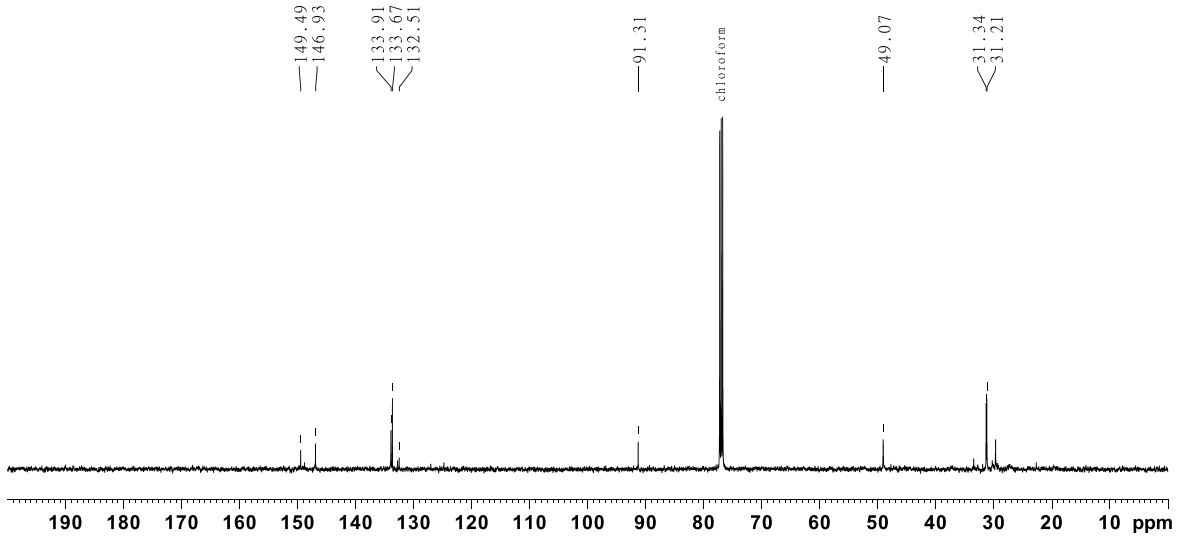

Figure SII.18: 125 MHz ^{13}C-NMR spectrum of (12a*R*,12b*R*/12a*S*,12b*S*,*Z*)-4,9-diiodo-1,2,11,12,12a,12b-hexahydrodiindeno[7,1-*cd*:1',7'-*fg*][1,2]-diazocine (**5**).

SII.1.8 Synthesis of 3,4-dibromoaniline (17)[1]

To a solution of 3-bromoaniline (**16**, 15.0 g, 87.2 mmol) in 90 mL MeCN a solution of *N*-bromosuccinimide (15.6 g, 87.5 mmol) in 90 mL MeCN was added and stirred at room temperature for 16 h and poured on 200 g ice. After extraction with DCM (3 x 50 mL) the combined organic layers were dried over $MgSO_4$ and the solvent was removed under reduced pressure to afford the product as brown solid.

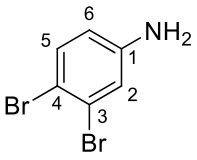

17

yield: 21.8 g (86.9 mmol, >99%) Lit. 95%[1]

mp.: 67 °C

^{1}H-NMR (500 MHz, $CDCl_3$, 300 K): δ = 7.31 (d, ^3J = 8.6 Hz, 1 H, *H*-5), 6.95 (d, ^4J = 2.7 Hz, 1 H, *H*-2), 6.48 (dd, ^3J = 8.6 Hz, ^4J = 2.7 Hz, 1 H, *H*-6), 3.72 (br. s, 2 H, -N*H*$_2$), 2.93 ppm.

^{13}C-NMR (125 MHz, $CDCl_3$, 300 K): δ = 146.61 (C-1), 133.76 (C-5), 1124.94 (C-3), 119.61 (C-2), 115.54 (C-6), 112.08 (C-4) ppm.

HR-MS (EI, 70 eV, DCM): m/z $[M]^+$ calculated for $C_6H_5{}^{79}Br_2N^+$: 248.8778; found: 248.87903 ± 0.60 ppm.

IR (ATR): $\tilde{\nu}$ = 3459 (w), 3405 (w), 3315 (w), 2166 (w), 1700 (w), 1618 (m), 1579 (m), 1458 (m), 1407 (w), 1289 (s), 1236 (w), 1190 (w), 1106 (w), 1005 (w), 855 (m), 817 (s), 637 (s) cm^{-1}.

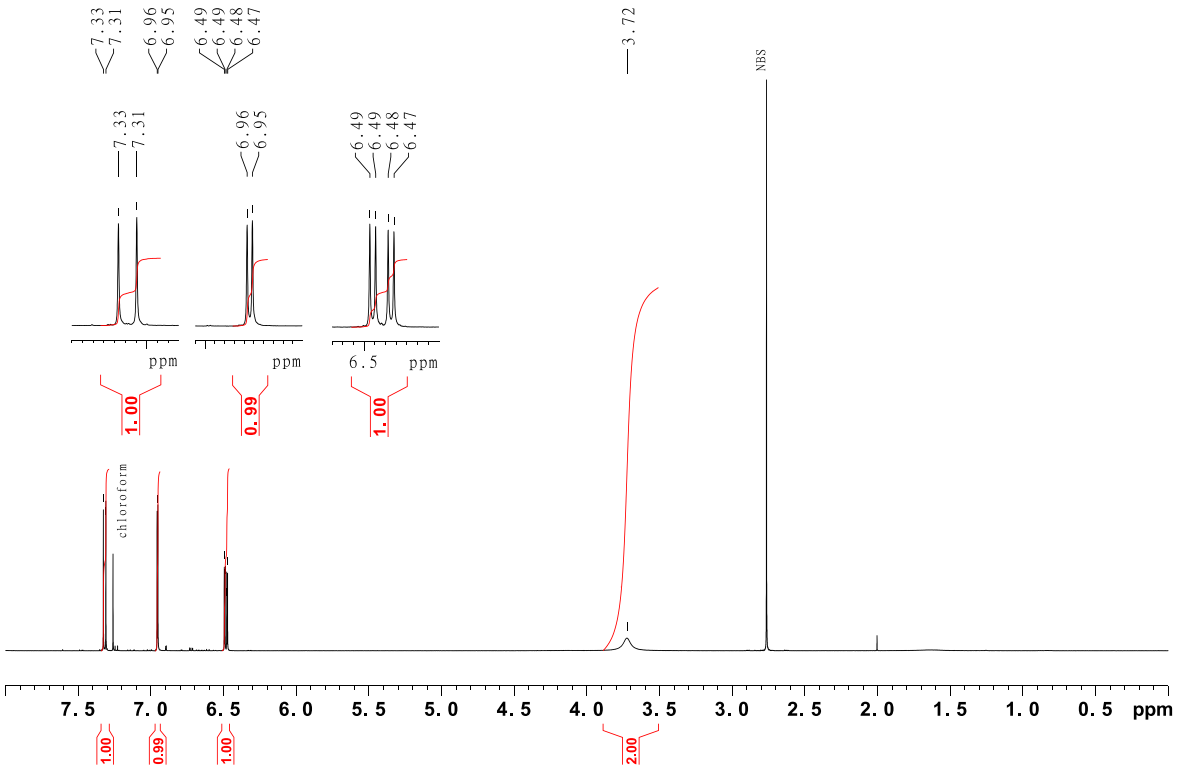

Figure SII.19: 500 MHz ^{1}H-NMR spectrum of 3,4-dibromoaniline (**17**).

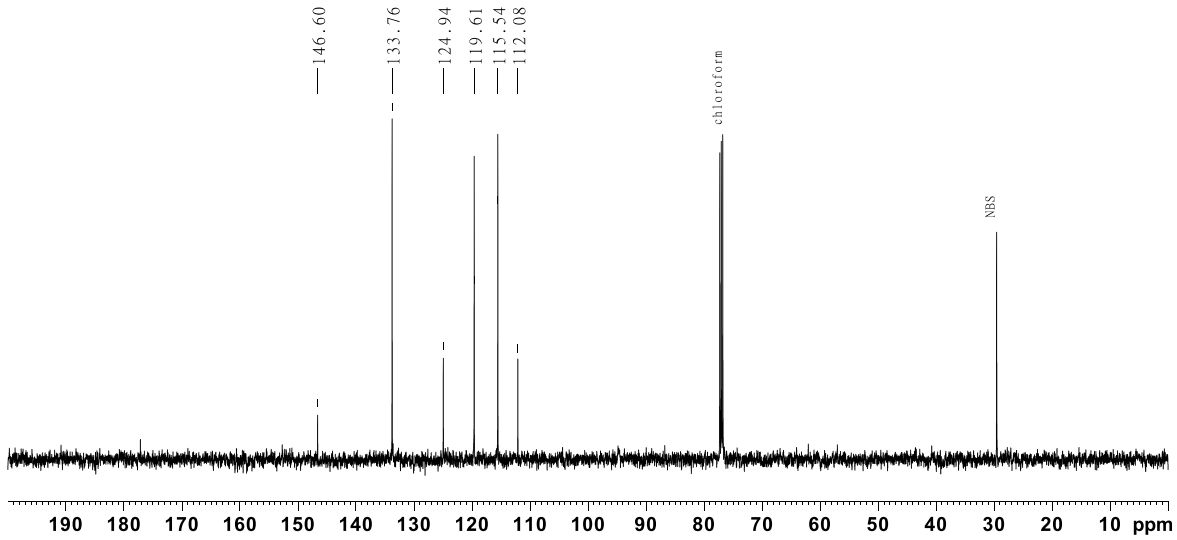

Figure SII.20: 125 MHz ^{13}C-NMR spectrum of 3,4-dibromoaniline (**17**).

SII.1.9 Synthesis of 3-(3,4-dibromophenyl)propionic acid (18)[2]

3,4-Dibromoaniline (**17**, 21.8 g, 86.9 mmol) was dissolved in 87 mL acetone and cooled to -5 °C. Then 30 mL hydrobromic acid were added. A solution of sodium nitrite (9.02 g, 567 mmol) in 130 mL dem. H_2O was added and the mixture was stirred for 10 min. Then methyl acrylate (75.9 mL, 72.1 g, 837 mmol) and Cu(I)Br (5.75 g, 40,1 mmol) were added and the reaction mixture was stirred for 16 h at room temperature. Acetone was removed under reduced pressure and the aqueous residue was extracted with toluene (3 x 100 mL). The combined organic layers were dried over $MgSO_4$ and the solvent was removed under reduced pressure. The residue was dissolved in 130 mL acetic acid, zinc powder (10.8 g, 165 mmol) was added and the mixture was stirred at room temperature for 4 h. The reaction mixture was filtered through Celite and dem. H_2O and $CHCl_3$ were added. The mixture was extracted with $CHCl_3$ (3 x 100 mL), the combined organic layers were dried over $MgSO_4$ and the solvent was removed under reduced pressure. Then 130 mL of 10% KOH in dem. H_2O were added and the reaction mixture was stirred under reflux for 2 h. After filtration through Celite the mixture was neutralized with conc. HCl. The precipitated solid was filtered off and dissolved in DCM, dried over MgSO4 and the solvent was removed under reduced pressure to obtain the product as brown solid.

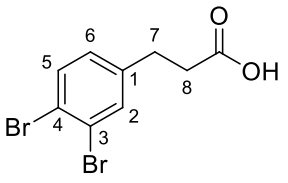

18

yield: 20.5 g (66.6 mmol, 76%) Lit. 50%[2]

mp.: 71 °C

^{1}H-NMR (500 MHz, $CDCl_3$, 300 K): δ = 7.51 (d, ^3J = 8.2 Hz, 1 H, *H*-5), 7.46 (d, ^4J = 2.0 Hz, 1 H, *H*-2), 6.99 (dd, ^3J = 8.2 Hz, ^4J = 2.0 Hz, 1 H, *H*-6), 2.86 (t, ^3J = 7.5 Hz, 2 H, *H*-8), 2.63 (t, ^3J = 7.6 Hz, 2 H, *H*-7) ppm.

^{13}C-NMR (125 MHz, $CDCl_3$, 300 K): δ = 177.73 (COOH), 141.25 (C-1), 133.78 (C-5), 133.64 (C-2), 128.74 (C-6), 124.92 (C-3), 122.61 (C-4), 35.15 (C-8), 29.72 (C-7) ppm.

HR-MS (EI, 70 eV, DCM): m/z $[M]^+$ calculated for $C_9H_8{}^{79}Br_2O_2^+$: 305.88911; found: 305.88888 ± 0.72 ppm.

IR (ATR): $\tilde{\nu}$ = 2921 (w), 1704 (s), 1584 (w), 1556 (w), 1461 (m), 1439 (m), 1408 (m), 1392 (s), 1294 (m), 1218 (m), 1190 (m), 1110 (m), 1010 (m), 924 (w), 873 (m), 821 (s), 666 (w), 431 (w) cm^{-1}.

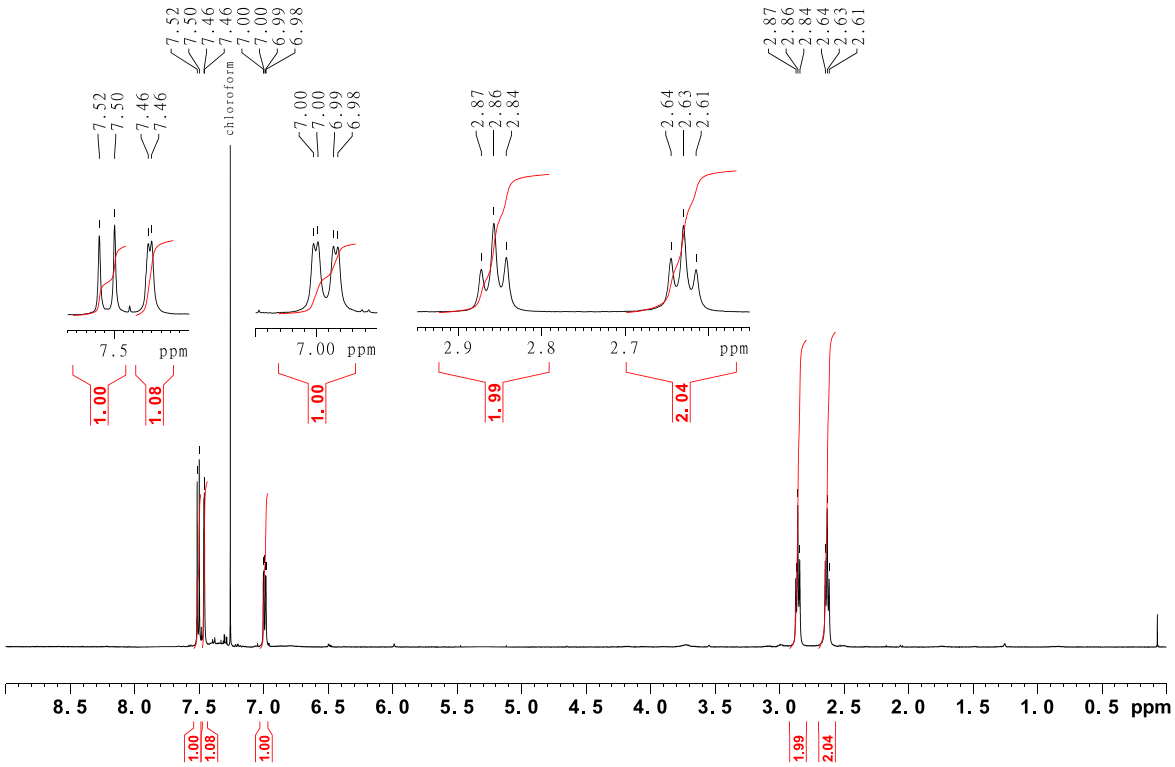

Figure SII.21: 500 MHz ^{1}H-NMR spectrum of 3-(3,4-dibromophenyl)propionic acid (**18**).

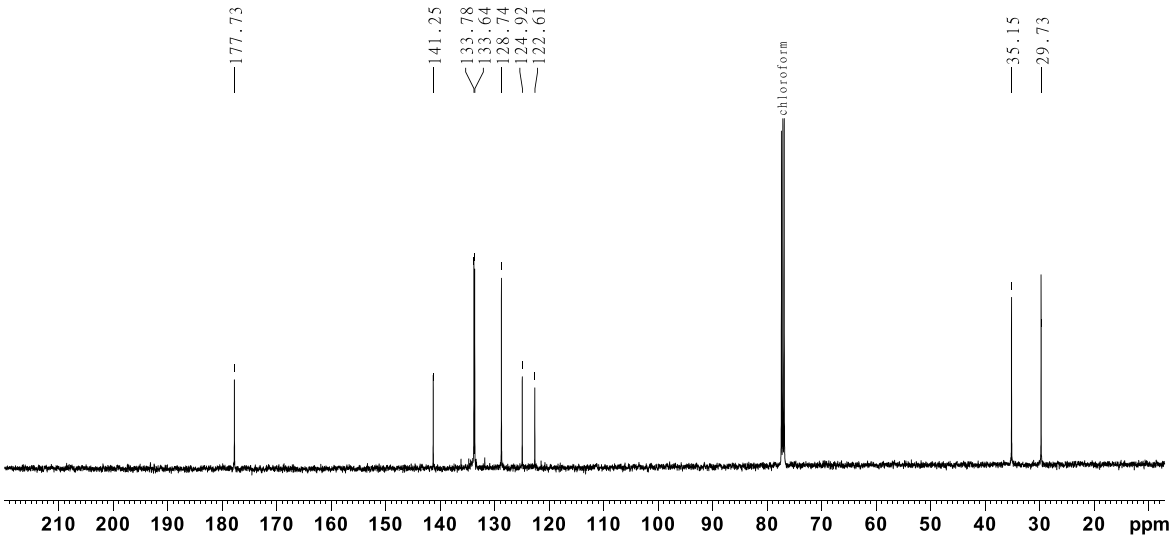

Figure SII.22: 125 MHz ^{13}C-NMR spectrum of 3-(3,4-dibromophenyl)propionic acid (**18**).

SII.1.10 Synthesis of 6,7-dibromo-2,3-dihydro-1*H*-inden-1-one (19) and 5,6-dibromo-2,3-dihydro-1*H*-inden-1-one

To 3-(3,4-dibromophenyl)propionic acid (**18**, 20.5 g, 66.6 mmol) was added 100 g trifluoromethanesulfonic acid under a nitrogen atmosphere and stirred at 100°C for 4 h. The reaction mixture was poured on ice and extracted with DCM (3 x 100 mL). The combined organic layers were dried over $MgSO_4$ and the solvent was removed under reduced pressure. The desired product (**19**) could be separated from the byproduct by column chromatography (silica gel, cyclohexane/EE, 4:1) to afford slightly yellow solid.

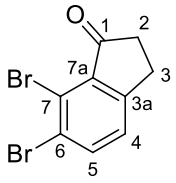

19

yield: 3.73 g (12.9 mmol, 20%)

mp.: 108 °C

R_f = 0.35 (cyclohexane/EE, 4:1)

^{1}H-NMR (500 MHz, $CDCl_3$, 300 K): δ = 7.79 (d, ^3J = 8.0 Hz, 1 H, *H*-5), 7.31 (d, ^3J = 8.1 Hz, 1 H, *H*-4), 3.04 (t, ^3J = 6.1 Hz, 2 H, *H*-3), 2.80-2.76 (m, 2 H, *H*-2) ppm.

^{13}C-NMR (125 MHz, $CDCl_3$, 300 K): δ = 202.67 (C-1), 156.54 (C-3a), 138.67 (C-5), 136.55 (C-7a), 126.79 (C-3), 126.28 (C-6), 122.17 (C-7), 37.22 (C-2), 24.42 (C-3) ppm.

HR-MS (ESI, DCM): m/z $[M+H]^+$ calculated for $C_9H_6{}^{79}Br_2O+H^+$: 288.88528; found: 288.88533 ± 1.69 ppm.

IR (ATR): $\tilde{\nu}$ = 3059 (w), 2921 (w), 2853 (w), 1703 (s), 1577 (w), 1557 (w), 1431 (s), 1384 (w), 1312 (w), 1274 (w), 1241 (w), 1213 (w), 1176 (s), 1118 (s), 838 (s), 789 (w), 674 (w), 565 (s), 526 (m), 442 (w) cm^{-1}.

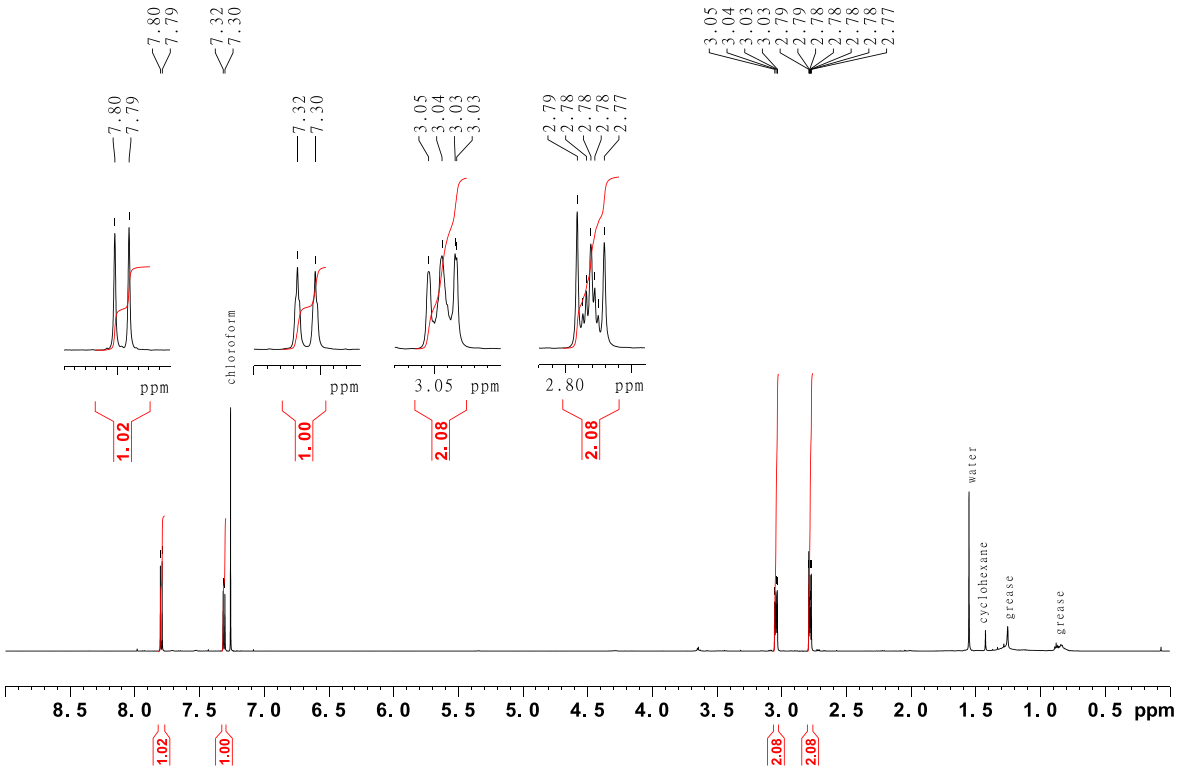

Figure SII.23: 500 MHz ^{1}H-NMR spectrum of 6,7-dibromo-2,3-dihydro-1*H*-inden-1-one (**19**).

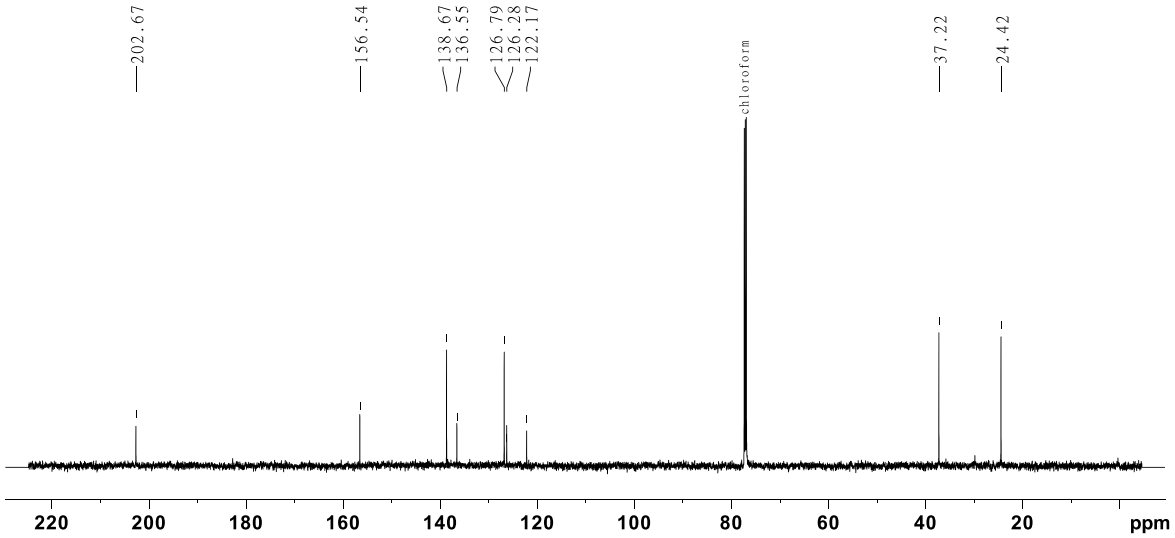

Figure SII.24: 125 MHz ^{13}C-NMR spectrum of 6,7-dibromo-2,3-dihydro-1*H*-inden-1-one (**19**).

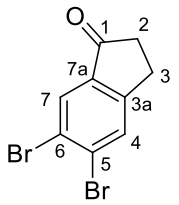

yield: 15.5 g (53.3 mmol, 80%)

mp.: 158 °C

R_f = 0.42 (cyclohexane/EE, 4:1)

^{1}H-NMR (500 MHz, $CDCl_3$, 300 K): δ = 7.98 (s, 1 H, *H*-7), 7.80 (s, 1 H, *H*-4), 3.11-3.07 (m, 2 H, *H*-3), 2.74-2.69 (m, 2 H, *H*-2) ppm.

^{13}C-NMR (125 MHz, $CDCl_3$, 300 K): δ = 204.40 (C-1), 154.55 (C-7a), 137.66 (C-3a), 132.12 (C-4), 128.59 (C-7), 124.49 (C-5, C-6), 36.54 (C-2), 25.29 (C-3) ppm.

HR-MS (ESI, DCM): m/z $[M+H]^+$ calculated for $C_9H_6{}^{79}Br_2O+H^+$: 288.88582; found: 288.88531 ± 1.75 ppm.

IR (ATR): $\tilde{\nu}$ = 3076 (w), 2925 (w), 2929 (w), 1702 (s), 1586 (s), 1567 (m), 1433 (s), 1372 (m), 1310 (m), 1296 (m), 1269 (m), 1231 (m), 1196 (s), 1145 (m), 1091 (m), 1036 (m), 986 (w), 895 (m), 877 (s), 812 (w), 677 (w), 618 (w), 592 (w), 541 (m), 512 (m), 403 (s) cm^{-1}.

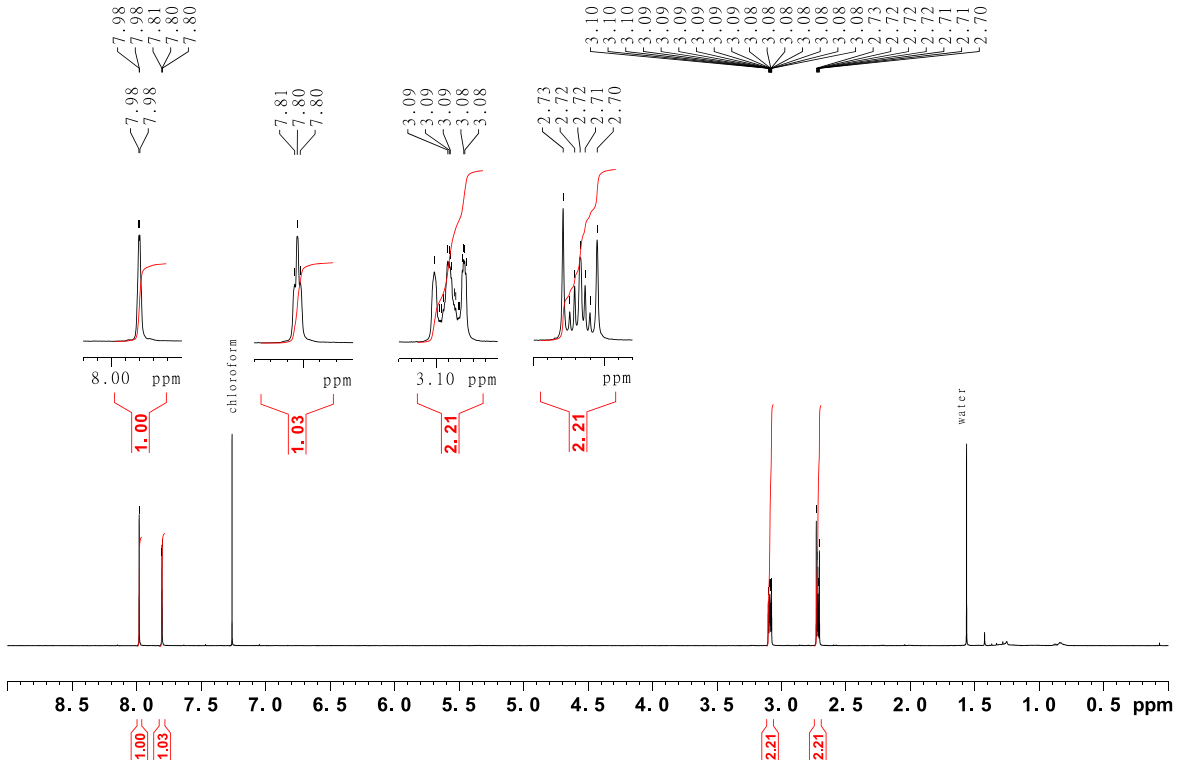

Figure SII.25: 500 MHz ^{1}H-NMR spectrum of 5,6-dibromo-2,3-dihydro-1*H*-inden-1-one.

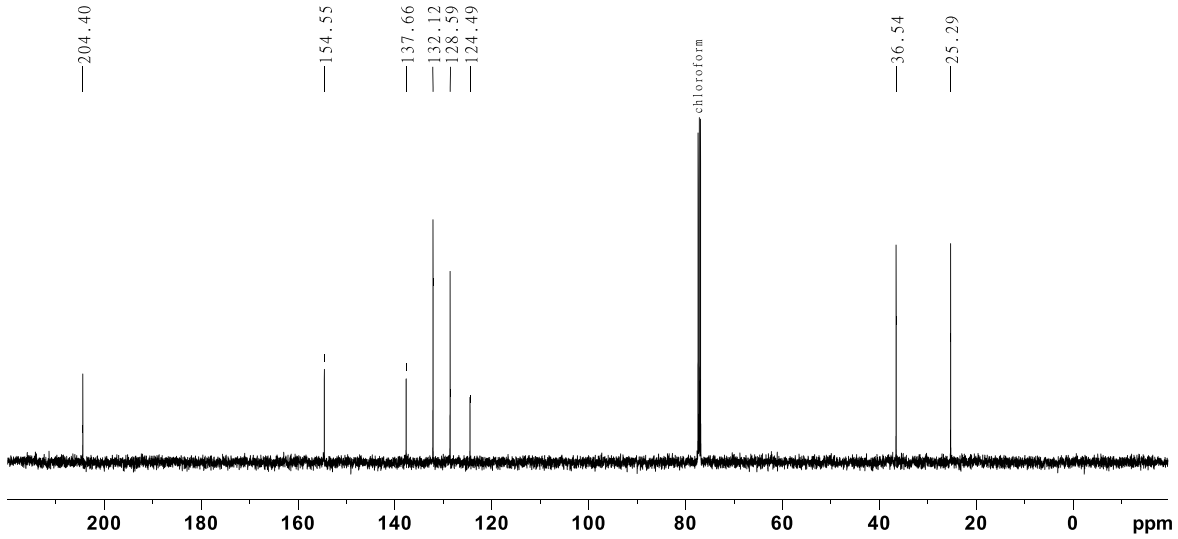

Figure SII.26: 125 MHz ^{13}C-NMR spectrum of 5,6-dibromo-2,3-dihydro-1*H*-inden-1-one.

SII.1.11 Synthesis of 4,5-dibromo-2,3-dihydro-1*H*-indene (20)

6,7-Dibromo-2,3-dihydro-1*H*-inden-1-one (**19**, 3.73 g, 12.9 mmol) was dissolved in 40 mL abs. DCM under a nitrogen atmosphere and cooled to 0 °C. Trifluoromethanesulfonic acid (4 mL, 6.85 g, 45.5 mmol) dissolved in 20 mL abd. DCM and triethylsilane (6 mL, 4,38 g, 37.7 mmol) dissolved in 20 mL were added dropwise subsequently. After 5 min. of stirring in at 0 °C trifluoromethanesulfonic acid (4 mL, 6.85 g, 45.5 mmol) and triethylsilane (6 mL, 4,38 g, 37.7 mmol) were added dropwise. After stirring at room temperature for 1 h triethylsilane (6 mL, 4.38 g, 37.7 mmol) were added stirred for another 2 h. The reaction mixture was poured on 100 mL cold saturated $NaHCO_3$ solution and extracted with DCM (3 x 50 mL). The combined organic layers were dried over $MgSO_4$ and the solvent was removed under reduced pressure. The crude product was purified by column chromatography (silica gel, cyclohexane/EE, 4:1) to afford a slightly yellow liquid still containing triethylsilane which could not be separated from the desired product.

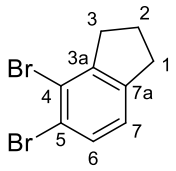

20

yield: 3.56 g (12.9 mmol, >99%)

***R*f =** 0.79 (cyclohexane/EE, 4:1)

^{1}H-NMR (500 MHz, $CDCl_3$, 300 K): δ = 7.37 (d, ^3J = 7.9 Hz, 1 H, *H*-6), 7.01 (d, ^3J = 7.9 Hz, 1 H, *H*-7), 3.01-2.95 (m, 4 H, *H*-1, *H*-3), 2.10 (q, ^3J = 7.7 Hz, 2 H, *H*-2) ppm.

^{13}C-NMR (125 MHz, $CDCl_3$, 300 K): δ = 147.30 (C-3a), 144.56 (C-7a), 131.37 (C-6), 124.23 (C-7), 122.03 (C-5), 121.78 (C-4), 36.20 (C-1/C-3), 33.87 (C-1/C-3), 24.53 (C-2) ppm.

HR-MS (EI, 70 eV, DCM): m/z $[M]^+$ calculated for $C_9H_8{}^{79}Br_2{}^+$: 273.89928; found: 273.89941 ± 0.13 ppm.

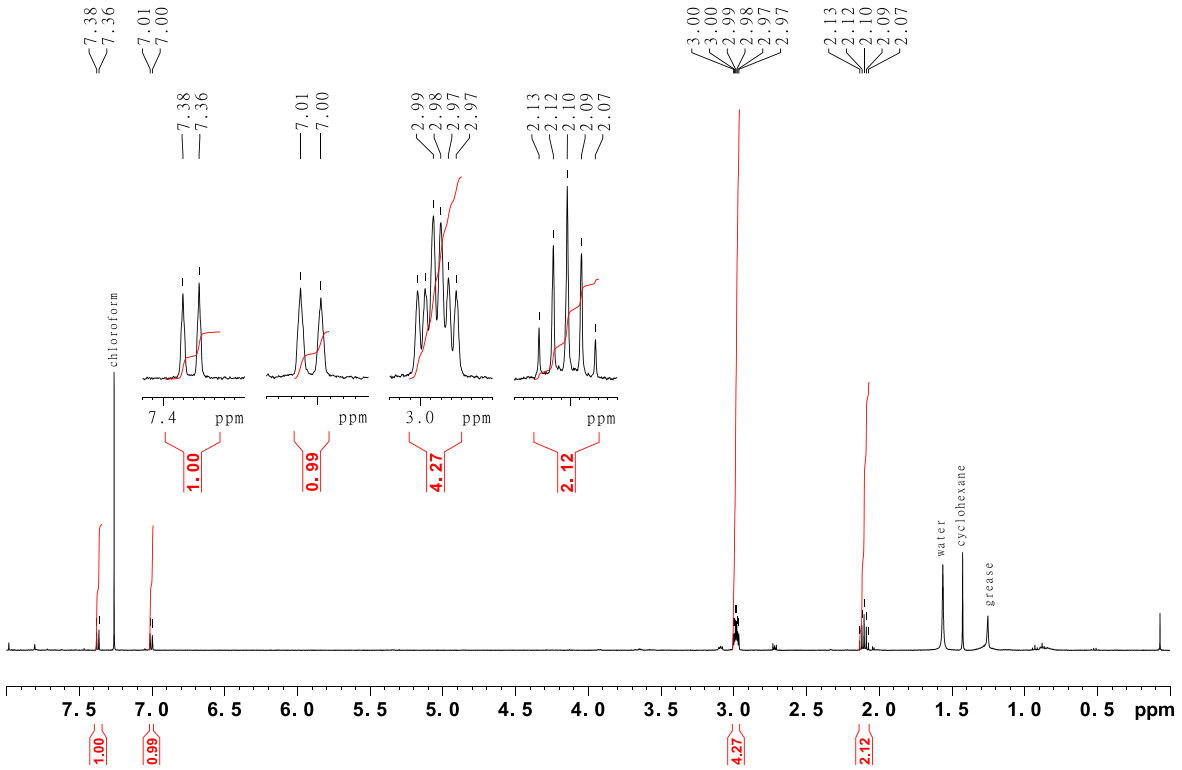

Figure SII.27: 500 MHz ^{1}H-NMR spectrum of 4,5-dibromo-2,3-dihydro-1*H*-indene (**20**).

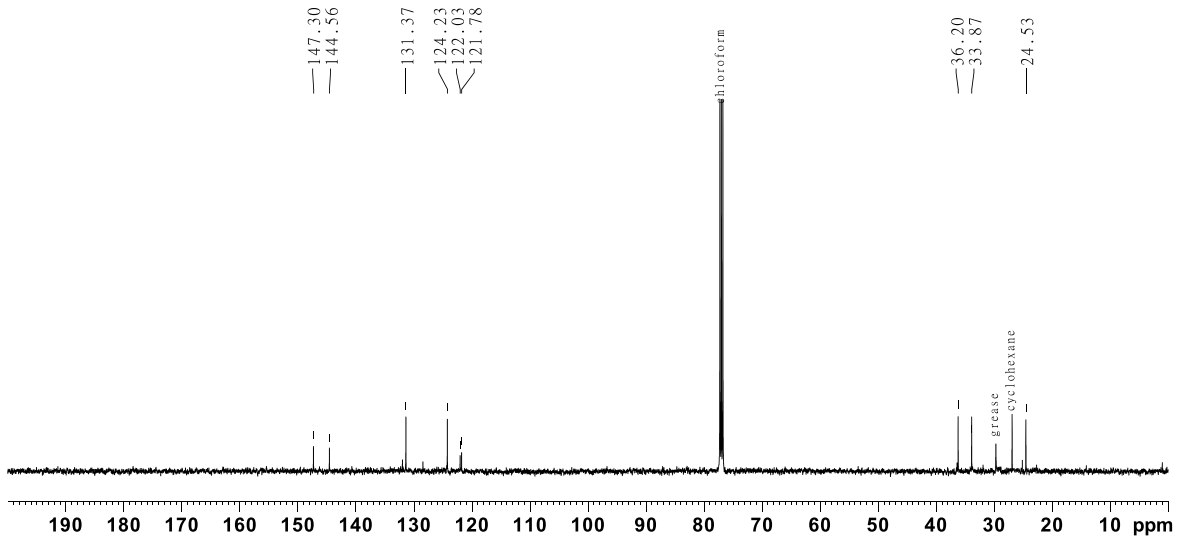

Figure SII.28: 125 MHz ^{13}C-NMR spectrum of 4,5-dibromo-2,3-dihydro-1*H*-indene (**20**).

SII.1.12 Synthesis of 4,5-dibromo-7-nitro-2,3-dihydro-1*H*-indene (15)

To 50 mL white fuming nitric acid cooled to 0 °C 4,5-dibromo-2,3-dihydro-1*H*-indene (**20**, 3.56 g, 12.9 mmol) dissolved in 5 mL DCM was added dropwise under a nitrogen atmosphere and stirred for 4 h at 0 °C. The reaction mixture was poured on ice extracted with DCM (5 x 50 mL), the organic layers were dried over $MgSO_4$ and the solvent was removed under reduced pressure. The crude product was purified by column chromatography (silica gel, cyclohexane/EE, 20:1) to afford the desired product isomer (**15**) as a yellow solid.

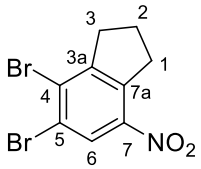

15

yield: 1.32 g (4.13 mmol, 32%)

mp.: 104 °C

^{1}H-NMR (500 MHz, $CDCl_3$, 300 K): δ = 8.26 (s, 1 H, *H*-6), 3.48 (t, ^3J = 7.5 Hz, 2 H, *H*-1/*H*-3), 3.10 (t, ^3J = 7.5 Hz, 2 H, *H*-1/*H*-3), 2.20 (q, ^3J = 7.6 Hz, 2 H, *H*-2) ppm.

^{13}C-NMR (125 MHz, $CDCl_3$, 300 K): δ = 150.58 (C-3a), 144.39 (C-7), 140.35 (C-7a), 129.13 (C-5), 126.87 (C-6), 122.94 (C-4), 36.75 (C-1/C-3), 35.33 (C-1/C-3), 23.81 (C-2) ppm.

HR-MS (ESI, DCM): m/z $[M+H]^+$ calculated for $C_9H_7{}^{79}Br_2NO_2+H^+$: 319.89163; found: 319.89130 ± 1.03 ppm.

IR (ATR): $\tilde{\nu}$ = 3085 (m), 2956 (m), 1739 (w), 1583 (w), 1525 (s), 1432 (m), 1401 (m), 1349 (s), 1310 (s), 1269 (m), 1195 (m), 1148 (m), 1050 (w), 952 (m), 914 (w), 850 (s), 754 (s), 689 (m) cm^{-1}.

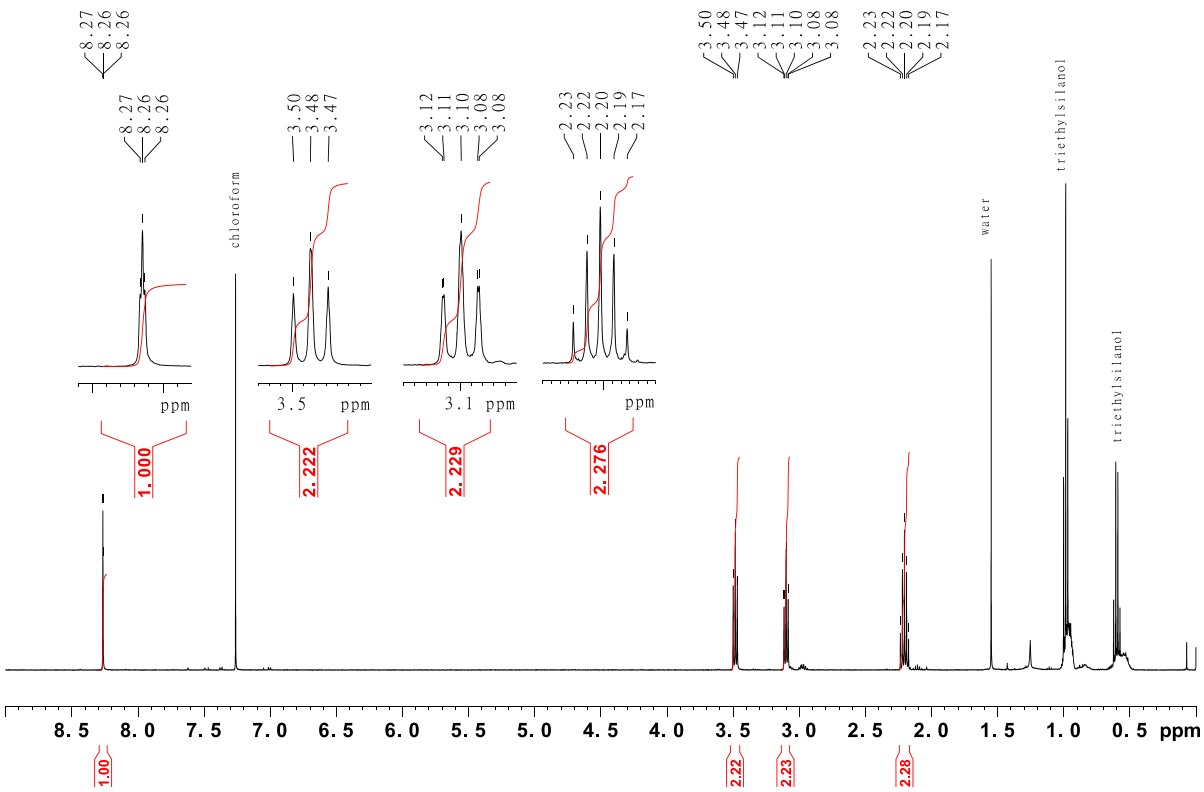

Figure SII.29: 500 MHz ^{1}H-NMR spectrum of 4,5-dibromo-7-nitro-2,3-dihydro-1*H*-indene (**15**).

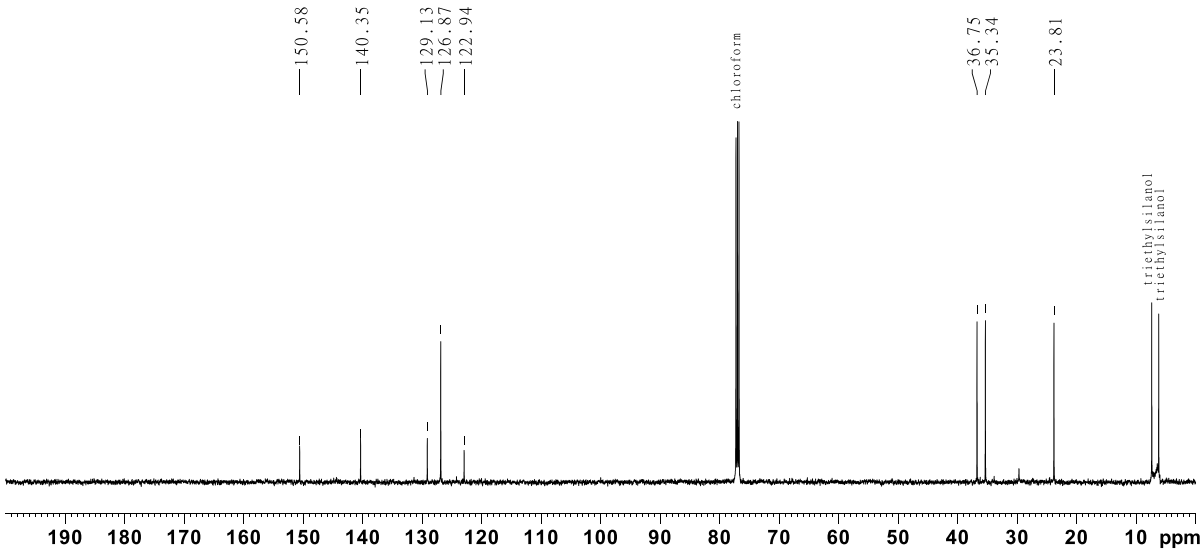

Figure SII.30: 125 MHz ^{13}C-NMR spectrum of 4,5-dibromo-7-nitro-2,3-dihydro-1*H*-indene (**15**).

SII.13 Synthesis of (1*R*,1'*S*)-4,4',5,5'-tetrabromo-7,7'-dinitro-2,2',3,3'-tetrahydro-1*H*,1'*H*-1,1'-diindene (22) and (1*R*,1'*R*/1*S*,1'*S*)-4,4',5,5'-tetrabromo-7,7'-dinitro-2,2',3,3'-tetrahydro-1*H*,1'*H*-1,1'-diindene (23)

4,5-Dibromo-7-nitro-2,3-dihydro-1*H*-indene (**15**, 1.32 g, 4.13 mmol) was dissolved in dry THF under nitrogen atmosphere, cooled to 0 °C and potassium butoxide (732 mg, 6.03 mmol) was added. The reaction was stirred for 30 s before bromine (830 mg, 0.28 mL, 5.20 mmol) was added rapidly. The reaction was stirred for further 10 min. and 150 g of ice were added. The aqueous solution was extracted with DCM (3 × 40 mL) and the combined organic layers were wash with saturated sodium thiosulfate solution, dried with over $MgSO_4$ and the solvent was removed under reduced pressure. The crude product was purified by column chromatography (silica gel, *n*-pentane/DCM, 3:1) to afford the pure *rac*-product **23** and a mixture of *rac*- **23** and *meso*-diastereomers **22**. The meso-diastereomer could not be obtained in a pure form.

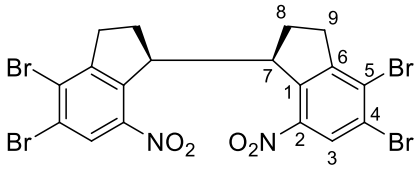

22

***R*f** = 0.23 (*n*-pentane/DCM, 4:1)

^{1}H-NMR (600 MHz, $CDCl_3$, 300 K): δ = 8.12 (s, 2 H, *H*-3), 4.59-4.56 (m, 2 H, *H*-7), 2.92-2.86 (m, 2 H, *H*-8/*H*-9), 2.55-2.37 (m, 4 H, *H*-8/*H*-9), 2.03-1.96 (m, 2 H, *H*-9b) ppm.

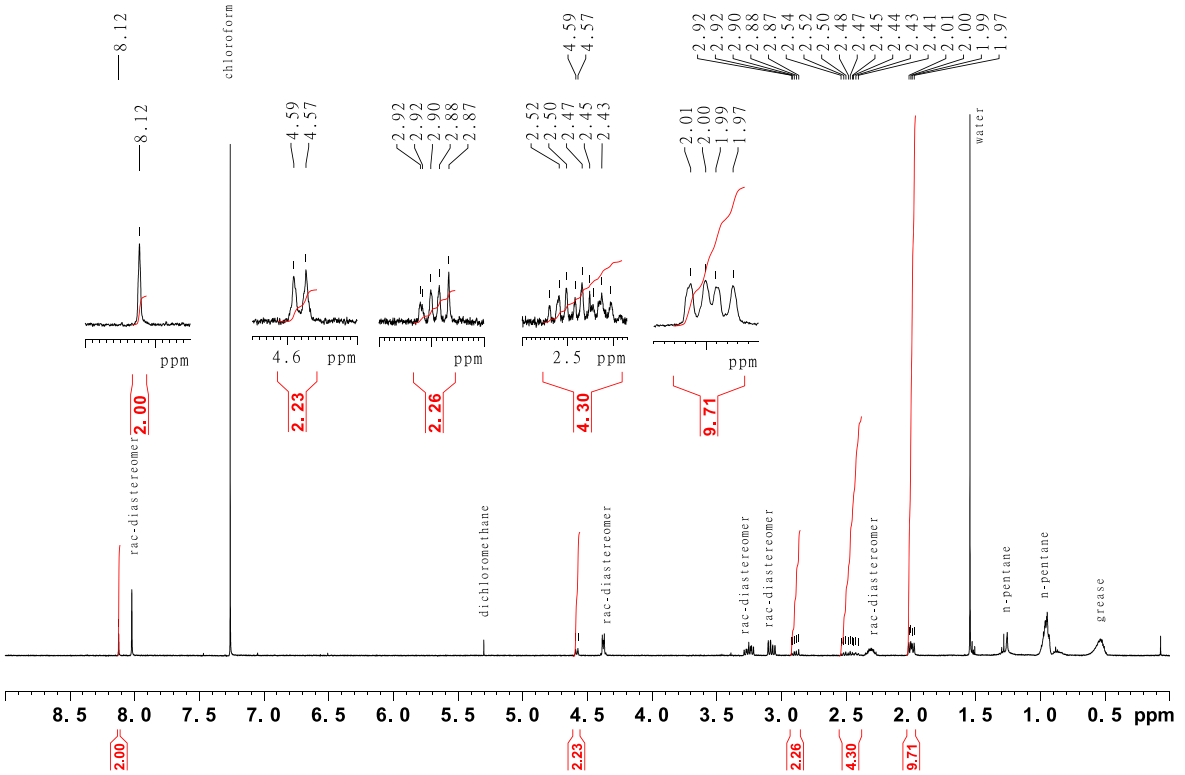

Figure SII.31: 500 MHz ^{1}H-NMR spectrum of (1*R*,1'*S*)-4,4',5,5'-tetrabromo-7,7'-dinitro-2,2',3,3'-tetrahydro-1*H*,1'*H*-1,1'-diindene (**22**) and (1*R*,1'*R*/1*S*,1'*S*)-4,4',5,5'-tetrabromo-7,7'-dinitro-2,2',3,3'-tetrahydro-1*H*,1'*H*-1,1'-diindene (**23**). The 1H signals of (1*R*,1'*S*)-4,4',5,5'-tetrabromo-7,7'-dinitro-2,2',3,3'-tetrahydro-1*H*,1'*H*-1,1'-diindene (**22**) are marked.

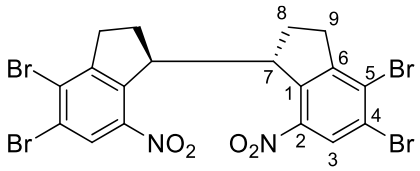

23

yield: 555 mg (867 µmol, 21%)

mp.: degradation over 240 °C

***R*f =** 0.28 (*n*-pentane/DCM, 4:1)

^{1}H-NMR (500.1 MHz, $CDCl_3$), 300 K): δ = 8.02 (s, 2 H, *H*-3), 4.40-4.35 (m, 2 H, *H*-7), 3.29-3.21 (m, 2 H, *H*-9a), 3.11-3.04 (m, 2 H, *H*-9b), 2.36-2.64 (m, 2 H, *H*-8a), 2.03-1.97 (m, 2 H, *H*-8b) ppm.

^{13}C-NMR (125.8 MHz, $CDCl^3$, 300 K): δ = 151.31 (C-6), 144.65 (C-2), 139.21 (C-1), 129.21 (C-5), 127.23 (C-3), 124.41 (C-4), 48.57 (C-7), 34.76 (C-9), 30.48 (C-8) ppm.

IR (ATR): $\tilde{\nu}$ = 2959 (w), 2878 (w), 1520 (s), 1430 (w), 1407 (m), 1385 (w), 1337 (s), 1302 (m), 1241 (m), 1180 (m), 1083 (s), 1030 (s), 1005 (s), 954 (m), 885 (m), 875 (m), 814 (m), 759 (s), 738 (m), 725 (m), 705 (m), 612 (w), 537 (w), 411 (w) cm^{-1}.

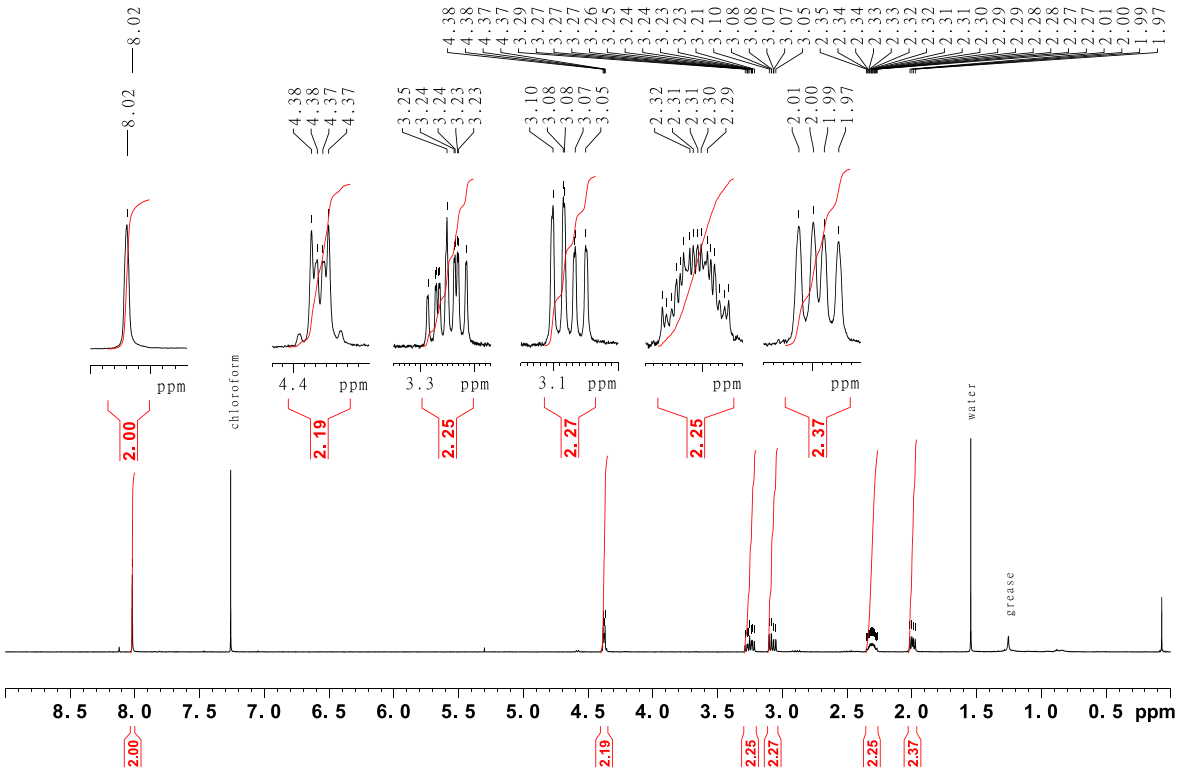

Figure SII.32: 500 MHz ^{1}H-NMR spectrum of (1*R*,1'*R*/1*S*,1'*S*)-4,4',5,5'-tetrabromo-7,7'-dinitro-2,2',3,3'-tetrahydro-1*H*,1'*H*-1,1'-diindene (**23**).

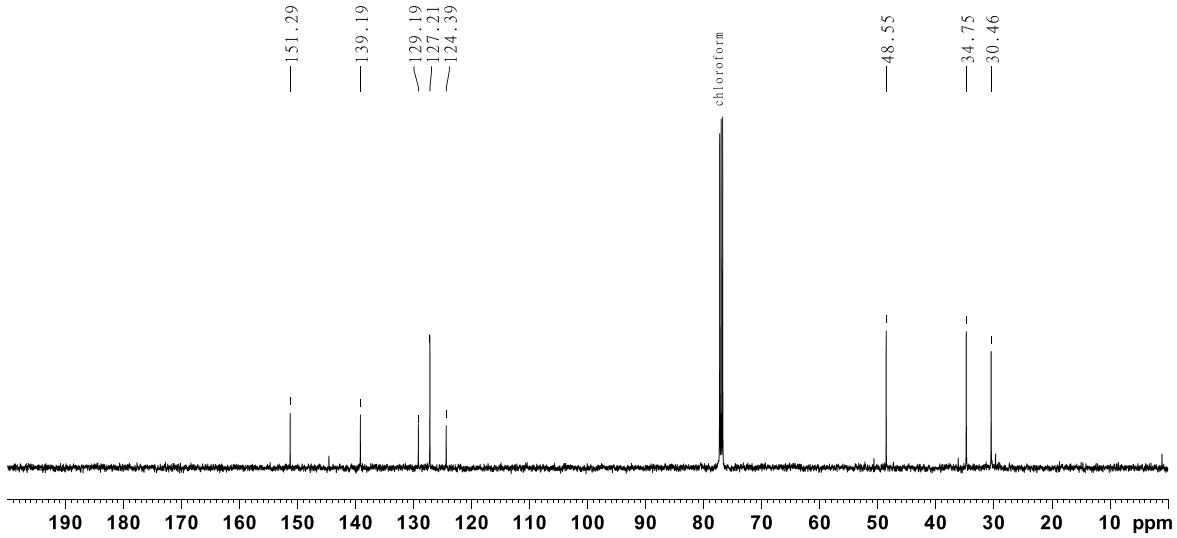

Figure SII.33: 125 MHz ^{13}C-NMR spectrum of (1*R*,1'*R*/1*S*,1'*S*)-4,4',5,5'-tetrabromo-7,7'-dinitro-2,2',3,3'-tetrahydro-1*H*,1'*H*-1,1'-diindene (**23**).

SII.14 Synthesis of (12a*R*,12b*R*/12a*S*,12b*S*,*Z*)-3,4,9,10-tetrabromo-1,2,11,12,12a,12b-hexahydrodiindeno[7,1-*cd*:1',7'-*fg*][1,2]-diazocine (6)

To a solution of (1R,1'R/1S,1'S)-4,4',5,5'-tetrabromo-7,7'-dinitro-2,2',3,3'-tetrahydro-1H,1'H-1,1'-diindene (**23**, 57.1 mg, 89.2 µmol) in 14 mL EtOH an aqueous solution of barium hydroxide [$Ba(OH)_2 \cdot 8\ H_2O$] (95.6 mg, 303 µmol) in 6 mL H_2O and zinc powder (105 mg, 1.61 mmol) and the mixture was stirred for 16 h under reflux. The reaction mixture was filtered through Celite and the solvent was removed under reduced pressure. The residue was dissolved in DCM and filtered through Celite and the solvent was removed under reduced pressure. The crude product was dissolved in 6 mL 0.1 M methanolic NaOH solution, $CuCl_2$ (1 mg, 7.43 µmol) was added and the reaction mixture was stirred at room temperature until completion while air was bubbled through the solution. The reaction was neutralized with 6 M HCl solution. Saturated sodium bicarbonate solution (20 mL) was added and the aqueous layer was extracted with DCM (3 × 10 mL). The combined organic layers were dried over $MgSO_4$ and the solvent was removed under reduced pressure. The crude product was purified by column chromatography (silica gel, *n*-pentane/DCM, 2:1) to afford an orange solid.

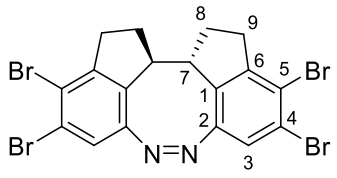

22

yield: 14.2 mg (24.6 µmol, 28%)

mp.: 209 °C

R_f = 0.54 (*n*-pentane/DCM, 2:1)

^{1}H-NMR (500.1 MHz, $CDCl_3$, 300 K): δ = 7.68 (s, 2 H, *H*-3), 3.09-2.96 (m, 6 H, *H*-7, *H*-9a, *H*-9b), 2.30-2.20 (m, 2 H, *H*-8a), 2.05-1.94 (m, 2 H, *H*-8b) ppm.

^{13}C-NMR (125.8 MHz, $CDCl_3$, 300 K): δ = 147.80 (C-2), 147.10 (C-6), 132.15 (C-1), 130.35 (C-3), 123.03 (C-4), 122.68 (C-5), 50.53 (C-7), 34.92 (C-9), 30.59 (C-8) ppm.

HR-MS (EI, 70 eV, DCM): m/z $[M]^+$ calculated for $C_{18}H_{12}{}^{79}Br_4N_2^+$: 571.77340; found: 571.77324 ± 0.28 ppm.

IR (ATR): $\tilde{\nu}$ = 2922 (m), 2854 (m), 1734 (w), 1456 (w), 1406 (w), 1377 (w), 1251 (w), 1093 (s), 863 (m), 798 (w), 743 (m), 661 (w), 435 (w) cm^{-1}.

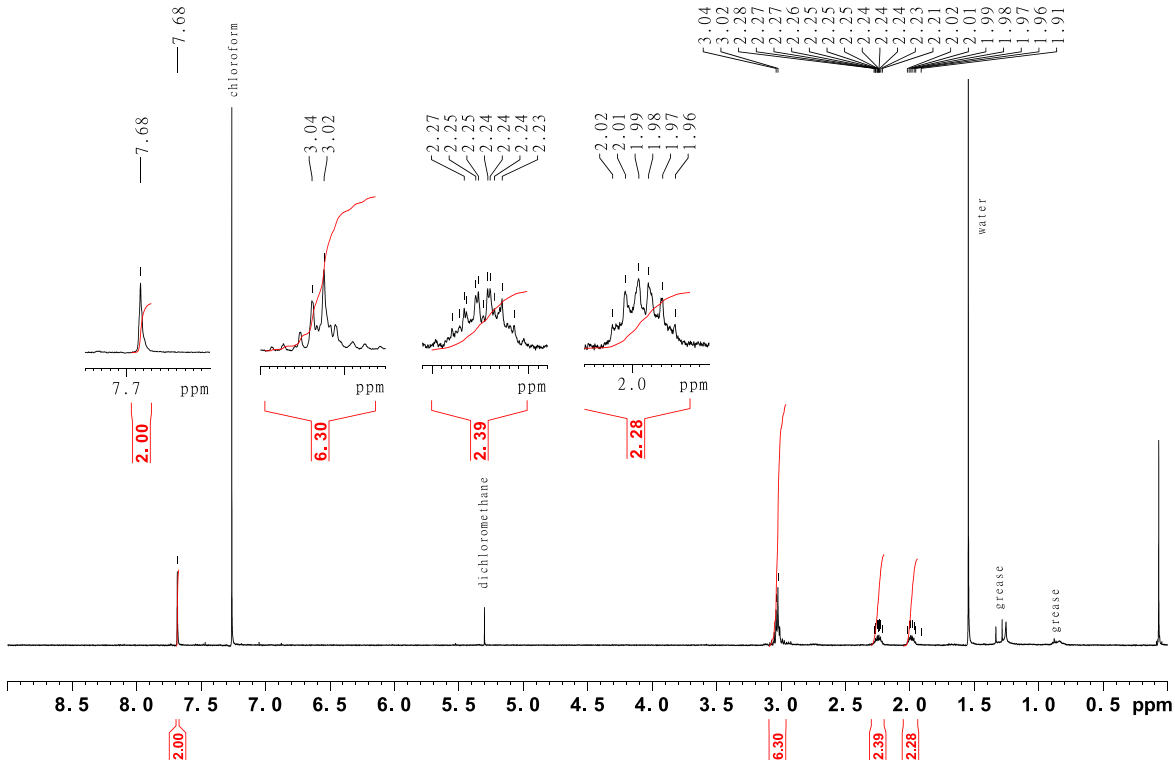

Figure SII.34: 500 MHz ^{1}H-NMR spectrum of (12a*R*,12b*R*/12a*S*,12b*S*,*Z*)-3,4,9,10-tetrabromo-1,2,11,12,12a,12b-hexahydrodiindeno[7,1-*cd*:1',7'-*fg*][1,2]-diazocine (**6**).

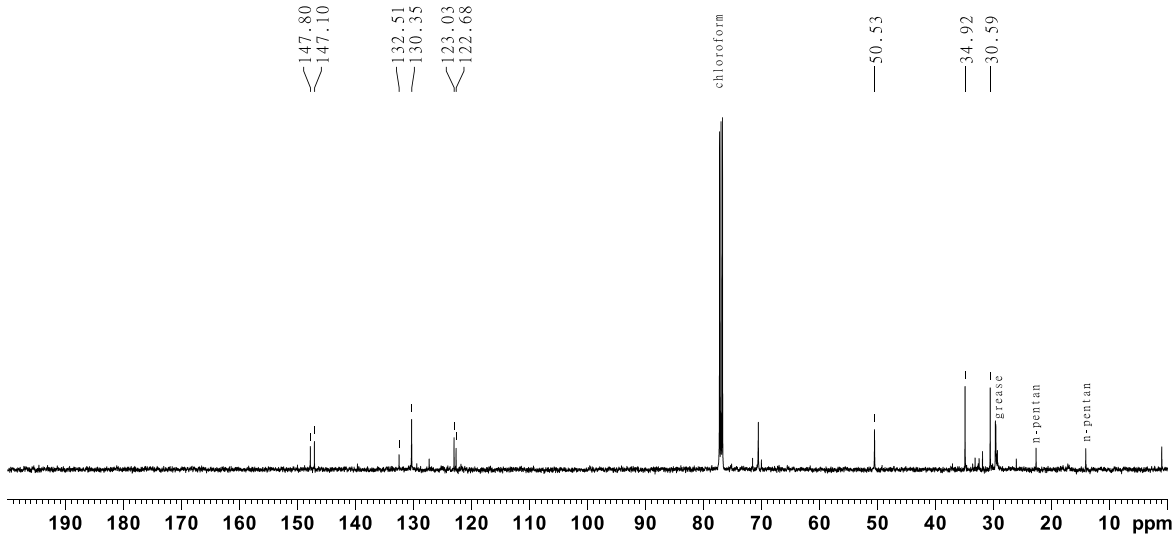

Figure SII.35: 125 MHz ^{13}C-NMR spectrum of (12a*R*,12b*R*/12a*S*,12b*S*,*Z*)-3,4,9,10-tetrabromo-1,2,11,12,12a,12b-hexahydrodiindeno[7,1-*cd*:1',7'-*fg*][1,2]-diazocine (**6**).

SIII. Photostationary states (PSS)

Photostationary states Γ of compounds **3-6** were measured via ^{1}H-NMR by integration of the different species after irradiation with different wavelengths (3 min. irradiation time). The values of the integrals are given in Table SIII.1. ^{1}H-NMR spectra were measured at 7.68 mM concentrations at 298 K. All spectra were measured at a Bruker AV600 spectrometer.

The following equation (1) was used for extrapolation of the photostationary state of **3** at 238 K.

$$PSS_{extrapol.} = PSS_{measured} \cdot e^{kt} \quad (1)$$

k is the rate constant at given temperature determined via Arrhenius plot (for details, see Supporting Information section IV) and t the measuring time of 132 s (transfer into the spectrometer after excitation with light and measuring time for 2 scans). Spectra were measured at Bruker DRX 500.

Table SIV.1: Measured photostationary states of compounds **3-6** in acetone-d$_6$ measured at 298 K except compound **3** which was measured at 238 K and extrapolated via equation 1.

	measured PSS	
	% *E* (385 nm)	% *Z* (530 nm)
3	86[b]	>99[b]
4	68	92
5	67	92
6	78	93

[b] measured at 238 K.

SIII.1 (12a*R*,12b*S*,*Z*)-4,9-dibromo-1,2,11,12,12a,12b-hexahydrodiindeno[7,1-*cd*:1',7'-*fg*][1,2]-diazocine (3)

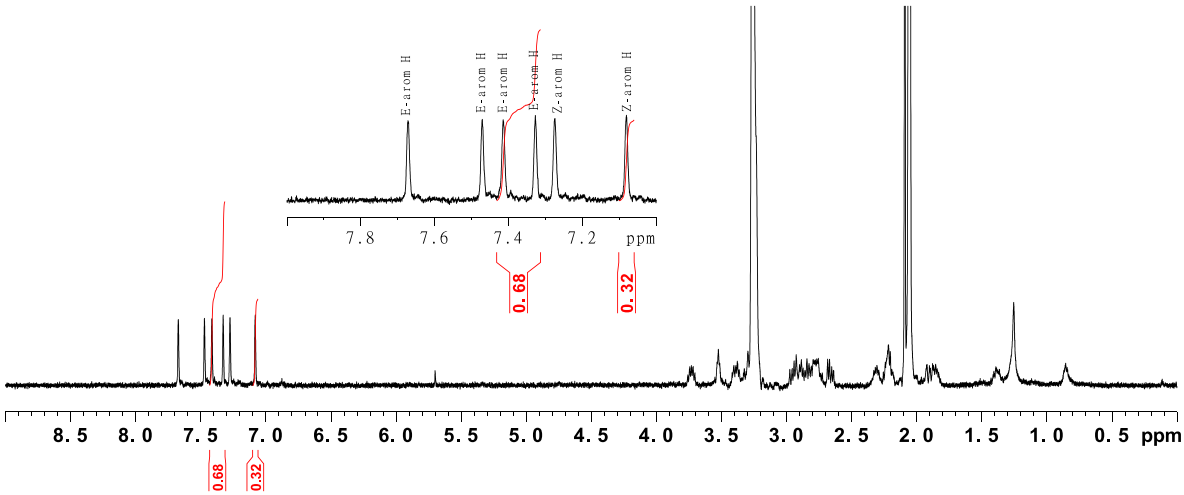

Figure SIII.1: ^{1}H-NMR spectra of unirradiated (12a*R*,12b*S*,*Z*)-4,9-dibromo-1,2,11,12,12a,12b-hexahydrodiindeno[7,1-*cd*:1',7'-*fg*][1,2]-diazocine **3** in acetone-d$_6$ at 238 K after irradiation with 385 nm.

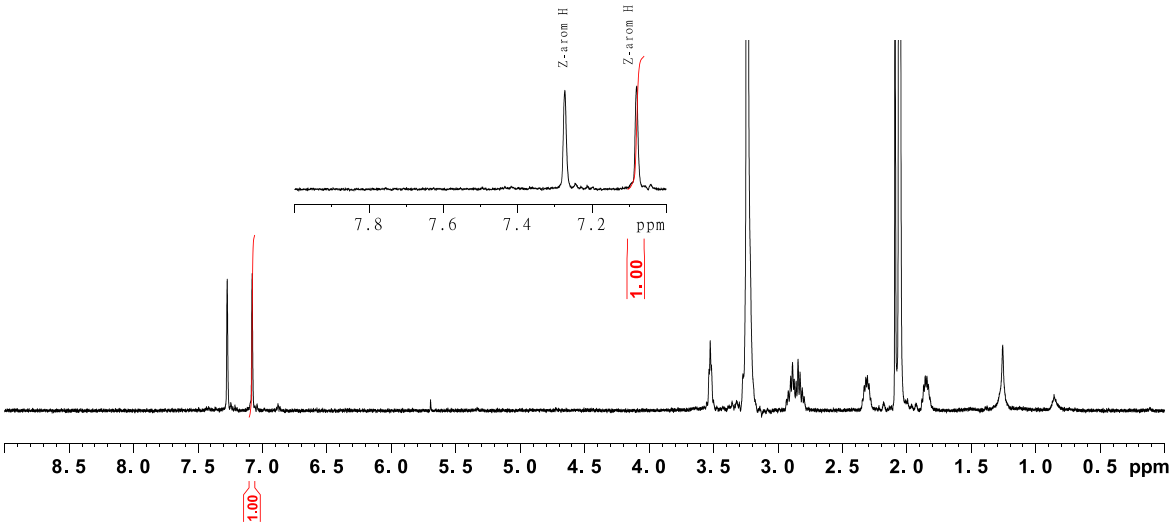

Figure SIII.2: ^{1}H-NMR spectra of (12a*R*,12b*S*,*Z*)-4,9-dibromo-1,2,11,12,12a,12b-hexahydrodiindeno[7,1-*cd*:1',7'-*fg*][1,2]-diazocine **3** in acetone-d_6 at 238 K after irradiation with 530 nm.

SIII.2 (12a*R*,12b*R*/12a*S*,12b*S*,*Z*)-4,9-dibromo-1,2,11,12,12a,12b-hexahydrodiindeno[7,1-*cd*:1',7'-*fg*][1,2]-diazocine (4)

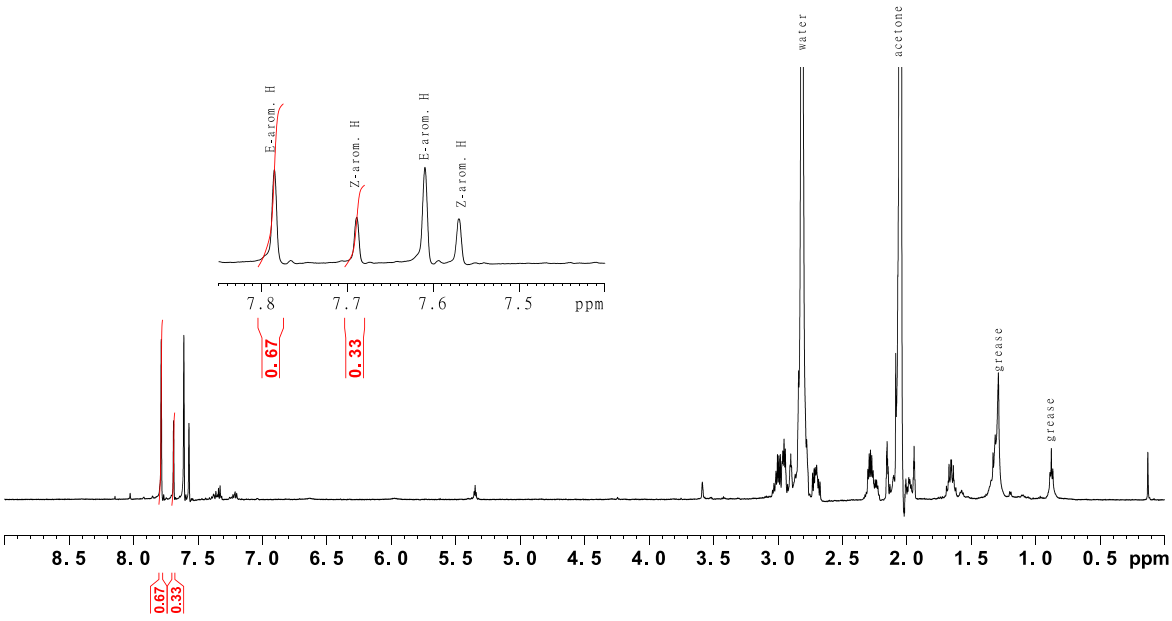

Figure SIII.3: 600 MHz ^{1}H-NMR spectra of (12a*R*,12b*R*/12a*S*,12b*S*,*Z*)-4,9-dibromo-1,2,11,12,12a,12b-hexahydrodiindeno[7,1-*cd*:1',7'-*fg*][1,2]-diazocine (**4**) in acetone-d_6 at 298 K after irradiation with 385 nm.

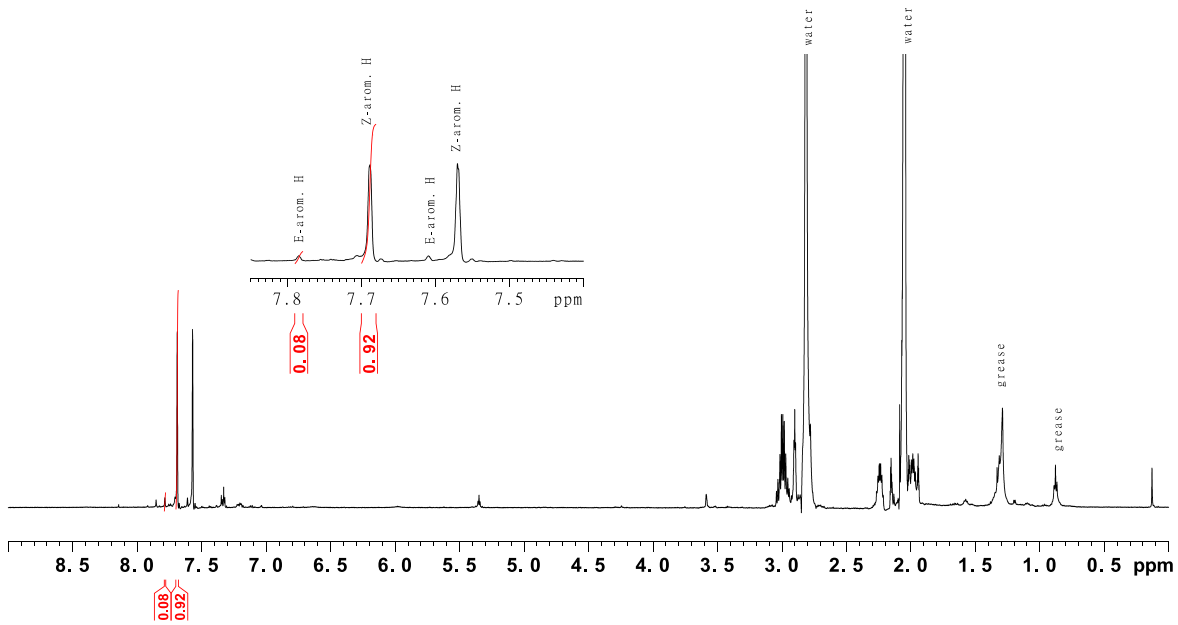

Figure SIII.4: 600 MHz ^{1}H-NMR spectra of (12a*R*,12b*R*/12a*S*,12b*S*,*Z*)-4,9-dibromo-1,2,11,12,12a,12b-hexahydrodiindeno[7,1-*cd*:1',7'-*fg*][1,2]-diazocine (**4**) in acetone-d_6 at 298 K after irradiation with 530 nm.

SIII.3 (12a*R*,12b*R*/12a*S*,12b*S*,*Z*)-4,9-diiodo-1,2,11,12,12a,12b-hexahydrodiindeno[7,1-*cd*:1',7'-*fg*][1,2]-diazocine (5)

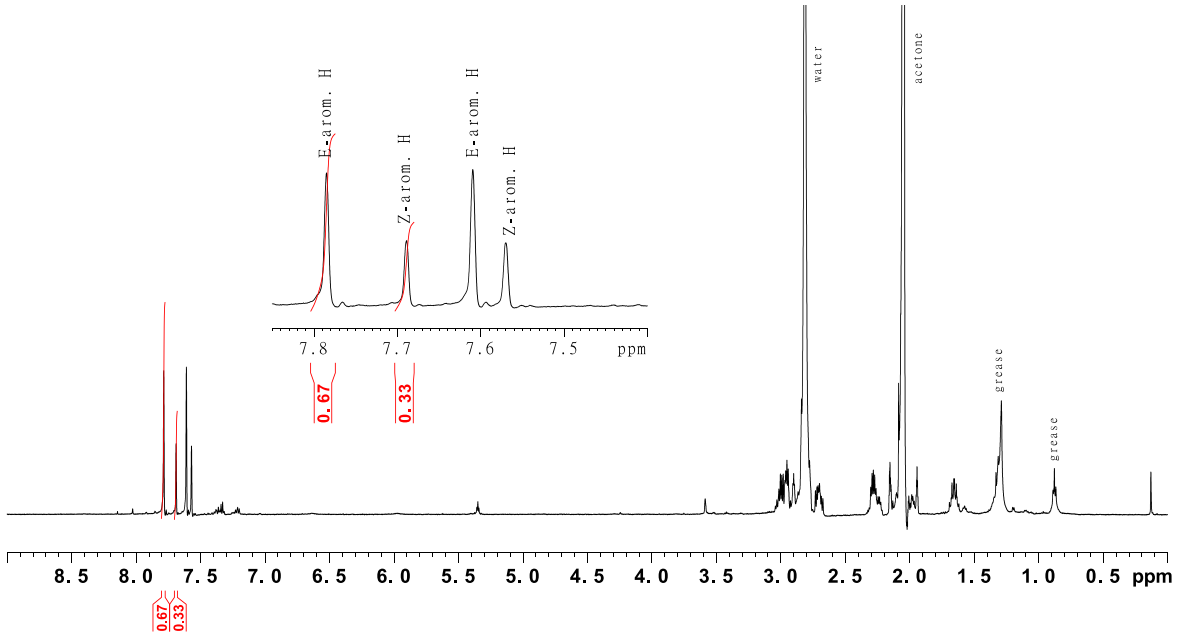

Figure SIII.5: 600 MHz ^{1}H-NMR spectra of (12a*R*,12b*R*/12a*S*,12b*S*,*Z*)-4,9-diiodo-1,2,11,12,12a,12b-hexahydrodiindeno[7,1-*cd*:1',7'-*fg*][1,2]-diazocine (**5**) in acetone-d_6 at 298 K after irradiation with 385 nm.

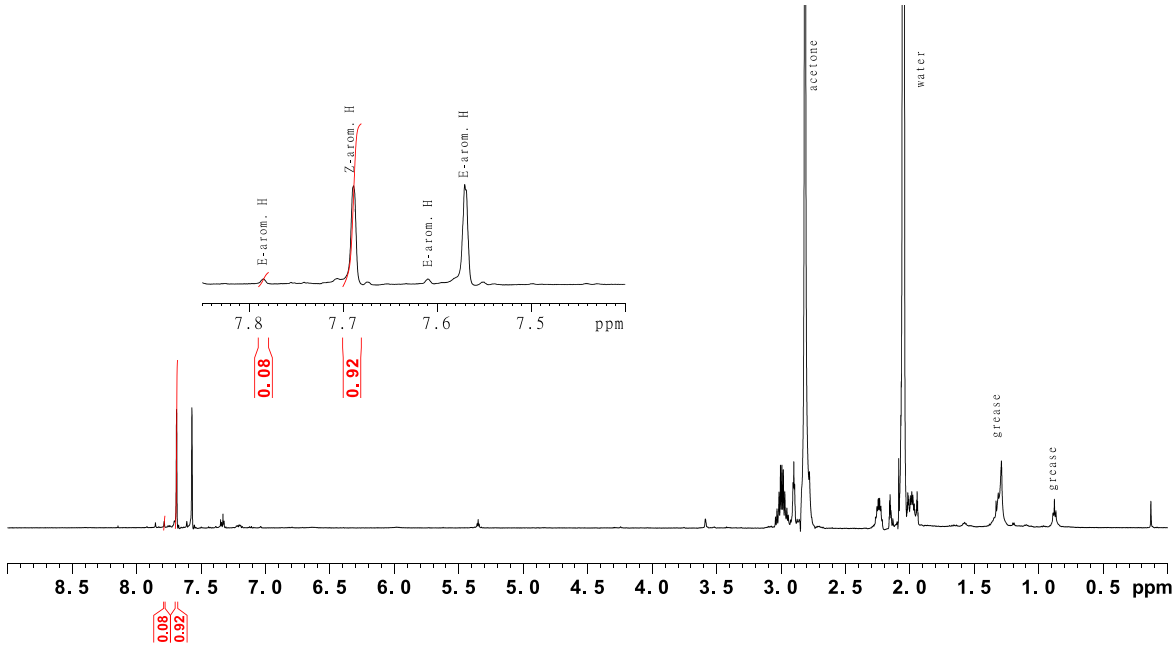

Figure SIII.6: 600 MHz ^{1}H-NMR spectra of (12a*R*,12b*R*/12a*S*,12b*S*,*Z*)-4,9-diiodo-1,2,11,12,12a,12b-hexahydrodiindeno[7,1-*cd*:1',7'-*fg*][1,2]-diazocine (**5**) in acetone-d_6 at 298 K after irradiation with 530 nm.

SIII.4 (12a*R*,12b*R*/12a*S*,12b*S*,*Z*)-3,4,9,10-tetrabromo-1,2,11,12,12a,12b-hexahydrodiindeno[7,1-*cd*:1',7'-*fg*][1,2]-diazocine (6)

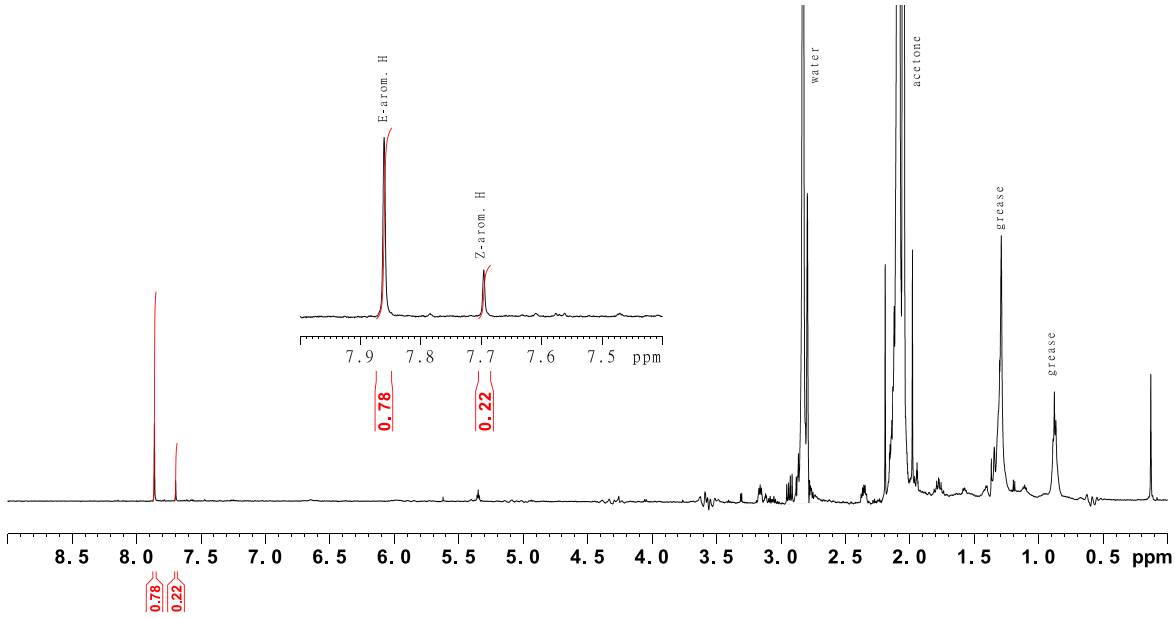

Figure SIII.7: ^{1}H-NMR spectra of (12a*R*,12b*R*/12a*S*,12b*S*,*Z*)-4,9-diiodo-1,2,11,12,12a,12b-hexahydrodiindeno[7,1-*cd*:1',7'-*fg*][1,2]-diazocine (**5**) in acetone-d_6 at 298 K after irradiation with 385 nm.

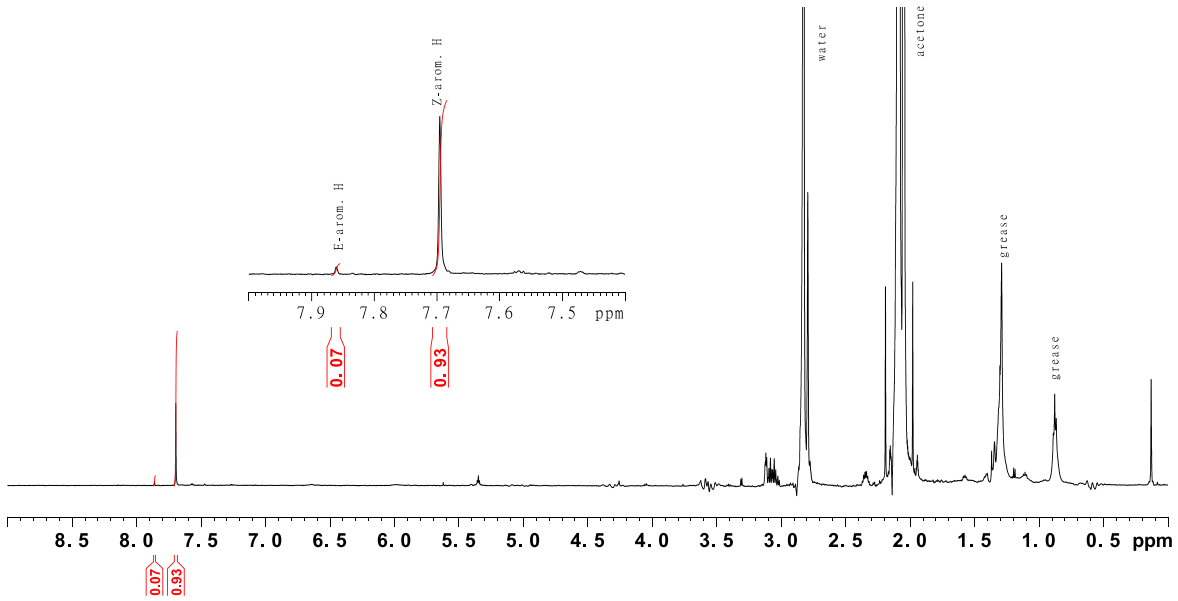

Figure SIII.8: ^{1}H-NMR spectra of (12a*R*,12b*R*/12a*S*,12b*S*,*Z*)-4,9-diiodo-1,2,11,12,12a,12b-hexahydrodiindeno[7,1-*cd*:1',7'-*fg*][1,2]-diazocine (**5**) in acetone-d_6 at 298 K after irradiation with 530 nm.

SIV. UV-vis experiments

All samples were irradiated to the photostationary state Γ with 385 nm in acetone. The extrapolated UV-vis spectra of the *E*-configurations were calculated from the UV-vis spectra of the PSS, the pure *Z*-configuration and the percentage of *E*-configuration measured by ^{1}H-NMR (for details see SIII) by the following equation (2):

$$A_{E,extrapol.} = \frac{A_{PSS} - [A_Z \cdot (1 - PSS)]}{PSS} \quad (2)$$

Thermal half-lives have been calculated with equation (3) following a first order kinetics of thermal relaxation. The thermal rate constant k has been obtained from the slope of the thermal relaxation plot.

$$t_{1/2} = \frac{ln\,2}{k} \quad (3)$$

SIV.1 (12a*R*,12b*S*,*Z*)-4,9-dibromo-1,2,11,12,12a,12b-hexahydrodiindeno[7,1-*cd*:1',7'-*fg*][1,2]-diazocine (3)

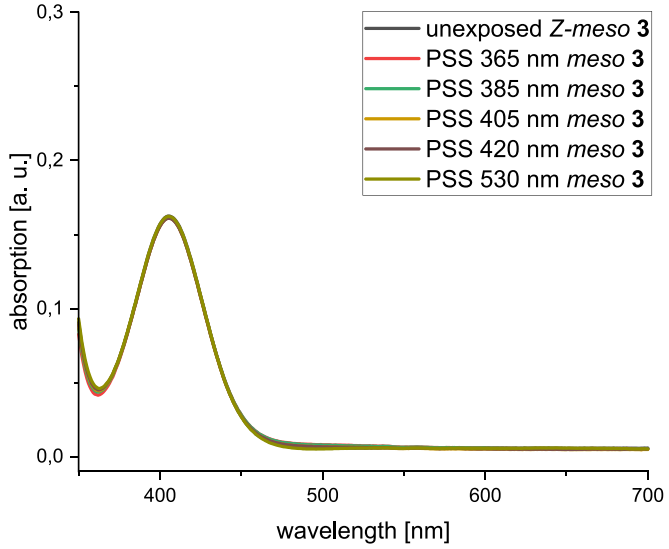

Figure SVII.1: UV-vis spectra of *meso*-DID **3** (250 µM) in acetone at 298 K before (black) and after irradiation with different wavelengths.

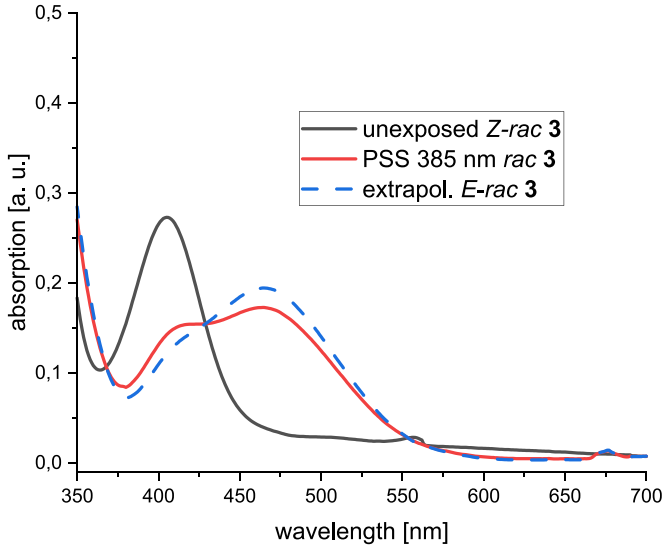

Figure SVII.2: UV-vis spectra of *meso*-DID **3** (250 µM) in acetone at 233 K before (black) and after irradiation with light at 385 nm (red).

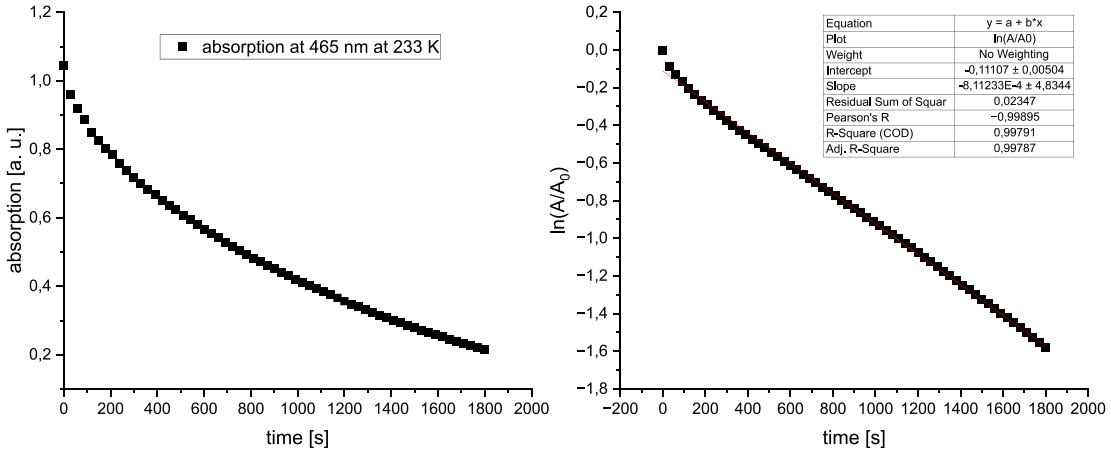

Figure SIV.3: Absorption of *meso*-DID **3** (250µM) in acetone at 233 K at 465 nm after irradiation with light at 385 nm (left) with the corresponding first order kinetics plot (right).

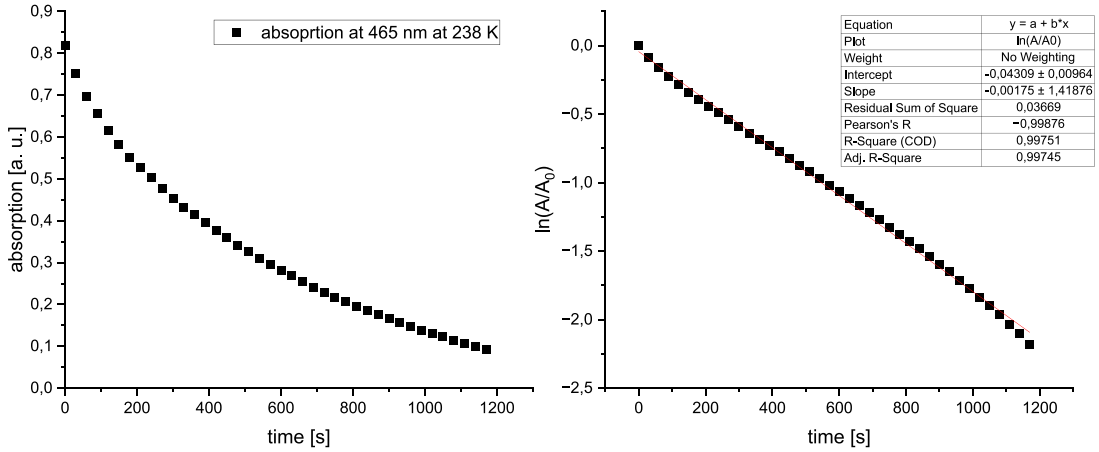

Figure SIV.4: Absorption of *meso*-DID **3** (250µM) in acetone at 238 K at 465 nm after irradiation with light at 385 nm (left) with the corresponding first order kinetics plot (right).

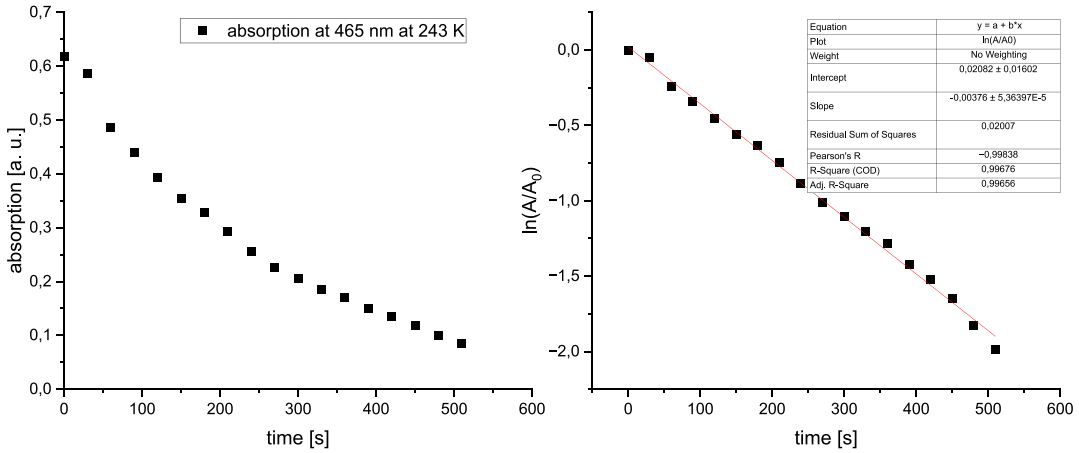

Figure SIV.5: Absorption of *meso*-DID **3** (250µM) in acetone at 243 K at 465 nm after irradiation with light at 385 nm (left) with the corresponding first order kinetics plot (right).

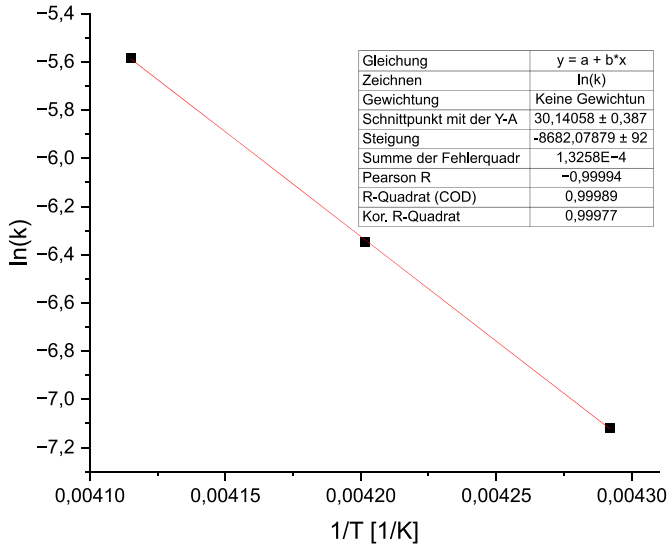

Figure SIV.6: Arrhenius plot of *meso*-DID **3** for determination of the rate constant at room temperature.

Table SIV.1: Rate constants and half-lives at given temperature of the back isomerization from *E-meso* DID **3** to *Z-meso* DID **3**.

temperature T	rate constant k	half-life $t_{1/2}$
K	s^{-1}	min.
233	$8.11*10^{-4}$	14.24
238	$1.75*10^{-3}$	6.60
243	$3.76*10^{-3}$	3.07
298	2.73	$3.48*10^{-3}$

SIV.2 (12a*R*,12b*R*/12a*S*,12b*S*,*Z*)-4,9-dibromo-1,2,11,12,12a,12b-hexahydrodiindeno[7,1-*cd*:1',7'-*fg*][1,2]-diazocine (4)

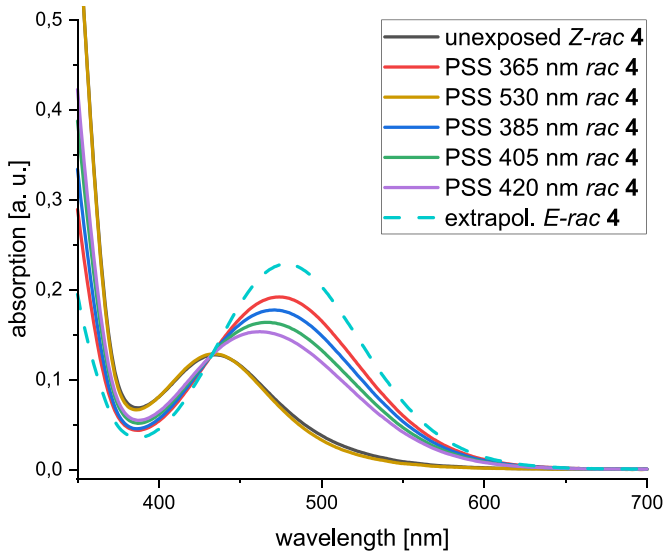

Figure SIV.7: UV-vis spectra of *rac*-DID **4** (250 µM) in acetone at 298 K before (black) and after irradiation at different wavelengths.

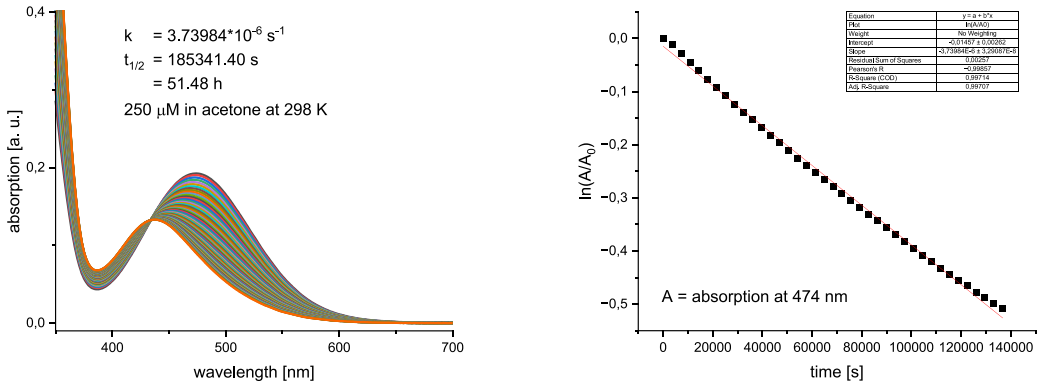

Figure SIV.8: UV-vis spectra of the half-life determination of *rac*-DID **4** (250 µM) in acetone at 298 K after irradiation with 385 nm (left) with the corresponding first order kinetics plot (right).

SIV.3 (12a*R*,12b*R*/12a*S*,12b*S*,*Z*)-4,9-diiodo-1,2,11,12,12a,12b-hexahydrodiindeno[7,1-*cd*:1',7'-*fg*][1,2]-diazocine (5)

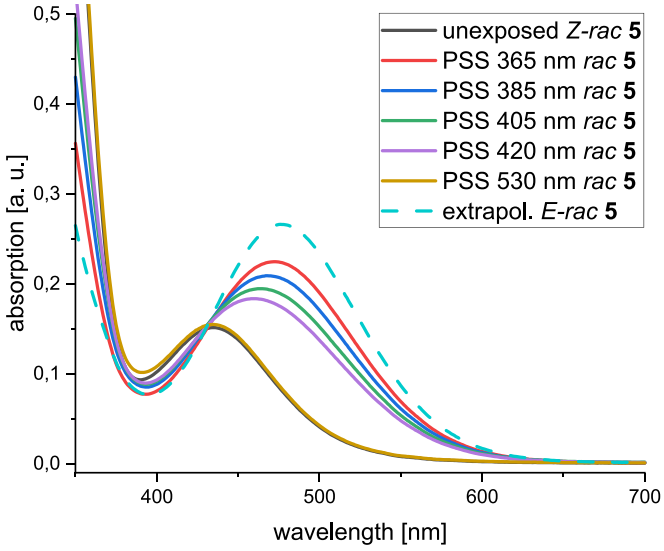

Figure SIV.9: UV-vis spectra of *rac*-DID **5** (250 µM) in acetone at 298 K before (black) and after irradiation at different wavelengths.

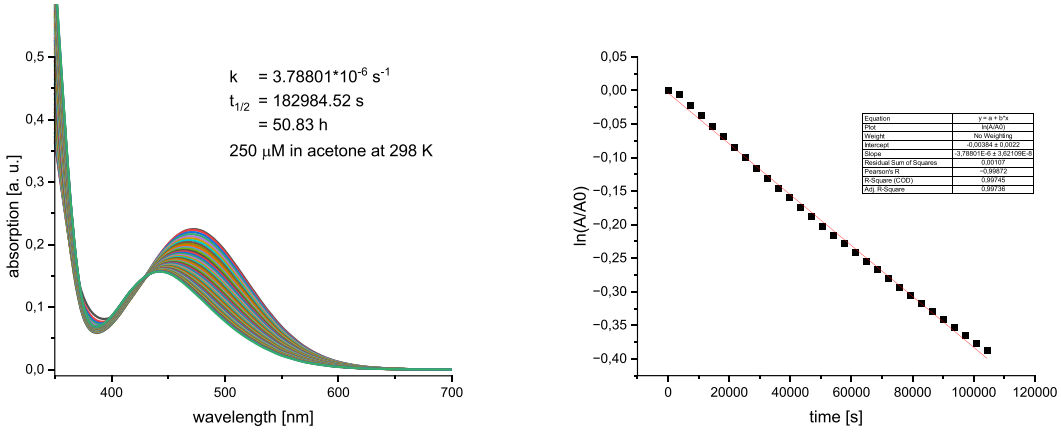

Figure SIV.10: UV-vis spectra of the half-life determination of *rac*-DID **5** (250 µM) in acetone at 298 K after irradiation with 385 nm (left) with the corresponding first order kinetics plot (right).

SIV.4 (12a*R*,12b*R*/12a*S*,12b*S*,*Z*)-3,4,9,10-tetrabromo-1,2,11,12,12a,12b-hexahydrodiindeno[7,1-*cd*:1',7'-*fg*][1,2]-diazocine (6)

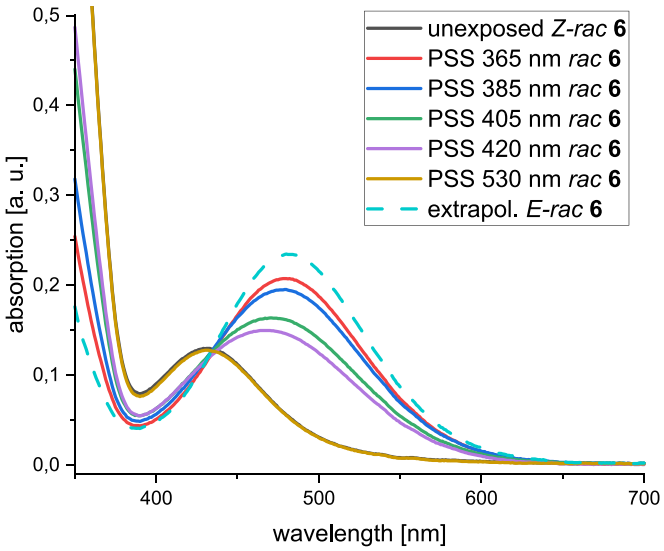

Figure SIV.11: UV-vis spectra of *rac*-DID **6** (250 µM) in acetone at 298 K before (black) and after irradiation at different wavelengths.

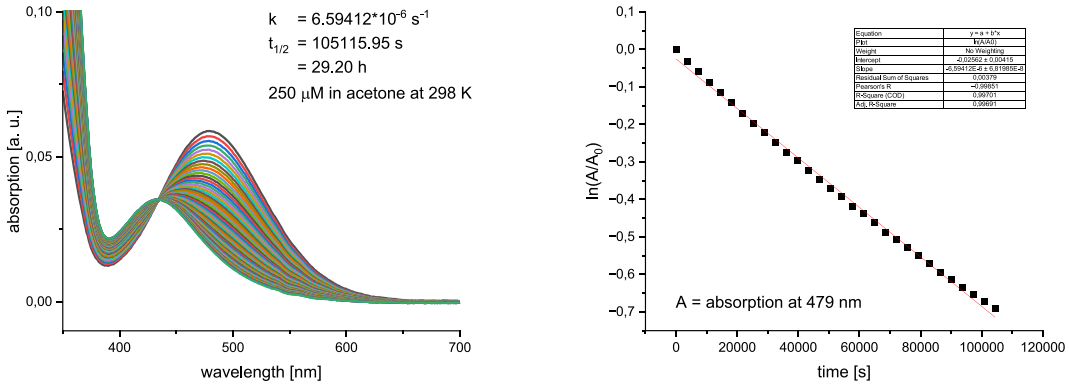

Figure SIV.12: UV-vis spectra of the half-life determination of *rac*-DID **6** (250 µM) in acetone at 298 K after irradiation with 385 nm (left) with the corresponding first order kinetics plot (right).

SV. Literature

[1] S. Bartoli, A. Cipollone, A. Squarcia, A. Madami, D. Fattori, *Synthesis* **2009**, *2009*, 1305-1308.

[2] R. Tirfoin, J. A. B. Abdalla, S. Aldridge, *Chem. Eur. J.* **2015**, *21*, 11813-11824.

8.2.3 Substituted Nitrogen-Bridged Diazocines

BEILSTEIN JOURNAL OF ORGANIC CHEMISTRY

Supporting Information

for

Substituted nitrogen-bridged diazocines

Pascal Lentes, Jeremy Rudtke, Thomas Griebenow and Rainer Herges

Beilstein J. Org. Chem. **2021,** *17,* 1503–1508. doi:10.3762/bjoc.17.107

Analytical equipment, experimental procedures, NMR and UV–vis spectra

Table of contents

I. Analytical equipment

NMR spectroscopy

NMR spectra were measured in deuterated solvents (Deutero). The spectra were referenced to the following solvent residual signals:

solvent	degree of deuteration	^{1}H signal (ppm)	^{13}C signal (ppm)
acetone-d_6	99.8 %	2.05 (quintet)	29.84 (septet)
chloroform-d_1	99.8 %	7.26 (singlet)	77.16 (triplet)
CD_3CN	99.5 %	1.94 (quintet)	/
water-d_2	99.9 %	4.79 (singlet)	/

Spectra were recorded with a Bruker AC 200 (^{1}H NMR: 200 MHz), a Bruker DRX 500 (^{1}H NMR: 500 MHz, ^{13}C NMR: 125 MHz), and a Bruker AV 600 (^{1}H NMR: 600 MHz, ^{13}C NMR: 150 MHz). The multiplicities of the signals were abbreviated with s (singlet), d (doublet), t (triplet), q (quartet), quint (quintet), m (multiplet) and br. (broad) in addition for broad signals.

Melting point

Melting points were measured with a Melting Point B-540 (Büchi) in melting point tubes without further correction.

Mass spectrometry

Mass spectra (EI) and high-resolution mass spectra (HR-EI) were measured with an AccuTOF GCv 4G (Joel) with an ionization energy of 70 eV. HR-ESI mass spectra were measured with a Q Exactive Plus (Thermo Scientific).

IR spectroscopy

Infrared spectra were measured with a Perkin-Elmer 1600 Series FT-IR spectrometer with an A531-G Golden-Gate-Diamond-ATR-unit. Signals were abbreviated with w (weak), m (medium), s (strong) for its intensity.

Chromatography

Silica gel (Merck, particle size 0.040-0.063 mm) was used for column chromatography purifications. R_f values were determined by thin layer chromatography on Polygeram® SilG/UV254 (Macherey Nagel, 0.2 mm particle size).

UV–vis spectroscopy

UV–vis spectra were measured with a Lambda 650 spectrometer (Perkin-Elmer) and quartz cuvettes of 10 mm optical path length were used.

Chemicals

All commercially available chemicals and solvents were used without purification.

Light sources

For exposure experiments with 400 nm, a custom-built LED light source was used. The irradiation wavelength of the 400 nm LED light source was measured via a mobile UV–vis spectrometer (USB4000-UV-vis, Ocean Optics, Largo, FL, USA).

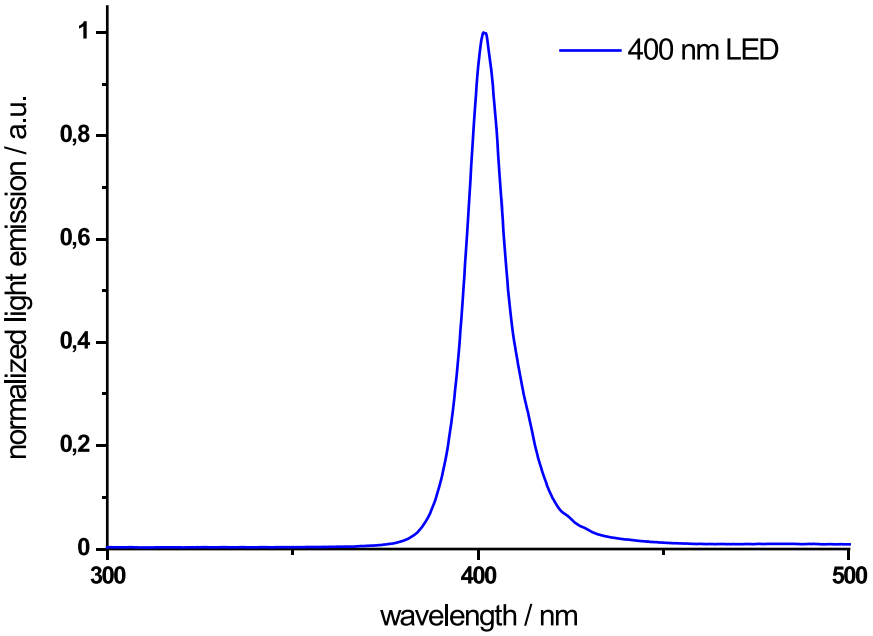

Figure S1: Emission spectrum of 400 nm LED light source. The full width at half maximum (FWHM) amounts to 12 nm (396–401 nm, maximum at 401 nm).

II. Syntheses

II.1 Synthesis of (9*H*-fluorene-9-yl)methyl (2-aminobenzyl)(2-aminophenyl)carbamate

(9*H*-Fluorene-9-yl)methyl (2-aminophenyl)(2-nitrobenzyl)carbamate[1] (6.80 g, 14.6 mmol) was dissolved in 500 mL of ethanol and 250 mL of a 1M NH_4Cl solution in water was added. It was heated to 75 °C and zink powder (7.64 g, 117 mmol, 8 equiv) was added. The reaction mixture was stirred at 75 °C for 1 h and then hot filtrated. The solvent was evaporated and to the residue were added 500 mL of DCM and 500 mL of deionized water. The organic layer was separated and extracted twice with DCM. The combined organic layers were dried over $MgSO_4$ and the solvent was evaporated. The crude product, a white powder (6.36 g, 14.6 mmol, quant.) was used without further purification.

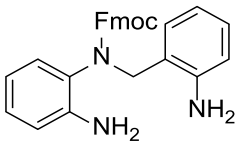

melting point: 75.7 °C

^{1}H NMR (600 MHz, acetone-d_6, 298 K): δ = 7.79 (d, ^{3}J = 6.9 Hz, 1 H, Ar-*H*), 7.54-6.31 (m, 14 H, Ar-*H*), 5.04-3.95 (m, 5 H, aliph. *H*) ppm.

^{13}C NMR (150 MHz, acetone-d_6, 298 K): δ = 131.28, 130.86, 130.47, 130.27, 129.76, 129.32, 128.77, 128.47, 128.44, 127.88, 127.85, 127.81, 126.60, 126.45, 126.25, 124.11, 123.92, 123.75, 121.30, 121.15, 120.69, 120.63, 119.96, 119.78, 117.64, 117.24, 116.65, 115.90, 68.71, 68.34, 67.87, 50.66, 49.63, 49.38, 47.96, 47.84 ppm.

IR (ATR): $\tilde{\nu}$ = 3353 (w), 3038 (w), 1618 (s), 1621 (m), 1501 (m), 1450 (m), 1409 (s), 1356 (w), 1310 (s), 1276 (s), 1215 (w), 1128 (m), 1069 (w), 1007 (w), 979 (m), 939 (w), 860 (w), 739 (s), 631 (m), 621 (w), 602 (w), 552 (w), 525 (m) cm^{-1}.

MS (ESI HR, $CHCl_3$/MeOH): *m/z* ($C_{28}H_{25}N_3O_2$+H^+) = calc.: 436.20195, found: 436.20159 ± 0.84 ppm.

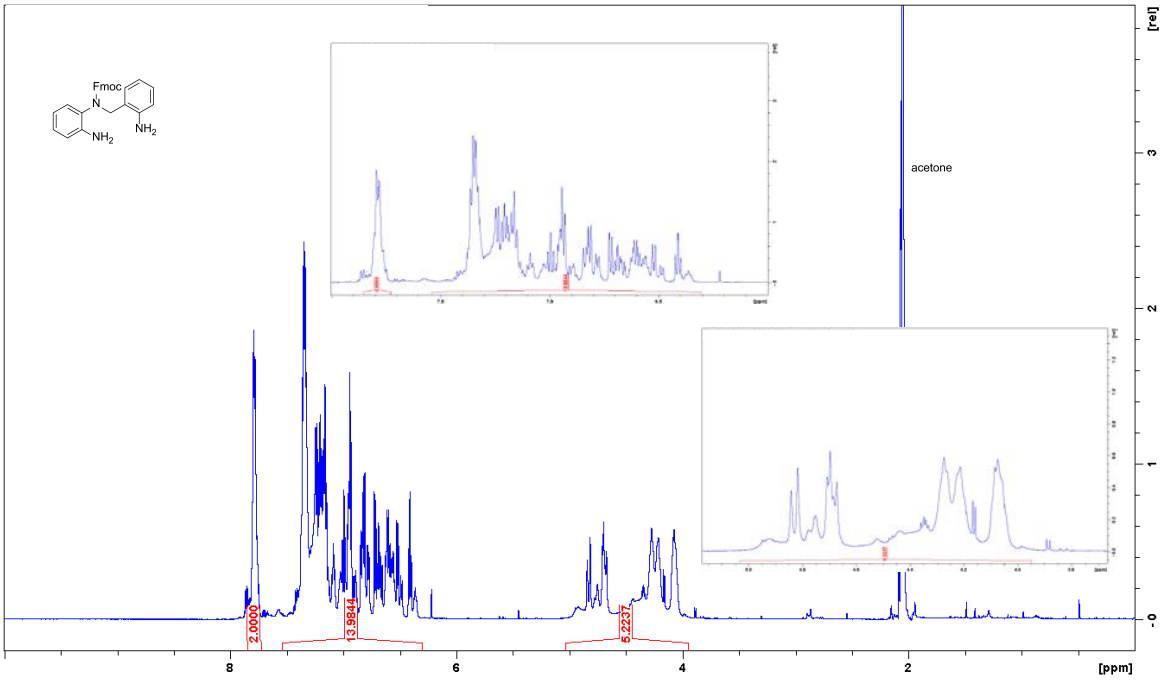

Figure S2: ^{1}H NMR spectrum of the given aniline compound.

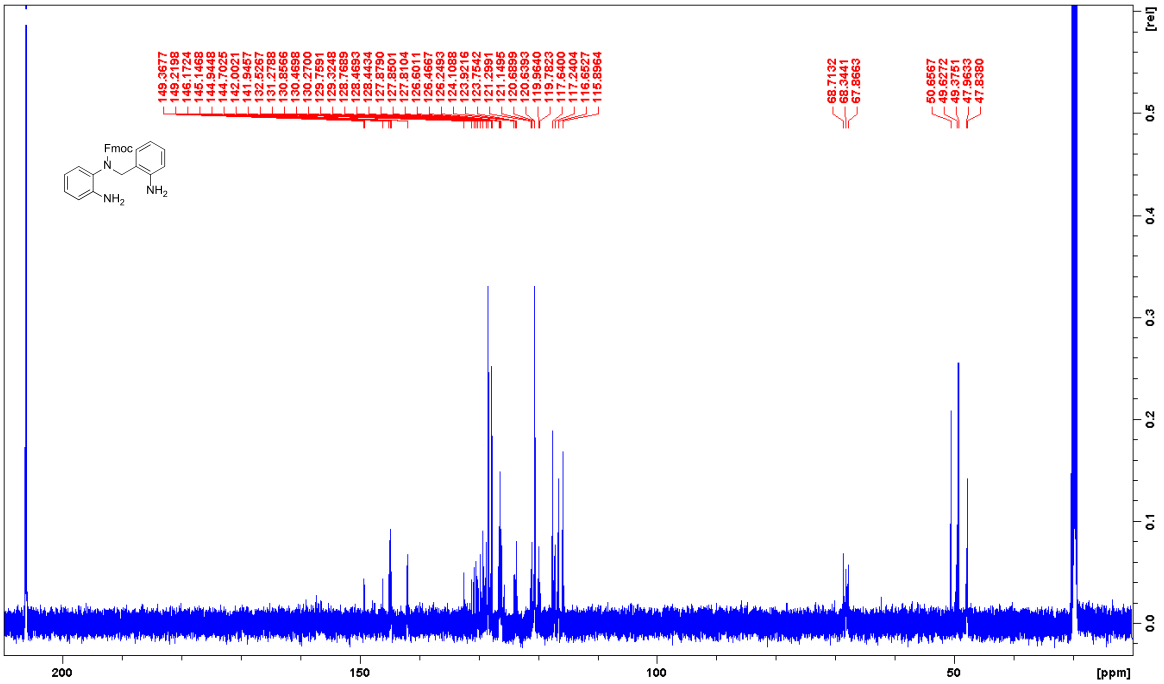

Figure S3: ^{13}C NMR spectrum of the given aniline compound.

II.2 Synthesis of (9*H*-fluorene-9-yl)methyl (*Z*)-dibenzo[*c*,*g*][1,2,5]triazocine-11(12*H*)-carboxylate (8c)

(9*H*-Fluorene-9-yl)methyl (2-aminobenzyl)(2-aminophenyl)carbamate (3.70 g, 8.50 mmol) was dissolved in 250 mL of acetic acid and *m*CPBA (3.81 g, 17.0 mmol, ≥ 77%) in 250 mL of acetic acid was added dropwise over a period of 2 h. The reaction mixture was stirred at rt over night and after that, the solvent was evaporated. To the residue were added 100 mL of DCM and 250 mL of half-concentrated $NaHCO_3$ solution in deionized water and the organic layer was separated. It was extracted twice with DCM and the combined organic layers were dried over $MgSO_4$. The solvent was evaporated and flash column chromatography on silica (0.040–0.063 mm, ethyl acetate/cyclohexane 1:3, R_f = 0.38) gave a yellow solid (**8c**, 2.28 g, 5.28 mmol, 62%).

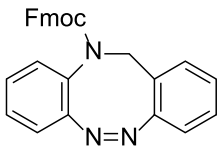

^{1}H NMR (200 MHz, acetone-d_6, 300 K): δ = 7.83 (d, ^3J = 7.2 Hz, 2 H, Ar-*H*), 7.73-6.73 (m 14 H, Ar-*H*), 5.12-3.94 (m, 5 H, aliph. *H*) ppm.

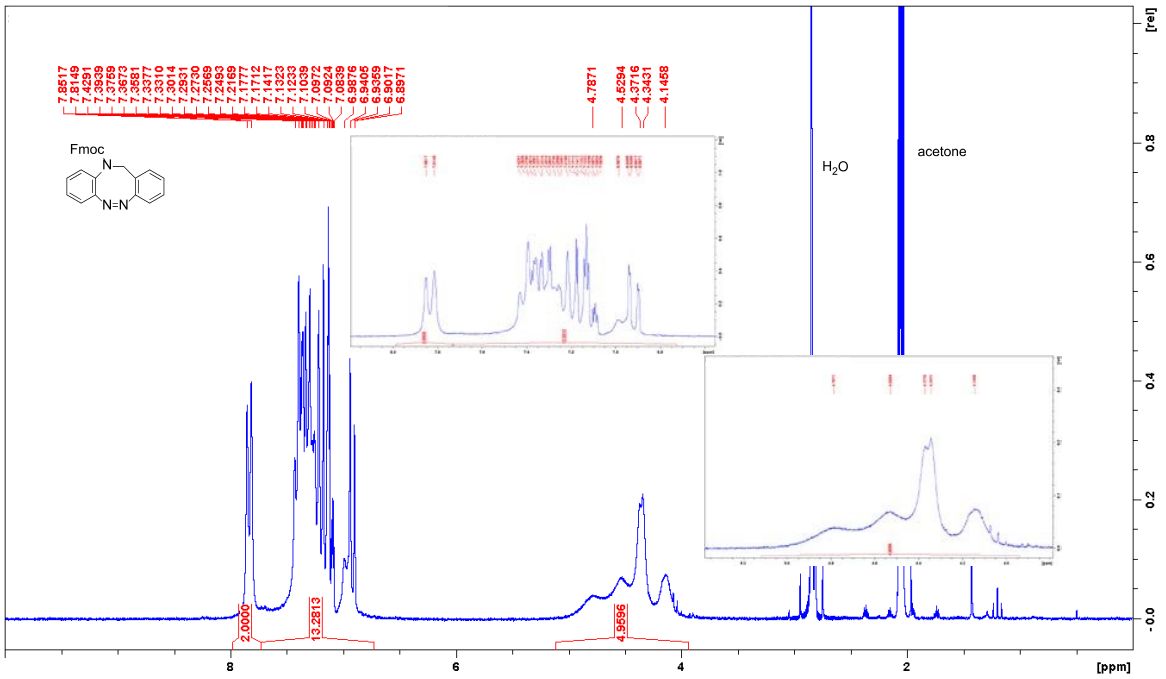

Figure S4: ^{1}H NMR spectrum of compound **8c**.

II.3 Synthesis of chloral[2]

Under a nitrogen atmosphere, 5 mL of concentrated H_2SO_4 was added to chloral hydrate (10.0 g, 60.5 mmol) and chloral (6.31 g, 42.8 mmol, 71%) was directly distilled out of the reaction mixture with a vigreux condenser.

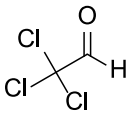

boiling point: 98 °C

^{1}H NMR (200 MHz, $CDCl_3$, 300 K): δ = 9.06 (s, 1 H, C*H*O) ppm.

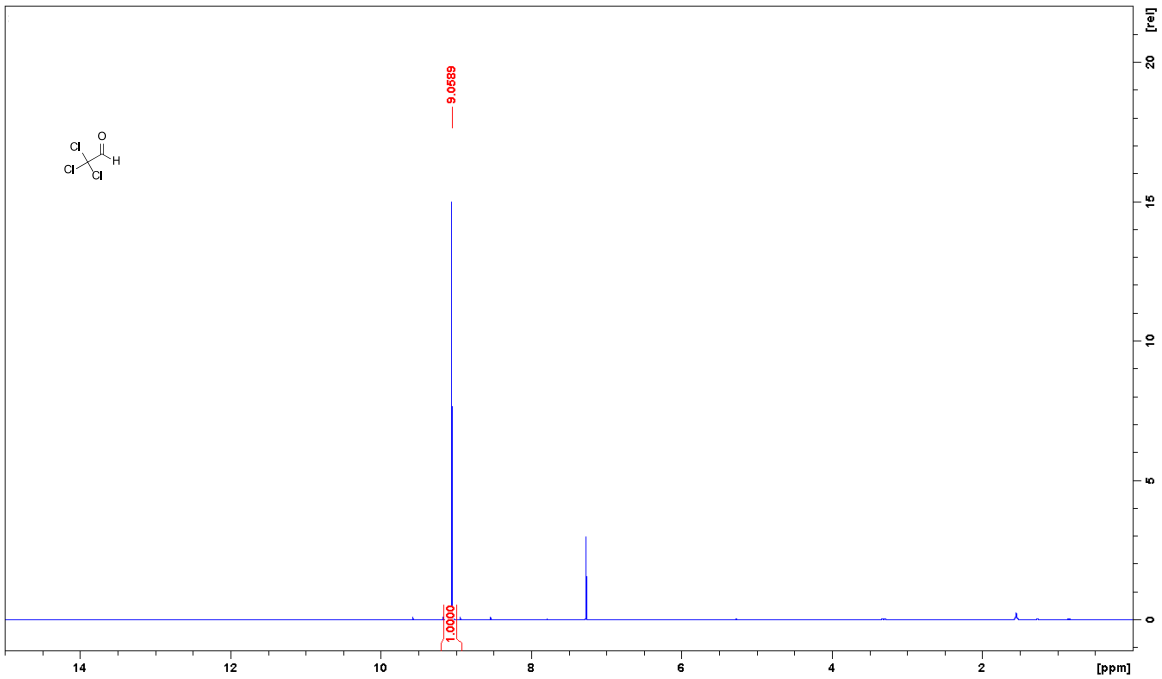

Figure S5: ^{1}H NMR spectrum of chloral.

II.4 Synthesis of (*Z*)-dibenzo[*c*,*g*][1,2,5]triazocine-11(12*H*)-carbaldehyde (11c)

Under a nitrogen atmosphere, (*Z*)-11,12-dihydrodibenzo[*c*,*g*][1,2,5]triazocine[1] **9c** (100 mg, 478 µmol) was dissolved in MeCN (10 mL anhydrous), and DIPEA (832 µL, 4.78 mmol) and chloral (466 µL, 4.78 mmol) were added. The reaction mixture was stirred at rt for 21 h. The solvent was removed and separation of the products by flash column chromatography on silica (0.040-0.063 mm, ethyl acetate/cyclohexane 1:2, R_f = 0.33) gave a pale yellow solid (**11c**, 86 mg, 362 µmol, 76%).

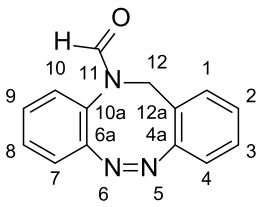

melting point: 206.5 °C

^{1}H NMR (500 MHz, acetone-d$_6$, 298 K): δ = 8.38 (s, 1 H, C*H*O), 7.38 (td, ^{3}J = 7.7 Hz, ^{4}J = 1.3 Hz, 1 H, *H*-2), 7.34-7.28 (m, 2 H, *H*-1, *H*-3), 7.24-7.17 (m, 2 H, *H*-8, *H*-9), 7.15 (dd, ^{3}J = 7.9 Hz, ^{4}J = 1.2 Hz, 1 H, *H*-4), 7.01 (dd, ^{3}J = 7.9 Hz, ^{4}J = 1.1 Hz, 1 H, *H*-7/10), 6.91 (dd, ^{3}J = 7.8 Hz, ^{4}J = 1.5 Hz, 1 H, *H*-7/10), 4.52 (m$_c$, 2 H, C*H*$_2$) ppm.

^{13}C NMR (125 MHz, acetone-d$_6$, 298 K): δ = 162.27 (*C*=O), 157.61 (*C*-12a), 152.96 (*C*-4a), 131.38 (*C*-1), 130.31 (*C*-2), 129.10 (*C*-8/9), 128.98 (*C*-8/9), 128.73 (*C*-3), 128.06 (*C*-4), 123.15 (*C*-6a/10a), 120.46 (*C*-7/10), 119.30 (*C*-7/10), 49.47 (*C*H$_2$) ppm.

IR (ATR): $\tilde{\nu}$=2251 (w), 1662 (s), 1587 (w), 1514 (w), 1476 (m), 1439 (w), 1367 (w), 1309 (s), 1273 (m), 1242 (m), 1152 (w), 1040 (w), 1015 (w), 944 (w), 916 (w), 857 (w), 804 (w), 774 (s), 755 (s), 727 (s), 687 (m), 661 (w),631 (w), 596 (w), 550 (s), 538 (m) cm^{-1}.

MS (ESI HR, $CHCl_3$/MeOH): *m/z* ($C_{14}H_{11}{}^{79}BrN_3O+H^+$) = calc.: 238.09749, found: 238.09758 ± 0.39 ppm.

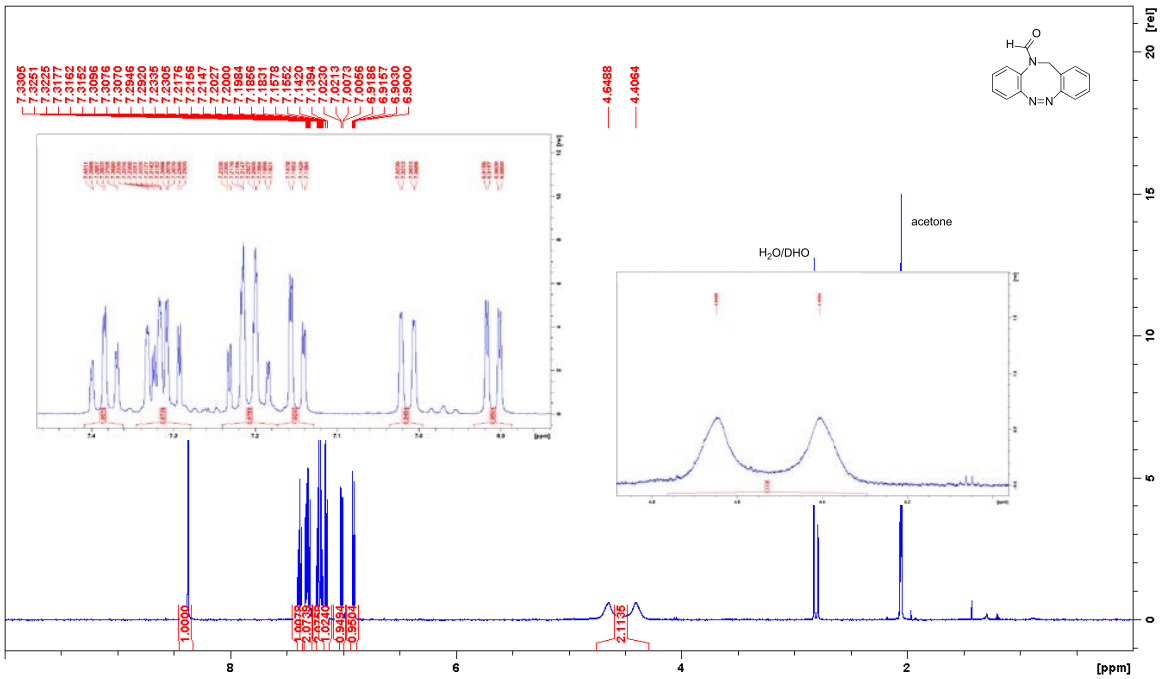

Figure S6: ^{1}H NMR spectrum of compound **11c**.

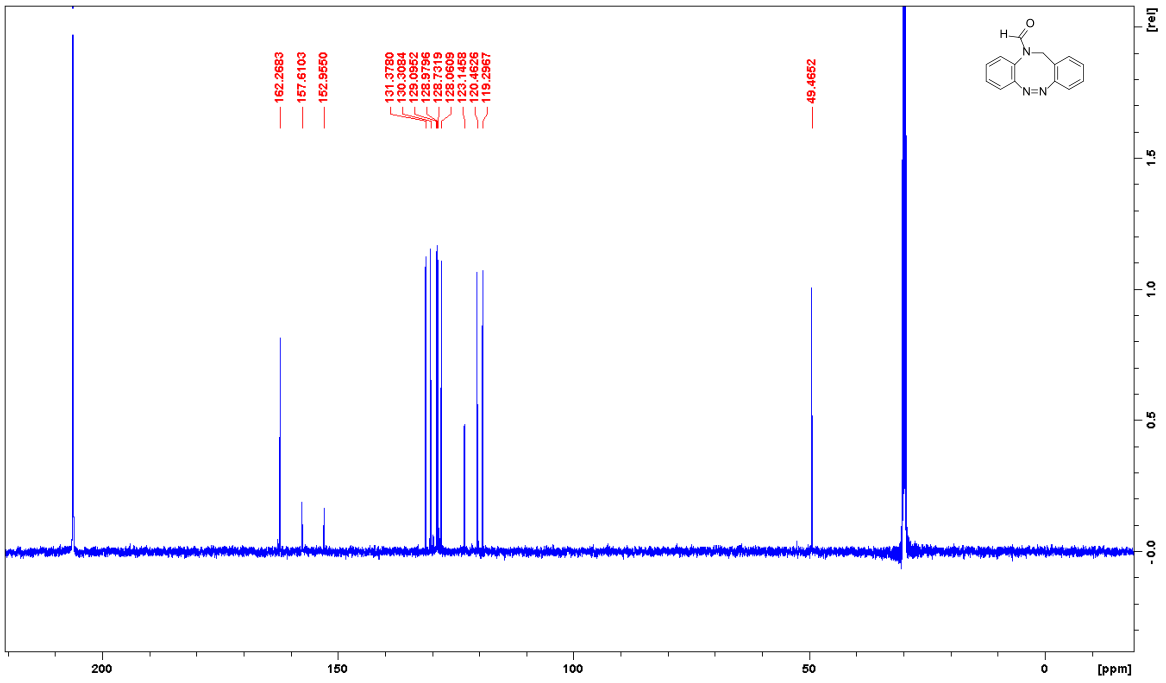

Figure S7: ^{13}C NMR spectrum of compound **11c**.

II.5 Synthesis of *tert*-butyl (2-((4-bromo-2-nitrobenzyl)amino)phenyl)carbamate (4a)

Under a nitrogen atmosphere, a solution of *tert*-butyl (2-aminophenyl)carbamate[1] (**2**, 2.62 g, 12.6 mmol) in 50 mL of abs. THF was prepared, and then triethylamine (4.30 mL, 13.5 mmol) and 4-bromo-1-(bromomethyl)-2-nitrobenzene[3] (**3a**, 3.72 g, 12.6 mmol) was added. The reaction mixture was refluxed

for 20 h and after that, the solvent was evaporated. Then, 50 mL of water and 50 mL of DCM were added to the residue. The organic layer was separated and it was extracted twice with 50 mL of DCM. The combined organic layers were dried over $MgSO_4$ and the solvent was evaporated. Recrystallization from cyclohexane/ethyl acetate 1:1 gave a yellow solid (**4a**, 3.03 g, 8.85 mmol, 71%).

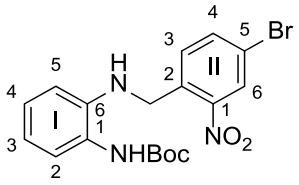

melting point: 151.1 °C

^{1}H NMR (500 MHz, acetone-d_6, 298 K): δ = 8.24 (d, ^4J = 2.0 Hz, 1 H, Ar^{II}-*H*-6), 7.83 (dd, ^3J = 8.4 Hz, ^4J = 2.0 Hz, 1 H, Ar^{II}-*H*-4), 7.73 (d, ^3J = 8.4 Hz, 1 H, Ar^{II}-*H*-3), 7.63 (s, 1 H, N*H*), 7.25 (d, ^3J = 7.6 Hz, 1 H, Ar^{I}-*H*-2), 6.93 (td, ^3J = 7.6 Hz, ^4J = 1.5 Hz, 1 H, Ar^{I}-*H*-4), 6.64 (td, ^3J = 7.6 Hz, ^4J = 1.3 Hz, 1 H, Ar^{I}-*H*-3), 6.50 (dd, ^3J = 7.6 Hz, ^4J = 1.1 Hz, 1 H, Ar^{I}-*H*-5), 5.59-5.42 (m, 1 H, N*H*), 4.76 (d, ^3J = 6.2 Hz, 2 H, CH_2), 1.47 (s, 9H, CH_3) ppm.

^{13}C NMR (125 MHz, acetone-d_6, 298 K): δ = 155.13 (*C*=O), 150.02 (Ar^{II}-*C*-1), 142.84 (Ar^{I}-*C*-6), 137.22 (Ar^{II}-*C*-4), 136.28 (Ar^{II}-*C*-2), 132.44 (Ar^{II}-*C*-3), 128.32 (Ar^{II}-*C*-6), 127.11 (Ar^{I}-*C*-4), 126.87 (Ar^{I}-*C*-2), 125.50 (Ar^{I}-*C*-1), 120.93 (Ar^{II}-*C*-5), 118.02 (Ar^{I}-*C*-3), 112.35 (Ar^{I}-*C*-5), 79.90 (*C*-(CH$_3$)$_3$), 45.09 (-CH$_2$), 28.58 (-*C*H$_3$) ppm.

IR (ATR): $\tilde{\nu}$ = 3400 (m), 3270 (w), 2976 (w), 1686 (m), 1604 (m), 1528 (s), 1462 (m), 1348 (w), 1151(s) 830 (m), 753 (m) cm^{-1}.

MS (EI, 70 eV): *m/z* (%) = 421.06 (3) [M]$^+$, 365.00 (13) [$C_{14}H_{12}BrN_3O_4$]$^+$, 321.01 (9) [$C_{13}H_{12}BrN_3O_2$]$^+$, 286.99 (18) [$C_{13}H_{10}BrN_3$]$^+$, 197.95 (14) [$C_7H_7BrN_2$]$^+$, 119.06 (32) [$C_7H_7N_2$]$^+$, 107.06 (32) [$C_6H_7N_2$]$^+$.

MS (HR) (EI, 70 eV): *m/z* ($C_{18}H_{20}{}^{79}BrN_3O_4$) = calc.: 421.06372, found: 421.06392 ± 0.49 ppm.

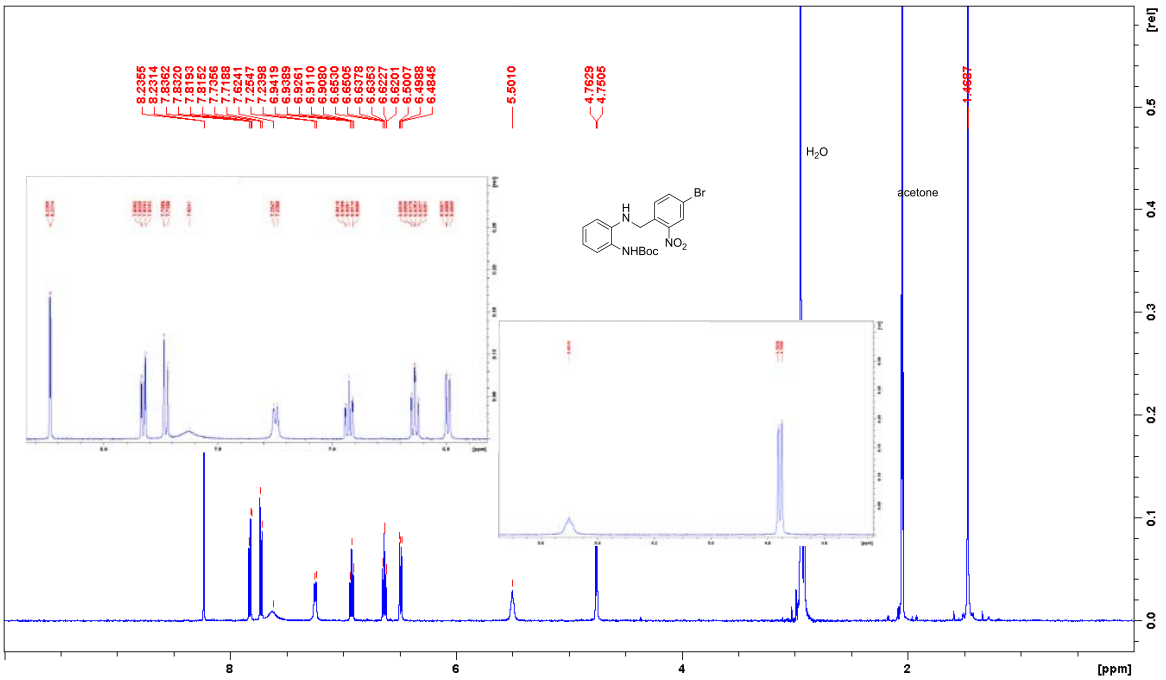

Figure S8: ^{1}H NMR spectrum of compound **4a**.

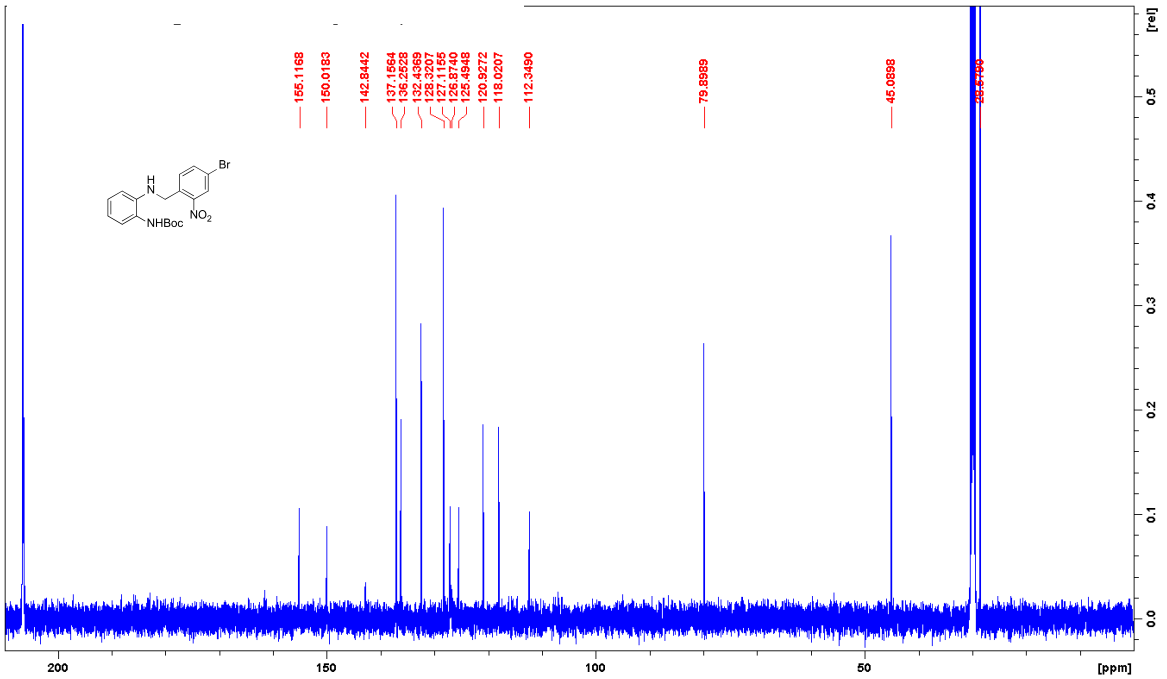

Figure S9: ^{13}C NMR spectrum of compound **4a**.

II.6 Synthesis of (9*H*-fluorene-9-yl)methyl (4-bromo-2-nitrobenzyl)(2-((*tert*-butoxycarbonyl)-amino)phenyl)carbamate (5a)

Under a nitrogen atmosphere, a solution of *tert*-butyl (2-((4-bromo-2-nitrobenzyl)amino)phenyl)-carbamate (**4a**, 1.70 g, 4.94 mmol) in anhydrous DMF (20 mL) was prepared, and then DIPEA (861 µL, 4.94 mmol) and 9-fluorenylmethoxycarbonyl chloride (2.40 g, 9.89 mmol) dissolved in anhydrous DMF (20 mL) were added. The reaction mixture was stirred at rt for 48 h and after that, the solvent was evaporated. Then, 50 mL of water and 50 mL of DCM were added to the residue. The organic layer was separated and it was extracted twice with DCM. The combined organic layers were dried over $MgSO_4$ and the solvent was evaporated. Flash column chromatography on silica (0.040–0.063 mm, ethyl acetate/cyclohexane 1:3, R_f = 0.44) gave a colorless solid (**5a**, 1.78 g, 2.76 mmol, 56%).

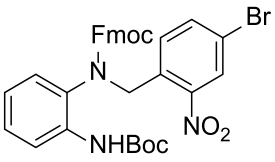

melting point: 164.3 °C

^{1}H NMR (500 MHz, acetone-d$_6$, 298 K): δ = 8.14 (d, ^4J = 2.1 Hz, 1 H), 8.03-7.66 (m, 5 H), 7.55-7.00 (m, 10 H), 5.27-4.88 (m, 2 H, aliph. *H*), 4.61-3.96 (m, 3 H, aliph. *H*), 1.46 (s, 9H, C*H*$_3$) ppm.

^{13}C NMR (125 MHz, acetone-d$_6$, 298 K): δ = 155.54 (*C*=O), 142.10, 137.03, 129.18, 128.49, 128.20, 127.86, 126.07, 124.43, 120.74, 80.46, 68.43, 47.83, 28.48 (*C*H$_3$) ppm.

IR (ATR): $\tilde{\nu}$ = 3380 (w), 2977 (w), 1719 (s), 1595 (w), 1535 (s), 1518 (s), 1477 (w), 1450 (m), 1390 (m), 1342 (m), 1292 (m), 1278 (m), 1218 (m), 1187 (m), 1153 (s), 1042 (w), 1025 (w), 976 (w), 942 (w), 933 (w), 885 (w), 843 (w), 801 (w), 756 (s), 739(s), 670 (w), 645 (w), 618 (m), 535 (m) cm^{-1}.

MS (ESI HR, CHCl$_3$/MeOH): *m/z* (C$_{33}$H$_{30}$^{79}BrN$_3$O$_6$+H$^+$) = calc.: 644.13907, found: 644.13932 ± 0.38 ppm.

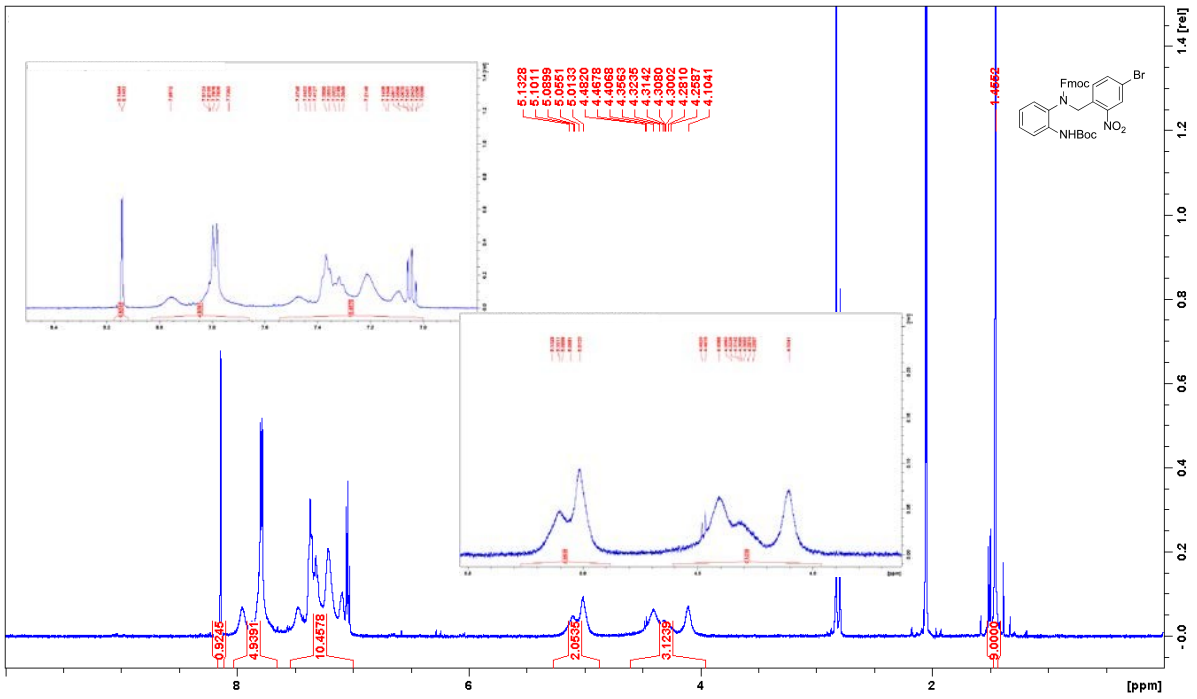

Figure S10: ^{1}H NMR spectrum of compound **5a**.

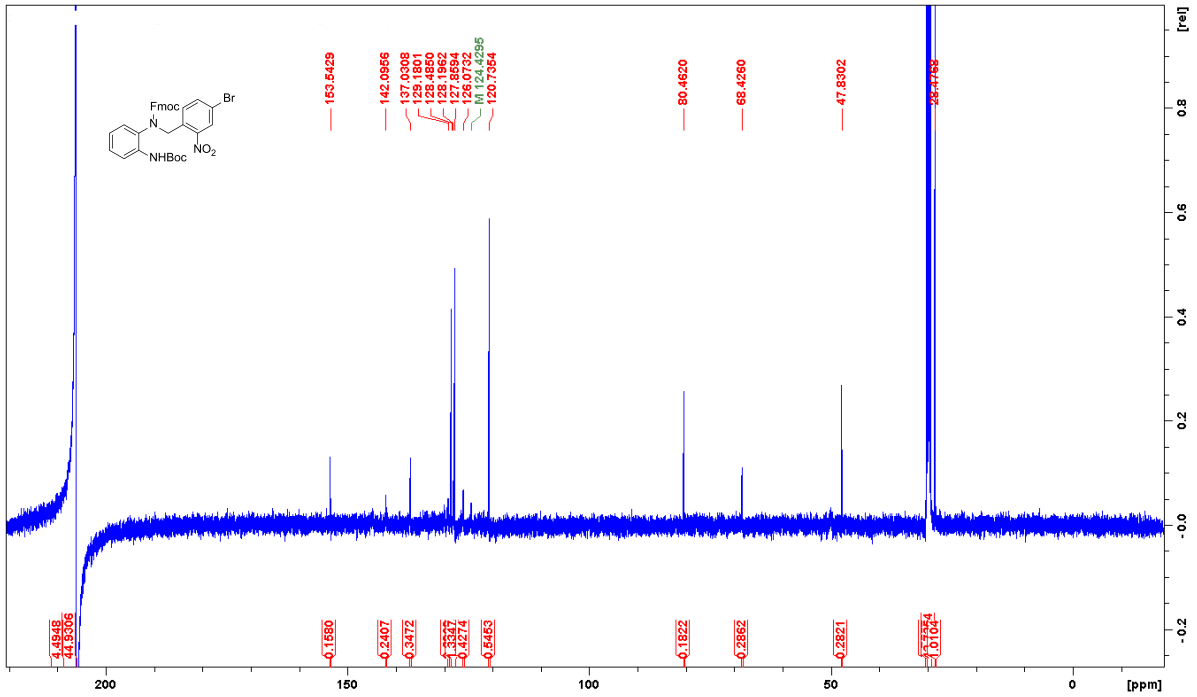

Figure S11: ^{13}C NMR spectrum of compound **5a**.

II.7 Synthesis of (9*H*-fluorene-9-yl)methyl (2-aminophenyl)(4-bromo-2-nitrobenzyl)carbamate (6a)

(9*H*-Fluorene-9-yl)methyl (4-bromo-2-nitrobenzyl)(2-((*tert*-butoxycarbonyl)amino)phenyl)carbamate (**5a**, 1.20 g, 1.86 mmol) was dissolved in 25 mL of DCM and 15 mL of TFA was added. The reaction mixture was stirred at rt for 16 h and then neutralized with saturated aqueous $NaHCO_3$. The organic layer was separated and it was extracted twice with DCM. The combined organic layers were dried over $MgSO_4$ and the solvent was evaporated. A pale yellow solid (**6a**, 1.01 g, 1.86 mmol, quant.) was obtained.

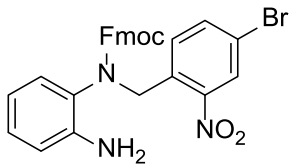

melting point: 79.6 °C

^{1}H NMR (500 MHz, acetone-d_6, 298 K): δ = 8.12 (d, ^4J = 1.8 Hz, 1 H), 7.98-7.58 (m, 4 H), 7.58-6.50 (m, 10 H), 5.58-3.89 (m, 5 H) ppm.

^{13}C NMR (125 MHz, acetone-d_6, 298 K): δ = 144.90, 142.13, 136.87, 133.24, 130.35, 129.02, 128.45, 128.05, 127.85, 127.81, 126.17, 124.44, 121.50 120.73, 120.68, 68.41, 49.68, 47.99, 47.90 ppm.

IR (ATR): $\tilde{\nu}$ = 3363 (w), 2251 (w), 1965 (s), 1621 (w), 1528 (s), 1503 (m), 1450 (w), 1404 (w), 1340 (m), 1299 (s), 1136 (m), 1101 (w), 1022 (w), 988 (w), 877 (m), 797 (w), 757 (s), 739 (s), 621 (w), 534 (w) cm^{-1}.

MS (ESI HR, $CHCl_3$/MeOH): *m/z* ($C_{28}H_{22}{}^{79}BrN_3O_4$+$H^+$) = calc.: 544.08665, found: 544.08639 ± 0.48 ppm.

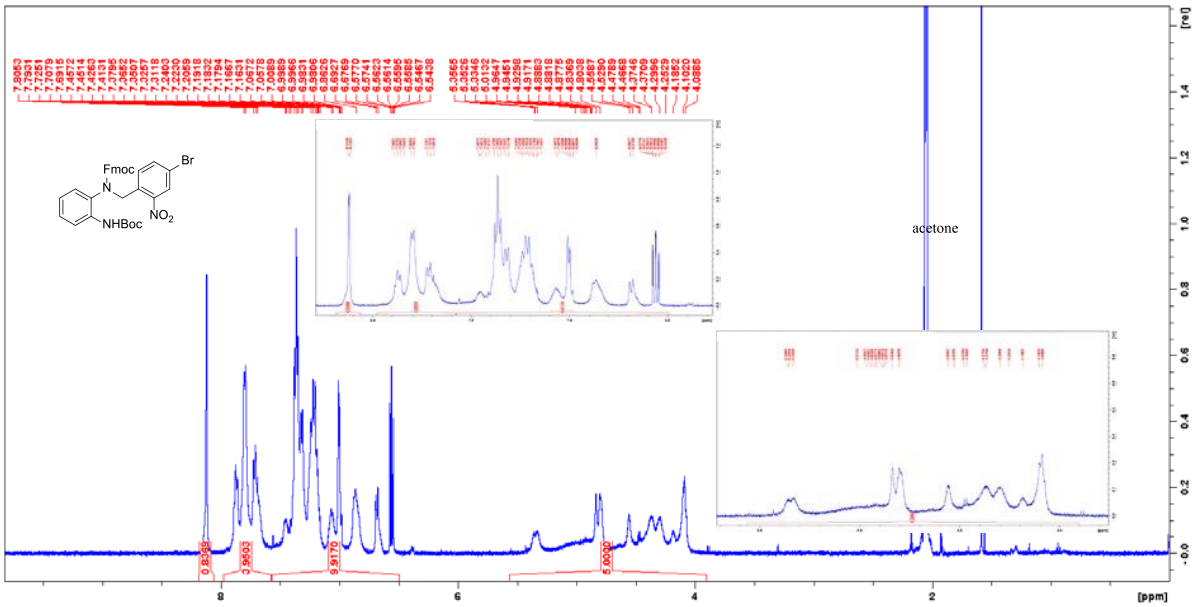

Figure S12: ^{1}H NMR spectrum of compound **6a**.

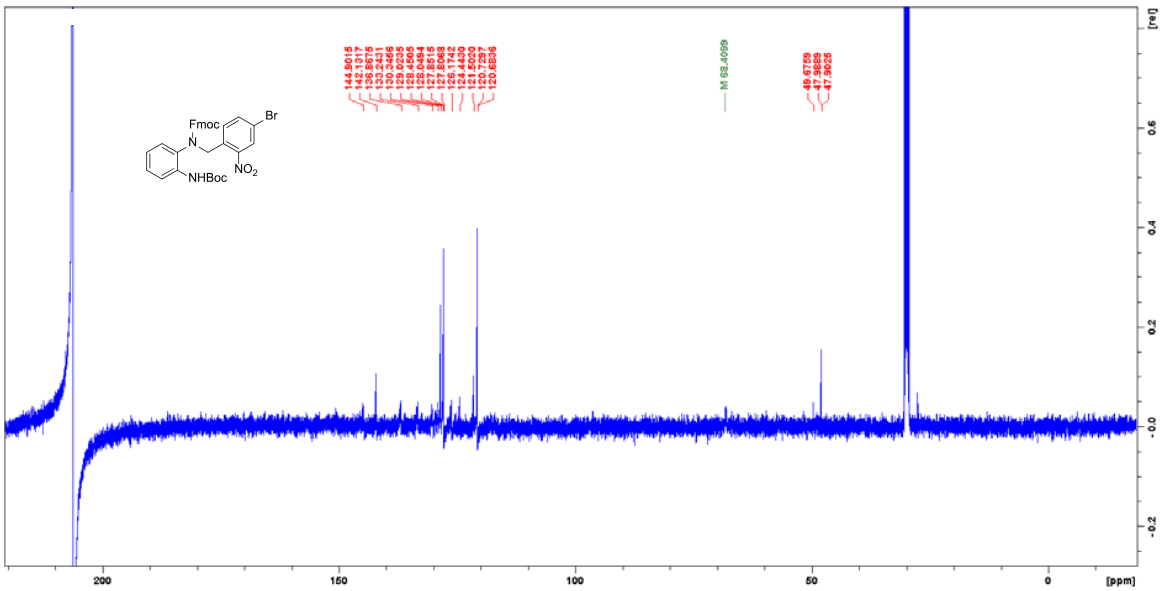

Figure S13: ^{13}C NMR spectrum of compound **6a**.

II.8 Synthesis of (9*H*-fluorene-9-yl)methyl (*Z*)-3-bromodibenzo[*c*,*g*][1,2,5]triazocine-11(12*H*)-carboxylate (8a)

(9*H*-Fluorene-9-yl)methyl (2-aminophenyl)(4-bromo-2-nitrobenzyl)carbamate (**6a**, 858 mg, 1.58 mmol) was suspended in 100 mL of ethanol and 50 mL of a 1M NH_4Cl solution in water was added. The reaction mixture was heated to 75 °C and zink powder (824 mg, 12.6 mmol, 8 equiv) was added. The reaction mixture was stirred at 75 °C for 1 h and then hot filtrated. The solvent was evaporated and DCM (50 mL) and deionized water (50 mL) were added to the residue. The organic layer was separated and it was extracted twice with DCM. The combined organic layers were dried over $MgSO_4$ and the solvent was evaporated. The crude product was dissolved in 50 mL of acetic acid and *m*CPBA (708 mg, 3.15 mmol, ≥ 77%) dissolved in 50 mL of acetic acid was added dropwise over a period of 2 h. The reaction mixture was stirred at rt overnight and after that, the solvent was evaporated. Then, 50 mL of DCM (50 mL) and half-concentrated $NaHCO_3$ (50 mL, dissolved in deionized water) were added to the residue and the organic layer was separated. It was extracted twice with DCM and the combined organic layers were dried over $MgSO_4$. The solvent was evaporated and flash column chromatography on silica (0.040–0.063 mm, ethyl acetate/cyclohexane 1:3, R_f = 0.51) gave a yellow solid (**8a**, 451 mg, 883 µmol, 56%).

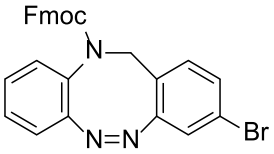

melting point: 91.4 °C

^{1}H NMR (500 MHz, acetone-d_6, 298 K): δ = 8.18-6.66 (m, 15 H, Ar-*H*), 5.13-3.87 (m, 5 H, aliph. *H*) ppm.

^{13}C NMR (125 MHz, acetone-d_6, 298 K): δ = 154.75, 142.11, 132.72, 131.30, 130.53, 129.56, 129.13, 128.56, 127.92, 126.14, 124.23, 122.63, 120.85, 119.66, 68.52, 52.74, 47.99, 47.78 ppm.

IR (ATR): $\tilde{\nu}$ = 2924 (w), 1702 (s), 1591 (w), 1476 (w), 1449 (m), 1390 (s), 1321 (s), 1295 (s), 1242 (w), 1128 (w), 1078 (w), 1041 (m), 102 (w), 866 (w), 818 (w), 757 (s), 737 (s), 694 (w), 670 (w), 650 (w), 621 (w), 604 (w), 549 (m), 513 (w) cm^{-1}.

MS (ESI HR, $CHCl_3$/MeOH): *m/z* ($C_{28}H_{20}{}^{79}BrN_3O_2$+$H^+$) = calc.: 510.08117, found: 510.08153 ± 0.7 ppm.

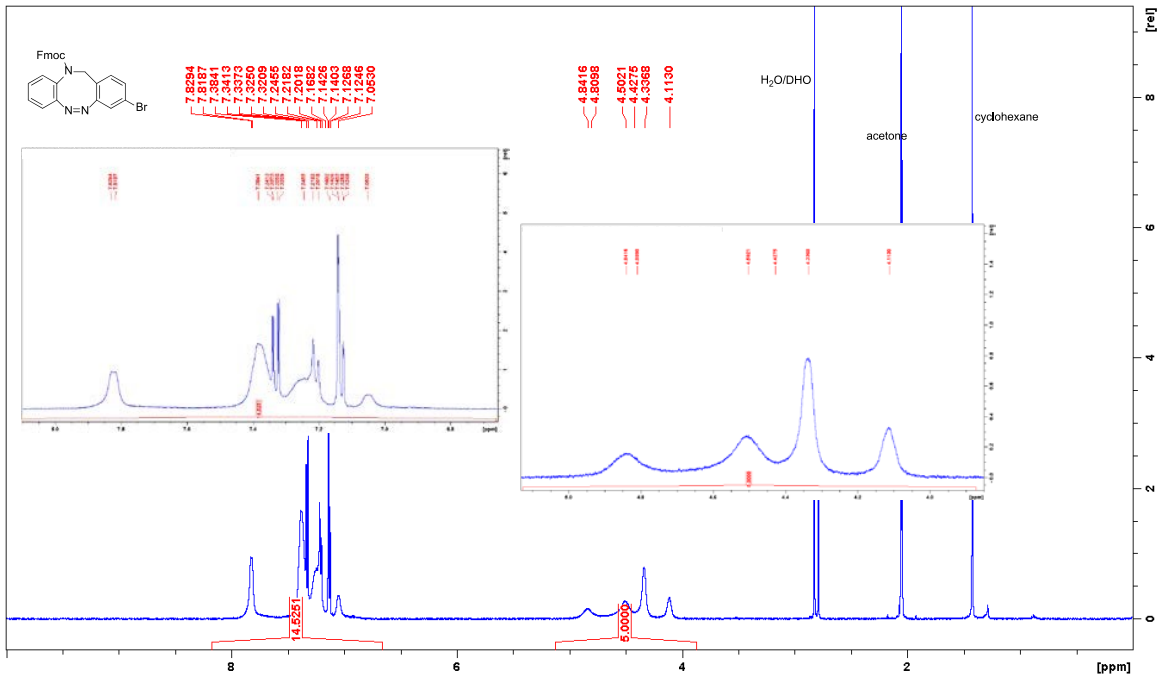

Figure S14: ^{1}H NMR spectrum of compound **8a**.

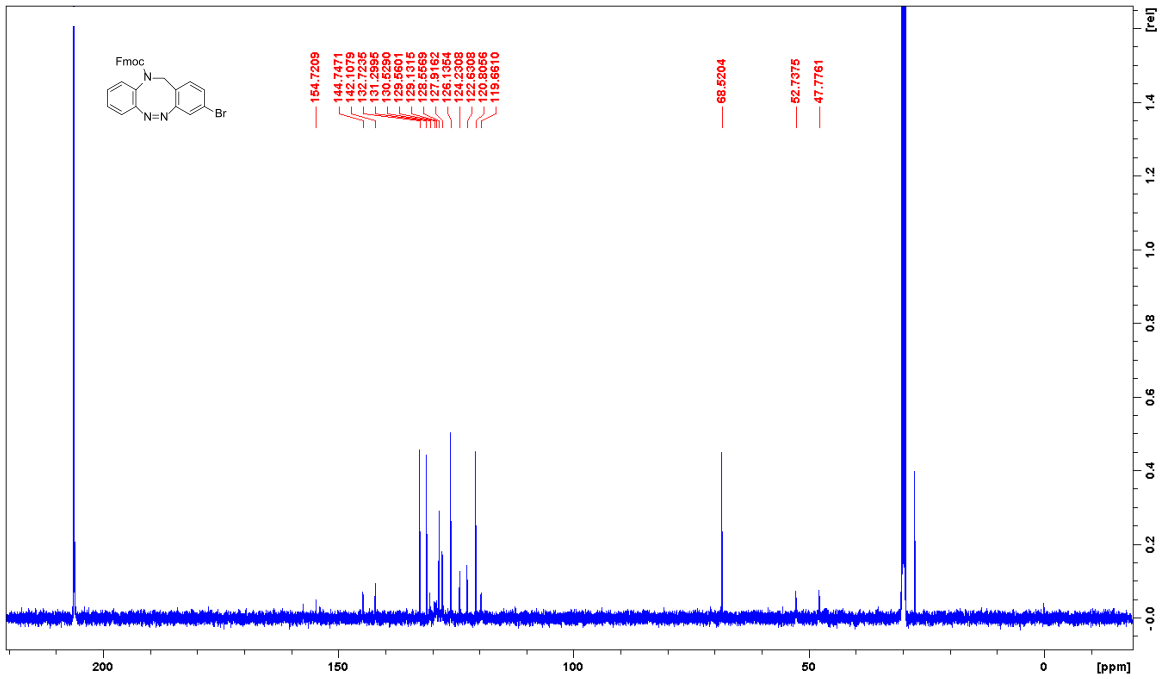

Figure S15: ^{13}C NMR spectrum of compound **8a**.

II.9 Synthesis of (*Z*)-3-bromo-11,12-dihydrodibenzo[*c*,*g*][1,2,5]triazocine (9a)

(9*H*-Fluorene-9-yl)methyl (*Z*)-3-bromodibenzo[*c*,*g*][1,2,5]triazocine-11(12*H*)-carboxylate (**8a**, 382 mg, 748 µmol) was dissolved in 10 mL of DCM and 25 mL of NEt_3 was added. The reaction mixture was stirred at rt for 22 h. The solvent was removed and flash column chromatography on silica (0.040–0.063 mm, ethyl acetate/cyclohexane 1:2, R_f = 0.54) gave a red solid (**9a**, 201 mg, 698 µmol, 93%).

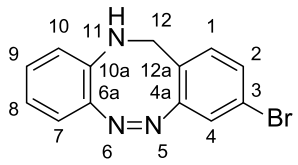

melting point: 160.3 °C

^{1}H NMR (500 MHz, acetone-d_6, 298 K): δ = 7.44 (dd, ^3J = 8.1 Hz, ^4J = 2.0 Hz, 1 H, *H*-2), 7.35 (d, ^4J = 2.0 Hz, 1 H, *H*-4), 7.31 (d, ^3J = 8.1 Hz, 1 H, *H*-1), 6.88 (td, ^3J = 7.7 Hz, ^4J = 1.6 Hz, 1 H, *H*-9), 6.75 (dd, ^3J = 8.0 Hz, ^4J = 1.6 Hz, 1 H, *H*-7), 6.65 (td, ^3J = 7.5 Hz, ^4J = 1.2 Hz, 1 H, *H*-8), 6.56 (dd, ^3J = 8.2 Hz, ^4J = 1.0 Hz, 1 H, *H*-10), 5.42 (m_c, 1 H, N*H*), 3.98 (m_c, 2 H, CH_2) ppm.

^{13}C NMR (125 MHz, acetone-d_6, 298 K): δ = 160.24 (*C*-4a), 144.64 (*C*-6a), 137.04 (*C*-10a), 132.43 (*C*-1), 131.85 (*C*-2), 129.06 (*C*-9), 124.00 (*C*-3), 123.56 (*C*-7), 122.67 (*C*-4), 121.76 (*C*-12a), 119.93 (*C*-10), 118.31 (*C*-8), 47.15 (*C*H$_2$) ppm.

IR (ATR): $\tilde{\nu}$ = 3322 (m), 2959 (w), 1601 (m), 1587 (m), 1568 (w), 1513 (m), 1480 (s), 1456 (m), 1422 (w), 1389 (m), 1363 (w), 1251 (m), 1191 (w), 1161 (m), 1119 (m), 1093 (m), 1072 (m), 956 (w), 898 (m), 831 (s), 812 (s); 768 (m), 741 (s), 720 (s), 703 (w), 651 (w), 604 (m), 560 (w), 513 (m) cm^{-1}.

MS (ESI HR, $CHCl_3$/MeOH): *m/z* ($C_{13}H_{10}{}^{79}BrN_3$+H^+) = calc.: 288.01309, found: 288.01278 ± 1.07 ppm.

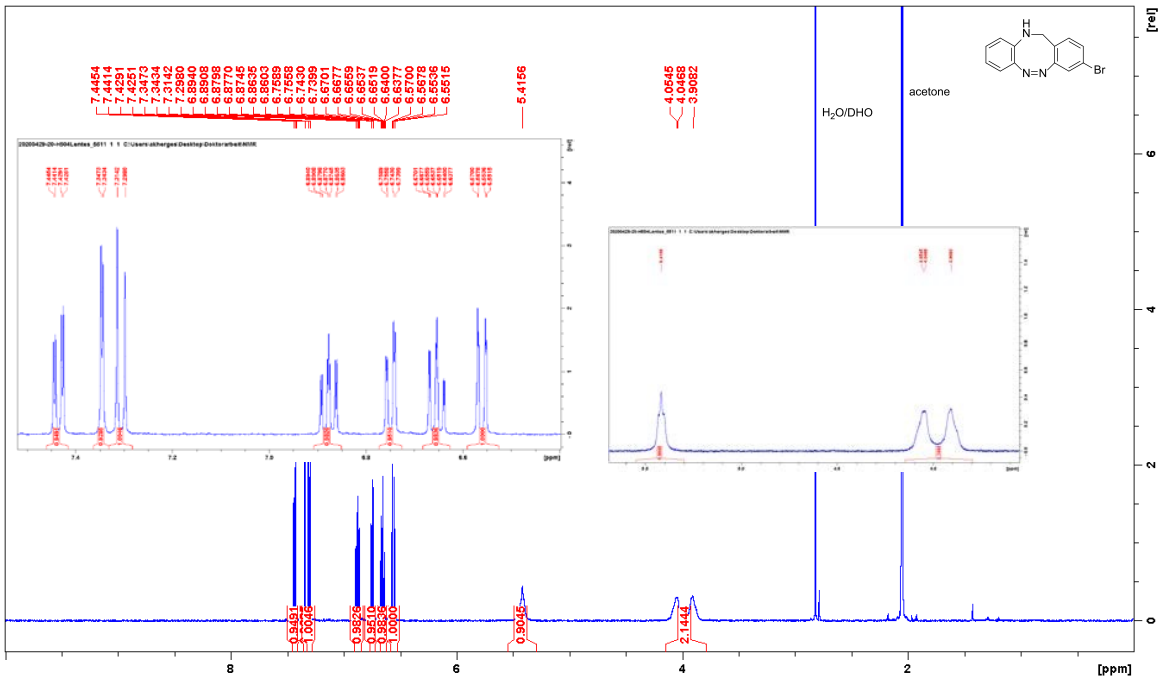

Figure S16: ^{1}H NMR spectrum of compound **9a**.

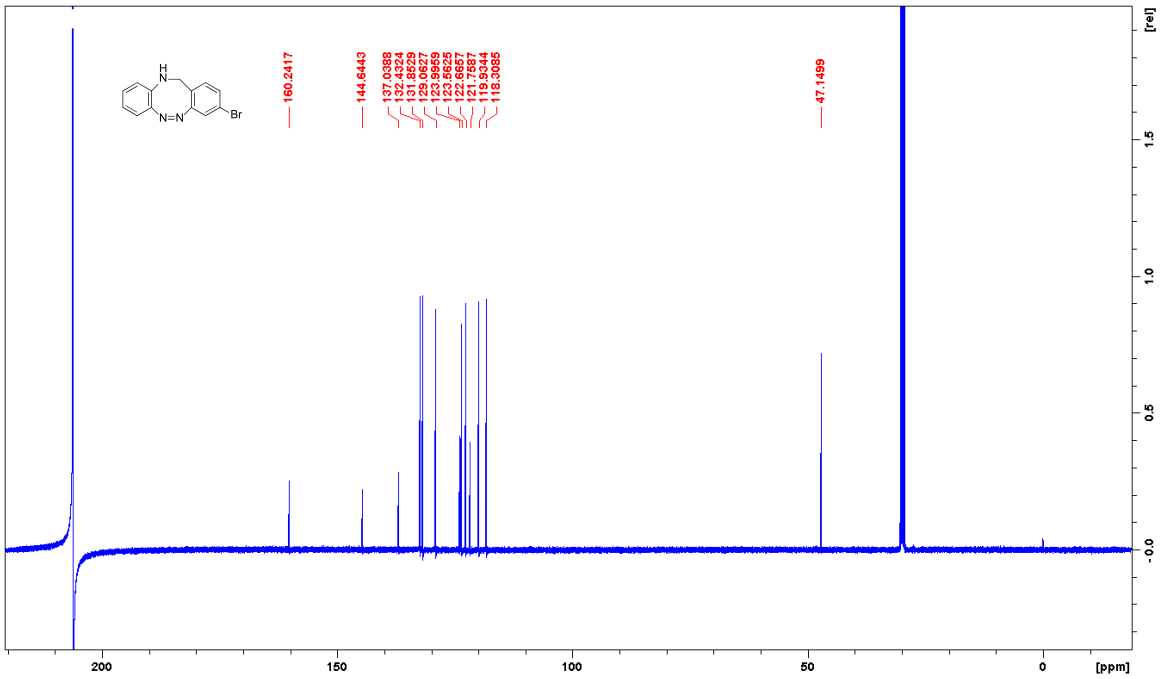

Figure S17: ^{13}C NMR spectrum of compound **9a**.

II.10 Synthesis of (*Z*)-1-(3-bromodibenzo[*c*,*g*][1,2,5]triazocin-11(12*H*)-yl)ethan-1-one (10a)

Under a nitrogen atmosphere, a solution of (*Z*)-3-bromo-11,12-dihydrodibenzo[*c*,*g*][1,2,5]triazocine (**9a**, 52 mg, 180 µmol) in anhydrous DMF (5 mL) was prepared, and then TEA (503 µL, 20 equiv) and HOAc (103 µL, 1.80 mmol) were added. The reaction mixture was cooled to 0 °C and T3P (1.08 mL, 1.80 mmol, 50% in ethyl acetate) was added dropwise. The ice bath was removed and it was stirred for 22 h. Then, 50 mL DCM and 50 mL deionized water were added and the organic layer was separated. It was extracted twice with DCM and the combined organic layers were dried over $MgSO_4$. The solvent was removed and flash column chromatography on silica (0.040–0.063 mm, ethyl acetate/ cyclohexane 1:1, R_f = 0.31) gave a pale yellow solid (**10a**, 51 mg, 154 µmol, 86%).

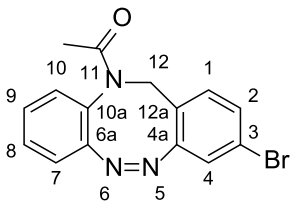

melting point: 164.9 °C

^{1}H NMR (500 MHz, acetone-d_6, 298 K): δ = 7.41 (td, ^3J = 7.5 Hz, ^4J = 1.8 Hz, 1 H, *H*-8/9), 7.34-7.36 (m, 3 H, *H*-2, Ar-*H*, Ar-*H*), 7.19 (d, ^3J = 7.2 Hz, 1 H, *H*-1), 7.12 (d, ^4J = 2.0 Hz, 1 H, *H*-4), 7.06 (dd, ^3J = 7.8 Hz, ^4J = 1.4 Hz, 1 H, *H*-7/10), 5.02 (d, ^2J = 14.5 Hz, 1 H, CH_2a), 4.32 (d, ^2J = 14.5 Hz, 1 H, CH_2b), 1.80 (s, 3 H, CH_3) ppm.

^{13}C NMR (125 MHz, acetone-d_6, 298 K): δ = 169.39 (*C*=O), 157.21 (*C*-4a), 154.16 (*C*-6a/10a), 132.77 (*C*-1), 131.29 (Ar-*C*), 130.29 (Ar-*C*), 130.26 (*C*-8/9), 129.57 (Ar-*C*), 129.45 (*C*-6a/10a), 124.74 (*C*-12a), 122.69 (*C*-4), 122.34 (*C*-3), 120.02 (*C*-7/10), 51.53 (CH_2), 20.04 (CH_3) ppm.

IR (ATR): $\tilde{\nu}$ = 3048 (w), 2924 (w), 1658 (s), 1590 (m), 1516 (w), 1475 (m), 1380 (s), 1338 (s), 1294 (m), 1242 (w), 1161 (w), 1115 (w), 1085 (w), 1070 (w), 1006 (w), 963 (w), 943 (w), 925 (w), 888 (w), 872 (w), 848 (m), 815 (s), 789 (w), 763 (s), 739 (m), 689 (w), 659 (m), 626 (w), 596 (m), 576 (m), 584 (s), 518 (m) cm^{-1}.

MS (ESI HR, $CHCl_3$/MeOH): *m/z* ($C_{15}H_{12}{}^{79}BrN_3$+H^+) = calc.: 330.02365, found: 330.02334 ± 0.95 ppm.

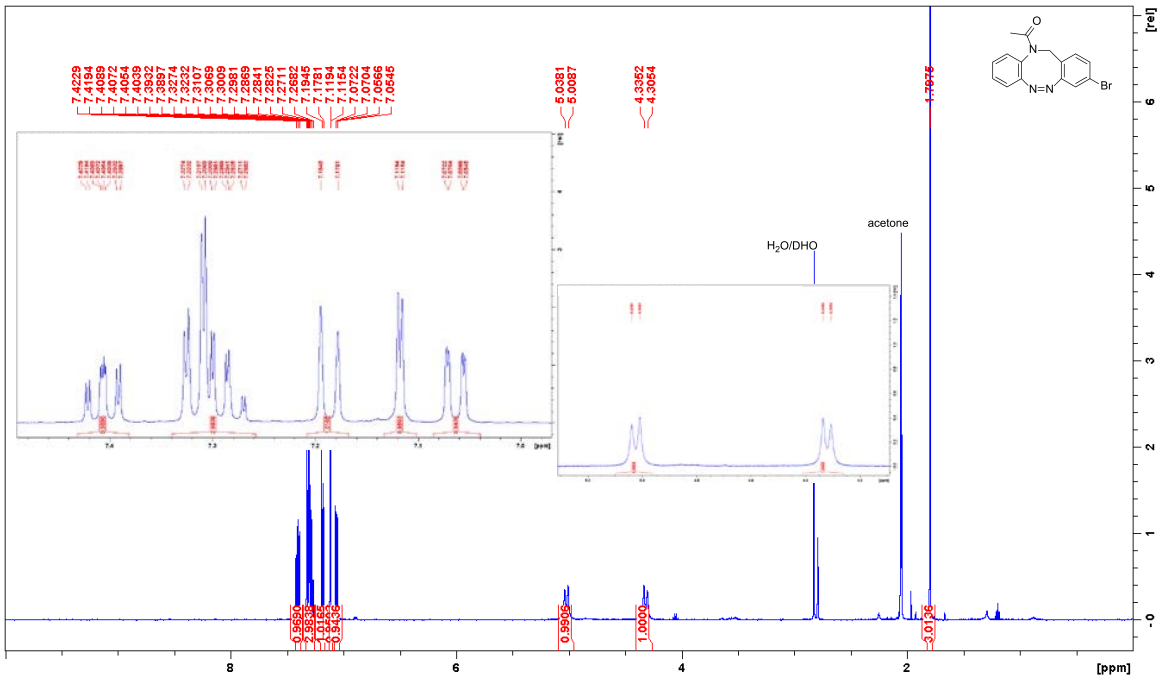

Figure S18: ^{1}H NMR spectrum of compound **10a**.

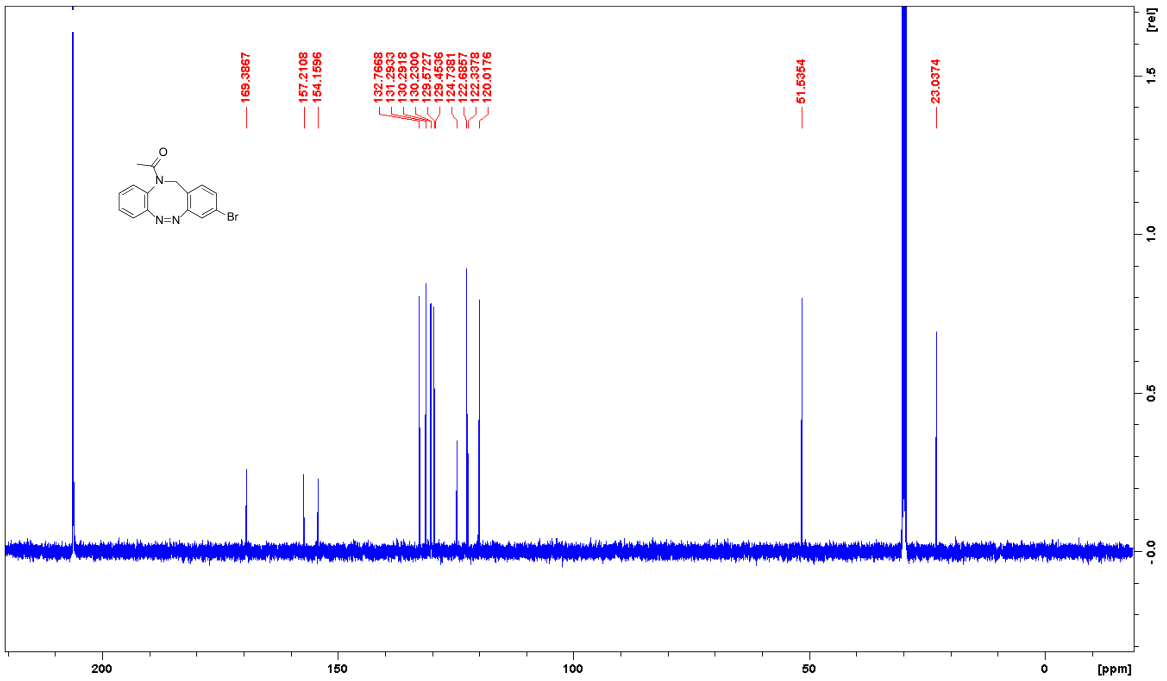

Figure S19: ^{13}C NMR spectrum of compound **10a**.

II.11 Synthesis of (*Z*)-3-bromodibenzo[*c*,*g*][1,2,5]triazocine-11(12*H*)-carbaldehyde (11a)

Under a nitrogen atmosphere, a solution of (*Z*)-3-bromo-11,12-dihydrodibenzo[*c*,*g*][1,2,5]triazocine (**9a**, 100 mg, 348 µmol) in anhydrous MeCN (6 mL) was prepared, and then DIPEA (604 µL, 3.48 mmol) and chloral (338 µL, 3.48 mmol) were added. The reaction mixture was stirred at rt for 20 h. The solvent was removed and flash column chromatography on silica (0.040–0.063 mm, ethyl acetate/cyclohexane 1:2, R_f = 0.35) gave a pale yellow solid (**11a**, 92 mg, 291 µmol, 84%).

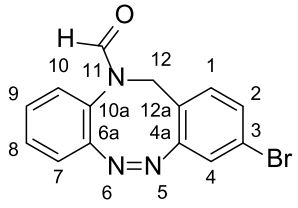

melting point: 201.8 °C

^{1}H NMR (500 MHz, acetone-d$_6$, 298 K): δ = 8.36 (s, 1 H, C*H*O), 7.39 (dd, ^3J = 8.2 Hz, ^4J = 2.0 Hz, 1 H, *H*-2), 7.36 (td, ^3J = 7.7 Hz, ^4J = 1.3 Hz, 1 H, *H*-8/9), 7.31 (d, ^3J = 8.1 Hz, 1 H, *H*-1), 7.28-7.23 (m, H, *H*-2, *H*-4, *H*-8/9), 7.18 (dd, ^3J = 7.9 Hz, ^4J = 1.2 Hz, 1 H, *H*-7/10), 6.97 (dd, ^3J = 7.8 Hz, ^4J = 1.4 Hz, 1 H, *H*-7/10), 4.52 (m$_c$, 2 H, C*H*$_2$) ppm.

^{13}C NMR (125 MHz, acetone-d$_6$, 298 K): δ = 162.30 (*C*HO), 158.37 (*C*-4a), 152.77 (*C*-6a/10a), 133.31 (*C*-1), 131.69 (*C*-2), 129.45 (*C*-8/9), 129.25 (*C*-8/9), 128.29 (*C*-7/10), 123.19 (*C*-3), 122.88 (*C*-12a), 122.21 (*C*-4), 120.51 (*C*-7/10), 48.98 (*C*H$_2$) ppm.

IR (ATR): $\tilde{\nu}$ = 3353 (w), 3038 (w), 1682 (s), 1621 (m), 1501 (s), 1450 (m), 1409 (s), 1356 (m), 1310 (s), 1276 (s), 1215 (m), 1128 (m), 1096 (w), 1007 (w), 979 (m), 939 (w), 860 (w), 739 (s), 631 (w), 621 (w), 552 (w), 525 (m) cm^{-1}.

MS (ESI HR, CHCl$_3$/MeOH): *m/z* (C$_{14}$H$_{10}$^{79}BrN$_3$O+H$^+$) = calc.: 316.00800, found: 316.00781 ± 0.59 ppm.

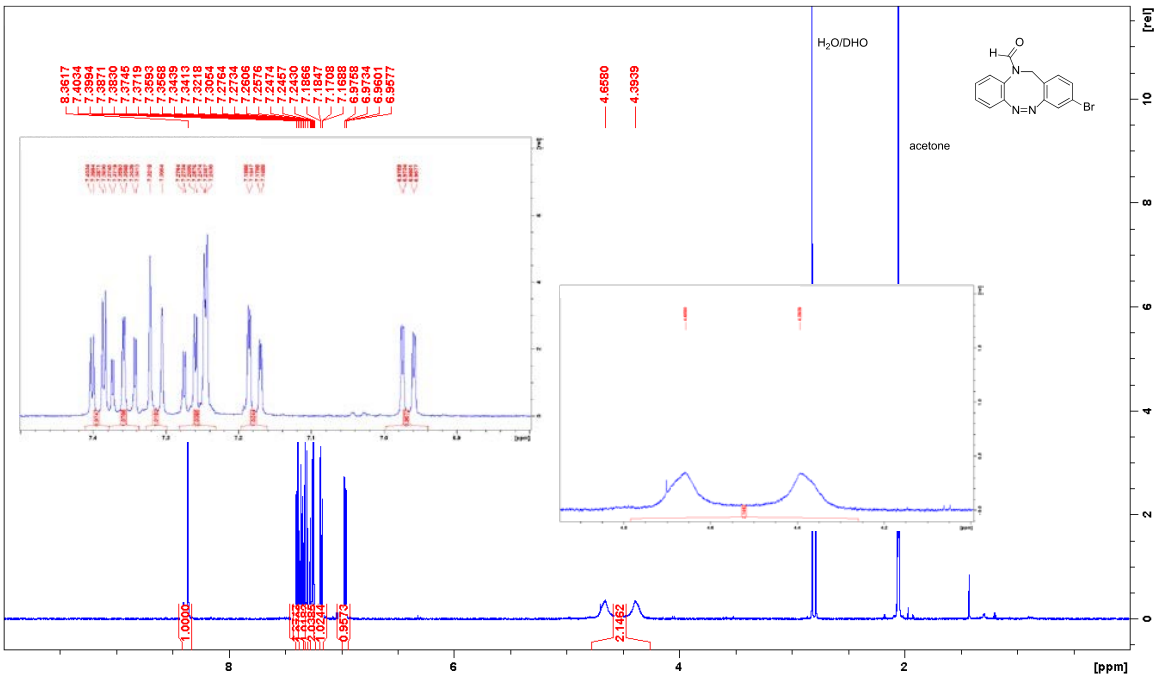

Figure S20: ^{1}H NMR spectrum of compound **11a**.

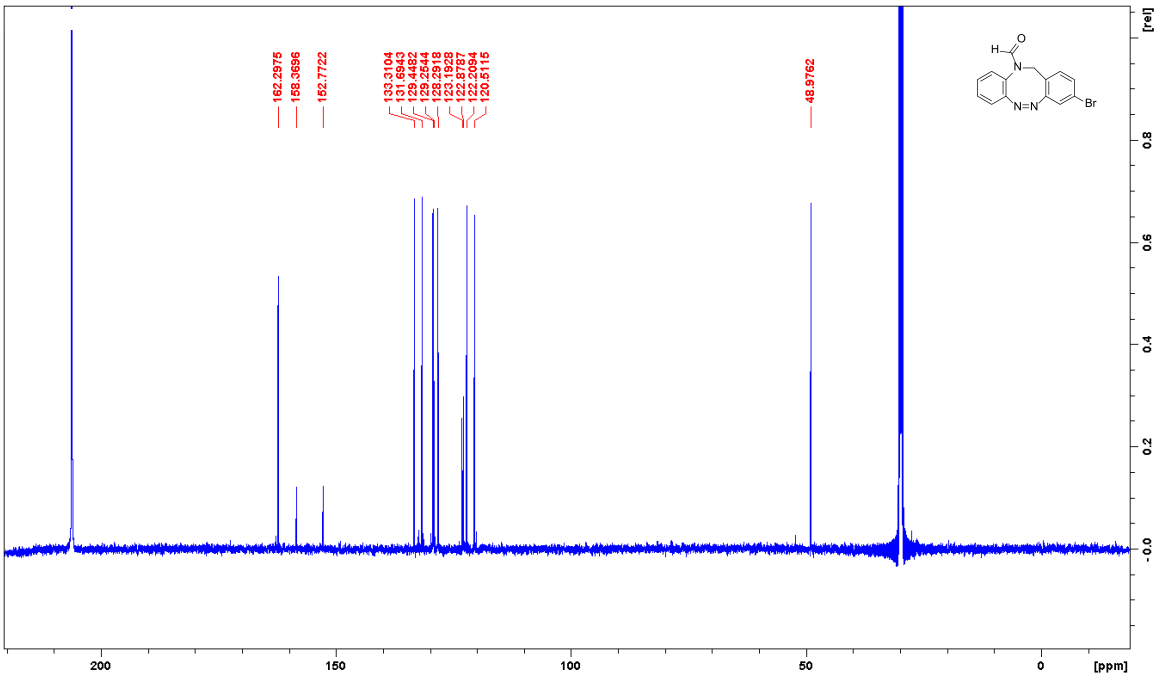

Figure S21: ^{13}C NMR spectrum of compound **11a**.

II.12 Synthesis of 1-(bromomethyl)-4-iodo-2-nitrobenzene (3b)

Under a nitrogen atmosphere, a solution of 4-iodo-1-methyl-2-nitrobenzene (5.00 g, 19.0 mmol) in anhydrous MeCN (21 mL) was prepared, and then NBS (4.00 g, 22.6 mmol) and AIBN (97.2 mg, 600 µmol) were added. The reaction mixture was refluxed for 24 h. The solvent was removed and flash column chromatography on silica (0.040–0.063 mm, ethyl acetate/cyclohexane 1:12, R_f = 0.43) gave a brown solid (**3b**, 1.07 g, 3.12 mmol, 16%).

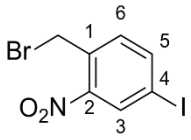

melting point: 103.9 °C

^{1}H NMR (500 MHz, $CDCl_3$, 298 K): δ = 8.35 (d, ^4J = 1.8 Hz, 1 H, *H*-3), 7.93 (dd, ^3J = 8.2 Hz, ^4J = 1.8 Hz, 1 H, *H*-5), 7.30 (d, ^3J = 8.2 Hz, *H*-6), 7.46 (s, 2 H, CH_2) ppm.

^{13}C NMR (125 MHz, $CDCl_3$, 298 K): δ = 148.06 (*C*-2), 142.77 (*C*-5), 134.29 (*C*-3), 133.91 (*C*-6), 132.58 (*C*-1), 93.60 (*C*-4), 28.18 (CH_2) ppm.

IR (ATR): $\tilde{\nu}$ = 3081 (w), 1702 (w), 1592 (w), 1555 (w), 1518 (s), 1476 (w), 1433 (m), 1342 (m), 1275 (w), 1223 (m), 1204 (w), 1164 (w), 1124 (w), 1077 (w), 971 (w), 897 (w), 889 (w), 870 (m), 837 (m), 804 (m), 762 (w), 705 (w), 681 (w), 627 (w), 611 (m), 567 (w) cm^{-1}.

MS (EI, 70 eV): *m/z*(%) = 341 (11) $[M]^+$, 262 (100) $[M\text{-}Br]^+$, 242 (5) $[M\text{-}BrO]^+$.

MS (EI, HR, 70 eV): *m/z* ($C_7H_5{}^{79}BrINO_2$+H^+) = calc.: 330.85483, found: 340.85328 ± 4.65 ppm.

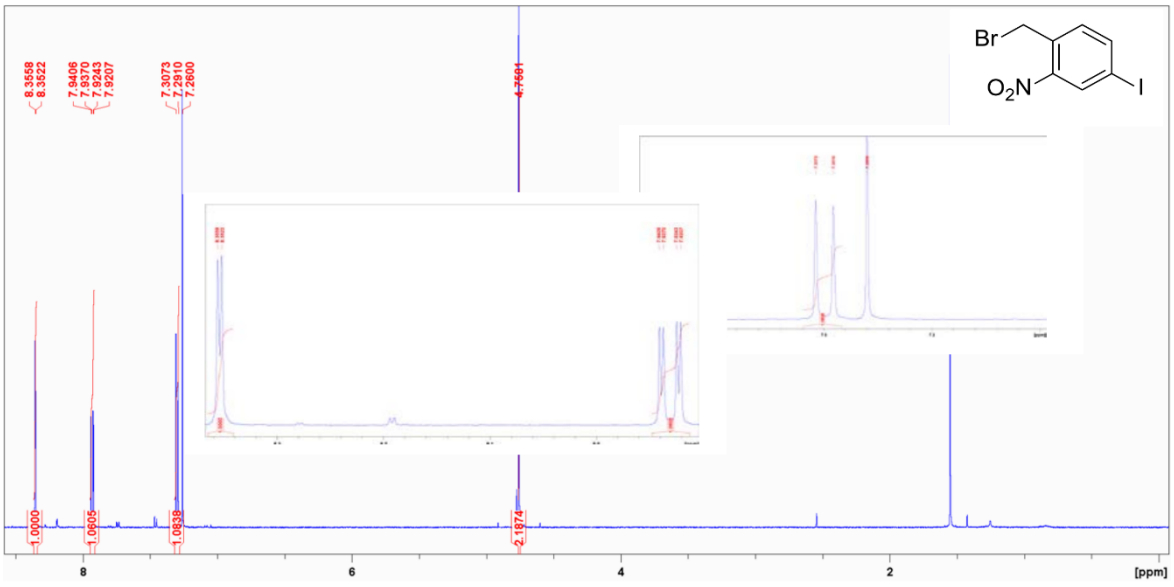

Figure S22: ^{1}H NMR spectrum of compound **3b**.

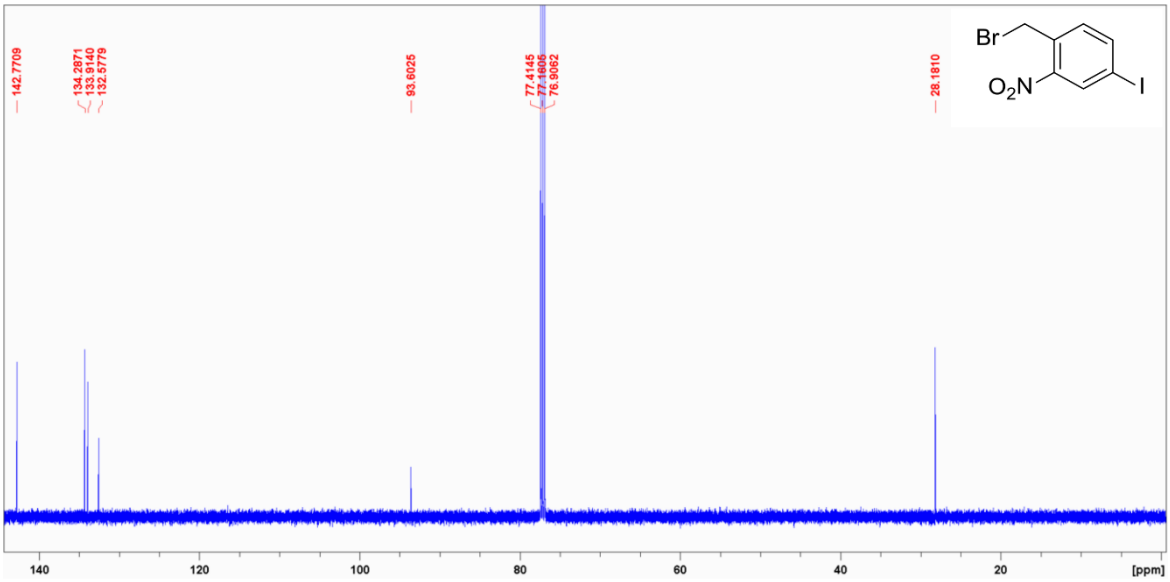

Figure S23: ^{13}C NMR spectrum of compound **3b**.

II.13 Synthesis of *tert*-butyl (2-((4-iodo-2-nitrobenzyl)amino)phenyl)carbamate (4b)

Under a nitrogen atmosphere, a solution of *tert*-butyl (2-aminophenyl)carbamate[1] (**2**, 651 mg, 3.12 mmol) in anhydrous THF (12 mL) was prepared, and then TEA (477 µL, 3.42 mmol) and 1-(bromomethyl)-4-iodo-2-nitrobenzene (**3b**, 1.07 g, 3.12 µmol) were added. The reaction mixture was refluxed for 20 h and after that, the solvent was removed. Deionized water and DCM were added, the organic layer was separated and it was extracted twice with DCM. The combined organic layers were dried over $MgSO_4$ and the solvent was evaporated. Recrystallization from ethyl acetate/cyclohexane 1:1 gave a yellow solid (**4b**, 1.41 g, 3.00 mmol, 96%).

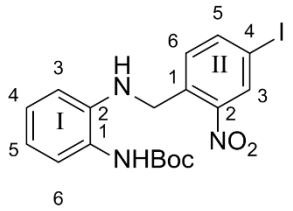

melting point: 143.5 °C

^{1}H NMR (500 MHz, $CDCl_3$, 298 K): δ = 8.38 (d, ^4J = 1.8 Hz, 1 H, Ar^{II}-*H*-3), 7.85 (dd, ^3J = 8.2 Hz, ^4J = 1.8 Hz, 1 H, Ar^{II}-*H*-5), 7.40 (d, ^3J = 8.2 Hz, 1H, Ar^{II}-*H*-6), 7.25 (d, ^3J = 7.7 Hz, 1 H, Ar^{I}-*H*-6), 7.01 (td, ^3J = 7.7 Hz, ^4J = 1.5 Hz, 1 H, Ar^{I}-*H*-4), 6.80 (t, ^3J = 7.7 Hz, 1 H, Ar^{I}-*H*-5), 6.52 (d, ^3J = 7.7 Hz, 1 H, Ar^{I}-*H*-3), 6.28 (br. s, 1 H, N*H*), 4.69 (s, 2 H, -CH_2), 1.51 (s, 9 H, tBu-*H*) ppm.

^{13}C NMR (125 MHz, $CDCl_3$, 298 K): δ = 154.39 (*C*=O),148.69 (Ar^{II}-*C*-2), 140.69 (Ar^{I}-*C*-2), 142.74 (Ar^{II}-*C*-5), 134.55 (Ar^{II}-*C*-1), 133.81 (Ar^{II}-*C*-3), 131.85 (Ar^{II}-*C*-6), 127.09 (Ar^{I}-*C*-4), 126.03 (Ar^{I}-*C*-6), 124.84 (Ar^{I}-*C*-1), 119.72 (Ar^{I}-*C*-5), 113.62 (Ar^{I}-*C*-3), 91.87 (Ar^{II}-*C*-4), 81.08 (-*C*-(CH_3)$_3$, 45.84 (-*C*H_2), 28.46 (-*C*H_3) ppm.

IR (ATR): $\tilde{\nu}$ = 3414 (w), 3314 (w), 2924 (w), 2847 (w), 1679 (m), 1606 (m), 1531 (m), 1503 (m), 1460 (m), 1392 (w), 1363 (w), 1343 (m), 1329 (m), 1305 (w), 1285 (w), 1271 (m), 1247 (m), 1159 (s), 1133 (w), 1085 (w), 1055 (w), 1029 (w), 990 (w), 937 (w), 906 (w), 890 (w), 869 (w), 837 (w), 821 (w), 783 (w), 774 (w), 754 (w), 741 (w), 717 (w), 692 (w), 647 (w), 599 (w), 523 (w) cm^{-1}.

MS (ESI HR, $CHCl_3$/MeOH): *m/z* ($C_{18}H_{20}IN_3O_4$+H^+) = calc.: 470.05713, found: 470.05680 ± 0.69 ppm.

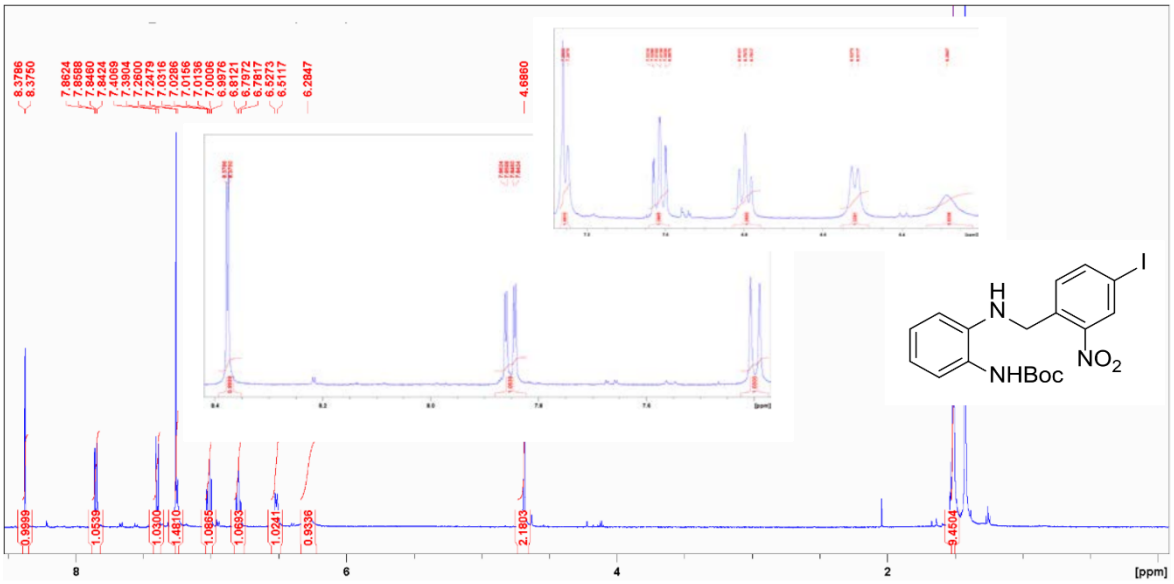

Figure S24: ^{1}H NMR spectrum of compound **4b**.

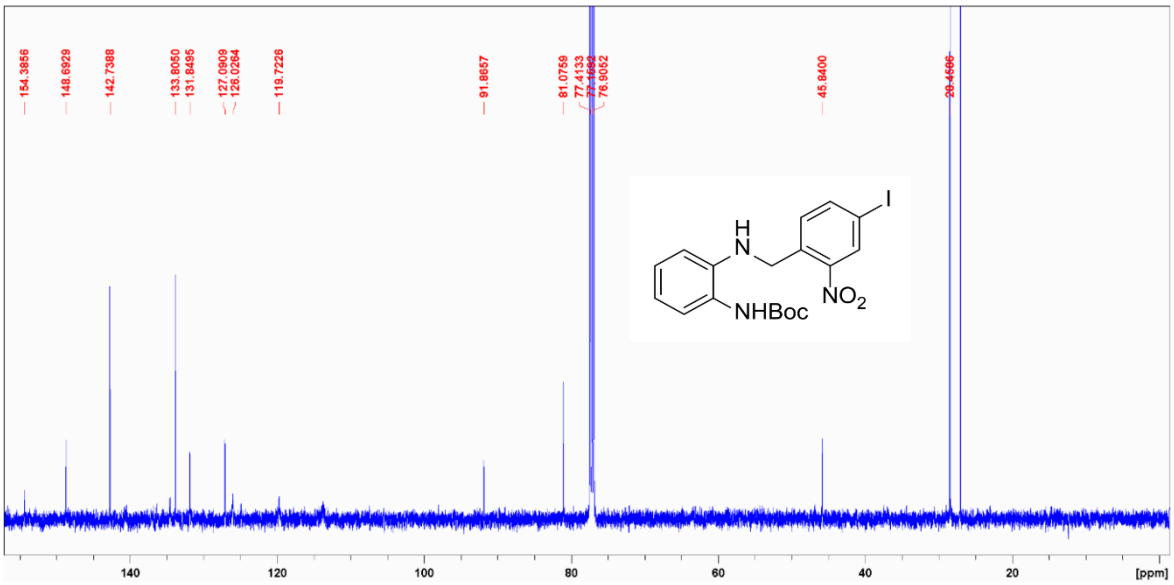

Figure S25: ^{13}C NMR spectrum of compound **4b**.

II.14 Synthesis of (9*H*-fluorene-9-yl)methyl (2-((*tert*-butoxycarbonyl)amino)phenyl)(4-iodo-2-nitrobenzyl)carbamate (5b)

Under a nitrogen atmosphere, a solution of *tert*-butyl (2-((4-iodo-2-nitrobenzyl)amino)phenyl)carbamate (**4b**, 1.41 g, 3.00 mmol) in anhydrous DMF (12 mL) was prepared, and then DIPEA (510 µL, 3.00 mmol) and Fmoc-chloride (1.55 g, 6.00 µmol) were added. The reaction mixture was stirred for 91 h at rt and after that, the solvent was evaporated. Deionized water and DCM were added, the organic layer was separated and it was extracted twice with DCM. The combined organic layers were dried over $MgSO_4$ and the solvent was evaporated. Flash column chromatography on silica (0.040–0.063 mm, ethyl acetate/cyclohexane 1:4, R_f = 0.45) gave a white solid (**5b**, 682 mg, 986 µmol, 33%).

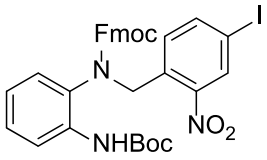

melting point: 131.6 °C

^{1}H NMR (500 MHz, acetone-d_6, 298 K): δ = 8.29 (d, ^{4}J = 1.7 Hz, 1 H, Ar-*H*), 8.14-7.55 (m, 5 H), 7.84-7.54-6.87 (m, 10 H), 5.12 (br. S, 1 H, -C*H*$_2$), 5.28-4.76 (m, 2 H), 4.73-3.96 (m, 3 H), 1.46 (s, 9 H, tBu-*H*) ppm.

^{13}C NMR (125 MHz, acetone-d_6, 298 K): δ = 153.53, 143.00, 142.08, 133.86, 129.96, 129.22, 128.48, 127.86, 126.06, 124.43, 122.55, 120.73, 92.68, 80.46, 68.42, 47.83, 28.60 ppm.

IR (ATR): $\tilde{\nu}$ = 2976 (w), 1706 (m), 1594 (w), 1524 (m), 1477 (s), 1449 1449, 1392 (w), 1366 (m), 1345 (m), 1295 (m), 1274 (m), 1239 (m), 1153 (s), 1046 (w), 1024 (m), 984 (w), 870 (w), 835 (w), 758 (m), 739 (s), 620 (w), 588 (w), 553 (w) cm^{-1}.

MS (ESI HR, $CHCl_3$/MeOH): *m/z* ($C_{33}H_{30}IN_3O_6$+H^+) = calc.: 692.12521, found: 692.12442 ± 1.14 ppm.

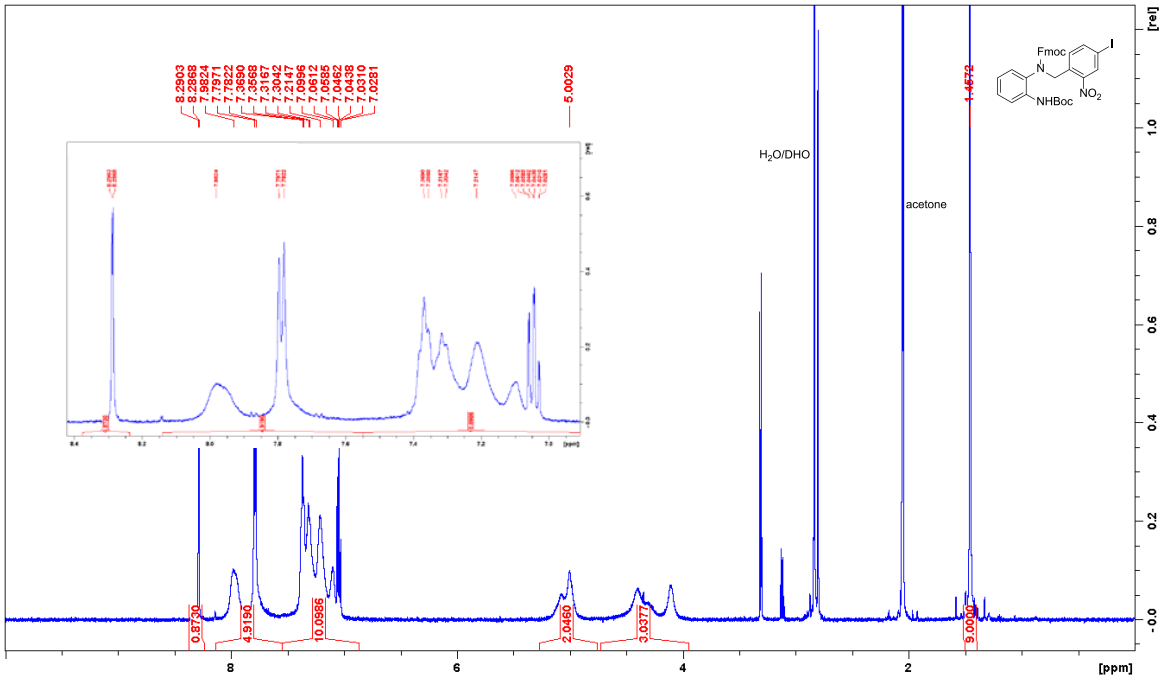

Figure S26: ^{1}H NMR spectrum of compound **5b**.

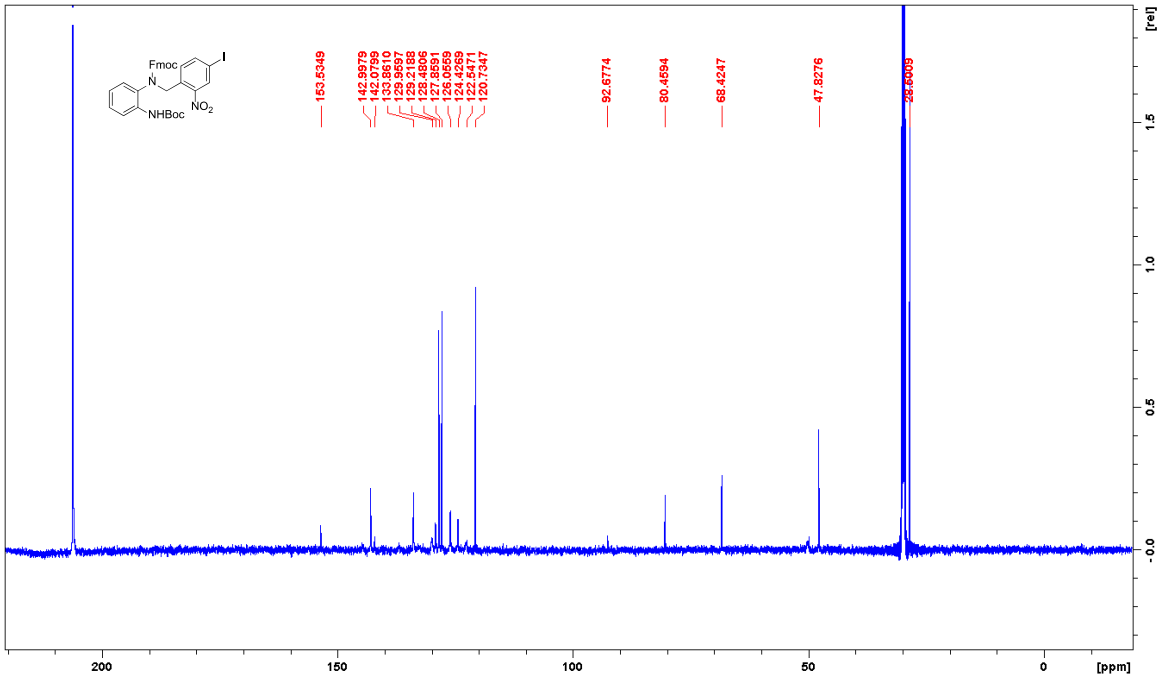

Figure S27: ^{13}C NMR spectrum of compound **5b**.

II.15 Synthesis of (9*H*-fluorene-9-yl)methyl (2-aminophenyl)(4-iodo-2-nitrobenzyl)carbamate (6b)

A solution of (9*H*-fluorene-9-yl)methyl (2-((*tert*-butoxycarbonyl)amino)phenyl)(4-iodo-2-nitrobenzyl)carbamate (**5b**, 2.15 g, 3.11 mmol) in DCM (20 mL) was prepared, and then TFA (12 mL) was added. The reaction mixture was stirred for 20 h at rt and after that, it was neutralized with saturated aqueous $NaHCO_3$ solution. The organic layer was separated and it was extracted twice with DCM. The combined organic layers were dried over $MgSO_4$ and the solvent was evaporated. A yellow solid (**6b**, 1.76 g, 2.97 mmol, 96%) was obtained.

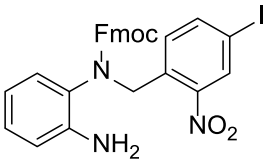

melting point: 85.7 °C

^{1}H NMR (500 MHz, $CDCl_3$, 298 K): δ = 8.24 (d, ^4J = 1.8 Hz, 1 H,), 7.87 (br. s, 1 H, 1 H), 7.71-7.62 (m, 2 H), 7.39-7.29 (m, 3 H), 7.24-7.07 (m, 5 H), 6.82-6.72 (m, 2 H), 6.70-6.65 (m, 1 H), 5.23 (br. s, 1 H, C*H*$_2$), 4.93 (br. s, 1 H, C*H*$_2$), 4.50-4.32 (m, 2 H, Fmoc-C*H*$_2$), 4.07 (br. s, 1 H, Fmoc-C*H*), 3.60 (br. s, 2 H, N*H*$_2$).

^{13}C NMR (125 MHz, $CDCl_3$, 298 K): δ = 156.20, 143.52, 142.32, 141.41, 133.50, 132.44, 128.81, 128.6, 127.78, 127.08, 125.27, 120.02, 118.99, 116.6, 68.05, 47.21 ppm.

IR (ATR): $\tilde{\nu}$ = 3360 (w), 3065 (w), 1696 (m), 1620 (w), 1525 (m), 1501 (w), 1450 (w), 1403 (w), 1340 (w), 1297 (m), 1271 (w), 1157 (w), 1137 (w), 1044 (w), 987 (w), 739 (s), 692 (w), 620 (w), 535 (w) cm^{-1}.

MS (ESI HR, $CHCl_3$/MeOH): *m/z* ($C_{28}H_{22}IN_3O_4$+H$^+$) = calc.: 592.07278, found: 592.07234 ± 0.73 ppm.

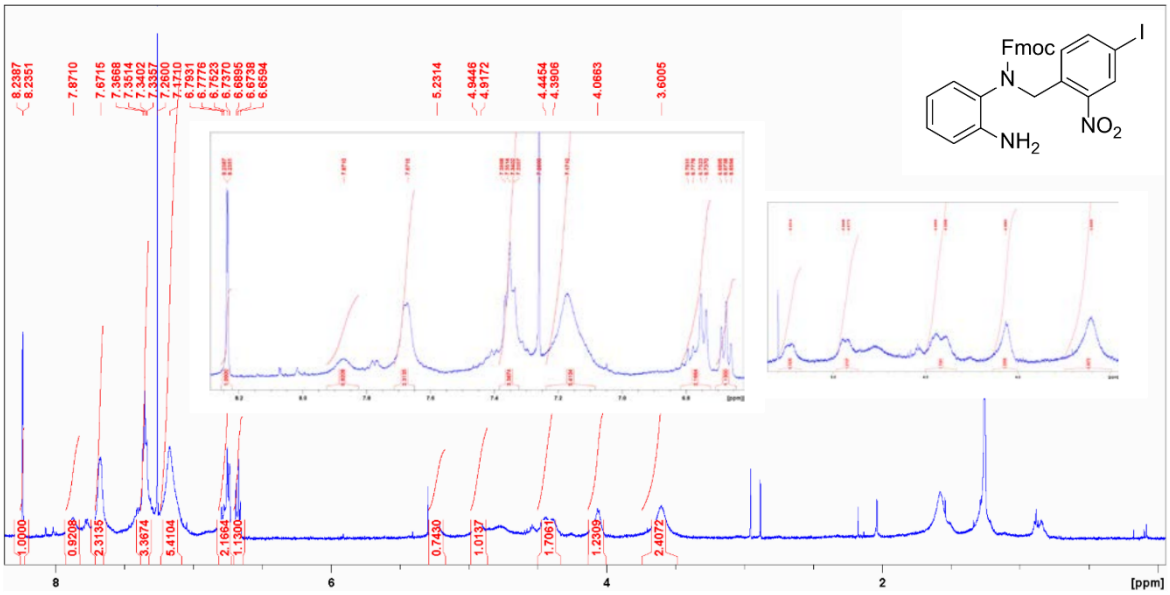

Figure S28: ^{1}H NMR spectrum of compound **6b**.

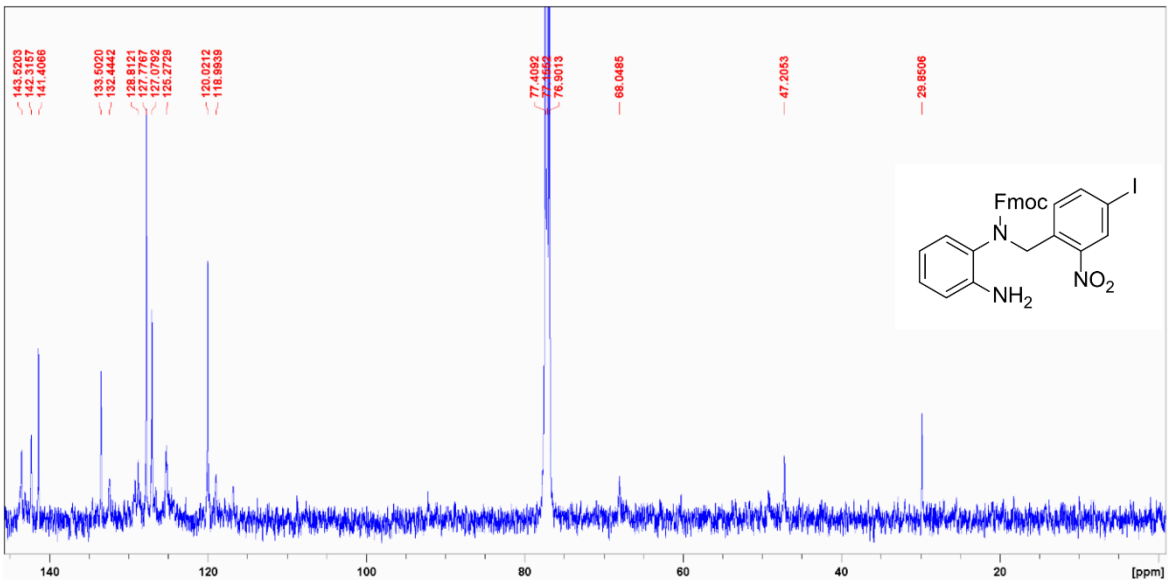

Figure S29: ^{13}C NMR spectrum of compound **6b**.

II.16 Synthesis of (9*H*-fluorene-9-yl)methyl (*Z*)-3-iododibenzo[*c*,*g*][1,2,5]triazocine-11(12*H*)-carboxylate (8b)

(9*H*-Fluorene-9-yl)methyl (2-aminophenyl)(4-iodo-2-nitrobenzyl)carbamate (**6b**, 1.55 g, 2.62mmol) was suspended in 250 mL of ethanol and $SnCl_2$·2 H_2O (2.96 g, 14.9mmol) was added. The reaction mixture was heated to 75 °C and zink powder (824 mg, 12.6 mmol, 8 eq) was added. It was stirred at rt over night and afterwards neutralized with saturated aqueous $NaHCO_3$ solution. The solvent was evaporated and to the residue was added DCM and deionized water. The organic layer was separated and it was extracted twice with DCM. The combined organic layers were dried over $MgSO_4$ and the solvent was evaporated. The crude product was dissolved in 150 mL of acetic acid and *m*CPBA (1.17 g, 3.15 mmol, ≥ 77%) in 150 mL of acetic acid was added dropwise over a period of 2 h. The reaction mixture was stirred at rt over night and after that, the solvent was evaporated. To the residue was added DCM and half-concentrated aqueous $NaHCO_3$ solution in deionized water and the organic layer was separated. It

was extracted twice with DCM and the combined organic layers were dried over $MgSO_4$. The solvent was evaporated and flash column chromatography on silica (0.040–0.063 mm, ethyl acetate/cyclohexane 1:4, R_f = 0.41) gave a yellow solid (**8b**, 833 mg, 1.49 mmol, 56%).

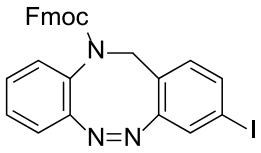

melting point: 87.6 °C

^{1}H NMR (600 MHz, acetone-d_6, 298 K): δ = 8.15-6.65 (m, 15 H, Ar-*H*), 5.05-3.99 (m, 5 H, aliph. *H*) ppm.

^{13}C NMR (150 MHz, acetone-d_6, 298 K): δ = 154.71, 153.87, 144.72, 142.08, 137.37, 132.64, 130.47, 129.54, 129.13, 128.53, 128.36, 127.89, 126.12, 124.68, 120.78, 119.69, 68.50, 52.85, 47.74 ppm. ppm.

IR (ATR): $\tilde{\nu}$ = 2925 (w), 2850 (w),2036 (w), 1703 (s), 1586 (w), 1477 (w), 1449 (m), 1390 (m), 1320 (s), 1295 (s), 1230 (m), 1129 (m), 1105 (m), 1041 (m), 1022 (m), 863 (w), 816 (w), 756 (s), 738 (s), 693 (w), 621 (m), 603 (w), 549 (m), 512 (w) cm^{-1}.

MS (ESI HR, $CHCl_3$/MeOH): *m/z* ($C_{28}H_{20}IN_3O_2$+H^+) = calc.: 558.06730, found: 558.06694 ± 0.63 ppm.

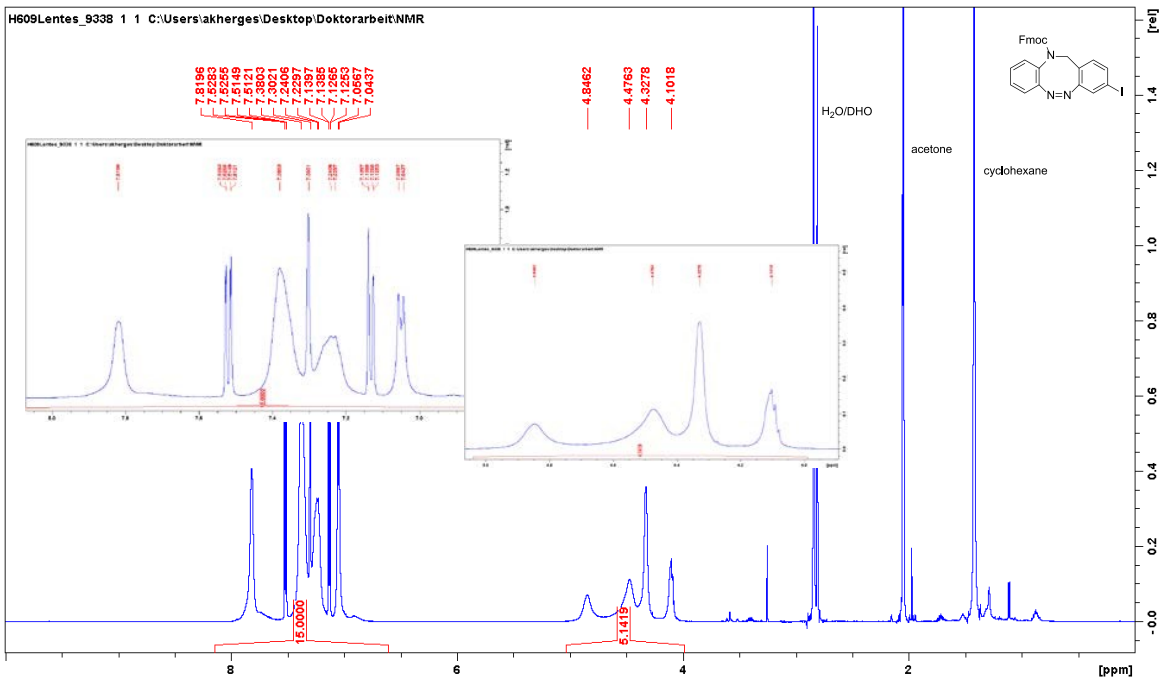

Figure S30: ^{1}H NMR spectrum of compound **8b**.

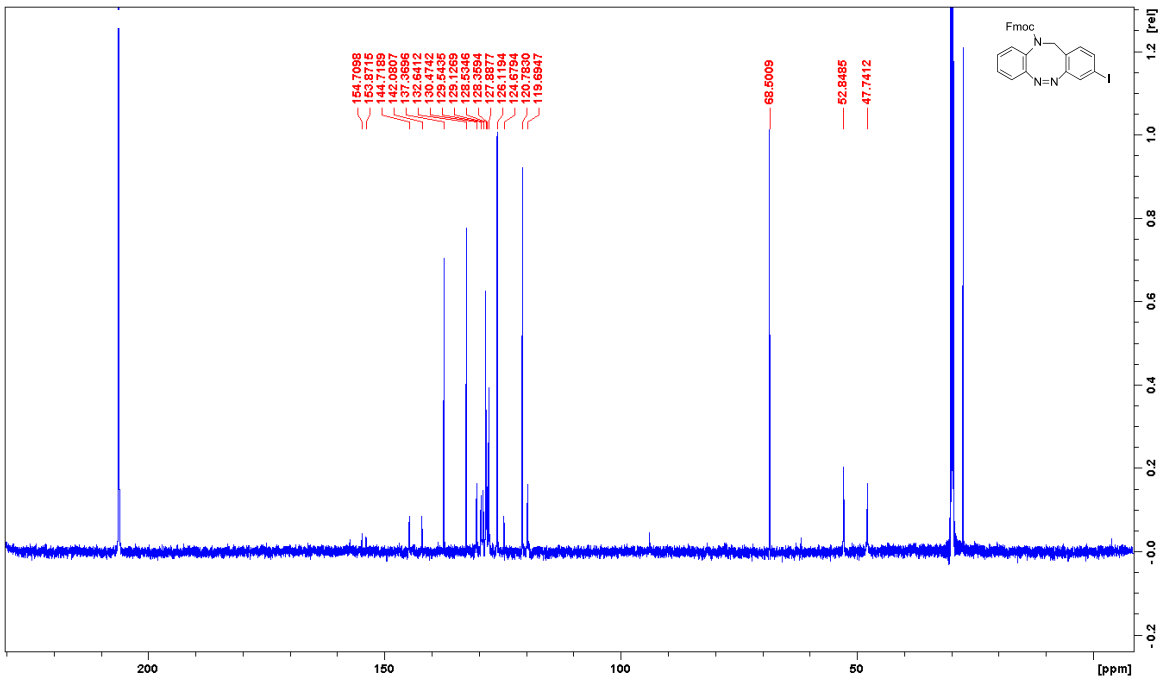

Figure S31: ^{13}C NMR spectrum of compound **8b**.

II.17 Synthesis of (*Z*)-3-iodo-11,12-dihydrodibenzo[*c*,*g*][1,2,5]triazocine (9b)

(9*H*-Fluorene-9-yl)methyl (*Z*)-3-iododibenzo[*c*,*g*][1,2,5]triazocine-11(12*H*)-carboxylate (**8b**, 813 mg, 1.46 mmol) was dissolved in 20 mL of DCM and 50 mL of NEt_3 was added. The reaction mixture was stirred at rt for 20 h. The solvent was removed and flash column chromatography on silica (0.040–0.063 mm, ethyl acetate/cyclohexane 1:3, R_f = 0.43) gave a red solid (**9b**, 410 mg, 1.22 mmol, 84%).

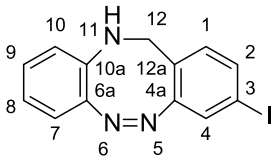

melting point: 165.2 °C

^{1}H NMR (500 MHz, acetone-d_6, 298 K): δ = 7.63 (dd, ^3J = 8.0 Hz, ^4J = 1.7 Hz, 1 H, *H*-2), 7.52 (d, ^4J = 1.7 Hz, 1 H, *H*-4), 7.16 (d, ^3J = 8.0 Hz, 1 H, *H*-1), 6.87 (td, ^3J = 7.6 Hz, ^4J = 1.6 Hz, 1 H, *H*-9), 6.75 (dd, ^3J = 8.0 Hz, ^4J = 1.5 Hz, 1 H, *H*-7), 6.65 (td, ^3J = 7.5 Hz, ^4J = 1.2 Hz, 1 H, *H*-8), 6.56 (dd, ^3J = 8.2 Hz, ^4J = 1.1 Hz, 1 H, *H*-10), 5.43 (m_c, 1 H, N*H*), 3.96 (m_c, 2 H, CH_2) ppm.

^{13}C NMR (125 MHz, acetone-d_6, 298 K): δ = 160.26 (*C*-4a), 144.64 (*C*-6a), 137.88 (*C*-2), 137.08 (*C*-10a), 132.44 (*C*-1), 129.06 (*C*-9), 128.50 (*C*-4), 124.49 (*C*-12a), 123.61 (*C*-7), 119.93 (*C*-10), 118.30 (*C*-8), 93.11 (*C*-3), 47.15 (CH_2) ppm.

IR (ATR): $\tilde{\nu}$ = 3323 (m), 2959 (w), 1601 (m), 1581 (m), 1561 (w), 1518 (m), 1479 (s), 1453 (m), 1383 (m), 1364 (w), 1322 (m), 1251 (w), 1161 (w), 1139 (w), 1117 (w), 1094 (m), 1068 (w), 949 (w), 896 (m), 831 (s), 806 (s), 764 (m), 742 (s), 720 (s), 701 (w), 645 (w), 600 (s), 559 (w), 511 (m) cm^{-1}.

MS (ESI HR, $CHCl_3$/MeOH): *m/z* ($C_{13}H_{10}IN_3$+H^+) = calc.: 335.99922, found: 335.99888 ± 1.02 ppm.

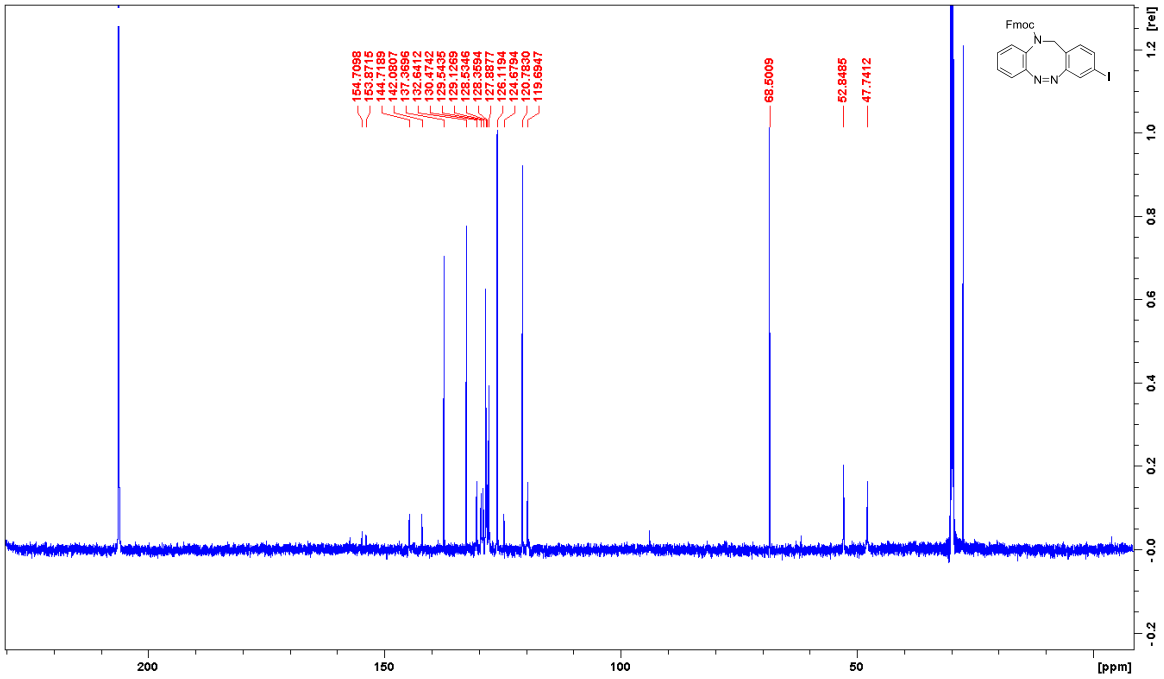

Figure S31: ^{13}C NMR spectrum of compound **8b**.

II.17 Synthesis of (*Z*)-3-iodo-11,12-dihydrodibenzo[*c*,*g*][1,2,5]triazocine (9b)

(9*H*-Fluorene-9-yl)methyl (*Z*)-3-iododibenzo[*c*,*g*][1,2,5]triazocine-11(12*H*)-carboxylate (**8b**, 813 mg, 1.46 mmol) was dissolved in 20 mL of DCM and 50 mL of NEt_3 was added. The reaction mixture was stirred at rt for 20 h. The solvent was removed and flash column chromatography on silica (0.040–0.063 mm, ethyl acetate/cyclohexane 1:3, R_f = 0.43) gave a red solid (**9b**, 410 mg, 1.22 mmol, 84%).

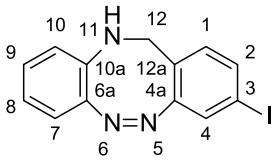

melting point: 165.2 °C

^{1}H NMR (500 MHz, acetone-d_6, 298 K): δ = 7.63 (dd, ^3J = 8.0 Hz, ^4J = 1.7 Hz, 1 H, *H*-2), 7.52 (d, ^4J = 1.7 Hz, 1 H, *H*-4), 7.16 (d, ^3J = 8.0 Hz, 1 H, *H*-1), 6.87 (td, ^3J = 7.6 Hz, ^4J = 1.6 Hz, 1 H, *H*-9), 6.75 (dd, ^3J = 8.0 Hz, ^4J = 1.5 Hz, 1 H, *H*-7), 6.65 (td, ^3J = 7.5 Hz, ^4J = 1.2 Hz, 1 H, *H*-8), 6.56 (dd, ^3J = 8.2 Hz, ^4J = 1.1 Hz, 1 H, *H*-10), 5.43 (m_c, 1 H, N*H*), 3.96 (m_c, 2 H, CH_2) ppm.

^{13}C NMR (125 MHz, acetone-d_6, 298 K): δ = 160.26 (*C*-4a), 144.64 (*C*-6a), 137.88 (*C*-2), 137.08 (*C*-10a), 132.44 (*C*-1), 129.06 (*C*-9), 128.50 (*C*-4), 124.49 (*C*-12a), 123.61 (*C*-7), 119.93 (*C*-10), 118.30 (*C*-8), 93.11 (*C*-3), 47.15 (CH_2) ppm.

IR (ATR): $\tilde{\nu}$ = 3323 (m), 2959 (w), 1601 (m), 1581 (m), 1561 (w), 1518 (m), 1479 (s), 1453 (m), 1383 (m), 1364 (w), 1322 (m), 1251 (w), 1161 (w), 1139 (w), 1117 (w), 1094 (m), 1068 (w), 949 (w), 896 (m), 831 (s), 806 (s), 764 (m), 742 (s), 720 (s), 701 (w), 645 (w), 600 (s), 559 (w), 511 (m) cm^{-1}.

MS (ESI HR, $CHCl_3$/MeOH): *m/z* ($C_{13}H_{10}IN_3$+H^+) = calc.: 335.99922, found: 335.99888 ± 1.02 ppm.

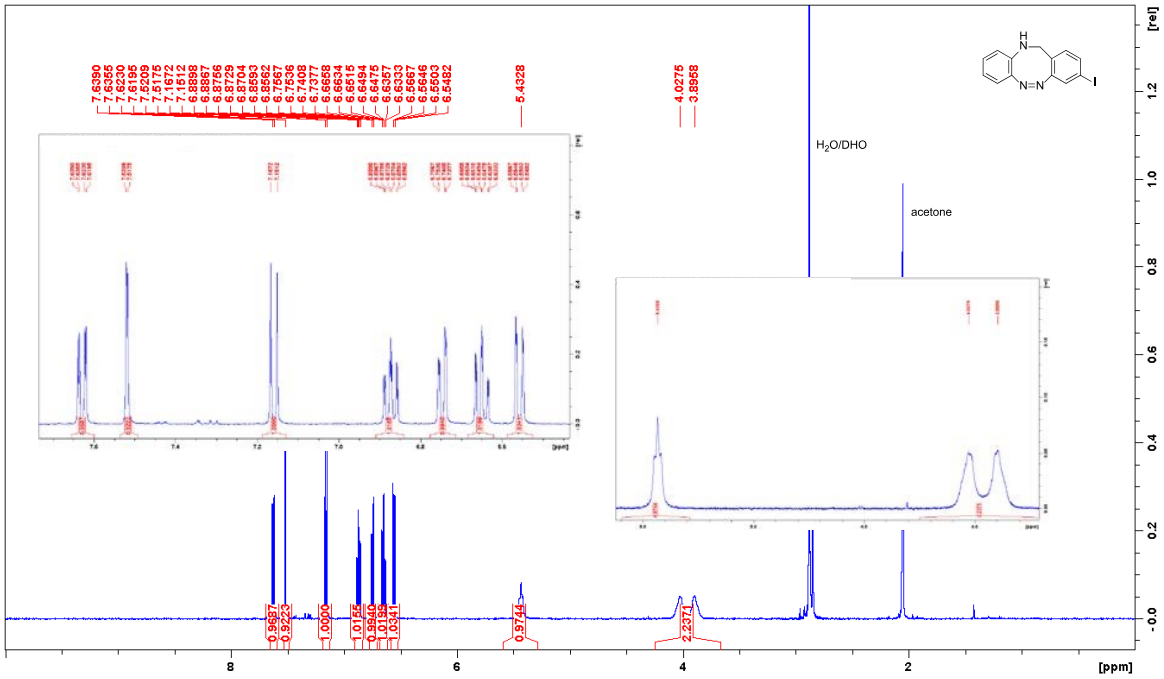

Figure S32: ^{1}H NMR spectrum of compound **9b**.

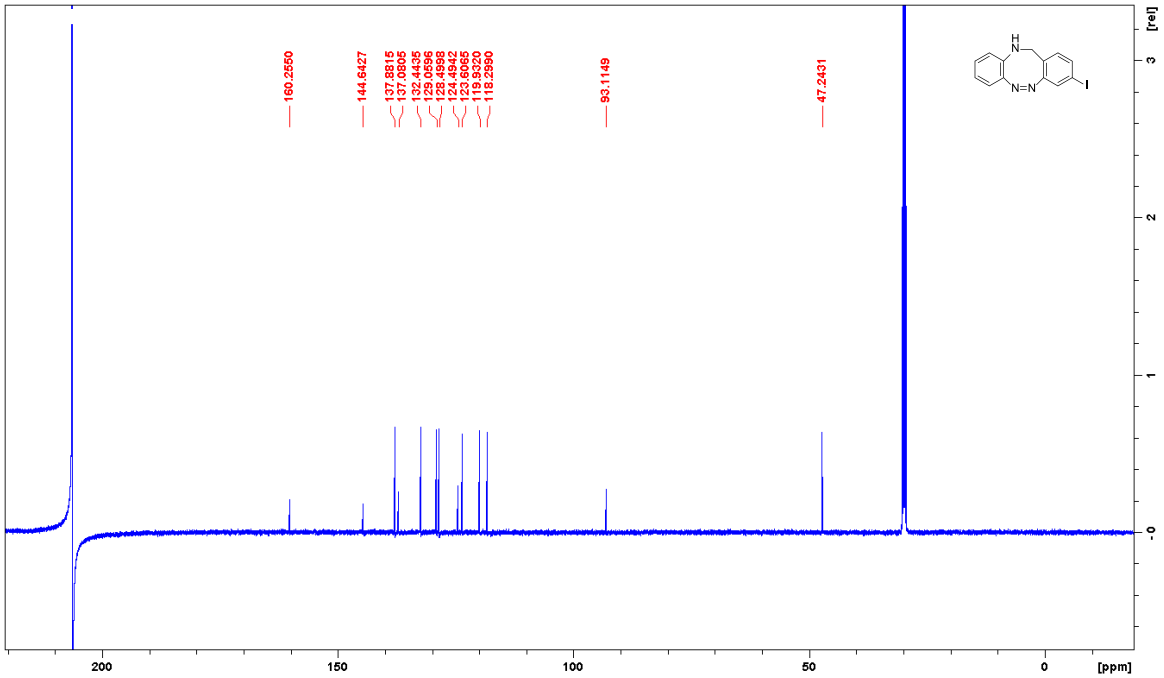

Figure S33: ^{13}C NMR spectrum of compound **9b**.

II.18 Synthesis of (*Z*)-3-iododibenzo[*c*,*g*][1,2,5]triazocine-11(12*H*)-carbaldehyde (11b)

Under a nitrogen atmosphere, a solution of (*Z*)-3-iodo-11,12-dihydrodibenzo[*c*,*g*][1,2,5]triazocine (**9b**, 50.0 mg, 149 µmol) in anhydrous MeCN (5 mL) was prepared, and then DIPEA (260 µL, 1.49 mmol) and chloral (146 µL, 1.49 mmol) were added. The reaction mixture was stirred at rt for 22 h. The solvent

was removed and flash column chromatography on silica (0.040–0.063 mm, ethyl acetate/cyclohexane 1:2, R_f = 0.20) gave a pale yellow solid (**11b**, 28 mg, 77.1 µmol, 52%).

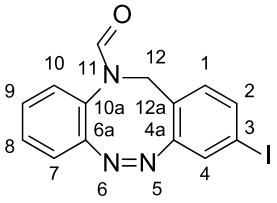

melting point: 208.9 °C

^{1}H NMR (500 MHz, acetone-d_6, 298 K): δ = 8.35 (s, 1 H, C*H*O), 7.58 (dd, ^3J = 8.0 Hz, ^4J = 1.7 Hz, 1 H, *H*-2), 7.41 (d, ^4J = 1.7 Hz, 1 H, *H*-4), 7.36 (td, ^3J = 7.7 Hz, ^4J = 1.3 Hz, 1 H, *H*-9), 7.26 (td, ^3J = 7.5 Hz, ^4J = 1.5 Hz, 1 H, *H*-8), 7.18 (dd, ^3J = 7.9 Hz, ^4J = 1.3 Hz, 1 H, *H*-7), 7.15 (d, ^3J = 8.0 Hz, 1 H, *H*-1), 6.96 (dd, ^3J = 7.8 Hz, ^4J = 1.4 Hz, 1 H, *H*-10), 4.50 (m_c, 2 H, CH_2) ppm.

^{13}C NMR (125 MHz, acetone-d_6, 298 K): δ = 162.37 (*C*=O), 158.26 (*C*-4a), 152.78 (*C*-6a), 137.80 (*C*-2), 133.25 (*C*-1), 129.44 (*C*-8), 129.28 (*C*-9), 128.28 (*C*-7), 128.19 (*C*-12a), 127.93 (*C*-4), 123.30 (*C*-10a), 120.54 (*C*-10), 94.57 (*C*-3), 49.12 (CH_2) ppm.

IR (ATR): $\tilde{\nu}$ = 3070 (w), 3045 (w), 2880 (w), 1935 (w), 1668 (s), 1538 (m), 1513 (w), 1475 (m), 1387 (w), 1358 (m), 1313 (s), 1277 (m), 1242 (m), 1209 (w), 1117 (m), 1038 (m), 1012 (w), 956 (m), 028 (w), 892 (w), 828 (s), 810 (s), 759 (s), 741 (m), 692 (m), 666 (m), 647 (w), 605 (w), 562 (s), 516 (m) cm^{-1}.

MS (ESI HR, $CHCl_3$/MeOH): *m/z* ($C_{14}H_{10}IN_3O+H^+$) = calc.: 363.99413, found: 363.99426 ± 0.36 ppm.

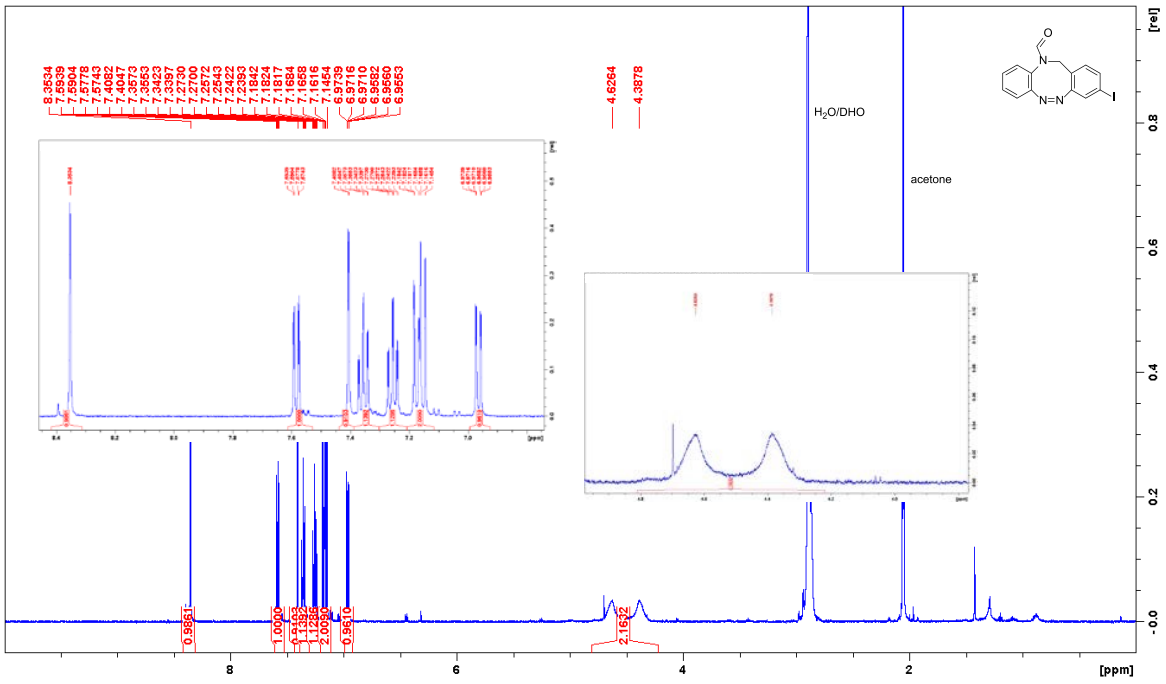

Figure S34: ^{1}H NMR spectrum of compound **11b**.

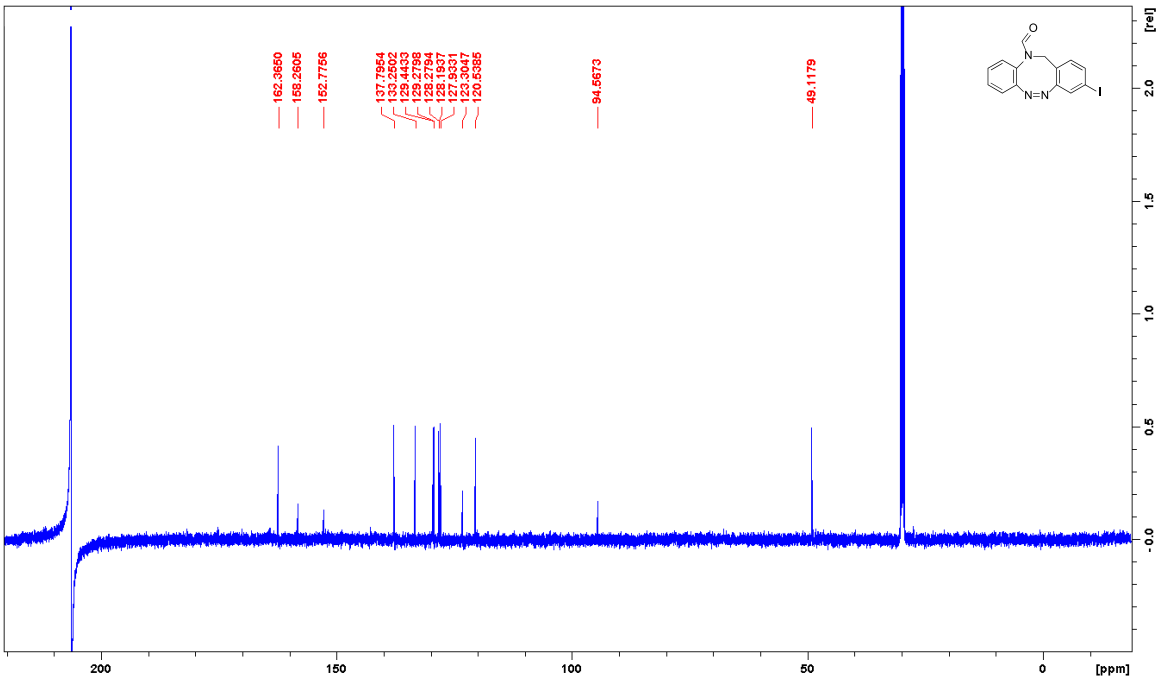

Figure S35: ^{13}C NMR spectrum of compound **11b**.

II.19 Synthesis of (*Z*)-1-(3-iododibenzo[*c*,*g*][1,2,5]triazocine-11(12*H*)-yl)ethan-1-one (10b)

Under a nitrogen atmosphere, a solution of (*Z*)-3-iodo-11,12-dihydrodibenzo[*c*,*g*][1,2,5]triazocine (**9b**, 100 mg, 298 µmol) in anhydrous DMF (5 mL) was prepared, and then TEA (832 µL, 20 equiv) and HOAcl (171 µL, 2.98 mmol) were added. The reaction mixture was cooled to 0 °C and T3P (1.78 mL, 2.98 mmol, 50% in ethyl acetate) was added dropwise. The ice bath was removed and it was stirred for 21 h. Then, 50 mL DCM and 50 mL deionized water were added and the organic layer was separated. It was extracted twice with DCM and the combined organic layers were dried over $MgSO_4$. The solvent was removed and flash column chromatography on silica (0.040–0.063 mm, ethyl acetate/cyclohexane 1:2, R_f = 0.13) gave a pale yellow solid (**10b**, 68 mg, 180 µmol, 60%).

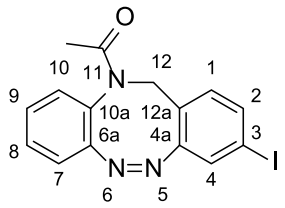

melting point: 170.0 °C

^{1}H NMR (500 MHz, acetone-d_6, 298 K): δ = 7.51 (dd, ^3J = 8.1 Hz, ^4J = 1.8 Hz, 1 H, *H*-2), 7.51 (td, ^3J = 7.4 Hz, ^4J = 1.8 Hz, 1 H, *H*-8/9), 7.34-7.26 (m, 3 H, *H*-4, Ar-*H*, Ar-*H*), 7.06 (dd, ^3J = 8.0 Hz, ^4J = 1.3 Hz, 1 H, *H*-7/10), 7.03 (d, ^3J = 8.1 Hz, 1 H, *H*-1), 5.03 (d, ^2J = 14.5 Hz, 1 H, CH_2a), 4.30 (d, ^2J = 14.9 Hz, 1 H, CH_2b), 1.79 (s, 3 H, CH_3) ppm.

^{13}C NMR (125 MHz, acetone-d_6, 298 K): δ = 169.50 (*C*=O), 157.09 (*C*-4a), 154.15 (*C*-6a/10a), 137.40 (*C*-2), 132.73 (*C*-1), 130.32 (*C*-7/10), 130.19 (Ar-*C*), 129.58 (Ar-*C*), 129.44 (*C*-6a/10a), 128.43 (*C*-4), 125.19 (*C*-12a), 120.05 (*C*-7/10), 93.56 (*C*-6a/10a), 51.65 (CH_2), ppm.

IR (ATR): $\tilde{\nu}$ = 3058 (w), 3012 (w), 2928 (w), 2251 (w), 1652 (s), 1583 (w), 1556 (w), 1513 (w), 1473 (m), 1434 (w), 1378 (s), 1336 (s), 1297 (m), 1250 (w), 1111 (m), 1084 (m), 1031 (m), 1009 (w), 971 (m), 917 (w), 842 (m), 824 (s), 768 (s), 691 (m), 653 (m), 598 (s), 582 (s), 534 (w), 515 (m) cm^{-1}.

MS (ESI HR, $CHCl_3$/MeOH): *m/z* ($C_{15}H_{12}IN_3O+H^+$) = calc.: 378.00978, found: 378.00937 ± 1.08 ppm.

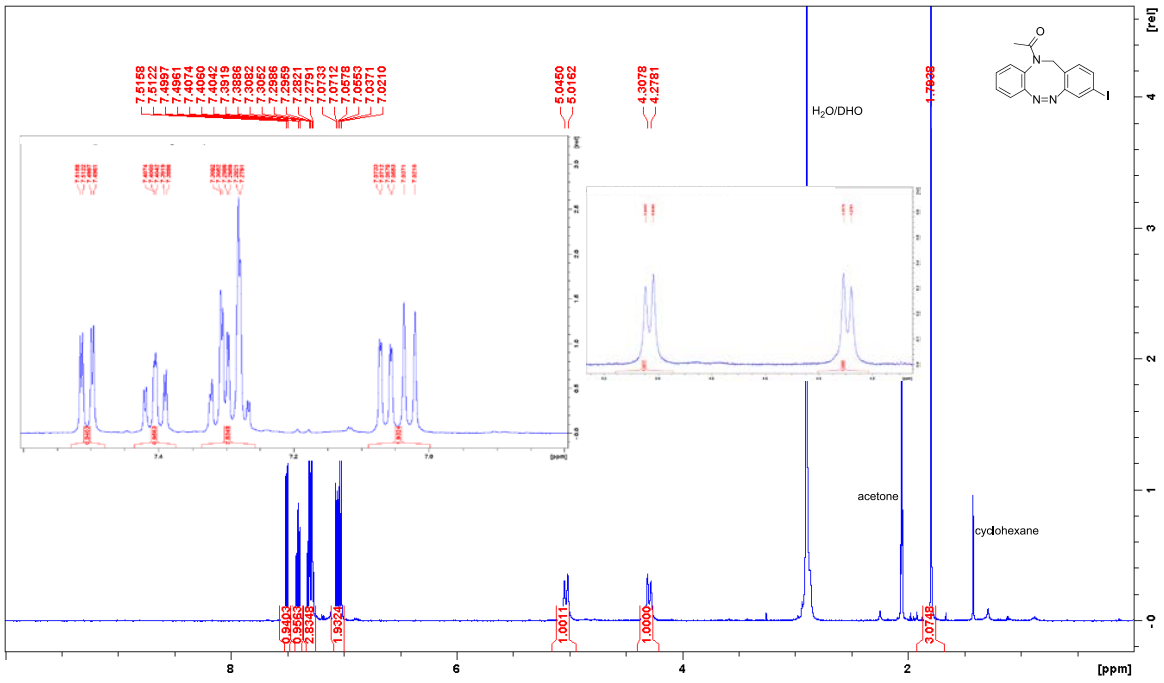

Figure S36: ^{1}H NMR spectrum of compound **10b**.

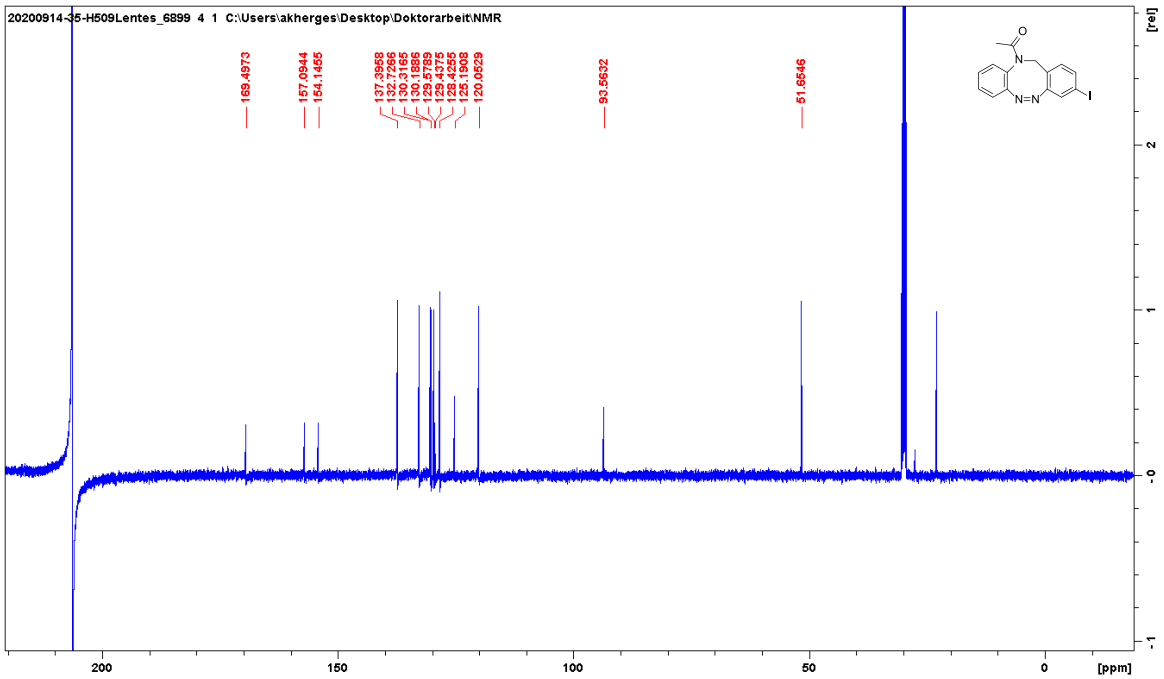

Figure S37: ^{13}C NMR spectrum of compound **10b**.

III. UV–vis switching experiments

All samples were irradiated to the photostationary state (PSS) with 400 nm in the given solvent or solvent mixture. The extrapolated UV–vis spectra of the *E* compounds were calculated from the UV–vis spectra of the PSS and the percentage of the *E* compounds which were measured by ^{1}H NMR (for details see SIV) by the following equation (1):

$$A_{E,\text{extrapol.}} = \left\{A_{PSS} - \left(A_Z \cdot \left[1 - \frac{100\%}{\%\text{PSS}}\right]\right)\right\} / \left(\frac{100\%}{\%\text{PSS}}\right) \quad (1)$$

The rate constants *k* of the thermal *E*→*Z* isomerization of all compounds were determined with first oder kinetic plots by the following equation (2):

$$A_t = A_0 \cdot e^{-kt} \quad (2)$$

Half-lifes ($t_{1/2}$) were calculated with equation 3:

$$t_{1/2} = \frac{\ln(2)}{k} \quad (3)$$

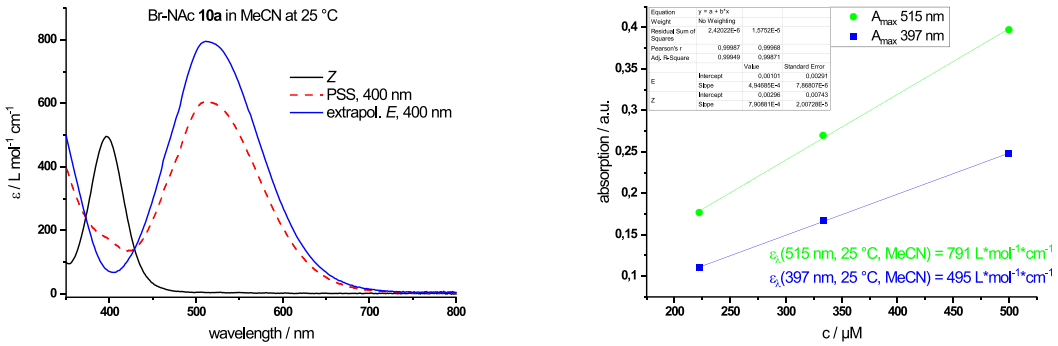

Figure S38: UV–vis spectra of Br-NAc-diazocine **10a** in MeCN at 25 °C before (black) and after irradiation with 400 nm (dashed red). The extrapolated *E* spectrum is given in blue (left) and molar extinction coefficient (ε) determination of the maxiumum absorption (λ_{max}) of the $n\pi^*$-transitions of the *E* (green) and *Z* (blue) isomers (right).

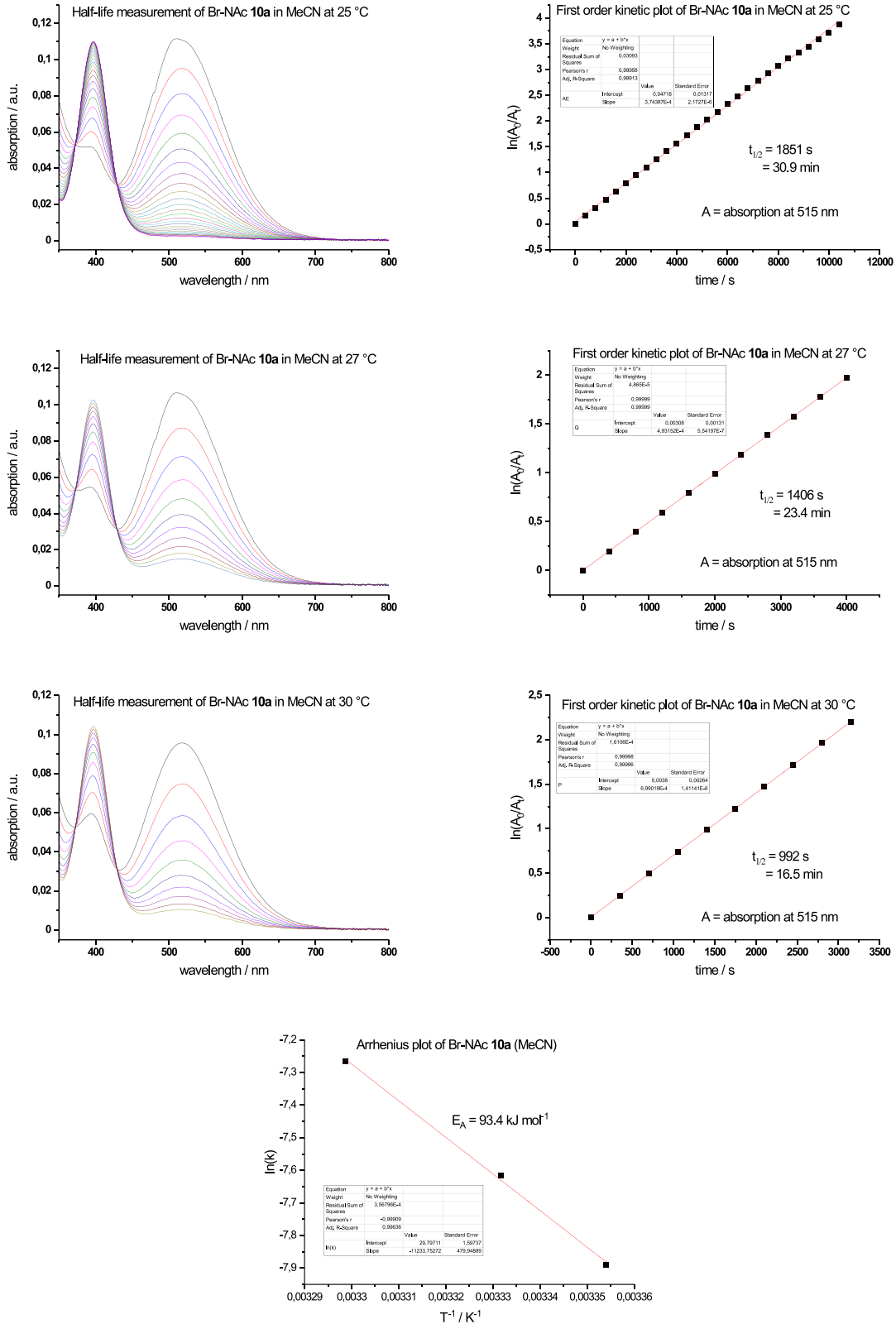

Figure S39: UV–vis spectra of the half-life determination of Br-NAc-diazocine **10a** in MeCN at different temperatures (left) with corresponding first order kinetic plots (right) and Arrhenius plot (bottom).

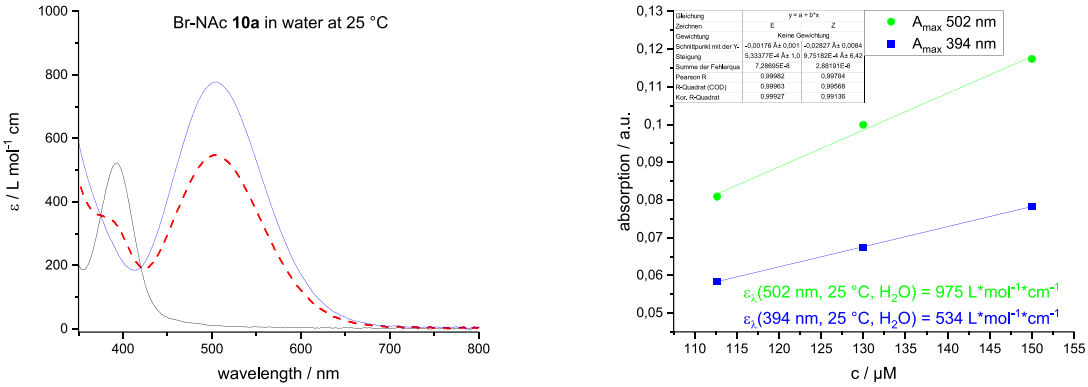

Figure S40: UV–vis spectra of Br-NAc-diazocine **10a** in water at 25 °C before (black) and after irradiation with 400 nm (dashed red). The extrapolated *E* spectrum is given in blue (left) and molar extinction coefficient (ε) determination of the maxiumum absorption (λ_{max}) of the $n\pi^*$-transitions of the *E* (green) and *Z* (blue) isomers (right).

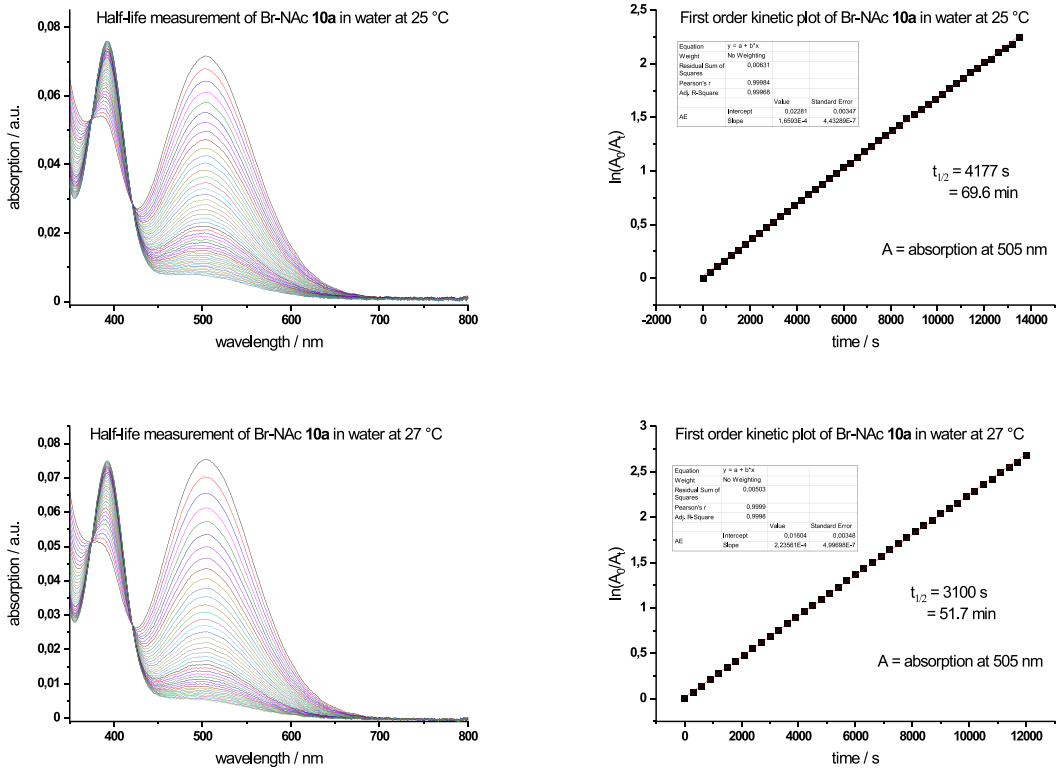

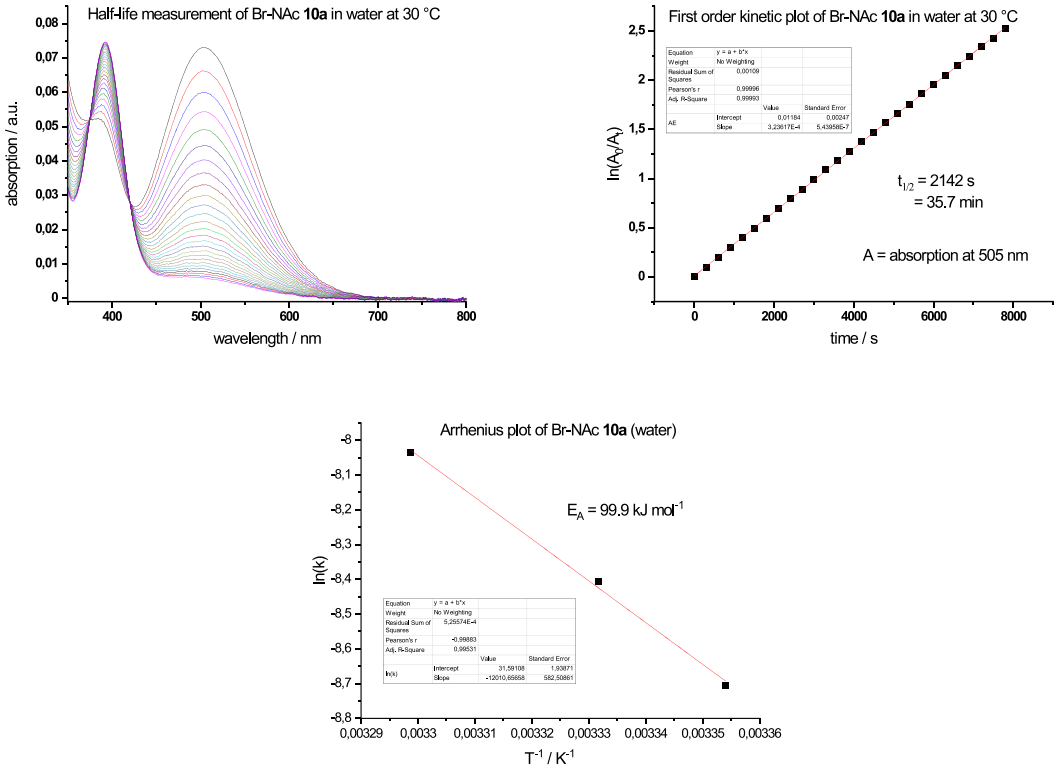

Figure S41: UV–vis spectra of the half-life determination of Br-NAc-diazocine **10a** in water at different temperatures (left) with corresponding first order kinetic plots (right) and Arrhenius plot (bottom).

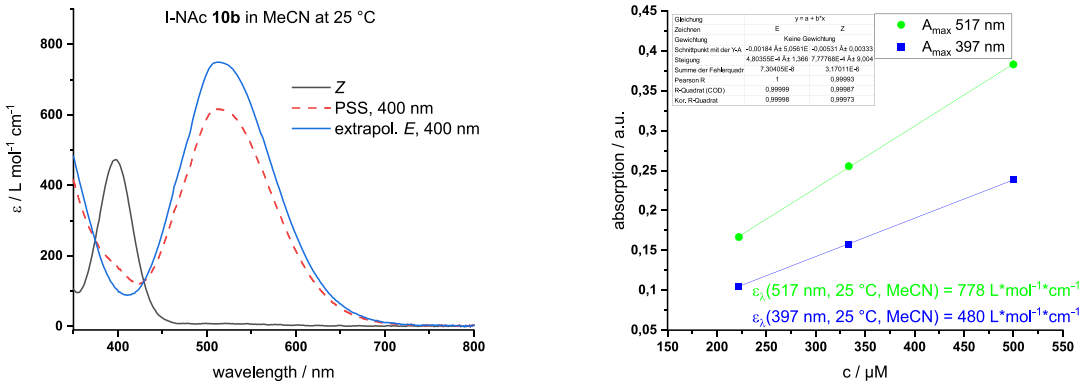

Figure S42: UV–vis spectra of I-NAc-diazocine **10b** in MeCN at 25 °C before (black) and after irradiation with 400 nm (dashed red). The extrapolated *E* spectrum is given in blue (left) and molar extinction coefficient (ε) determination of the maxiumum absorption (λ_{max}) of the $n\pi^*$-transitions of the *E* (green) and *Z* (blue) isomers (right).

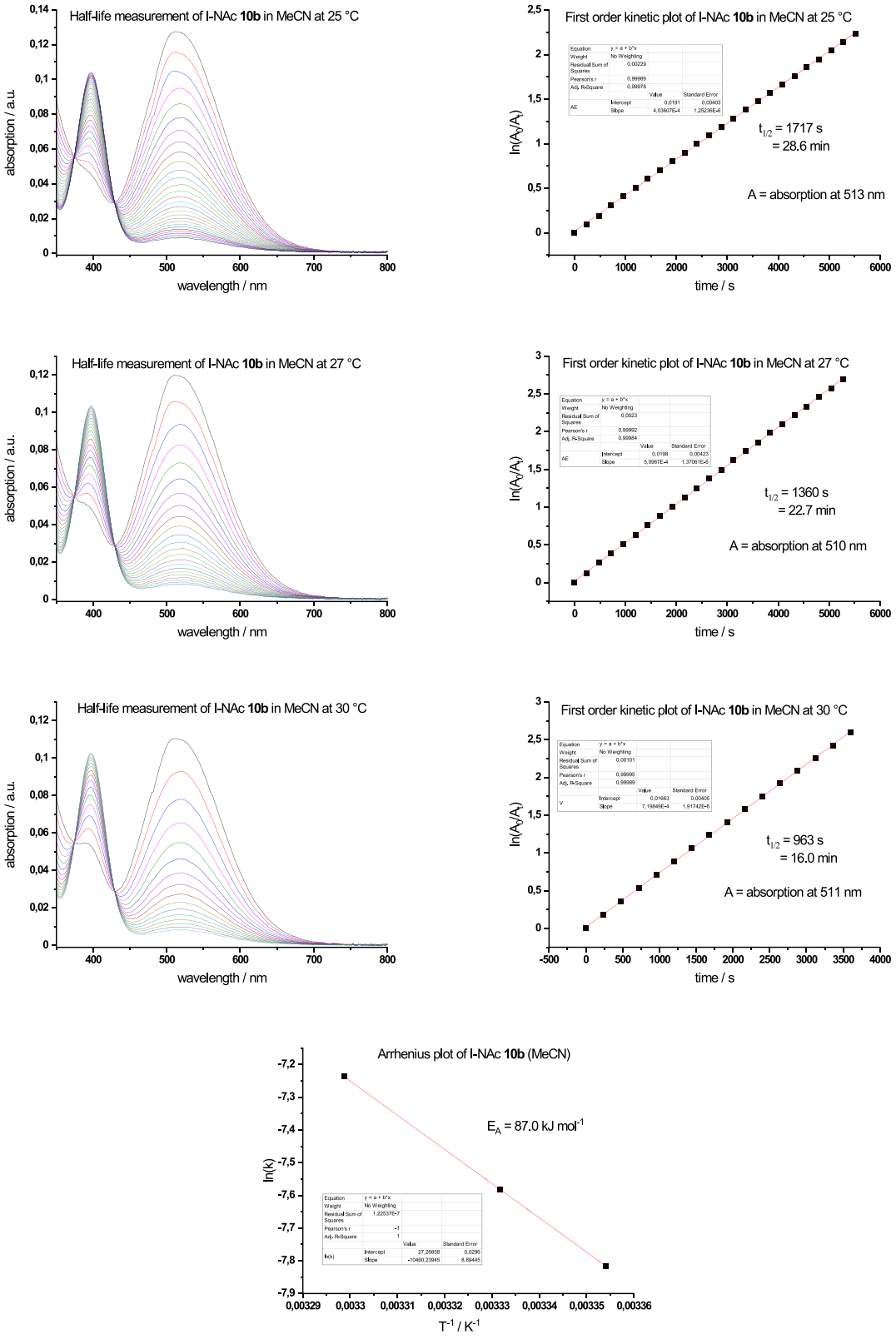

Figure S43: UV–vis spectra of the half-life determination of I-NAc-diazocine **10b** in MeCN at different temperatures (left) with corresponding first order kinetic plots (right) and Arrhenius plot (bottom).

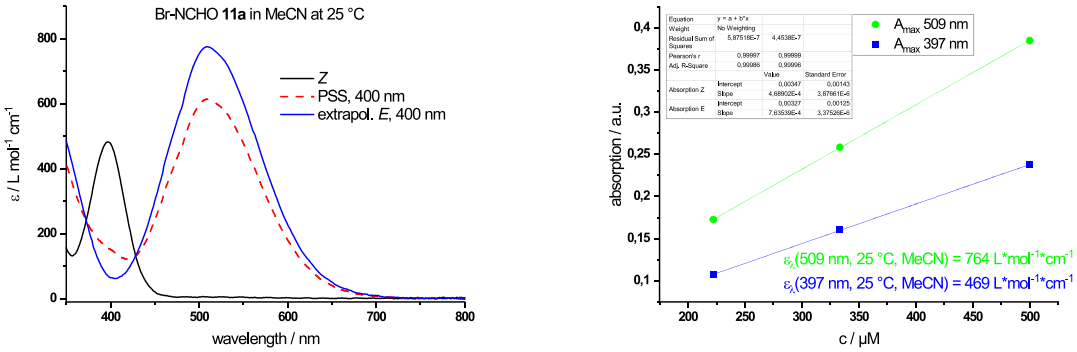

Figure S44: UV–vis spectra of Br-NCHO-diazocine **11a** in MeCN at 25 °C before (black) and after irradiation with 400 nm (dashed red). The extrapolated *E* spectrum is given in blue (left) and molar extinction coefficient (ε) determination of the maxiumum absorption (λ_{max}) of the $n\pi^*$-transitions of the *E* (green) and *Z* (blue) isomers (right).

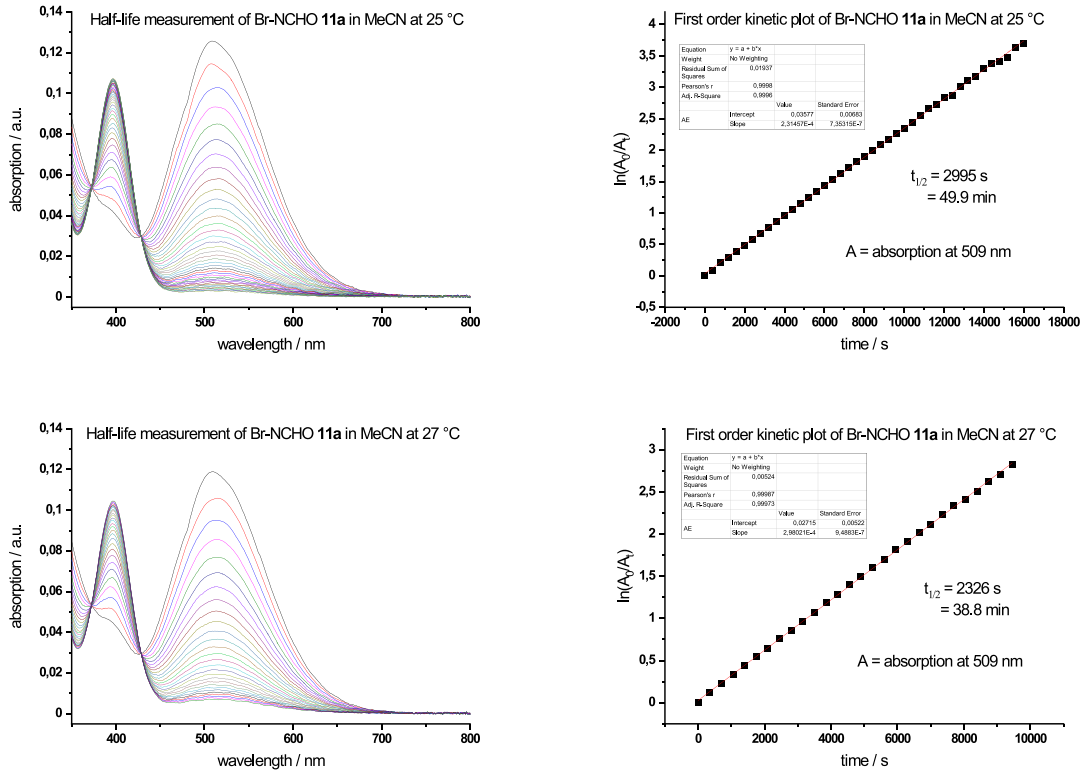

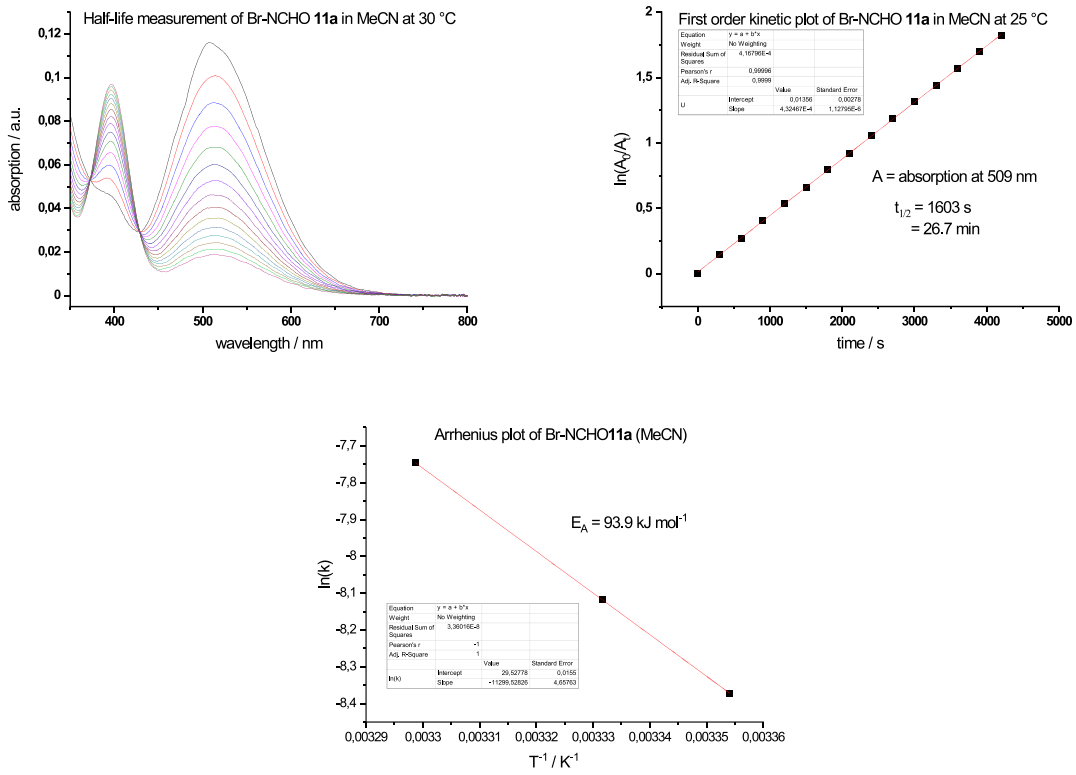

Figure S45: UV–vis spectra of the half-life determination of Br-NCHO-diazocine **11a** in MeCN at different temperatures (left) with corresponding first order kinetic plots (right) and Arrhenius plot (bottom).

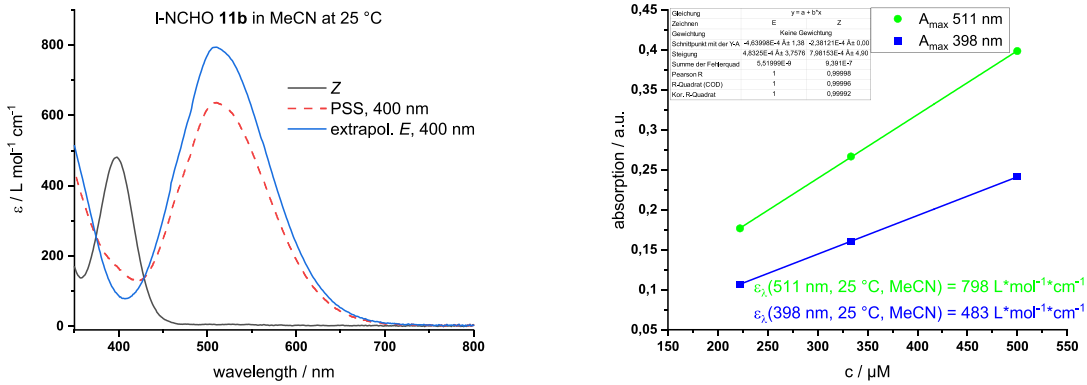

Figure S46: UV–vis spectra of I-NCHO-diazocine **11b** in MeCN at 25 °C before (black) and after irradiation with 400 nm (dashed red). The extrapolated *E* spectrum is given in blue (left) and molar extinction coefficient (ε) determination of the maxiumum absorption (λ_{max}) of the $n\pi^*$-transitions of the *E* (green) and *Z* (blue) isomers (right).

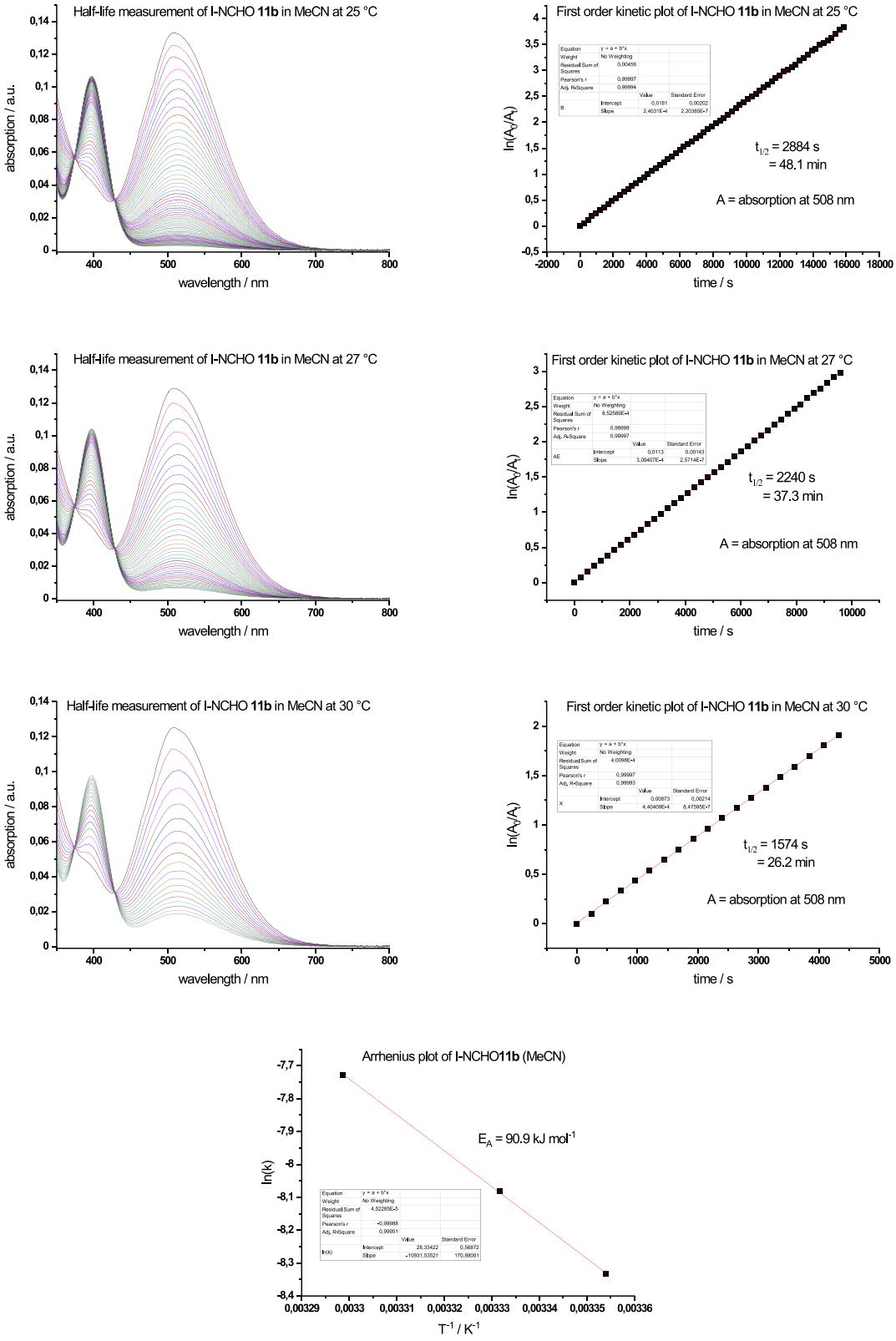

Figure S47: UV–vis spectra of the half-life determination of I-NCHO-diazocine **11b** in MeCN at different temperatures (left) with corresponding first order kinetic plots (right) and Arrhenius plot (bottom).

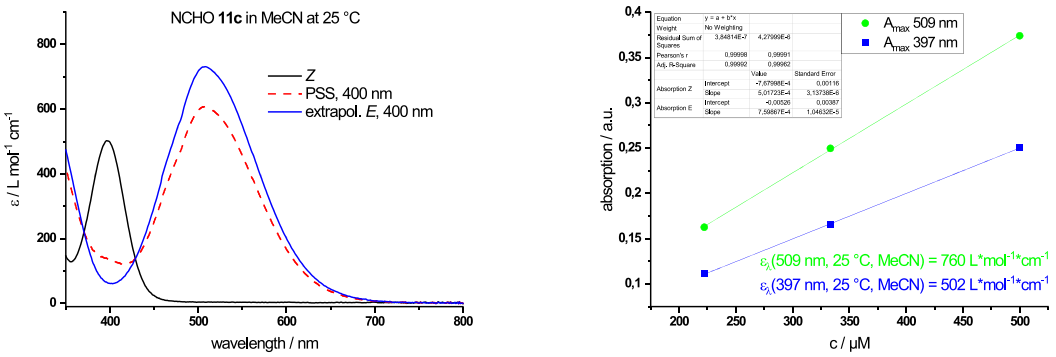

Figure S48: UV–vis spectra of NCHO-diazocine **11c** in MeCN at 25 °C before (black) and after irradiation with 400 nm (dashed red). The extrapolated *E* spectrum is given in blue (left) and molar extinction coefficient (ε) determination of the maxiumum absorption (λ_{max}) of the $n\pi^*$-transitions of the *E* (green) and *Z* (blue) isomers (right).

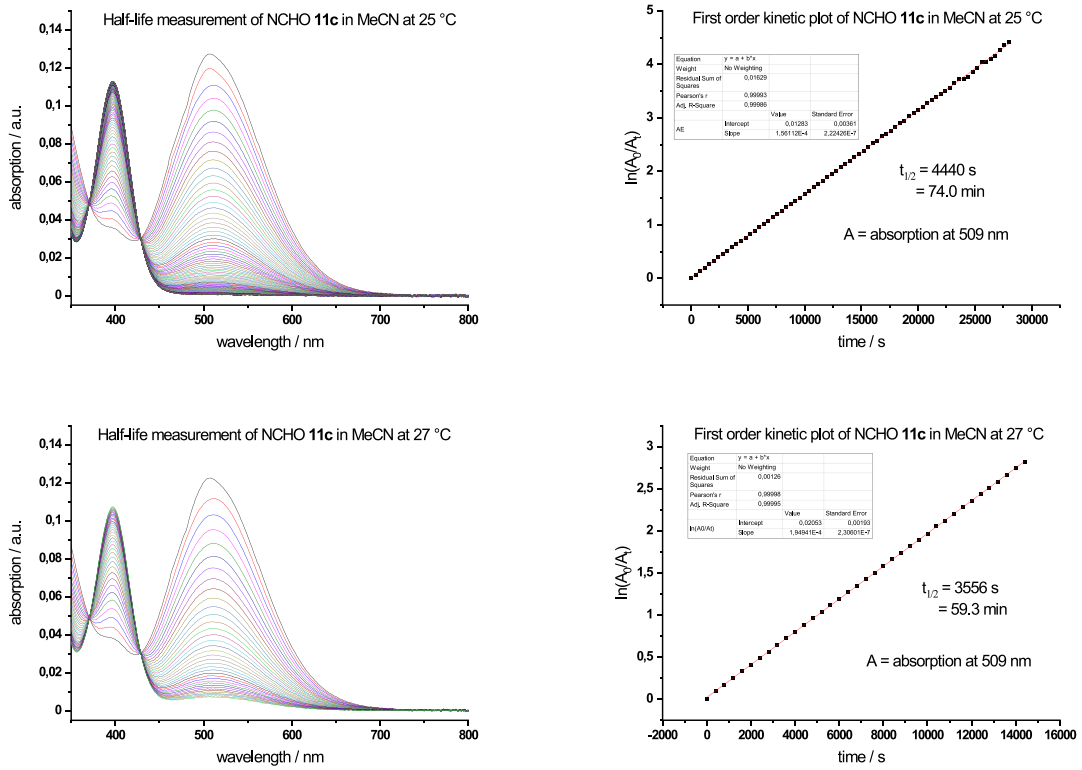

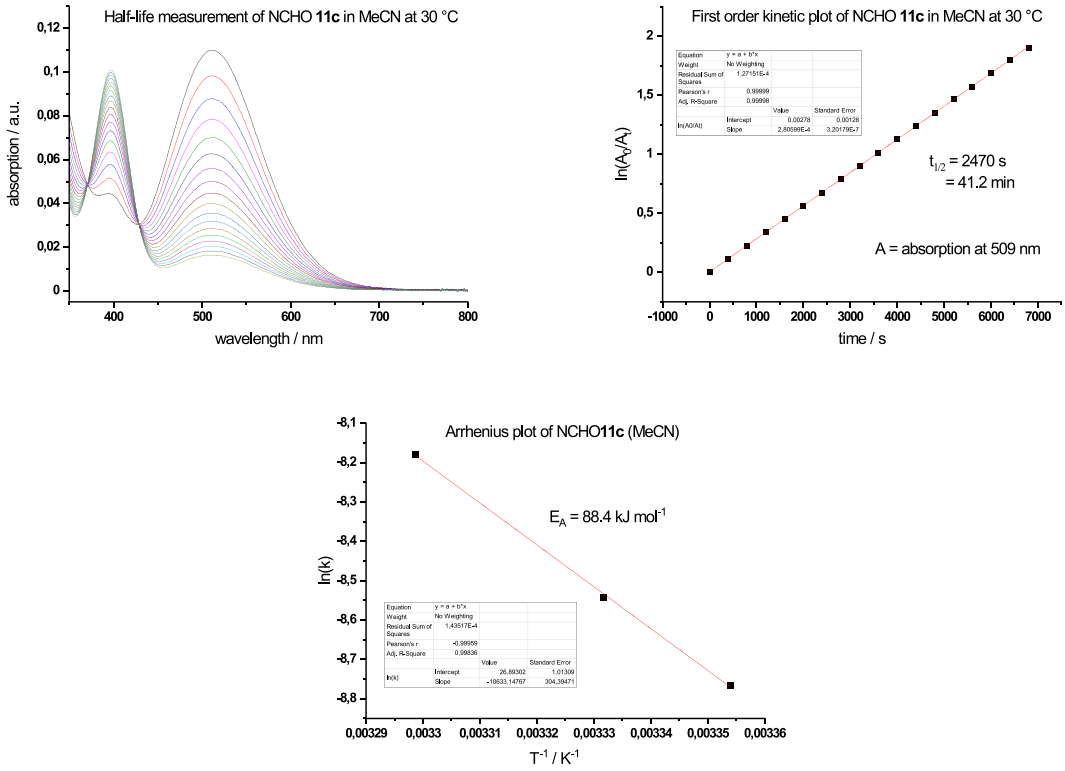

Figure S49: UV–vis spectra of the half-life determination of NCHO-diazocine **11c** in MeCN at different temperatures (left) with corresponding first order kinetic plots (right) and Arrhenius plot (bottom).

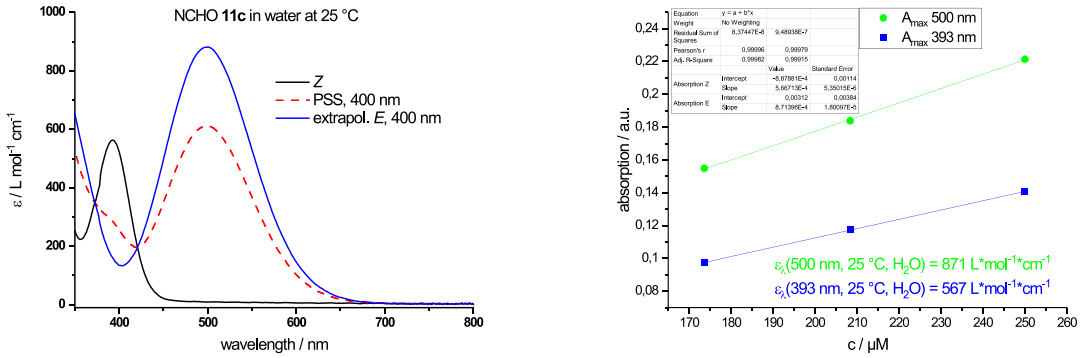

Figure S50: UV–vis spectra of NCHO-diazocine **11c** in water at 25 °C before (black) and after irradiation with 400 nm (dashed red). The extrapolated *E* spectrum is given in blue (left) and molar extinction coefficient (ε) determination of the maxiumum absorption (λ_{max}) of the $n\pi^*$-transitions of the *E* (green) and *Z* (blue) isomers (right).

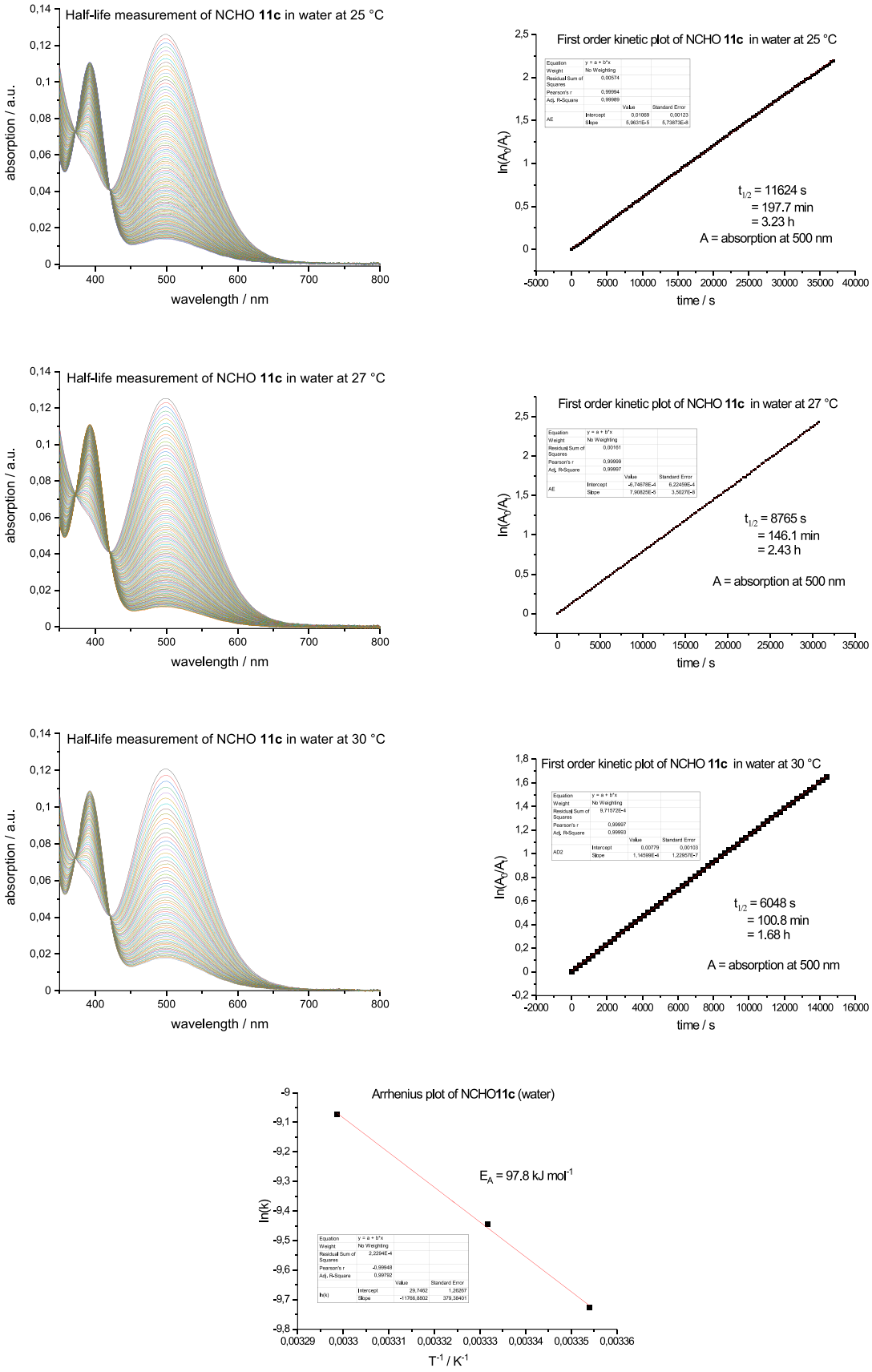

Figure S51: UV–vis spectra of the half-life determination of NCHO-diazocine **11c** in water at different temperatures (left) with corresponding first order kinetic plots (right) and Arrhenius plot (bottom).

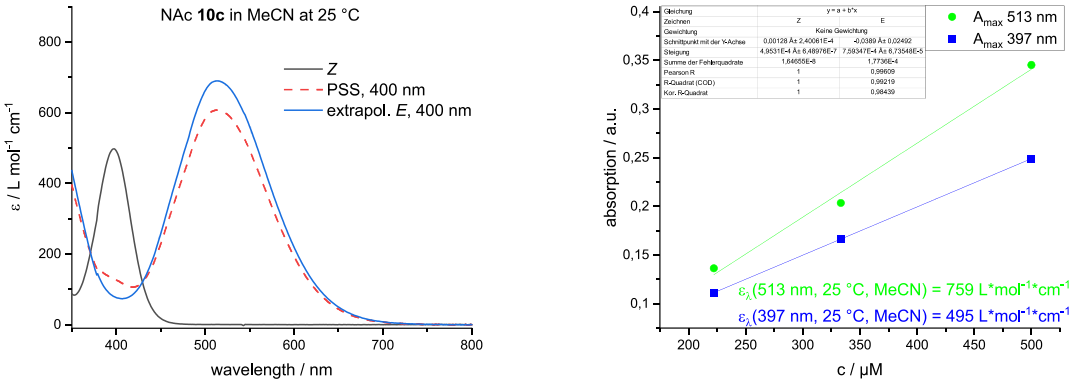

Figure S52: UV–vis spectra of NAc-diazocine **10c** in MeCN at 25 °C before (black) and after irradiation with 400 nm (dashed red). The extrapolated *E* spectrum is given in blue (left) and molar extinction coefficient (ε) determination of the maxiumum absorption (λ_{max}) of the $n\pi^*$-transitions of the *E* (green) and *Z* (blue) isomers (right).

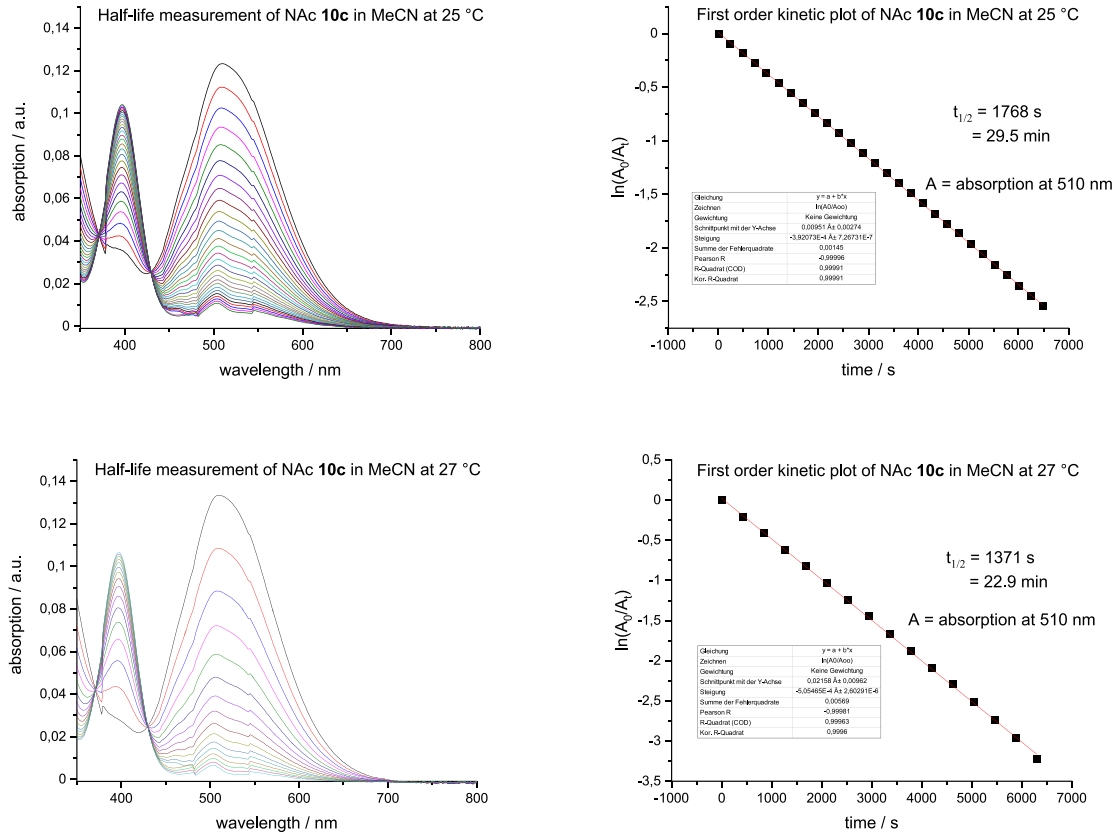

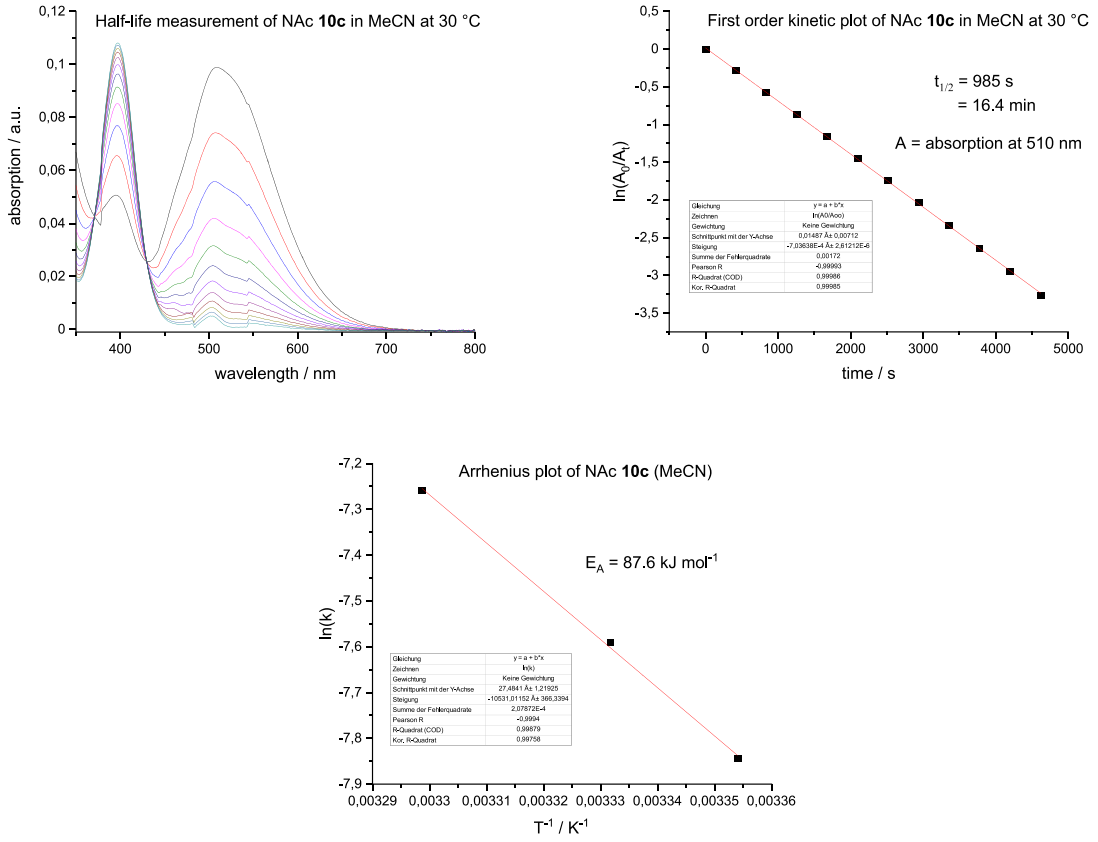

Figure S53: UV–vis spectra of the half-life determination of NAc-diazocine **10c** in MeCN at different temperatures (left) with corresponding first order kinetic plots (right) and Arrhenius plot (bottom).

IV. ^{1}H NMR switching experiments

Photostationary states (PSS) of compounds **10** and **11** were measured via ^{1}H NMR by integration of the different species after irradiation with 400 nm. The value of the integrals and the extrapolated values is given in Table S1. ^{1}H NMR und UV–vis spectra (SIII) were measured at 250 µM concentrations, except of Br-NCHO diazocine **11a** (150 µM due to solubility limit). The following equation was used for extrapolation of the photostationary states:

$$PSS_{\text{extrapol.}} = \text{PSS} \cdot e^{kt} \quad (2)$$

k is the rate constant at 25 °C (see SIII) and *t* the measuring time (180 s): 60 s preparation (transfer into the spectrometer and shimming) and ~120 s measuring time for 32 scans. All spectra were measured at a Bruker AV 600 spectrometer.

Table S1: Measured and extrapolated photostationary states of compounds **10** and **11** in MeCN and water.

	CD_3CN		D_2O	
	measured PSS / %	extrapolated PSS / %	measured PSS / %	extrapolated PSS / %
Br-NAc **10a**	76	81	68	70
I-NAc **10b**	76	82	-	-
NCHO **11c**	83	85	68	69
Br-NCHO **11a**	79	82	-	-
I-NCHO **11b**	77	80	-	-
NAc **10c**	82	88	-	-

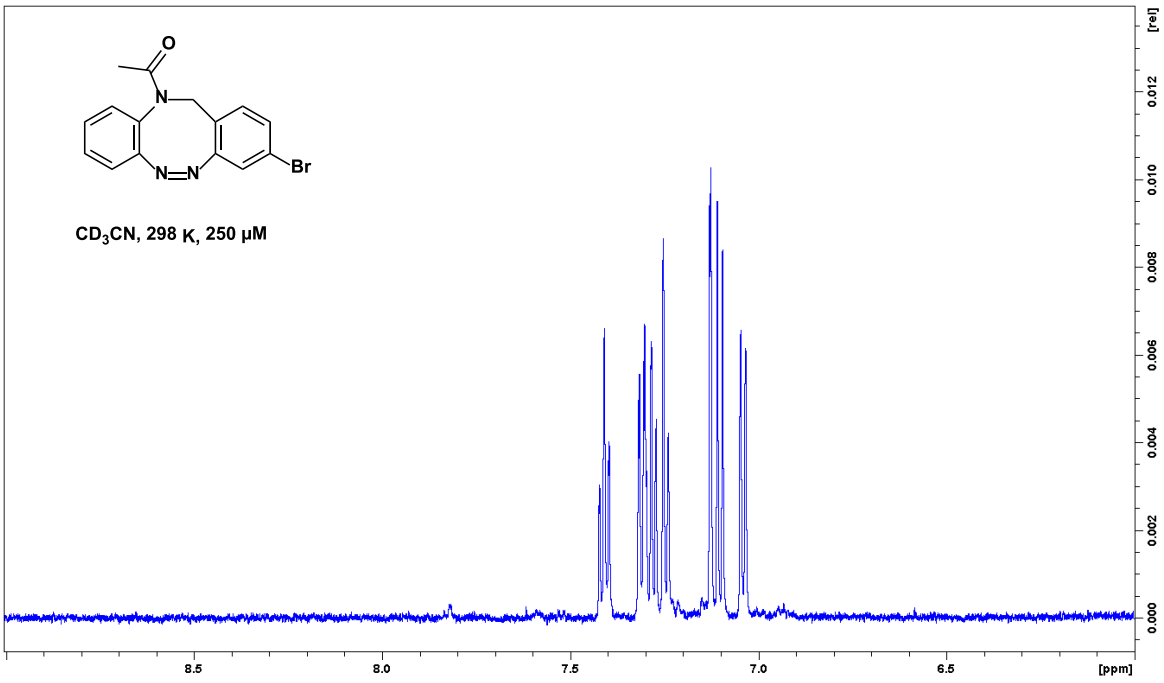

Figure S54: ^1H NMR spectrum (aromatic region) of Br-NAc diazocine **10a** in CD_3CN at 298 K.

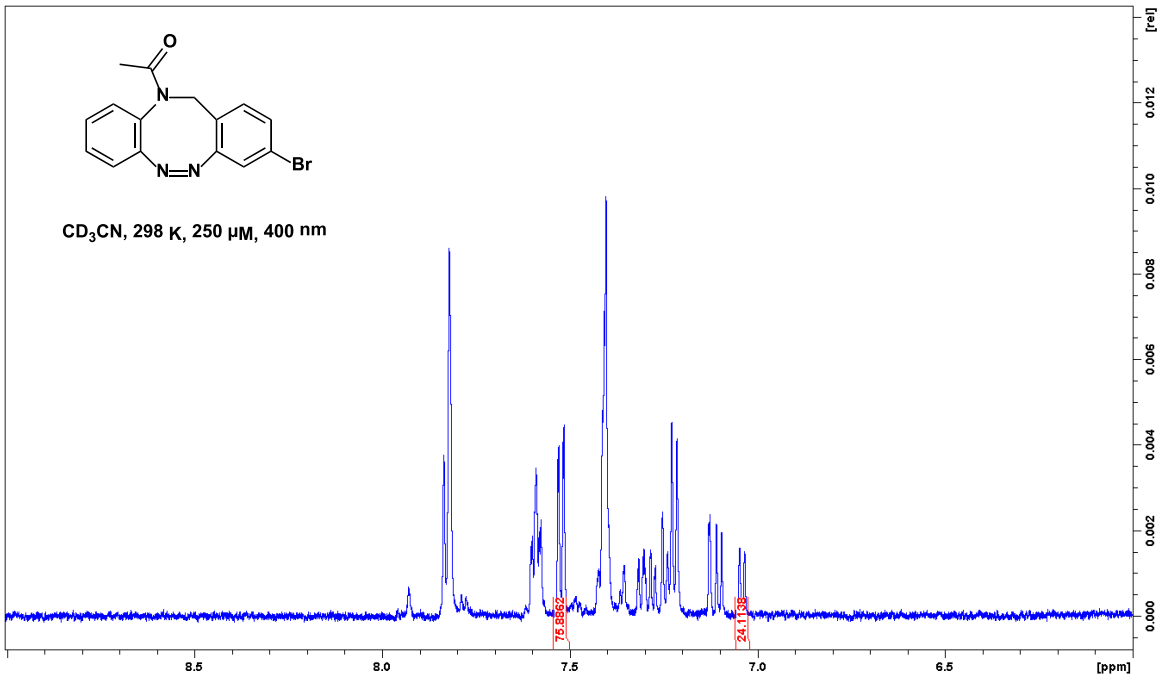

Figure S55: ^{1}H NMR spectrum (aromatic region) of Br-NAc diazocine **10a** in CD_3CN at 298 K after irradiation with 400 nm.

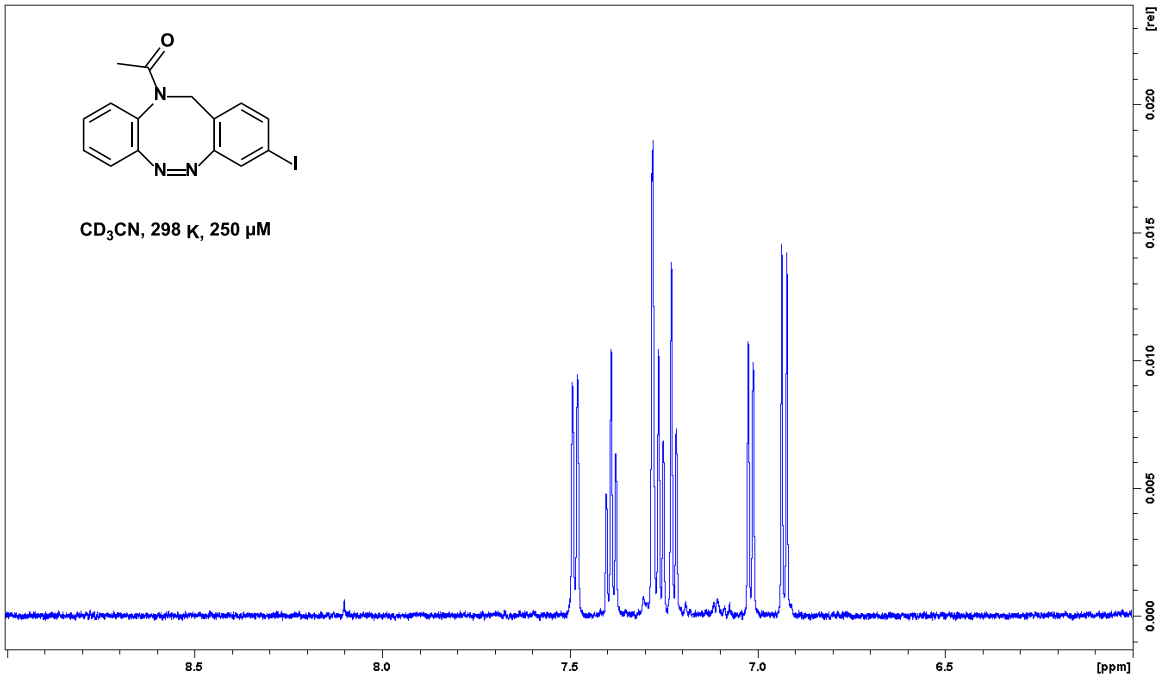

Figure S56: ^{1}H NMR spectrum (aromatic region) of I-NAc diazocine **10b** in CD_3CN at 298 K.

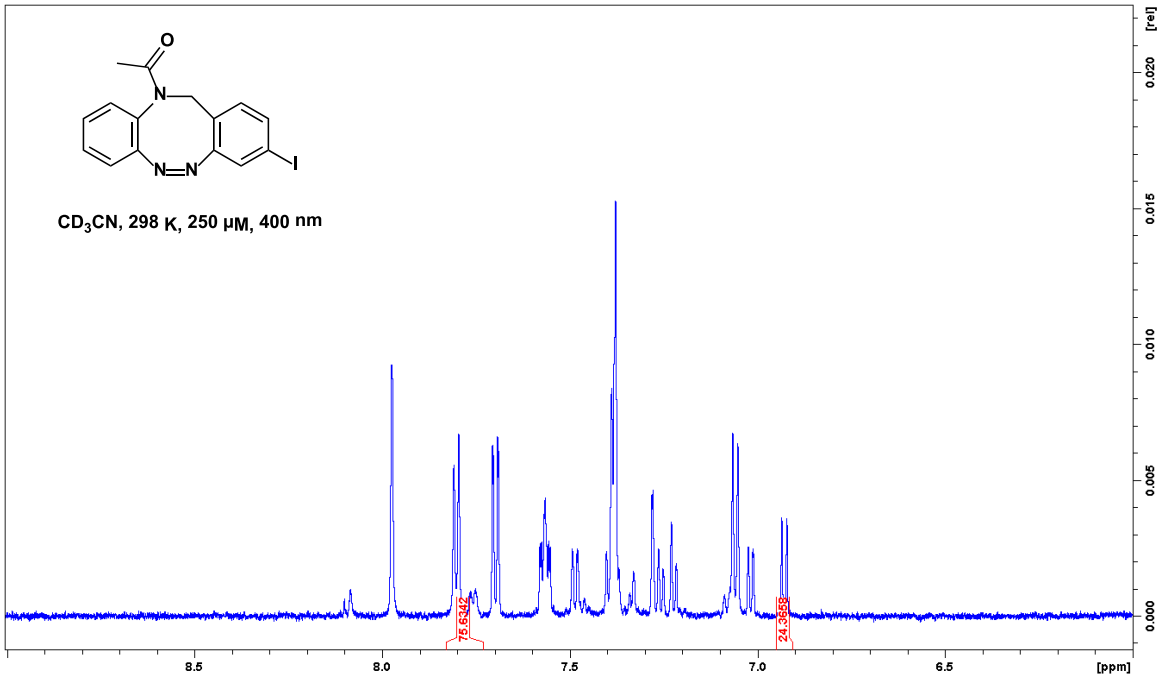

Figure S57: ^{1}H NMR spectrum (aromatic region) of **I-NAc** diazocine **10b** in CD_3CN at 298 K after irradiation with 400 nm.

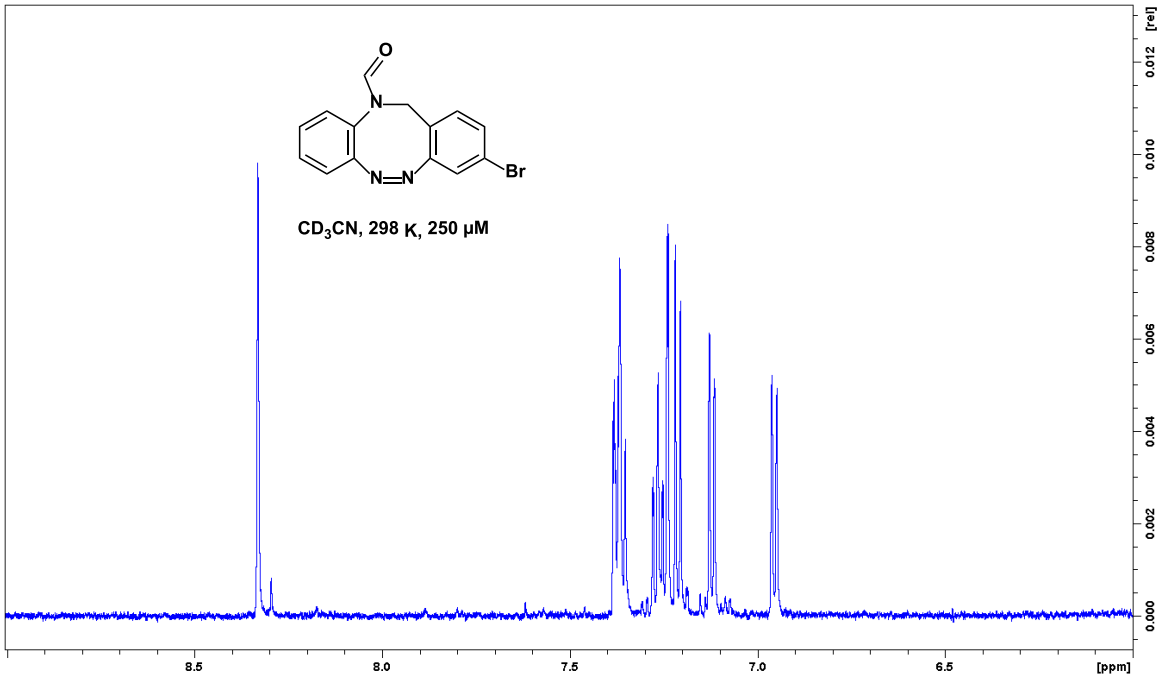

Figure S58: ^{1}H NMR spectrum (aromatic region) of Br-NCHO diazocine **11a** in CD_3CN at 298 K.

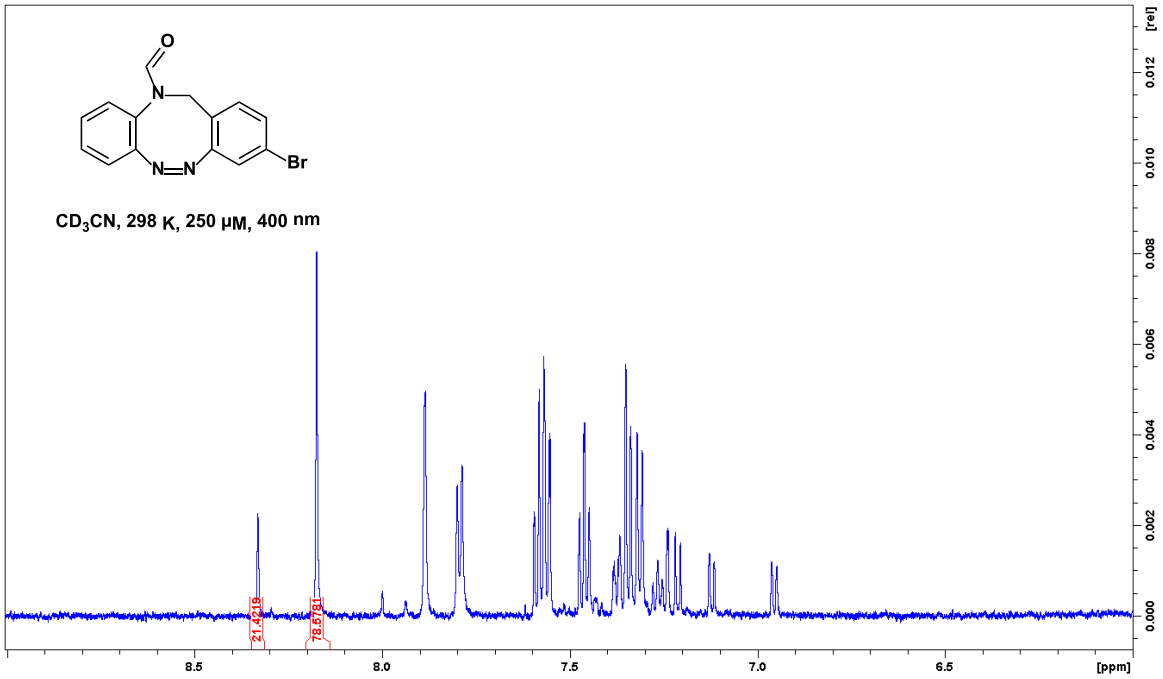

Figure S59: ^{1}H NMR spectrum (aromatic region) of Br-NCHO diazocine **11a** in CD_3CN at 298 K after irradiation with 400 nm.

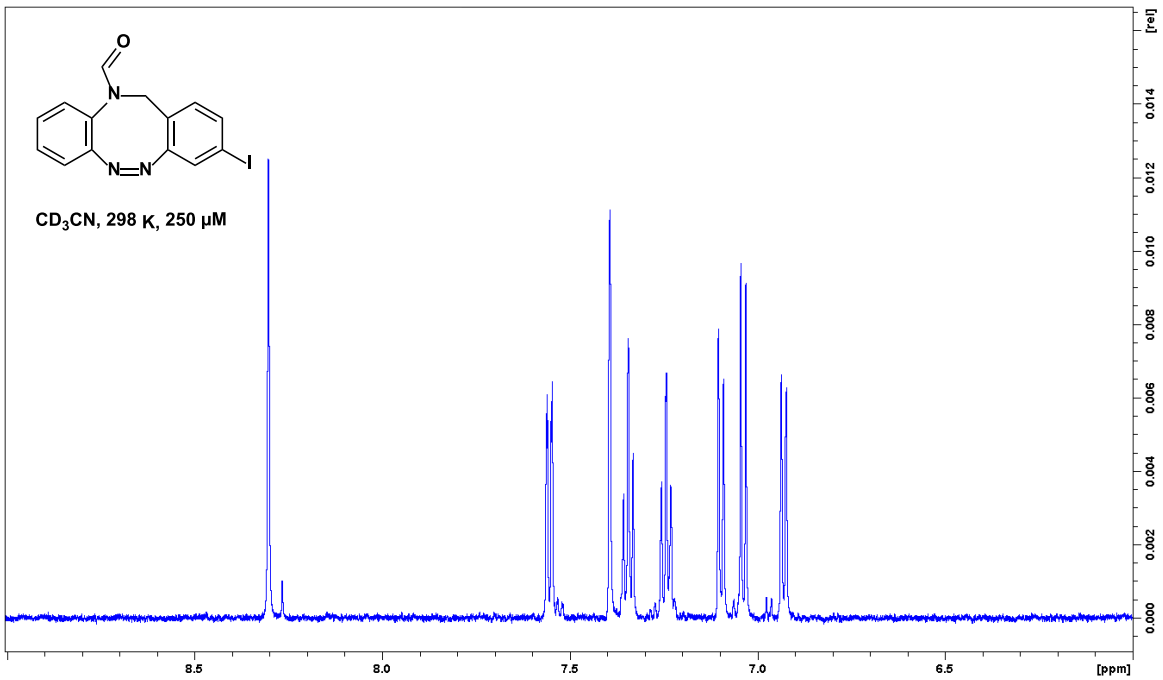

Figure S60: ^{1}H NMR spectrum (aromatic region) of I-NCHO diazocine **11b** in CD_3CN at 298 K.

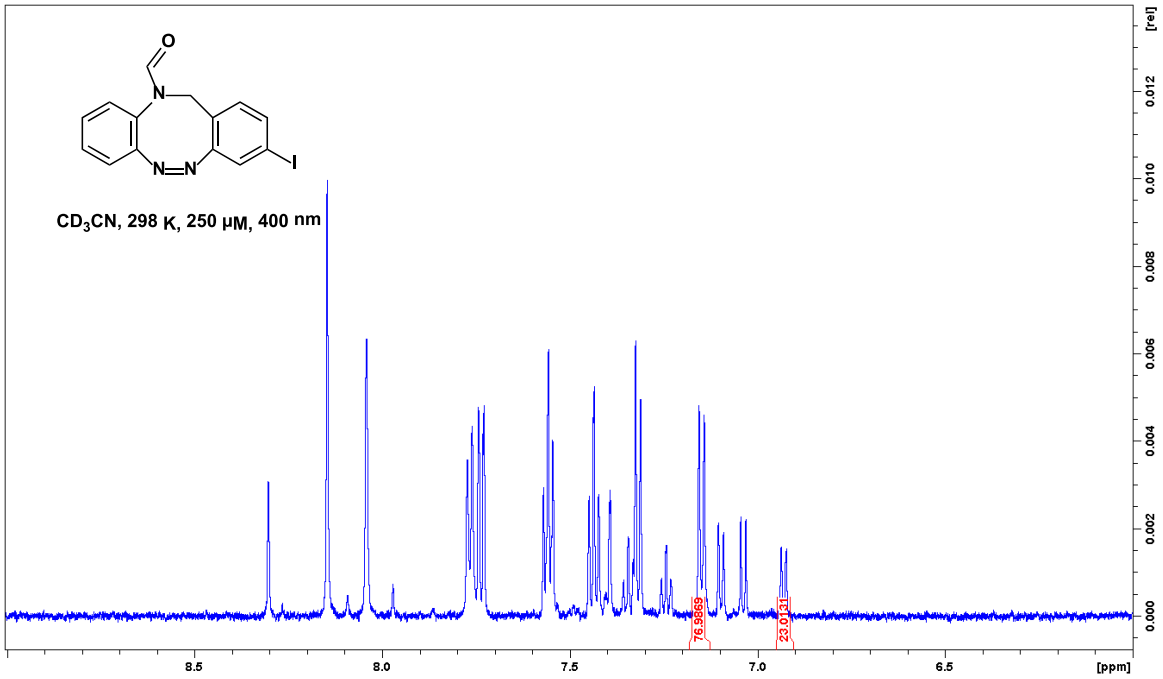

Figure S61: ^{1}H NMR spectrum (aromatic region) of **I-**NCHO diazocine **11b** in CD_3CN at 298 K after irradiation with 400 nm.

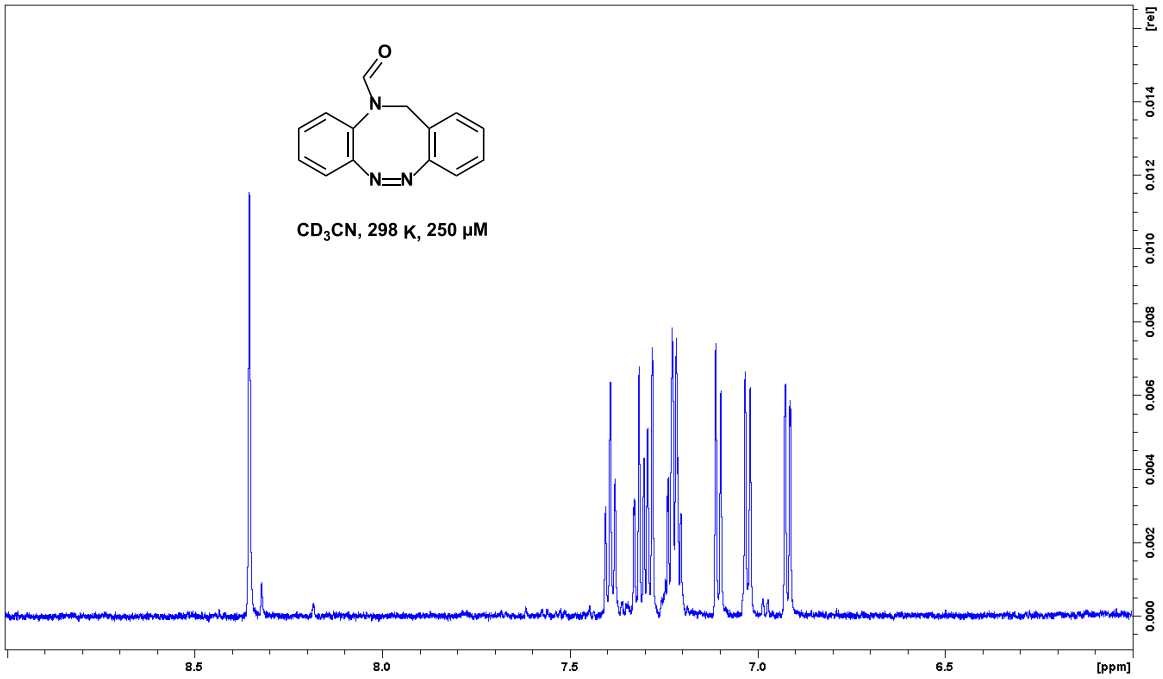

Figure S62: ^{1}H NMR spectrum (aromatic region) of NCHO diazocine **11c** in CD_3CN at 298 K.

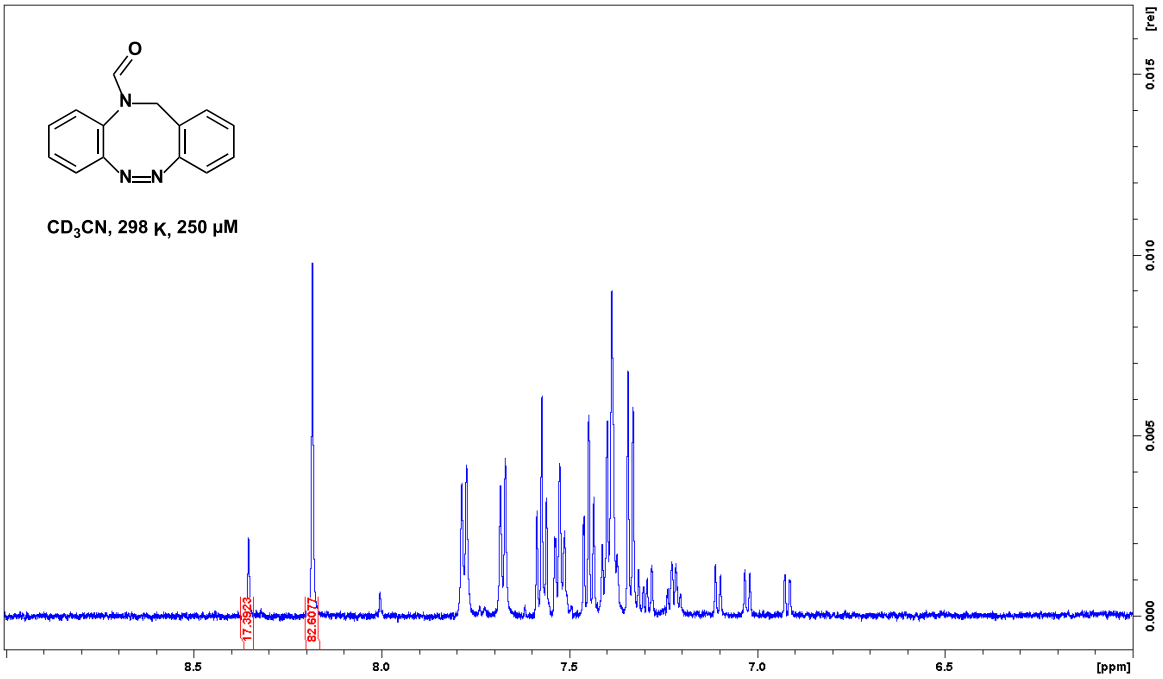

Figure S63: ^{1}H NMR spectrum (aromatic region) of NCHO diazocine **11c** in CD_3CN at 298 K after irradiation with 400 nm.

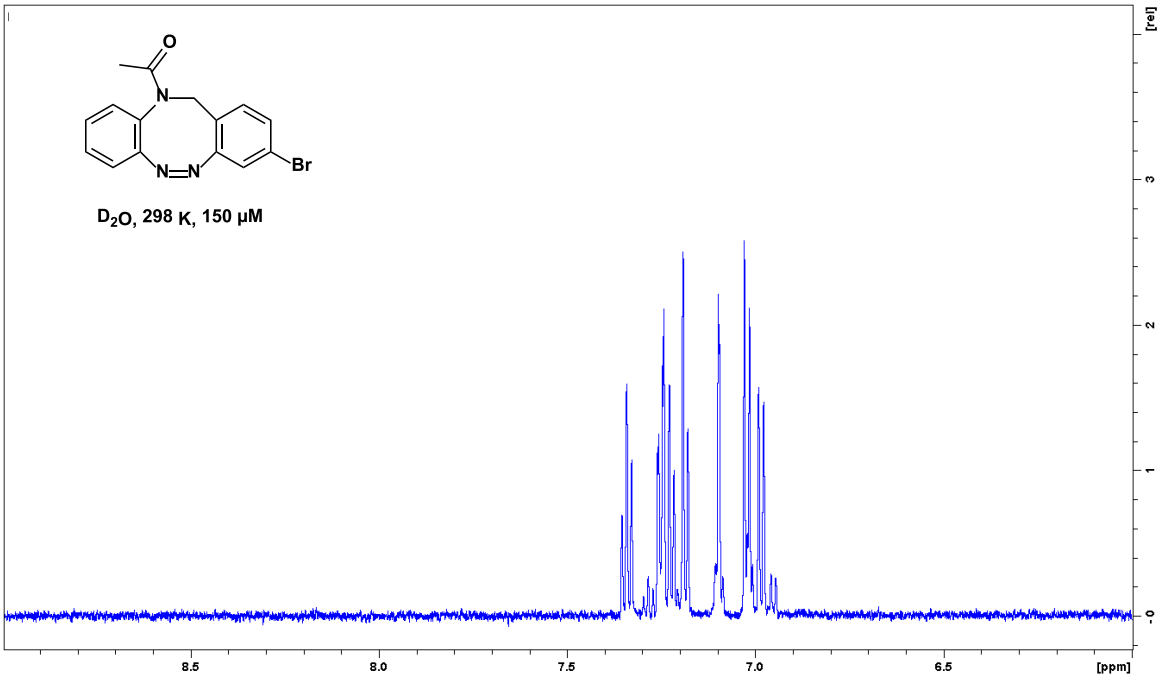

Figure S64: ^{1}H NMR spectrum (aromatic region) of Br-NAc diazocine **10a** in D_2O at 298 K.

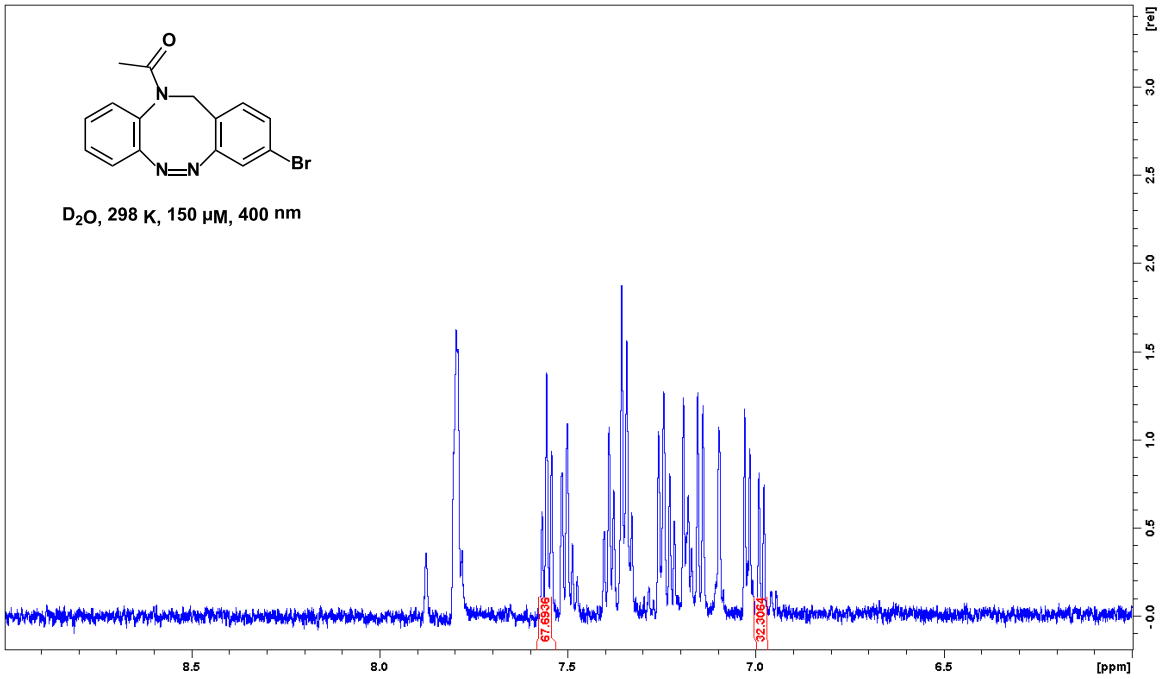

Figure S65: ^{1}H NMR spectrum (aromatic region) of Br-NAc diazocine **10a** in D_2O at 298 K after irradiation with 400 nm.

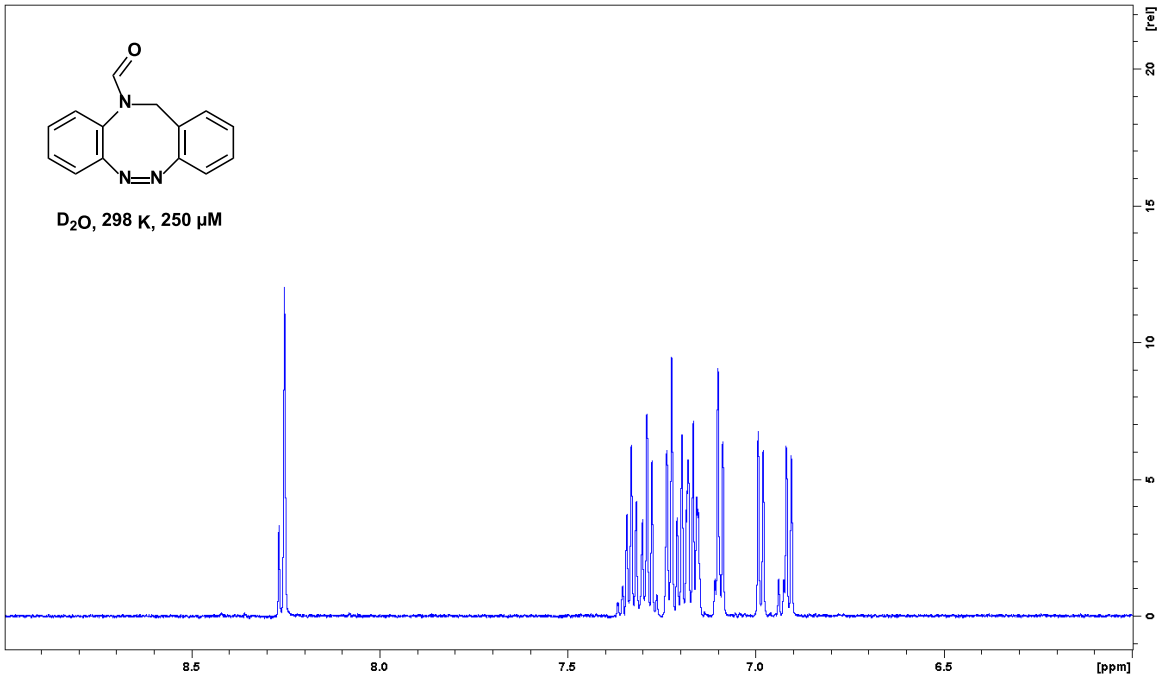

Figure S66: ^{1}H NMR spectrum (aromatic region) of NCHO diazocine **11c** in D_2O at 298 K.

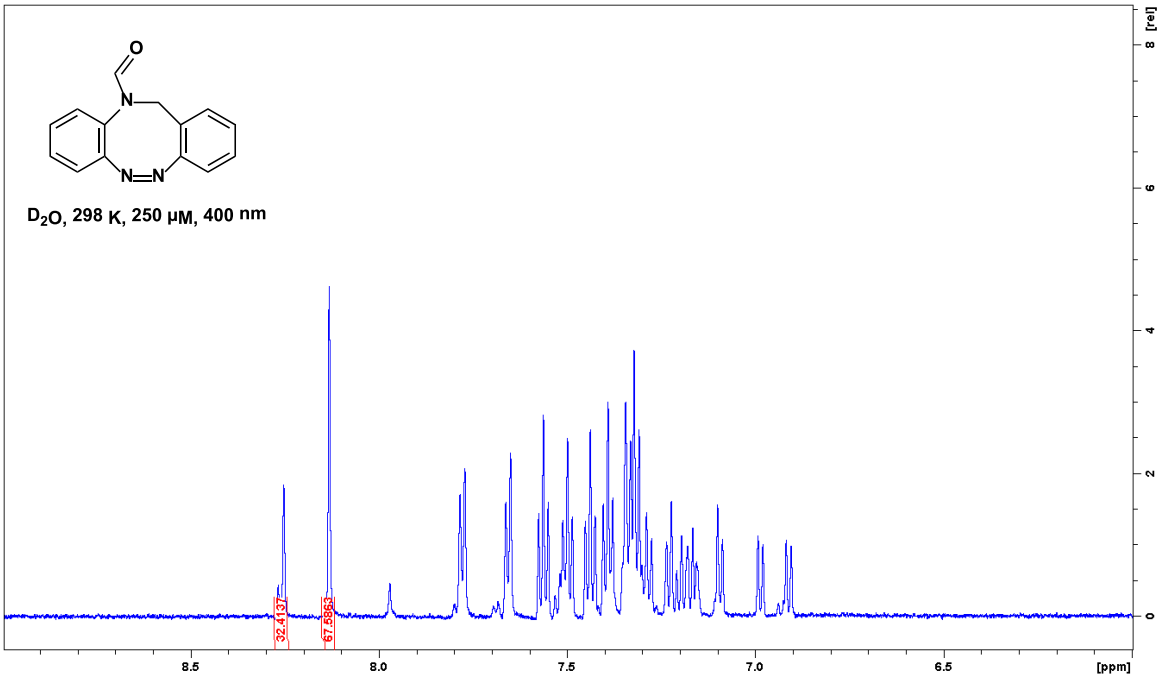

Figure S67: ^{1}H NMR spectrum (aromatic region) of NCHO diazocine **11c** in D_2O at 298 K after irradiation with 400 nm.

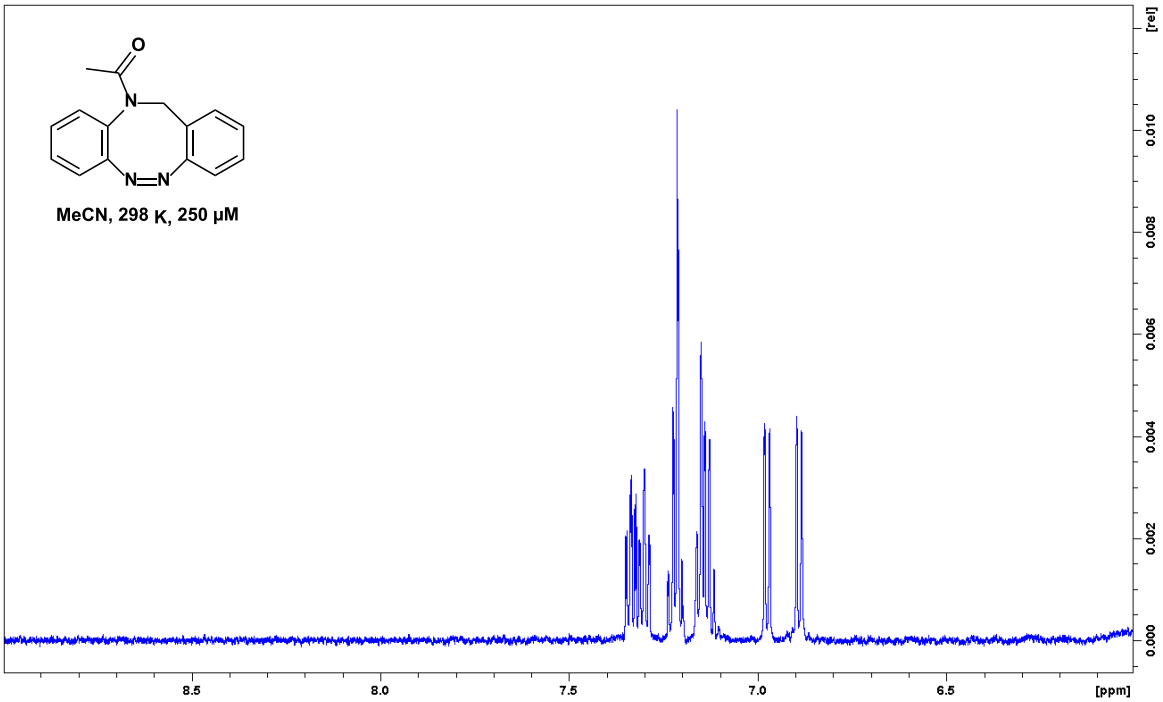

Figure S68: ^{1}H NMR spectrum (aromatic region) of NAc diazocine **10c** in MeCN at 298 K.

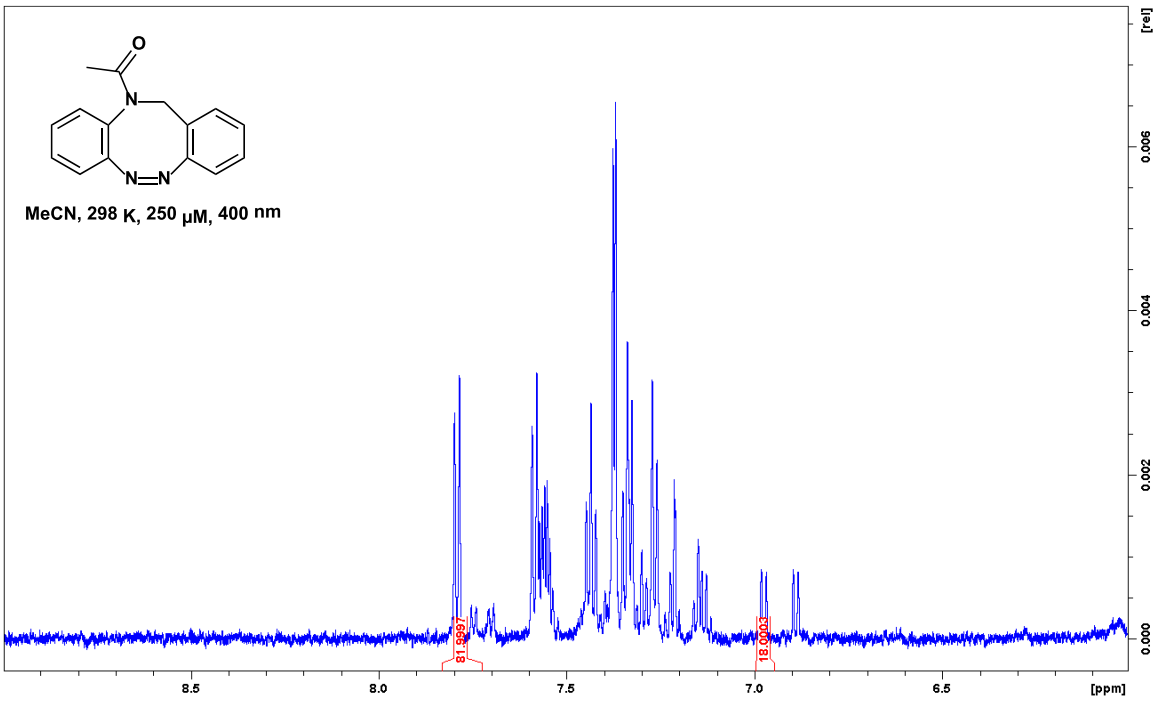

Figure S69: ^{1}H NMR spectrum (aromatic region) of NAc diazocine **10c** in MeCN at 298 K after irradiation with 400 nm.

[1] Lentes, P.; Stadler, E.; Röhricht, F.; Brahms, A.; Gröbner, J.; Sönnichsen, F. D.; Gescheidt, G.; Herges, R. *J. Am. Chem. Soc.* 2019, 141, 34, 13592–13600.
[2] Liebig, J. *Justus Liebigs Ann. Chem.* **1832**, *1*, 182–230.
[3] Schehr, M.; Hugenbusch, D.; Moje, T.; Näther, C.; Herges, R. *Beilstein J. Org. Chem.* **2018**, *14*, 2799–2904.

8.2.4 *N*-Acetyl Diazocine Derivatives via Cross-Coupling

Supporting Information

for

N-Acetyl Diazocine Derivatives via Cross-Coupling

Thomas Brandt, Pascal Lentes, Jeremy Rudtke, Michael Hösgen, Christian Näther, Rainer Herges

Otto-Diels-Institute for Organic Chemistry, Christian-Albrechts-Universität Kiel, 24118 Germany

*email: rherges@oc.uni-kiel.de

Table of Contents

I. Analytical Equipment

NMR spectroscopy

NMR spectra were measured in deuterated solvents (Deutero). The spectra were referenced to the following solvent residual signals:

solvent	degree of deuteration	^{1}H signal ppm	^{13}C-signal ppm
acetone-d_6	99.8%	2.05 (quintet)	29.84 (septet)
chloroform-d_1	99.8%	7.26 (singlet)	77.16 (triplet)
acetonitrile-d_3	99.8%	1.94 (singlet)	1.32 (septet), 118.26 (mulitplet)
water-d_2	99.9%	4.79 (singlet)	-

The spectra were recorded with a Bruker DRX 500 (^{1}H-NMR: 500 MHz, ^{13}C-NMR: 125 MHz) and a Bruker AV 600 (^{1}H-NMR: 600 MHz, ^{13}C-NMR: 150 MHz). The Multiplicities of the signals were abbreviated with s (singlet), d (doublet), t (triplet), q (quartet), quint. (quintet), m (multiplet), and br. (broad) in addition for broad signals. DEPT data were used to assign carbon types. Structural assignments were made with additional information from HSQC and HMBC experiments. Baseline correction of the spectra in D_2O was performed with Baseline Correction "Witthaker Smoother" tool and Signal Suppression tool in MestReNova 14.3.1 NMR analytic software by Mestrelab Research. Spectra were plotted with TopSpin 4.1.0 NMR analytic software by Bruker. Major impuritites in the 1D-NMR spectra used for compound characterization have been identified as far as possible and labeled accordingly.

Melting Point

Melting Points were measured with a Melting Point B-560 (Büchi) in melting point tubes without further correction.

Mass spectrometry

Mass spectra (EI) and high-resolution mass spectra (HR-EI) were measured with an AccuTOF GCv 4G EI-time of flight mass spectrometer from the company Joel. An ionization energy of 70 eV was used.
HR-ESI mass spectra were measured with a Q Exactive Plus Hybrid Quadrupole-Orbitrap ESI-mass spectrometer of the company Thermo Scientific was used.

IR spectroscopy

Infrared spectra were measured with a Perkin-Elmer 1600 FT-IR spectrometer with an A531-G Golden-Gate-Diamond-ATR-unit. Signals were abbreviated with w (weak), m (medium) or s (strong) for its intensity.

UV-vis spectroscopy

UV-vis spectra were measured with a Shimadzu UV-2600 i UV-vis spectrometer. Quartz cuvettes of 10 mm optical path length were used.

Chromatography

Silica gel (Merck, particle size 0.040-0.063 mm) was used for column chromatography purifications. R_f values were determined via thin layer chromatography on Polygram® SilG/UV254 (Macherey Nagel, 0.2 mm particle size).

Chemicals

All commercially available chemicals were used without further purification.

Light sources

For irradiation different custom-built light sources with a wavelength of 405 nm and 530 nm were used (Sahlmann Photochemistry Solutions & in-house built). Irradiation wavelengths for all (405 nm and 530 nm) LED units were measured via a mobile UV-vis spectrometer (USB4000-UV-VIS, Ocean Optics, Largo, FL, USA). All emission spectra were normalized. Figure SI1 shows the normalized emission spectra of all LED units used.

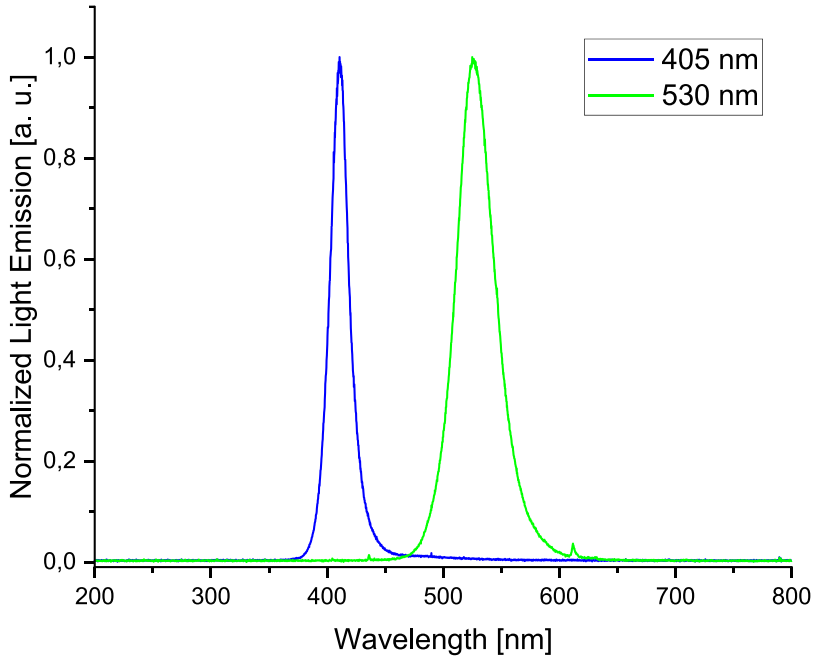

Figure SI.1: Emission spectra of all LED units used. For better comparison all datasets were normalized to its maximum.

The full width at half maximum (FWHM) amounts to 19 nm (401-420 nm, maximum at 410 nm) for the 405 nm LED unit and to 38 nm (509-547 nm, maximum at 525 nm) for the 530 nm LED unit.

II. Syntheses

II.1 Synthesis of halogenated *N*-acetyl diazocines

The halogenated *N*-acetyl diazocine precursors **2-4** were synthesized following the procedure of LENTES *et al.*[1] (Scheme 1). Therefore, the dianiline and bromide building blocks were connected in a nucleophile substitution in the first step followed by Fmoc-protection of the secondary amine. After cleaving the Boc-protecting group the nitro-group was reduced using stannous chloride and zink. In the following the oxidative azo-cyclization adapted from the procedure of MAIER *et al.*[2] was performed to receive the Fmoc-protected *N*-acetyl diazocine intermediates. After the Fmoc-group was cleaved the acetyl protecting group was introduced as final step.

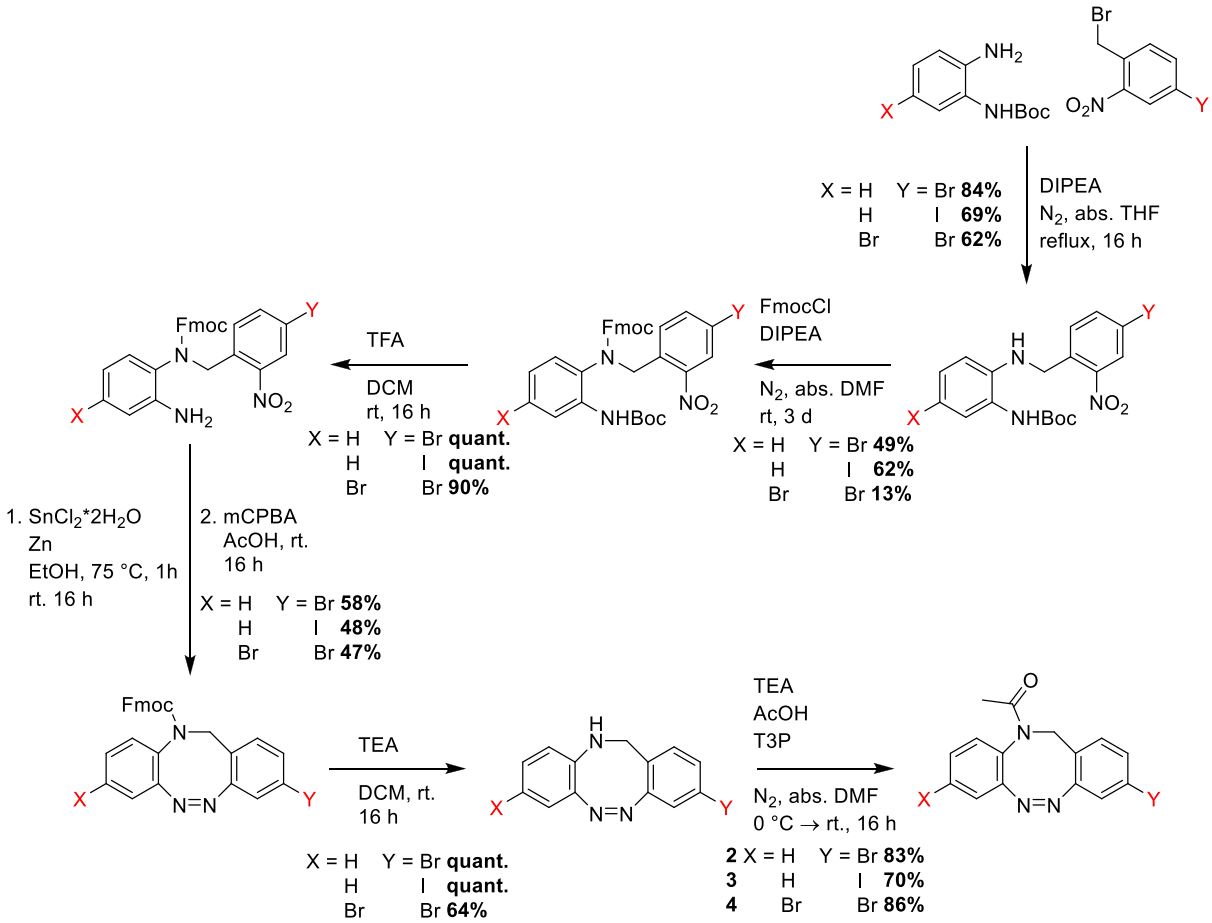

Scheme S1: Synthesis of the halogenated *N*-acetyl diazocine precursors **2-4** for the cross-coupling reactions according to the procedure of LENTES *et al.*[1]

For the synthesis of dibromo-*N*-acetyl diazocine **4** the Boc-protected dianiline building block **5** was prepared from commercially available 5-bromo-2-nitroaniline **6**. In the first step the Boc protecting group was introduced after deprotonation of the aniline with sodium hydride. The nitro group was reduced with sodium dithionite and sodium hydrogencarbonate subsequently to obtain dianiline building block **5**.

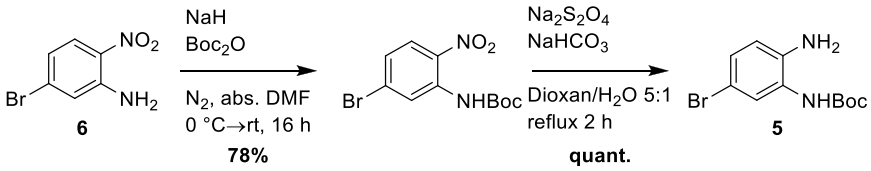

Scheme S2: Synthesis of dianiline building block **5** from *o*-nitroaniline **6**.

II.1.1 Synthesis of *tert*-butyl-(2-((4-bromo-2-nitrobenzyl)amino)phenyl)carbamate[1]

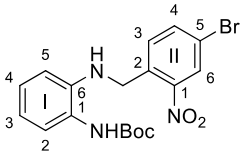

Under a nitrogen atmosphere triethylamine (3.87 mL, 27.9 mmol) and 4-bromo-1-(bromomethyl)-2-nitrobenzene (7.50 g, 25.4 mmol) were added to solution of tert-butyl-(2-aminophenyl)carbamate (5.30 g, 25.4 mmol) in 100 mL abs. THF. The reaction mixture was heated to reflux with an oil bath and stirred for 16 h at that temperature. Afterwards the solvent was evaporated and 100 mL of deionized water and 100 mL DCM were added to the residue. The organic layer was separated and the aqueous layer was extracted twice with 50 mL of DCM. The combined organic layers were dried over $MgSO_4$ and the solvent was evaporated. Recrystallization from cyclohexane/ethyl acetate (1:1) gave the product as yellow solid (9.06 g, 21.4 mmol, 84%, lit. 71%[1]).

melting point: 147 °C

^{1}H-NMR (500 MHz, acetone-d_6, 298 K): δ = 8.24 (d, ^4J = 2.0 Hz, 1 H, Ar^{II}-*H*-6), 7.83 (dd, ^3J = 8.4 Hz, ^4J = 2.1 Hz, 1 H, Ar^{II}-*H*-4), 7.73 (d, ^3J = 8.4 Hz, 1 H, Ar^{II}-*H*-3), 7.63 (br. s, 1 H, N*H*), 7.25 (d, ^3J = 7.7 Hz, 1 H, Ar^{I}-*H*-2), 6.93 (td, ^3J = 7.8 Hz, ^4J = 1.5 Hz, 1 H, Ar^{I}-*H*-4), 6.64 (td, ^3J = 7.6 Hz, ^4J = 1.3 Hz, 1 H, Ar^{I}-*H*-3), 6.50 (dd, ^3J = 7.6 Hz, ^4J = 2.1 Hz, 1 H, Ar^{I}-*H*-5), 5.51 (br. s, 1 H, N*H*), 4.76 (s, 2 H, CH_2), 1.47 (s, 9 H, CH_3) ppm.

^{13}C{^{1}H}-NMR (125 MHz, acetone-d_6, 298 K): δ = 155.0 (*C*=O), 150.0 (Ar^{II}-*C*-1), 142.7 (Ar^{I}-*C*-6), 137.1 (Ar^{II}-*C*-4), 136.2 (Ar^{II}-*C*-6), 132.4 (Ar^{II}-*C*-3), 128.3 (Ar^{II}-*C*-6), 127.1 (Ar^{I}-*C*-4), 126.8 (Ar^{I}-*C*-2), 125.5 (Ar^{I}-*C*-1), 120.9 (Ar^{II}-*C*-5), 118.0 (Ar^{I}-*C*-3), 112.4 (Ar^{I}-*C*-5), 79.9 (*C*-(CH$_3$)$_3$), 45.1 (-*C*H$_2$), 28.6 (-*C*H$_3$) ppm.

IR (ATR): $\tilde{\nu}$ = 3398 (m), 3270 (m), 2975 (w), 1707 (w), 1684 (s), 1604 (m), 1528 (s), 1502 (s), 1462 (m), 1421 (w), 1393 (w), 1346 (m), 1336 (m), 1307 (w), 1242 (s), 1153 (s), 1083 (w), 1066 (w), 1052 (m), 1028 (w), 906 (w), 874 (w), 845 (w), 831 (m), 792 (w), 754 (s), 717 (w), 647 (w), 616 (w) cm^{-1}.

HR-MS (ESI, DCM): *m/z* [M+H]$^+$ calculated for $C_{18}H_{20}O_4N_3{}^{79}Br+H^+$: 422.0710; found: 422.0700 ± 2.36 ppm.

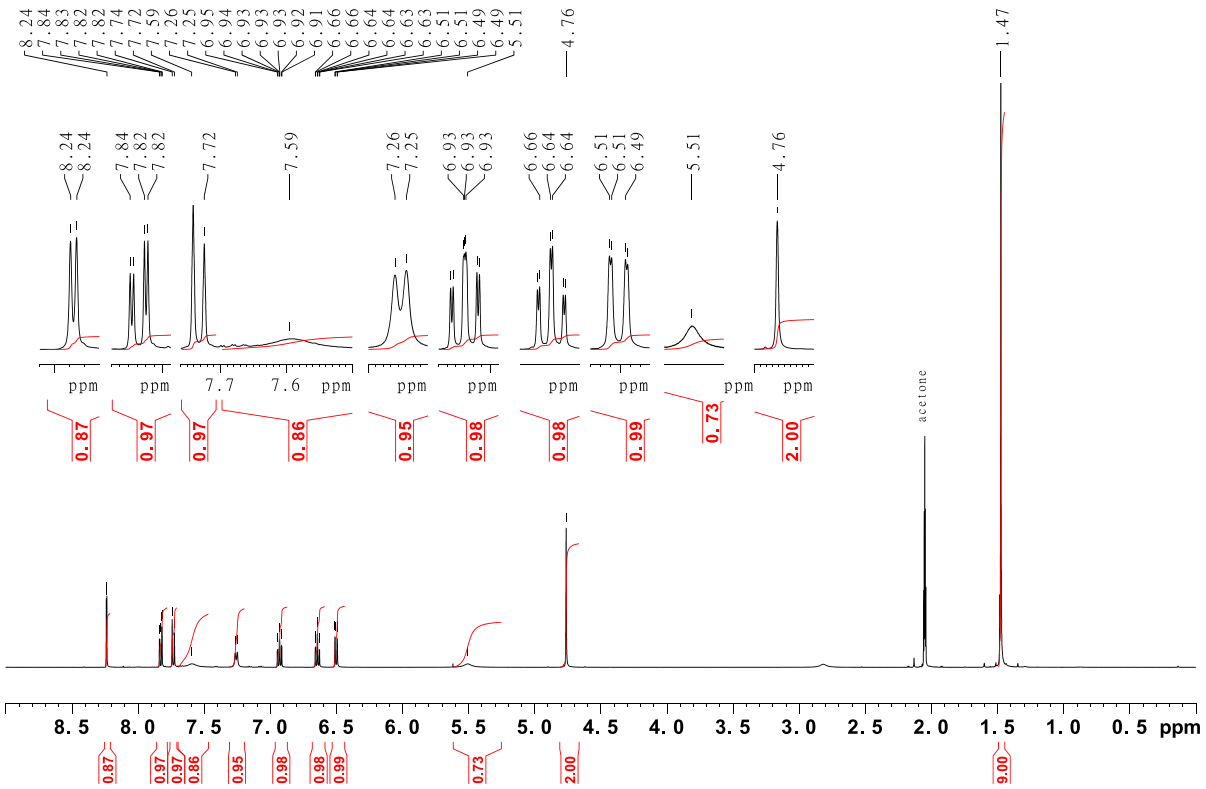

Figure SII.1: 500 MHz ^{1}H-NMR spectrum of *tert*-butyl-(2-((4-bromo-2-nitrobenzyl)amino)phenyl)carbamate.

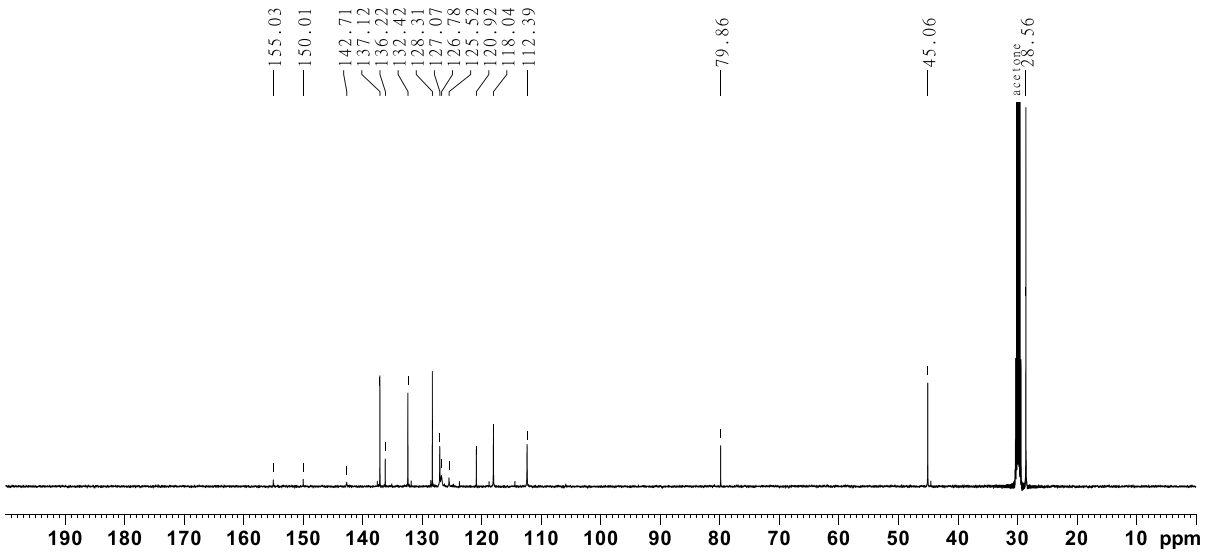

Figure SII.2: 125 MHz ^{13}C{^{1}H}-NMR spectrum of *tert*-butyl-(2-((4-bromo-2-nitrobenzyl)amino)phenyl)carbamate.

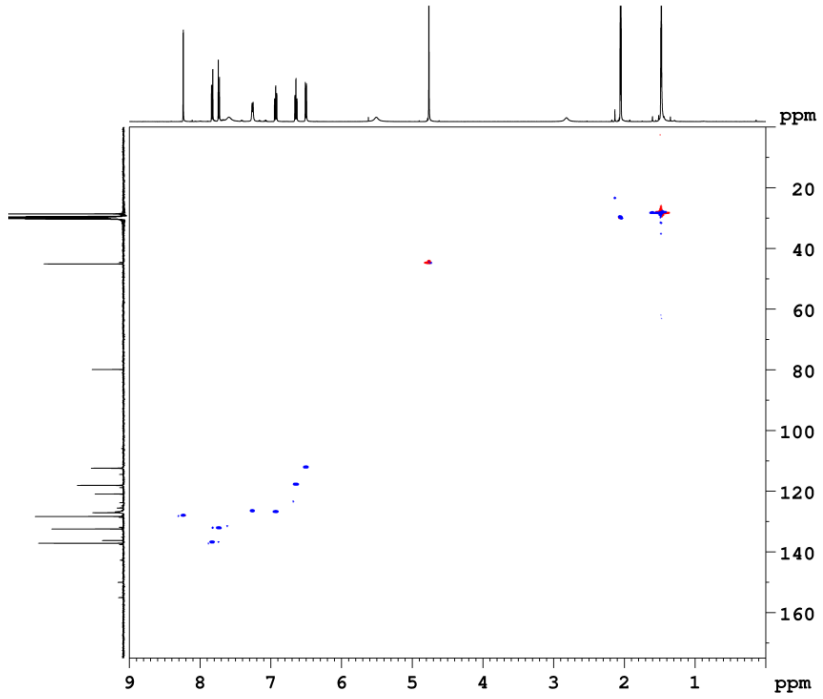

Figure SII.3: 500 MHz ^{1}H-^{13}C HSQC spectrum of *tert*-butyl-(2-((4-bromo-2-nitrobenzyl)amino)phenyl)carbamate.

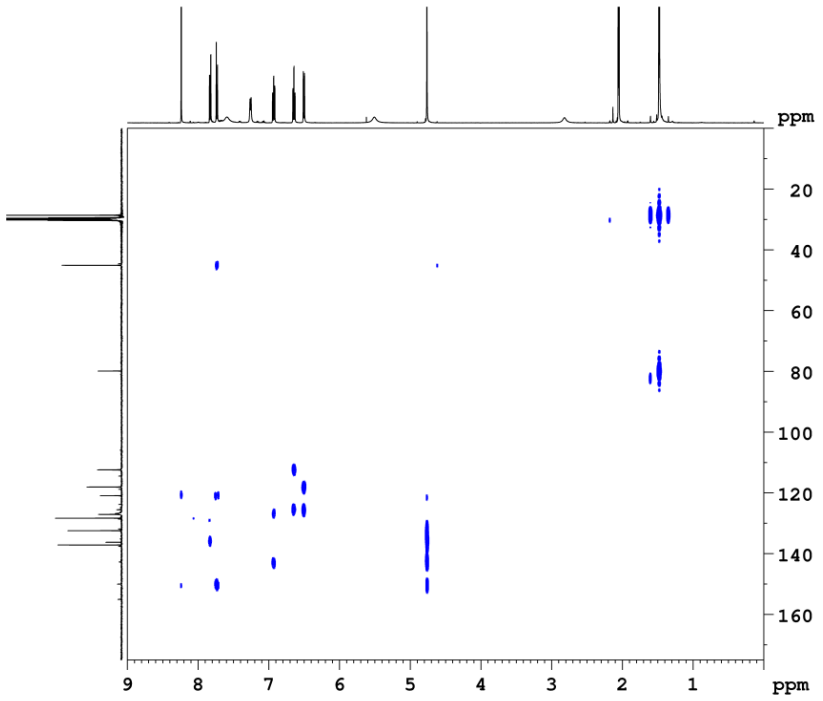

Figure SII.4: 500 MHz HMBC spectrum of *tert*-butyl-(2-((4-bromo-2-nitrobenzyl)amino)phenyl)carbamate.

II.1.2 Synthesis of (9*H*-fluoren-9-yl)methyl-(4-bromo-2-nitrobenzyl)(2-((*tert*-butoxycarbonyl)amino)phenyl)carbamate[1]

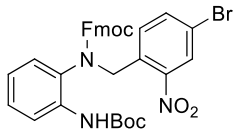

DIPEA (3.21 mL, 18.9 mmol) and 9-Fluorenylmethoxycarbonyl chlorid (9.77 g, 37.8 mmol) were added to a solution of *tert*-butyl-(2-((4-bromo-2-nitrobenzyl)amino)phenyl)carbamate (8.00 g, 18.9 mmol) in 50 mL abs. DMF under a nitrogen atmosphere. The reaction mixture was stirred for 48 h at rt. and the solvent was evaporated subsequently. 100 mL of deionized water and 100 mL of DCM were added to the residue. The organic layer was separated and the aqueous layer was extracted twice with 100 mL DCM. The combined organic layers were dried over $MgSO_4$ and the solvent was evaporated. Column chromatography on silica (ethyl acetate/cyclohexane 1:4, R_f = 0.34) gave a colorless solid (5.91 g, 9.18 mmol, 49%, lit. 56%[1]).

melting point: 157 °C

^{1}H-NMR (500 MHz, acetone-d_6, 298 K): δ = 8.14 (d, ^4J = 2.1 Hz, 1 H), 8.05-7.61 (m,5 H), 7.53-7.01 (m,10 H), 5.24-4.92 (m, 2 H, aliph.-*H*), 4.56-4.00 (m, 3 H, aliph.-*H*), 1.45 (s, 9 H, CH_3) ppm.

^{13}C{^{1}H}-NMR (125 MHz, acetone-d_6, 298 K): δ = 153.5 (*C*=O), 142.1, 137.0, 129.2, 128.5, 128.2, 127.8, 126.1, 124.4, 120.7, 80.4, 68.4, 47.8, 28.5 (*C*H_3) ppm.

IR (ATR): $\tilde{\nu}$ = 3381 (m), 2974 (w), 2348 (w), 2253 (w), 1717 (s), 1596 (m), 1536 (m), 1518 (s), 1450 (m), 1390 (m), 1365 (w), 1292 (m), 1278 (w), 1234 (m), 1217 (w), 1152 (s), 1042 (w), 1024 (w), 976 (m), 942 (w), 884 (m), 842 (w), 756 (s), 739 (w), 634 (w), 617 (m), 543(m) cm^{-1}.

HR-MS (ESI, DCM): *m/z* $[M+H]^+$ calculated for $C_{33}H_{30}O_6N_3{}^{79}Br+H^+$: 644.1391; found: 644.1393 ± 0.41 ppm.

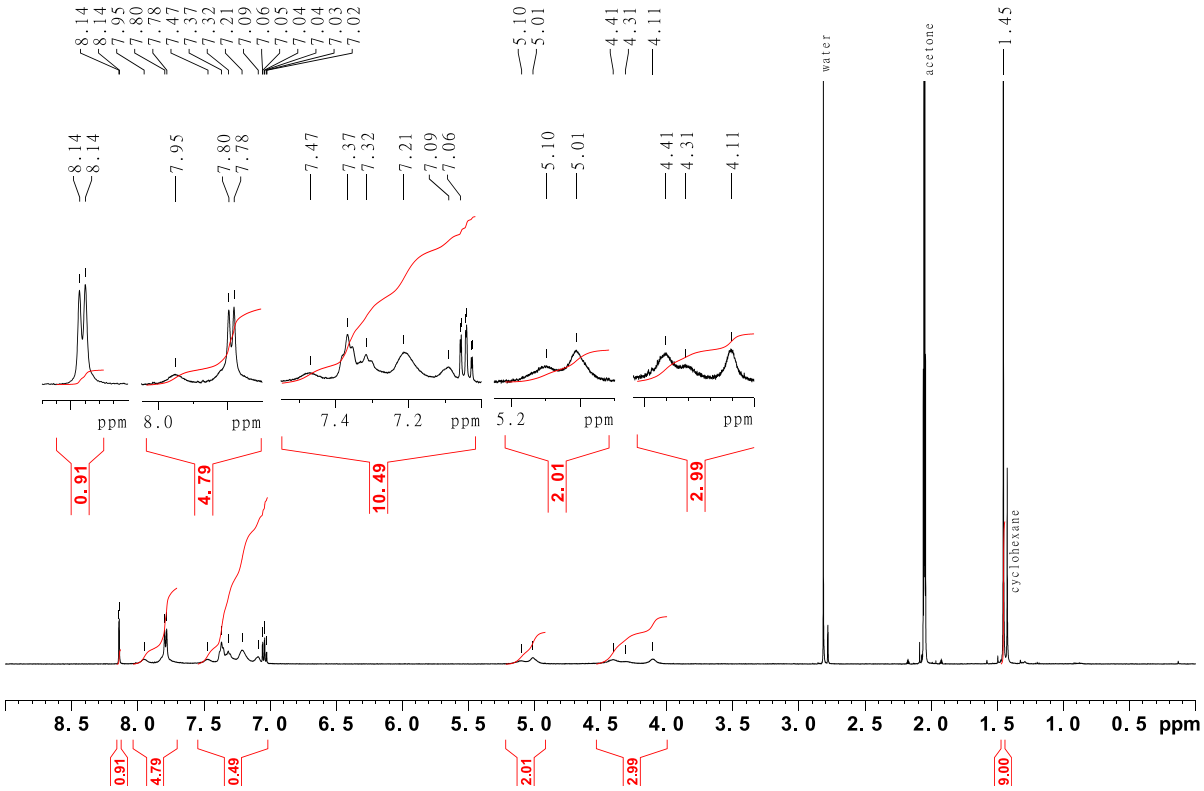

Figure SII.5: 500 MHz ^{1}H-NMR spectrum of (9*H*-fluoren-9-yl)methyl-(4-bromo-2-nitrobenzyl)(2-((*tert*-butoxycarbonyl)amino)phenyl)carbamate.

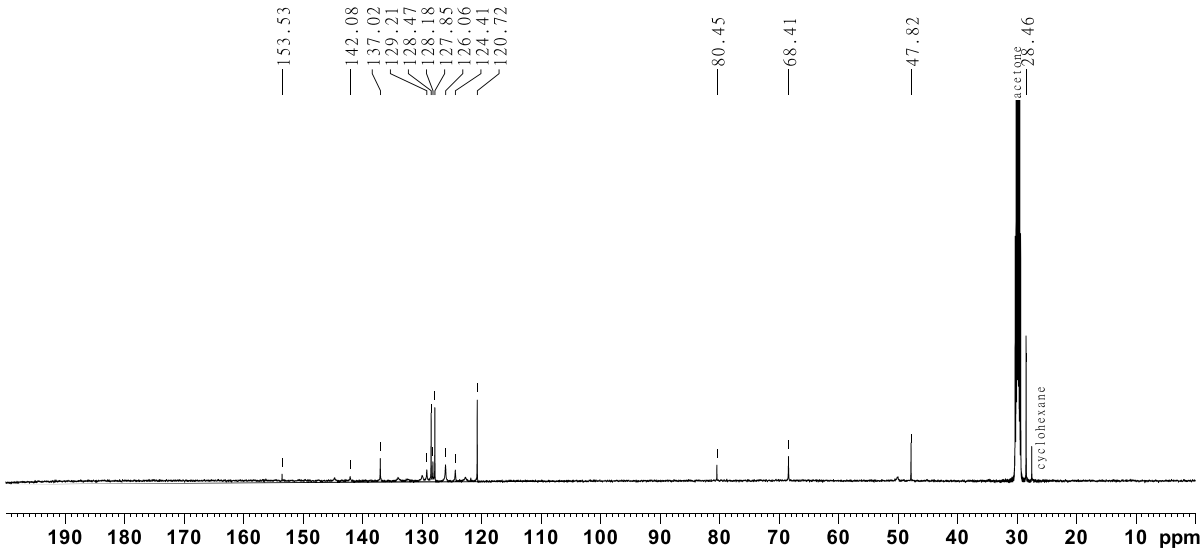

Figure SII.6: 125 MHz ^{13}C{^{1}H}-NMR spectrum of (9*H*-fluoren-9-yl)methyl-(4-bromo-2-nitrobenzyl)(2-((*tert*-butoxycarbonyl)amino)phenyl)carbamate.

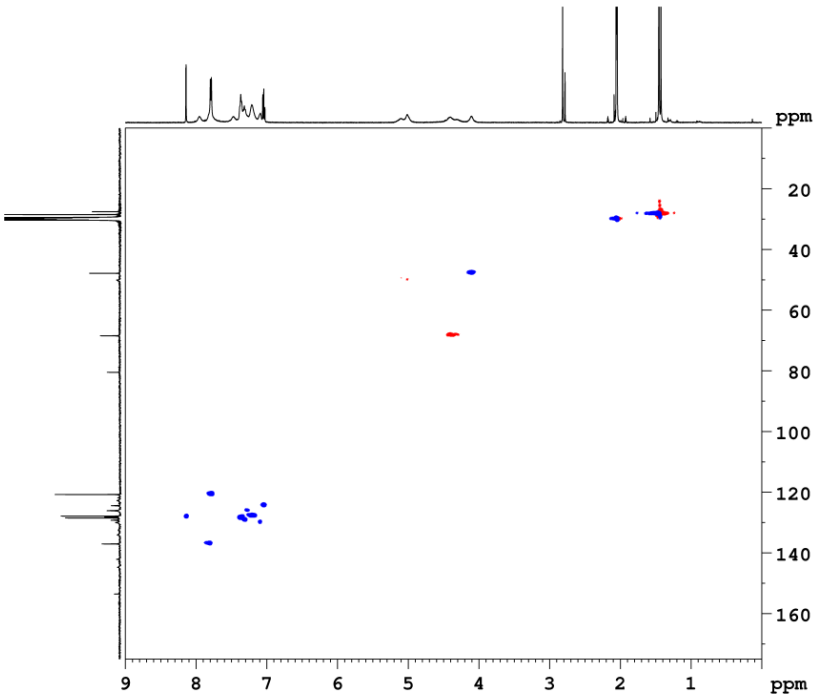

Figure SII.7: 500 MHz ^{1}H-^{13}C HSQC spectrum of (9*H*-fluoren-9-yl)methyl-(4-bromo-2-nitrobenzyl)(2-((*tert*-butoxycarbonyl)amino)phenyl)carbamate.

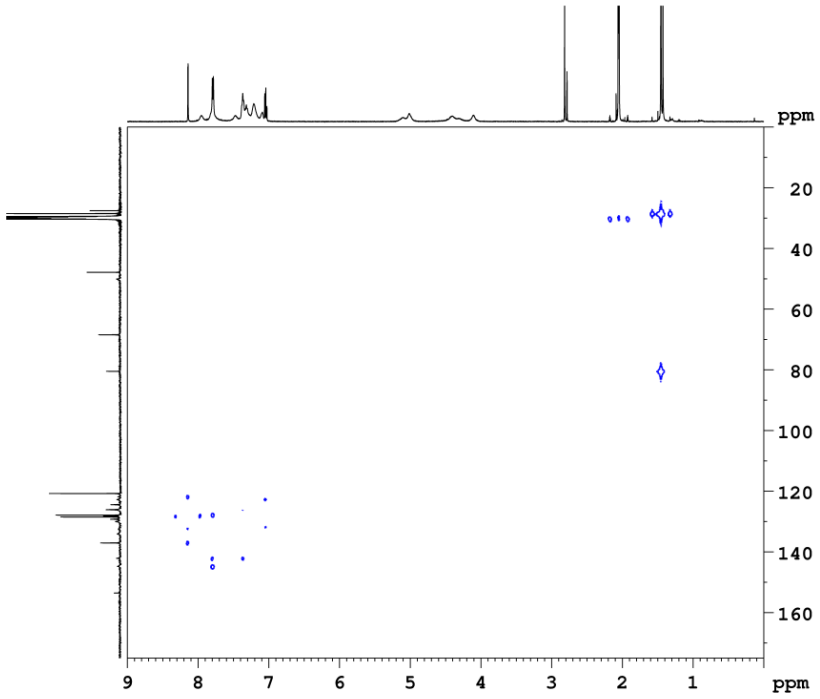

Figure SII.8: 500 MHz HMBC spectrum of (9*H*-fluoren-9-yl)methyl-(4-bromo-2-nitrobenzyl)(2-((*tert*-butoxycarbonyl)amino)phenyl)carbamate.

II.1.3 Synthesis of (9*H*-fluoren-9-yl)methyl-(2-aminophenyl)(4-bromo-2-nitrobenzyl)carbamate[1]

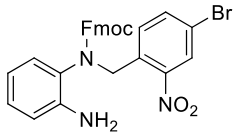

(9*H*-fluoren-9-yl)methyl-(4-bromo-2-nitrobenzyl)(2-((*tert*-butoxycarbonyl)amino)phenyl)carbamate (5.00 g, 7.76 mol) was dissolved in 100 mL DCM and 30 mL TFA was added. The reaction mixture was stirred at rt. for 16 h and neutralized with saturated aqueous $NaHCO_3$ subsequently. The organic layer was separated and the aqueous layer was extracted twice with 100 mL. The combined organic layers were dried over $MgSO_4$ and the solvent was evaporated to obtain a pale yellow solid (4.22 g, 7.75 mmol, quant., lit. quant.[1]) which was used without further purification.

melting point: 156 °C

^{1}H-NMR (600 MHz, acetone-d_6, 298 K): δ = 8.12 (s, 1 H), 7.92-7.63 (m,4 H), 7.50-6.52 (m,10 H), 5.60-4.02 (m, 5 H, aliph.-*H*) ppm.

^{13}C{^{1}H}-NMR (150 MHz, acetone-d_6, 298 K): δ = 144.7, 142.1, 136.9, 133.2, 130.3, 129.0, 128.4, 127.84, 127.79, 126.1, 124.4, 121.5, 120.72, 120.67, 68.0, 49.66, 47.97, 47.89 ppm.

IR (ATR): $\tilde{\nu}$ = 3425 (w), 3353 (w), 2348 (w), 2185 (w), 2163 (s), 2052 (m), 1978 (m), 1712 (s), 1619 (m), 1521 (s), 1503 (w), 1451 (w), 1433 (m), 1340 (m), 1253 (s), 1189 (w), 1172 (m), 1150 (w), 1102 (m), 1063 (m), 1051 (w), 876 (m), 764 (m), 745 (s), 659 (m), 638 (w), 621(m), 568 (w), 543 (m) cm^{-1}.

HR-MS (ESI, DCM): *m/z* $[M+H]^+$ calculated for $C_{28}H_{22}O_4N_3{}^{79}Br+H^+$: 544.0867; found: 544.0870 ± 0.58 ppm.

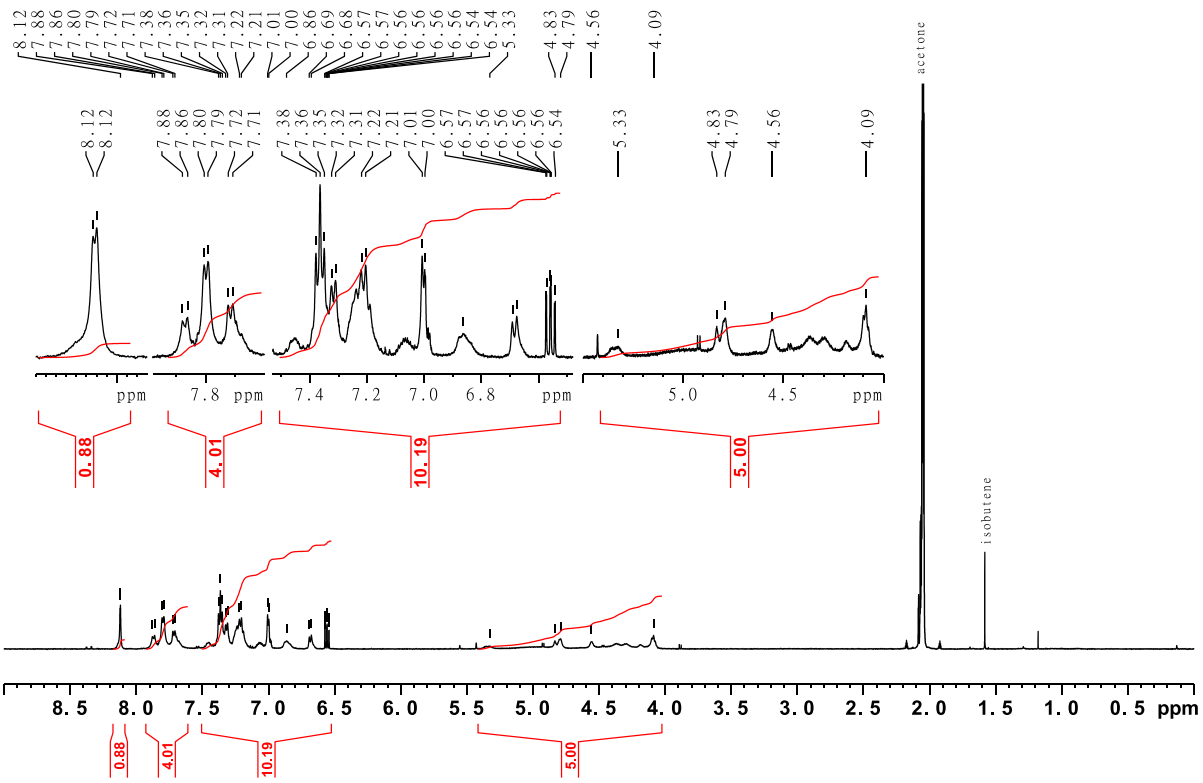

Figure SII.9: 600 MHz ^{1}H-NMR spectrum of (9*H*-fluoren-9-yl)methyl-(2-aminophenyl)(4-bromo-2-nitrobenzyl)carbamate.

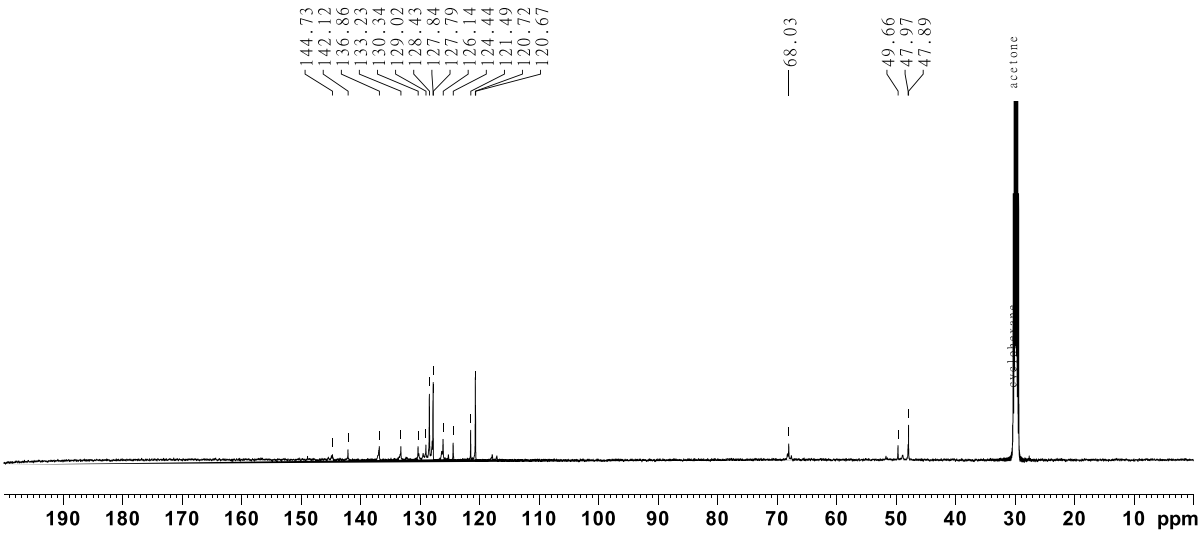

Figure SII.10: 150 MHz ^{13}C{^{1}H}-NMR spectrum of (9*H*-fluoren-9-yl)methyl-(2-aminophenyl)(4-bromo-2-nitrobenzyl)carbamate.

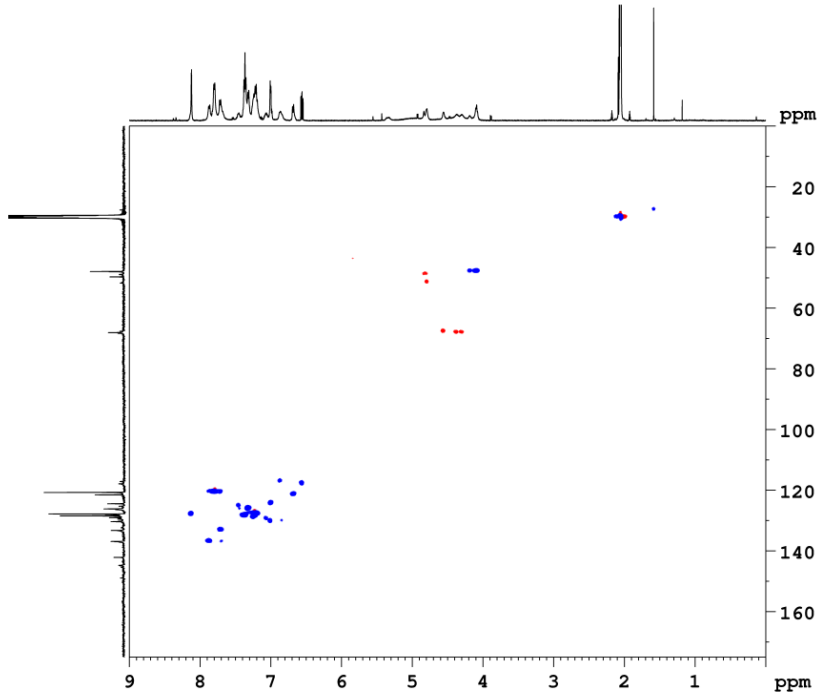

Figure SII.11: 600 MHz ^{1}H-^{13}C HSQC spectrum of (9*H*-fluoren-9-yl)methyl-(2-aminophenyl)(4-bromo-2-nitrobenzyl)carbamate.

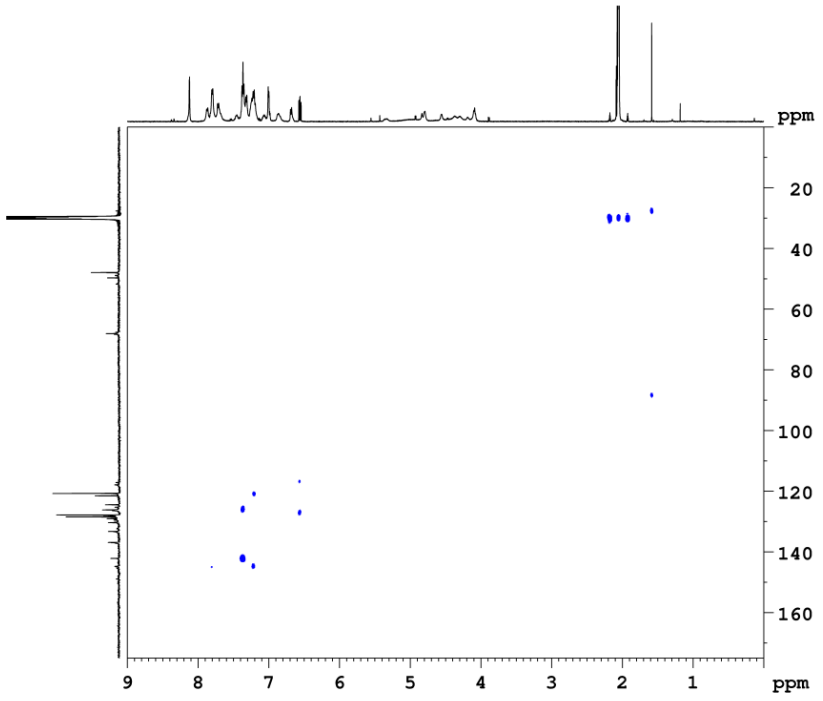

Figure SII.12: 600 MHz HMBC spectrum of (9*H*-fluoren-9-yl)methyl-(2-aminophenyl)(4-bromo-2-nitrobenzyl)carbamate.

II.1.4 Synthesis of (9*H*-fluoren-9-yl)methyl-(*Z*)-3-bromodibenzo[c,g][1,2,5]triazocin-11-(12*H*)-carboxylate[1]

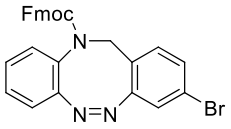

(9*H*-fluoren-9-yl)methyl-(2-aminophenyl)(4-bromo-2-nitrobenzyl)carbamate (4.18 g, 7.68 mmol) was suspended in 250 mL EtOH and $SnCl_2 \cdot 2\ H_2O$ (10.4 g, 46.1 mmol) was added. The reaction mixture was heated to 75 °C with an oil bath and zinc-powder (4.02 g, 61.4 mmol) was added. The reaction mixture was stirred at 75 °C for 1 h and cooled to rt. afterwards. It was stirred at rt. for 16 h and neutralized with saturated aqueous $NaHCO_3$ solution subsequently. The solvent was evaporated and 100 mL water and 100 mL DCM were added to the residue. The organic layer was separated and the aqueous layer was extracted twice with 100 mL DCM. The combined organic layers were dried over $MgSO_4$ and the solvent was evaporated. The residue was dissolved in 300 mL of acetic acid and *m*CPBA (2.66 g, 15.4 mmol) dissolved in 300 mL acetic acid was added dropwise to the reaction mixture. The reaction mixture was stirred at rt. for 16 h and the solvent was evaporated in the following. 100 mL DCM and 100 mL half-concentrated aqueous $NaHCO_3$ solution were added to the residue. The organic layer was separated and the aqueous layer was extracted twice with 100 mL DCM. The combined organic layers were dried over $MgSO_4$ and the solvent was evaporated. After column chromatography on silica (ethyl acetate/cyclohexane = 1:4, R_f = 0.43) the product could be obtained as yellow solid (2.27 g, 4.45 mmol, 58%, lit. 56%[1]).

melting point: 175 °C

^{1}H-NMR (600 MHz, acetone-d_6, 298 K): δ = 7.99-7.77 (s, 2 H, Ar-*H*), 7.50-6.95 (m, 13 H, Ar-*H*), 4.99-3.95 (m, 5 H, aliph.-*H*) ppm.

^{13}C{^{1}H}-NMR (150 MHz, acetone-d_6, 298 K): δ = 154.7, 142.1, 132.7, 131.3, 130.5, 129.5, 129.1, 128.5, 127.9, 126.1, 124.2, 122.6, 120.8, 119.7, 68.5, 52.7, 47.8 ppm.

IR (ATR): $\tilde{\nu}$ = 2946 (w), 2320 (w), 2256 (w), 2178 (w), 2038 (w), 1999 (w), 1701 (s), 1591 (m), 1475 (m), 1447 (m), 1389 (s), 1316 (s), 1243 (m), 1132 (m), 1074 (w), 1042 (m), 1023 (m), 1003 (w), 976 (w), 864 (w), 843 (w), 822 (m), 755 (s), 736 (s), 698 (m), 622 (m), 547 (m), 515 (w), 503 (m) cm^{-1}.

HR-MS (ESI, DCM): *m/z* $[M+H]^+$ calculated for $C_{28}H_{22}O_3N_2{}^{79}Br+H^+$: 510.0812, found: 510.0817 ± 0.55 ppm.

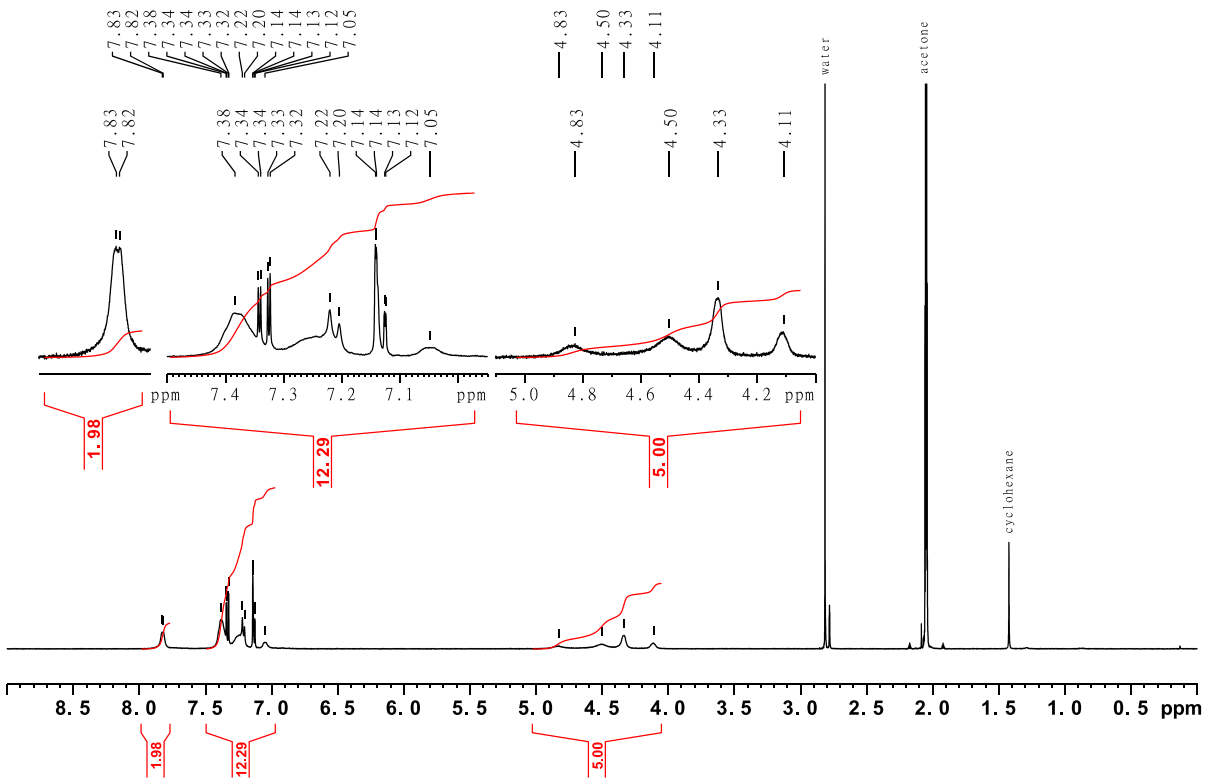

Figure SII.13: 600 MHz ^{1}H-NMR spectrum of (9*H*-fluoren-9-yl)methyl-(*Z*)-3-bromodibenzo[c,g][1,2,5]triazocin-11-(12*H*)-carboxylate.

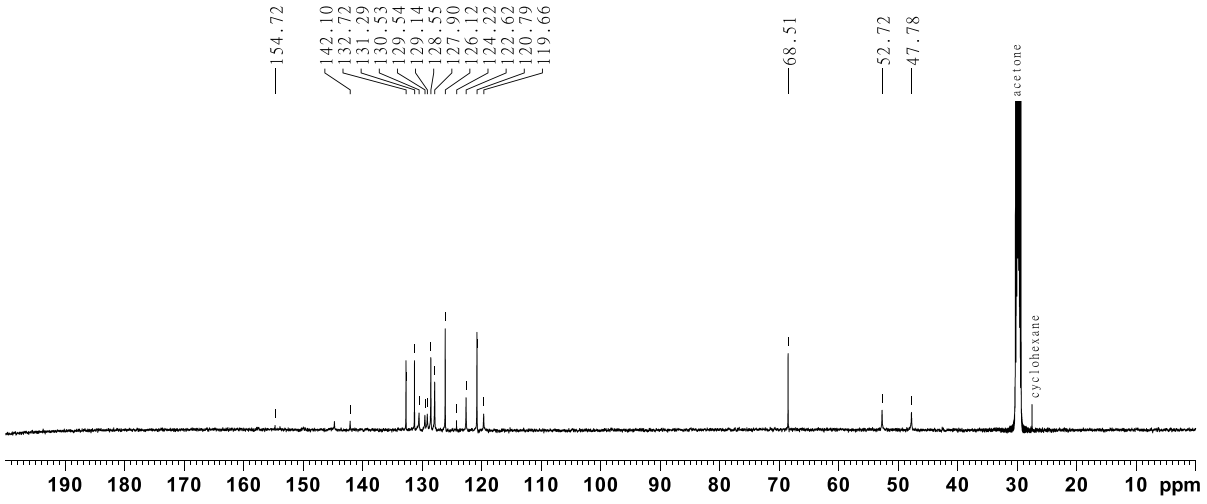

Figure SII.14: 150 MHz ^{13}C{^{1}H}-NMR spectrum of (9*H*-fluoren-9-yl)methyl-(*Z*)-3-bromodibenzo[c,g][1,2,5]triazocin-11-(12*H*)-carboxylate.

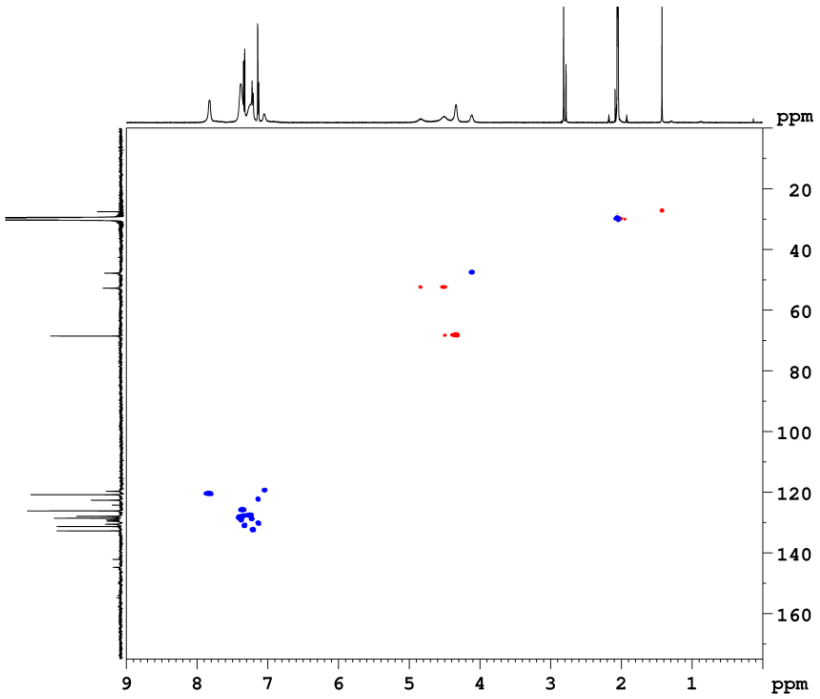

Figure SII.15: 600 MHz ^{1}H-^{13}C HSQC spectrum of (9*H*-fluoren-9-yl)methyl-(*Z*)-3-bromodibenzo[c,g][1,2,5]triazocin-11-(12*H*)-carboxylate.

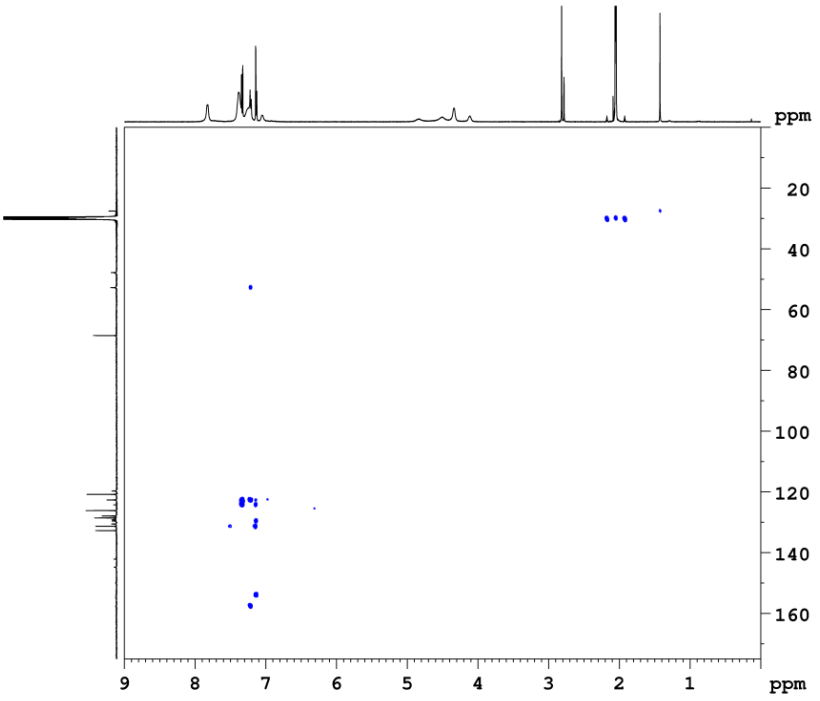

Figure SII.16: 600 MHz HMBC spectrum of (9*H*-fluoren-9-yl)methyl-(*Z*)-3-bromodibenzo[c,g][1,2,5]triazocin-11-(12*H*)-carboxylate.

II.1.5 Synthesis of (*Z*)-bromo-11,12-dihydrodibenzo[c,g][1,2,5]triazocine[1]

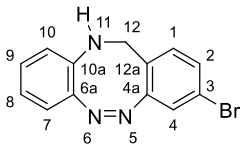

9*H*-fluoren-9-yl)methyl-(*Z*)-3-bromodibenzo[c,g][1,2,5]triazocin-11-(12*H*)-carboxylate (1.63 g, 3.19 mmol) was dissolved in 50 mL of DCM and 50 mL NEt_3 was added. The reaction mixture was stirred at rt. for 16 h. the solvent was evaporated and column chromatography on silica (ethyl acetate/cyclohexane 1:2, R_f = 0.32) gave a red solid (893 mg, 3.17 mmol, quant., lit. 93%[1]).

melting point: 149 °C

^{1}H-NMR (500 MHz, acetone-d_6, 298 K): δ = 7.42 (dd, ^3J = 8.1 Hz, ^4J = 2.0 Hz, 1 H, *H*-2), 7.33 (d, ^4J = 2.1 Hz, 1 H, *H*-4), 7.31 (d, ^3J = 8.1 Hz, 1 H, *H*-1), 6.87 (td, ^3J = 7.7 Hz, ^4J = 1.6 Hz, 1 H, *H*-9), 6.74 (dd, ^3J = 8.0 Hz, ^4J = 1.6 Hz, 1 H, *H*-7), 6.64 (td, ^3J = 7.4 Hz, ^4J = 1.2 Hz, 1 H, *H*-8), 6.56 (dd, ^3J = 8.1 Hz, ^4J = 1.1 Hz, 1 H, *H*-10), 5.51 (s, 1 H, N*H*-), 4.04 (s, 1 H, -*H*-12), 3.88 (s, 1 H, -*H*-12') ppm.

^{13}C{^{1}H}-NMR (125 MHz, acetone-d_6, 298 K): δ = 160.1 (*C*-4a), 144.5 (*C*-6a), 137.0 (*C*-10a), 132.4 (*C*-1), 131.8 (*C*-2), 129.1 (*C*-9), 124.0 (*C*-3), 123.5 (*C*-7), 122.6 (*C*-4), 121.7 (*C*-12a), 119.9 (*C*-10), 118.2 (*C*-8), 47.0 (*C*-12) ppm.

IR (ATR): $\tilde{\nu}$ = 3317 (s), 3026 (w), 2959 (w), 2878 (w), 1601 (m), 1587 (m), 1567 (w), 1511 (m), 1481 (s), 1455 (w), 1389 (m), 1363 (w), 1321 (s), 1272 (w), 1251 (s), 1191 (w), 1161 (m), 1139 (w), 1119 (w), 1093 (m), 1072 (m), 1034 (w), 956 (w), 898 (m), 831 (m), 812 (s), 740 (s), 720 (m), 702 (w), 651 (w), 603 (w) cm^{-1}.

HR-MS (ESI, DCM): *m/z* $[M+H]^+$ calculated for $C_{13}H_{10}N_3{}^{79}Br+H^+$: 288.01301; found: 288.0127 ± 1.44 ppm.

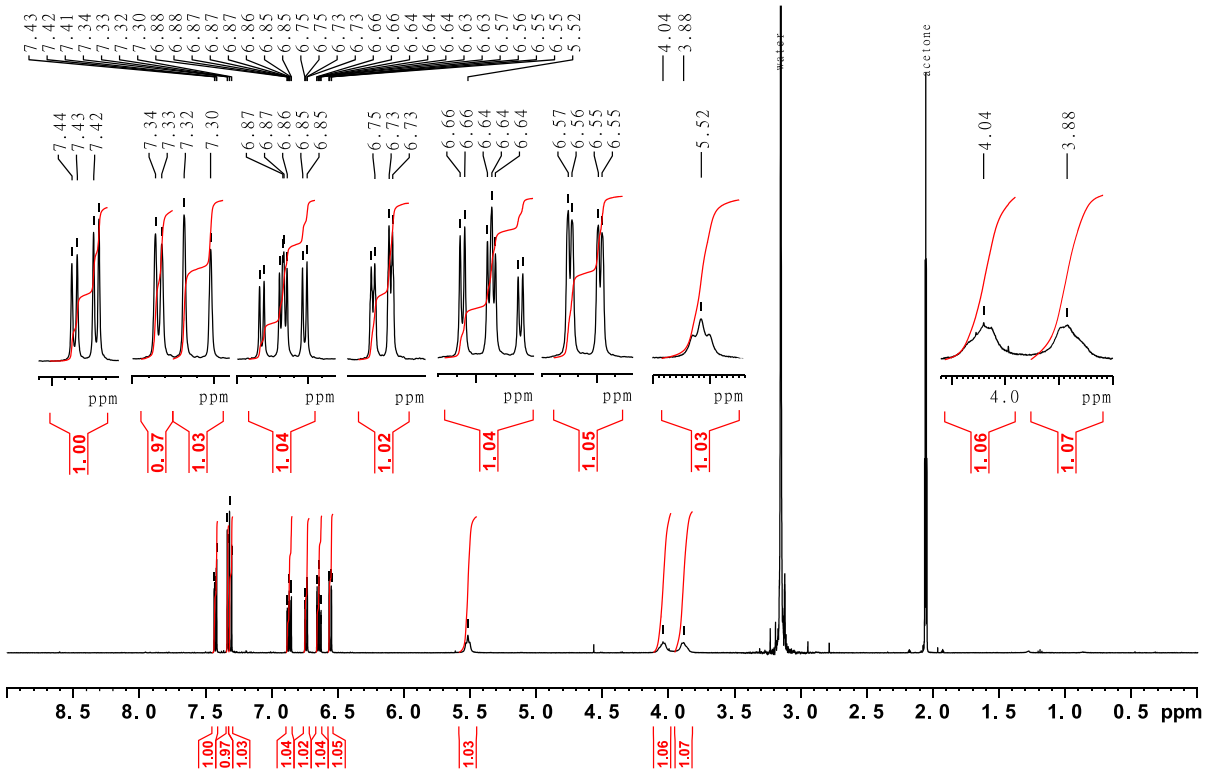

Figure SII.17: 500 MHz ^{1}H-NMR spectrum of (*Z*)-bromo-11,12-dihydrodibenzo[c,g][1,2,5]triazocine.

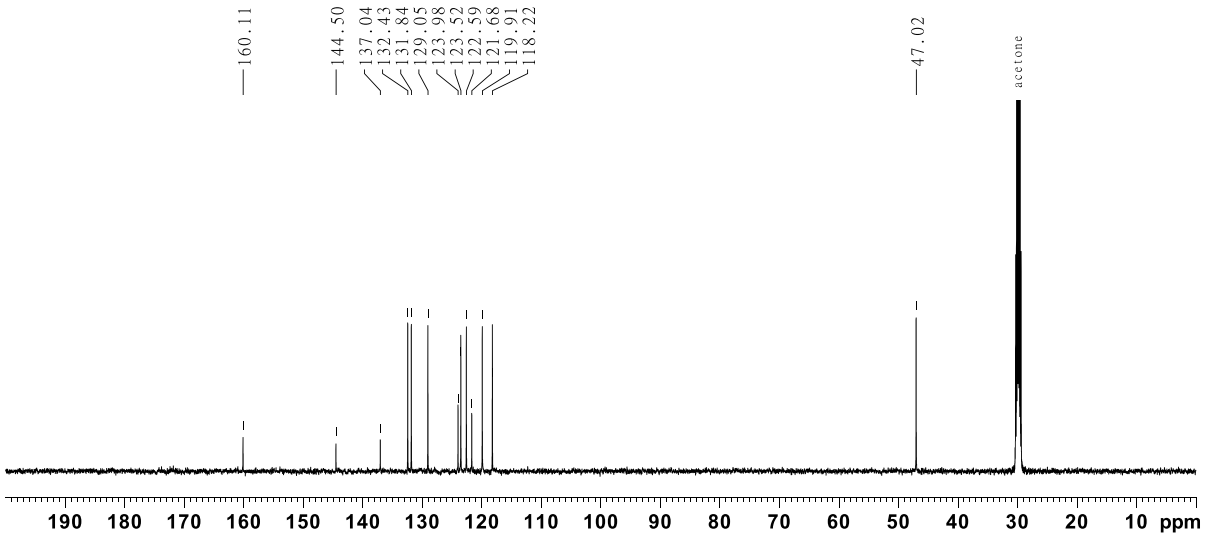

Figure SII.18: 125 MHz ^{13}C{^{1}H}-NMR spectrum of (*Z*)-bromo-11,12-dihydrodibenzo[c,g][1,2,5]triazocine.

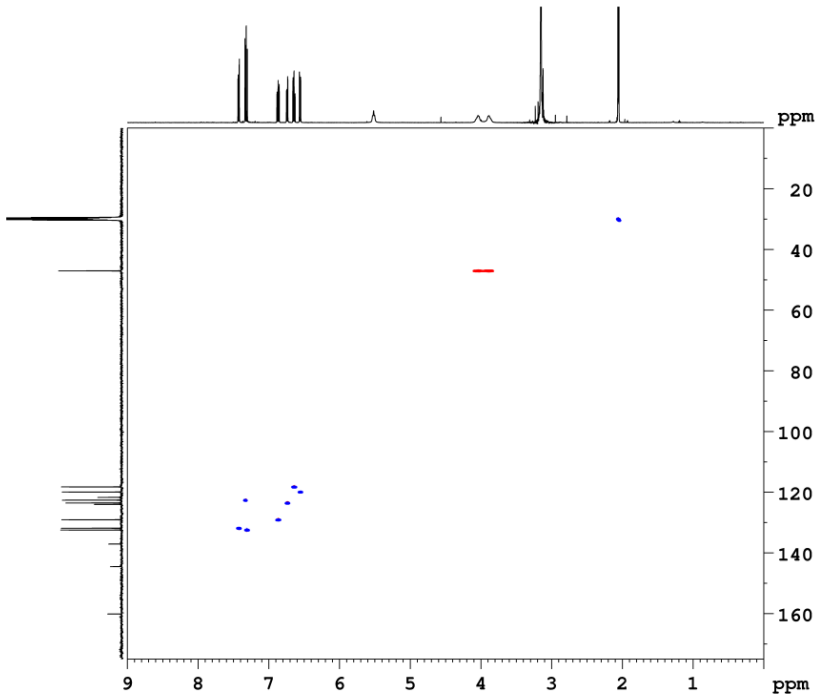

Figure SII.19: 500 MHz ^{1}H-^{13}C HSQC spectrum of (*Z*)-bromo-11,12-dihydrodibenzo[c,g][1,2,5]triazocine.

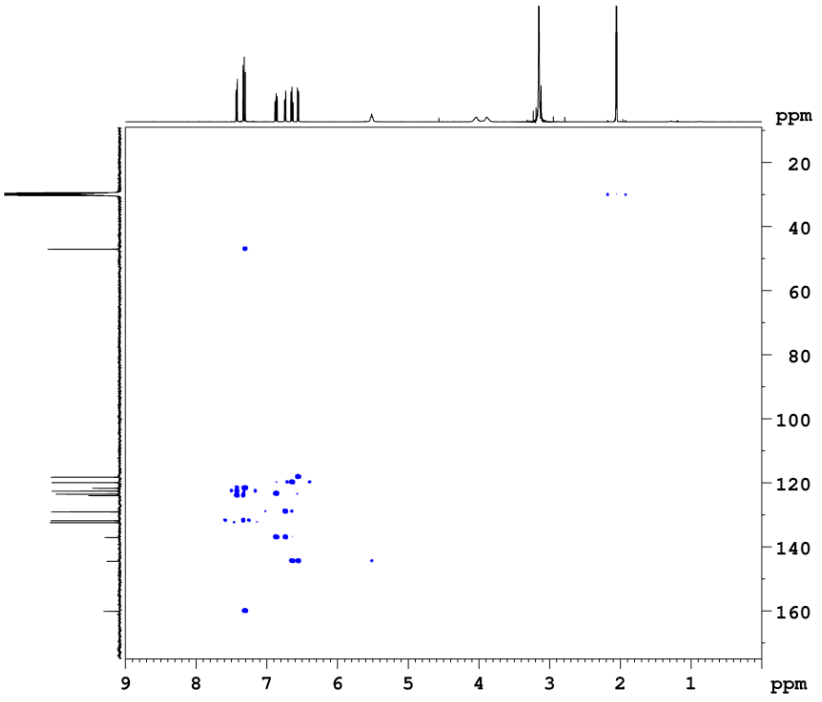

Figure SII.20: 500 MHz HMBC spectrum of (*Z*)-bromo-11,12-dihydrodibenzo[c,g][1,2,5]triazocine.

II.1.6 Synthesis of (*Z*)-1-(3-bromodibenzo[c,g][1,2,5]triazocin-11(12*H*)-yl)-ethan-1-one (2)[1]

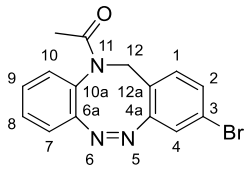

(*Z*)-bromo-11,12-dihydrodibenzo[c,g][1,2,5]triazocine (500 mg, 1.8 mmol) were dissolved in 50 mL anhydrous DMF under a nitrogen atmosphere. NEt_3 (5 mL, 36 mmol) and AcOH (1.03 mL, 18 mmol) were added. The reaction mixture was cooled to 0 °C and T3P (10 mL, 18 mmol, 50% in ethyl acetate) was added dropwise. The reaction mixture was stirred at rt. for 16 h. 100 mL DCM and 100 mL deionized water were added and the organic layer was separated. The aqueous layer was extracted twice with 100 mL DCM and the combined organic layers were dried over $MgSO_4$. The solvent was removed and column chromatography on silica (ethyl acetate/cyclohexane 1:1, R_f = 0.39) gave a yellow solid (492 mg, 1.49 mmol, 83%, lit. 86%[1]).

melting point: 163 °C

^{1}H-NMR (600 MHz, acetone-d_6, 298 K): δ = 7.40 (dd, ^3J = 7.4 Hz, ^4J = 1.6 Hz, 1 H, *H*-8/9), 7.34-7.27 (m, 3 H, *H*-2, *H*-7/10, *H*-8/9), 7.18 (d, ^3J = 8.2 Hz, 1 H, *H*-1), 7.11 (d, ^4J = 2.0 Hz, 1 H, *H*-4), 7.06 (dd, ^3J = 7.8 Hz, ^4J = 0.9 Hz, 1 H, *H*-10), 5.02 (d, ^2J = 14.8 Hz, 1 H, *H*-12a), 4.32 (d, ^2J = 14.7 Hz, 1 H, *H*-12b), 1.79 (s, 3 H, CH_3) ppm.

^{13}C{^{1}H}-NMR (150 MHz, acetone-d_6, 198 K): δ = 169.4 (*C*=O), 157.2 (*C*-4a), 154.1 (*C*-6a/10a), 132.8 (*C*-1), 131.3 (*C*-2), 130.28 (*C*-8/9), 130.22 (*C*-8/9), 129.56 (*C*-7/10), 129.44 (*C*-6a/10a), 124.7 (*C*-12a), 122.7 (*C*-4), 122.3 (*C*-3), 120.0 (*C*-7/10), 51.5 (*C*-12), 23.0 (*C*H_3) ppm.

IR (ATR): $\tilde{\nu}$ = 3049 (m), 2928 (m), 1658 (s), 1590 (m), 1518 (w), 1475 (m), 1380 (s), 1338 (s), 1294 (m), 1242 (w), 1161 (m), 1115 (w), 1085 (m), 1031 (m), 1007 (w), 962 (m), 925 (w), 887 (w), 872 (w), 847 (m), 815 (s), 782 (w), 762 (s), 738 (m), 689 (w), 659 (m), 629 (w), 584s (w), 532 (w), 441 (s), 405 (m) cm^{-1}.

HR-MS (ESI, DCM): *m/z* $[M+H]^+$ calculated for $C_{15}H_{12}N_3O^{79}Br+H^+$: 330.0237; found: 330.0233 ± 1.18 ppm.

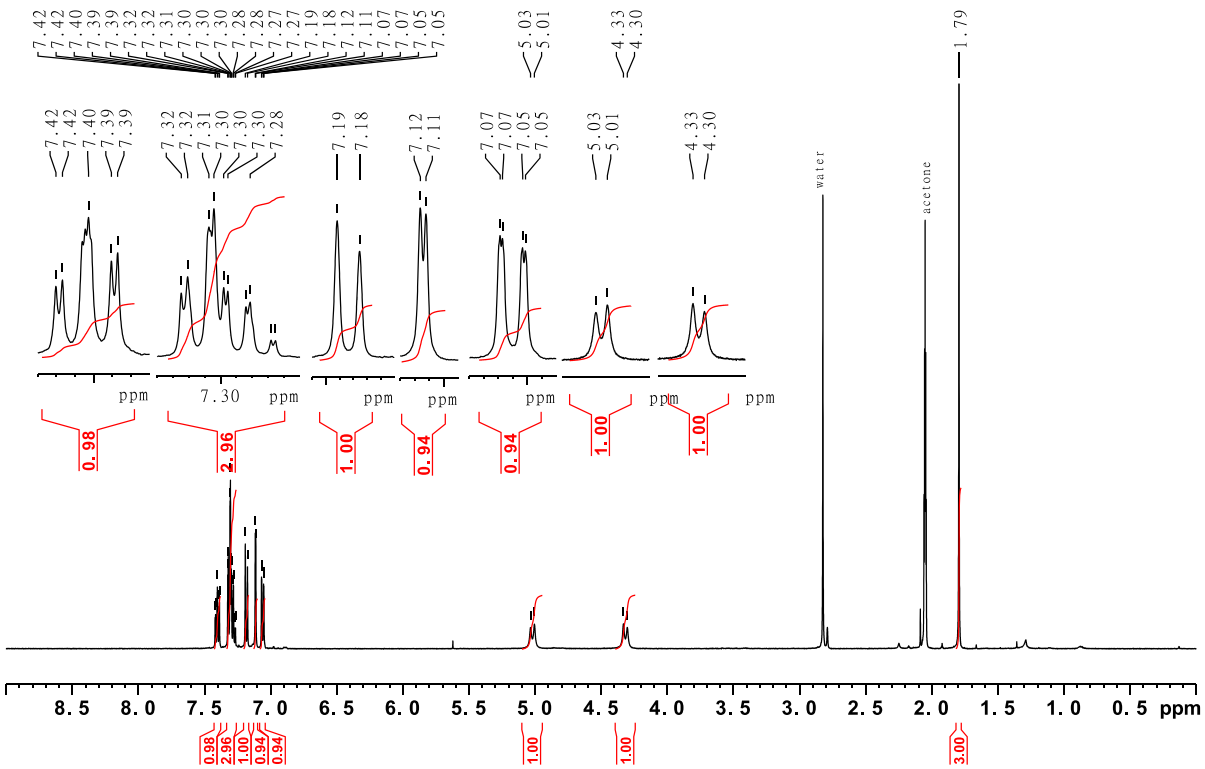

Figure SII.21: 600 MHz ^{1}H-NMR spectrum of (*Z*)-1-(3-bromodibenzo[c,g][1,2,5]triazocin-11(12*H*)-yl)-ethan-1-one (**2**).

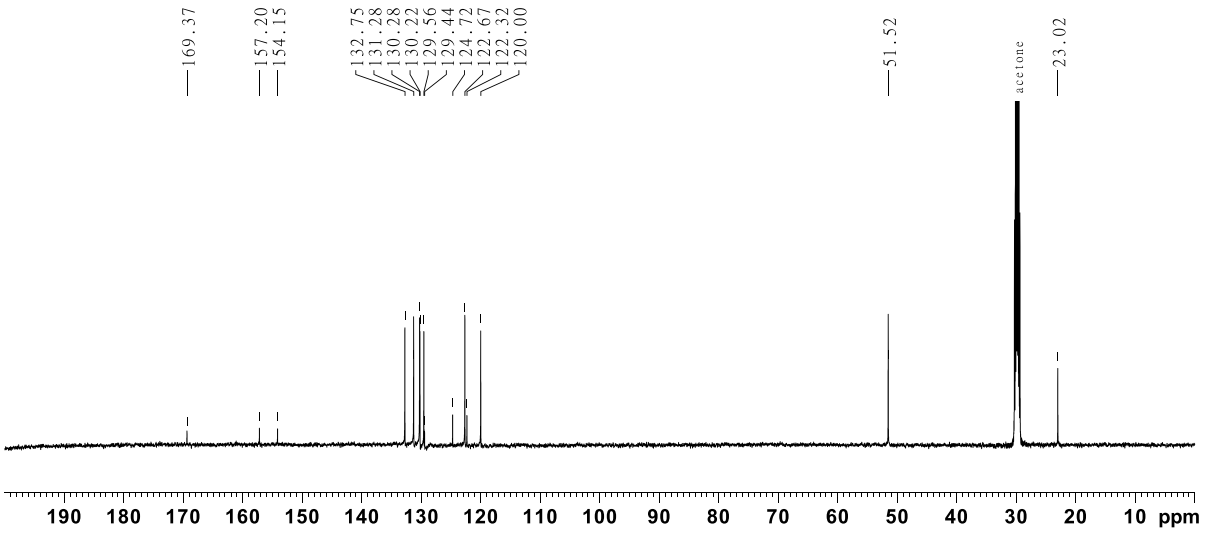

Figure SII.22: 150 MHz ^{13}C{^{1}H}-NMR spectrum of (*Z*)-1-(3-bromodibenzo[c,g][1,2,5]triazocin-11(12*H*)-yl)-ethan-1-one (**2**).

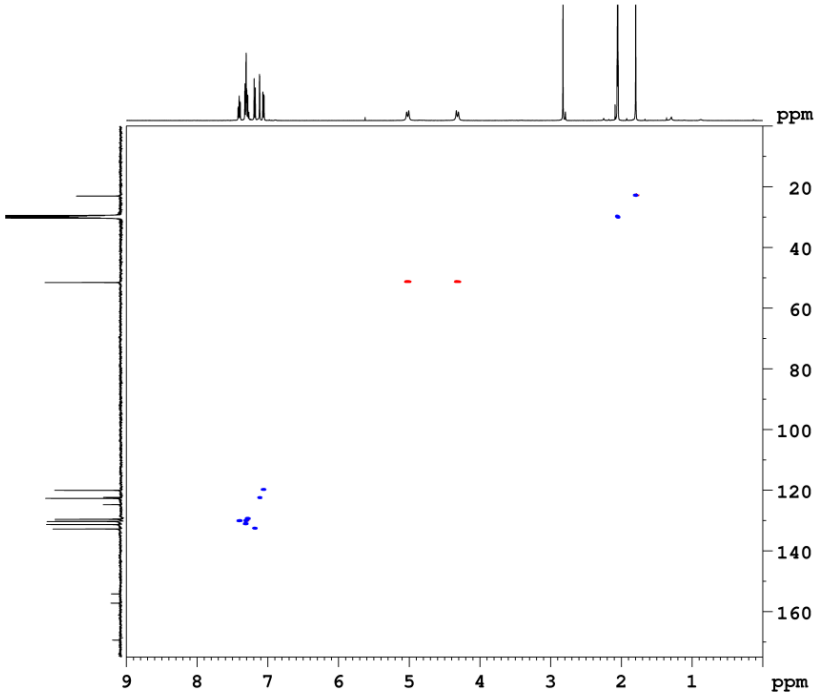

Figure SII.23: 600 MHz ^{1}H-^{13}C HSQC spectrum of (*Z*)-1-(3-bromodibenzo[c,g][1,2,5]triazocin-11(12*H*)-yl)-ethan-1-one (**2**).

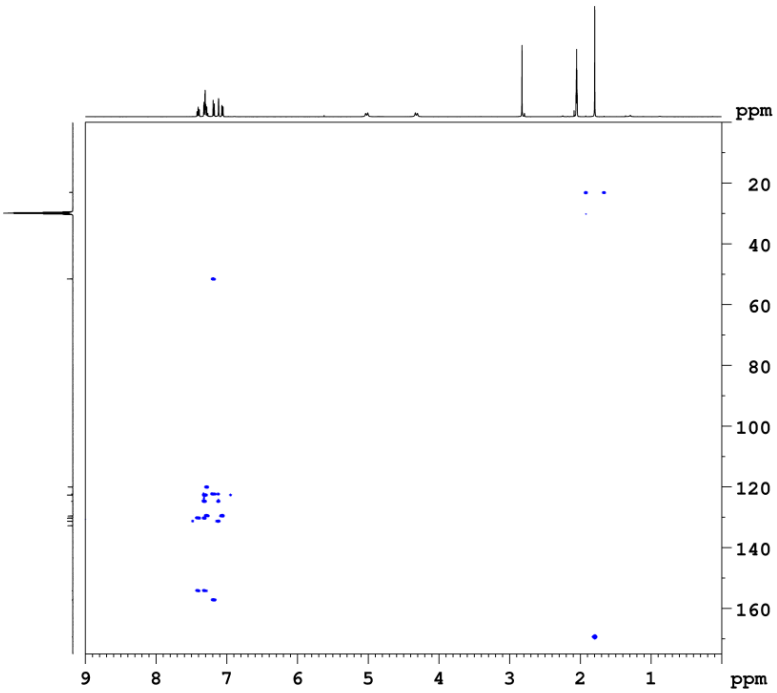

Figure SII.24: 600 MHz HMBC spectrum of (*Z*)-1-(3-bromodibenzo[c,g][1,2,5]triazocin-11(12*H*)-yl)-ethan-1-one (**2**).

II.1.7 Synthesis of *tert*-butyl-(2-((4-iodo-2-nitrobenzyl)amino)phenyl)carbamate[1]

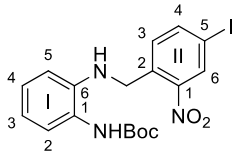

Under a nitrogen atmosphere triethylamine (4.25 mL, 24.9 mmol) and 1-(bromomethyl)-4-iodo-2-nitrobenzene (7.81 g, 22.9 mmol) were added to solution of tert-butyl-(2-aminophenyl)carbamate (4.77 g, 22.9 mmol) in 100 mL abs. THF. The reaction mixture was heated to reflux with an oil bath and stirred for 16 h at that temperature. Afterwards the solvent was evaporated and 100 mL of deionized water and 100 mL DCM were added to the residue. The organic layer was separated and the aqueous layer was extracted twice with 50 mL of DCM. The combined organic layers were dried over $MgSO_4$ and the solvent was evaporated. Recrystallization from cyclohexane/ethyl acetate (1:1) gave the product as yellow solid (7.39 g, 15.7 mmol, 69%, lit. 96%[1]).

melting point: 109 °C

^{1}H-NMR (500 MHz, $CDCl_3$, 298 K): δ = 8.37 (d, ^4J = 1.7 Hz, 1 H, Ar^{II}-*H*-3), 7.85 (dd, ^3J = 8.3 Hz, ^4J = 1.6 Hz, 1 H, Ar^{II}-*H*-5), 7.38 (d, ^3J = 8.2 Hz, 1 H, Ar^{II}-*H*-6), 7.24 (d, ^3J = 7.6 Hz, 1 H, Ar^{I}-*H*-6), 7.00 (td, ^3J = 8.0 Hz, ^4J = 1.3 Hz, 1 H, Ar^{I}-*H*-4), 6.75 (t, ^3J = 7.6 Hz, 1 H, Ar^{I}-*H*-5), 6.43 (d, ^3J = 8.0 Hz, 1 H, Ar^{I}-*H*-3), 6.18 (br. s, 1 H, N*H*), 4.68 (s, 2 H, CH_2), 1.51 (s, 9 H, *t*Bu-*H*) ppm.

^{13}C{^{1}H}-NMR (125 MHz, $CDCl_3$, 298 K): δ = 154.4 (*C*=O), 148.6 (Ar^{II}-*C*-2), 142.7 (Ar^{II}-*C*-5), 141.5 (Ar^{I}-*C*-2), 135.3 (Ar^{II}-*C*-1), 133.8 (Ar^{II}-*C*-3), 131.5 (Ar^{II}-*C*-6), 127.1 (Ar^{I}-*C*-4), 126.0 (Ar^{I}-*C*-6), 124.3 (Ar^{I}-*C*-1), 118.9 (Ar^{I}-*C*-5), 112.9 (Ar^{I}-*C*-3), 91.6 (Ar^{II}-*C*-4), 81.0 (-*C*-(CH_3)$_3$), 45.4 (-*C*H_2), 28.5 (-*C*H_3), ppm.

IR (ATR): $\tilde{\nu}$ = 3374 (m), 2974 (m), 2931 (w), 2169 (w), 2051 (w), 1978 (w), 1684 (m), 1605 (m), 1509 (s), 1446 (m), 1391 (w), 1366 (w), 1342 (m), 1307 (w), 1272 (w), 1244 (m), 1152 (s), 1047 (m), 1024 (m), 934 (w), 869 (w), 823 (w), 743 (s), 715 (w), 637 (w) cm^{-1}..

HR-MS (ESI, DCM): *m/z* $[M+H]^+$ calculated for $C_{18}H_{20}O_4N_3{}^{127}I+H^+$: 470.0571; found: 470.0572 ± 0.08 ppm.

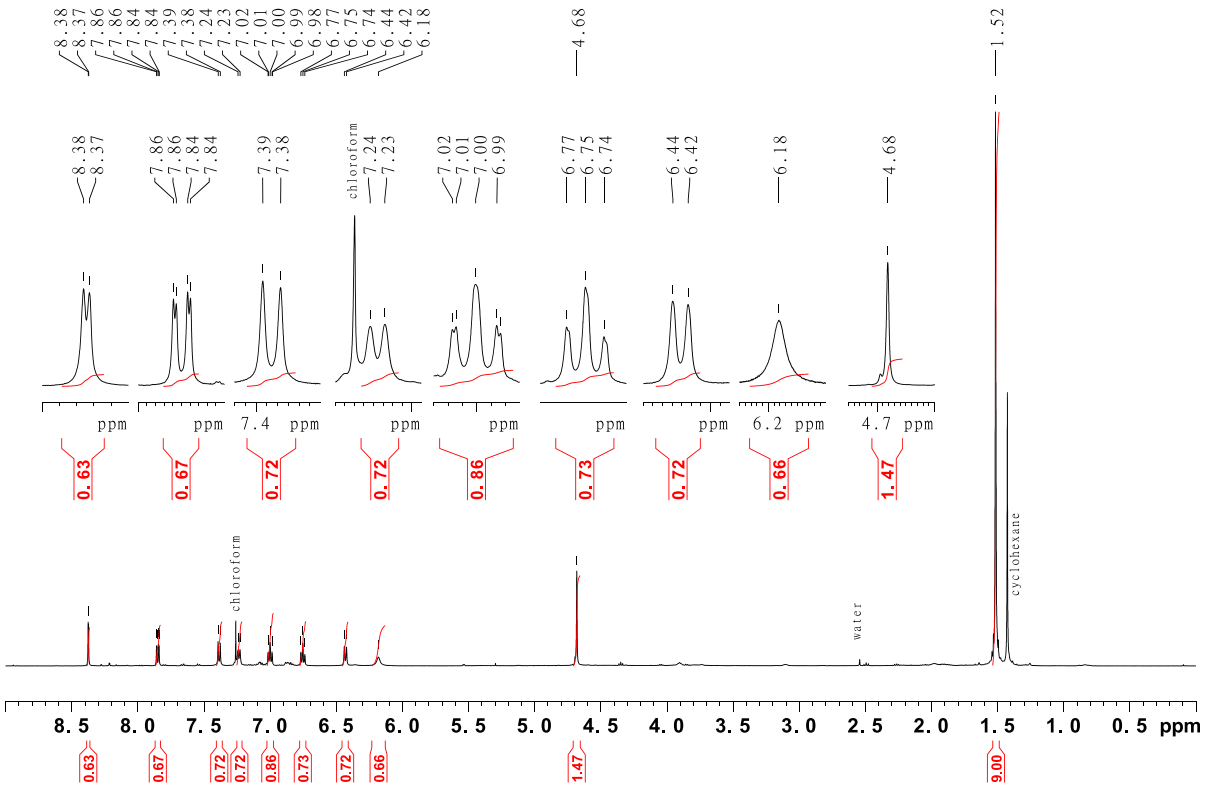

Figure SII.25: 500 MHz ^{1}H-NMR spectrum of *tert*-butyl-(2-((4-iodo-2-nitrobenzyl)amino)phenyl)carbamate.

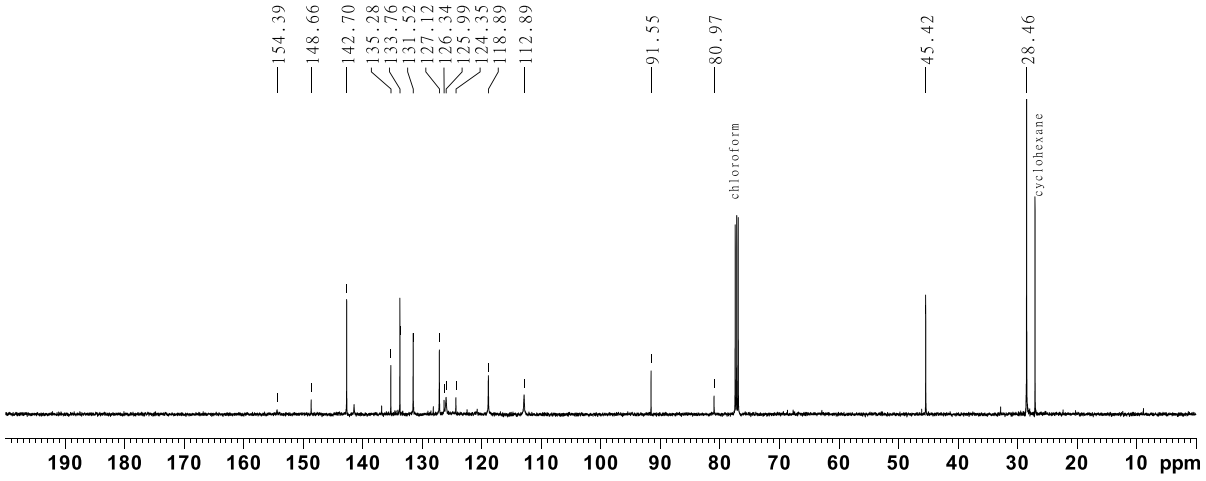

Figure SII.26: 125 MHz ^{13}C{^{1}H}-NMR spectrum of *tert*-butyl-(2-((4-iodo-2-nitrobenzyl)amino)phenyl)carbamate.

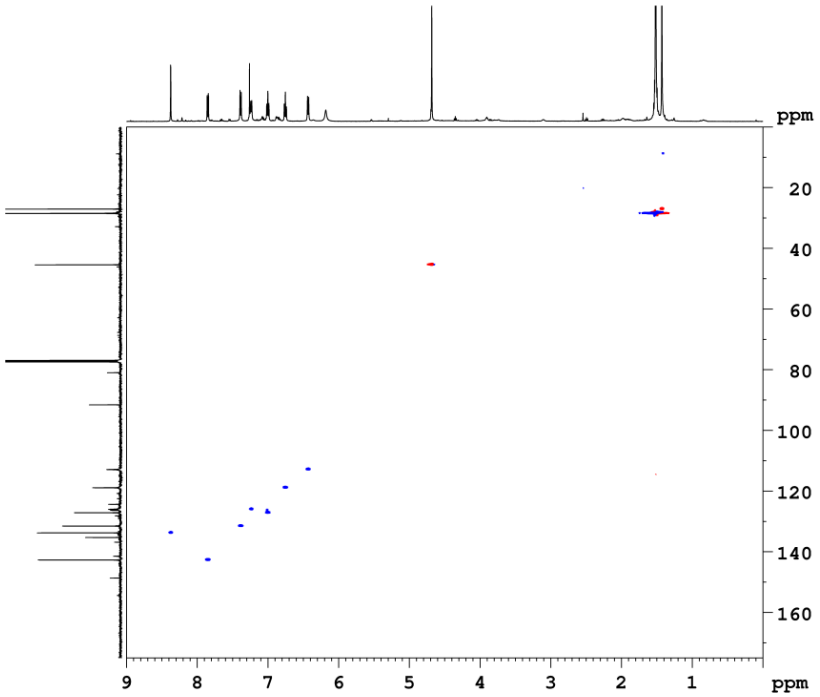

Figure SII.27: 500 MHz ^{1}H-^{13}C HSQC spectrum of *tert*-butyl-(2-((4-iodo-2-nitrobenzyl)amino)phenyl)carbamate.

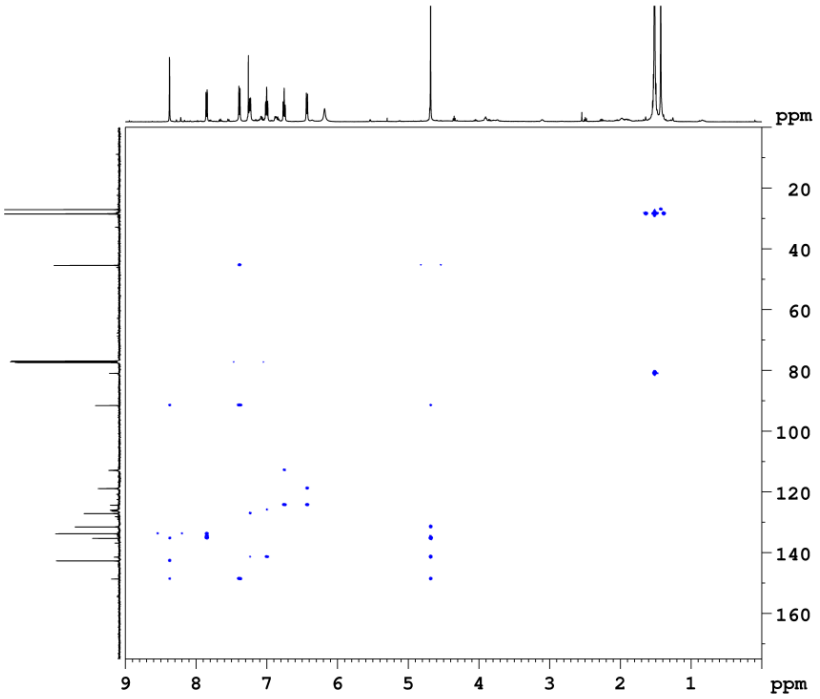

Figure SII.28: 500 MHz HMBC spectrum of *tert*-butyl-(2-((4-iodo-2-nitrobenzyl)amino)phenyl)carbamate.

II.1.8 Synthesis of (9*H*-fluoren-9-yl)methyl-(4-iodo-2-nitrobenzyl)(2-((*tert*-butoxycarbonyl)amino)phenyl)carbamate[1]

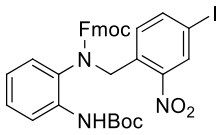

DIPEA (2.67 mL, 15.7 mmol) and 9-Fluorenylmethoxycarbonyl chlorid (8.12 g, 31.4 mmol) were added to a solution of *tert*-butyl-(2-((4-iodo-2-nitrobenzyl)amino)phenyl)carbamate (7.39 g, 15.7 mmol) in 50 mL abs. DMF under a nitrogen atmosphere. The reaction mixture was stirred for 48 h at rt. and the solvent was evaporated subsequently. 100 mL of deionized water and 100 mL of DCM were added to the residue. The organic layer was separated and the aqueous layer was extracted twice with 100 mL DCM. The combined organic layers were dried over $MgSO_4$ and the solvent was evaporated. Column chromatography on silica (ethyl acetate/cyclohexane 1:4, R_f = 0.48) gave a slightly yellow solid (6.66 g, 9.63 mmol, 62%, lit. 33%[1]).

melting point: 99 °C

^{1}H-NMR (600 MHz, acetone-d_6, 298 K): δ = 8.29 (d, ^4J = 1.8 Hz, 1 H, Ar-*H*), 8.08-7.70 (m, 5 H), 7.40-7.02 (m, 10 H), 5.18-4.93 (m, 2 H), 4.53-4.01 (m, 3 H), 1.45 (s, 9 H, *t*Bu-*H*) ppm.

^{13}C{^{1}H}-NMR (150 MHz, acetone-d_6, 298 K): δ = 153.5, 143.0, 133.9, 129.2, 128.5, 127.9, 126.1, 124.4, 120.7, 92.7, 80.4, 68.4, 47.8, 28.5 ppm.

IR (ATR): $\tilde{\nu}$ = 3314 (w), 3066 (w), 2051 (w), 2024 (w), 2012 (w), 1709 (s), 1595 (m), 1525 (s), 1477 (w), 1449 (s), 1401 (m), 1345 (m), 1296 (m), 1216 (m), 1155 (m), 1043 (m), 981 (w), 940 (w), 870 (m), 838 (w), 757 (w), 749 (w), 738 (s), 620 (m), 573 (w), 538 (m), 494 (w) cm^{-1}.

HR-MS (ESI, DCM): *m/z* $[M+H]^+$ calculated for $C_{30}H_{30}O_6N_3{}^{127}I+H^+$: 692.1252; found: 692.1259 ± 1.00 ppm.

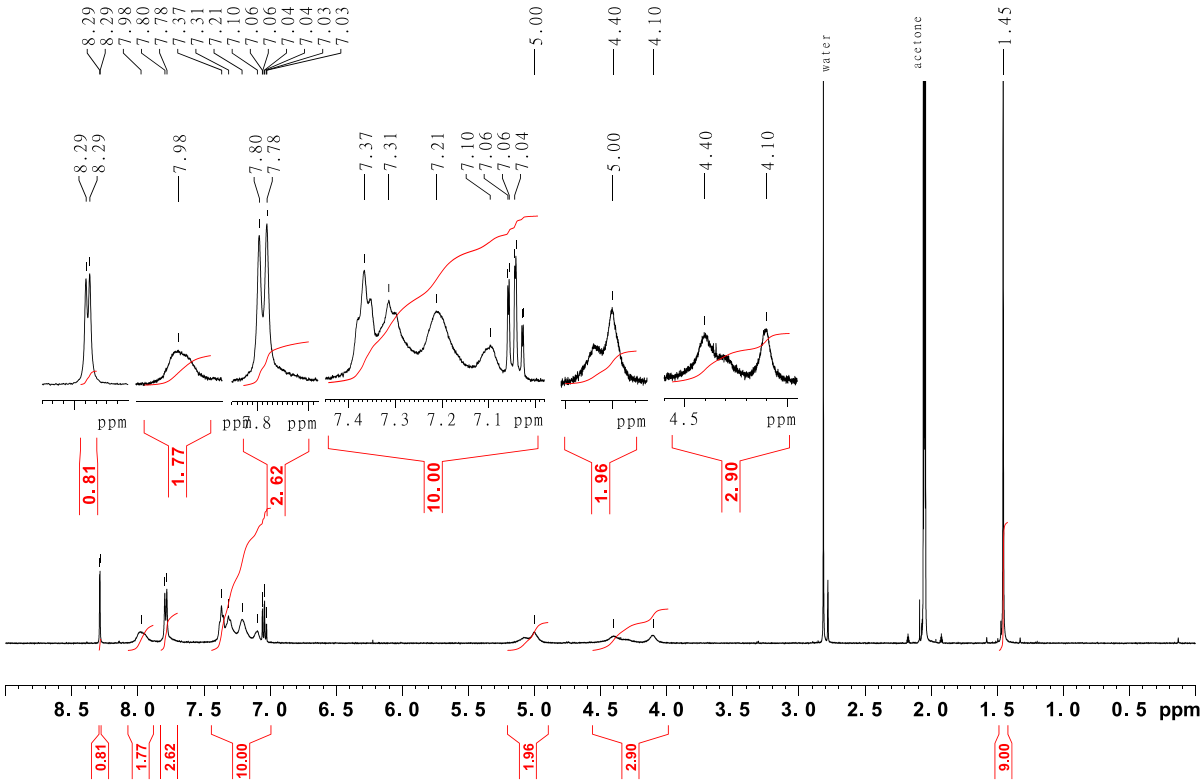

Figure SII.29: 600 MHz ^{1}H-NMR spectrum of (9*H*-fluoren-9-yl)methyl-(4-iodo-2-nitrobenzyl)(2-((*tert*-butoxycarbonyl)amino)phenyl)carbamate.

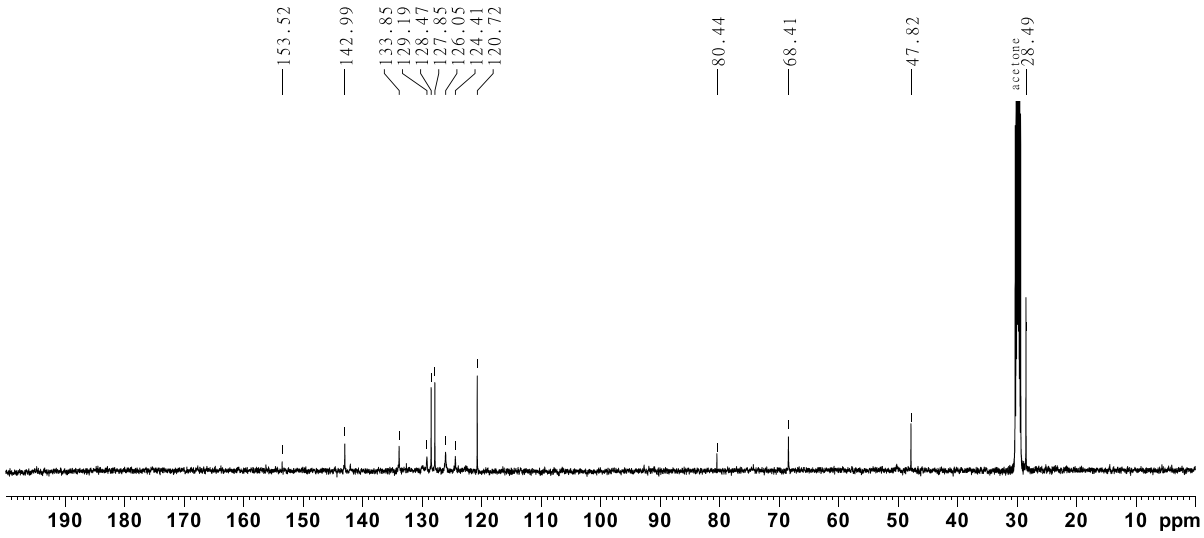

Figure SII.30: 150 MHz ^{13}C{^{1}H}-NMR spectrum of (9*H*-fluoren-9-yl)methyl-(4-iodo-2-nitrobenzyl)(2-((*tert*-butoxycarbonyl)amino)phenyl)carbamate.

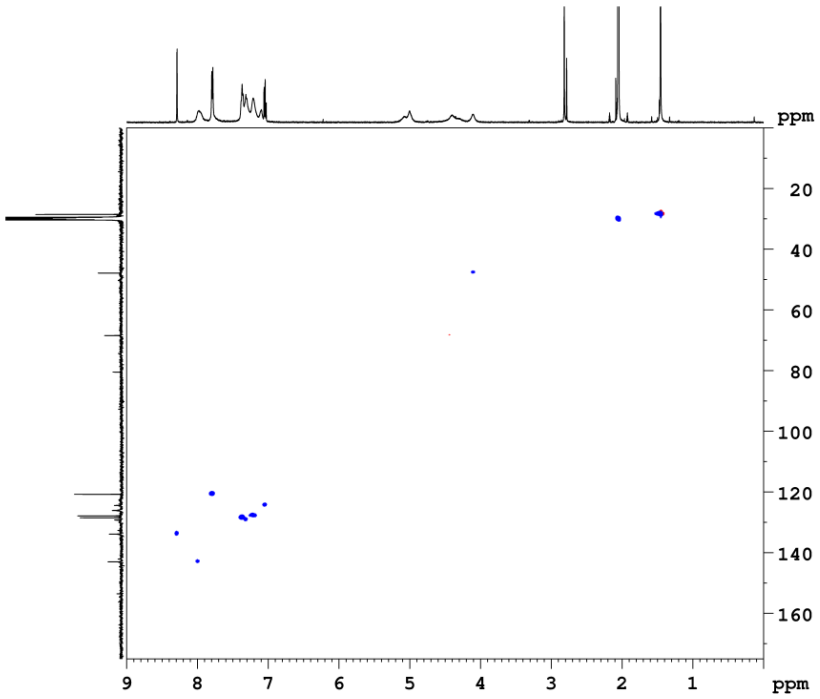

Figure SII.31: 600 MHz ^{1}H-^{13}C HSQC spectrum of (9*H*-fluoren-9-yl)methyl-(4-iodo-2-nitrobenzyl)(2-((*tert*-butoxycarbonyl)amino)phenyl)carbamate.

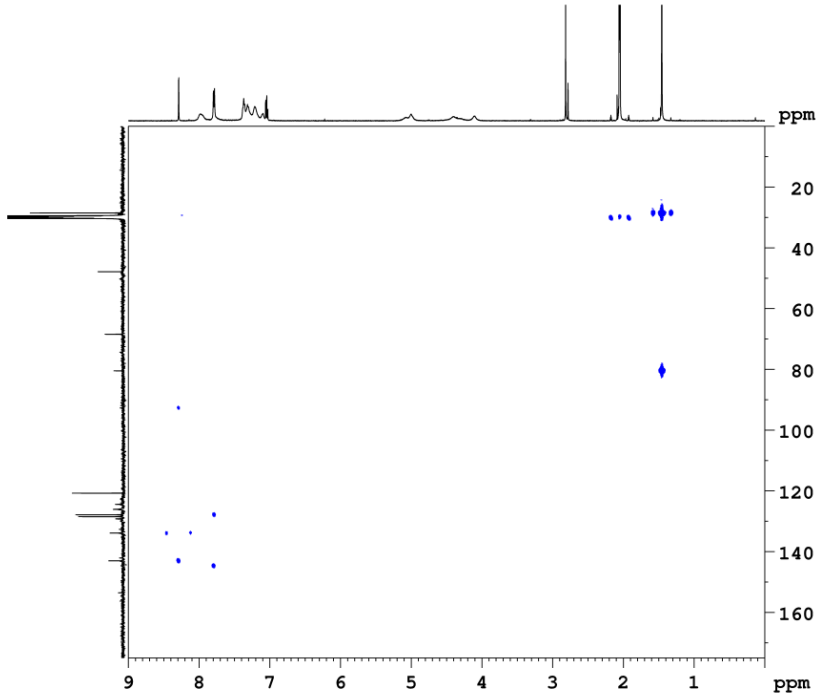

Figure SII.32: 600 MHz HMBC spectrum of (9*H*-fluoren-9-yl)methyl-(4-iodo-2-nitrobenzyl)(2-((*tert*-butoxycarbonyl)amino)phenyl)carbamate.

II.1.9 Synthesis of (9*H*-fluoren-9-yl)methyl-(2-aminophenyl)(4-iodo-2-nitrobenzyl)carbamate[1]

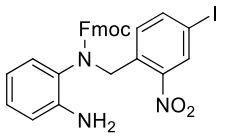

(9*H*-fluoren-9-yl)methyl-(4-iodo-2-nitrobenzyl)(2-((*tert*-butoxycarbonyl)amino)phenyl)carbamate (6.66 g, 9.63 mol) was dissolved in 100 mL DCM and 30 mL TFA was added. The reaction mixture was stirred at rt. for 16 h and neutralized with saturated aqueous $NaHCO_3$ subsequently. The organic layer was separated and the aqueous layer was extracted twice with 100 mL. The combined organic layers were dried over $MgSO_4$ and the solvent was evaporated to obtain a pale yellow solid (5.74 g, 9.60 mmol, quant., lit. 96%[1]) which was used without further purification.

melting point: 86 °C

^{1}H-NMR (500 MHz, $CDCl_3$, 298 K): δ = 8.24 (d, ^4J = 1.5 Hz, 1 H), 7.87 (br. s, 1 H), 7.72-7.62 (m, 2 H), 7.38-7.32 (m, 3 H), 7.22-7.10 (m, 5 H), 6.78-6.72 (m, 2 H), 6.69-6.65 (m, 1 H), 5.21 (br. s, 1 H, -CH_2), 5.04-3.98 (m, 4 H) ppm.

^{13}C{^{1}H}-NMR (125 MHz, $CDCl_3$, 298 K): δ = 155.2, 143.6, 142.3, 141.4, 133.5, 132.4, 129.2, 128.8, 127.8, 127.1, 125.3, 120.0, 119.0, 92.16, 68.0, 47.2 ppm.

IR (ATR): $\tilde{\nu}$ = 3370 (w), 3039 (w), 2252 (w), 2168 (w), 1978 (w), 1695 (s), 1620 (m), 1525 (s), 1503 (w), 1477 (w), 1449 (m), 1402 (w), 1339 (m), 1297 (m), 1156 (w), 1136 (w), 1043 (w), 987 (w), 870 (m), 795 (w), 756 (w), 738 (s), 692 (w), 620 (m), 534 (w), 501 (w), 480 (w) cm^{-1}.

HR-MS (ESI, DCM): *m/z* $[M+H]^+$ calculated for $C_{28}H_{22}O_4N_3{}^{127}I+H^+$: 592,0729; found: 592.0732 ± 0.78 ppm.

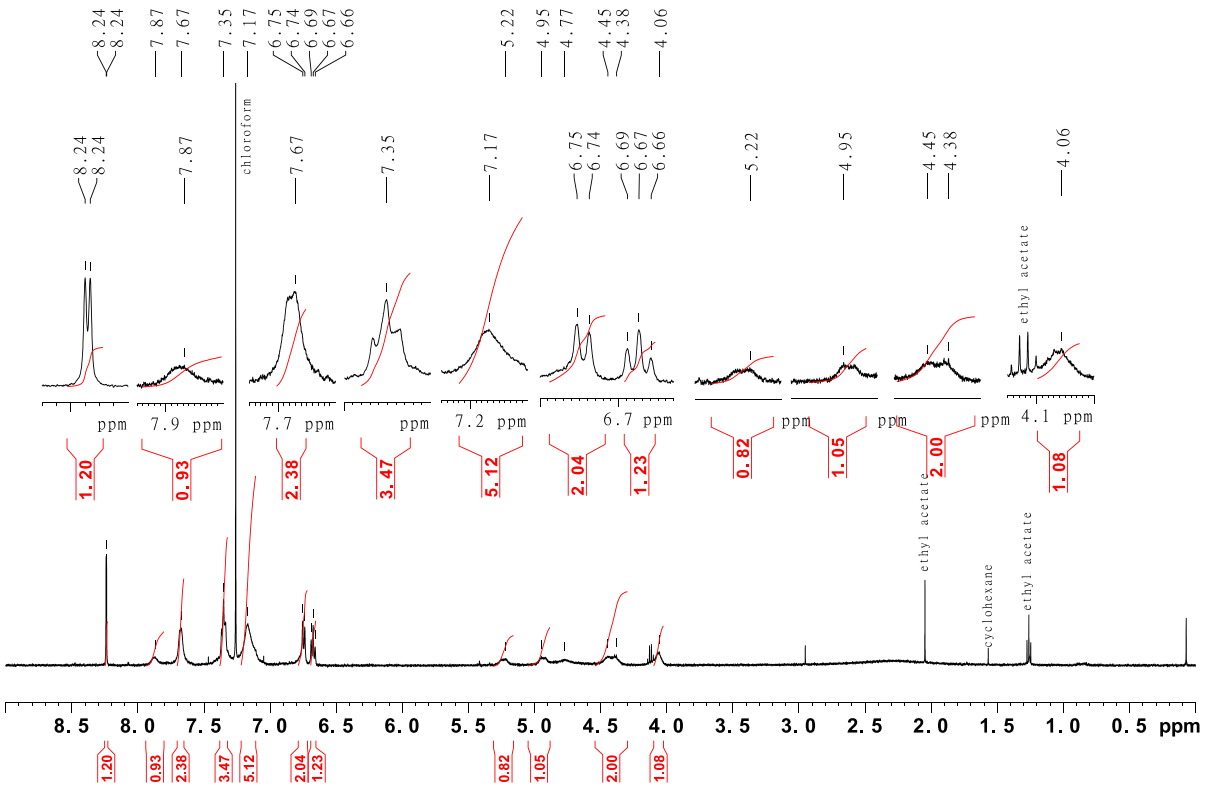

Figure SII.33: 500 MHz ^{1}H-NMR spectrum of (9*H*-fluoren-9-yl)methyl-(2-aminophenyl)(4-iodo-2-nitrobenzyl)carbamate.

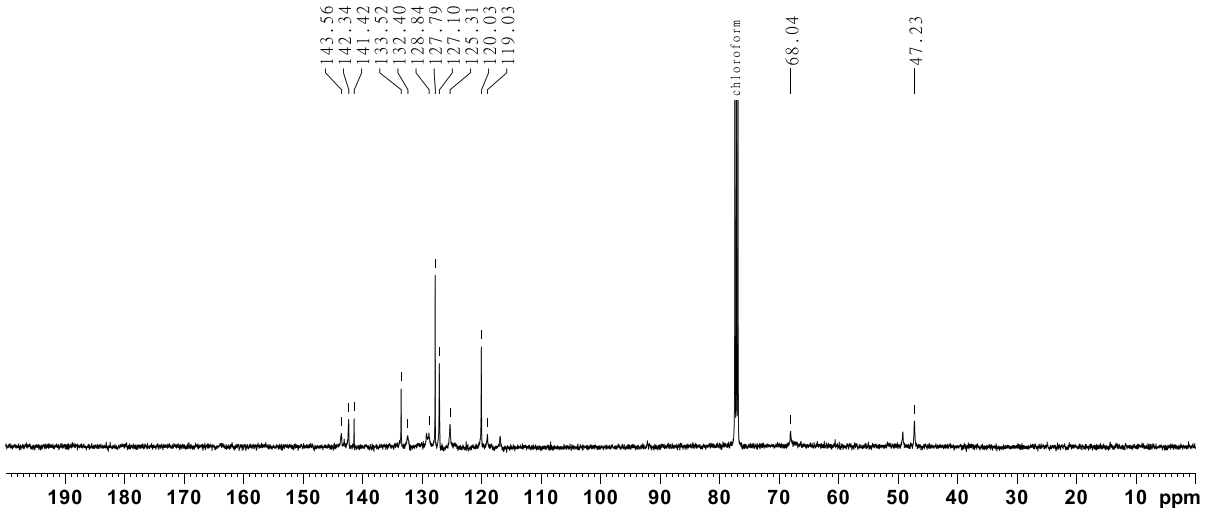

Figure SII.34: 125 MHz ^{13}C{^{1}H}-NMR spectrum of (9*H*-fluoren-9-yl)methyl-(2-aminophenyl)(4-iodo-2-nitrobenzyl)carbamate.

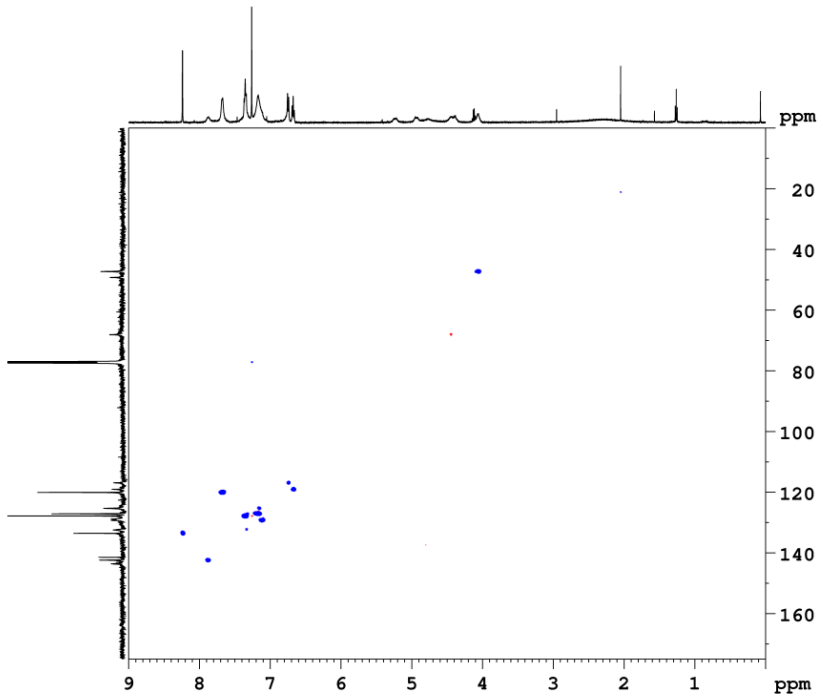

Figure SII.35: 500 MHz ^{1}H-^{13}C HSQC spectrum of (9*H*-fluoren-9-yl)methyl-(2-aminophenyl)(4-iodo-2-nitrobenzyl)carbamate.

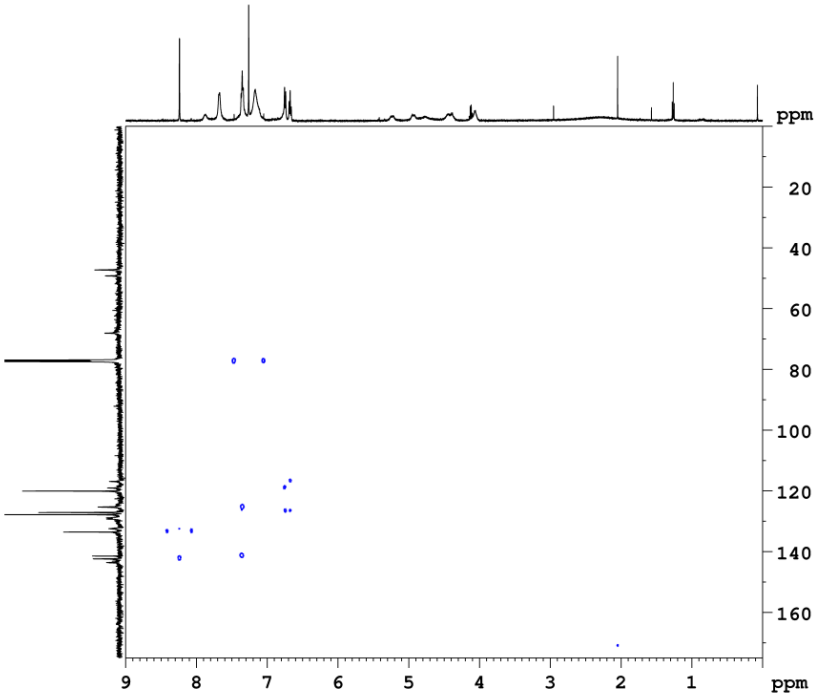

Figure SII.36: 500 MHz HMBC spectrum of (9*H*-fluoren-9-yl)methyl-(2-aminophenyl)(4-iodo-2-nitrobenzyl)carbamate.

II.1.10 Synthesis of (9*H*-fluoren-9-yl)methyl-(*Z*)-3-iododibenzo[c,g][1,2,5]triazocin-11-(12*H*)-carboxylate[1]

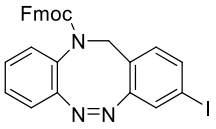

(9*H*-fluoren-9-yl)methyl-(2-aminophenyl)(4-iodo-2-nitrobenzyl)carbamate (5.74 g, 9.71 mmol) was suspended in 250 mL EtOH and $SnCl_2 \cdot 2\ H_2O$ (13.2 g, 46.1 mmol) was added. The reaction mixture was heated to 75 °C with an oil bath and zinc-powder (5.08 g, 77.7 mmol) was added. The reaction mixture was stirred at that temperature for 1 h and then cooled to rt. It was stirred at rt. for 16 h and neutralized with saturated aqueous $NaHCO_3$ solution subsequently. The solvent was evaporated and 100 mL water and 100 mL DCM were added to the residue. The organic layer was separated and the aqueous layer was extracted twice with 100 mL DCM. The combined organic layers were dried over $MgSO_4$ and the solvent was evaporated. The residue was dissolved in 300 mL of acetic acid and *m*CPBA (3.35 g, 19.42 mmol) dissolved in 300 mL acetic acid was added dropwise to the reaction mixture. The reaction mixture was stirred at rt. for 16 h and the solvent was evaporated in the following. 100 mL DCM and 100 mL half-concentrated aqueous $NaHCO_3$ solution were added to the residue. The organic layer was separated and the aqueous layer was extracted twice with 100 mL DCM. The combined organic layers were dried over $MgSO_4$ and the solvent was evaporated. After column chromatography on silica (ethyl acetate/cyclohexane = 1:4, R_f = 0.38) the product could be obtained as yellow solid (2.59 g, 4.66 mmol, 48%, lit. 56%[1]).

melting point: 167 °C

^{1}H-NMR (500 MHz, $CDCl_3$, 298 K): δ = 7.97-6.98 (m, 15 H, Ar-*H*), 4.99-3.99 (m, 5 H, aliph. H), ppm.

^{13}C{^{1}H}-NMR (125 MHz, $CDCl_3$, 298 K): δ = 154.4, 152.6, 144.7, 142.1, 137.4, 132.6, 130.5, 129.5, 129.1 128.54, 128.36, 127.9, 126.1, 124.8, 120.8, 119.7, 93.4, 68.5, 52.8, 47.8 ppm.

IR (ATR): $\tilde{\nu}$ = 3071 (w), 2945 (w), 2255 (w), 2037 (w), 1700 (s), 1585 (m), 1485 (m), 1448 (s), 1315 (s), 1130 (s), 1072 (m), 1041 (m), 1021 (m), 976 (w), 878 (w), 863 (m), 820 (m), 753 (s), 735 (s), 696 (m), 670 (w), 640 (w), 546 (s), 512 (m), 487 (w), 464 (w), 434 (m) cm^{-1}.

HR-MS (ESI, DCM): *m/z* $[M+H]^+$ calculated for $C_{28}H_{20}O_2N_3{}^{127}I+H^+$: 558.0673; found: 558.0667 ± 1.09 ppm.

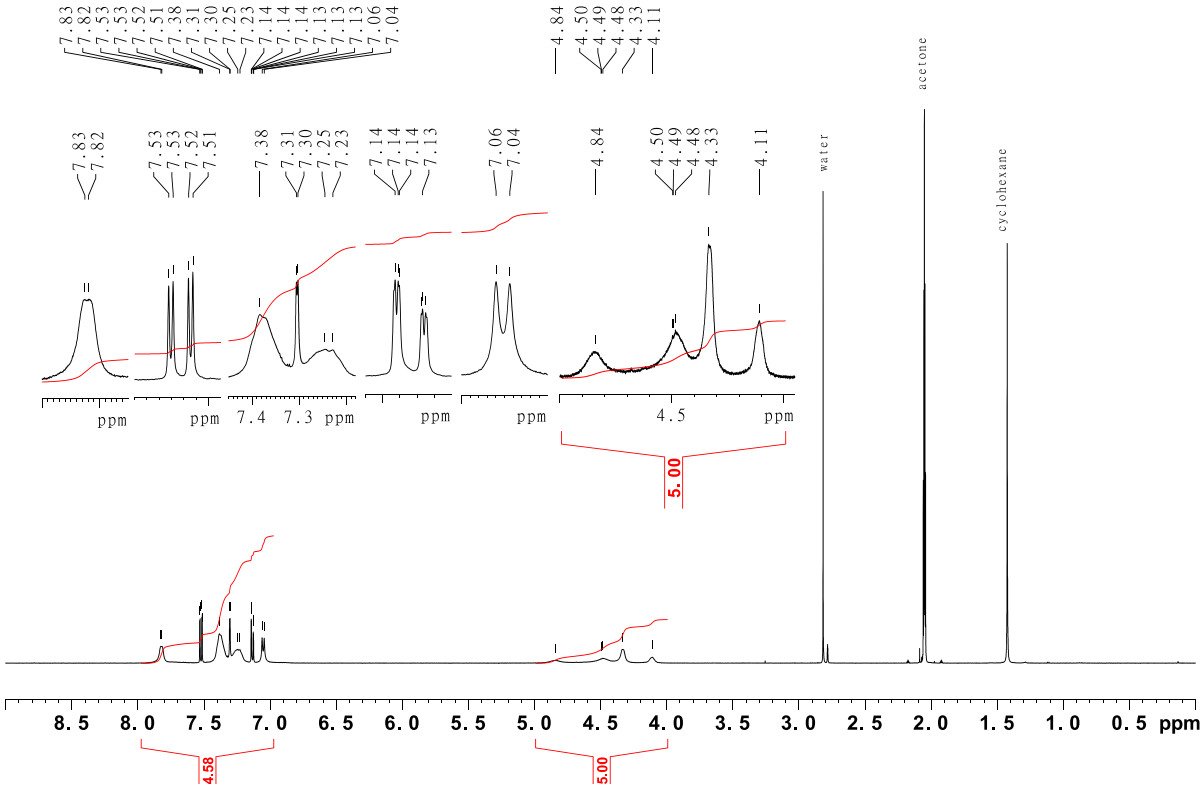

Figure SII.37: 500 MHz ^{1}H-NMR spectrum of (9*H*-fluoren-9-yl)methyl-(*Z*)-3-iododibenzo[c,g][1,2,5]triazocin-11-(12*H*)-carboxylate.

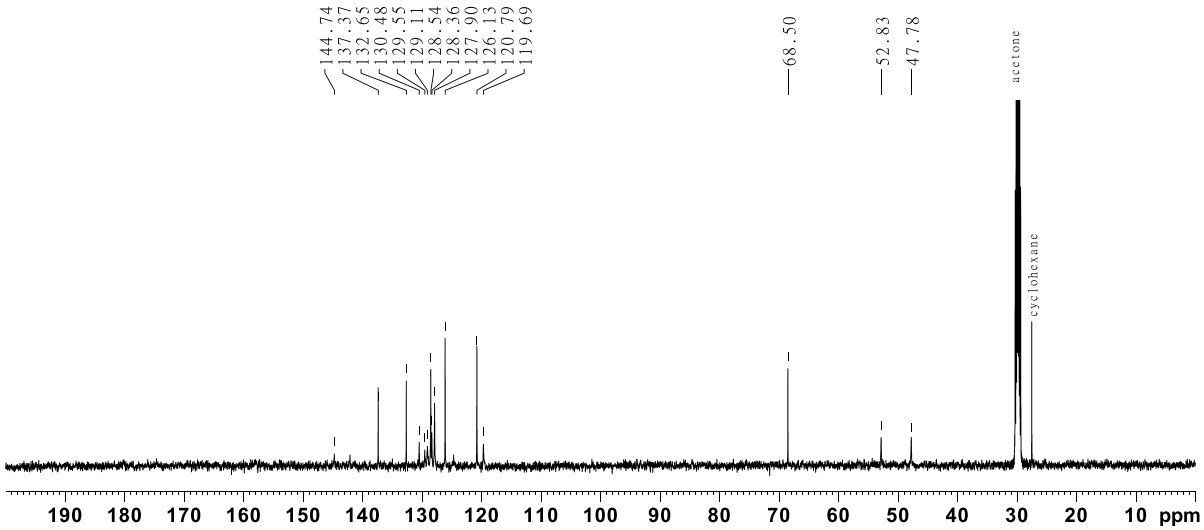

Figure SII.38: 125 MHz ^{13}C{^{1}H}-NMR spectrum of (9*H*-fluoren-9-yl)methyl-(*Z*)-3-iododibenzo[c,g][1,2,5]triazocin-11-(12*H*)-carboxylate.

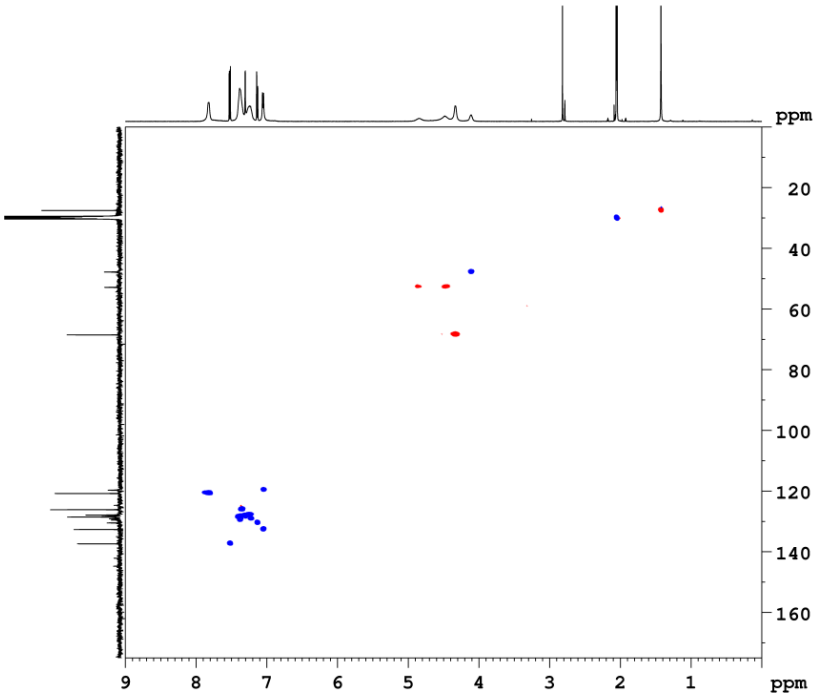

Figure SII.39: 500 MHz ^{1}H-^{13}C HSQC spectrum of (9*H*-fluoren-9-yl)methyl-(*Z*)-3-iododibenzo[c,g][1,2,5]triazocin-11-(12*H*)-carboxylate.

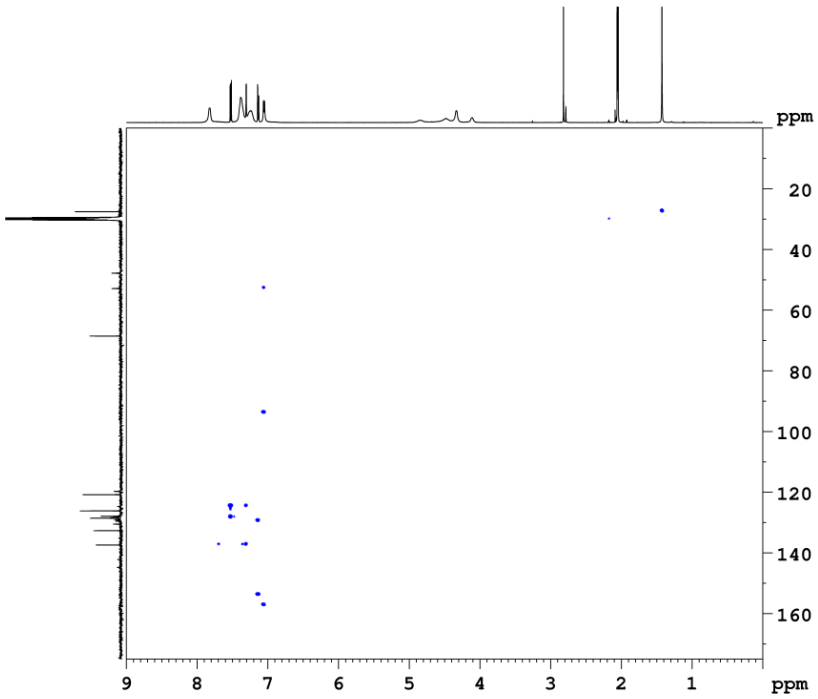

Figure SII.40: 500 MHz HMBC spectrum of (9*H*-fluoren-9-yl)methyl-(*Z*)-3-iododibenzo[c,g][1,2,5]triazocin-11-(12*H*)-carboxylate.

II.1.11 Synthesis of (*Z*)-3-iodo-11,12-dihydrodibenzo[c,g][1,2,5]triazocine[1]

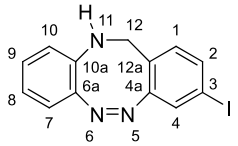

(9*H*-fluoren-9-yl)methyl-(*Z*)-3-iododibenzo[c,g][1,2,5]triazocin-11-(12*H*)-carboxylate (2.09 g, 3.75 mmol) was dissolved in 50 mL of DCM and 50 mL NEt_3 was added. The reaction mixture was stirred at rt. for 16 h. the solvent was evaporated and column chromatography on silica (ethyl acetate/cyclohexane 1:3, R_f = 0.25) gave a red solid (1.25 g, 3.72 mmol, quant., lit. 84%[1]).

melting point: 151 °C

^{1}H-NMR (500 MHz, acetone-d_6, 298 K): δ = 7.63 (dd, ^3J = 8.0 Hz, ^4J = 1.8 Hz, 1 H, *H*-2), 7.52 (d, ^4J = 1.6 Hz, 1 H, *H*-4), 7.16 (d, ^3J = 7.8 Hz, 1 H, *H*-1), 6.88 (td, ^3J = 8.3 Hz, ^4J = 1.6 Hz, 1 H, *H*-9), 6.75 (dd, ^3J = 8.0 Hz, ^4J = 1.6 Hz, 1 H, *H*-7), 6.65 (td, ^3J = 7.9 Hz, ^4J = 1.2 Hz, 1 H, *H*-8), 6.56 (dd, ^3J = 8.2 Hz, ^4J = 1.0 Hz, 1 H, *H*-10), 5.42 (m_c, 1 H, -N*H*), 3.97 (m_c, ^{2} H, -CH_2) ppm.

^{13}C{^{1}H}-NMR (125 MHz, acetone-d_6, 298 K): δ = 160.3 (*C*-4a), 144.6 (*C*-6a), 137.9 (*C*-2), 137.1 (*C*-10a), 131.8 (*C*-1), 129.0 (*C*-9), 128.5 (*C*-4), 124.5 (*C*-12a), 123.6 (*C*-7), 119.9 (*C*-10), 118.3 (*C*-8), 93.1 (*C*-3), 47.2 (CH_2) ppm.

IR (ATR): $\tilde{\nu}$ = 3381 (m), 3042 (w), 2255 (w), 2169 (w), 1597 (m), 1582 (m), 1514 (w), 1479 (s), 1385 (w), 1315 (m), 1246 (w), 1161 (m), 1145 (w), 1117 (w), 1066 (m), 970 (w), 938 (w), 912 (m), 875 (w), 835 (m), 810 (m), 749 (s), 721 (w), 703 (w), 650 (w), 601 (m), 543 (w), 501 (w), 466 (m), 454 (w) cm^{-1}.

HR-MS (ESI, DCM): *m/z* $[M+H]^+$ calculated for $C_{13}H_{10}N_3{}^{127}I+H^+$: 335.9992; found: 335.9986 ± 0.57 ppm.

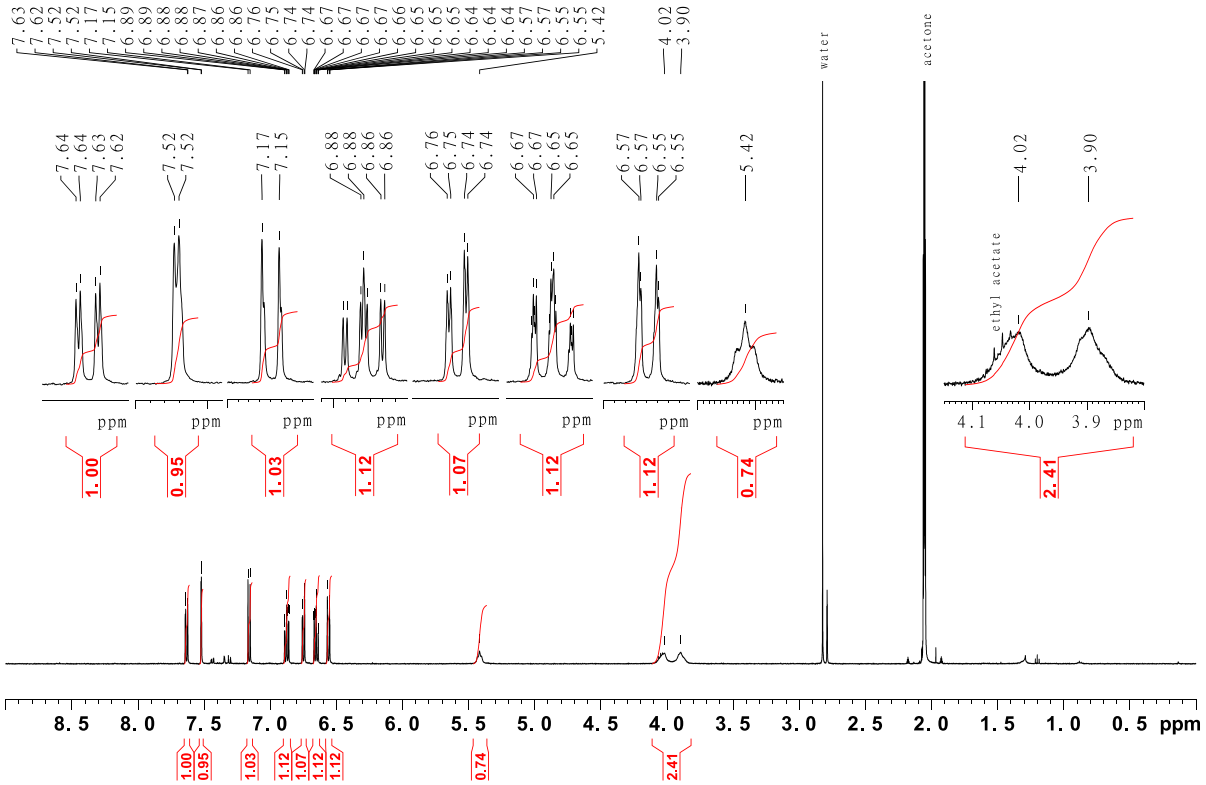

Figure SII.41: 500 MHz ^{1}H-NMR spectrum of (*Z*)-3-iodo-11,12-dihydrodibenzo[c,g][1,2,5]triazocine.

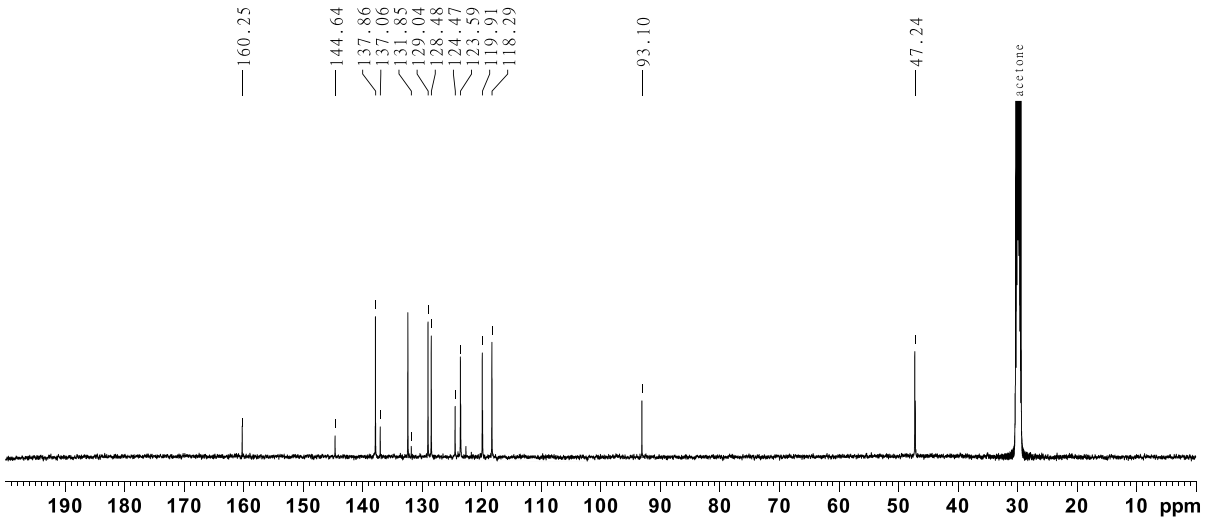

Figure SII.42: 125 MHz ^{13}C{^{1}H}-NMR spectrum of (*Z*)-3-iodo-11,12-dihydrodibenzo[c,g][1,2,5]triazocine.

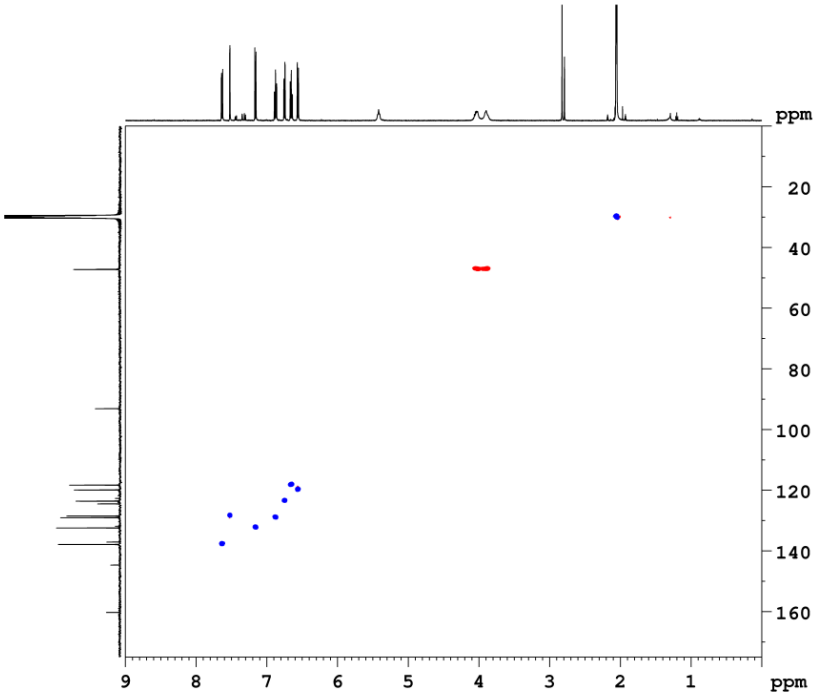

Figure SII.43: 500 MHz ^{1}H-^{13}C HSQC spectrum of (*Z*)-3-iodo-11,12-dihydrodibenzo[c,g][1,2,5]triazocine.

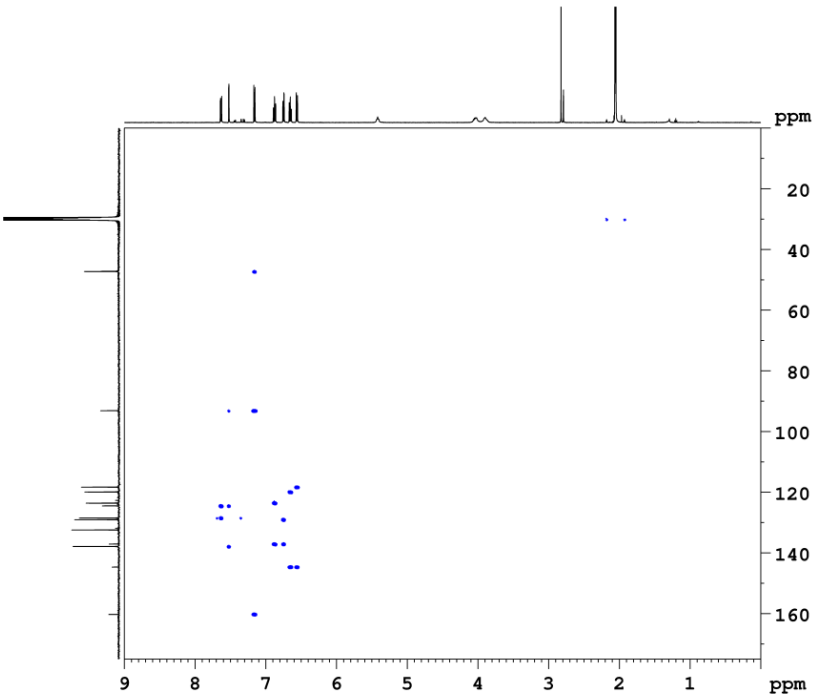

Figure SII.44: 500 MHz HMBC spectrum of (*Z*)-3-iodo-11,12-dihydrodibenzo[c,g][1,2,5]triazocine.

II.1.12 Synthesis of (*Z*)-1-(3-iododibenzo[c,g][1,2,5]triazocin-11(12*H*)-yl)-ethan-1-one (3)[1]

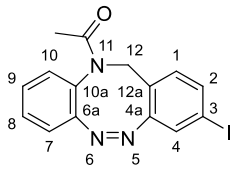

(*Z*)-3-iodo-11,12-dihydrodibenzo[c,g][1,2,5]triazocine (603 mg, 1.8 mmol) were dissolved in 50 mL anhydrous DMF under a nitrogen atmosphere. NEt_3 (2.5 mL, 3.6 mmol) and AcOH (1.03 mL, 18 mmol) were added. The reaction mixture was cooled to 0 °C and T3P (10 mL, 18 mmol, 50% in ethyl acetate) was added dropwise. The reaction mixture was stirred at rt. for 16 h. 100 mL DCM and 100 mL deionized water were added and the organic layer was separated. The aqueous layer was extracted twice with 100 mL DCM and the combined organic layers were dried over $MgSO_4$. The solvent was removed and column chromatography on silica (ethyl acetate/cyclohexane 1:1, R_f = 0.39) gave a yellow solid (476 mg, 1.26 mmol, 70%, lit. 60%[1]).

melting point: 179 °C

^{1}H-NMR (600 MHz, acetone-d_6, 298 K): δ = 7.51 (dd, ^3J = 8.0 Hz, ^4J = 1.8 Hz, 1 H, *H*-2), 7.40 (td, ^3J = 7.5 Hz, ^4J = 1.6 Hz, 1 H, *H*-8/9), 7.32-7.26 (m, 3 H, *H*-4, *H*-7/10, *H*-8/9), 7.06 (dd, ^3J = 7.8 Hz, ^4J = 1.1 Hz, 1 H, *H*-7/10), 7.03 (d, ^3J = 8.1 Hz, 1 H, *H*-1), 5.02 (d, ^2J = 14.6 Hz, 1 H, *H*-12), 4.29 (d, ^2J = 14.7 Hz, 1 H, *H*-12'), 1.79 (s, 3 H, CH_3), ppm.

^{13}C{^{1}H}-NMR (150 MHz, acetone-d_6, 298 K): δ = 169.4 (*C*=O), 157.1 (*C*-4a), 154.2 (*C*-6a/10a), 137.4 (*C*-2), 132.7 (*C*-1), 130.28 (*C*-7/10), 130.18 (*C*-8/9), 129.54 (*C*-8/9), 129.45 (*C*-6a/10a), 128.4 (*C*-4), 125.2 (*C*-12a), 120.0 (*C*-7/10), 93.5 (*C*-3), 51.6 (*C*-12), 23.0 (*C*H_3) ppm.

IR (ATR): $\tilde{\nu}$ = 3057 (w), 3010 (w), 2930 (w), 2021 (w), 1654 (s), 1582 (m), 1554 (w), 1513 (w), 1473 (m), 1432 (w), 1377 (s), 1336 (s), 1296 (m), 1250 (w), 1110 (m), 1084 (m), 1030 (m), 1009 (w), 970 (m), 917 (w), 842 (m), 823 (s), 767 (s), 735 (w), 652 (m), 598 (m), 582 (m), 514 (m), 485 (m), 470 (w), 437 (s) cm^{-1}.

HR-MS (ESI, DCM): *m/z* $[M+H]^+$ calculated for $C_{15}H_{11}ON_3{}^{127}I+H^+$: 378.0098; found: 378.0090 ± 2.03 ppm.

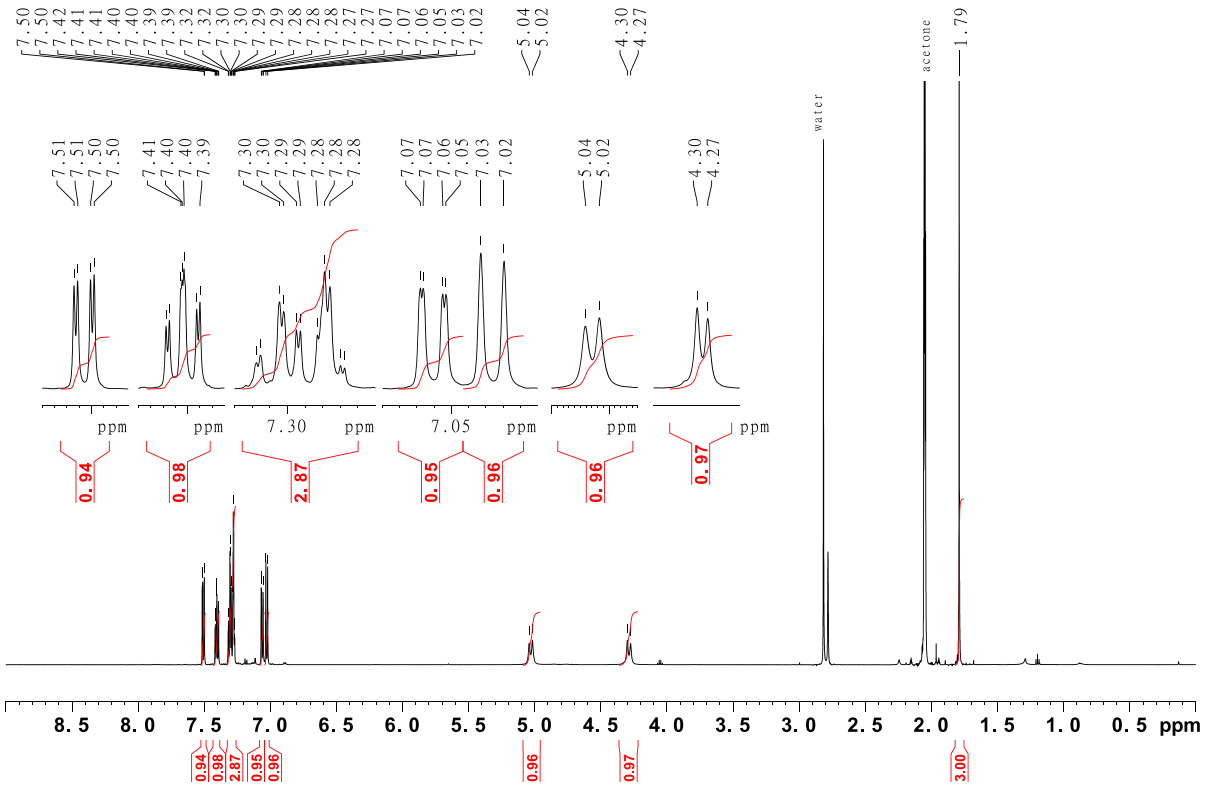

Figure SII.45: 600 MHz ^{1}H-NMR spectrum of (*Z*)-1-(3-iododibenzo[c,g][1,2,5]triazocin-11(12*H*)-yl)-ethan-1-one (**3**).

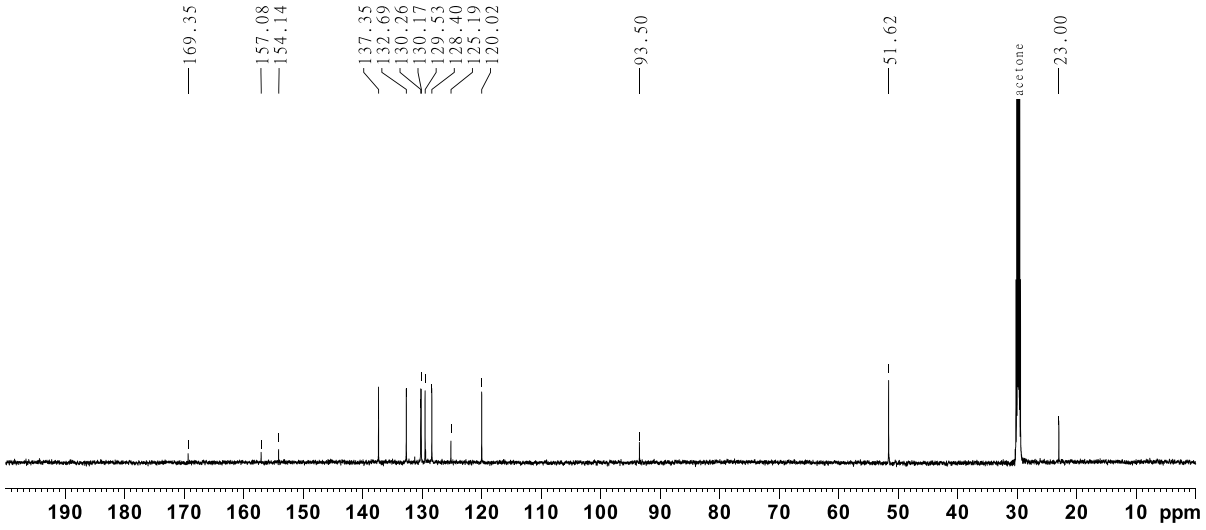

Figure SII.46: 150 MHz ^{13}C{^{1}H}-NMR spectrum of (*Z*)-1-(3-iododibenzo[c,g][1,2,5]triazocin-11(12*H*)-yl)-ethan-1-one (**3**).

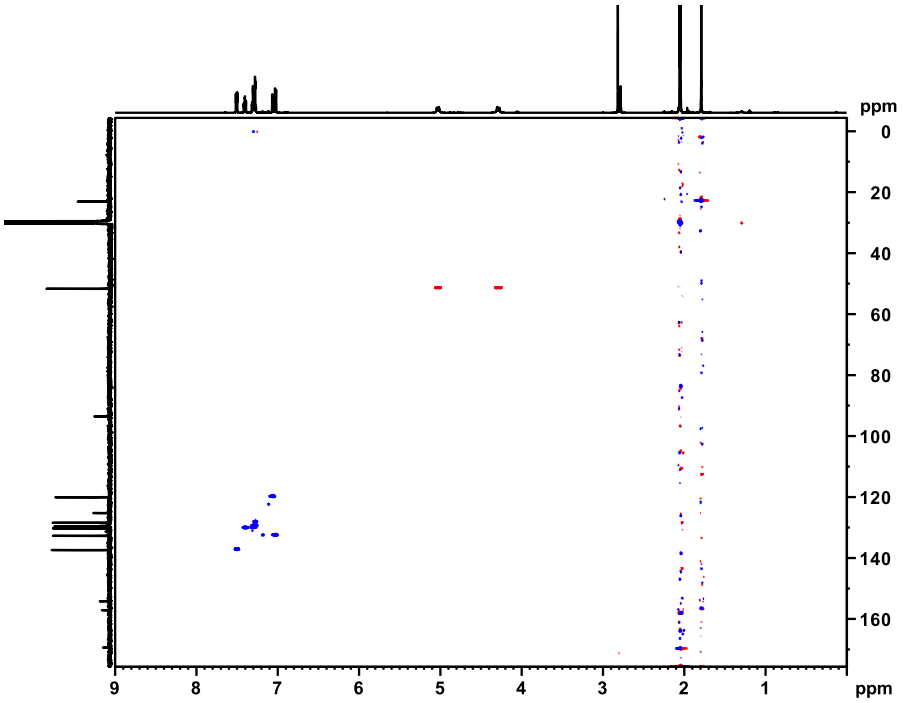

Figure SII.47: 600 MHz ^{1}H-^{13}C HSQC spectrum of (*Z*)-1-(3-iododibenzo[c,g][1,2,5]triazocin-11(12*H*)-yl)-ethan-1-one (**3**).

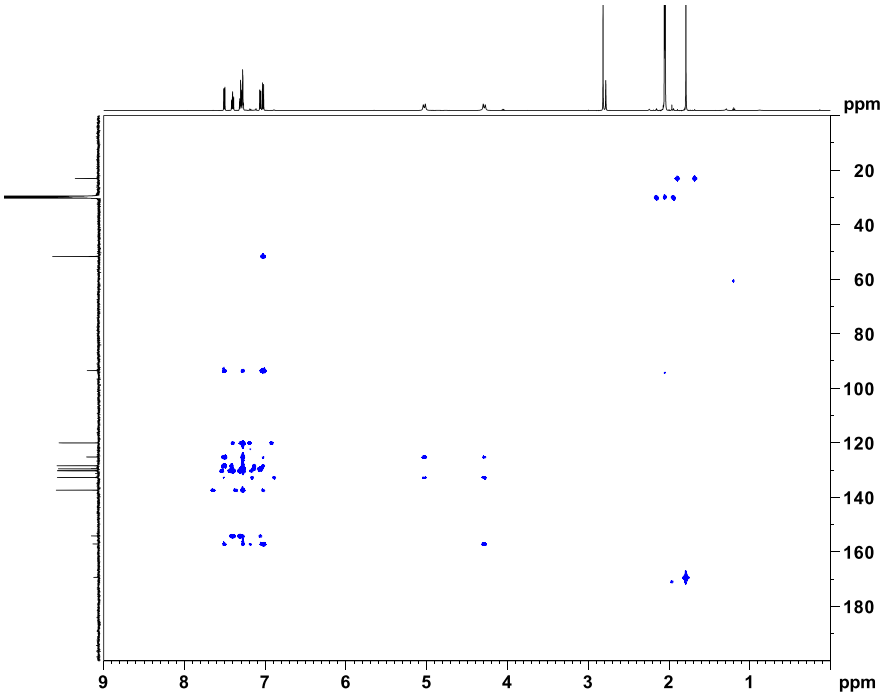

Figure SII.48: 600 MHz HMBC spectrum of (*Z*)-1-(3-iododibenzo[c,g][1,2,5]triazocin-11(12*H*)-yl)-ethan-1-one (**3**).

II.1.13 Synthesis of *tert*-butyl-(5-bromo-2-nitrophenyl)carbamate

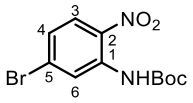

Under a nitrogen atmosphere NaH (444 mg, 18.5 mmol, 60% in mineral oil) was suspended in 10 mL anhydrous DMF and 5-bromo-2nitroaniline (**6**, 1.00 g, 4.61 mmol) was added at 0 °C. The reaction mixture was stirred at 0 °C for 10 min. and at rt. for 30 min. Di-*tert*-butyldicarbonate (1.00 g, 4.66 mmol) dissolved in 10 mL anhydrous DMF was added dropwise and the reaction mixture was stirred at rt. for 16 h and poured on ice subsequently. The organic layer was separated and the aqueous layer was extracted twice with 50 mL ethyl acetate. The combined organic layers were dried over $MgSO_4$ and the solvent was evaporated. After column chromatography on silica (ethyl acetate/cyclohexane 1:10, R_f = 0.70) the product could be obtained as pale green solid (1.14 g, 3.60 mmol, 78%).

melting point: 83 °C

^{1}H-NMR (500 MHz, $CDCl_3$, 298 K): δ = 9.73 (br. s, 1 H, N*H*), 8.85 (d, ^4J = 2.1 Hz, 1 H, *H*-6), 8.06 (d, ^3J = 9.1 Hz, 1 H, *H*-3), 7.21 (dd, ^3J = 9.0 Hz, ^4J = 2.2 Hz, 1 H, *H*-4), 1.55 (s, 10 H, CH_3) ppm.

^{13}C{^{1}H}-NMR (125 MHz, $CDCl_3$, 198 K): δ = 151.9 (*C*=O), 137.0 (*C*-1), 134.6 (*C*-2), 131.5 (*C*-4), 127.1 (*C*-6), 125.2 (*C*-5), 123.4 (*C*-3), 82.6 (*C*-(CH_3)$_3$), 28.3 (*C*H_3), ppm.

IR (ATR): $\tilde{\nu}$ = 3356 (w), 3115 (w), 2980 (w), 1729 (m), 1605 (m), 1569 (m), 1537 (w), 1489 (m), 1470 (m), 1427 (m), 1392 (w), 1368 (w), 1327 (m), 1298 (m), 1244 (m), 1204 (w), 1144 (s), 1093 (w), 1073 (m), 1049 (w), 1027 (w), 923 (w), 837 (m), 818 (m), 773 (w), 761 (w), 750 (m), 672 (m), 603 (w), 583 (w) cm^{-1}.

MS (EI, 70 eV): *m/z*(%) = 318.00 [$C_{11}H_{13}{}^{81}BrN_2O_4$]$^+$, 316.01 [$C_{11}H_{13}{}^{79}BrN_2O_4$]$^+$, 260.95 [$C_8H_8{}^{79}BrN_2O_3$]$^+$, 215.95 [$C_6H_3{}^{79}BrN_2O_2$]$^+$, 185.95 [$C_6H_3{}^{79}BrN_1O_1$]$^+$, 169.94 [$C_6H_3{}^{79}BrN$]$^+$, 90.03 [$C_6H_3{}^{79}BrN$]$^+$.

HR-MS (EI, 70 eV, acetone): m/z [M]$^+$ calculated for $C_{11}H_{13}N_2O_4{}^{79}Br^+$: 316.0057; found.: 316.0059 ± 0.44 ppm.

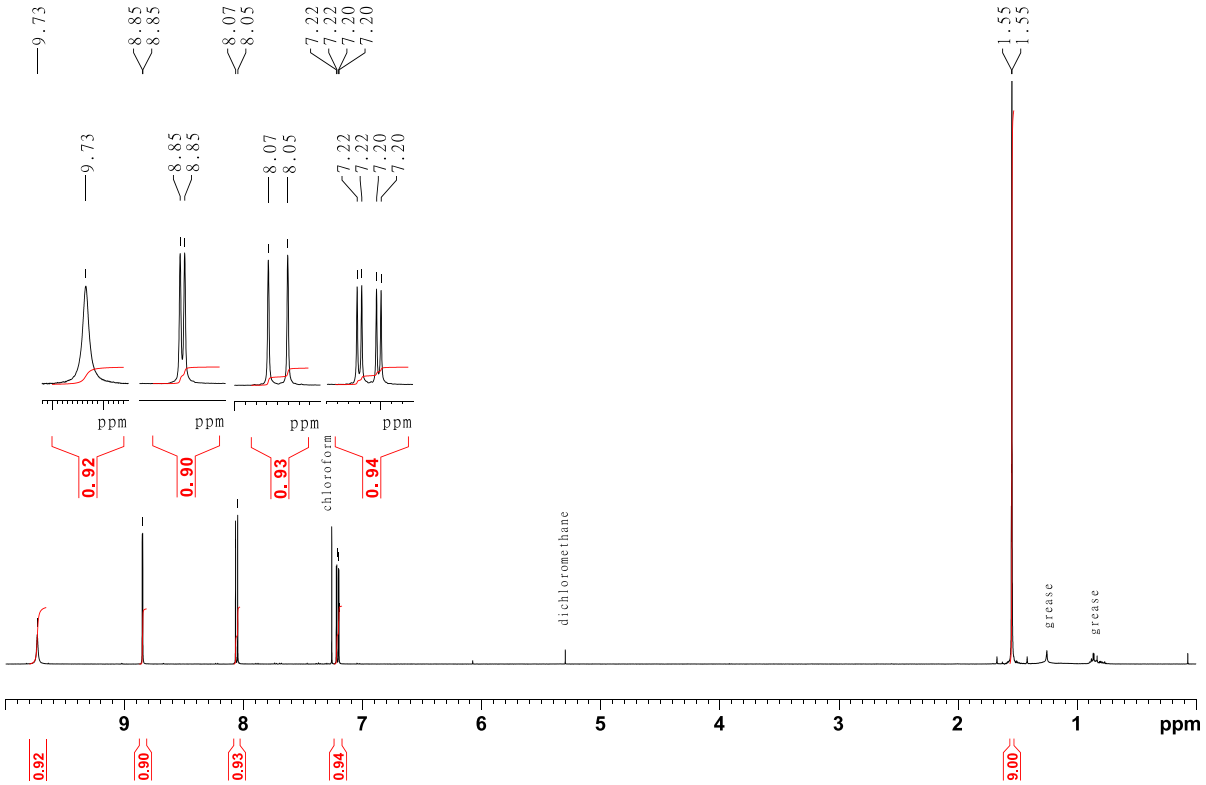

Figure SII.49: 500 MHz ^{1}H-NMR spectrum of *tert*-butyl-(5-bromo-2-nitrophenyl)carbamate.

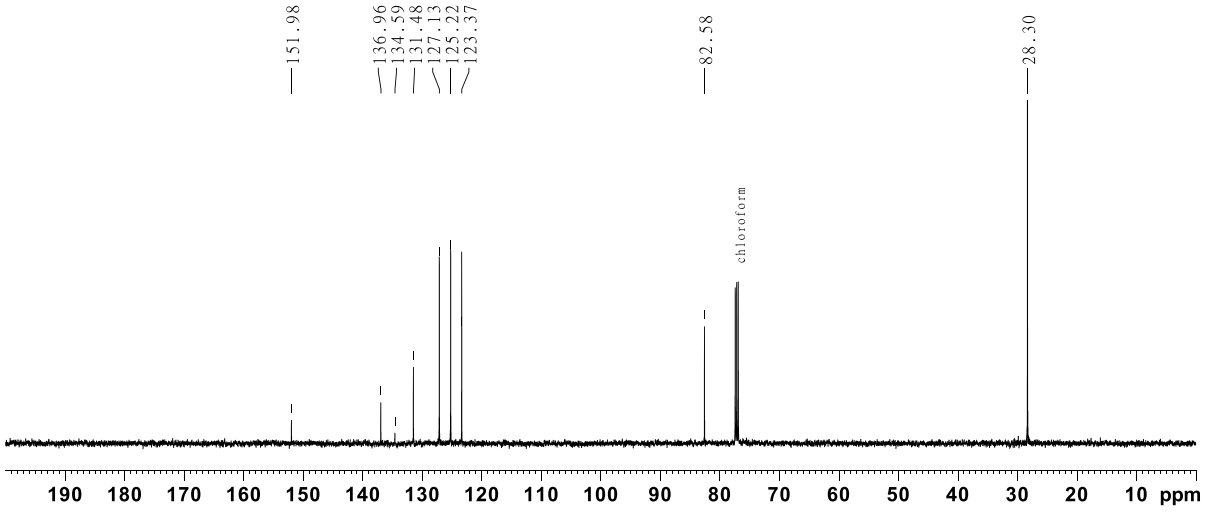

Figure SII.50: 125 MHz ^{13}C{^{1}H}-NMR spectrum of *tert*-butyl-(5-bromo-2-nitrophenyl)carbamate.

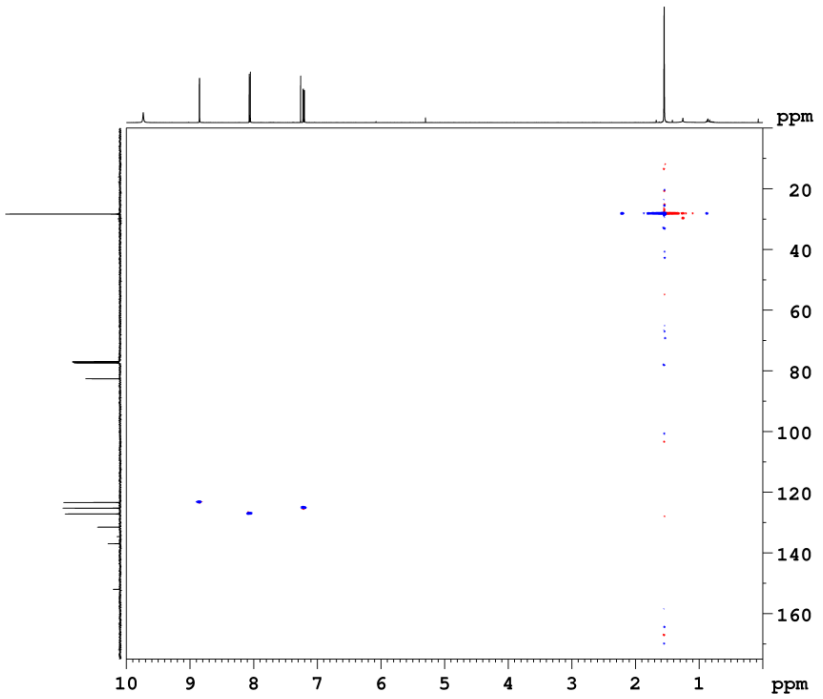

Figure SII.51: 500 MHz ^{1}H-^{13}C HSQC spectrum of *tert*-butyl-(5-bromo-2-nitrophenyl)carbamate.

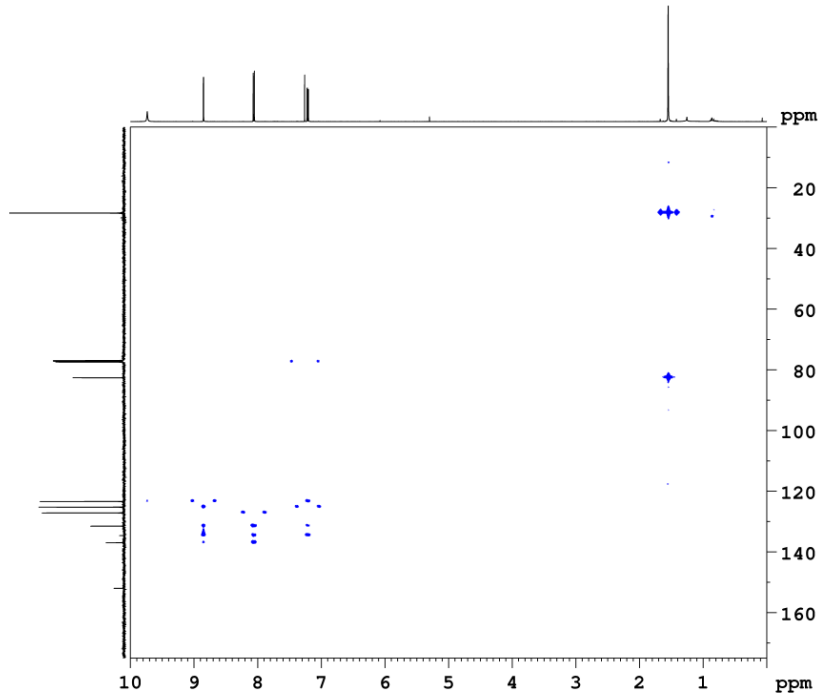

Figure SII.52: 500 MHz HMBC spectrum of *tert*-butyl-(5-bromo-2-nitrophenyl)carbamate.

II.1.14 Synthesis of *tert*-butyl-(2-amino-5-bromophenyl)carbamate (5)

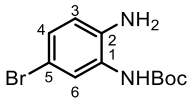

tert-butyl-(5-bromo-2-nitrophenyl)carbamate (1.80 g, 5.70 mmol), sodium dithionite (3.97 g, 22.7 mmol) and sodium bicarbonate (4.79 g, 57.0 mmol) were suspended in 48 mL 1,4-dioxane/deionized water mixture (5:1), heated to reflux with an oil bath and stirred at given temperature for 2 h. After cooling down 100 mL deionized water were added and the reaction mixture was extracted three times with 50 mL ethyl acetate. After drying the combined organic layers over $MgSO_4$ and evaporation of the solvent the product could be obtained as yellow solid (1.58 g, 5.53 mmol, 97 %)

melting point: 141 °C

^{1}H-NMR (500 MHz, $CDCl_3$, 298 K): δ = 7.52 (s, 1 H, *H*-6), 7.08 (dd, ^3J = 2.4 Hz, ^4J = 8.4 Hz, 1 H, *H*-4), 6.67 (d, ^4J = 8.4 Hz, 1 H, *H*-3), 6.32 (s, 1 H, -N*H*), 3.71(s, 2 H, -N*H*2), 1.51 (s, 9 H, -CH_3) ppm.

^{13}C{^{1}H}-NMR (125 MHz, $CDCl_3$, 298 K): δ = 153.5 (*C*=O), 137.8 (*C*-2), 128.6 (*C*-4), 126.8 (*C*-6), 119.3 (*C*-3), 111.8 (*C*-1), 81.2 (*C*-$(CH_3)_3$), 28.4 (*C*H_3) ppm.

IR (ATR): $\tilde{\nu}$ = 3440 (w), 3359 (m), 3295 (m), 2980 (m), 2929 (w), 2163 (w), 1980 (w), 1673 (s), 1634 (m), 1589 (m), 1515 (s), 1488 (m), 1454 (w), 1416 (s), 1389 (m), 1362 (m), 1322 (m), 1282 (s), 1248 (s), 1224 (w), 1149 (s), 1049 (m), 1024 (m), 882 (m), 857 (m), 817 (w), 807 (m), 777 (m), 760 (w), 742 (m), 627 (m), 601 (m), 556 (s) cm^{-1}.

MS (EI, 70 eV): m/z (%) = 288.02991 $[C_{11}H_{15}{}^{79}BrN_2O_2]^+$, 286.03176 $[C_{11}H_{15}{}^{79}BrN_2O_2]^+$, 229.97 $[C_7H_6{}^{79}BrN_2O_2]^+$, 185.98 $[C_6H_6{}^{79}BrN^2]^+$.

HR-MS (EI, 70 eV, acetone): m/z $[M]^+$ calculated for $C_{11}H_{15}{}^{79}BrN_2O_2{}^+$: 286.0318; found: 286.0317 ± 0.24 ppm.

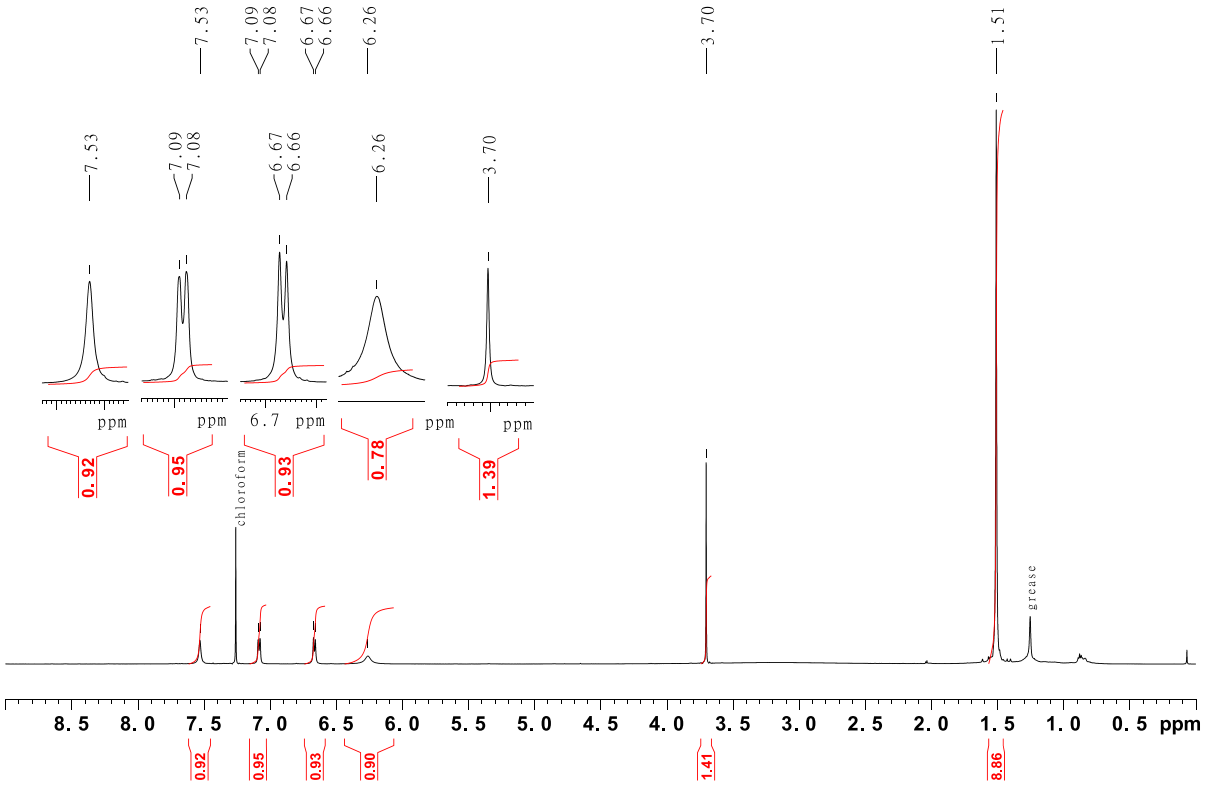

Figure SII.53: 500 MHz ^{1}H-NMR spectrum of *tert*-butyl-(2-amino-5-bromophenyl)carbamate (**5**).

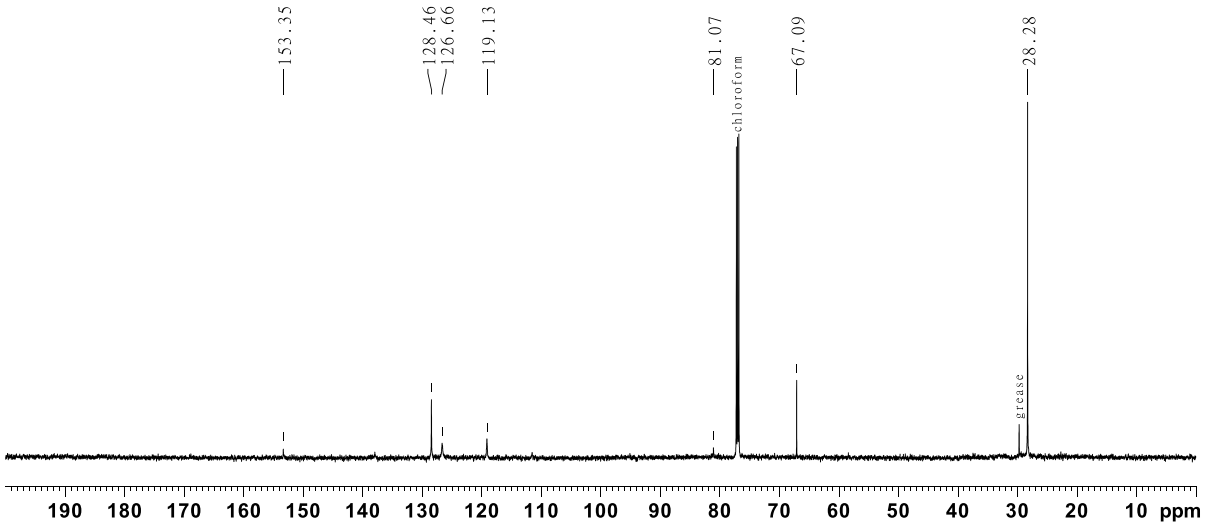

Figure SII.54: 125 MHz ^{13}C{^{1}H}-NMR spectrum of *tert*-butyl-(2-amino-5-bromophenyl)carbamate (**5**).

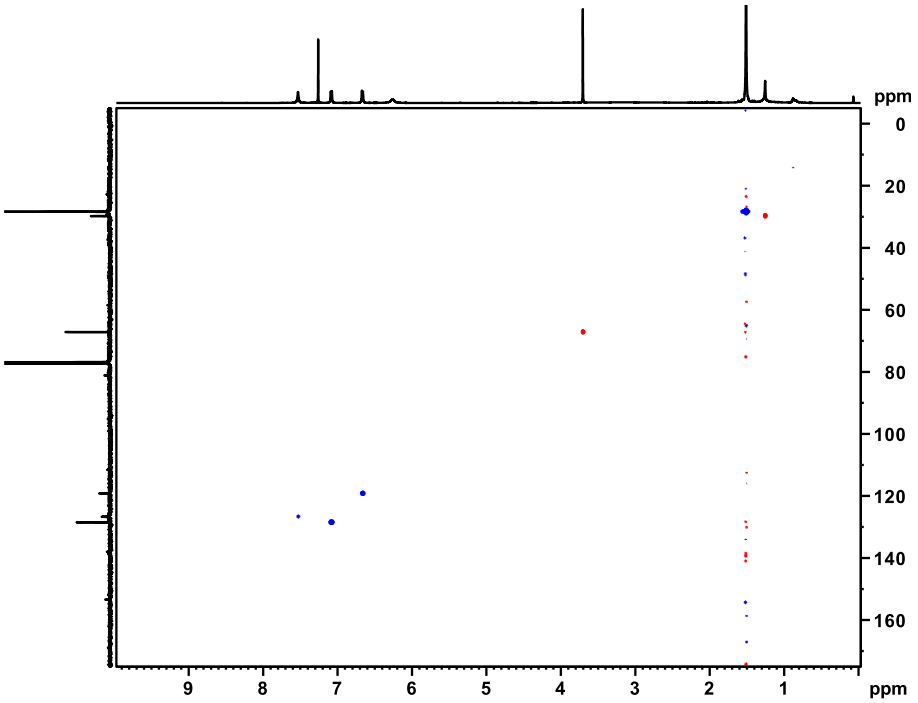

Figure SII.55: 500 MHz ^{1}H-^{13}C HSQC spectrum of *tert*-butyl-(2-amino-5-bromophenyl)carbamate (**5**).

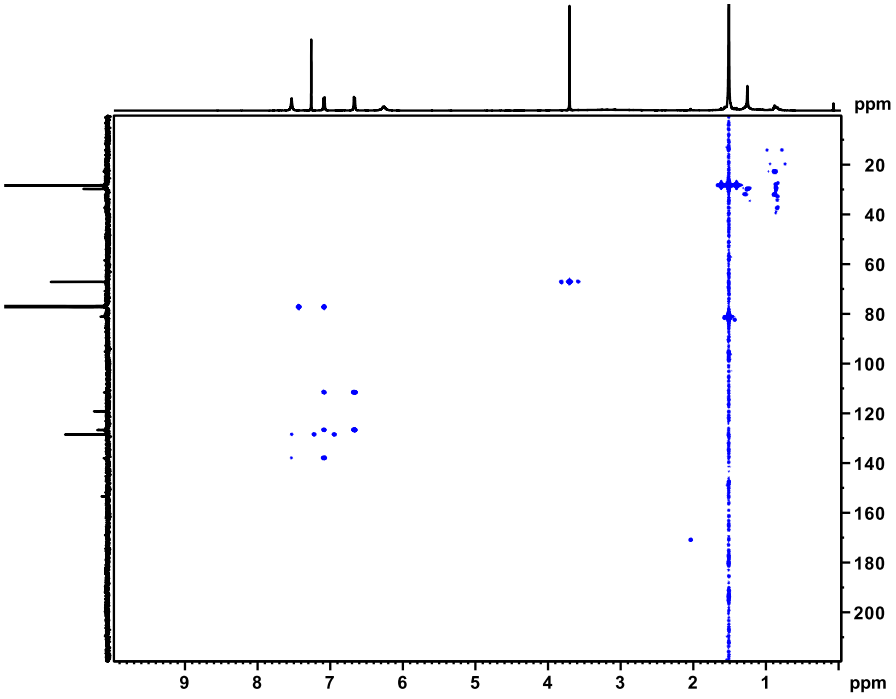

Figure SII.56: 500 MHz HMBC spectrum of *tert*-butyl-(2-amino-5-bromophenyl)carbamate (**5**).

II.1.15 Synthesis of *tert*-butyl-(5-bromo-2-((4-bromo-2-nitrobenzyl)amino)phenyl)carbamate

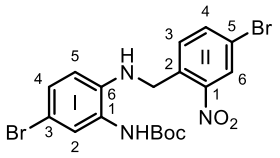

Under a nitrogen atmosphere triethylamine (3.06 mL, 18.0 mmol) and 1-(bromomethyl)-4-bromo-2-nitrobenzene (5.17 g, 17.5 mmol) were added to solution of *tert*-butyl-(2-amino-5-bromophenyl)carbamate (5.02 g, 17.5 mmol) in 100 mL abs. THF. The reaction mixture was heated to reflux with an oil bath and stirred for 16 h at given temperature. Afterwards the solvent was evaporated and 100 mL of deionized water and 100 mL DCM were added to the residue. The organic layer was separated and the aqueous layer was extracted twice with 50 mL of DCM. The combined organic layers were dried over $MgSO_4$ and the solvent was evaporated. Recrystallization from cyclohexane/ethyl acetate (1:1) gave the product as yellow solid (7.39 g, 15.7 mmol, 62%).

melting point: 186 °C

^{1}H-NMR (500 MHz, $CDCl_3$, 298 K): δ = 8.22 (d, ^4J = 2.0 Hz, 1 H, Ar^{II}-*H*-3), 7.68 (dd, ^4J = 2.1 Hz, ^3J = 8.3 Hz, 1 H, Ar^{II}-*H*-4), 7.49-7.43 (m, 2 H, Ar^{II}-*H*-3, Ar^{I}-*H*-2), 7.08 (dd, ^4J = 2.2 Hz, ^3J = 8.6 Hz, 1 H, Ar^{I}-*H*-4), 6.32 (s, 1 H, Ar^{I}-*H*-5), 6.20 (br. s, 1 H, -CON*H*), 4.98 (br. S, 1 H, -N*H*), 4.74-4.41 (m, 3 H, -CH_2, -N*H*), 1.51 (s, 9 H, -CH_3) ppm.

^{13}C{^{1}H}-NMR (125 MHz, $CDCl_3$, 198 K): δ = 153.9 (*C*=O), 148.8 (Ar^{II}-*C*-1), 140.1 (Ar^{I}-*C*-2), 136.9 (Ar^{II}-*C*-4), 133.9 (Ar^{II}-*C*-5), 131.4 (Ar^{II}-*C*-3), 129.5 (Ar^{I}-*C*-4), 128.30 (Ar^{II}-*C*-6), 128.15 (Ar^{I}-*C*-6), 126.1 (Ar^{I}-*C*-1), 121.5 (Ar^{II}-*C*-2), 114.6 (Ar^{II}-*C*-3), 110.90 (Ar^{II}-*C*-5), 81.5 (-*C*-(CH_3)$_3$), 45.6 (-*C*H_2), 28.4 (-*C*H_3) ppm.

IR (ATR): $\tilde{\nu}$ = 3421 (m), 2982 (m), 2211 (w), 1685 (s), 1594 (m), 1527 (s), 1497 (m), 1366 (m), 1342 (m), 1281 (m), 1243 (s), 1152 (s), 1054 (w), 875 (s), 857 (w), 831 (w), 807 (m), 790 (w), 751 (m), 627 (w), 551 (m) cm^{-1}.

HR-MS (ESI, DCM): m/z $[M+H]^+$ calculated for $C_{18}H_{19}{}^{79}Br_2N_3O_4+H^+$: 499.9815; found: 499.9808 ± 151 ppm.

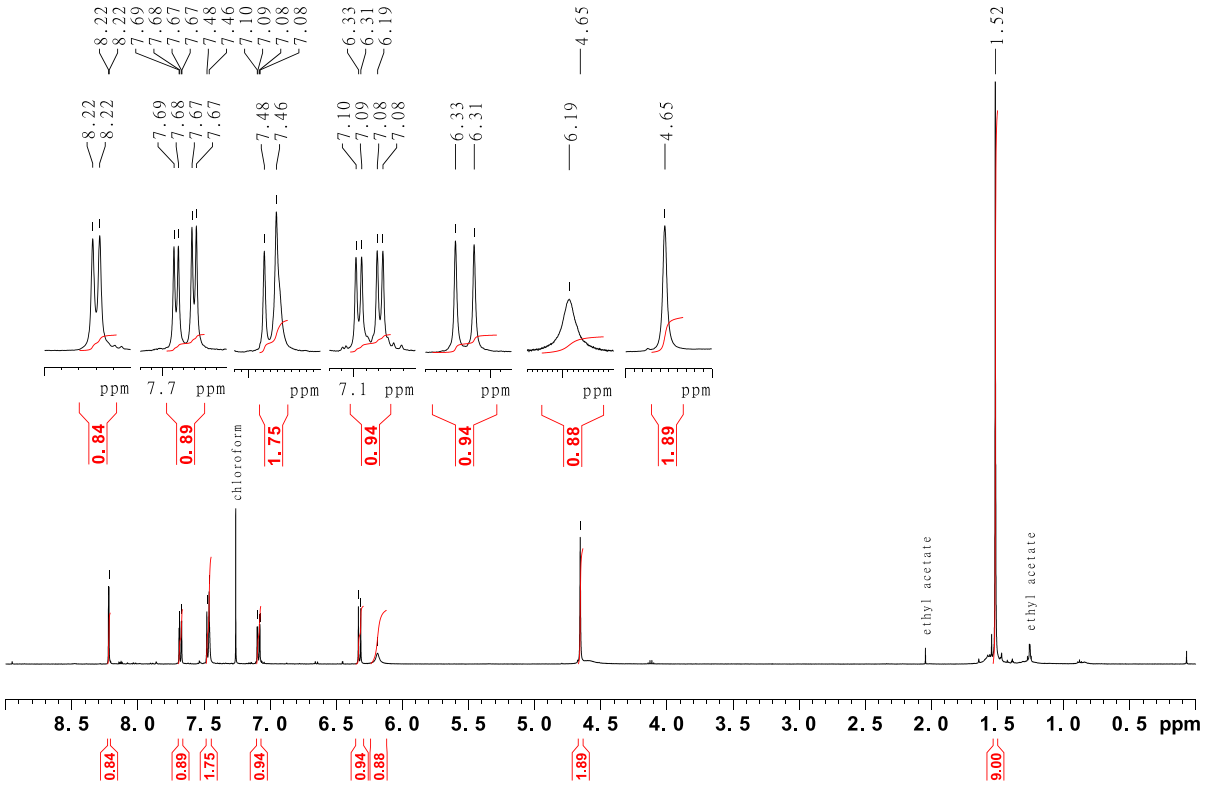

Figure SII.57: 500 MHz ^{1}H-NMR spectrum of *tert*-butyl-(5-bromo-2-((4-bromo-2-nitrobenzyl)amino)phenyl)carbamate.

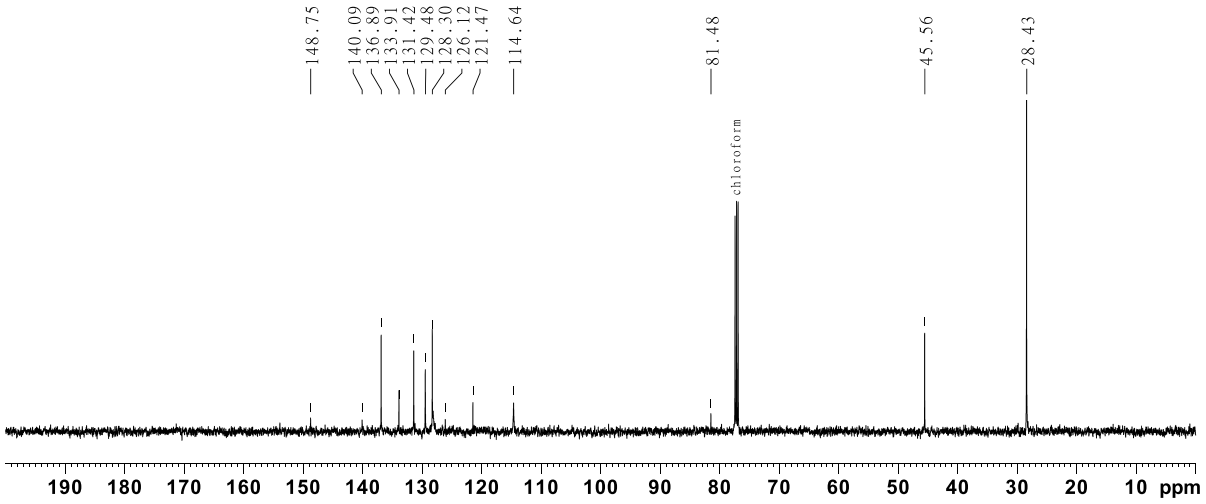

Figure SII.58: 125 MHz ^{13}C{^{1}H}-NMR spectrum of *tert*-butyl-(5-bromo-2-((4-bromo-2-nitrobenzyl)amino)phenyl)carbamate.

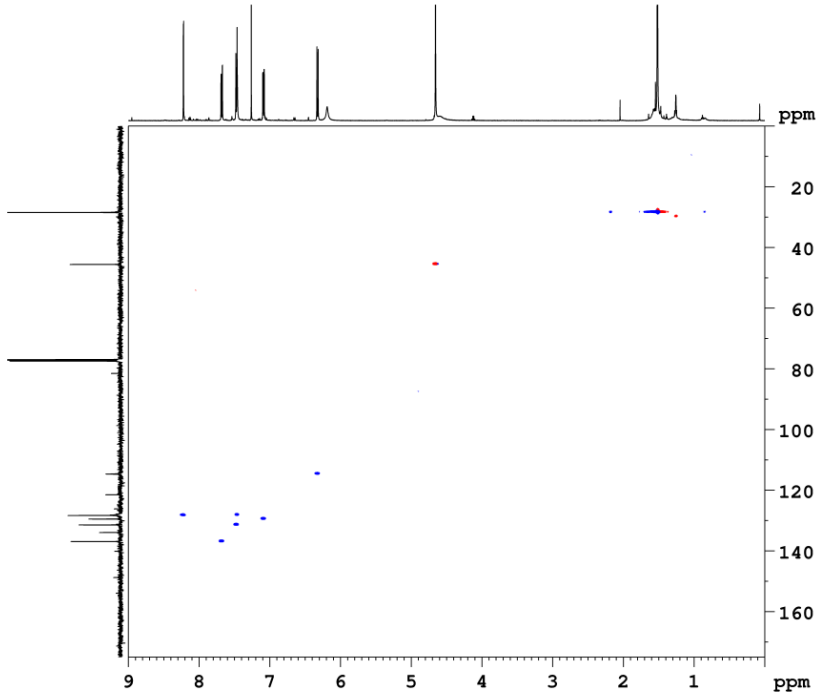

Figure SII.59: 500 MHz ^{1}H-^{13}C HSQC spectrum of *tert*-butyl-(5-bromo-2-((4-bromo-2-nitrobenzyl)amino)phenyl)carbamate.

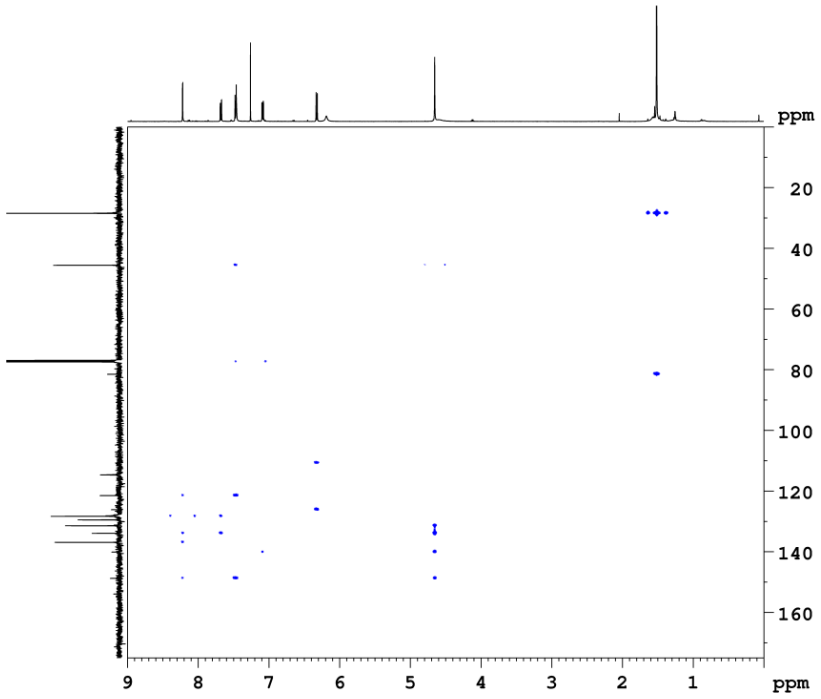

Figure SII.60: 500 MHz HMBC spectrum of *tert*-butyl-(5-bromo-2-((4-bromo-2-nitrobenzyl)amino)phenyl)carbamate.

II.1.16 Synthesis of (9*H*-fluoren-2-yl)methyl-(4-bromo-2-((*tert*-butoxycarbonyl)amino)phenyl)(4-bromo-2-nitrobenzyl)carbamate

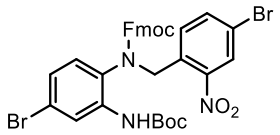

DIPEA (820 µL, 5 mmol) and 9-Fluorenylmethoxycarbonyl chlorid (2.50 g, 4.83 mmol) were added to a solution of *tert*-butyl-(5-bromo-2-((4-bromo-2-nitrobenzyl)amino)phenyl)carbamate (2.42 g, 4.83 mmol) in 50 mL abs. DMF under a nitrogen atmosphere. The reaction mixture was stirred for 48 h at rt. and the solvent was evaporated subsequently. 100 mL of deionized water and 100 mL of DCM were added to the residue. The organic layer was separated and the aqueous layer was extracted twice with 100 mL DCM. The combined organic layers were dried over $MgSO_4$ and the solvent was evaporated. Column chromatography on silica (ethyl acetate/cyclohexane 1:4, R_f = 0.34) gave a colorless solid (302 mg, 418 µmol, 13%).

melting point: 88 °C

^{1}H-NMR (500 MHz, $CDCl_3$, 298 K): δ = 8.16 (br. s, 1 H, -CON*H*), 8.06 (s, 1 H, Ar-*H*), 7.66 (d, ^3J = 7.4 Hz, 2 H, Ar-*H*), 7.58 (br. s, 1 H, Ar-*H*), 7.38-7.33 (m, 2 H, Ar-*H*), 7.25-6.98 (s, 6 H, Ar-*H*), 6.61 (br. s, 1 H, Ar-*H*), 6.32 (br. s, 1 H, Ar-*H*), 5.09 (br. s, 1 H, -CH_2), 4.78 (br. s, 1 H, -CH_2), 4.52 (br. s, 2 H, Fmoc-CH_2), 4.05 (s, 1 H, Fmoc-C*H*), 1.46 (s, 9 H, -CH_3) ppm.

^{13}C{^{1}H}-NMR (125 MHz, $CDCl_3$, 298 K): δ = 155.6, 143.3, 141.4, 136.5, 129.0, 128.08, 127.86, 127.1, 126.5, 124.7, 123.3, 120.1, 81.6, 68.2, 47.0, 28.4 ppm.

IR (ATR): $\tilde{\nu}$ = 2929 (w), 2166 (w), 1713 (s), 1583 (m), 1531 (s), 1512 (s), 1450 (m), 1392 (w), 1347 (w), 1276 (w), 1233 (m), 1151 (s), 1022 (w), 877 (m), 758 (s), 749 (s), 739 (s), 621 (w), 545 (w) cm^{-1}.

HR-MS (ESI, $CHCl_3$/MeOH): *m/z* $[M+H]^+$ calculated for $C_{33}H_{29}O_6N_3Br_2+H^+$: 722.0496; found: 722.0490 ± 0.82 ppm.

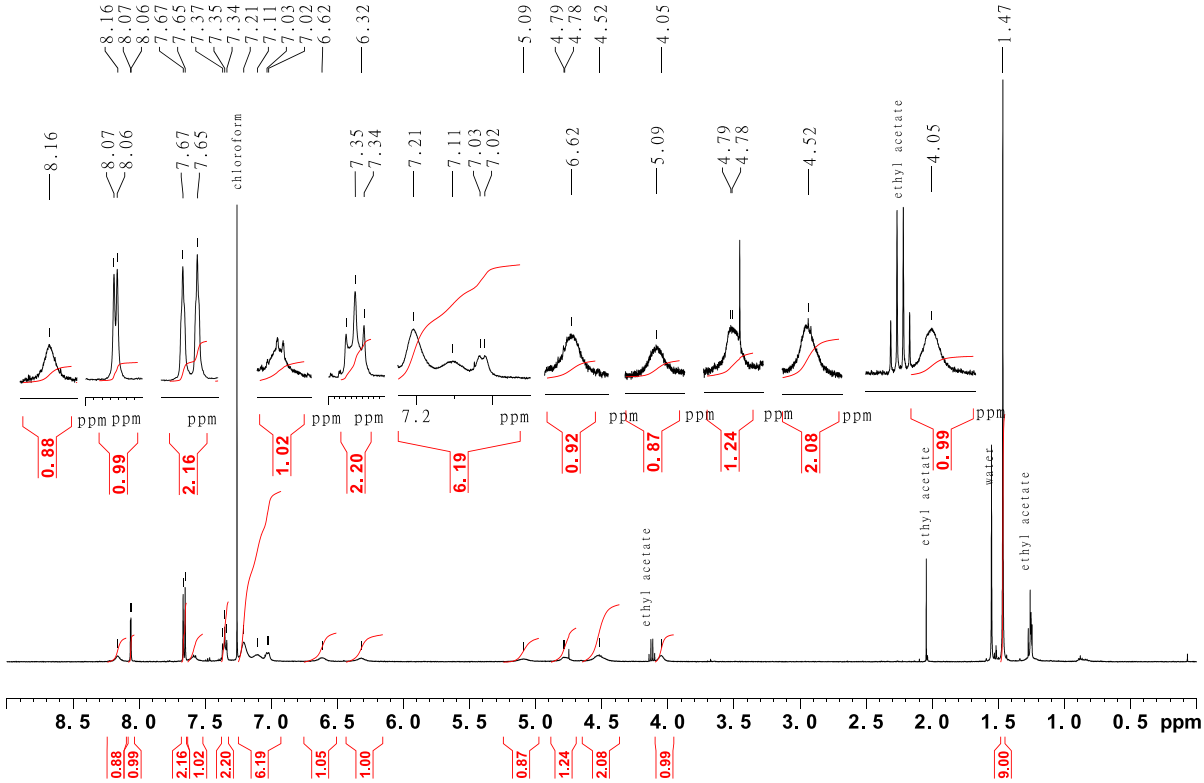

Figure SII.61: 500 MHz ^{1}H-NMR spectrum of (9*H*-fluoren-2-yl)methyl-(4-bromo-2-((*tert*-butoxycarbonyl)amino)phenyl)(4-bromo-2-nitrobenzyl)carbamate.

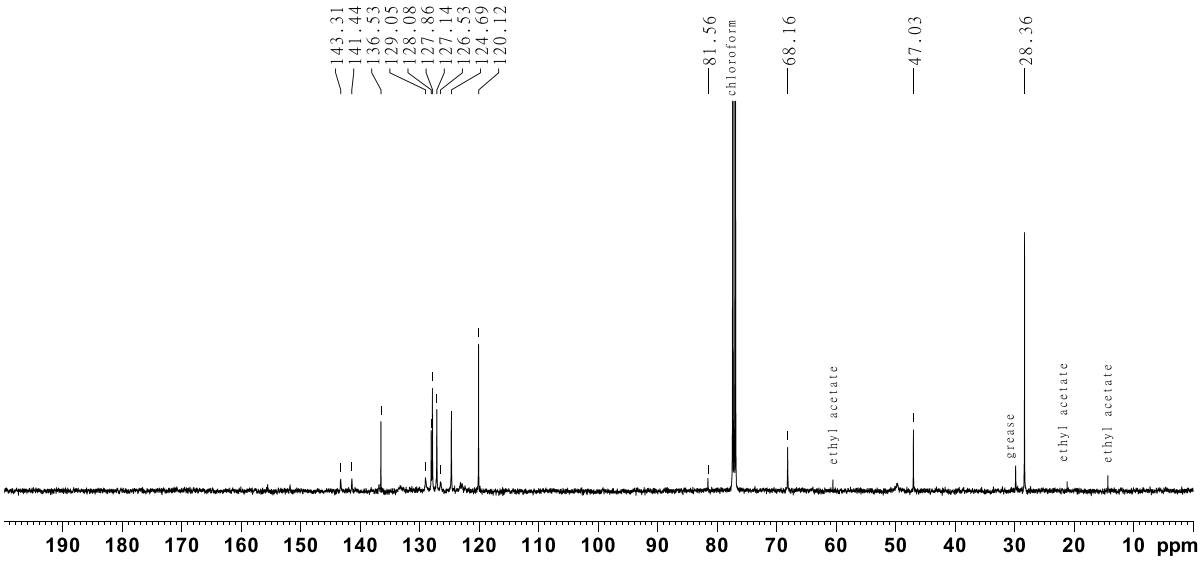

Figure SII.62: 125 MHz ^{13}C{^{1}H}-NMR spectrum of (9*H*-fluoren-2-yl)methyl-(4-bromo-2-((*tert*-butoxycarbonyl)amino)phenyl)(4-bromo-2-nitrobenzyl)carbamate.

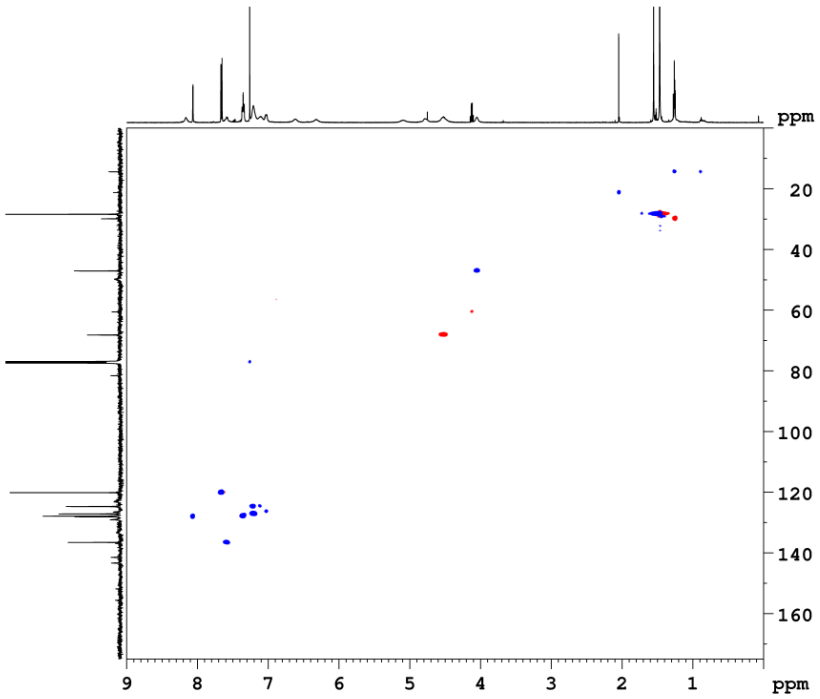

Figure SII.63: 500 MHz ^{1}H-^{13}C HSQC spectrum of (9*H*-fluoren-2-yl)methyl-(4-bromo-2-((*tert*-butoxycarbonyl)amino)phenyl)(4-bromo-2-nitrobenzyl)carbamate.

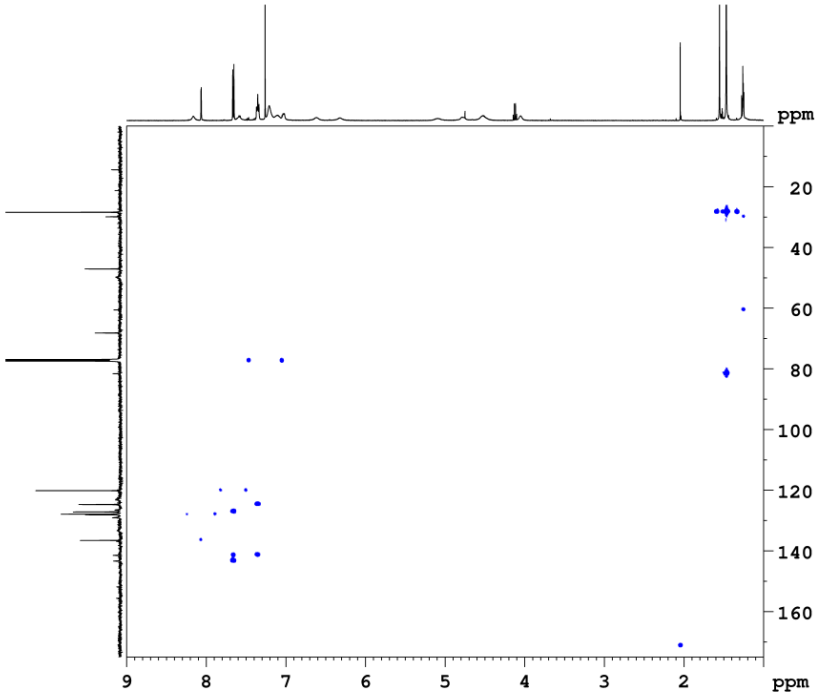

Figure SII.64: 500 MHz HMBC spectrum of (9*H*-fluoren-2-yl)methyl-(4-bromo-2-((*tert*-butoxycarbonyl)amino)phenyl)(4-bromo-2-nitrobenzyl)carbamate.

II.1.17 Synthesis of (9*H*-fluoren-9-yl)methyl-(2-amino-4-bromophenyl)(4-bromo-2-nitrobenzyl)carbamate

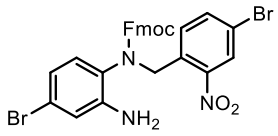

(9*H*-fluoren-2-yl)methyl-(4-bromo-2-((*tert*-butoxycarbonyl)amino)phenyl)(4-bromo-2-nitrobenzyl)carbamate (599 mg, 828 µmol) was dissolved in 25 mL DCM and 10 mL TFA was added. The reaction mixture was stirred at rt. for 16 h and neutralized with saturated aqueous $NaHCO_3$ subsequently. The organic layer was separated and the aqueous layer was extracted twice with 100 mL. The combined organic layers were dried over $MgSO_4$ and the solvent was evaporated to obtain a pale yellow solid (518 mg, 827 µmol, quant.) which was used without further purification.

melting point: 185 °C

^{1}H-NMR (600 MHz, $CDCl_3$, 298 K): δ = 8.06 (d, ^4J = 1.9 Hz, 1 H, Ar-*H*), 7.73-7.61 (m, 3 H, Ar-*H*), 7.39-7.33 (m, 3 H, Ar-*H*), 7.25-7.11 (m, 4 H, Ar-*H*), 6.82 (br. s, 1 H, Ar-*H*), 6.70 (br. s, 1 H, Ar-*H*), 6.47 (br. s, 1 H, Ar-*H*), 5.11 (br. s, 1 H, -C*H*$_2$), 4.88 (br. s, 1 H, -C*H*2), 4.49 (d, ^2J = 19.9 Hz 2 H, Fmoc-C*H*$_2$), 4.07 (br. s, 1 H, Fmoc-C*H*), 3.50 (br. s, 2 H, -N*H*$_2$) ppm.

^{13}C{^{1}H}-NMR (150 MHz, $CDCl_3$, 298 K): δ = 143.2, 140.9, 135.9, 132.3, 129.8, 127.41, 127.25, 126.6, 124.4, 122.3, 119.5, 67.7, 48.3, 46.7 ppm.

IR (ATR): $\tilde{\nu}$ = 3388 (m), 2925 (m), 2850 (w), 1704 (s), 1621 (m), 1523 (s), 1496 (s), 1450 (m), 1413 (s), 1394 (w), 1351 (m), 1297 (s), 1278 (w), 1229 (m), 1198 (w), 1182 (w), 1161 (m), 1139 (m), 1101 (w), 1066 (w), 1025 (m), 992 (m), 889 (w), 877 (m), 857 (w), 792 (m), 763 (s), 738 (s), 698 (w), 620 (w), 589 (w), 538 (w), 503 (w) cm^{-1}.

HR-MS (ESI, $CHCl_3$/MeOH): *m/z* $[M+H]^+$ calculated for $C_{28}H_{21}O_4N_3Br_2+H^+$: 621.9972; found: 621.9975 ± 0.49 ppm.

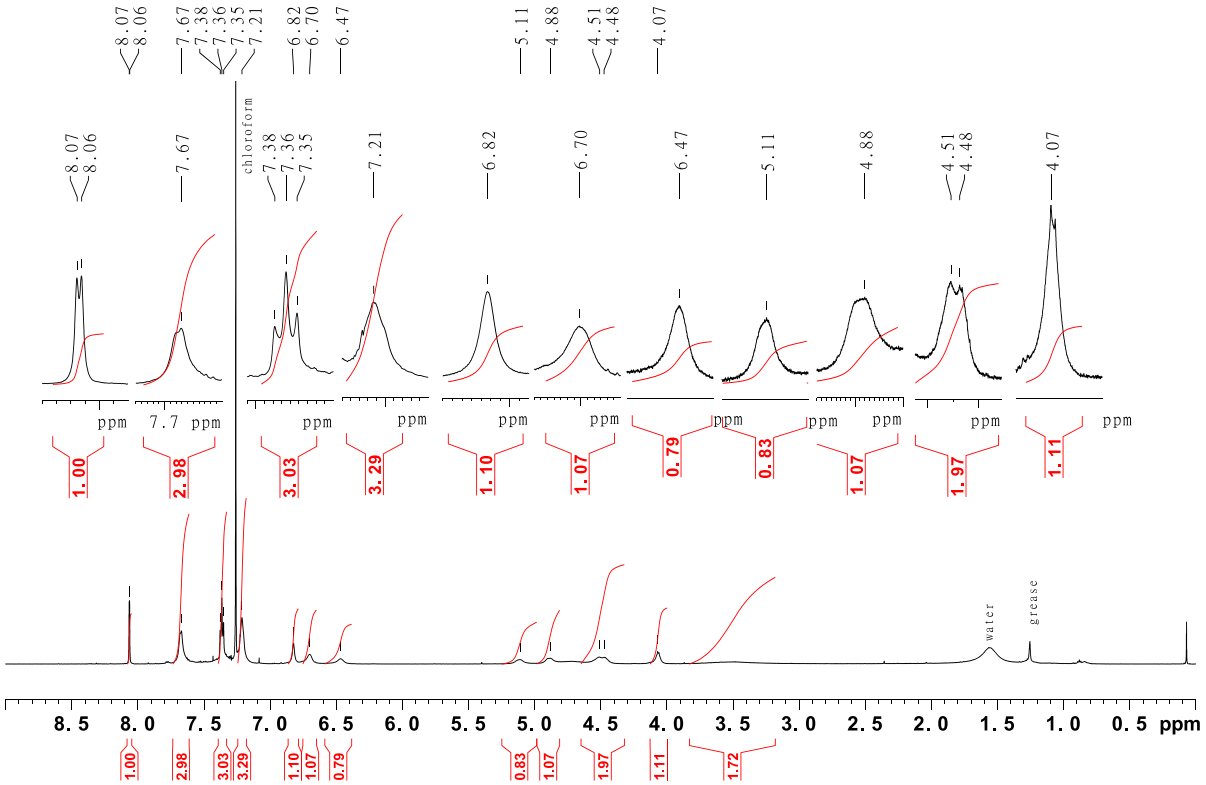

Figure SII.65: 600 MHz ^{1}H-NMR spectrum of (9*H*-fluoren-9-yl)methyl-(2-amino-4-bromophenyl)(4-bromo-2-nitrobenzyl)carbamate.

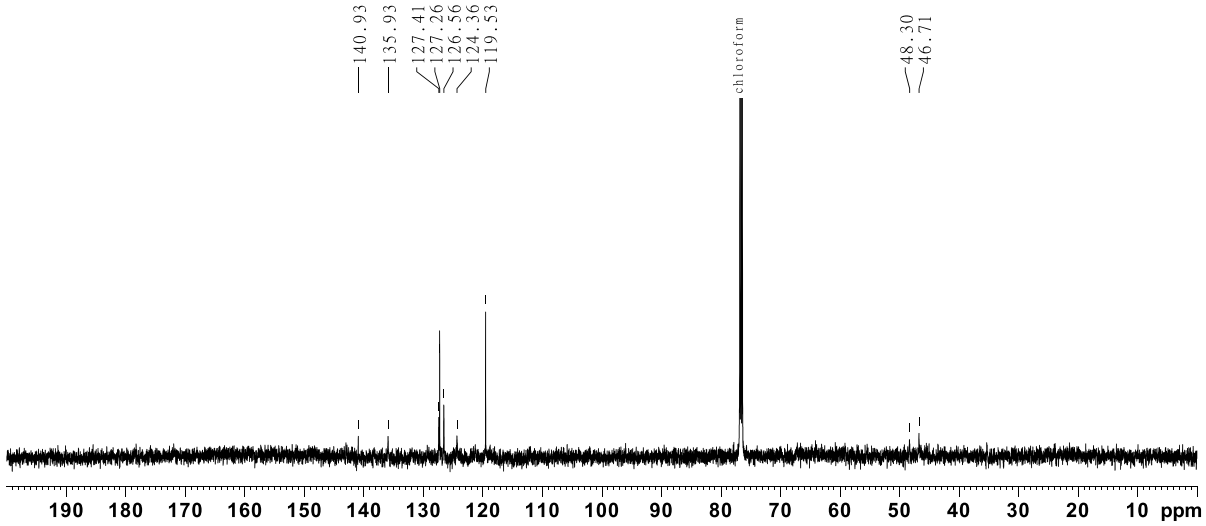

Figure SII.66: 150 MHz ^{13}C{^{1}H}-NMR spectrum of (9*H*-fluoren-9-yl)methyl-(2-amino-4-bromophenyl)(4-bromo-2-nitrobenzyl)carbamate.

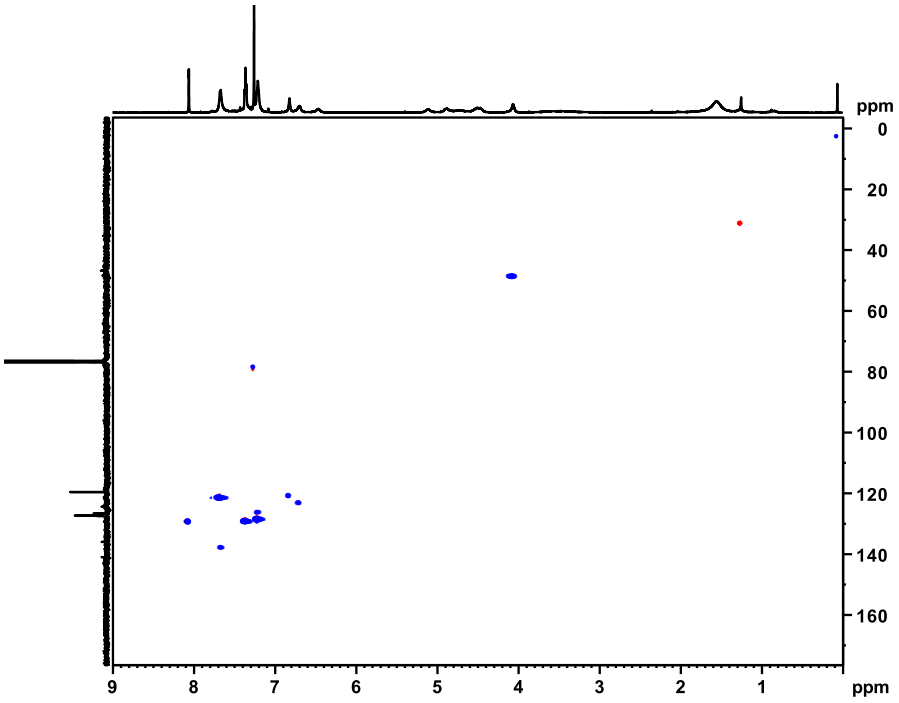

Figure SII.67: 600 MHz ^{1}H-^{13}C HSQC spectrum of (9*H*-fluoren-9-yl)methyl-(2-amino-4-bromophenyl)(4-bromo-2-nitrobenzyl)carbamate.

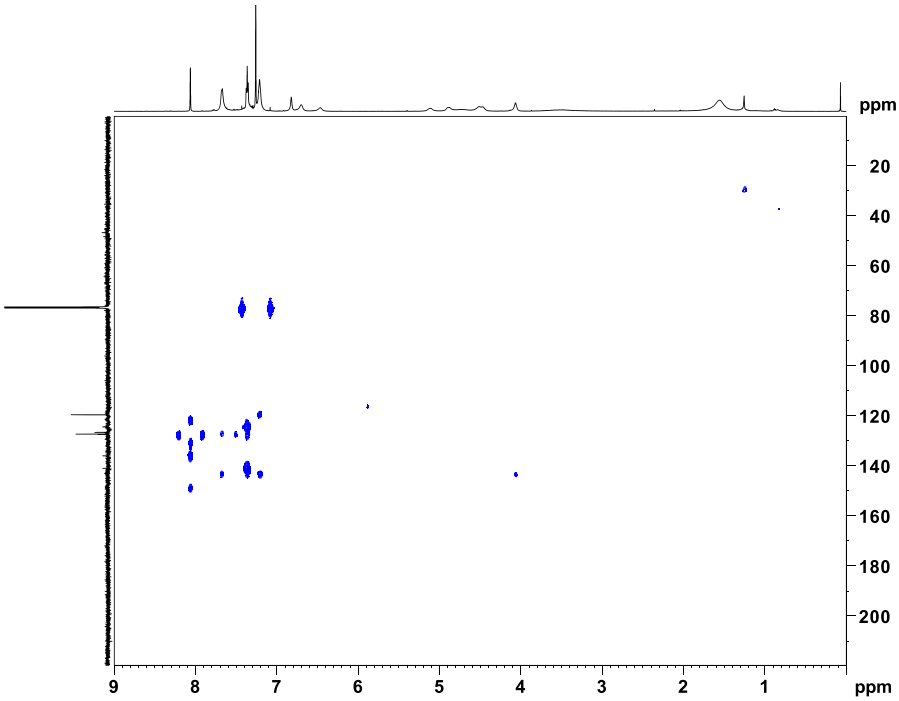

Figure SII.68: 600 MHz HMBC spectrum of (9*H*-fluoren-9-yl)methyl-(2-amino-4-bromophenyl)(4-bromo-2-nitrobenzyl)carbamate.

II.1.18 Synthesis of (9*H*-fluoren-9-yl)methyl-(*Z*)-3,8-dibromodibenzo[c,g][1,2,5]triazocin-11(12*H*)carboxylate

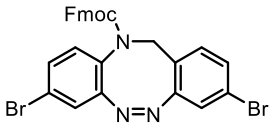

(9*H*-fluoren-9-yl)methyl-(2-amino-4-bromophenyl)(4-bromo-2-nitrobenzyl)carbamate (500 mg, 802 µmol) was suspended in 50 mL EtOH and $SnCl_2 \cdot 2\ H_2O$ (1.09 g, 4.81 mmol) was added. The reaction mixture was heated to 75 °C with an oil bath, zinc-powder (420 mg, 6.42 mmol) was added and it was stirred at given temperature. After cooling to rt the reaction mixture was stirred at for 16 h and neutralized with saturated aqueous $NaHCO_3$ solution subsequently. The solvent was evaporated and 100 mL water and 100 mL DCM were added to the residue. The organic layer was separated and the aqueous layer was extracted twice with 100 mL DCM. The combined organic layers were dried over $MgSO_4$ and the solvent was evaporated. The residue was dissolved in 25 mL of acetic acid and *m*CPBA (277 mg, 1.60 mmol) dissolved in 25 mL acetic acid was added dropwise to the reaction mixture. The reaction mixture was stirred at rt. for 16 h and the solvent was evaporated in the following. 50 mL DCM and 50 mL half-concentrated aqueous $NaHCO_3$ solution were added to the residue. The organic layer was separated and the aqueous layer was extracted twice with 50 mL DCM. The combined organic layers were dried over $MgSO_4$ and the solvent was evaporated. After column chromatography on silica (ethyl acetate/cyclohexane = 1:4, R_f = 0.58) the product could be obtained as yellow solid (63.6 mg, 108 µmol, 14%).

melting point: 91 °C

^{1}H-NMR (600 MHz, $CDCl_3$, 298 K): δ = 7.81-6.58 (m, 14 H, Ar-*H*), 4.92-4.03 (m, 5 H, -CH_2, -CH_2', Fmoc-CH_2, Fmoc-C*H*) ppm.

^{13}C{^{1}H}-NMR (150 MHz, $CDCl_3$, 298 K): δ = 152.8, 143.4, 141.3, 131.23, 131.19, 130.94, 130.71, 127.7, 127.0, 124.8, 122.21, 122.00, 119.9, 67.7, 52.0, 46.9 ppm.

IR (ATR): $\tilde{\nu}$ = 2922 (s), 2853 (m), 2360 (w), 2347 (w), 2228 (w), 2169 (w), 2019 (w), 1980 (w), 1961 (w), 1705 (s), 1590 (w), 1464 (w), 1450 (m), 1390 (m), 1317 (m), 1296 (w), 1228 (m), 1176 (m), 1071 (m), 1026 (m), 870 (m), 818 (m), 757 (m), 737 (s), 655 (w), 620 (m), 590 (w), 547 (m), 521 (w), 458 (m) cm^{-1}.

HR-MS (ESI, DCM): *m/z* $[M+H]^+$ calculated for $C_{28}H_{19}O_2N_3Br_2+H^+$: 587.99169; found: 587.99067 ± 1.74 ppm.

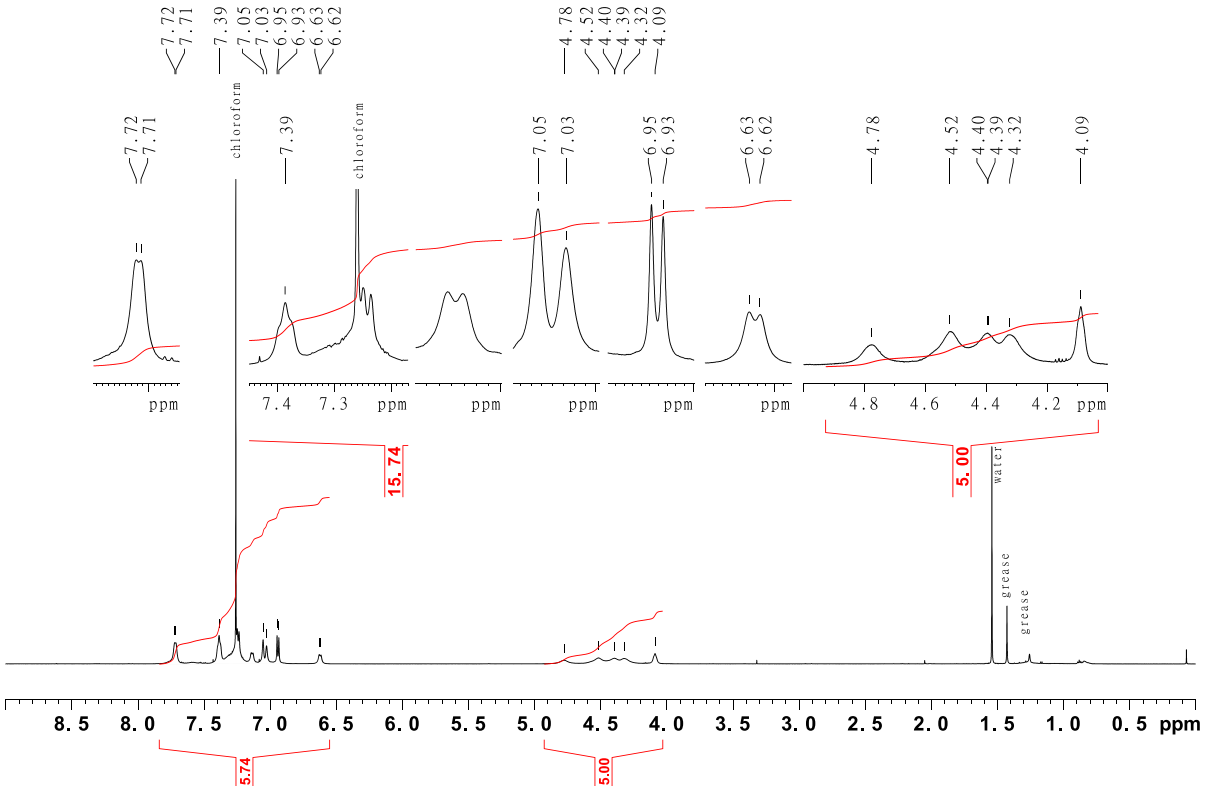

Figure SII.69: 600 MHz ^{1}H-NMR spectrum of (9*H*-fluoren-9-yl)methyl-(*Z*)-3,8-dibromodibenzo[c,g][1,2,5]triazocin-11(12*H*)carboxylate.

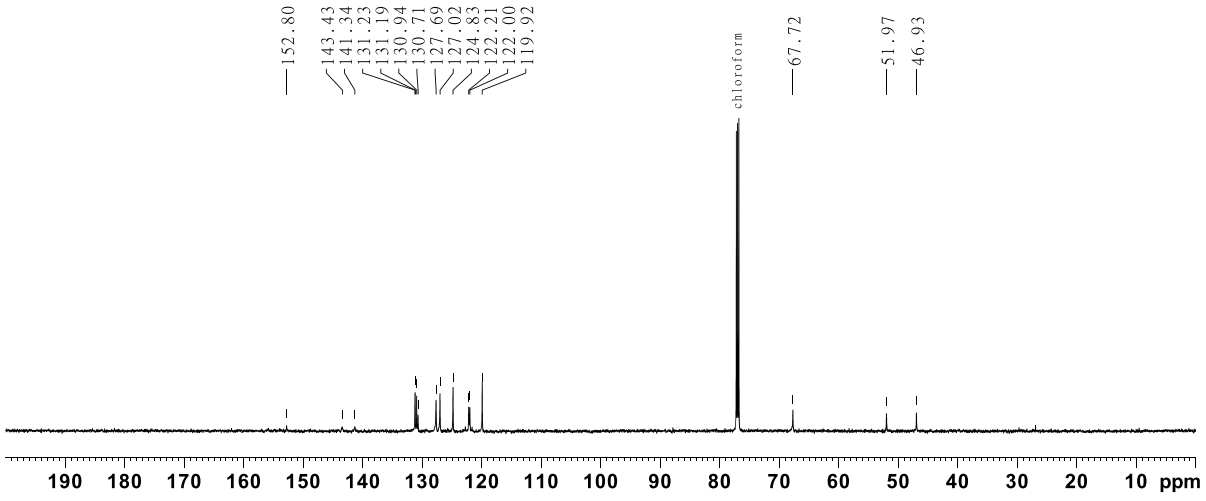

Figure SII.70: 150 MHz ^{13}C{^{1}H}-NMR spectrum of (9*H*-fluoren-9-yl)methyl-(*Z*)-3,8-dibromodibenzo[c,g][1,2,5]triazocin-11(12*H*)carboxylate.

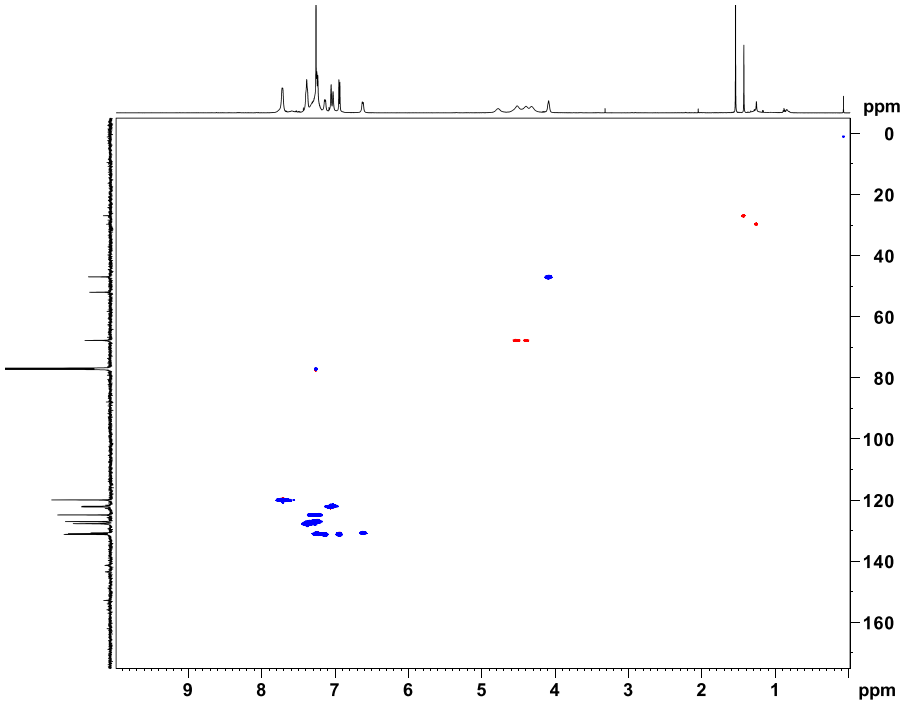

Figure SII.71: 600 MHz ^{1}H-^{13}C HSQC spectrum of (9*H*-fluoren-9-yl)methyl-(*Z*)-3,8-dibromodibenzo[c,g][1,2,5]triazocin-11(12*H*)carboxylate.

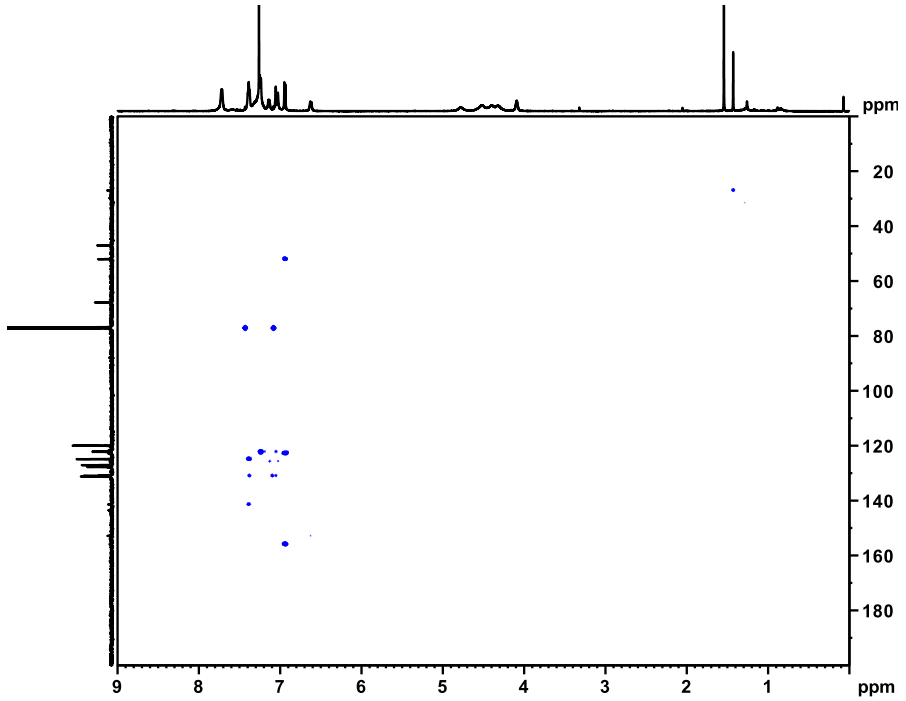

Figure SII.72: 600 MHz HMBC spectrum of (9*H*-fluoren-9-yl)methyl-(*Z*)-3,8-dibromodibenzo[c,g][1,2,5]triazocin-11(12*H*)carboxylate.

II.1.19 Synthesis of (*Z*)-3,8-dibromo-11,12-dihydrodibenzo[c,g][1,2,5]triazocine

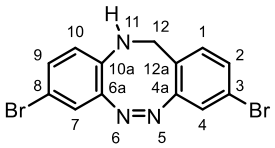

(9*H*-fluoren-9-yl)methyl-(*Z*)-3,8-dibromodibenzo[c,g][1,2,5]triazocin-11(12*H*)carboxylate (30.0 g, 50.9 µmol) was dissolved in 50 mL of DCM and 50 mL NEt_3 was added. The reaction mixture was stirred at rt. for 16 h. the solvent was evaporated and column chromatography on silica (ethyl acetate/cyclohexane 1:3, R_f = 0.32) gave a red solid (12.0 mg, 32.7 µmol, 64%).

melting point: 191 °C

^{1}H-NMR (600 MHz, $CDCl_3$, 298 K): δ = 7.38 (dd, ^3J = 8.1 Hz, ^4J = 2.0 Hz, 1 H, *H*-2), 7.33 (d, ^4J = 1.9 Hz, 1 H, *H*-4), 7.10 (d, ^3J = 8.1 Hz, 1 H, *H*-1), 7.00 (dd, ^3J = 8.6 Hz, ^4J = 2.3 Hz, 1 H, *H*-9), 6.96 (d, ^4J = 2.2 Hz, 1 H, *H*-10), 6.31 (d, ^3J = 8.6 Hz, 1 H, *H*-7), 4.08-3.81 (m, 3 H, -N*H,* *H*-12) ppm.

^{13}C{^{1}H}-NMR (150 MHz, $CDCl_3$, 298 K): δ = 158.6 (*C*-4a), 144.4 (*C*-6a), 134.3 (*C*-10-a), 131.8 (*C*-2), 131.4 (*C*-9), 130.8 (*C*-1), 125.7 (*C*-10), 122.8 (*C*-4), 122.3 (*C*-3), 121.6 (*C*-12a), 120.5 (*C*-7), 110.3 (*C*-8), 47.1 (CH_2) ppm.

IR (ATR): $\tilde{\nu}$ = 3307 (m), 2920 (m), 2360 (w), 2177 (w), 2020 (w), 1735 (w), 1588 (m), 1563 (w), 1520 (w), 1501 (w), 1479 (s), 1451 (w), 1378 (m), 1316 (m), 1269 (m), 1244 (m), 1192 (w), 1160 (m), 1120 (m), 1091 (m), 1056 (m), 967 (w), 904 (w), 858 (m), 831 (m), 806 (m), 775 (m), 720 (w), 696 (w), 518 (s) cm^{-1}.

HR-MS (ESI, EtOAc): *m/z* $[M+H]^+$ calculated for $C_{13}H_9N_3{}^{79}Br_2+H^+$: 365.9236; found: 365.9233 ± 0.89 ppm.

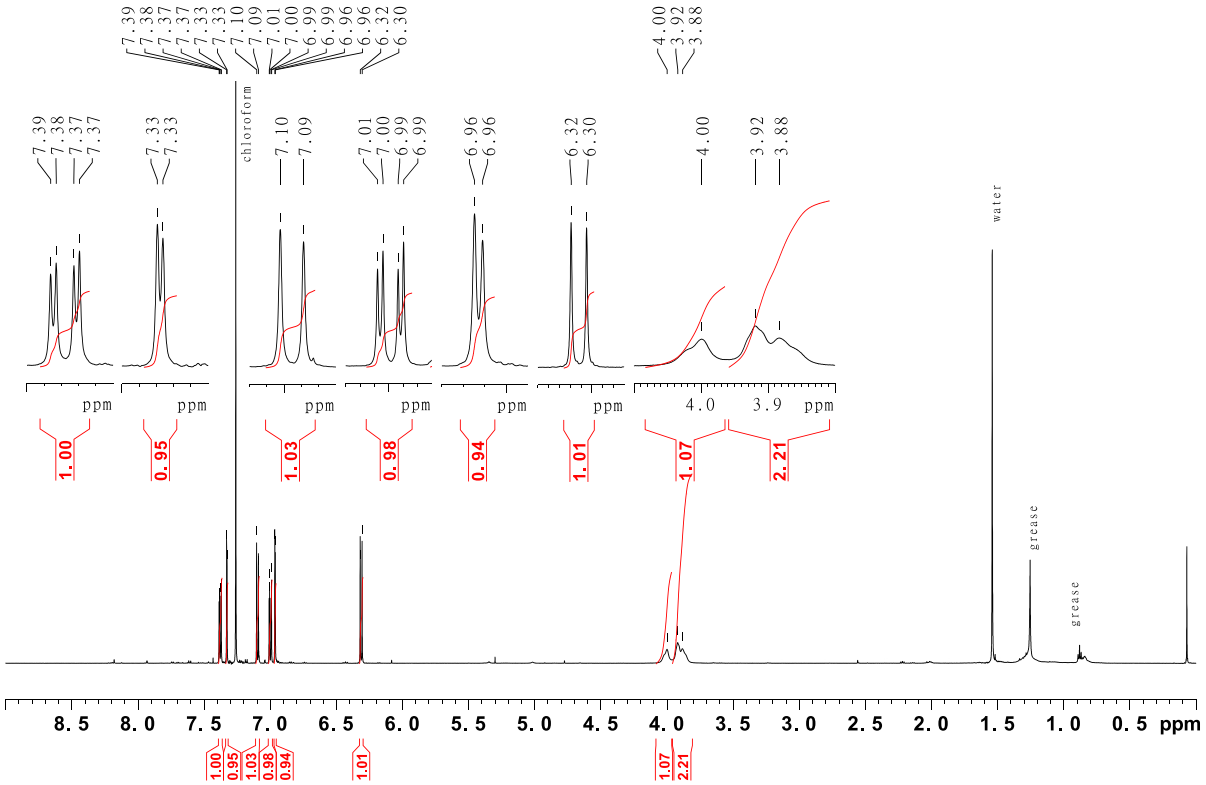

Figure SII.73: 600 MHz ^{1}H-NMR spectrum of (*Z*)-3,8-dibromo-11,12-dihydrodibenzo[c,g][1,2,5]triazocine.

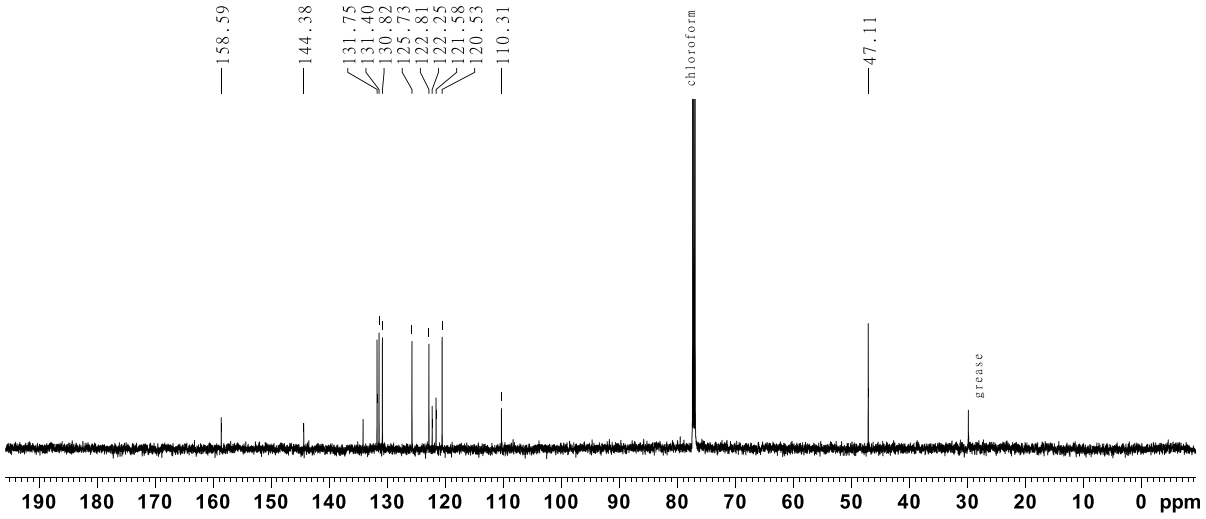

Figure SII.74: 150 MHz ^{13}C{^{1}H}-NMR spectrum of (*Z*)-3,8-dibromo-11,12-dihydrodibenzo[c,g][1,2,5]triazocine.

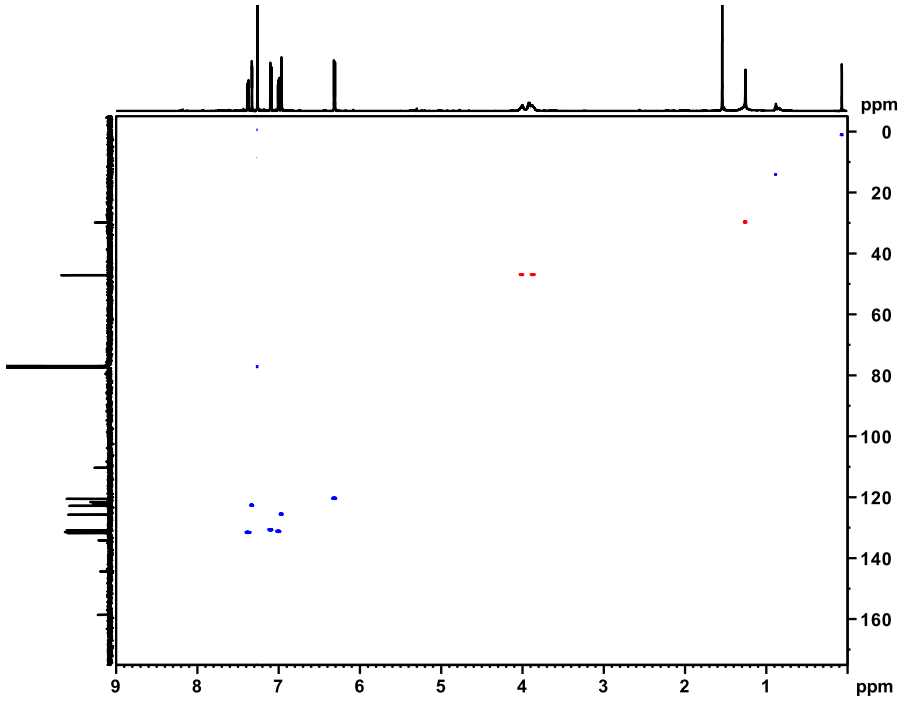

Figure SII.75: 600 MHz ^{1}H-^{13}C HSQC spectrum of (*Z*)-3,8-dibromo-11,12-dihydrodibenzo[c,g][1,2,5]triazocine.

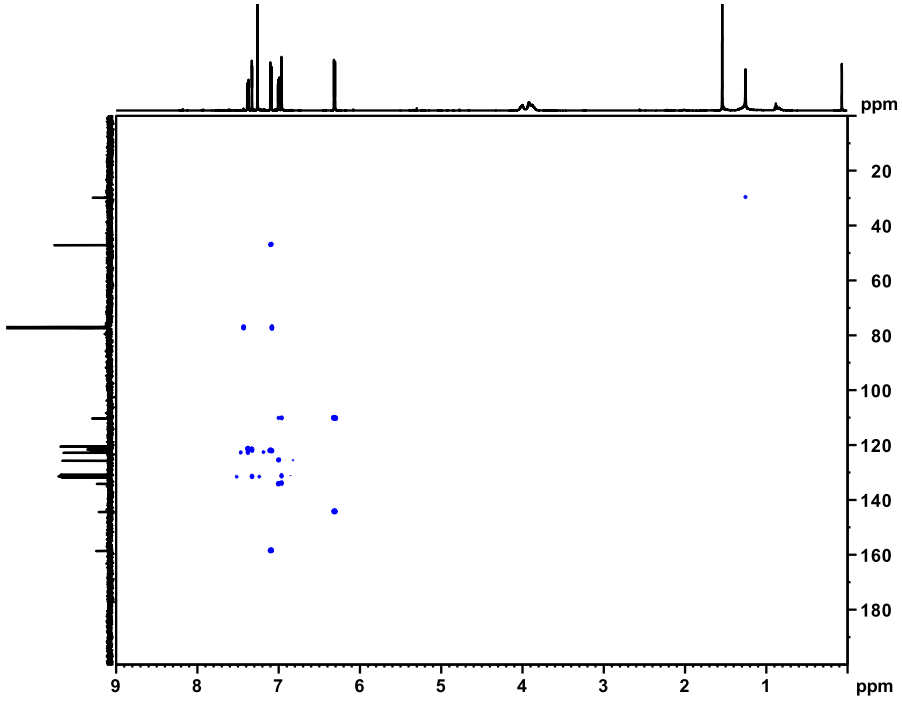

Figure SII.76: 600 MHz HMBC spectrum of (*Z*)-3,8-dibromo-11,12-dihydrodibenzo[c,g][1,2,5]triazocine.

II.1.20 Synthesis of (Z)-(3,8-dibromodibenzo[c,g][1,2,5]triazocin-11(12H)-yl)ethan-1-one (4)

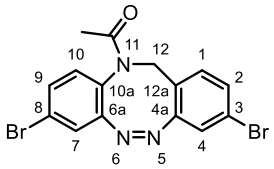

(*Z*)-3,8-dibromo-11,12-dihydrodibenzo[c,g][1,2,5]triazocine (12.0 mg, 32.7 µmol) were dissolved in 1 mL anhydrous DMF under a nitrogen atmosphere. NEt_3 (36.4 µL, 261 µmol) and AcOH (19.0 µL, 32.7 µmol) were added. The reaction mixture was cooled to 0 °C and T3P (167 µL, 327 µmol, 50% in ethyl acetate) was added dropwise. The reaction mixture was stirred at rt. for 16 h. 10 mL DCM and 10 mL deionized water were added and the organic layer was separated. The aqueous layer was extracted twice with 10 mL DCM and the combined organic layers were dried over $MgSO_4$. The solvent was removed and column chromatography on silica (ethyl acetate/cyclohexane 1:1, R_f = 0.37) gave a yellow solid (11.5 mg, 28.1 µmol, 86%).

melting point: 222 °C

^{1}H-NMR (500 MHz, $CDCl_3$, 298 K): δ = 7.32 (dd, ^3J = 8.4 Hz, ^4J = 2.2 Hz, 1 H, *H*-9), 7.25 (dd, ^3J = 8.2 Hz, ^4J = 2.0 Hz, 1 H, *H*-2), 7.12 (d, ^4J = 2.1 Hz, 1 H, *H*-7), 7.07 (d, ^4J = 1.8 Hz, 1 H, *H*-4), 6.95 (d, ^3J = 8.2 Hz, 1 H, *H*-1), 6.92 (d, ^3J = 8.4 Hz, 1 H, *H*-10), 5.01 (d, ^2J = 15.2 Hz, 1 H, *H*-12), 4.28 (d, ^2J = 14.5 Hz, 1 H, *H*-12'), 1.91 (s, 3 H, -C*H*$_3$) ppm.

^{13}C{^{1}H}-NMR (125 MHz, $CDCl_3$, 198 K): δ = 169.8 (*C*=O), 155.8 (*C*-4a), 153.5 (*C*-6a), 131.9 (*C*-9), 131.44 (*C*-1), 131.17 (*C*-2), 130.3 (*C*-10), 127.6 (*C*-10a), 122.93 (*C*-8), 122.68 (*C*-7), 122.59 (*C*-12a), 122.44 (*C*-4), 51.4 (*C*-12), 23.2 (*C*H$_3$) ppm.

IR (ATR): $\tilde{\nu}$ = 2920 (m), 2851 (w), 1654 (s), 1589 (m), 1557 (w), 1523 (w), 1469 (m), 1372 (s), 1332 (m), 1291 (m), 1268 (w), 1241 (w), 1159 (m), 1112 (m), 1075 (m), 1034 (w), 968 (m), 940 (w), 925 (w), 882 (m), 858 (m), 844 (s), 807 (s), 760 (m), 731 (m), 689 (w), 657 (m), 601 (m), 572 (s), 465 (s) cm^{-1}.

HR-MS (ESI, DCM): *m/z* [M+H]$^+$ calculated for $C_{15}H_{11}O_1N_3Br_2$+H$^+$: 407.9342; found: 407.9335 ± 1.62 ppm.

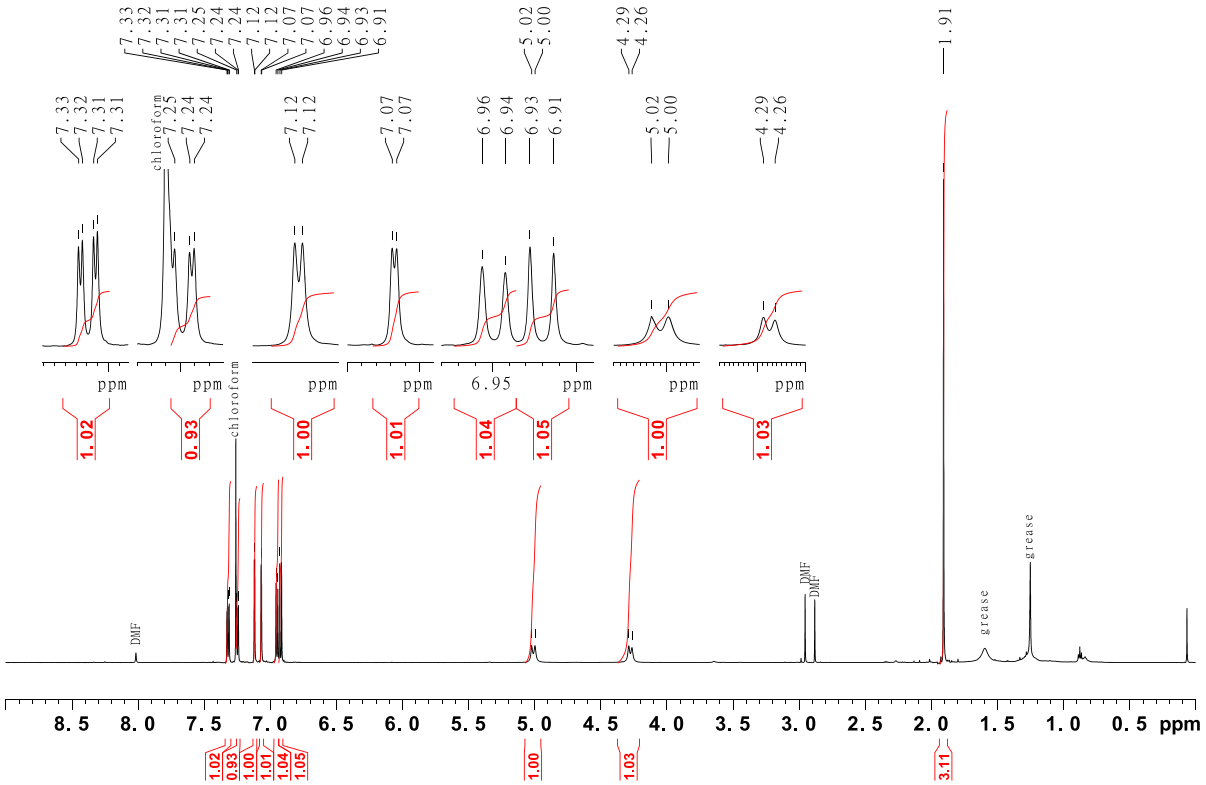

Figure SII.77: 500 MHz ^{1}H-NMR spectrum of (Z)-(3,8-dibromodibenzo[c,g][1,2,5]triazocin-11(12H)-yl)ethan-1-one (**4**).

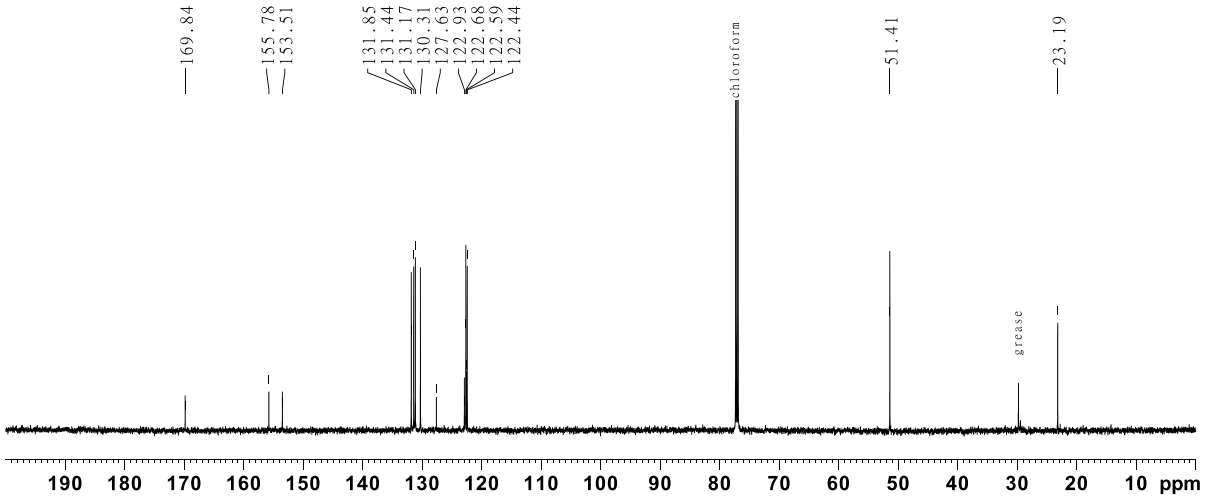

Figure SII.78: 125 MHz ^{13}C{^{1}H}-NMR spectrum of (Z)-(3,8-dibromodibenzo[c,g][1,2,5]triazocin-11(12H)-yl)ethan-1-one (**4**).

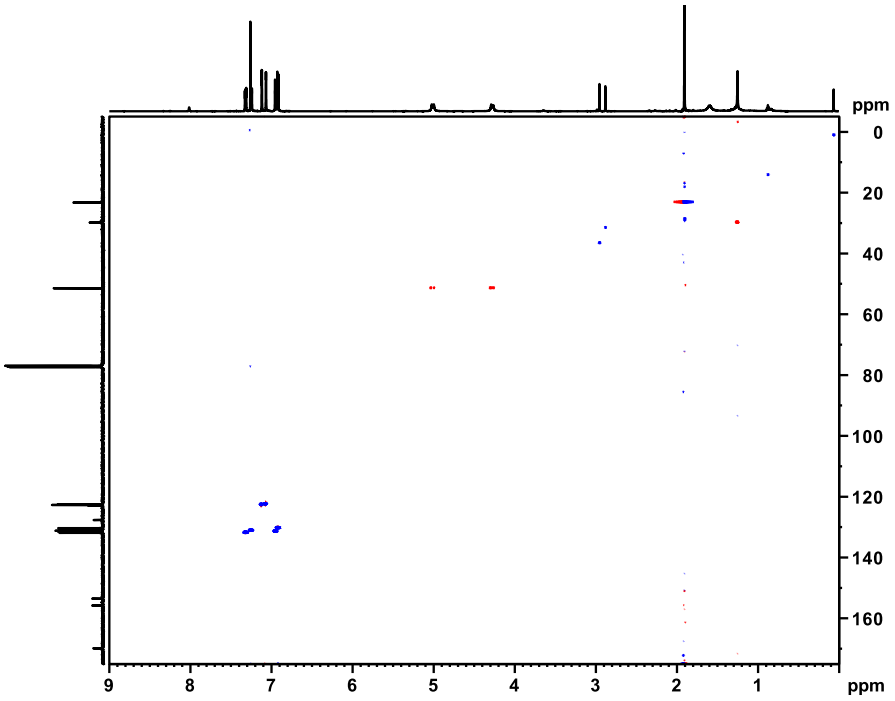

Figure SII.79: 500 MHz ^{1}H-^{13}C HSQC spectrum of (Z)-(3,8-dibromodibenzo[c,g][1,2,5]triazocin-11(12H)-yl)ethan-1-one (**4**).

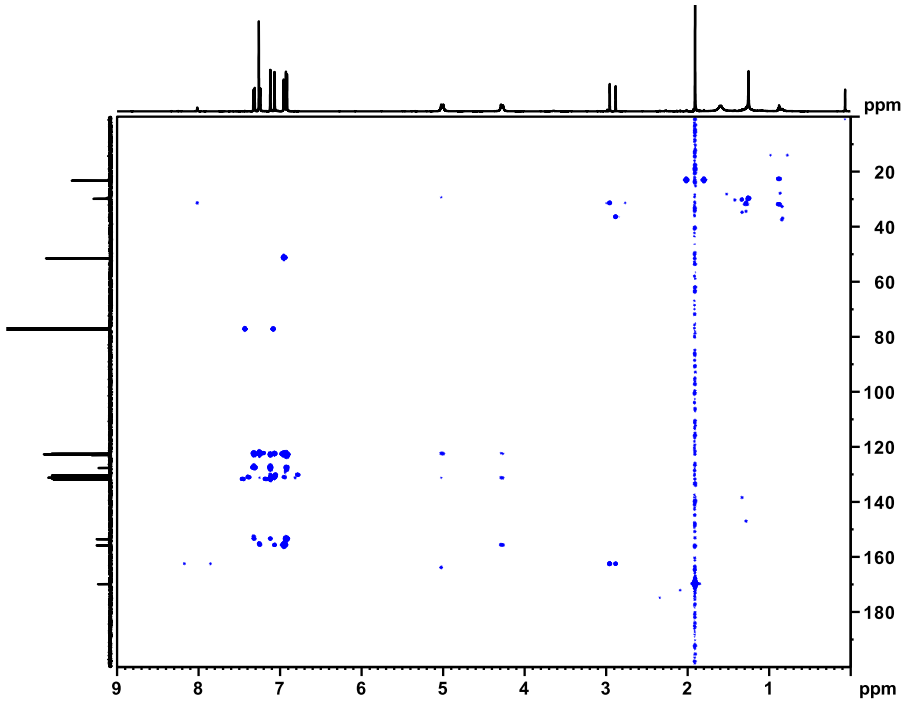

Figure SII.80: 500 MHz HMBC spectrum of (Z)-(3,8-dibromodibenzo[c,g][1,2,5]triazocin-11(12H)-yl)ethan-1-one (**4**).

II.2 Syntheses of diazocine derivatives via cross-coupling reactions

II.2.1 Synthesis of (*Z*)-1-(3-phenyldibenzo[c,g][1,2,5]triazocin-11(12*H*)-yl)ethan-1-one (7)

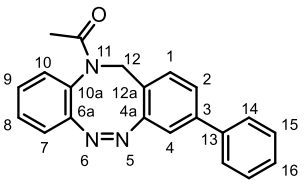

Preparation via Stille-coupling:

Halogenated *N*-acetyl-diazocine (**2**: 20.0 mg, 60.6 µmol, **3**: 23.0 mg, 60.6 µmol) and $Pd(PtBu_3)_2$ (3.1 mg, 6.06 µmol) were dissolved in 2 mL anhydrous THF and stirred at rt. for 10 min. Ph_3SnCl (23.4 mg, 60.6 µmol) was added and the reaction mixture was heated to 65 °C with an oil bath and stirred for 16 h at given temperature. After cooling to rt. deionized water and DCM were added and the reaction mixture was extracted with 10 mL DCM twice. The combined organic layers were dried over $MgSO_4$ and the solvent was evaporated. Column chromatography on silica (ethyl acetate/cyclohexane 1:1, R_f = 0.39) gave a mixture of starting material and product. The yield was determined via NMR (from bromide **2**: 1.9 mg, 5.67 µmol, 10%; from iodide **3**: 1.9 mg, 5.67 µmol, 10%).

Preparation via Suzuki-coupling:

Halogenated *N*-acetyl-diazocine (**2**: 20.0 mg, 60.6 µmol, **3**: 23.0 mg, 60.6 µmol), phenylboronic acid (14.8 mg, 121 µmol), $Pd(PPh_3)_4$ (2.45 mg, 2.12 µmol) and potassium carbonate (33.4 mg, 212 µmol) were dissolved in 2.4 mL of toluene/MeOH/deionized H_2O (5 : 1 : 2) under a nitrogen atmosphere, heated to 85 °C with an oil bath and stirred for 16 h at given temperature. After cooling to rt. the reaction mixture was extracted with 10 mL of DCM twice, dried over $MgSO_4$ and the solvent was evaporated. Column chromatography on silica (ethyl acetate/cyclohexane 1:1, R_f = 0.39) gave the product as yellow solid (from bromide **2**: 14.7 mg, 44.8 µmol, 74%; from iodide **3**: 16.5 mg, 50.3 µmol, 83%).

melting point: 187 °C

^{1}H-NMR (600 MHz, acetone-d_6, 298 K): δ = 7.61 (d, ^3J = 8.4 Hz, 2 H, *H*-14), 7.46-7.42 (m, 3 H, *H*-2, *H*-15), 7.38-7.23 (m, 5 H, *H*-16, *H*-7/8/9/10, *H*-7/8/9/10, *H*-1, *H*-8/9), 7.18 (d, ^4J = 1.8 Hz, 1 H, *H*-4), 7.04 (dd, ^3J = 7.8 Hz, ^4J = 1.2 Hz, 1 H, *H*-7/10), 5.11 (d, ^2J = 14.6 Hz, 1 H, *H*-12), 4.35 (d, ^2J = 14.6 Hz, 1 H, *H*-12'), 1.82 (s, 3 H, -C*H*$_3$) ppm.

^{13}C{^{1}H}-NMR (150 MHz, acetone-d_6, 298 K): δ = 169.4 (*C*=O), 156.8 (*C*-4a), 154.4 (*C*-6a), 142.1 (*C*-3), 140.0 (*C*-13), 131.5 (*C*-1), 130.13 (*C*-7/8/9/10), 130.08 (*C*-7/8/9/10), 129.84 (*C*-15), 129.69 (*C*-10a), 129.26 (*C*-8/9), 128.9 (*C*-16), 127.7 (*C*-14), 126.6 (*C*-2), 124.1 (*C*-12a), 120.0 (*C*-7/10), 118.0 (*C*-4), 51.8 (*C*-12), 23.1 (*C*H$_3$), ppm.

IR (ATR): $\tilde{\nu}$ = 2925 (m), 1656 (s), 1612 (w), 1590 (w), 1478 (m), 1448 (w), 1373 (s), 1335 (m), 1287 (w), 1157 (w), 1106 (w), 1076 (w), 1035 (w), 967 (w), 950 (w), 922 (w), 891 (w), 873 (w), 835 (m), 759 (s), 702 (m), 633 (m), 600 (w), 570 (m), 542 (w), 514 (m), 491 (m), 451 (w), 439 (w), 405 (m) cm^{-1}.

HR-MS (ESI, acetone): *m/z* [M+H]$^+$ calculated for $C_{21}H_{17}ON_3$+H$^+$: 328.1444; found: 328.1440 ± 1.35 ppm.

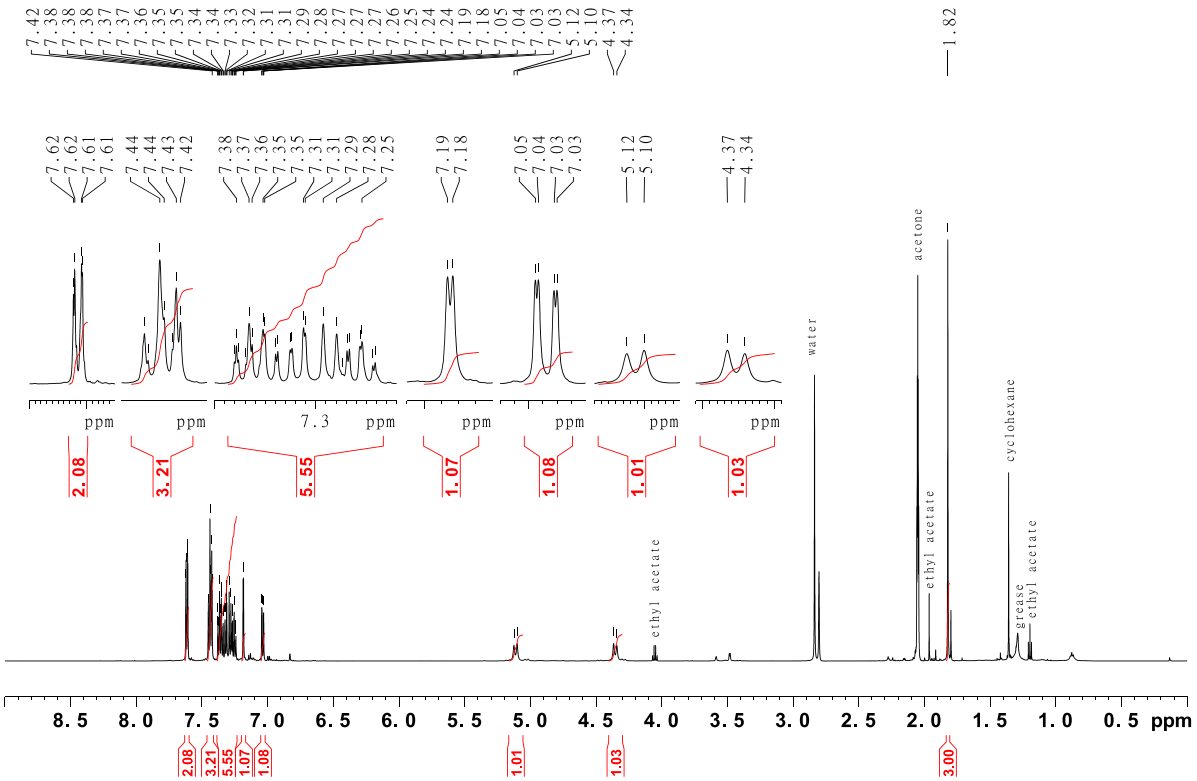

Figure SII.81: 600 MHz ^{1}H-NMR spectrum of (*Z*)-1-(3-phenyldibenzo[c,g][1,2,5]triazocin-11(12*H*)-yl)ethan-1-one (**7**).

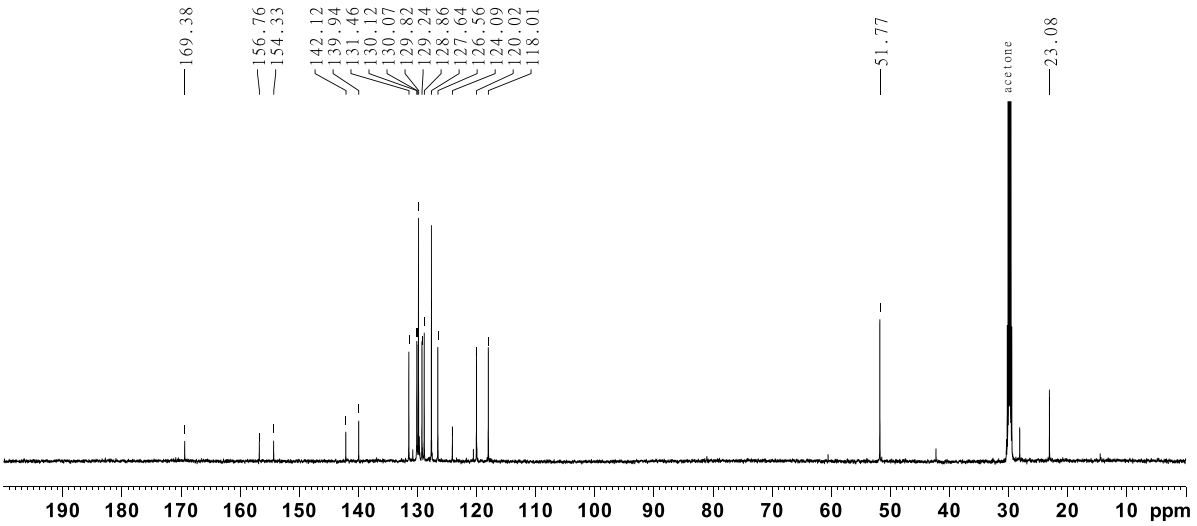

Figure SII.82: 150 MHz ^{13}C{^{1}H}-NMR spectrum of (*Z*)-1-(3-phenyldibenzo[c,g][1,2,5]triazocin-11(12*H*)-yl)ethan-1-one (**7**).

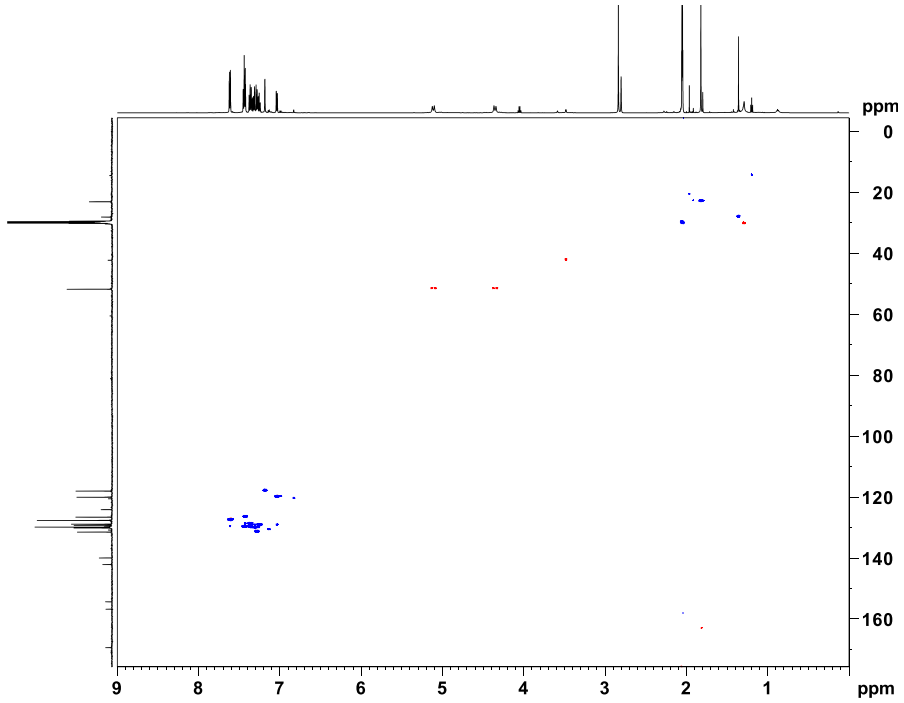

Figure SII.83: 600 MHz ^{1}H-^{13}C HSQC spectrum of (*Z*)-1-(3-phenyldibenzo[c,g][1,2,5]triazocin-11(12*H*)-yl)ethan-1-one (**7**).

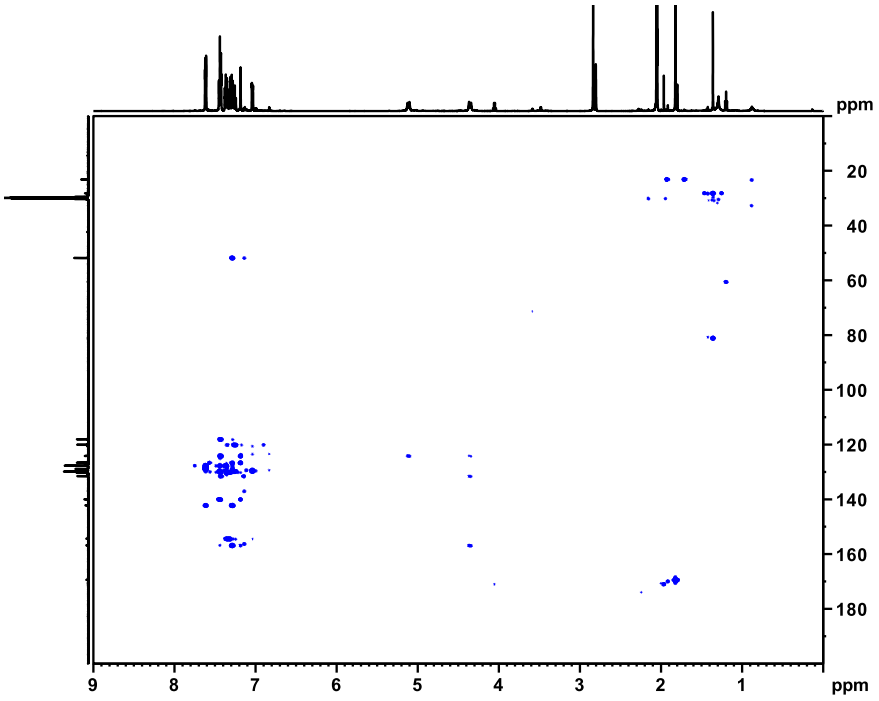

Figure SII.84: 600 MHz HMBC spectrum of (*Z*)-1-(3-phenyldibenzo[c,g][1,2,5]triazocin-11(12*H*)-yl)ethan-1-one (**7**).

II.2.2 Synthesis of (*Z*)-1-(3-vinyldibenzo[c,g][1,2,5]triazocin-11(12*H*)-yl)ethan-1-one (8)

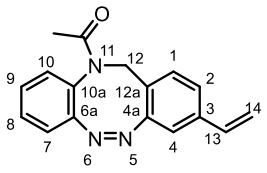

Preparation via Stille-coupling:

Halogenated *N*-acetyl-diazocine (**2**: 20.0 mg, 60.6 µmol, **3**: 23.0 mg, 60.6 µmol), $Pd(OAc)_2$ and PPh_3 (12.7 mg, 48.5 µmol) were dissolved in 2 mL anhydrous DMF and stirred at rt. for 15 min. vinyltributyltin (57.7 mg, 181 µmol) was added and the reaction mixture was heated to 100 °C with an oil bath and stirred for 16 h at given temperature. After cooling to rt. brine and ethyl acetate were added and the organic layer was separated. The aqueous layer was extracted with 10 mL ethyl acetate twice. The combined organic layers were dried over $MgSO_4$ and the solvent was evaporated. Column chromatography on silica (ethyl acetate/cyclohexane 1:1, R_f = 0.41) gave the product as yellow solid (from bromide **2**: 10.9 mg, 39.4 µmol, 65%; from iodide **3**: 11.8 mg, 43.0 µmol, 71%).

Tin-free preparation following the DENMARK-procedure[3]:

PdBr2 (1.60 mg, 6.06 µmol) and JohnPhos (1.8 mg, 6.06 µmol) were suspended in 2 mL anhydrous THF, 1,3,5,7-tetramethyl-1,3,5,7-tetravinylcyclotetrasiloxane (D_4^V, 13.4 µL, 38.8 µmol) and TBAF (1 M in THF, 242 µL, 242 µmol) were added and the reaction mixture was stirred for 10 min. at rt. The halogenated *N*-acetyl diazocine (**2**: 20.0 mg, 60.6 µmol, **3**: 23.0 mg, 60.6 µmol) was added, the reaction mixture was heated to 50 °C with an oil bath, stirred for 16 h at given temperature and the solvent was evaporated subsequently. After column chromatography on silica (ethyl acetate/cyclohexane, R_f = 0.39) the product could be obtained as yellow solid (from bromide **2**: 12.4 mg, 44.8 µmol, 74%; from iodide **3**: 13.0 mg, 46.9 µmol, 78%).

melting point: 144 °C

^{1}H-NMR (500 MHz, acetone-d_6, 298 K): δ = 7.35 (td, ^3J = 7.6 Hz, ^4J = 1.4 Hz, 1 H, *H*-8), 7.29 (dd, ^3J = 7.9 Hz, ^4J = 1.7 Hz, 1 H, *H*-10), 7.25 (dd, ^3J = 7.3 Hz, ^4J = 1.4 Hz, 1 H, *H*-7), 7.22 (dd, ^3J = 7.9 Hz, ^4J = 1.8 Hz, 1 H, *H*-2), 7.17 (d, ^3J = 7.9 Hz, 1 H, *H*-1), 7.02-6.97 (m, 2 H, *H*-4, *H*-9), 6.68 (dd, ^2J = 17.6 Hz, ^3J = 10.9 Hz, 1 H, *H*-13), 5.81 (dd, ^2J = 17.6 Hz, ^4J = 0.7 Hz, 1 H, *H*-14), 5.27 (dd, ^3J = 10.9 Hz, ^4J = 0.7 Hz, 1 H, *H*-14'), 5.04 (d, ^2J = 14.5 Hz, 1 H, *H*-12), 4.30 (d, ^2J = 14.7 Hz, 1 H, *H*-12'), 1.80 (s, 3 H, -CH_3) ppm.

^{13}C{^{1}H}-NMR (125 MHz, acetone-d_6, 298 K): δ = 169.3 (*C*=O), 156.5 (*C*-4a), 154.3 (*C*-6a), 139.0 (*C*-3), 136.3 (*C*-13), 131.1 (*C*-1), 130.11 (*C*-10), 130.04 (*C*-8), 129.7 (*C*-10a), 129.2 (*C*-7), 126.0 (*C*-2), 124.5 (*C*-12a), 120.0 (*C*-9), 117.4 (*C*-4), 116.0 (*C*-14), 51.8 (*C*-12), 23.1 (*C*H$_3$), ppm.

IR (ATR): $\tilde{\nu}$ = 2956 (w), 2922 (m), 1651 (s), 1591 (w), 1513 (w), 1479 (m), 1450 (w), 1431 (w), 1378 (s), 1339 (s), 1303 (m), 1252 (w), 1147 (w), 1109 (w), 1077 (w), 1031 (w), 995 (m), 962 (w), 926 (w), 911 (m), 885 (w), 845 (m), 766 (m), 742 (m), 665 (m), 630 (w), 601 (w), 585 (m), 570 (w), 529 (w) cm^{-1}.

HR-MS (ESI, acetone): *m/z* [M+H]$^+$ calculated for $C_{17}H_{15}ON_3$+H$^+$: 278.1288 found: 278.1287 ± 0.49 ppm.

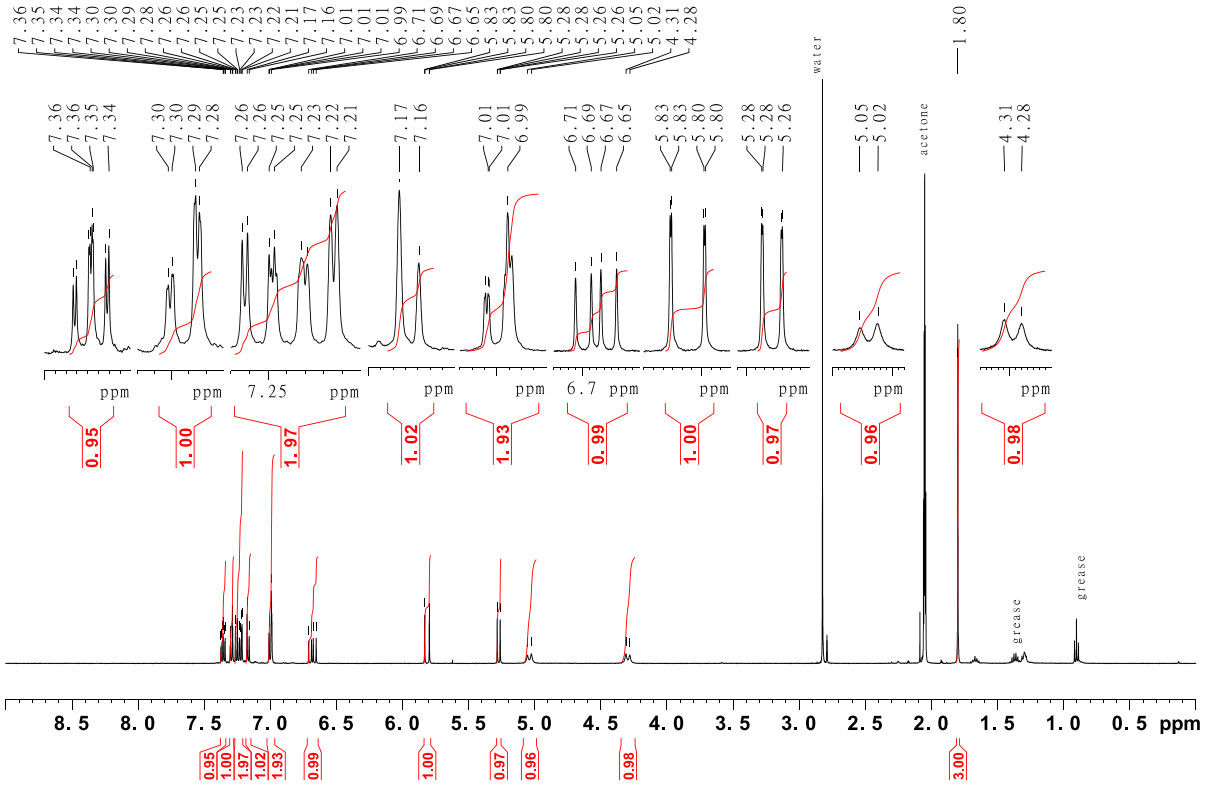

Figure SII.85: 500 MHz ^{1}H-NMR spectrum of (*Z*)-1-(3-vinyldibenzo[c,g][1,2,5]triazocin-11(12*H*)-yl)ethan-1-one (**8**).

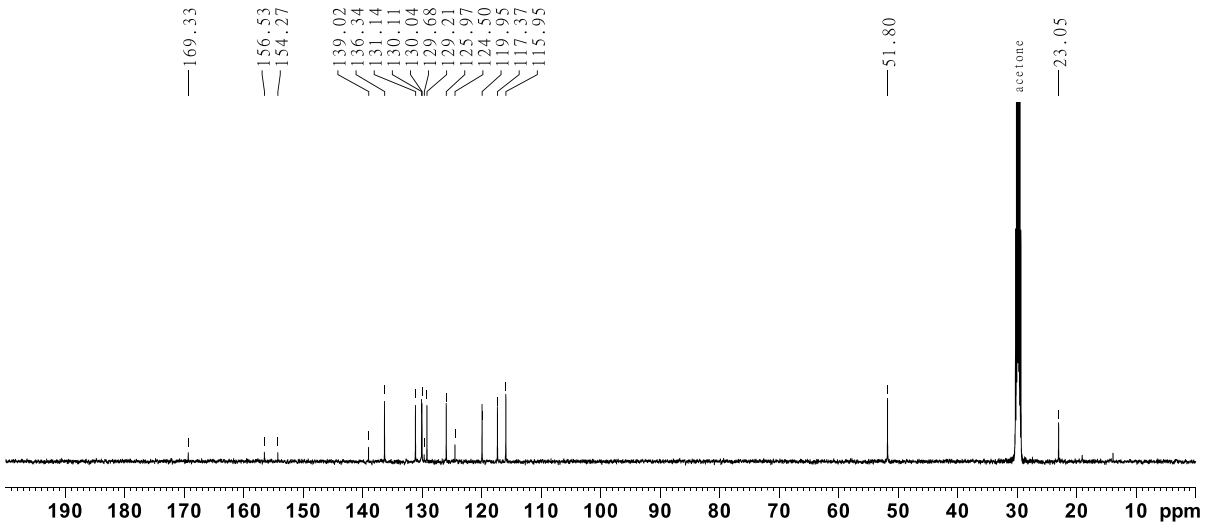

Figure SII.86: 125 MHz ^{13}C{^{1}H}-NMR spectrum of (*Z*)-1-(3-vinyldibenzo[c,g][1,2,5]triazocin-11(12*H*)-yl)ethan-1-one (**8**).

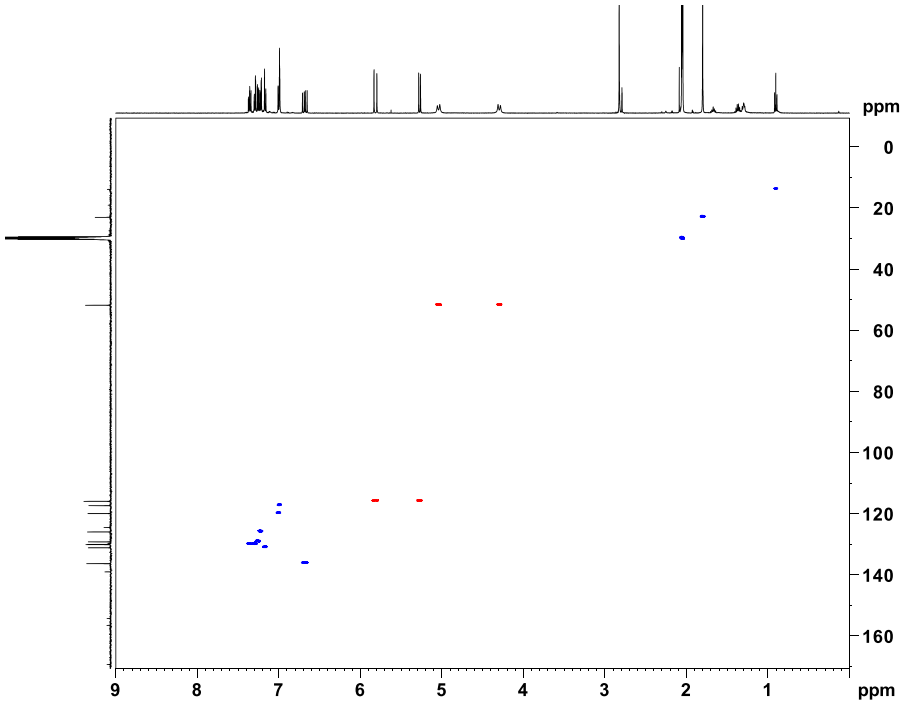

Figure SII.87: 500 MHz ^{1}H-^{13}C HSQC spectrum of (*Z*)-1-(3-vinyldibenzo[c,g][1,2,5]triazocin-11(12*H*)-yl)ethan-1-one (**8**).

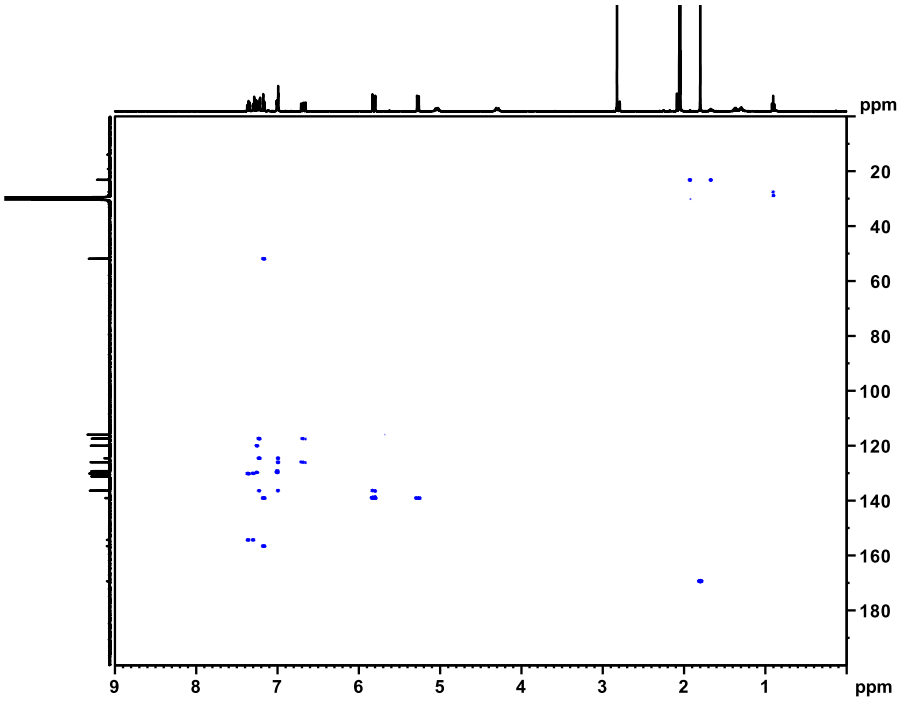

Figure SII.88: 500 MHz HMBC spectrum of (*Z*)-1-(3-vinyldibenzo[c,g][1,2,5]triazocin-11(12*H*)-yl)ethan-1-one (**8**).

II.2.3 Synthesis of (*Z*)-1-(3-(2,6-dimethylphenyl)dibenzo[c,g][1,2,5]triazocin-11(12*H*)-yl)ethan-1-one (9)

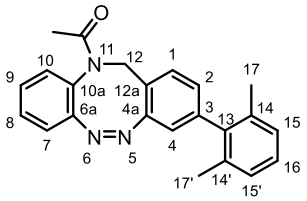

Halogenated *N*-acetyl-diazocine (**2**: 20.0 mg, 60.6 µmol, **3**: 23.0 mg, 60.6 µmol), phenylboronic acid (18.2 mg, 121 µmol), $Pd(PPh_3)_4$ (2.45 mg, 2.12 µmol) and potassium carbonate (33.4 mg, 212 µmol) were dissolved in 2.4 mL of toluene/MeOH/deionized H_2O (5 : 1 : 2) under a nitrogen atmosphere, heated to 85 °C with an oil bath and stirred for 16 h at given temperature. After cooling to rt. the reaction mixture was extracted with 10 mL of DCM twice, dried over $MgSO_4$ and the solvent was evaporated. Column chromatography on silica (ethyl acetate/cyclohexane 1:1, R_f = 0.40) gave the product as yellow solid (from bromide **2**: 14.6 mg, 41.1 µmol, 68%; from iodide **3**: 15.9 mg, 44.8 µmol, 74%).

melting point: 203 °C

^{1}H-NMR (600 MHz, acetone-d_6, 298 K): δ = 7.35 (td, ^3J = 7.5 Hz, ^4J = 1.5 Hz, 1 H, *H*-8), 7.29-7.24 (m, 3 H, *H*-1, *H*-9, *H*-10), 7.12 (t, ^3J = 7.3 Hz, 1 H, *H*-14), 7.10 (d, ^3J = 7.2 Hz, 1 H, *H*-15), 7.01 (d, ^3J = 6.6 Hz, 1 H, *H*-15'), 6.99 (dd, ^3J = 7.9 Hz, ^4J = 1.1 Hz, 1 H, *H*-7), 6.88 (dd, ^3J = 7.7 Hz, ^4J = 1.7 Hz, 1 H, *H*-2), 6.60 (d, ^4J = 1.6 Hz, 1 H, *H*-4), 5.01 (d, ^2J = 14.2 Hz, 1 H, *H*-12), 4.38 (d, ^2J = 14.3 Hz, 1 H, *H*-12'), 2.08 (s, 3 H, *H*-17), 1.80 (s, 3 H, -CH_3), 1.55 (s, 3 H, -17') ppm.

^{13}C{^{1}H}-NMR (150 MHz, acetone-d_6, 298 K): δ = 169.3 (*C*=O), 157.1 (*C*-4a), 154.7 (*C*-6a), 142.6 (*C*-3), 141.0 (*C*-13), 136.5 (*C*-14'), 136.1 (*C*-14), 131.3 (*C*-1), 130.3 (*C*-10), 130.0 (*C*-10a), 129.8 (*C*-8), 129.0 (*C*-9), 128.8 (*C*-2), 128.30 (*C*-16), 128.21 (*C*-17), 128.17 (*C*-17'), 123.6 (*C*-12a), 119.72 (*C*-4), 119.64 (*C*-7), 52.0 (*C*-12), 23.2 (*C*H$_3$), 20.8 (*C*-17), 20.4 (*C*-17') ppm.

IR (ATR): $\tilde{\nu}$ = 3751 (w), 2922 (m), 2300 (w), 1728 (w), 1651 (s), 1613 (w), 1589 (w), 1509 (w), 1482 (m), 1464 (w), 1380 (s), 1339 (s), 1297 (w), 1244 (w), 1169 (w), 1104 (w), 1069 (m), 1033 (m), 987 (w), 966 (m), 928 (w), 877 (m), 856 (w), 833 (s), 777 (s), 742 (m), 663 (w), 637 (m), 599 (m), 581 (m) cm^{-1}.

HR-MS (ESI, acetone): *m/z* $[M+H]^+$ calculated for $C_{23}H_{21}ON_3+H^+$: 356.1757; found: 356.1755 ± 0.75 ppm.

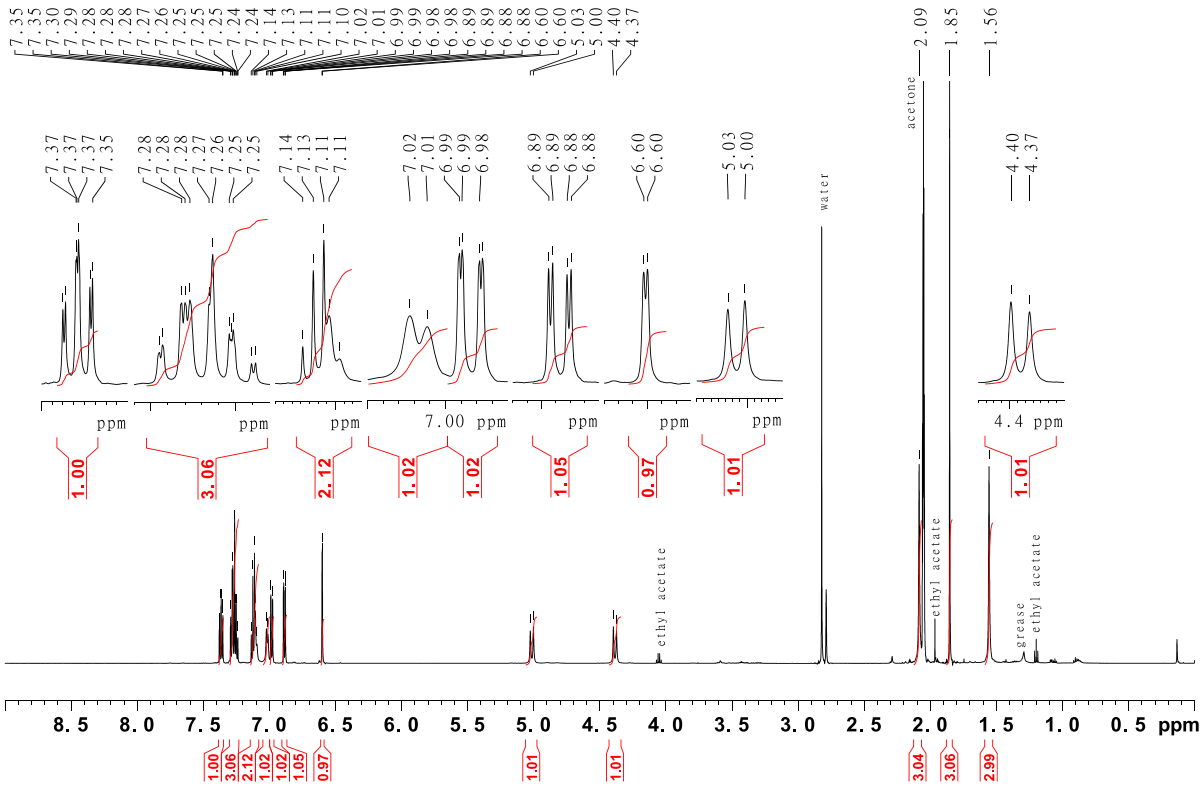

Figure SII.89: 600 MHz ^{1}H-NMR spectrum of (*Z*)-1-(3-(2,6-dimethylphenyl)dibenzo[c,g][1,2,5]triazocin-11(12*H*)-yl)ethan-1-one (**9**).

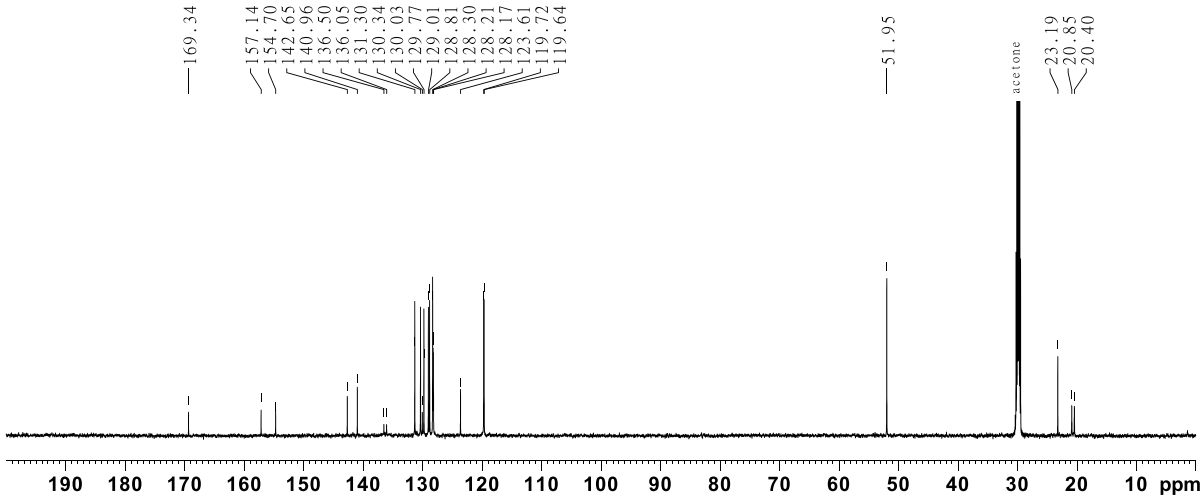

Figure SII.90: 150 MHz ^{13}C{^{1}H}-NMR spectrum of (*Z*)-1-(3-(2,6-dimethylphenyl)dibenzo[c,g][1,2,5]triazocin-11(12*H*)-yl)ethan-1-one (**9**).

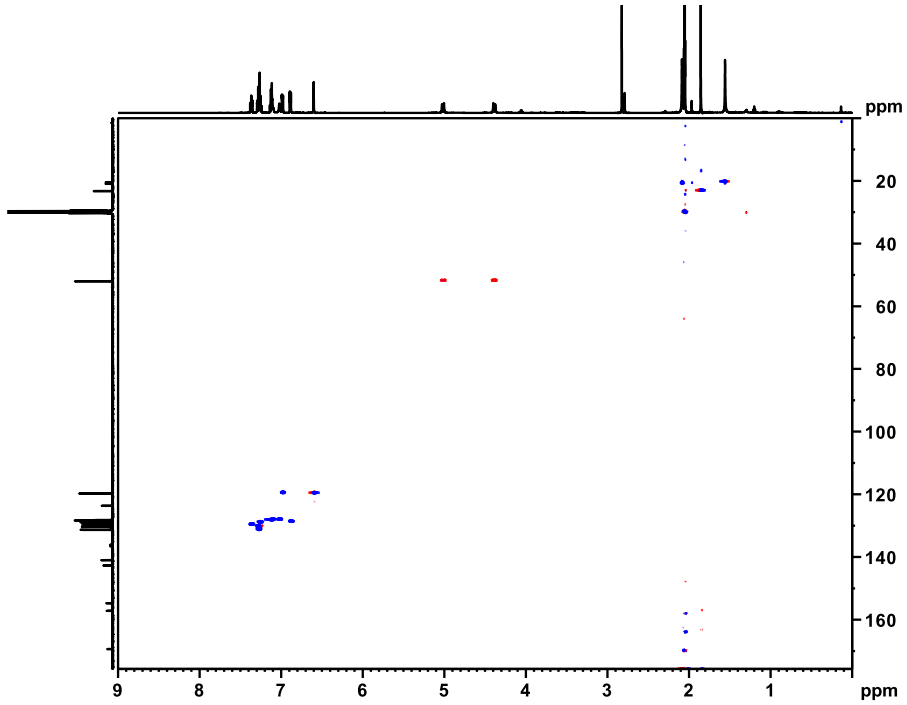

Figure SII.91: 600 MHz ^{1}H-^{13}C HSQC spectrum of (*Z*)-1-(3-(2,6-dimethylphenyl)dibenzo[c,g][1,2,5]triazocin-11(12*H*)-yl)ethan-1-one (**9**).

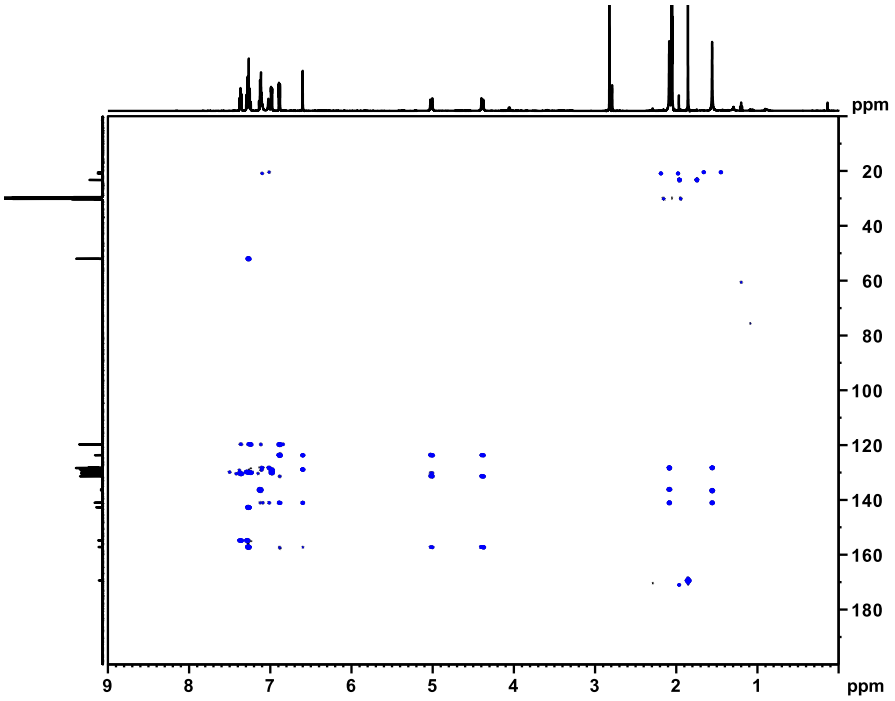

Figure SII.92: 600 MHz HMBC spectrum of (*Z*)-1-(3-(2,6-dimethylphenyl)dibenzo[c,g][1,2,5]triazocin-11(12*H*)-yl)ethan-1-one (**9**).

II.2.4 Synthesis of (*Z*)-1-(3-(2-bromophenyl)dibenzo[c,g][1,2,5]triazocin-11(12*H*)-yl)ethan-1-one (10)

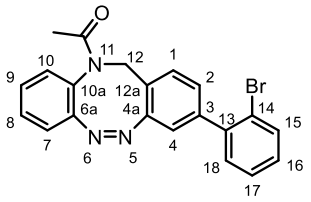

Halogenated *N*-acetyl-diazocine (**3**: 23.0 mg, 60.6 µmol), (2-bromophenyl)boronic acid (24.3 mg, 121 µmol), $Pd(PPh_3)_4$ (2.45 mg, 2.12 µmol) and potassium carbonate (33.4 mg, 212 µmol) were dissolved in 2.4 mL of toluene/MeOH/deionized H_2O (5 : 1 : 2) under a nitrogen atmosphere, heated to 85 °C with an oil bath and stirred for 16 h at given temperature. After cooling to rt. the reaction mixture was extracted with 10 mL of DCM twice, dried over $MgSO_4$ and the solvent was evaporated. Column chromatography on silica (ethyl acetate/cyclohexane 1:1, R_f = 0.45) gave the product as yellow solid (from iodide **3**: 20.2 mg, 49.7 µmol, 82%).

melting point: 119 °C

^{1}H-NMR (600 MHz, acetone-d_6, 298 K): δ = 7.69 (d, ^3J = 9.5 Hz, 1 H, Ar-*H*), 7.43 (td, ^3J = 7.5 Hz, ^4J = 1.2 Hz, 1 H, Ar-*H*), 7.38 (td, ^3J = 7.7 Hz, ^4J = 1.3 Hz, 1 H, Ar-*H*), 7.33-7.25 (m, 5 H), 7.16 (dd, ^3J = 7.9 Hz, ^4J = 1.8 Hz, 1 H, *H*-2), 7.04 (dd, ^3J = 7.8 Hz, ^4J = 1.2 Hz, 1 H, Ar-*H*), 6.94 (d, ^4J = 1.7 Hz, 1 H, *H*-4), 5.11 (d, ^2J = 14.4 Hz, 1 H, *H*-12), 4.37 (d, ^2J = 14.6 Hz, 1 H, *H*-12'), 1.83 (s, 3 H, -CH_3) ppm.

^{13}C{^{1}H}-NMR (150 MHz, acetone-d_6, 298 K): δ = 169.4 (*C*=O), 156.0 (*C*-4a), 154.5 (*C*-6a), 142.2 (*C*-Ar), 141.7 (*C*-3), 134.1 (*C*-Ar), 1320 (*C*-Ar), 130.7 (*C*-1), 130.5 (*C*-Ar), 130.15 (*C*-Ar), 130.06 (*C*-8), 129.7 (*C*-Ar), 129.3 (*C*-Ar), 128.8 (*C*-Ar), 124.6 (*C*-12a), 122.7 (*C*-Ar), 120.7 (*C*-4), 120.0 (*C*-Ar), 116.6 (*C*-Ar), 51.9 (*C*-12), 23.1 (*C*H_3) ppm.

IR (ATR): $\tilde{\nu}$ = 2922 (m), 2852 (w), 1654 (s), 1592 (w), 1485 (m), 1464 (m), 1433 (w), 1369 (s), 1334 (s), 1288 (w), 1242 (w), 1066 (w), 1023 (m), 971 (w), 933 (w), 879 (w), 842 (m), 752 (s), 729 (w), 699 (w), 659 (m), 603 (w), 569 (m), 533 (m), 430 (m) cm^{-1}.

HR-MS (ESI, DCM): *m/z* $[M+H]^+$ calculated for $C_{21}H_{16}ON_3{}^{79}Br+H^+$: 406.0550 found: 406.0547 ± 0.54 ppm.

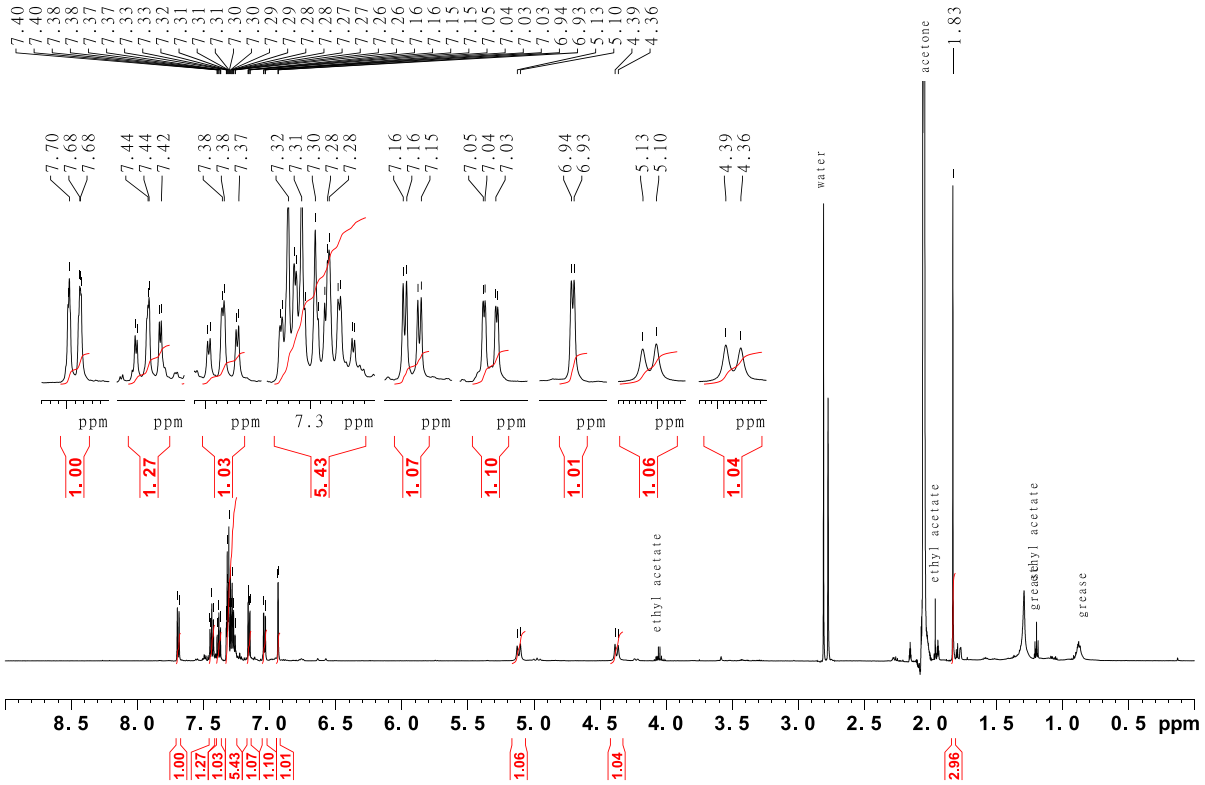

Figure SII.93: 600 MHz ^{1}H-NMR spectrum of (*Z*)-1-(3-(2-bromophenyl)dibenzo[c,g][1,2,5]triazocin-11(12*H*)-yl)ethan-1-one (**10**).

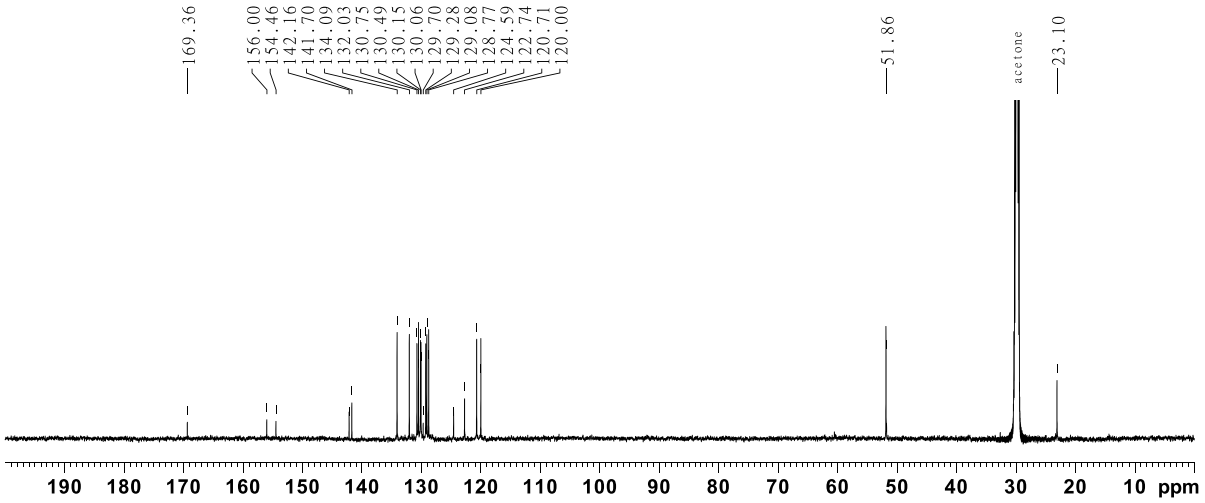

Figure SII.94: 150 MHz ^{13}C{^{1}H}-NMR spectrum of (*Z*)-1-(3-(2-bromophenyl)dibenzo[c,g][1,2,5]triazocin-11(12*H*)-yl)ethan-1-one (**10**).

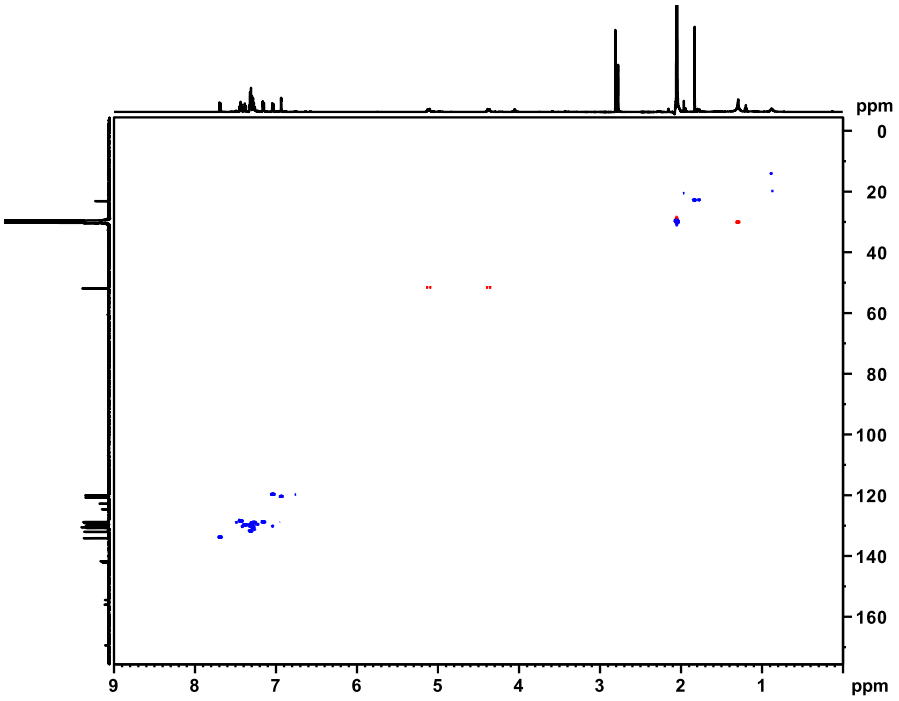

Figure SII.95: 600 MHz ^{1}H-^{13}C HSQC spectrum of (*Z*)-1-(3-(2-bromophenyl)dibenzo[c,g][1,2,5]triazocin-11(12*H*)-yl)ethan-1-one (**10**).

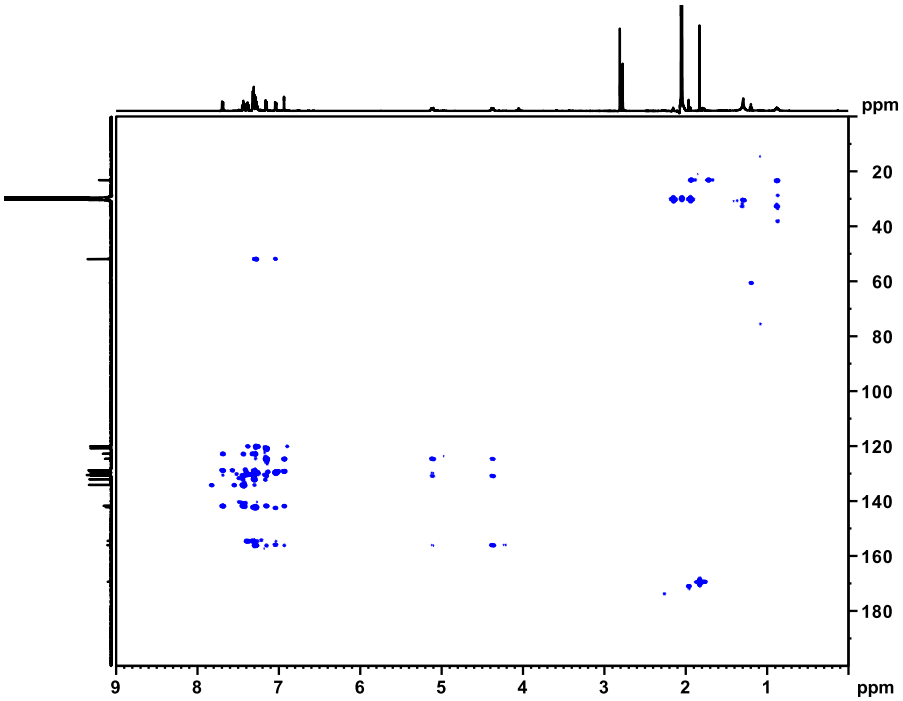

Figure SII.96: 600 MHz HMBC spectrum of (*Z*)-1-(3-(2-bromophenyl)dibenzo[c,g][1,2,5]triazocin-11(12*H*)-yl)ethan-1-one (**10**).

II.2.5 Synthesis of (*Z*)-1-(3-(4-fluorophenyl)dibenzo[c,g][1,2,5]triazocin-11(12*H*)-yl)ethan-1-one (11)

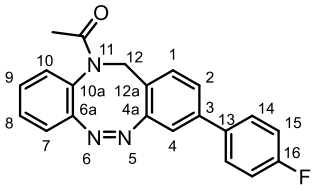

Halogenated *N*-acetyl-diazocine (**2**: 20.0 mg, 60.6 µmol, **3**: 23.0 mg, 60.6 µmol), (2,6-dimethylphenyl)boronic acid (17.0 mg, 121 µmol), $Pd(PPh_3)_4$ (2.45 mg, 2.12 µmol) and potassium carbonate (33.4 mg, 212 µmol) were dissolved in 2.4 mL of toluene/MeOH/deionized H_2O (5 : 1 : 2) under a nitrogen atmosphere, heated to 85 °C with an oil bath and stirred for 16 h at given temperature. After cooling to rt. the reaction mixture was extracted with 10 mL of DCM twice, dried over $MgSO_4$ and the solvent was evaporated. Column chromatography on silica (ethyl acetate/cyclohexane 1:1, R_f = 0.38) gave the product as yellow solid (from bromide **2**: 16.9 mg, 49.1 µmol, 81%; from iodide **3**: 18.4 mg, 53.3 µmol, 88%).

melting point: 203 °C

^{1}H-NMR (600 MHz, acetone-d_6, 298 K): δ = 7.67 (dd, ^3J = 8.9 Hz, ^3J = 5.3 Hz, 2 H, *H*-14), 7.41 (dd, ^3J = 7.9 Hz, ^4J = 1.9 Hz, 1 H, *H*-2), 7.36 (td, ^3J = 7.6 Hz, ^4J = 1.3 Hz, 1 H, *H*-8), 7.32 (dd, ^3J = 7.9 Hz, ^4J = 1.1 Hz, 1 H, *H*-10), 7.29 (d, ^3J = 7.9 Hz, 1 H, *H*-1), 7.26 (td, ^3J = 7.5 Hz, ^4J = 1.4 Hz, 1 H, *H*-9), 7.21 (t, ^3J = 8.8 Hz, 2 H, *H*-15), 7.17 (d, ^4J = 1.8 Hz, 1 H, *H*-4), 7.03 (dd, ^3J = 7.8 Hz, ^3J = 1.3 Hz, 1 H, *H*-7), 5.11 (d, ^2J = 14.6 Hz, 1 H, *H*-12), 4.35 (d, ^2J = 14.6 Hz, 1 H, *H*-12'), 1.81 (s, 3 H, -CH_3) ppm.

^{13}C{^{1}H}-NMR (150 MHz, acetone-d_6, 298 K): δ = 169.4 (*C*=O), 163.7 (^1J = 247.3 Hz, *C*-16) 156.8 (*C*-4a), 154.4 (*C*-6a), 141.1 (*C*-3), 136.4 (*C*-13), 131.5 (*C*-1), 130.14 (*C*-10), 130.09 (*C*-8), 129.7 (^3J = 8.2 Hz, *C*-14), 129.3 (*C*-9), 126.5 (*C*-2), 124.2 (*C*-12a), 120.0 (*C*-7), 118.0 (*C*-4), 116.6 (^2J = 21.7 Hz, *C*-15), 51.8 (*C*-12), 23.1 (*C*H_3) ppm.

IR (ATR): $\tilde{\nu}$ = 3065 (w), 2924 (m), 2852 (w), 2254 (w), 2038 (w), 1654 (s), 1606 (w), 1518 (m), 1475 (m), 1382 (s), 1290 (m), 1222 (s), 1164 (m), 1107 (w), 1034 (w), 1016 (m), 974 (m), 914 (w), 878 (w), 843 (m), 809 (s), 783 (w), 759 (s), 739 (s), 703 (w), 635 (m), 593 (s), 536 (m) cm^{-1}.

HR-MS (ESI, acetone): *m/z* $[M+H]^+$ calculated for $C_{21}H_{15}FON_3+H^+$: 346.1350; found: 346.1347 ± 0.33 ppm.

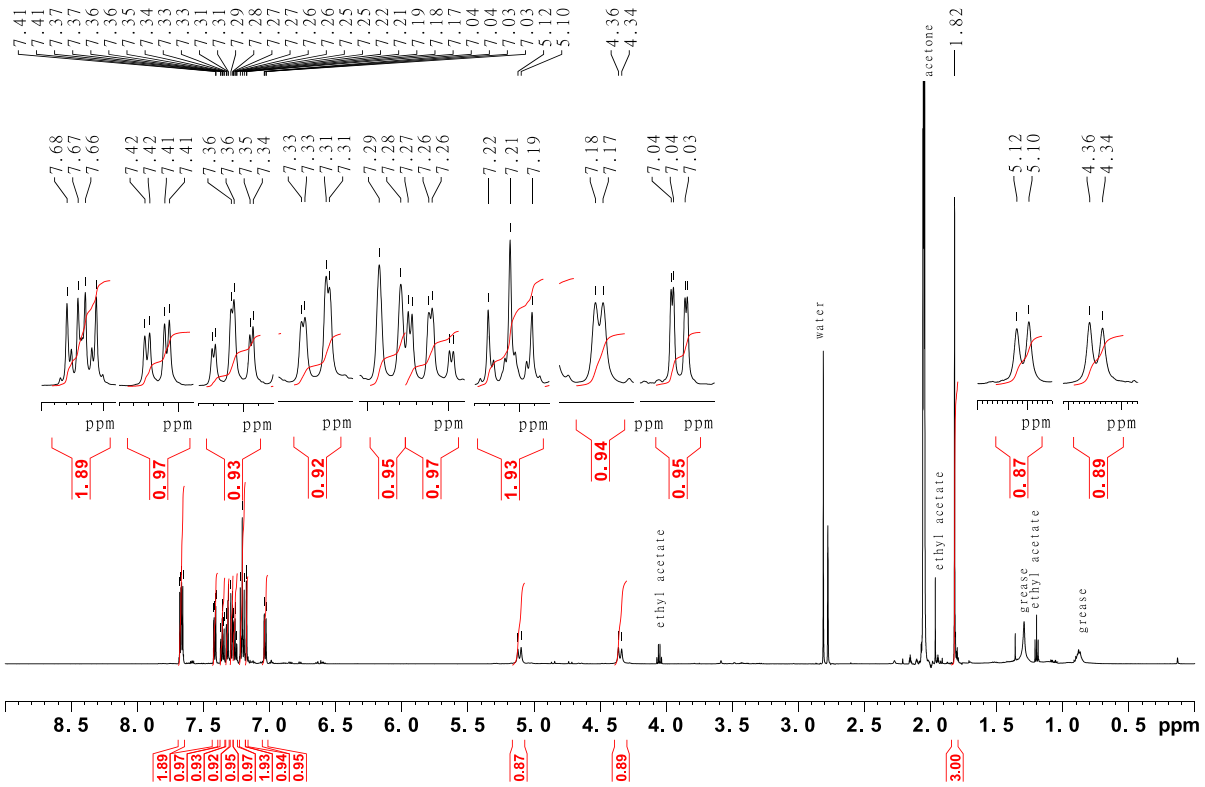

Figure SII.97: 600 MHz ^{1}H-NMR spectrum of (*Z*)-1-(3-(4-fluorophenyl)dibenzo[c,g][1,2,5]triazocin-11(12*H*)-yl)ethan-1-one (**11**).

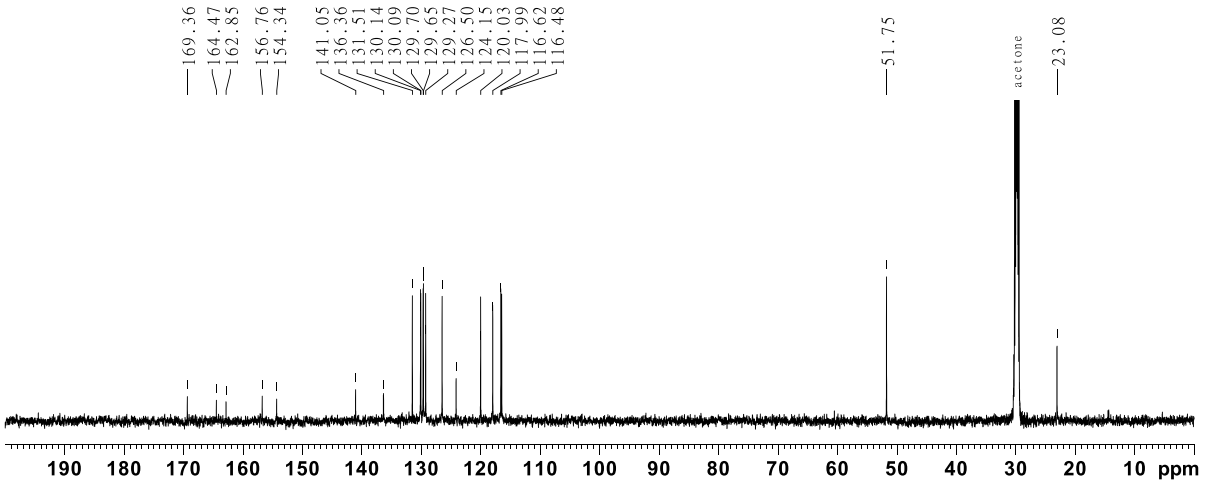

Figure SII.98: 150 MHz ^{13}C{^{1}H}-NMR spectrum of (*Z*)-1-(3-(4-fluorophenyl)dibenzo[c,g][1,2,5]triazocin-11(12*H*)-yl)ethan-1-one (**11**).

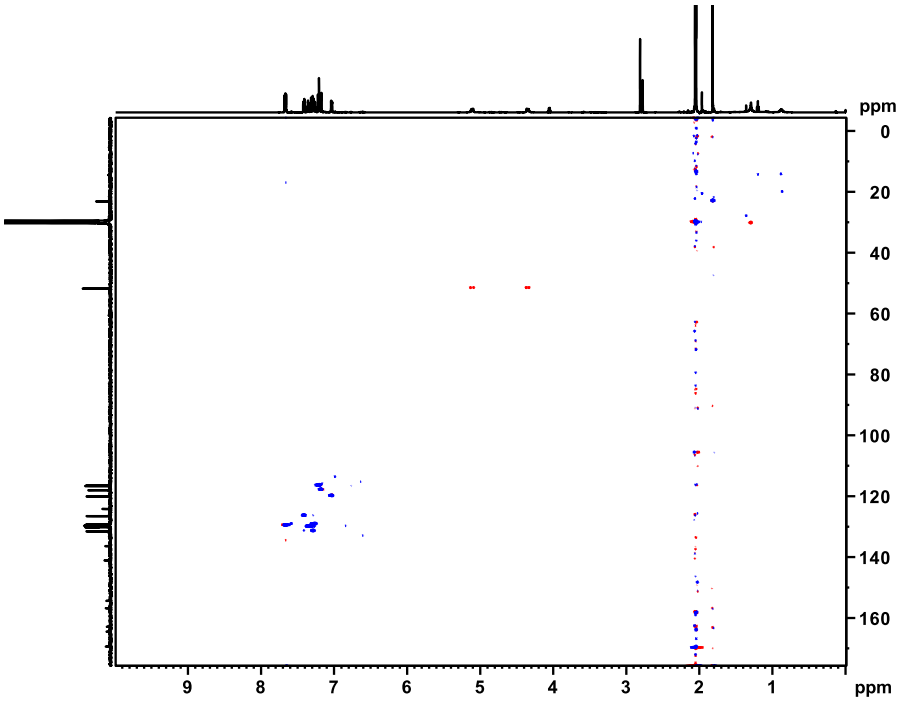

Figure SII.99: 600 MHz ^{1}H-^{13}C HSQC spectrum of (*Z*)-1-(3-(4-fluorophenyl)dibenzo[c,g][1,2,5]triazocin-11(12*H*)-yl)ethan-1-one (**11**).

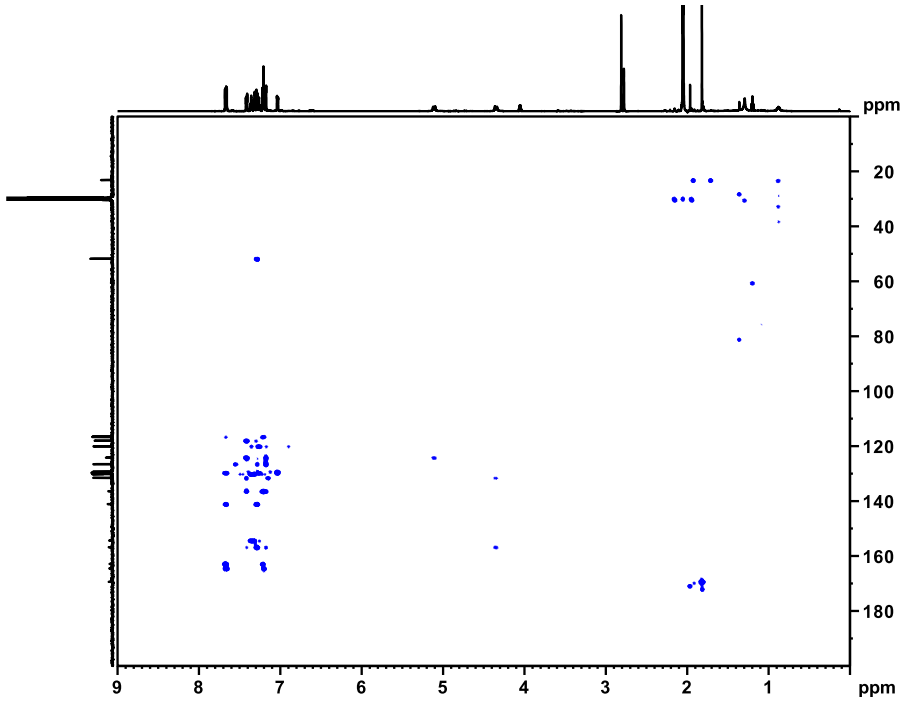

Figure SII.100: 600 MHz HMBC spectrum of (*Z*)-1-(3-(4-fluorophenyl)dibenzo[c,g][1,2,5]triazocin-11(12*H*)-yl)ethan-1-one (**11**).

II.2.6 Synthesis of (*Z*)-2-(11-acetyl-11,12-dihydrodibenzo[c,g][1,2,5]triazocin-3-yl)benzaldehyde (12)

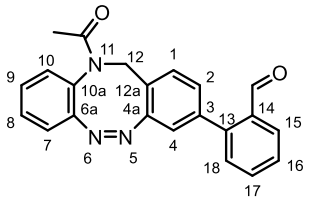

Halogenated *N*-acetyl-diazocine (**2**: 20.0 mg, 60.6 µmol, **3**: 23.0 mg, 60.6 µmol), (2-formylphenyl)boronic acid (18.1 mg, 121 µmol), $Pd(PPh_3)_4$ (2.45 mg, 2.12 µmol) and potassium carbonate (33.4 mg, 212 µmol) were dissolved in 2.4 mL of toluene/MeOH/deionized H_2O (5 : 1 : 2) under a nitrogen atmosphere, heated to 85 °C with an oil bath and stirred for 16 h at given temperature. After cooling to rt. the reaction mixture was extracted with 10 mL of DCM twice, dried over $MgSO_4$ and the solvent was evaporated. Column chromatography on silica (ethyl acetate/cyclohexane 1:1, R_f = 0.26) gave the product as yellow solid (from bromide **2**: 15.1 mg, 42.4 µmol, 70%; from iodide **3**: 16.6 mg, 46.7 µmol, 77%).

melting point: 160 °C

^{1}H-NMR (600 MHz, acetone-d_6, 298 K): δ = 9.71 (s, ^3J = 5.3 Hz, 1 H, C*H*O), 7.93 (dd, ^3J = 7.8 Hz, ^4J = 1.9 Hz, 1 H, *H*-15), 7.71 (td, ^3J = 7.6 Hz, ^4J = 1.4 Hz, 1 H, *H*-17), 7.58 (td, ^3J = 7.7 Hz, ^4J = 2.0 Hz, 1 H, *H*-16), 7.44-7.38 (m, 2 H, *H*-8, *H*-18), 7.37-7.33 (m, 2 H, *H*-1, *H*-10), 7.29 (td, ^3J = 7.3 Hz, ^4J = 1.5 Hz, 1 H, *H*-9), 7.22 (dd, ^3J = 7.8 Hz, ^4J = 1.9 Hz, 1 H, *H*-2), 7.05 (dd, ^3J = 7.8 Hz, ^3J = 1.5 Hz, 1 H, *H*-7), 6.99 (d, ^4J = 1.7 Hz, 1 H, *H*-4), 5.14 (d, ^2J = 14.6 Hz, 1 H, *H*-12), 4.41 (d, ^2J = 14.7 Hz, 1 H, *H*-12'), 1.83 (s, 3 H, -CH_3) ppm.

^{13}C{^{1}H}-NMR (150 MHz, acetone-d_6, 298 K): δ = 191.4 (*C*HO), 169.4 (*C*=O), 156.3 (*C*-4a), 154.4 (*C*-6a), 144.7 (*C*-13), 139.29 (*C*-3), 134.62 (*C*-14), 134.57 (*C*-17), 131.6 (*C*-18), 131.1 (*C*-1), 130.26 (*C*-10), 130.10 (*C*-8), 129.85 (*C*-2), 129.66 (*C*-10a), 129.39 (*C*-9), 129.26 (*C*-16), 128.34 (*C*-15), 125.1 (*C*-12a), 121.2 (*C*-4), 119.9 (*C*-7), 51.8 (*C*-12), 23.1 (*C*H_3) ppm.

IR (ATR): $\tilde{\nu}$ = 3751 (w), 3038 (w), 2924 (m), 2855 (w), 2753 (w), 2255 (w), 1688 (s), 1661 (s), 1600 (m), 1511 (w), 1474 (m), 1456 (w), 1430 (w), 1381 (s), 1337 (s), 1295 (w), 1253 (m), 1194 (m), 1163 (w), 1107 (m), 1074 (w), 1042 (w), 1005 (w), 928 (w), 839 (m), 768 (s), 741 (m), 630 (m), 576 (m), 439 (m) cm^{-1}.

HR-MS (ESI, acetone): *m/z* $[M+H]^+$ calculated for $C_{22}H_{18}O_2N_3+H^+$: 356.1394 found: 356.1387 ± 1.76 ppm.

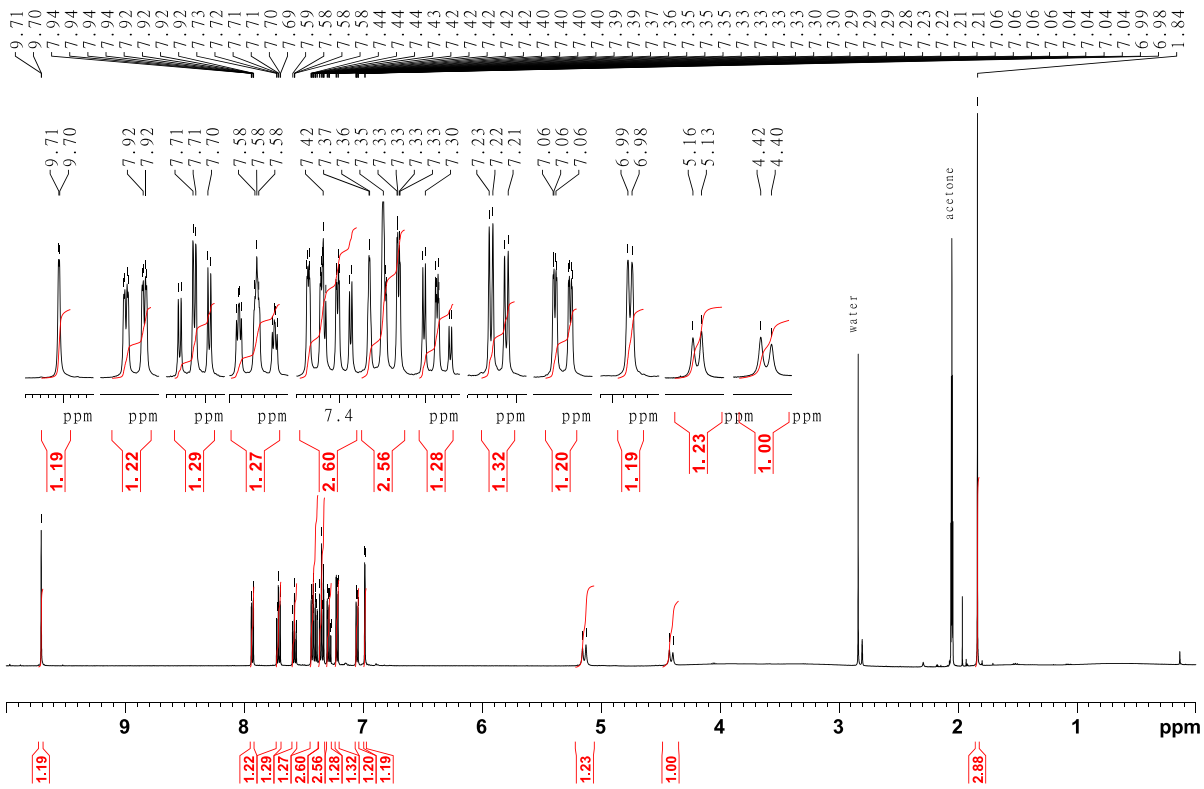

Figure SII.101: 600 MHz ^{1}H-NMR spectrum of (*Z*)-2-(11-acetyl-11,12-dihydrodibenzo[c,g][1,2,5]triazocin-3-yl)benzaldehyde (**12**).

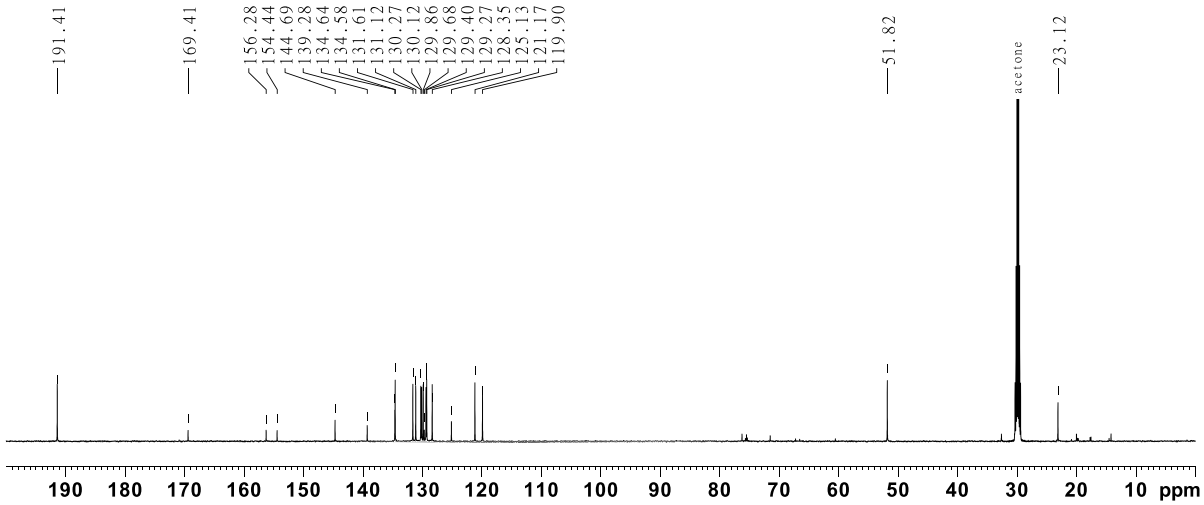

Figure SII.102: 150 MHz ^{13}C{^{1}H}-NMR spectrum of (*Z*)-2-(11-acetyl-11,12-dihydrodibenzo[c,g][1,2,5]triazocin-3-yl)benzaldehyde (**12**).

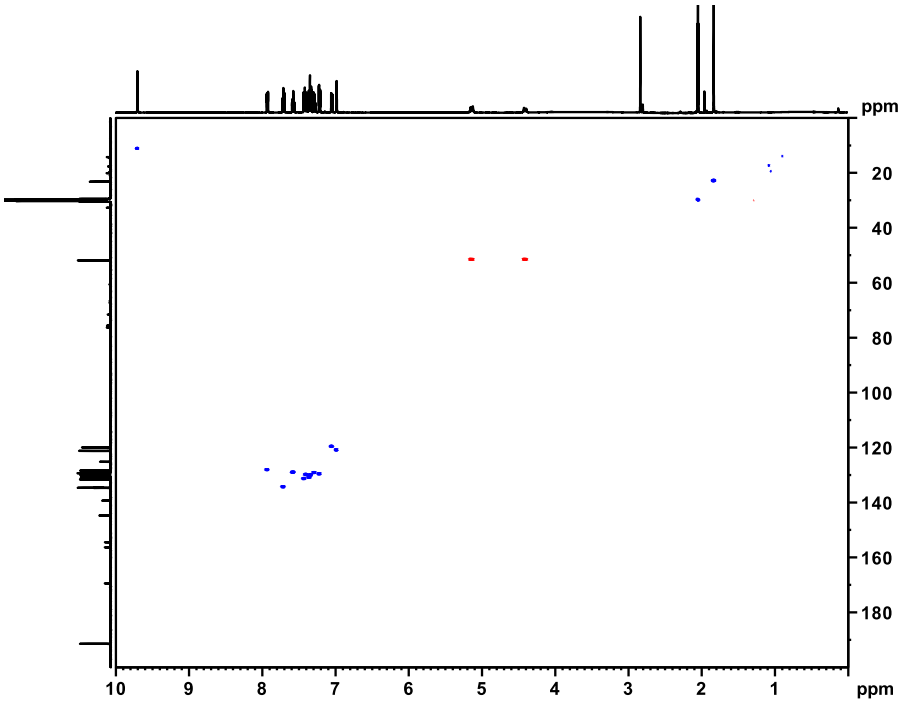

Figure SII.103: 600 MHz ^{1}H-^{13}C HSQC spectrum of (*Z*)-2-(11-acetyl-11,12-dihydrodibenzo[c,g][1,2,5]triazocin-3-yl)benzaldehyde (**12**).

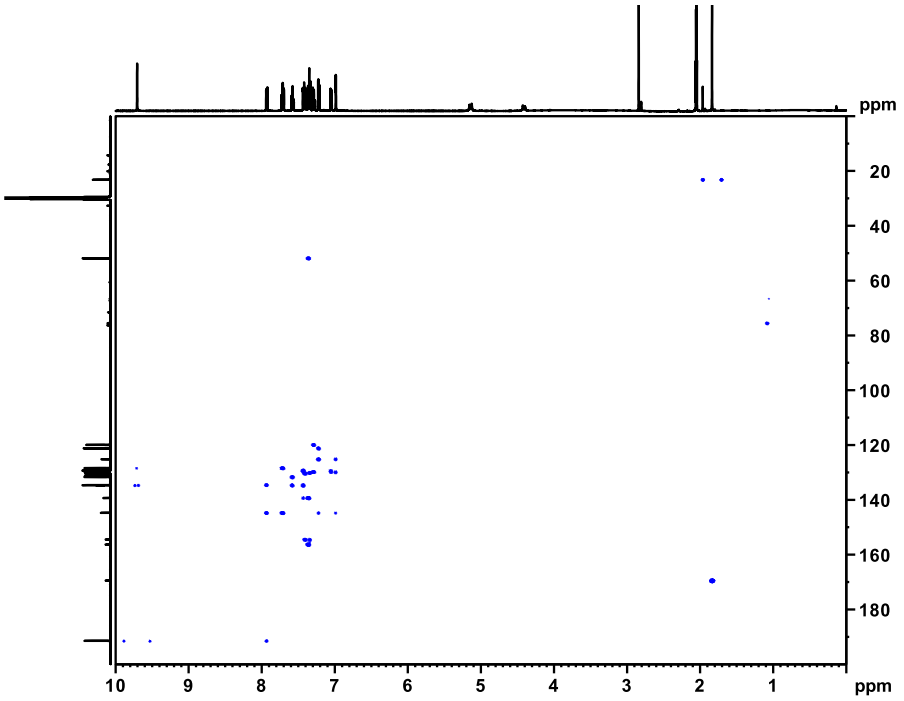

Figure SII.104: 600 MHz HMBC spectrum of (*Z*)-2-(11-acetyl-11,12-dihydrodibenzo[c,g][1,2,5]triazocin-3-yl)benzaldehyde (**12**).

II.2.7 Synthesis of (*Z*)-2-(11-acetyl-11,12-dihydrodibenzo[c,g][1,2,5]triazocin-3-yl)benzoic acid (13)

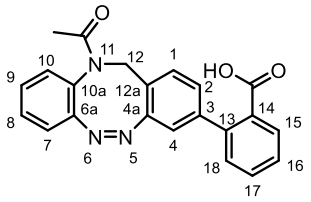

Halogenated *N*-acetyl-diazocine (**2**: 20.0 mg, 60.6 µmol, **3**: 23.0 mg, 60.6 µmol), 2-boronobenzoic acid (20.1 mg, 121 µmol), $Pd(PPh_3)_4$ (2.45 mg, 2.12 µmol) and potassium carbonate (33.4 mg, 212 µmol) were dissolved in 2.4 mL of dry DMF under a nitrogen atmosphere, heated to 100 °C with an oil bath and stirred for 16 h at given temperature. After cooling to rt. the reaction mixture was extracted with 10 mL of DCM twice, dried over $MgSO_4$ and the solvent was evaporated. Column chromatography on silica (ethyl acetate/cyclohexane 1:1 + 1% AcOH, R_f = 0.33) gave the product as yellow solid (from bromide **2**: 17.1 mg, 46.1 µmol, 76%; from iodide **3**: 17.6 mg, 47.3 µmol, 79%).

melting point: 190 °C

^{1}H-NMR (600 MHz, acetone-d_6, 298 K): δ = 7.84 (dd, ^3J = 7.7 Hz, ^4J = 1.0 Hz, 1 H, *H*-15/17), 7.56 (td, ^3J = 7.6 Hz, ^4J = 1.4 Hz, 1 H, *H*-15/17), 7.47 (td, ^3J = 7.6 Hz, ^4J = 1.2 Hz, 1 H, *H*-16), 7.36 (td, ^3J = 7.7 Hz, ^4J = 1.3 Hz, 1 H, *H*-8), 7.31 (dd, ^3J = 7.9 Hz, ^4J = 1.1 Hz, 1 H, *H*-10), 7.29-7.24 (m, 2 H, *H*-9, *H*-18), 7.21 (d, ^3J = 7.9 Hz, 1 H, *H*-1), 7.12 (dd, ^3J = 7.8 Hz, ^4J = 1.2 Hz, 1 H, *H*-2), 7.02 (dd, ^3J = 7.8 Hz, ^3J = 1.2 Hz, 1 H, *H*-7), 6.89 (d, ^4J = 1.6 Hz, 1 H, *H*-4), 5.11 (d, ^2J = 14.5 Hz, 1 H, *H*-12), 4.33 (d, ^2J = 14.5 Hz, 1 H, *H*-12'), 1.82 (s, 3 H, -CH_3) ppm.

^{13}C{^{1}H}-NMR (150 MHz, acetone-d_6, 298 K): δ = 169.4 (*C*=O, COOH), 155.9 (*C*-4a), 154.4 (*C*-6a), 142.8 (*C*-3), 141.3 (*C*-13), 132.6 (*C*-14), 132.0 (*C*-15/17), 131.5 (*C*-18), 130.76 (*C*-15/17), 130.55 (*C*-1), 130.10 (*C*-10), 130.02 (*C*-8), 129.6 (*C*-10a), 129.2 (*C*-9), 128.6 (*C*-16), 128.5 (*C*-2), 123.9 (*C*-12a), 120.08 (*C*-7), 120.01 (*C*-4), 51.9 (*C*-12), 23.1 (*C*H_3) ppm.

IR (ATR): $\tilde{\nu}$ = 2921 (s), 2852 (m), 2022 (w), 1713 (m), 1613 (s), 1591 (w), 1516 (w), 1477 (s), 1448 (w), 1377 (s), 1235 (s), 1135 (m), 1078 (m), 1014 (w), 977 (w), 922 (w), 877 (w), 834 (m), 756 (s), 739 (w), 720 (w), 691 (w), 628 (m), 603 (w), 575 (m), 533 (w), 488 (w), 439 (m), 409 (m) cm^{-1}.

HR-MS (ESI, DCM): *m/z* [M+H]$^+$ calculated for $C_{22}H_{17}O_3N_3$+H$^+$: 372.1343 found: 372.1337 ± 1.64 ppm.

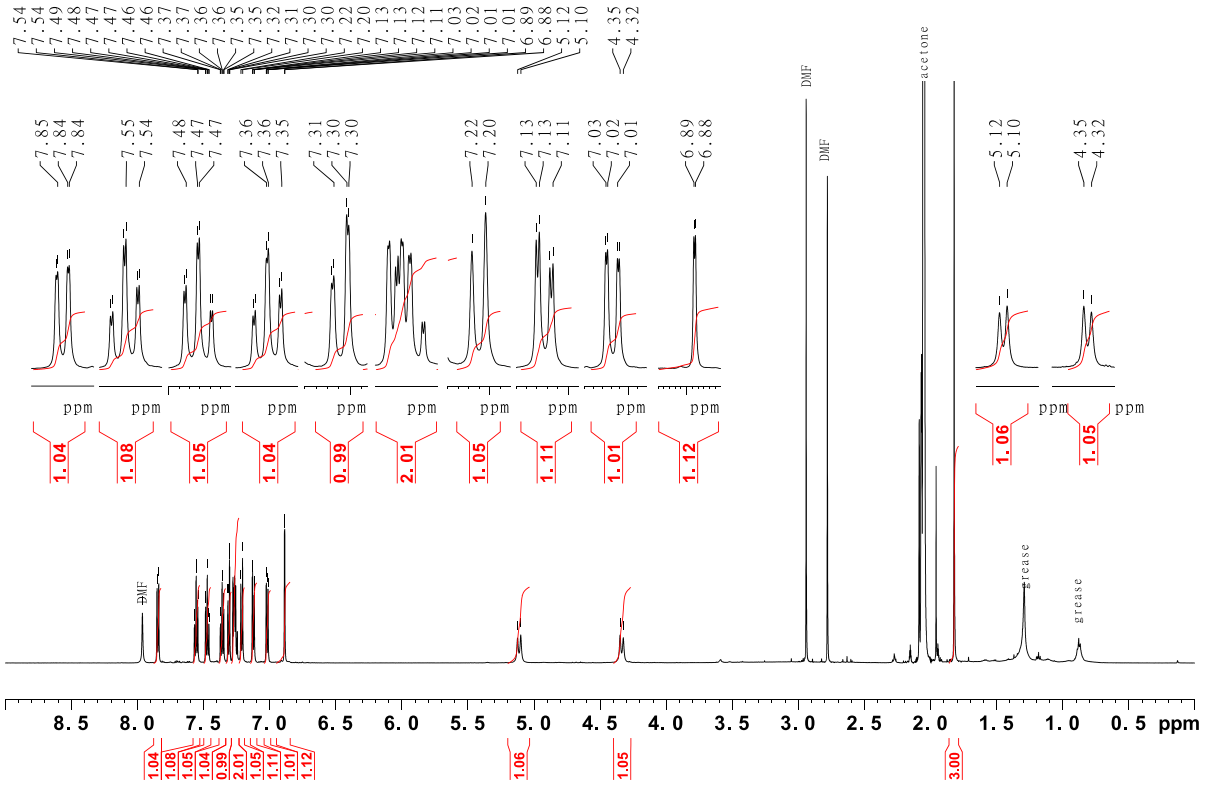

Figure SII.105: 600 MHz ^{1}H-NMR spectrum of (*Z*)-2-(11-acetyl-11,12-dihydrodibenzo[c,g][1,2,5]triazocin-3-yl)benzoic acid (**13**).

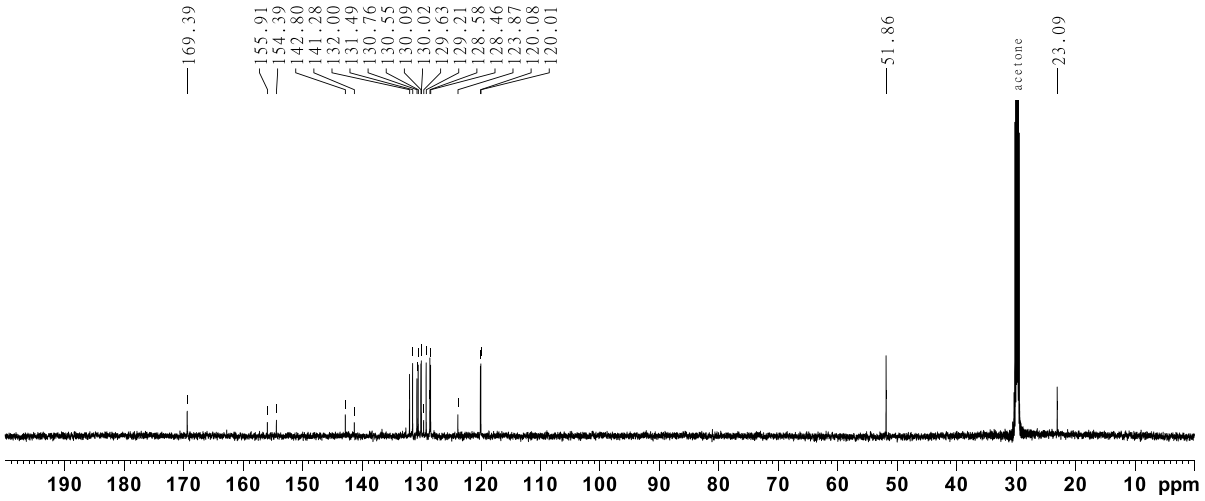

Figure SII.106: 150 MHz ^{13}C{^{1}H}-NMR spectrum of (*Z*)-2-(11-acetyl-11,12-dihydrodibenzo[c,g][1,2,5]triazocin-3-yl)benzoic acid (**13**).

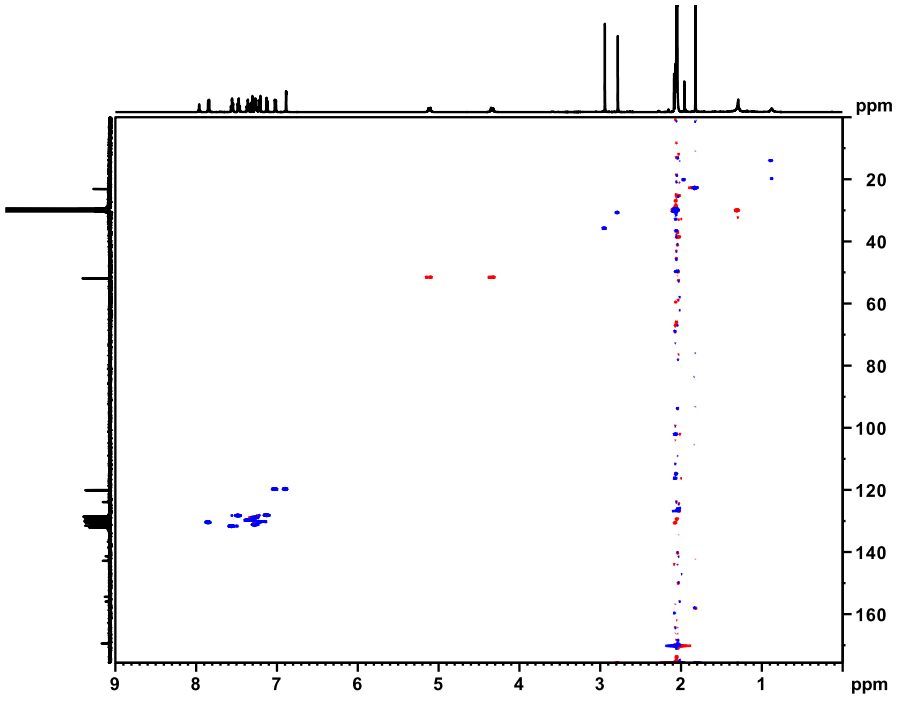

Figure SII.107: 600 MHz ^{1}H-^{13}C HSQC spectrum of (*Z*)-2-(11-acetyl-11,12-dihydrodibenzo[c,g][1,2,5]triazocin-3-yl)benzoic acid (**13**).

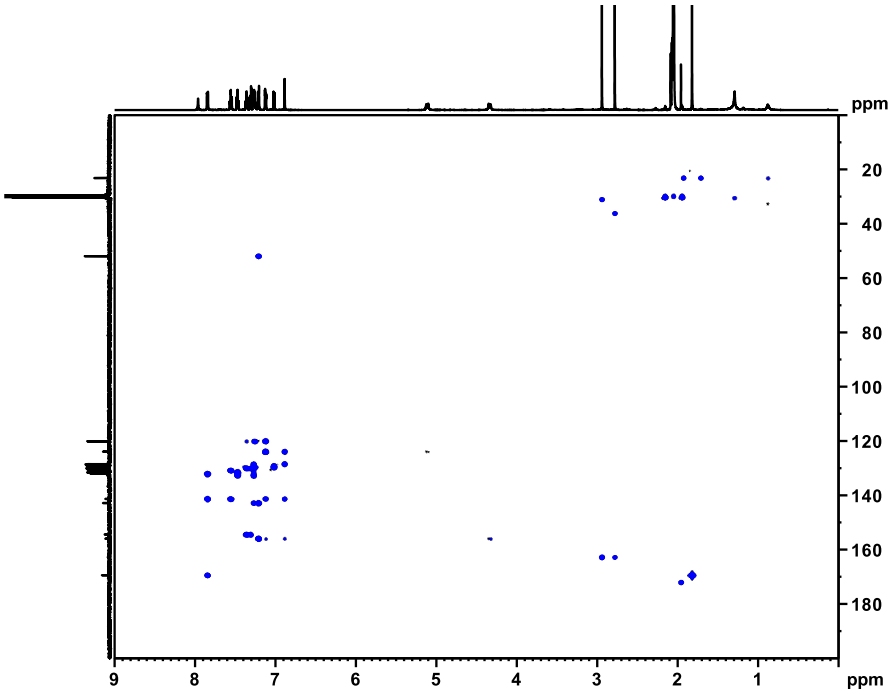

Figure SII.108: 600 MHz HMBC spectrum of (*Z*)-2-(11-acetyl-11,12-dihydrodibenzo[c,g][1,2,5]triazocin-3-yl)benzoic acid (**13**).

II.2.8 Synthesis of (*Z*)-1-(3-(pyridine-4-yl)dibenzo[c,g][1,2,5]triazocin-11(12*H*)-ethan-1-one (14)

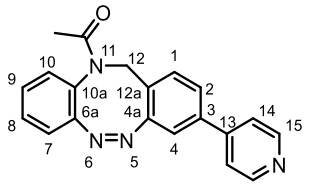

Halogenated *N*-acetyl-diazocine (**2**: 20.0 mg, 60.6 µmol, **3**: 23.0 mg, 60.6 µmol), pyridine-4-boronic acid (14.8 mg, 121 µmol), $Pd(PPh_3)_4$ (2.45 mg, 2.12 µmol) and potassium carbonate (33.4 mg, 212 µmol) were dissolved in 2.4 mL of toluene/MeOH/deionized H_2O (5 : 1 : 2) under a nitrogen atmosphere, heated to 85 °C with an oil bath and stirred for 16 h at given temperature. After cooling to rt. the reaction mixture was extracted with 10 mL of DCM twice, dried over $MgSO_4$ and the solvent was evaporated. Column chromatography on silica (ethyl acetate/cyclohexane 1:1, R_f = 0.07) gave the product as yellow solid (from bromide **2**: 1.4 mg, 4.26 µmol, 7%; from iodide **3**: 3.8 mg, 11.6 µmol, 19%).

melting point: 223 °C

^{1}H-NMR (600 MHz, acetone-d_6, 298 K): δ = 8.62 (dd, ^3J = 6.1 Hz, ^4J = 1.6 Hz, 2 H, *H*-15), 7.61 (dd, ^3J = 6.1 Hz, ^4J = 1.6 Hz, 2 H, *H*-14), 7.56 (dd, ^3J = 8.0 Hz, ^4J = 1.9 Hz, 1 H, *H*-2), 7.38-7.32 (4 H, *H*-1, *H*-4, *H*-8, *H*-9), 7.27 (dd, ^3J = 7.8 Hz, ^4J = 1.4 Hz, 1 H, *H*-7), 7.05 (dd, ^3J = 7.8 Hz, ^4J = 1.2 Hz, 1 H, *H*-10), 5.15 (d, ^2J = 14.6 Hz, 1 H, *H*-12), 4.38 (d, ^2J = 14.4 Hz, 1 H, *H*-12'), 1.81 (s, 3 H, -CH_3) ppm.

^{13}C{^{1}H}-NMR (150 MHz, acetone-d_6, 298 K): δ = 169.4 (*C*=O), 156.8 (*C*-4a), 154.3 (*C*-6a), 151.4 (*C*-15), 146.7 (*C*-13), 139.2 (*C*-3), 131.8 (*C*-1), 130.21 (*C*-8/9), 130.16 (*C*-8/9), 129.57 (*C*-10a), 129.41 (*C*-7), 126.7 (*C*-2), 126.1 (*C*-12a), 122.0 (*C*-14), 120.1 (*C*-10), 118.3 (*C*-4), 51.8 (*C*-12), 23.0 (*C*H_3) ppm.

IR (ATR): $\tilde{\nu}$ = 2922 (m), 2851 (w), 1726 (m), 1655 (s), 1599 (m), 1543 (w), 1513 (w), 1478 (m), 1451 (w), 1420 (w), 1379 (s), 1336 (s), 1291 (w), 1246 (w), 1074 (m), 1045 (w), 995 (w), 964 (w), 922 (w), 876 (m), 846 (w), 817 (s), 767 (m), 738 (m), 711 (m), 624 (s), 602 (w), 573 (m), 547 (m), 512 (m) cm^{-1}.

HR-MS (ESI, DCM): *m/z* $[M+H]^+$ calculated for $C_{20}H_{16}ON_4+H^+$: 329.1397; found: 329.1393 ± 1.07 ppm.

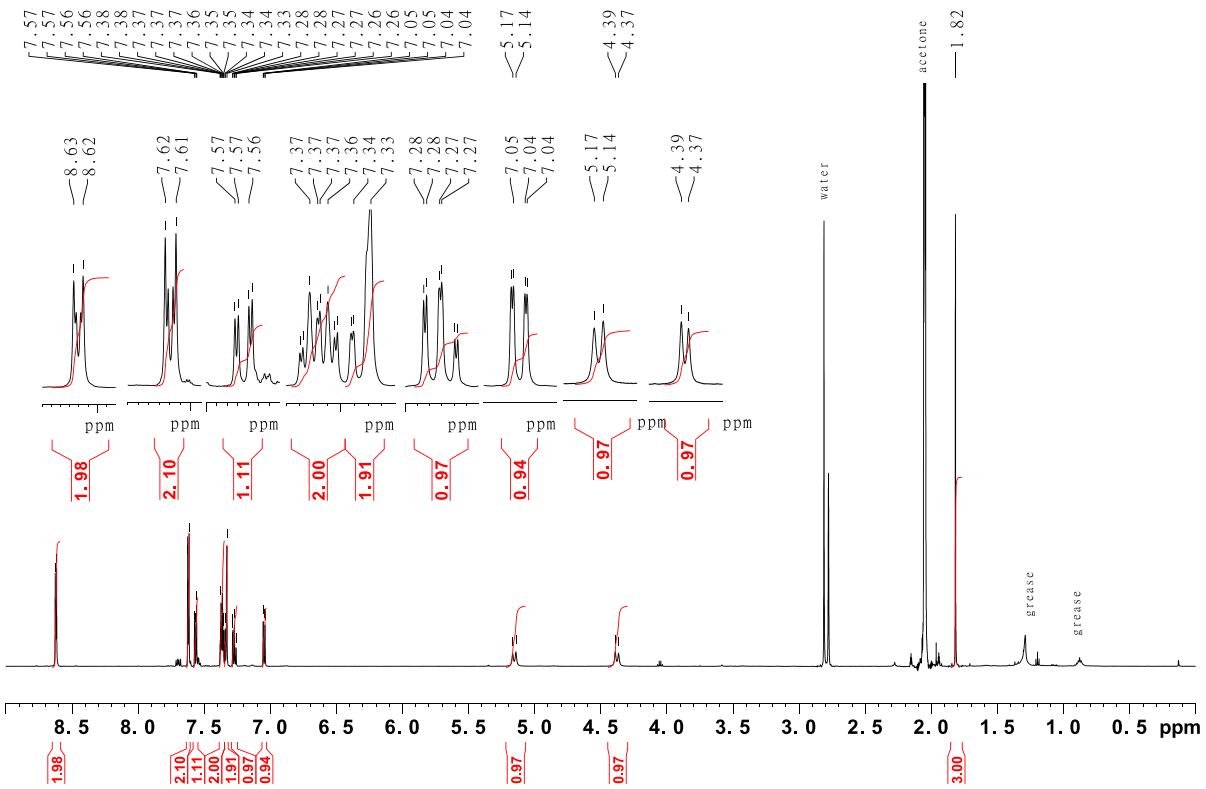

Figure SII.109: 600 MHz ^{1}H-NMR spectrum of (*Z*)-1-(3-(pyridine-4-yl)dibenzo[c,g][1,2,5]triazocin-11(12*H*)-ethan-1-one (**14**).

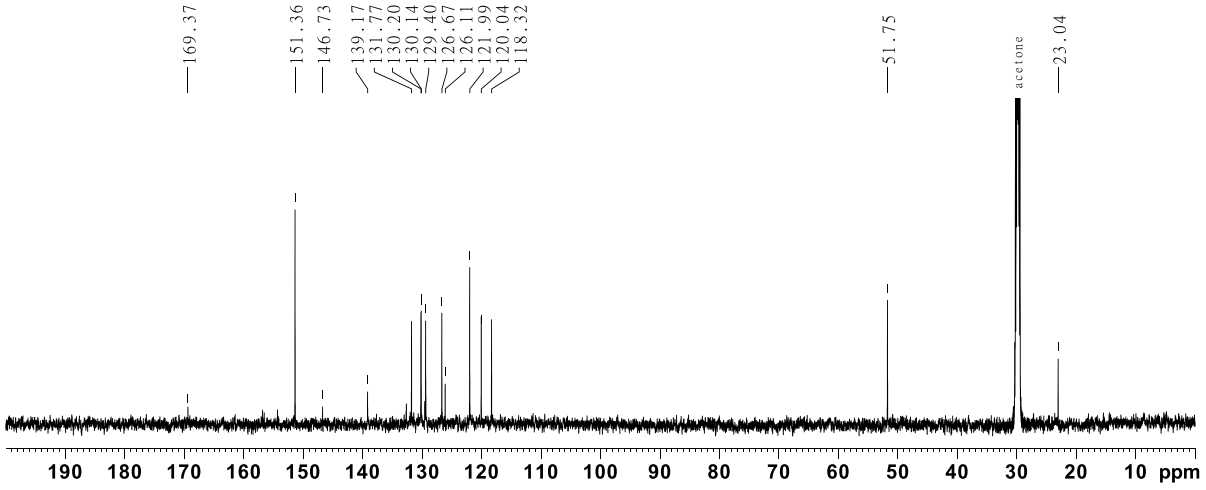

Figure SII.110: 150 MHz ^{13}C{^{1}H}-NMR spectrum of (*Z*)-1-(3-(pyridine-4-yl)dibenzo[c,g][1,2,5]triazocin-11(12*H*)-ethan-1-one (**14**).

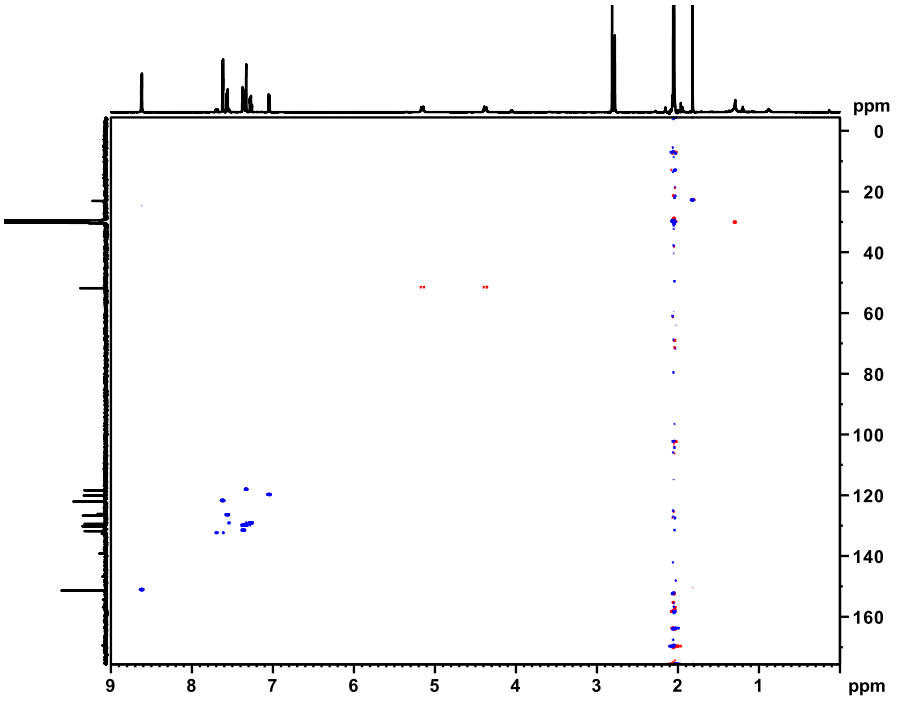

Figure SII.111: 600 MHz ^{1}H-^{13}C HSQC spectrum of (*Z*)-1-(3-(pyridine-4-yl)dibenzo[c,g][1,2,5]triazocin-11(12*H*)-ethan-1-one (**14**).

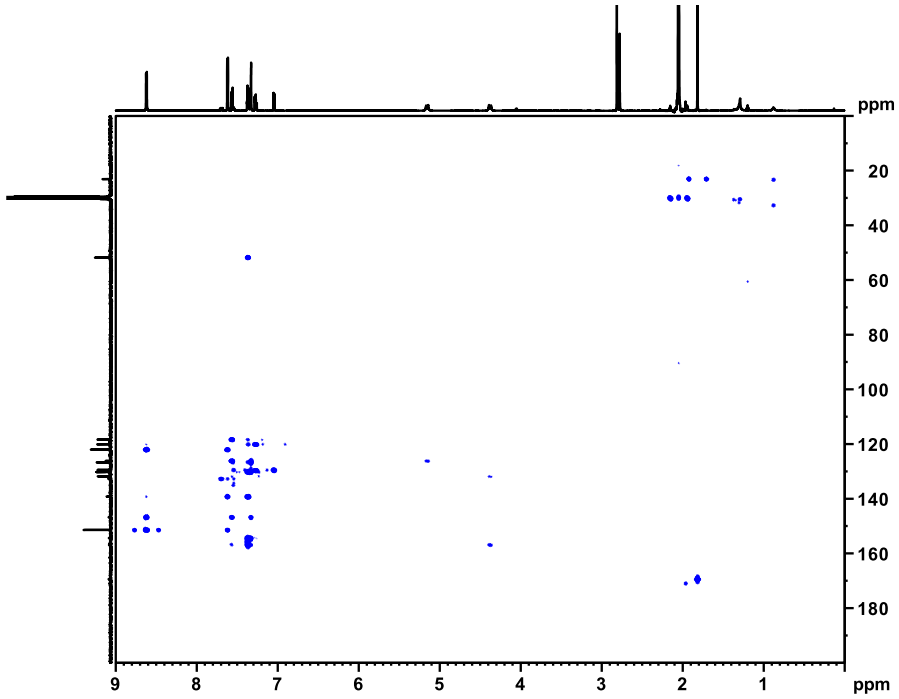

Figure SII.112: 600 MHz HMBC spectrum of (*Z*)-1-(3-(pyridine-4-yl)dibenzo[c,g][1,2,5]triazocin-11(12*H*)-ethan-1-one (**14**).

II.2.9 Synthesis of (*Z*)-1-(3-benzyldibenzo[c,g][1,2,5]triazocin-11(12*H*)-ethan-1-one (17)

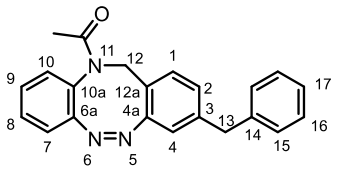

Halogenated *N*-acetyl-diazocine (**2**, 20.0 mg, 60.6 µmol, **3**: 23.0 mg, 60.6 µmol) 2-benzyl-4,4,5,5-tetramethyl-1,3,2-dioxoborolan (26.4 mg, 121 µmol), $Pd(PPh_3)_4$ (2.45 mg, 2.12 µmol) and potassium carbonate (33.4 mg, 212 µmol) were dissolved in 2.4 mL of toluene/MeOH/deionized H_2O (5 : 1 : 2) under a nitrogen atmosphere, heated to 85 °C with an oil bath and stirred for 16 h at given temperature. After cooling to rt. the reaction mixture was extracted with 10 mL of DCM twice, dried over $MgSO_4$ and the solvent was evaporated. Column chromatography on silica (ethyl acetate/cyclohexane 1:1, R_f = 0.33) gave the product as yellow solid (from bromide **2**: 9.4 mg, 27.5 µmol, 45%; from iodide **3**: no product could be obtained).

melting point: 147 °C

^{1}H-NMR (600 MHz, $CDCl_3$, 298 K): δ = 7.29-7.23 (m, 3 H, *H*-10, *H*-16), 7.19 (t, ^3J = 7.1 Hz, 1 H, *H*-17), 7.15 (td, ^3J = 7.7 Hz, ^4J = 1.5 Hz, 1 H, *H*-8), 7.04-7.00 (m, 3 H, *H*-9, *H*-15), 6.95 (d, ^3J = 8.1 Hz, 1 H, *H*-1), 6.88 (dd, ^3J = 7.9 Hz, ^4J = 1.4 Hz, 1 H, *H*-7), 6.86 (dd, ^3J = 8.0 Hz, ^4J = 1.7 Hz, 1 H, *H*-2), 6.68 (d, ^4J = 1.3 Hz, 1 H, *H*-4), 5.02 (d, ^2J = 14.6 Hz, 1 H, *H*-12), 4.31 (d, ^2J = 14.4 Hz, 1 H, *H*-12'), 3.88 (s, 2 H, *H*-13), 1.91 (s, 3 H, -CH_3) ppm.

^{13}C{^{1}H}-NMR (150 MHz, $CDCl_3$, 298 K): δ = 170.2 (*C*=O), 155.6 (*C*-4a), 153.2 (*C*-6a), 142.3 (*C*-3), 140.0 (*C*-14), 130.2 (*C*-1), 129.05 (*C*-10/16), 128.96 (*C*-15), 128.91 (*C*-9), 128.69 (*C*-10/16), 128.3 (*C*-2), 128.14 (*C*-8), 126.5 (*C*-17), 121.6 (*C*-12a), 119.57 (*C*-4), 119.46 (*C*-7), 51.8 (*C*-12), 41.4 (*C*-13) 23.4 (*C*H_3) ppm.

IR (ATR): $\tilde{\nu}$ = 2924 (m), 2853 (w), 2256 (m), 1654 (s), 1611 (w), 1593 (w), 1513 (w), 1482 (m), 1453 (m), 1437 (w), 1386 (s), 1337 (s), 1286 (w), 1245 (w), 1200 (m), 1147 (w), 1074 (m), 1040 (m), 974 (w), 914 (m), 902 (w), 772 (s), 739 (m), 723 (s), 703 (m), 644 (w), 623 (w), 607 (s), 591 (s), 462 (m) cm^{-1}.

HR-MS (ESI, EtOAc): *m/z* $[M+Na]^+$ calculated for $C_{22}H_{19}ON_3$+Na^+: 364.1420; found: 364.1418 ± 0.75 ppm.

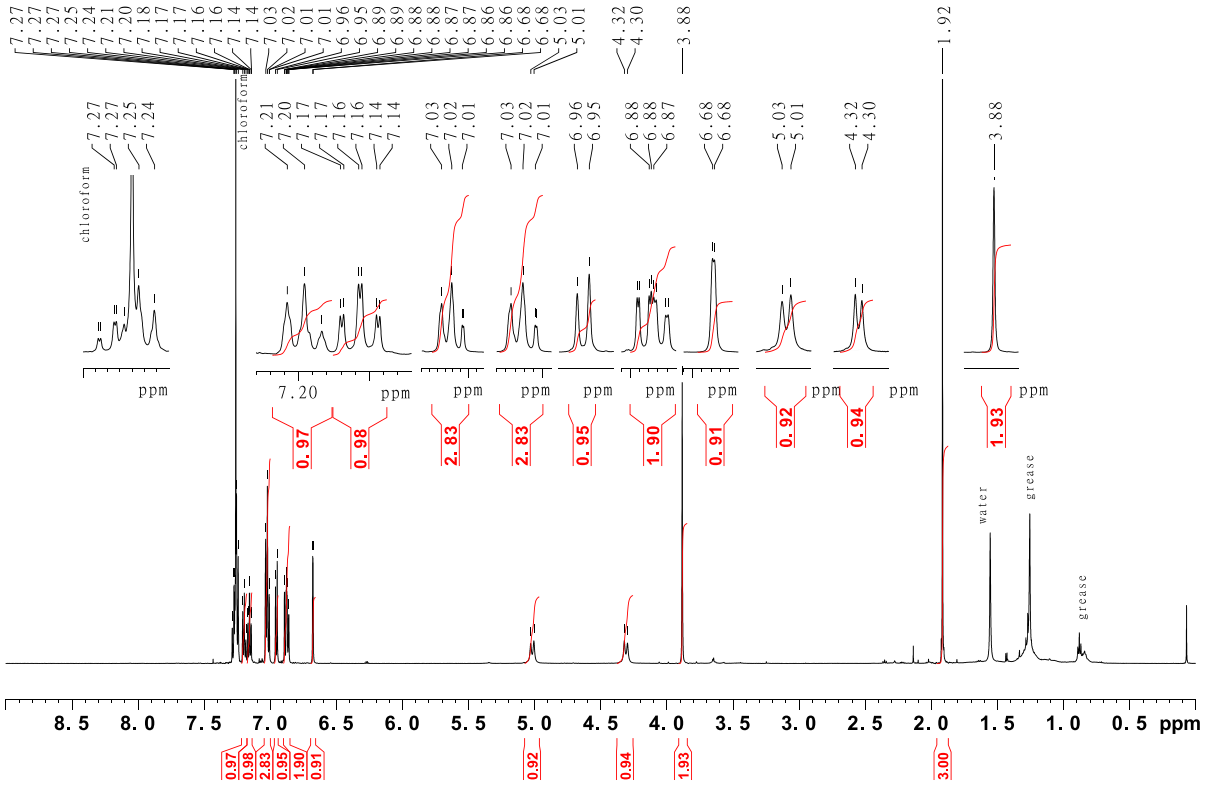

Figure SII.113: 600 MHz ^{1}H-NMR spectrum of (*Z*)-1-(3-benzyldibenzo[c,g][1,2,5]triazocin-11(12*H*)-ethan-1-one (**17**).

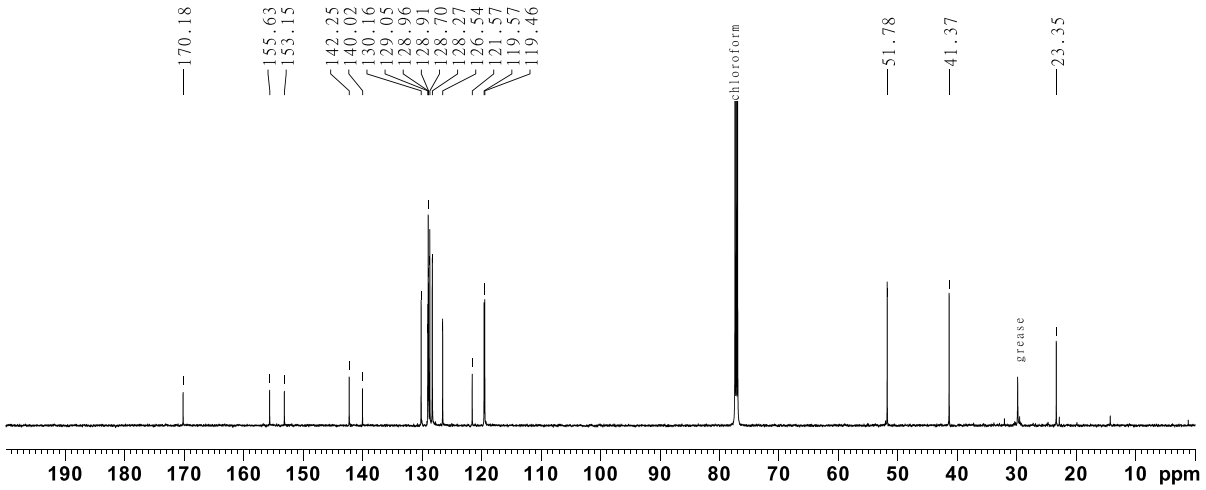

Figure SII.114: 150 MHz ^{13}C{^{1}H}-NMR spectrum of (*Z*)-1-(3-benzyldibenzo[c,g][1,2,5]triazocin-11(12*H*)-ethan-1-one (**17**).

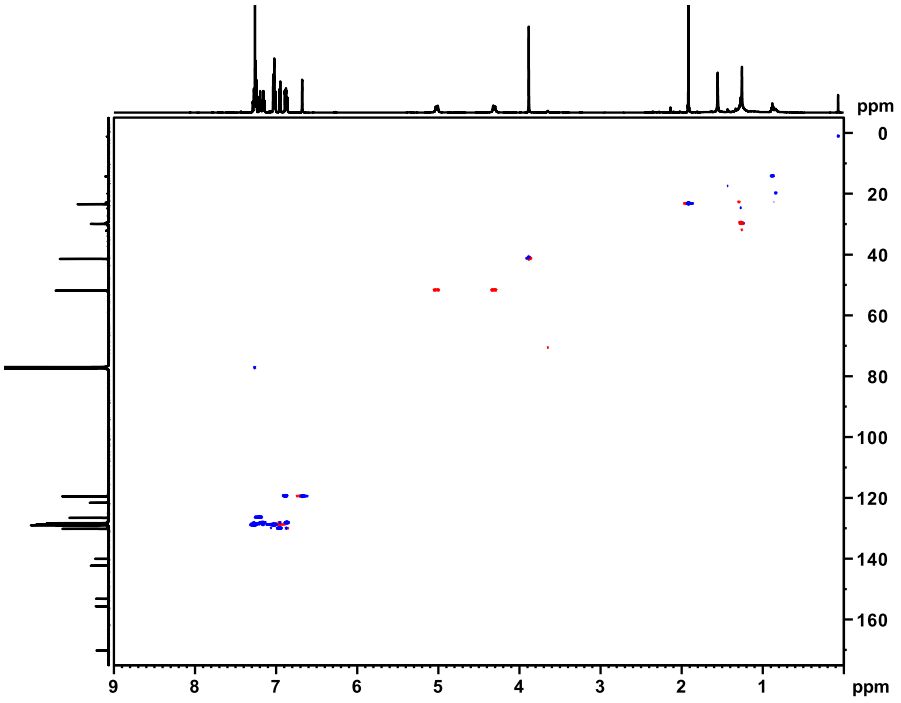

Figure SII.115: 600 MHz ^{1}H-^{13}C HSQC spectrum of (*Z*)-1-(3-benzyldibenzo[c,g][1,2,5]triazocin-11(12*H*)-ethan-1-one (**17**).

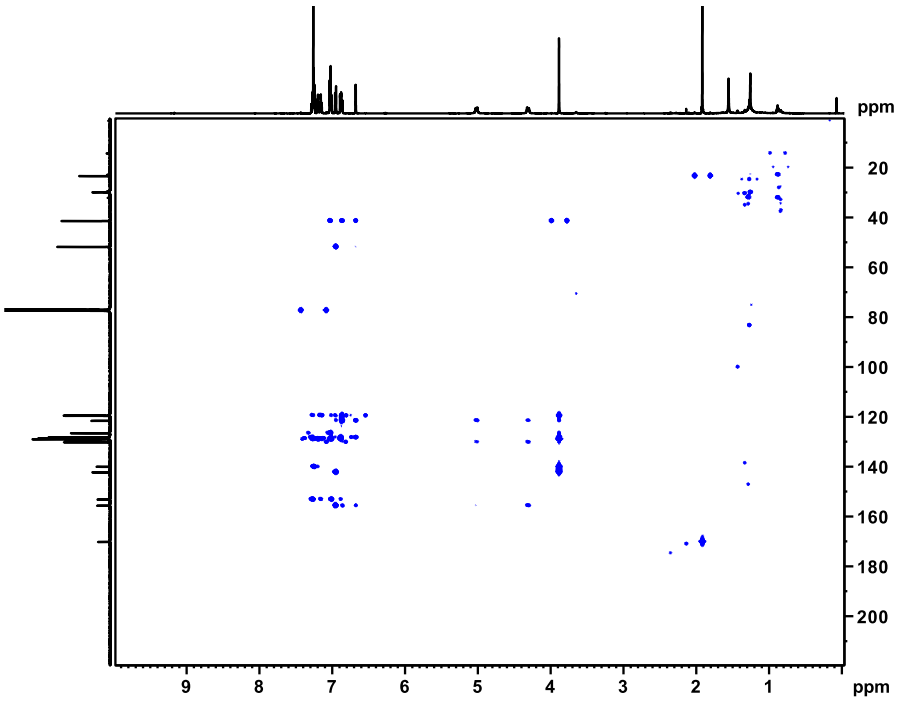

Figure SII.116: 600 MHz HMBC spectrum of (*Z*)-1-(3-benzyldibenzo[c,g][1,2,5]triazocin-11(12*H*)-ethan-1-one (**17**).

II.2.11 Synthesis of *tert*-butyl-(*Z*)-(11-acetyl-11,12-dihydrodiebenzo[c,g][1,2,5]triazocin-3-yl)carbamate (19)

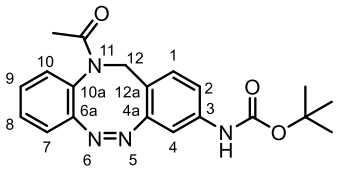

Halogenated *N*-acetyl-diazocine (**2**, 20.0 mg, 60.6 µmol, **3**: 23.0 mg, 60.6 µmol), *tert*-butyl carbamate (10.6 mg, 90.9 µmol), Xantphos Pd G3 (2.90 mg, 3.03 µmol) and caesium carbonate (19.7 mg, 60.6 µmol) were dissolved in 2.4 mL of dry 1,4-dioxane under a nitrogen atmosphere, heated to 100 °C with an oil bath and stirred for 16 h at given temperature. After cooling to rt. deionized H_2O and 5 mL ethyl acetate were added and the reaction mixture was extracted with 10 mL of ethyl acetate twice, dried over $MgSO_4$ and the solvent was evaporated. Column chromatography on silica (ethyl acetate/cyclohexane 1:1, R_f = 0.30) gave the product as yellow solid (from bromide **2**: no product could be obtained; from iodide **3**: 15.8 mg, 43.1 µmol, 72%).

melting point: 217°C

^{1}H-NMR (600 MHz, acetone-d_6, 298 K): δ = 8.56 (s, 1 H, -N*H*), 7.36 (td, ^3J = 7.6 Hz, ^4J = 1.7 Hz, 1 H, *H*-8), 7.28-7.20 (m, 4 H, *H*-2, *H*-4, *H*-9, *H*-10), 7.08 (d, ^3J = 8.2 Hz, 1 H, *H*-1), 7.00 (dd, ^3J = 7.7 Hz, ^4J = 1.3 Hz, 1 H, *H*-7), 4.93 (d, ^2J = 14.4 Hz, 1 H, *H*-12), 4.25 (d, ^2J = 14.5 Hz, 1 H, *H*-12'), 1.80 (s, 3 H, -CH_3), 1.45 (s, 9 H, -C(CH_3)$_3$) ppm.

^{13}C{^{1}H}-NMR (150 MHz, acetone-d_6, 298 K): δ = 170.9 (-NHC=O), 169.3 (*C*=O), 156.8 (*C*-4a), 154.2 (*C*-6a), 141.1 (*C*-3), 131.3 (*C*-1), 130.1 (*C*-10), 129.9 (*C*-8), 129.1 (*C*-9), 119.9 (*C*-7), 118.3 (*C*-12a), 117.5 (*C*-2/4), 108.9 (*C*-2/4), 80.5 (*C*(CH$_3$)$_3$), 51.7 (*C*-12), 28.4 (C(*C*H$_3$)$_3$) 23.2 (*C*H$_3$) ppm.

IR (ATR): $\tilde{\nu}$ = 3304 (m), 2976 (w), 2923 (m), 2164 (s), 1722 (s), 1638 (s), 1615 (m), 1590 (m), 1528 (s), 1479 (m), 1394 (s), 1367 (w), 1310 (m), 1239 (s), 1159 (s), 1075 (m), 1059 (m), 1034 (w), 974 (w), 953 (w), 917 (w), 881 (m), 856 (w), 829 (m), 796 (m), 763 (m), 694 (w), 618 (m), 570 (m), 449 (m) cm^{-1}.

HR-MS (ESI, DCM): *m/z* [M+H]$^+$ calculated for $C_{20}H_{22}O_3N_4$+H$^+$: 367.1765; found: 367.1761 ± 1.02 ppm.

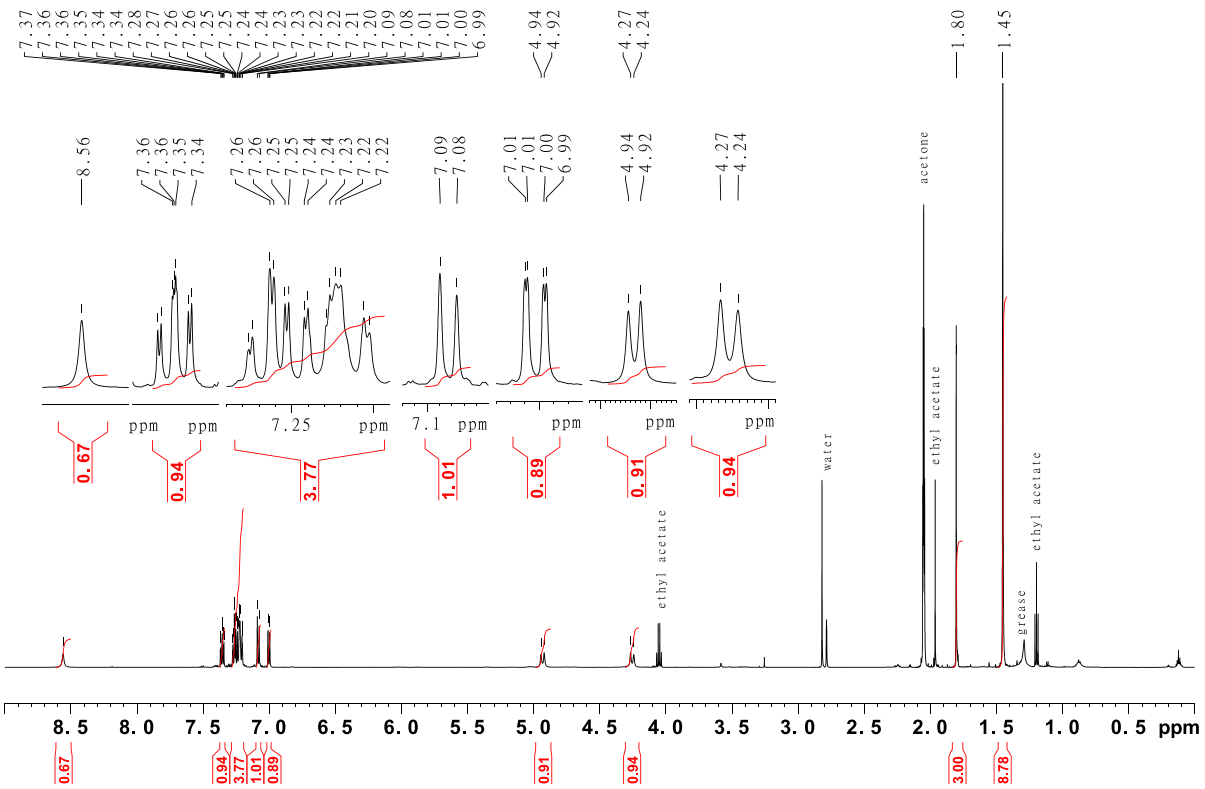

Figure SII.117: 600 MHz ^{1}H-NMR spectrum of *tert*-butyl-(*Z*)-(11-acetyl-11,12-dihydrodiebenzo[c,g][1,2,5]triazocin-3-yl)carbamate (**19**).

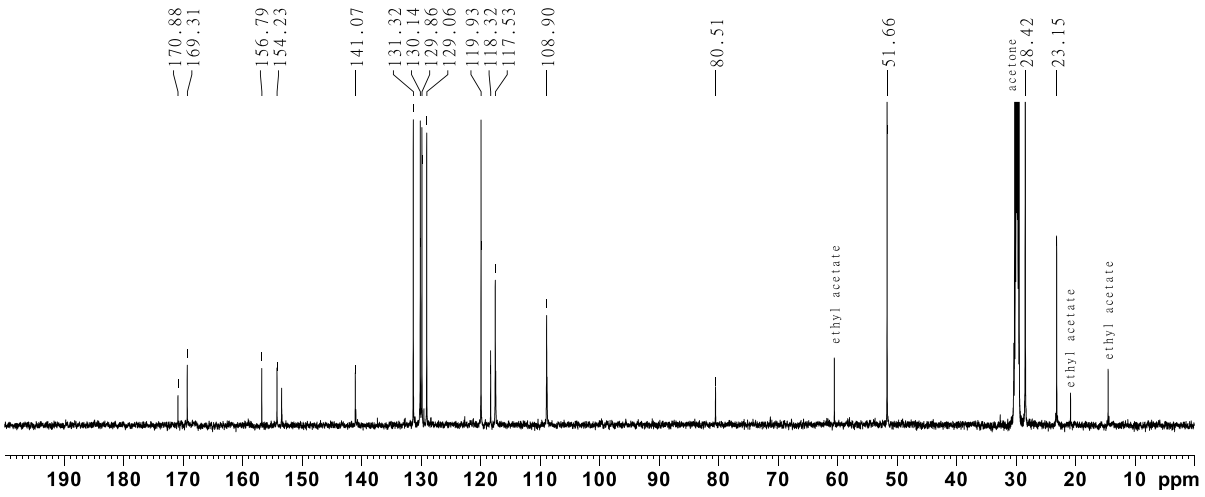

Figure SII.118: 150 MHz ^{13}C{^{1}H}-NMR spectrum of *tert*-butyl-(*Z*)-(11-acetyl-11,12-dihydrodiebenzo[c,g][1,2,5]triazocin-3-yl)carbamate (**19**).

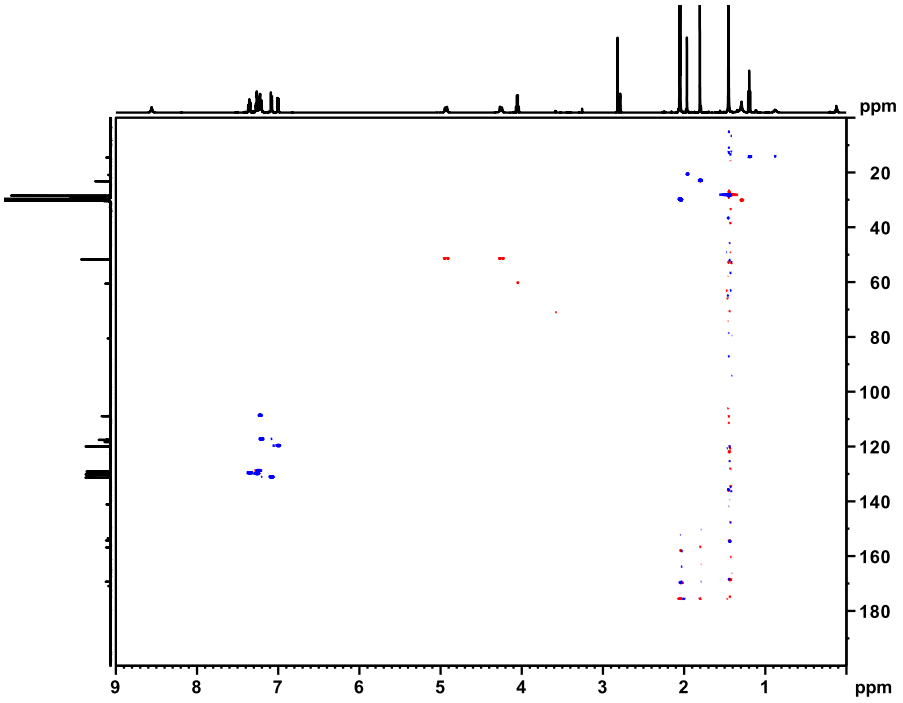

Figure SII.119: 600 MHz ^{1}H-^{13}C HSQC spectrum of *tert*-butyl-(*Z*)-(11-acetyl-11,12-dihydrodiebenzo[c,g][1,2,5]triazocin-3-yl)carbamate (**19**).

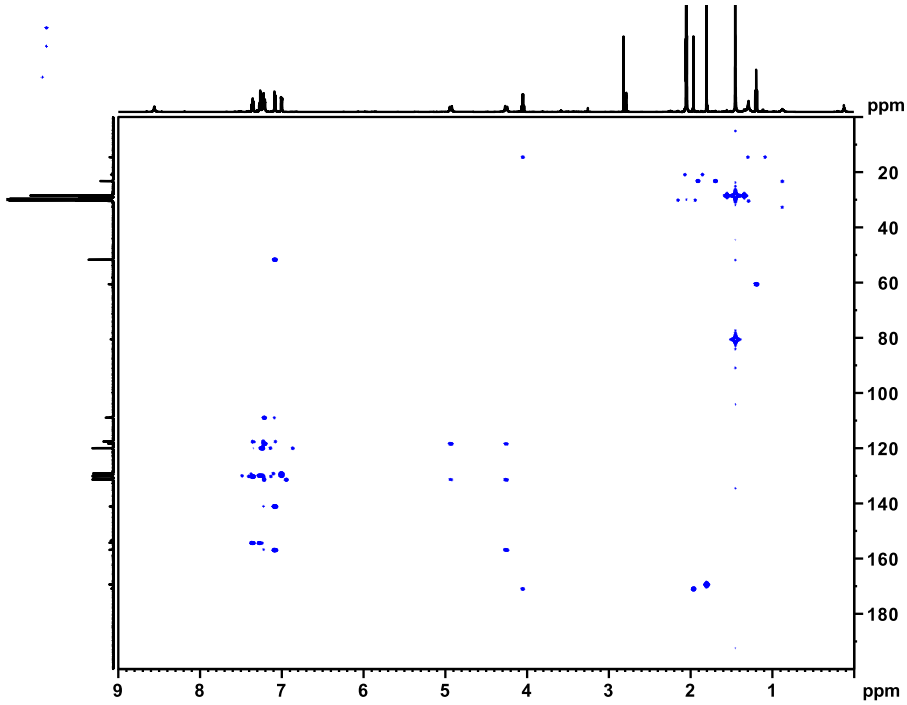

Figure SII.120: 600 MHz HMBC spectrum of *tert*-butyl-(*Z*)-(11-acetyl-11,12-dihydrodiebenzo[c,g][1,2,5]triazocin-3-yl)carbamate (**19**).

II.2.12 Synthesis of (*Z*)-1-(3-(diphenylamino)dibenzo[c,g][1,2,5]triazocin-11(12*H*)-yl)ethan-1-one (20)

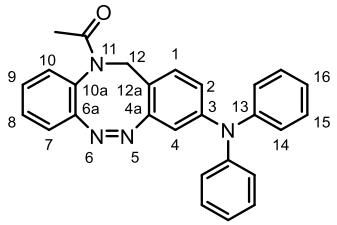

Halogenated *N*-acetyl-diazocine (2, 20.0 mg, 60.6 µmol, 3: 23.0 mg, 60.6 µmol), diphenylamine (15.4 mg, 90.9 µmol), Xantphos Pd G3 (2.90 mg, 3.03 µmol) and caesium carbonate (19.7 mg, 60.6 µmol) were dissolved in 2.4 mL of dry 1,4-dioxane under a nitrogen atmosphere, heated to 100 °C with an oil bath and stirred for 16 h at given temperature. After cooling to rt. deionized H_2O and 5 mL ethyl acetate were added and the reaction mixture was extracted with 10 mL of ethyl acetate twice, dried over $MgSO_4$ and the solvent was evaporated. Column chromatography on silica (ethyl acetate/cyclohexane 1:1, R_f = 0.30) gave the product as yellow solid (from bromide **2**: 6.30 mg, 15.1 µmol, 25%, **3**: 11.8 mg, 28.2 µmol, 47%).

melting point: 160 °C

^{1}H-NMR (500 MHz, acetone-d_6, 298 K): δ = 7.46 (td, ^3J = 7.9 Hz, ^4J = 1.9 Hz, 1 H, *H*-9), 7.32-7.27 (m, 6 H, *H*-7, *H*-8, *H*-14/15), 7.10-7.06 (m, 2 H, *H*-16), 7.04 (d, ^3J = 8.3 Hz, 1 H, *H*-1), 6.98-6.93 (5 H, *H*-10, *H*-14/15), 6.66 (dd, ^3J = 8.3 Hz, ^4J = 2.4 Hz, 1 H, *H*-2), 6.44 (d, ^4J = 2.4 Hz, 1 H, *H*-4), 4.77 (d, ^2J = 14.3 Hz, 1 H, *H*-12), 4.26 (d, ^2J = 14.3 Hz, 1 H, *H*-12'), 1.81 (s, 3 H, -CH_3) ppm.

^{13}C{^{1}H}-NMR (125 MHz, acetone-d_6, 298 K): δ = 169.3 (*C*=O), 157.4 (*C*-4a), 154.5 (*C*-6a), 149.2 (*C*-3), 147.9 (*C*-13), 131.9 (*C*-1), 130.42 (*C*-14/15), 130.34 (*C*-7), 130.04 (*C*-10a), 129.8 (*C*-9), 129.1 (*C*-8), 125.6 (*C*-14/15), 124.7 (*C*-16), 121.5 (*C*-2), 119.8 (*C*-10), 118.2 (*C*-12a), 112.8 (*C*-4), 51.6 (*C*-12) 23.2 (*C*H_3) ppm.

IR (ATR): $\tilde{\nu}$ = 2921 (w), 2228 (w), 2185 (w), 2084 (w), 2021 (w), 1659 (s), 1610 (w), 1592 (s), 1481 (s), 1384 (s), 1333 (s), 1304 (w), 1290 (m), 1265 (s), 1221 (w), 1171 (w), 1095 (w), 1075 (w), 1029 (w), 977 (w), 901 (w), 840 (w), 811 (m), 758 (m), 745 (m), 697 (s), 631 (m), 586 (m), 508 (s), 483 (m) cm^{-1}.

HR-MS (ESI, DCM): *m/z* [M+H]$^+$ calculated for $C_{27}H_{22}ON_4$+H$^+$: 419.1866; found: 419.1863 ± 0.85 ppm.

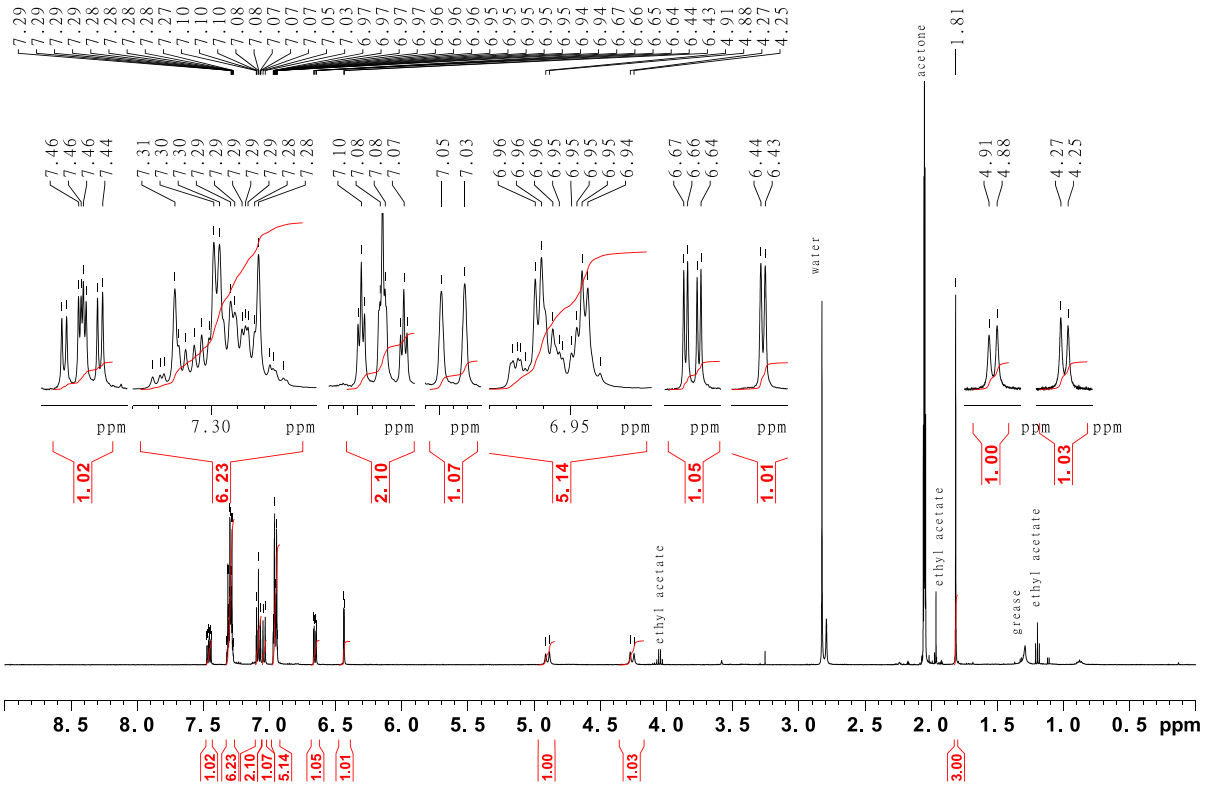

Figure SII.121: 500 MHz ^{1}H-NMR spectrum of (*Z*)-1-(3-(diphenylamino)dibenzo[c,g][1,2,5]triazocin-11(12*H*)-yl)ethan-1-one (**20**).

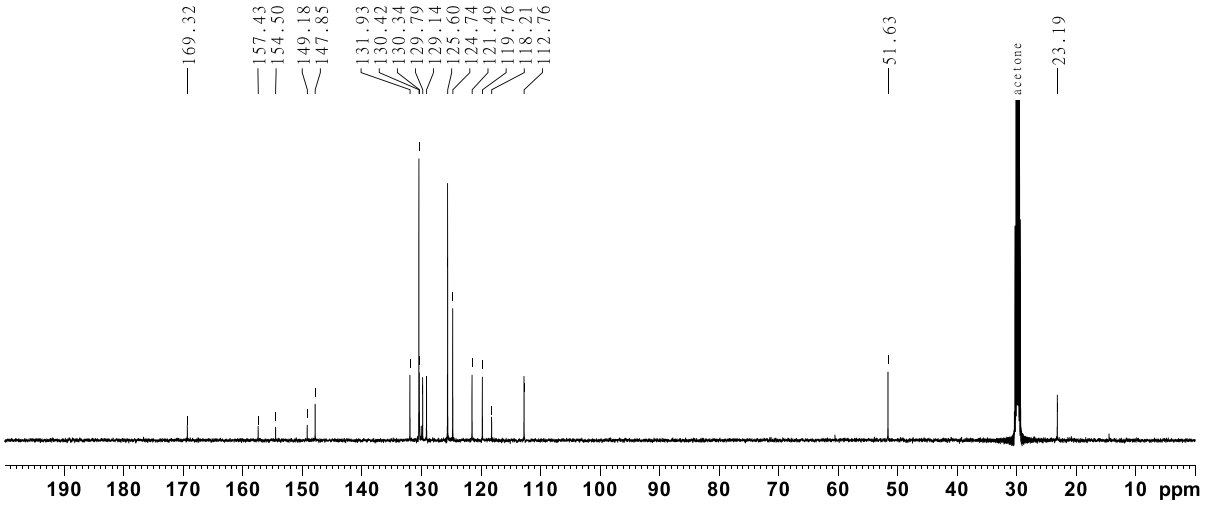

Figure SII.122: 125 MHz ^{13}C{^{1}H}-NMR spectrum of (*Z*)-1-(3-(diphenylamino)dibenzo[c,g][1,2,5]triazocin-11(12*H*)-yl)ethan-1-one (**20**).

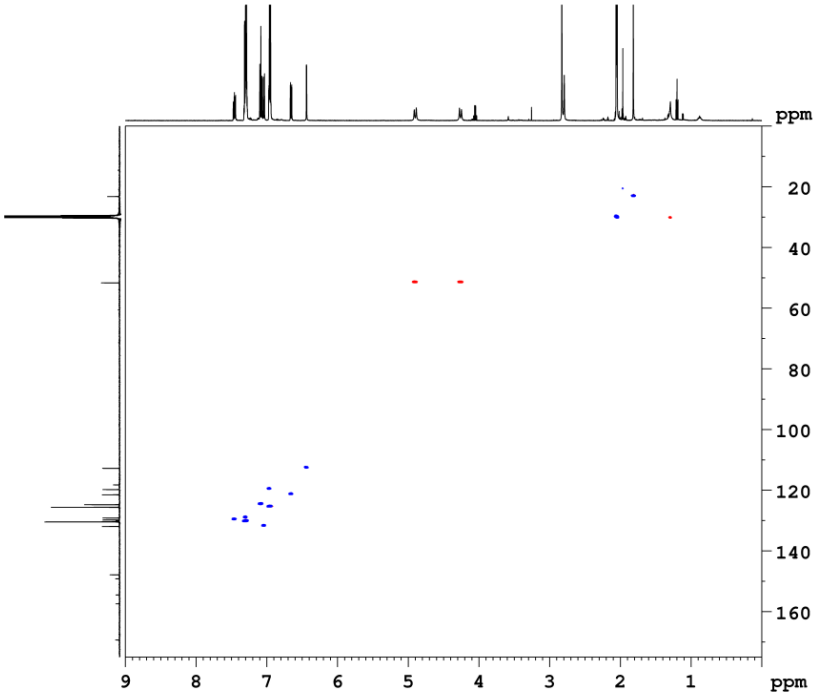

Figure SII.123: 500 MHz ^{1}H-^{13}C HSQC spectrum of (*Z*)-1-(3-(diphenylamino)dibenzo[c,g][1,2,5]triazocin-11(12*H*)-yl)ethan-1-one (**20**).

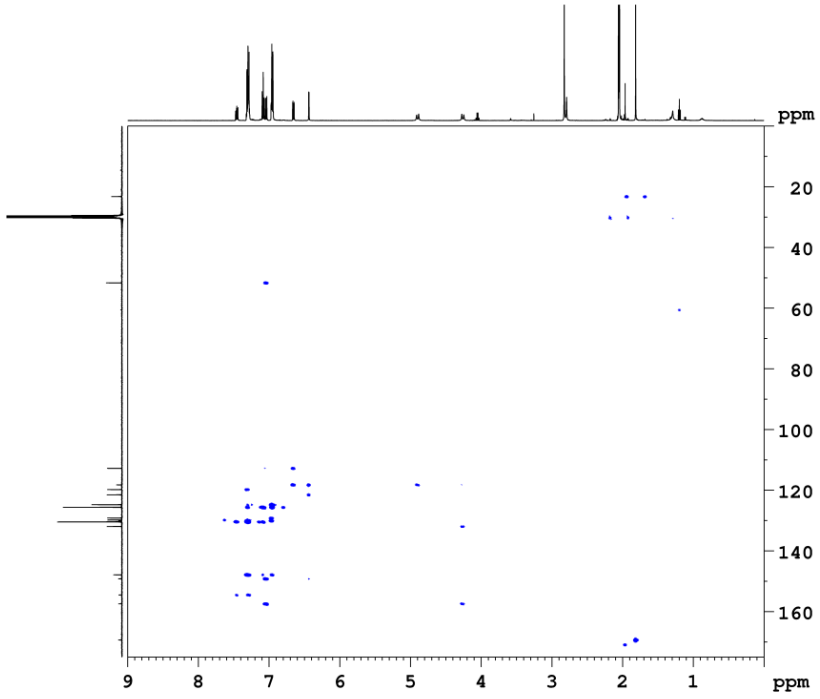

Figure SII.124: 500 MHz HMBC spectrum of (*Z*)-1-(3-(diphenylamino)dibenzo[c,g][1,2,5]triazocin-11(12*H*)-yl)ethan-1-one (**20**).

II.2.13 Synthesis of (*Z*)-1-(3-aminodibenzo[c,g][1,2,5]triazocin-11(12*H*)-yl)ethan-1-one (21)

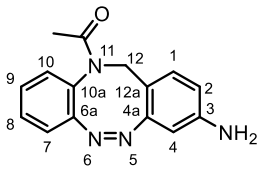

Tert-butyl-(*Z*)-(11-acetyl-11,12-dihydrodiebenzo[c,g][1,2,5]triazocin-3-yl)carbamate (**21**, 17.3 mg, 47.2 µmol) was dissolved in 25 mL dichloromethane and 5 mL of trifluoroacetic acid were added. The reaction mixture was stirred at room temperature for 16 h and then neutralized with saturated aqueous $NaHCO_3$ solution. The organic layer was separated and the aqueous layer was extracted twice with 10 mL dichloromethane, dried over $MgSO_4$ and the solvent was evaporated. Column chromatography on silica (ethyl acetate/cyclohexane 1:1, R_f = 0.15) gave the product as yellow solid (7.50 mg, 28.2 µmol, 60%).

melting point: 178 °C

^{1}H-NMR (600 MHz, $CDCl_3$, 298 K): δ = 7.27-7.24 (m, 1 H, *H*-8), 7.14 (td, ^3J = 7.7 Hz, ^4J = 1.4 Hz, 1 H, *H*-9), 6.99 (dd, ^3J = 7.9 Hz, ^4J = 0.9 Hz, 1 H, *H*-10), 6.87 (dd, ^3J = 7.8 Hz, ^4J = 1.2 Hz, 1 H, *H*-7), 6.80 (d, ^3J = 8.2 Hz, , 1 H, *H*-1), 6.33 (dd, ^3J = 8.1 Hz, ^4J = 2.4 Hz, 1 H, *H*-2), 6.16 (d, ^4J = 2.4 Hz, 1 H, *H*-4), 4.86 (d, ^2J = 14.3 Hz, 1 H, *H*-12), 4.27 (d, ^2J = 14.3 Hz, 1 H, *H*-12'), 3.72 (br. s, 2 H, -NH_2), 1.92 (s, 3 H, -CH_3) ppm.

^{13}C{^{1}H}-NMR (150 MHz, $CDCl_3$, 298 K): δ = 170.0 (*C*=O), 156.6 (*C*-4a), 152.9 (*C*-6a), 146.8 (*C*-3), 131.0 (*C*-1), 129.0 (*C*-10a), 128.82 (*C*-10), 128.67 (*C*-8), 127.9 (*C*-9), 119.3 (*C*-7), 113.9 (*C*-2), 113.2 (*C*-12a), 104.9 (*C*-4), 51.5 (*C*-12) 23.3 (*C*H_3) ppm.

IR (ATR): $\tilde{\nu}$ = 3346 (m), 2922 (m), 2852 (w), 1653 (s), 1608 (s), 1504 (w), 1480 (s), 1389 (s), 1372 (w), 1349 (s), 1326 (w), 1283 (m), 1241 (w), 1209 (w), 1148 (w), 1091 (w), 1071 (w), 975 (w), 907 (w), 867 (w), 827 (m), 802 (w), 760 (m), 742 (m), 718 (w), 696 (w), 605 (m), 585 (w), 541 (w), 515 (m) cm^{-1}.

HR-MS (ESI, EtOAc): *m/z* [M+Na]$^+$ calculated for $C_{15}H_{14}ON_4$+Na$^+$: 289.1060; found: 289.1057 ± 0.98 ppm.

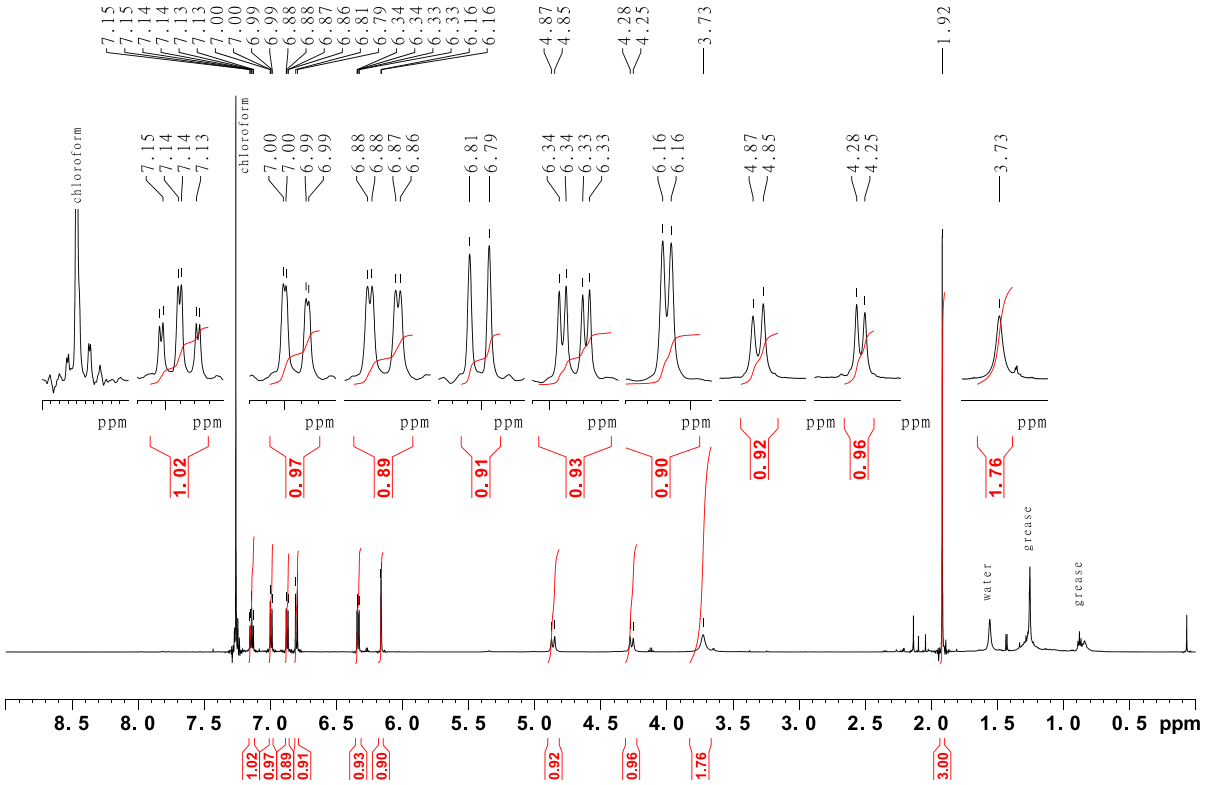

Figure SII.125: 600 MHz ^{1}H-NMR spectrum of (*Z*)-1-(3-aminodibenzo[c,g][1,2,5]triazocin-11(12*H*)-yl)ethan-1-one (**21**).

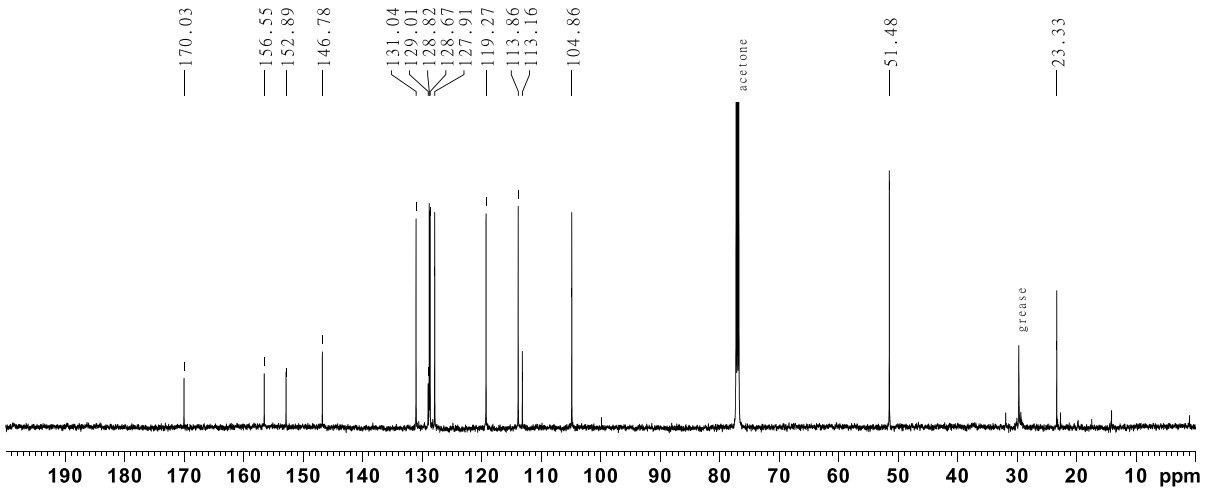

Figure SII.126: 150 MHz ^{13}C{^{1}H}-NMR spectrum of (*Z*)-1-(3-aminodibenzo[c,g][1,2,5]triazocin-11(12*H*)-yl)ethan-1-one (**21**).

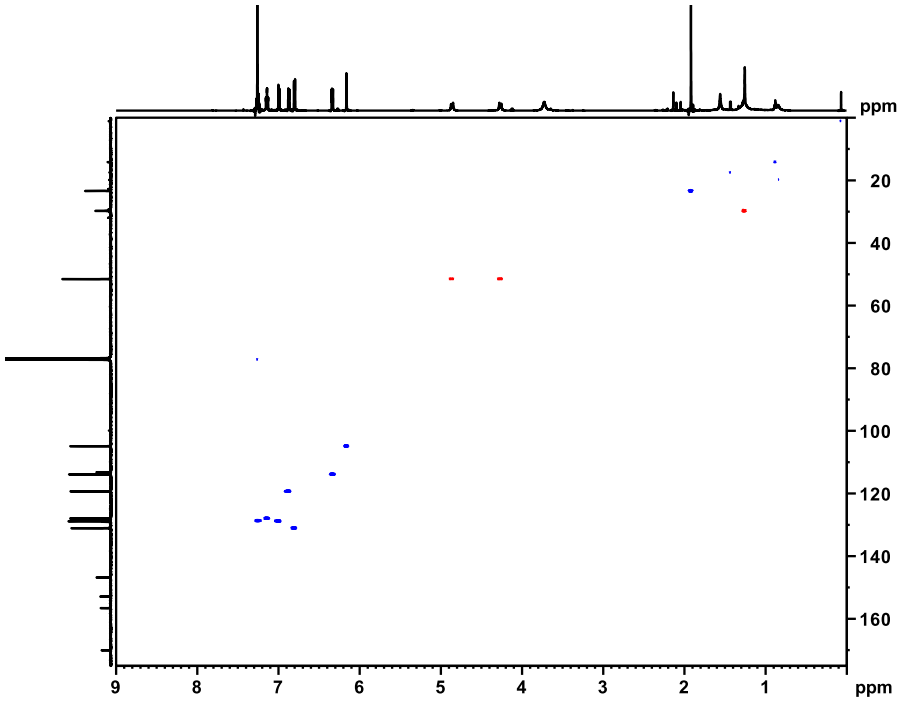

Figure SII.127: 600 MHz ^{1}H-^{13}C HSQC spectrum of (*Z*)-1-(3-aminodibenzo[c,g][1,2,5]triazocin-11(12*H*)-yl)ethan-1-one (**21**).

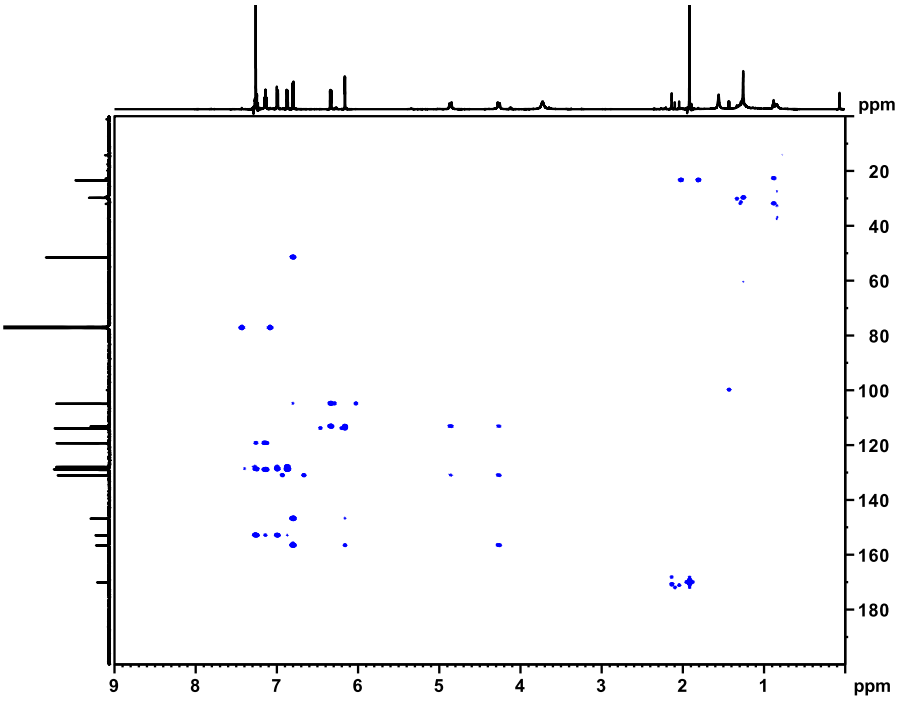

Figure SII.128: 600 MHz HMBC spectrum of (*Z*)-1-(3-aminodibenzo[c,g][1,2,5]triazocin-11(12*H*)-yl)ethan-1-one (**21**).

II.2.14 Synthesis of (*Z*)-11-acetyl-11,12-dihydrodibenzo[c,g][1,2,5]triazocine-3-carbonitrile (23)

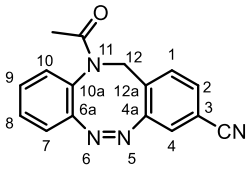

Halogenated *N*-acetyl-diazocine (**2**: 20.0 mg, 60.6 µmol, **3**: 23.0 mg, 60.6 µmol), 1,1'-bis(diphenylphosphino)ferrocene (1.00 mg, 1.81 µmol), $Pd(dba)_2$ (1.00 mg, 1.21 µmol) and zinc cyanide (3.55 mg, 30.3 µmol) were dissolved in 2.4 mL of dry DMAC under a nitrogen atmosphere, heated to 130 °C with an oil bath and stirred for 16 h at given temperature. After cooling to rt. the reaction mixture was extracted with 10 mL of DCM twice, dried over $MgSO_4$ and the solvent was evaporated. Column chromatography on silica (ethyl acetate/cyclohexane 1:1, R_f = 0.23) gave the product as yellow solid (from bromide **2**: 10.2 mg, 36.9 µmol, 61%; from iodide **3**: 13.6 mg, 49.1 µmol, 81%).

melting point: 194 °C

^{1}H-NMR (600 MHz, acetone-d_6, 298 K): δ = 7.56 (dd, ^3J = 7.9 Hz, ^4J = 1.7 Hz, 1 H, *H*-2), 7.47 (d, ^3J = 8.0 Hz, 1 H, *H*-1), 7.42 (td, ^3J = 7.9 Hz, ^4J = 1.4 Hz, 1 H, *H*-8), 7.37 (d, ^4J = 1.5 Hz, 1 H, *H*-4), 7.35 (dd, ^3J = 8.0 Hz, ^4J = 1.1 Hz, 1 H, *H*-10), 7.31 (td, ^3J = 7.4 Hz, ^4J = 1.4 Hz, 1 H, *H*-9), 7.09 (dd, ^3J = 7.9 Hz, ^4J = 1.1 Hz, 1 H, *H*-7), 5.21 (d, ^2J = 15.1 Hz, 1 H, *H*-12), 4.41 (d, ^2J = 15.0 Hz, 1 H, *H*-12'), 1.80 (s, 3 H, -CH_3) ppm.

^{13}C{^{1}H}-NMR (150 MHz, acetone-d_6, 298 K): δ = 169.4 (*C*=O), 156.3 (*C*-4a), 154.1 (*C*-6a), 132.1 (*C*-1), 131.9 (*C*-2), 130.9 (*C*-12a), 130.6 (*C*-8), 130.2 (*C*-10), 129.8 (*C*-9), 129.1 (*C*-10a), 123.7 (*C*-4), 120.1 (*C*-7), 118.1 (-*C*N), 113.2 (*C*-3), 51.8 (*C*-12) 22.9 (*C*H_3) ppm.

IR (ATR): $\tilde{\nu}$ = 3058 (w), 2923 (m), 2853 (w), 2233 (m), 1662 (s), 1589 (w), 1556 (w), 1521 (w), 1475 (m), 1448 (w), 1377 (s), 1340 (w), 1299 (m), 1228 (w), 1148 (w), 1109 (w), 1078 (w), 1032 (w), 1019 (w), 973 (w), 930 (w), 884 (w), 844 (w), 832 (w), 813 (w), 770 (m), 741 (m), 693 (w), 634 (w), 596 (m) cm^{-1}.

HR-MS (ESI, DCM): *m/z* $[M+H]^+$ calculated for $C_{16}H_{12}ON_4+H^+$: 277.1084; found: 277.1080 ± 1.40 ppm.

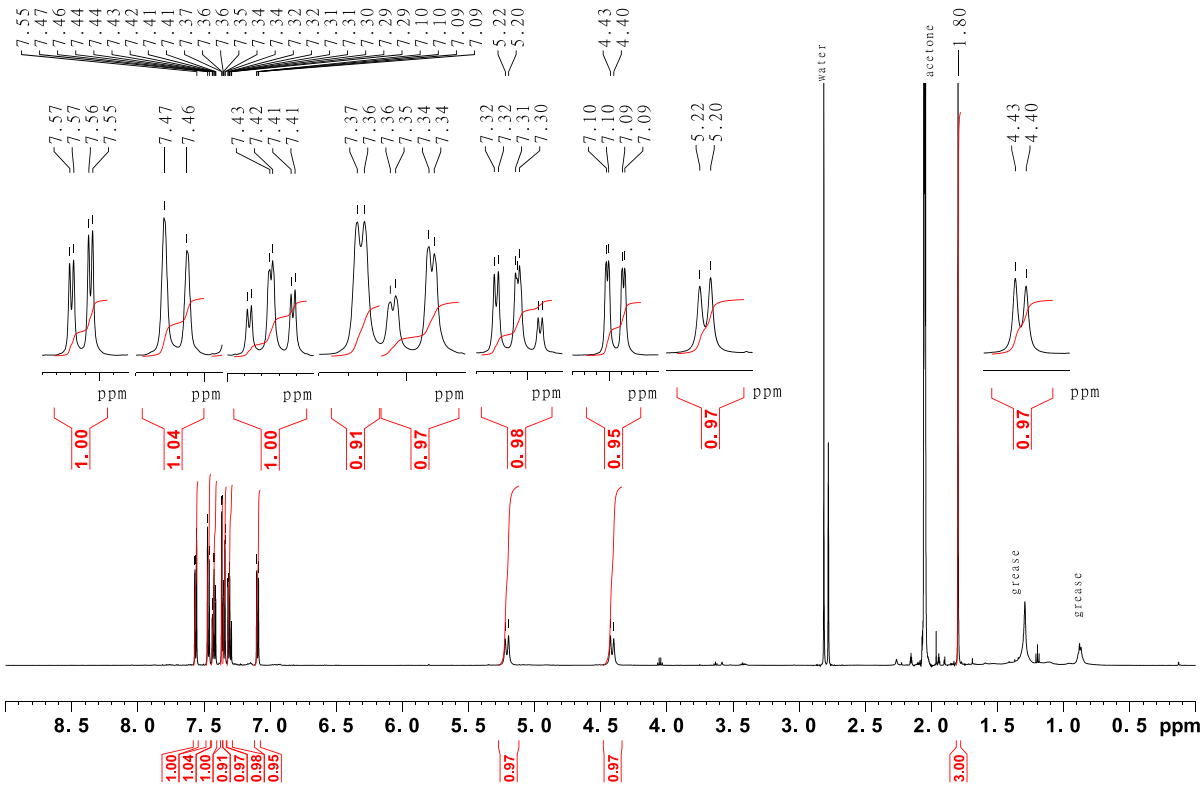

Figure SII.129: 600 MHz ^{1}H-NMR spectrum of (*Z*)-11-acetyl-11,12-dihydrodibenzo[c,g][1,2,5]triazocine-3-carbonitrile (**23**).

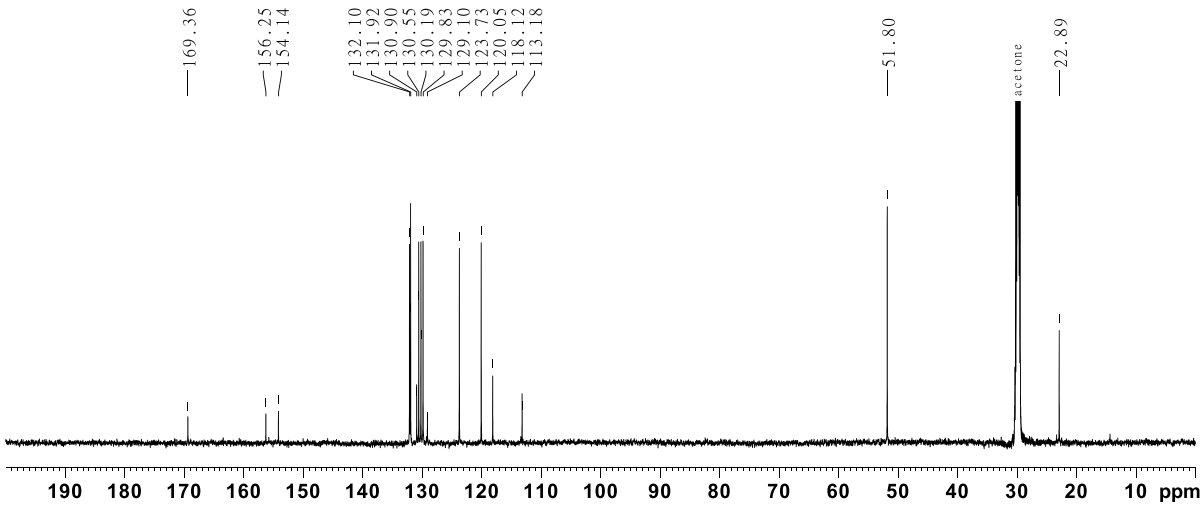

Figure SII.130: 150 MHz ^{13}C{^{1}H}-NMR spectrum of (*Z*)-11-acetyl-11,12-dihydrodibenzo[c,g][1,2,5]triazocine-3-carbonitrile (**23**).

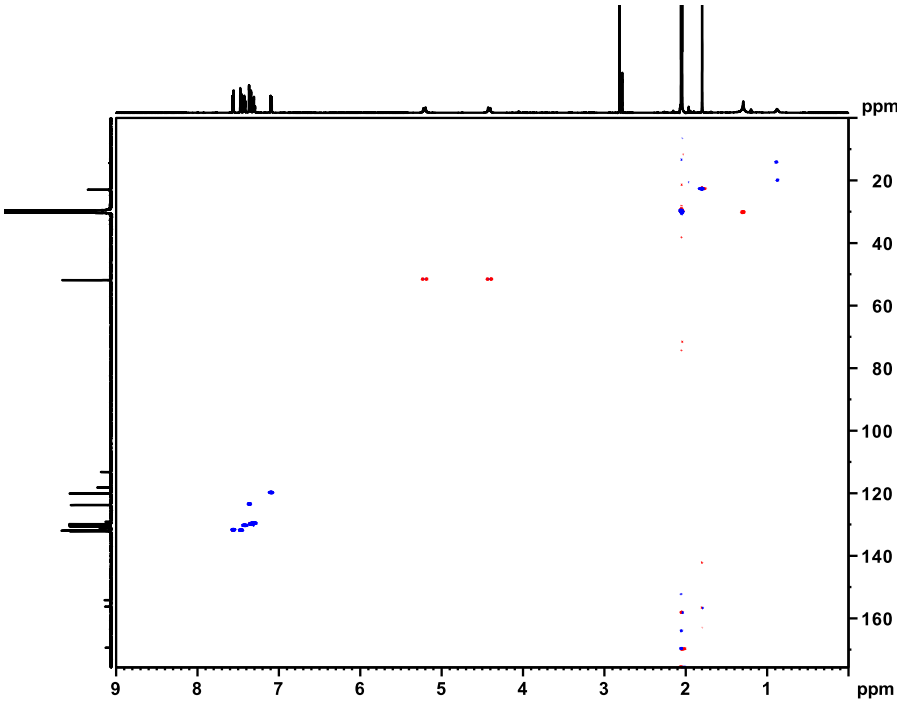

Figure SII.131: 600 MHz ^{1}H-^{13}C HSQC spectrum of *Z*)-11-acetyl-11,12-dihydrodibenzo[c,g][1,2,5]triazocine-3-carbonitrile (**23**).

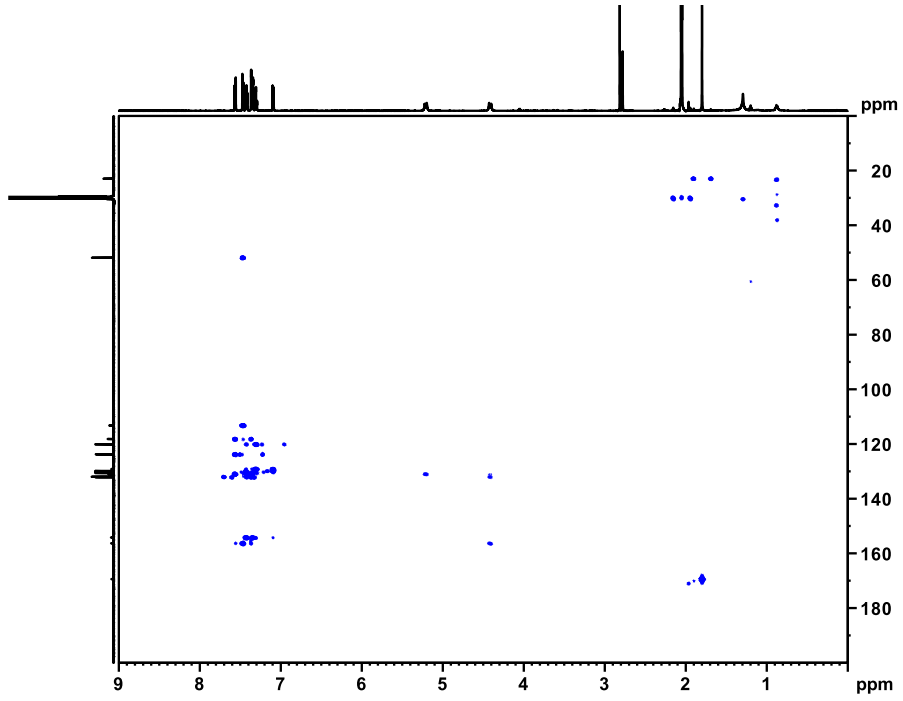

Figure SII.132: 600 MHz HMBC spectrum of *Z*)-11-acetyl-11,12-dihydrodibenzo[c,g][1,2,5]triazocine-3-carbonitrile (**23**).

III. UV-vis switching experiments

All samples were irradiated to the photostationary state (PSS) with 405 nm in acetonitrile or water. The UV-vis spectra were measured at 250 µM concentrations at 25 °C, except pyridine-substituted *N*-acetyl-diazocine **14** (2.55 mM due to low synthesis yield).

III.1 (Z)-(3,8-dibromodibenzo[c,g][1,2,5]triazocin-11(12H)-yl)ethan-1-one (4)

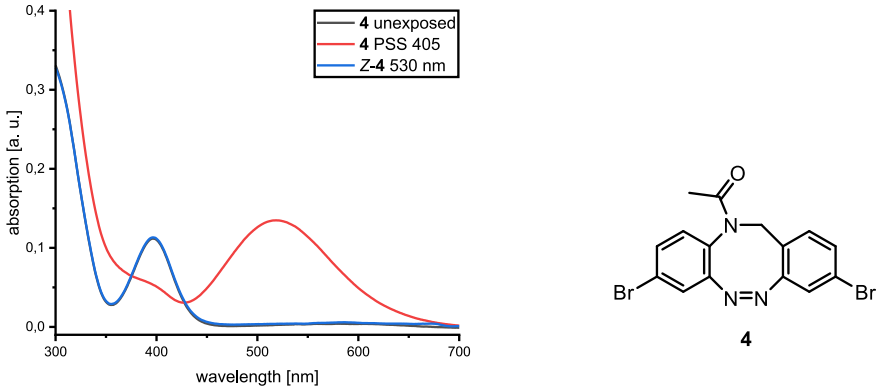

Figure SIII.1: UV-vis spectra of **4** in MeCN at 25 °C. The unexposed sample is plotted in black, the spectra of the PSS between *Z*-**4** and *E*-**4** after irradiation with 405 nm in red and the spectra of *Z*-**4** after irradiation with 530 nm in blue.

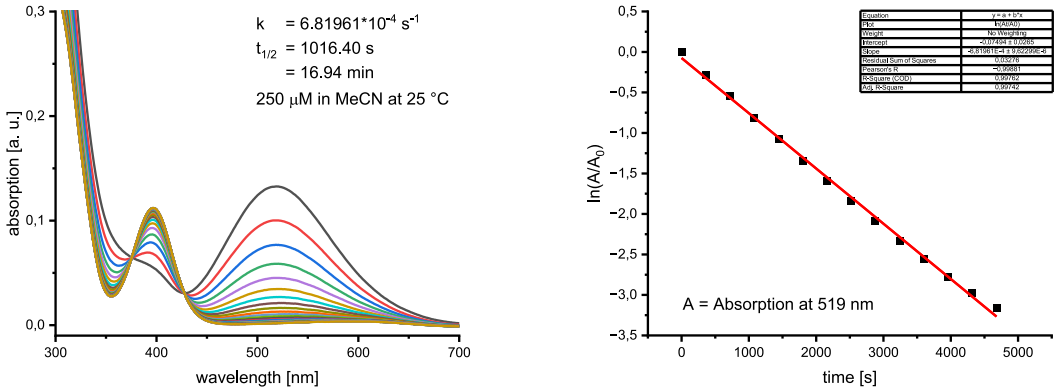

Figure SIII.2: UV-vis spectra of the half-life determination of **4** in MeCN at 25 °C (left) with the corresponding first order kinetics plot (right).

III.2 (*Z*)-1-(3-phenyldibenzo[c,g][1,2,5]triazocin-11(12*H*)-yl)ethan-1-one (7)

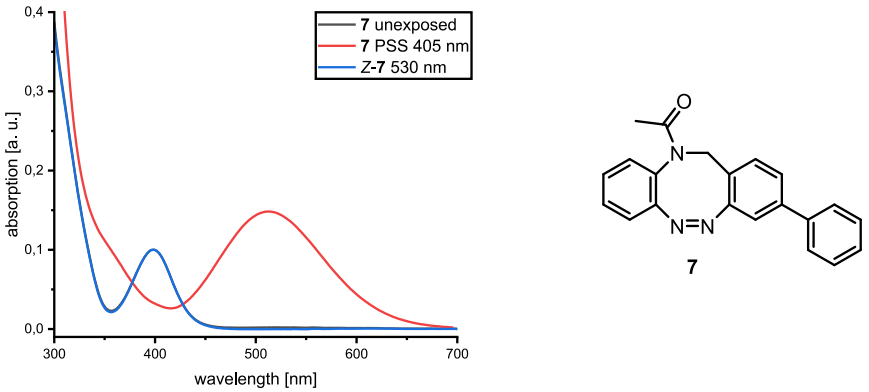

Figure SIII.3: UV-vis spectra of **7** in MeCN at 25 °C. The unexposed sample is plotted in black, the spectra of the PSS between *Z*-**7** and *E*-**7** after irradiation with 405 nm in red and the spectra of *Z*-**7** after irradiation with 530 nm in blue.

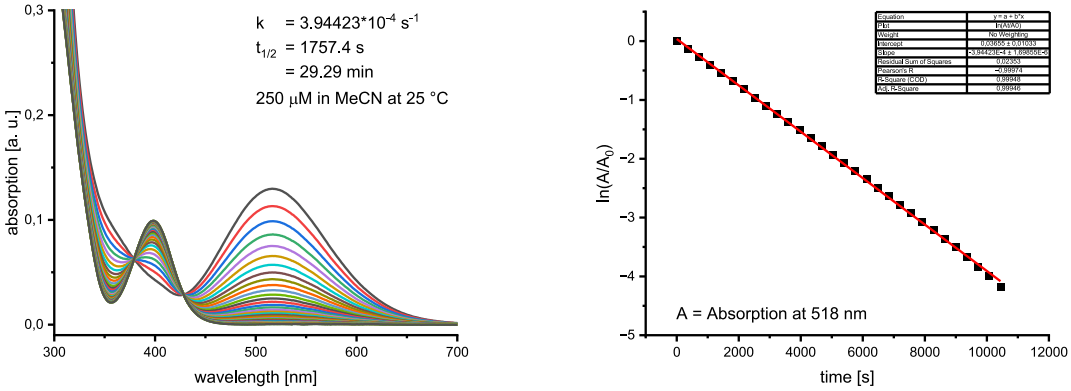

Figure SIII.4: UV-vis spectra of the half-life determination of **7** in MeCN at 25 °C (left) with the corresponding first order kinetics plot (right).

III.3 (*Z*)-1-(3-vinyldibenzo[c,g][1,2,5]triazocin-11(12*H*)-yl)ethan-1-one (8)

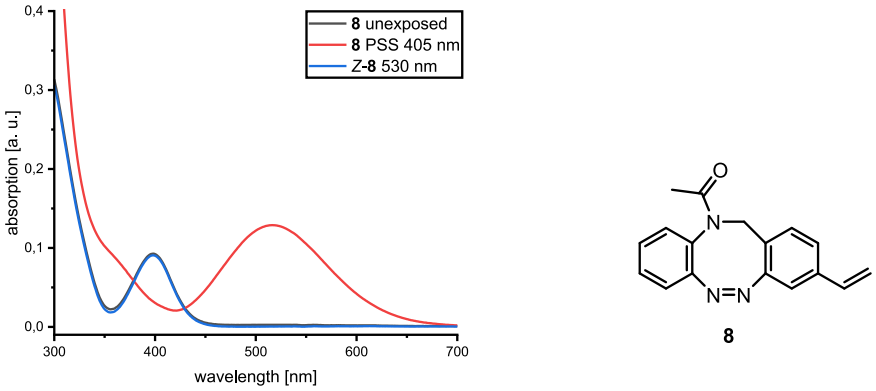

Figure SIII.5: UV-vis spectra of **8** in MeCN at 25 °C. The unexposed sample is plotted in black, the spectra of the PSS between *Z*-**8** and *E*-**8** after irradiation with 405 nm in red and the spectra of *Z*-**8** after irradiation with 530 nm in blue.

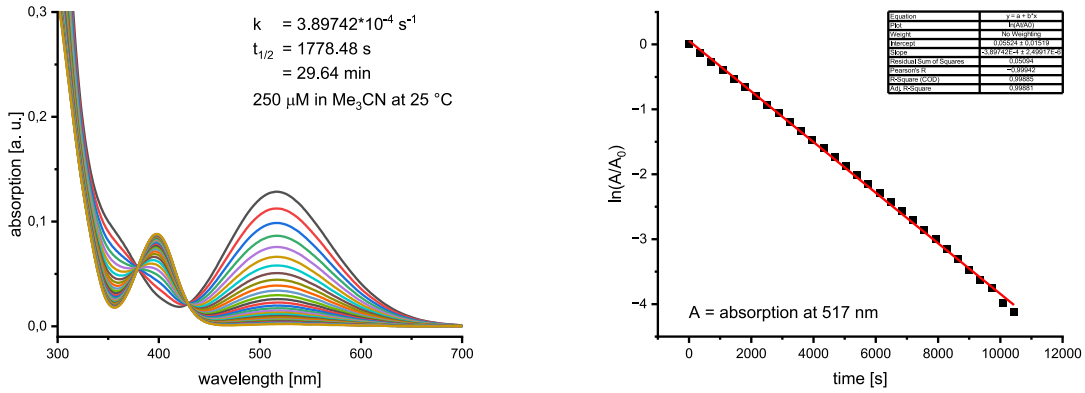

Figure SIII.6: UV-vis spectra of the half-life determination of **8** in MeCN at 25 °C (left) with the corresponding first order kinetics plot (right).

III.4 (*Z*)-1-(3-(2,6-dimethylphenyl)dibenzo[c,g][1,2,5]triazocin-11(12*H*)-yl)ethan-1-one (9)

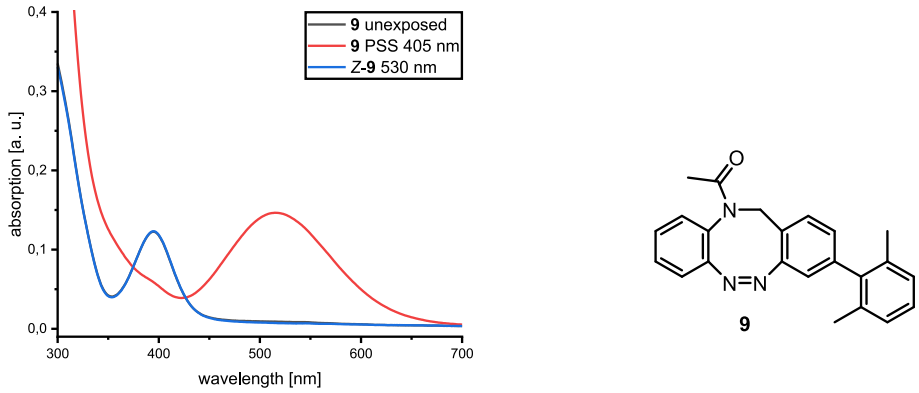

Figure SIII.7: UV-vis spectra of **9** in MeCN at 25 °C. The unexposed sample is plotted in black, the spectra of the PSS between *Z*-**9** and *E*-**9** after irradiation with 405 nm in red and the spectra of *Z*-**9** after irradiation with 530 nm in blue.

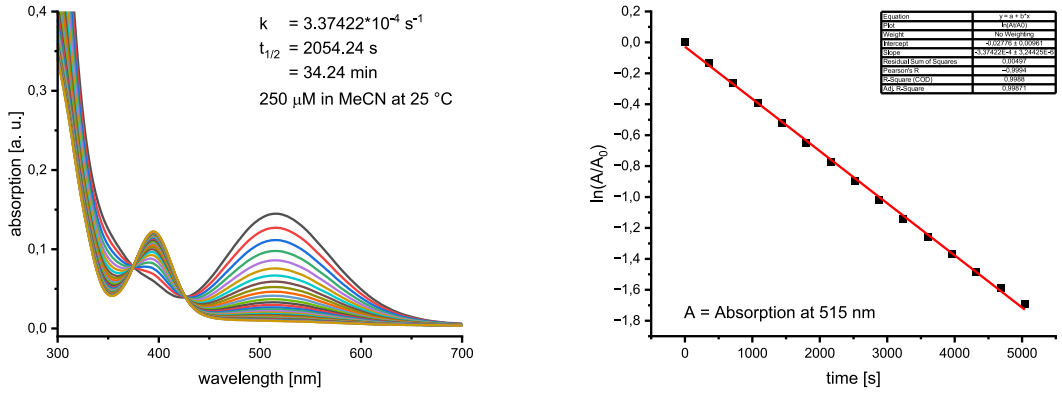

Figure SIII.8: UV-vis spectra of the half-life determination of **9** in MeCN at 25 °C (left) with the corresponding first order kinetics plot (right).

III.5 (*Z*)-1-(3-(2-bromophenyl)dibenzo[c,g][1,2,5]triazocin-11(12*H*)-yl)ethan-1-one (10)

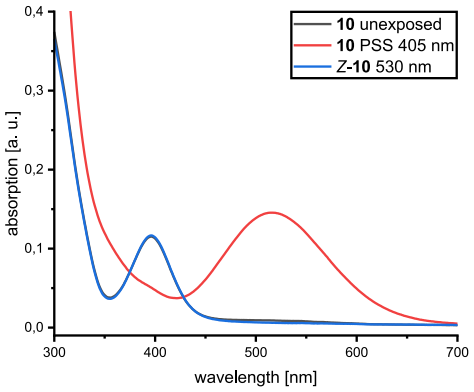

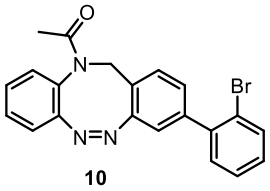

10

Figure SIII.9: UV-vis spectra of **10** in MeCN at 25 °C. The unexposed sample is plotted in black, the spectra of the PSS between *Z*-**10** and *E*-**10** after irradiation with 405 nm in red and the spectra of *Z*-**10** after irradiation with 530 nm in blue.

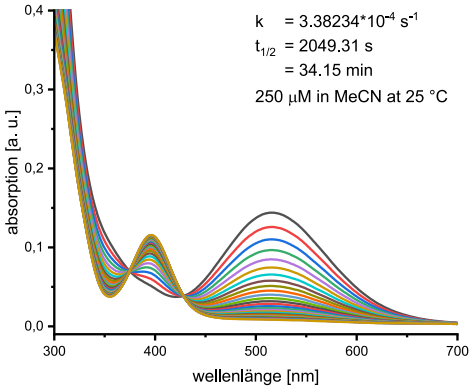

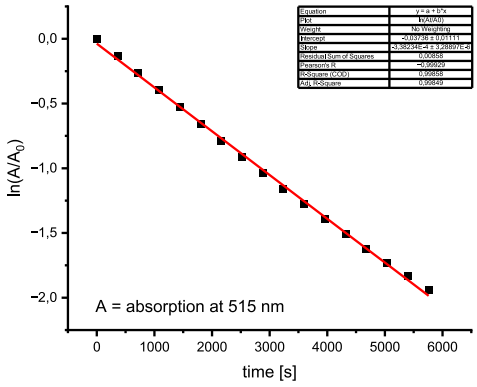

Figure SIII.10: UV-vis spectra of the half-life determination of **10** in MeCN at 25 °C (left) with the corresponding first order kinetics plot (right).

III.6 (*Z*)-1-(3-(4-fluorophenyl)dibenzo[c,g][1,2,5]triazocin-11(12*H*)-yl)ethan-1-one (11)

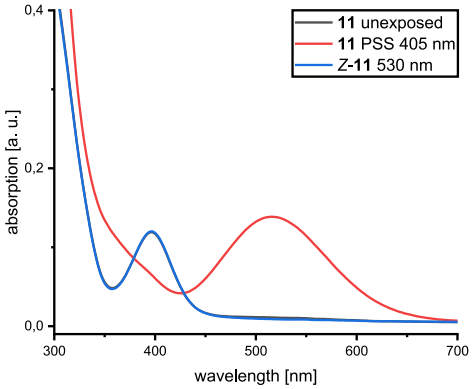

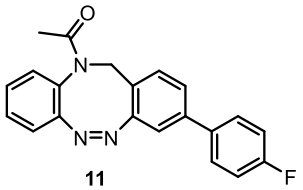

11

Figure SIII.11: UV-vis spectra of **11** in MeCN at 25 °C. The unexposed sample is plotted in black, the spectra of the PSS between *Z*-**11** and *E*-**11** after irradiation with 405 nm in red and the spectra of *Z*-**11** after irradiation with 530 nm in blue.

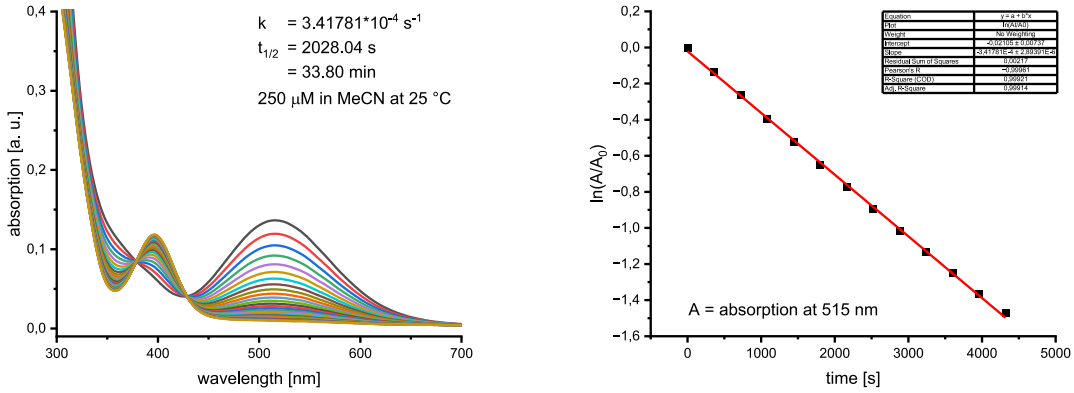

Figure SIII.12: UV-vis spectra of the half-life determination of **11** in MeCN at 25 °C (left) with the corresponding first order kinetics plot (right).

III.7 (*Z*)-2-(11-acetyl-11,12-dihydrodibenzo[c,g][1,2,5]triazocin-3-yl)benzaldehyde (12)

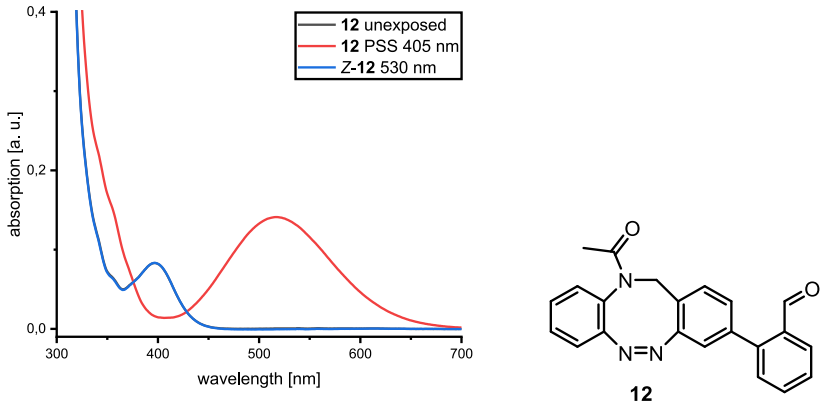

Figure SIII.13: UV-vis spectra of **12** in MeCN at 25 °C. The unexposed sample is plotted in black, the spectra of the PSS between *Z*-**12** and *E*-**12** after irradiation with 405 nm in red and the spectra of *Z*-**12** after irradiation with 530 nm in blue.

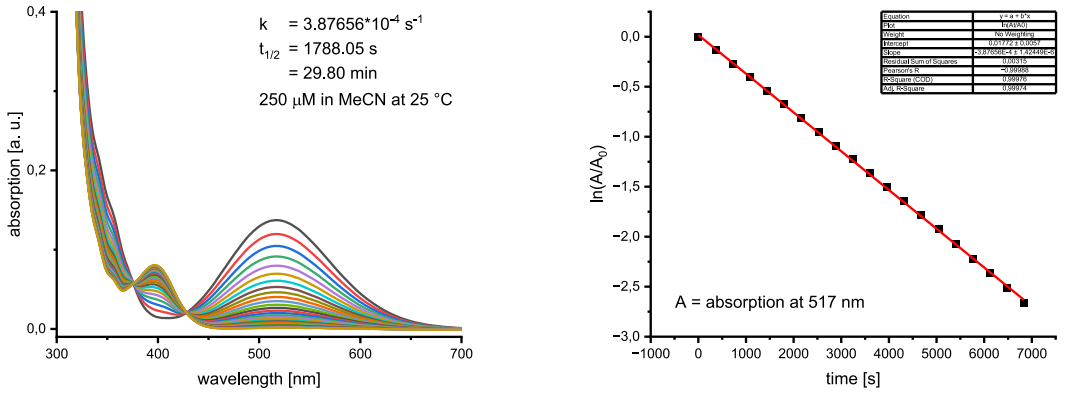

Figure SIII.14: UV-vis spectra of the half-life determination of **12** in MeCN at 25 °C (left) with the corresponding first order kinetics plot (right).

III.8 (*Z*)-2-(11-acetyl-11,12-dihydrodibenzo[c,g][1,2,5]triazocin-3-yl)benzoic acid (13)

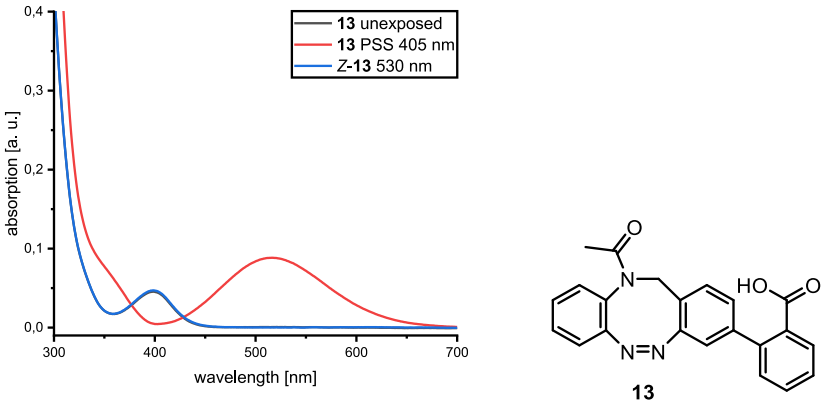

Figure SIII.15: UV-vis spectra of **13** in MeCN at 25 °C. The unexposed sample is plotted in black, the spectra of the PSS between *Z*-**13** and *E*-**13** after irradiation with 405 nm in red and the spectra of *Z*-**13** after irradiation with 530 nm in blue.

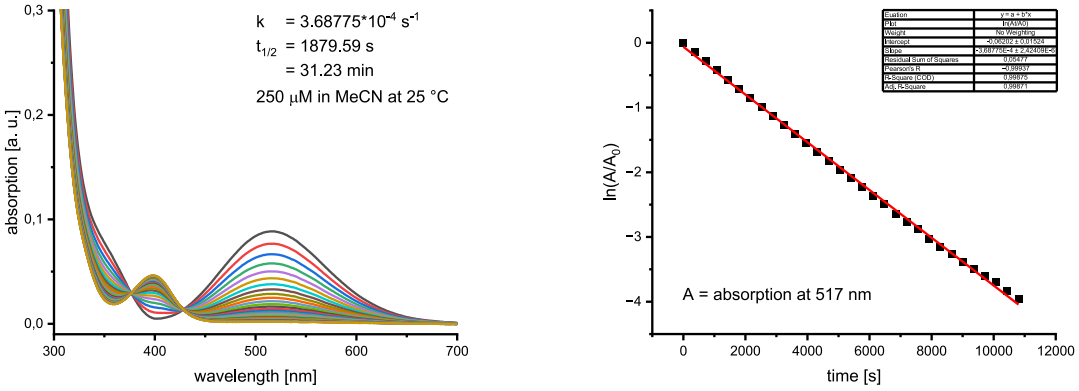

Figure SIII.16: UV-vis spectra of the half-life determination of **13** in MeCN at 25 °C (left) with the corresponding first order kinetics plot (right).

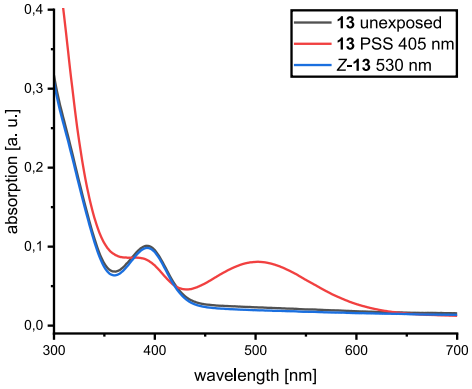

Figure SIII.17: UV-vis spectra of **13** in deionized water pH 9 at 25 °C. The unexposed sample is plotted in black, the spectra of the PSS between *Z*-**13** and *E*-**13** after irradiation with 405 nm in red and the spectra of *Z*-**13** after irradiation with 530 nm in blue.

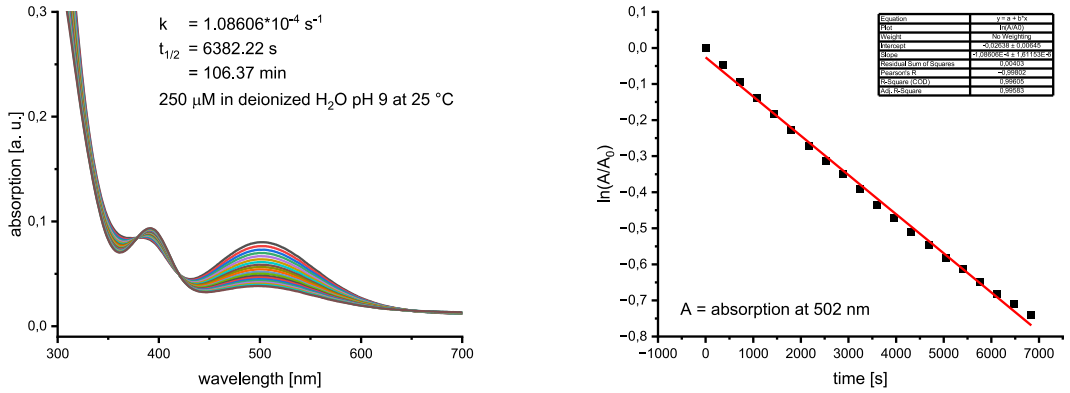

Figure SIII.18: UV-vis spectra of the half-life determination of **13** in deionized water pH 9 at 25 °C (left) with the corresponding first order kinetics plot (right).

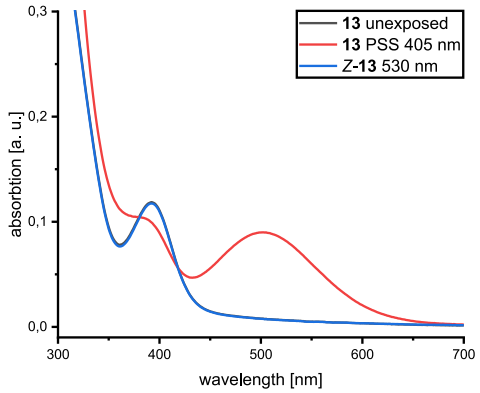

Figure SIII.19: UV-vis spectra of **13** in aqueous PBS buffer solution pH 7.4 at 25 °C. The unexposed sample is plotted in black, the spectra of the PSS between *Z*-**13** and *E*-**13** after irradiation with 405 nm in red and the spectra of *Z*-**13** after irradiation with 530 nm in blue.

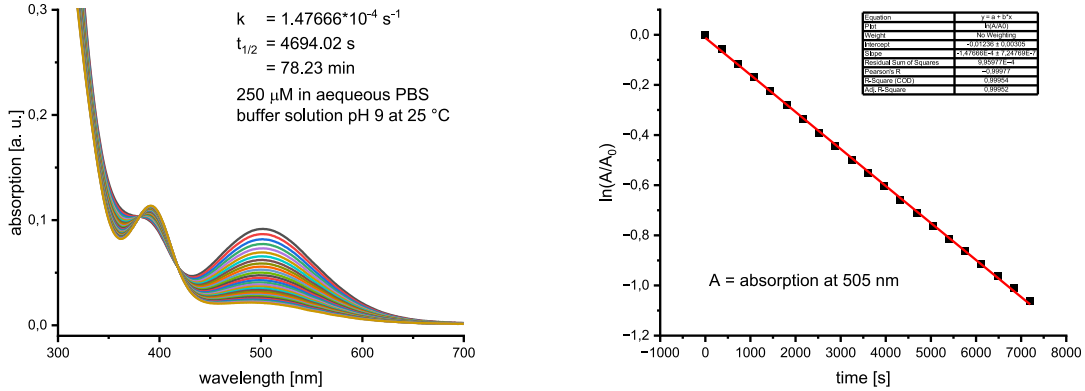

Figure SIII.20: UV-vis spectra of the half-life determination of **13** in aqueous PBS buffer solution pH 7.4 at 25 °C (left) with the corresponding first order kinetics plot (right).

III.9 (*Z*)-1-(3-(pyridine-4-yl)dibenzo[c,g][1,2,5]triazocin-11(12*H*)-ethan-1-one (14)

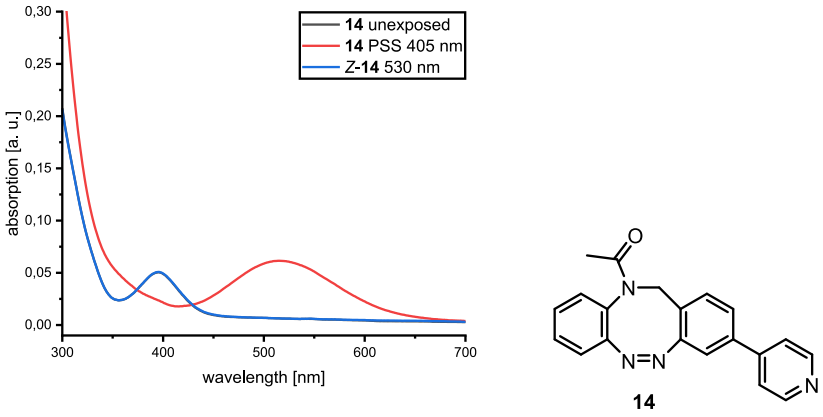

Figure SIII.21: UV-vis spectra of **14** in MeCN at 25 °C. The unexposed sample is plotted in black, the spectra of the PSS between *Z*-**14** and *E*-**14** after irradiation with 405 nm in red and the spectra of *Z*-**14** after irradiation with 530 nm in blue.

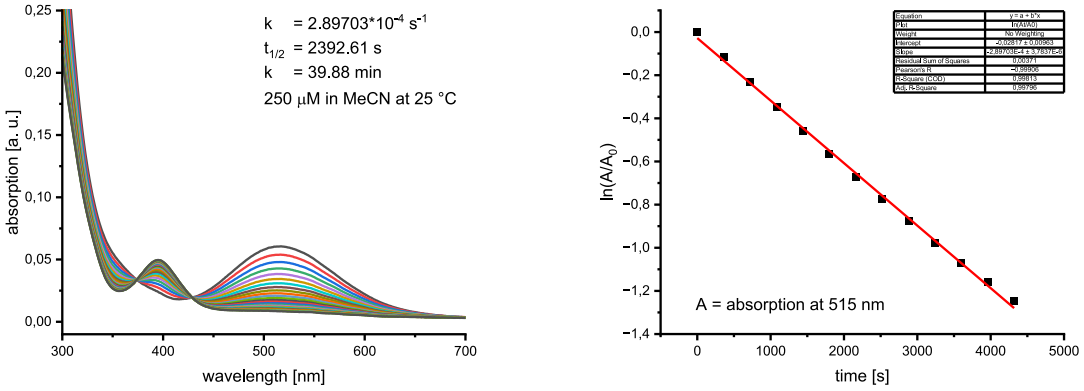

Figure SIII.22: UV-vis spectra of the half-life determination of **14** in MeCN at 25 °C (left) with the corresponding first order kinetics plot (right).

III.10 (*Z*)-1-(3-benzyldibenzo[c,g][1,2,5]triazocin-11(12*H*)-ethan-1-one (17)

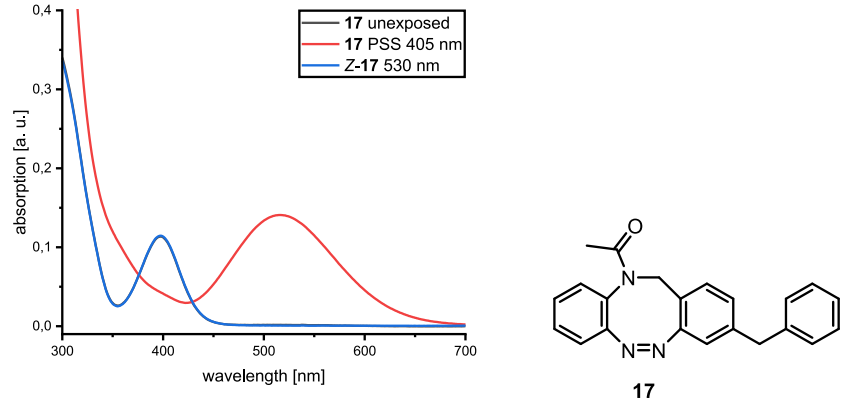

Figure SIII.23: UV-vis spectra of **17** in MeCN at 25 °C. The unexposed sample is plotted in black, the spectra of the PSS between *Z*-**17** and *E*-**17** after irradiation with 405 nm in red and the spectra of *Z*-**17** after irradiation with 530 nm in blue.

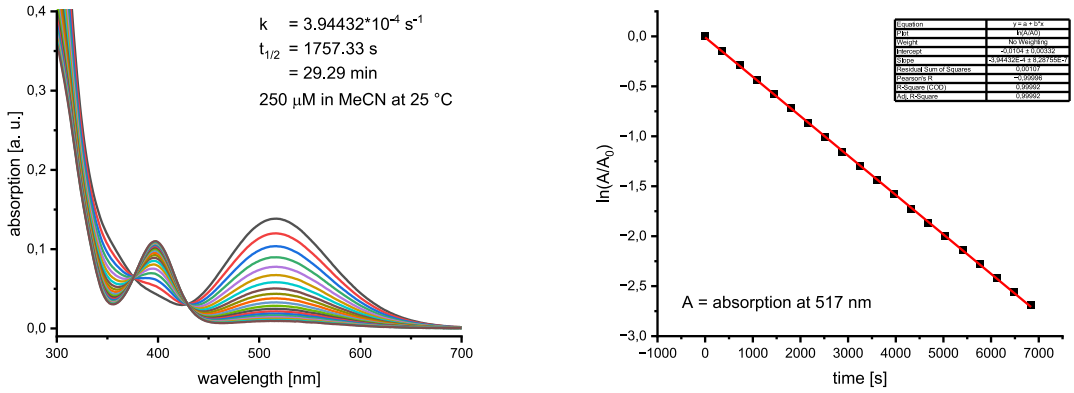

Figure SIII.24: UV-vis spectra of the half-life determination of **17** in MeCN at 25 °C (left) with the corresponding first order kinetics plot (right).

III.11 *tert*-butyl-(*Z*)-(11-acetyl-11,12-dihydrodiebenzo[c,g][1,2,5]triazocin-3-yl)carbamate (19)

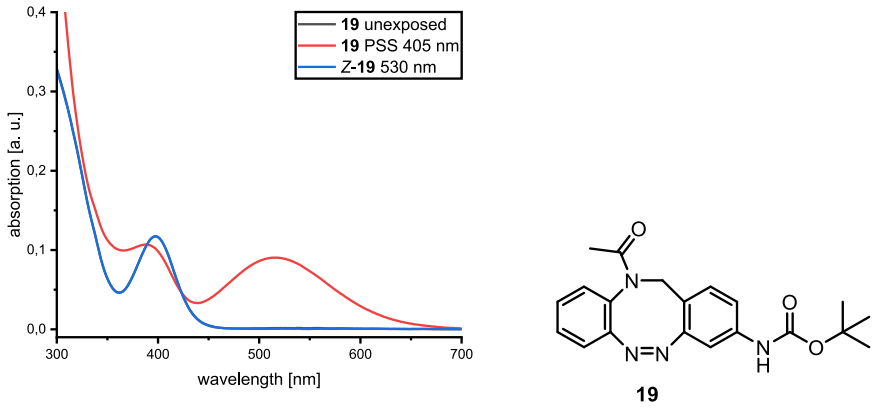

Figure SIII.25: UV-vis spectra of **19** in MeCN at 25 °C. The unexposed sample is plotted in black, the spectra of the PSS between *Z*-**19** and *E*-**19** after irradiation with 405 nm in red and the spectra of *Z*-**19** after irradiation with 530 nm in blue.

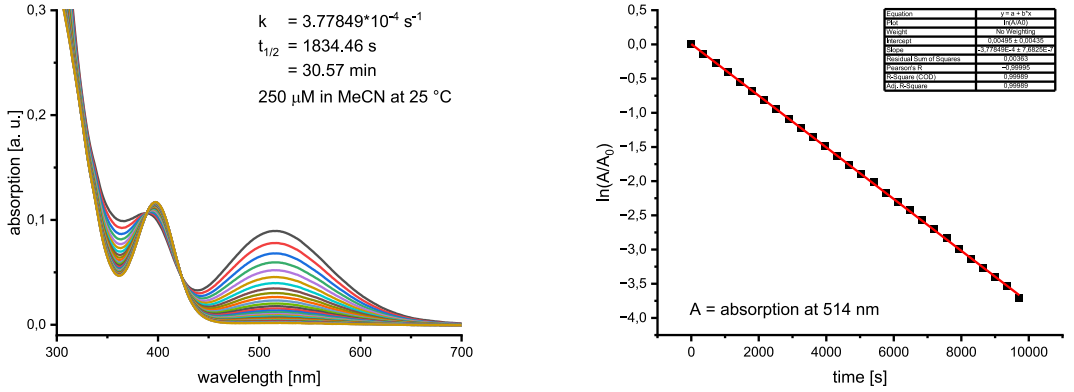

Figure SIII.26: UV-vis spectra of the half-life determination of **19** in MeCN at 25 °C (left) with the corresponding first order kinetics plot (right).

III.12 (*Z*)-1-(3-(diphenylamino)dibenzo[c,g][1,2,5]triazocin-11(12*H*)-yl)ethan-1-one (20)

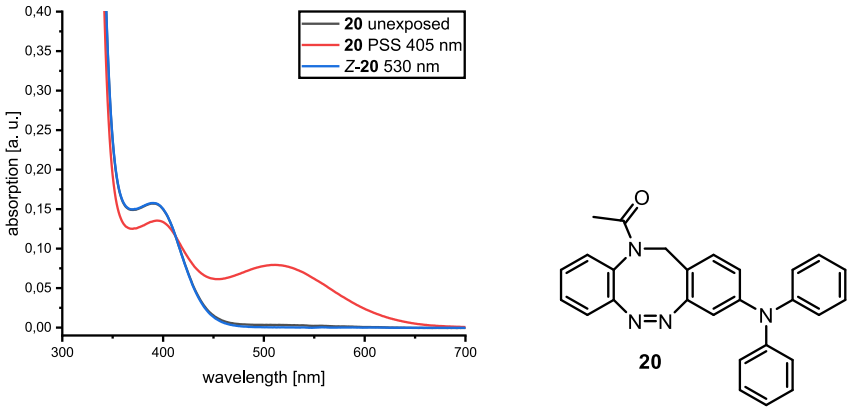

Figure SIII.27: UV-vis spectra of **20** in MeCN at 25 °C. The unexposed sample is plotted in black, the spectra of the PSS between *Z*-**20** and *E*-**20** after irradiation with 405 nm in red and the spectra of *Z*-**20** after irradiation with 530 nm in blue.

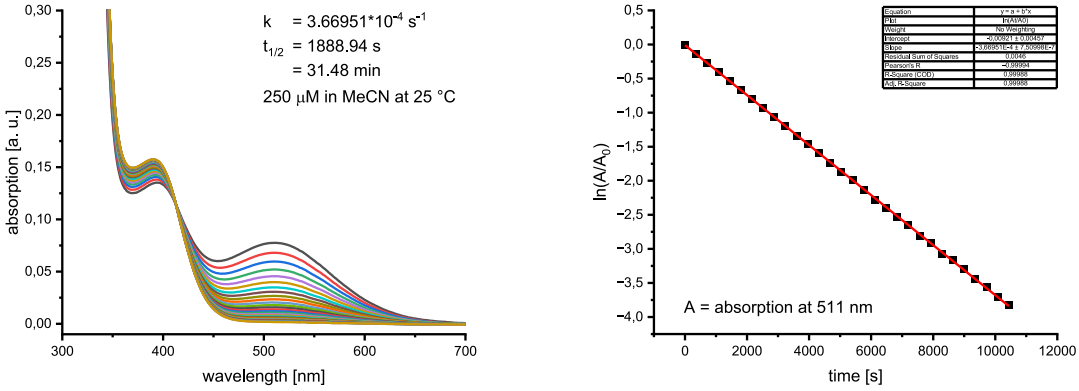

Figure SIII.28: UV-vis spectra of the half-life determination of **20** in MeCN at 25 °C (left) with the corresponding first order kinetics plot (right).

III.13 (*Z*)-1-(3-aminodibenzo[c,g][1,2,5]triazocin-11(12*H*)-yl)ethan-1-one (21)

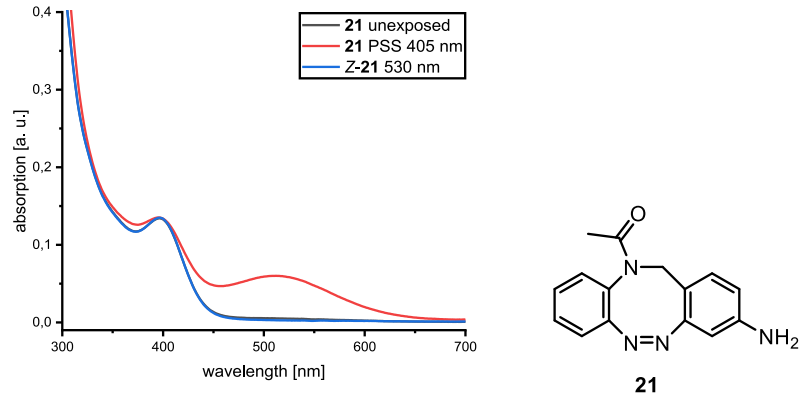

Figure SIII.29: UV-vis spectra of **21** in MeCN at 25 °C. The unexposed sample is plotted in black, the spectra of the PSS between *Z*-**21** and *E*-**21** after irradiation with 405 nm in red and the spectra of *Z*-**21** after irradiation with 530 nm in blue.

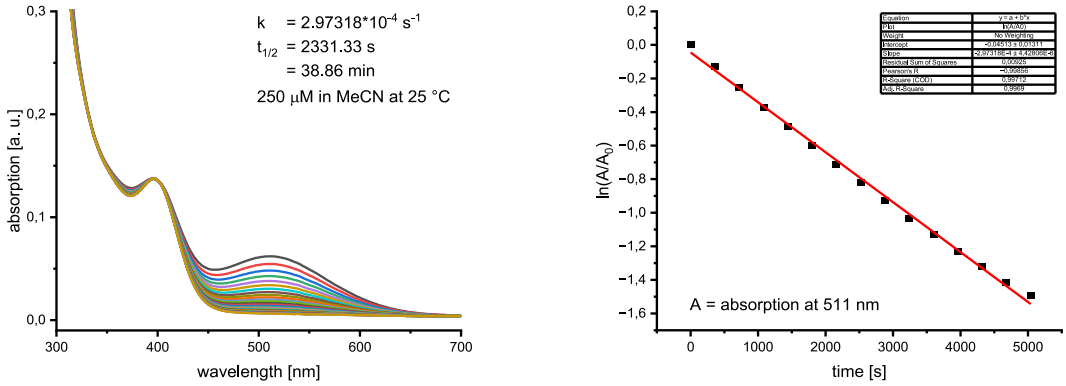

Figure SIII.30: UV-vis spectra of the half-life determination of **21** in MeCN at 25 °C (left) with the corresponding first order kinetics plot (right).

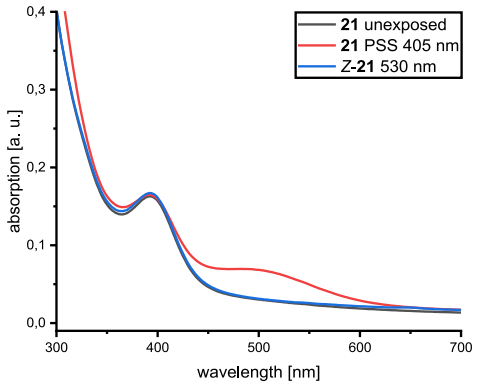

Figure SIII.31: UV-vis spectra of **21** in deionized water at 25 °C. The unexposed sample is plotted in black, the spectra of the PSS between *Z*-**21** and *E*-**21** after irradiation with 405 nm in red and the spectra of *Z*-**21** after irradiation with 530 nm in blue.

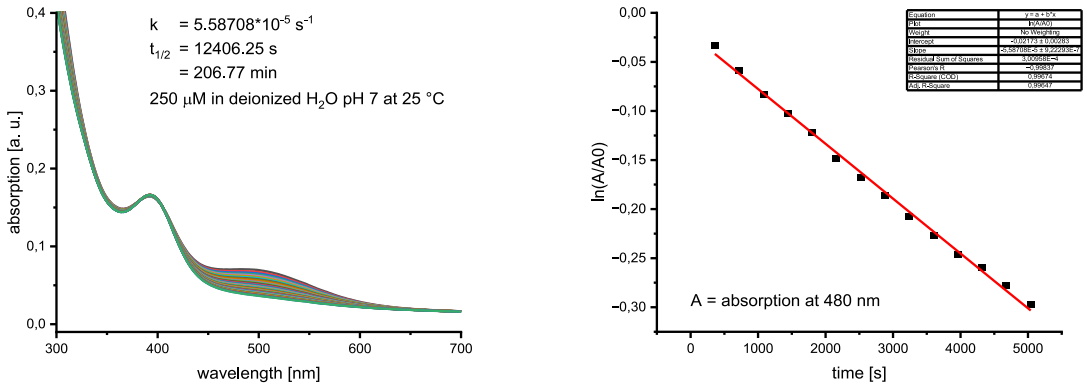

Figure SIII.32: UV-vis spectra of the half-life determination of **21** in deionized water at 25 °C (left) with the corresponding first order kinetics plot (right).

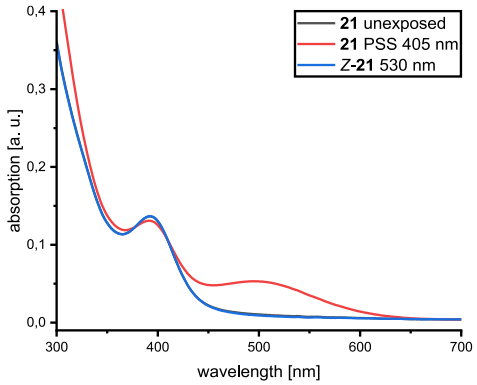

Figure SIII.33: UV-vis spectra of **21** in deionized water pH 3.5 at 25 °C. The unexposed sample is plotted in black, the spectra of the PSS between *Z*-**21** and *E*-**21** after irradiation with 405 nm in red and the spectra of *Z*-**21** after irradiation with 530 nm in blue.

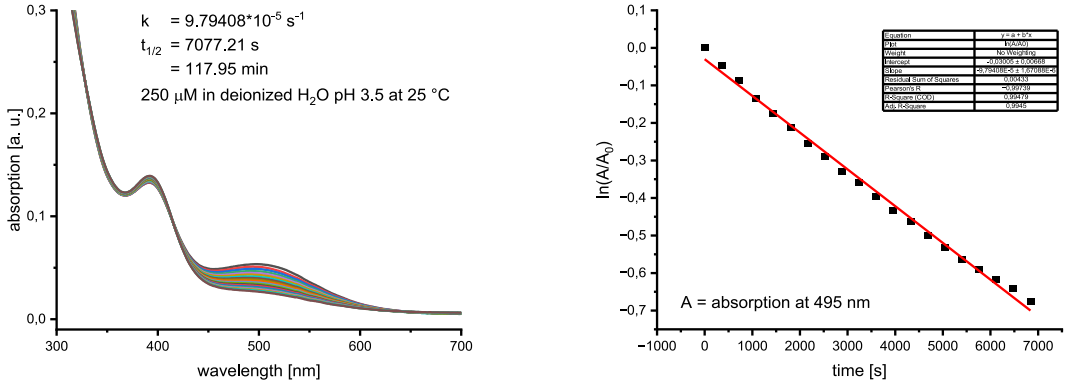

Figure SIII.34: UV-vis spectra of the half-life determination of **21** in deionized water pH 3.5 at 25 °C (left) with the corresponding first order kinetics plot (right).

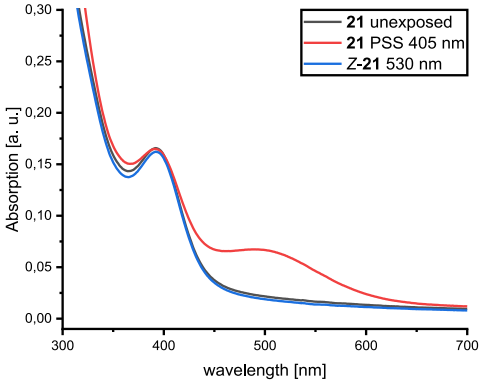

Figure SIII.35: UV-vis spectra of **21** in aqueous PBS buffer solution pH 7.4 at 25 °C. The unexposed sample is plotted in black, the spectra of the PSS between *Z*-**21** and *E*-**21** after irradiation with 405 nm in red and the spectra of *Z*-**21** after irradiation with 530 nm in blue.

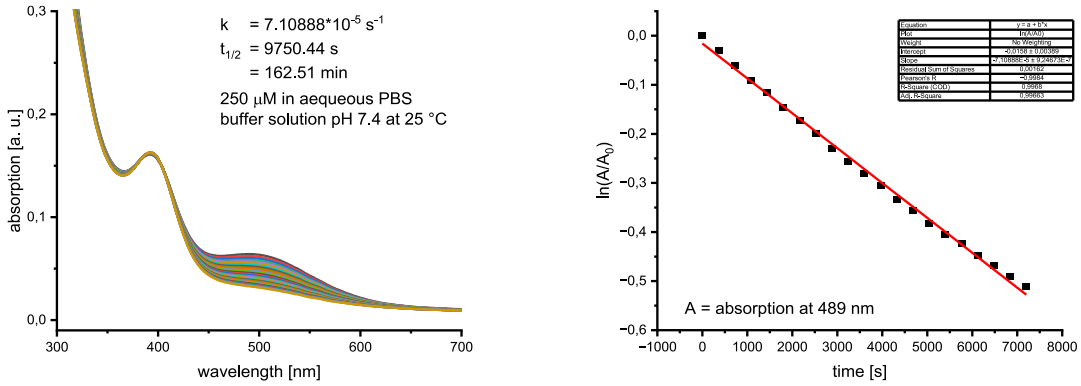

Figure SIII.36: UV-vis spectra of the half-life determination of **21** in aqueous PBS buffer solution pH 7.4 at 25 °C (left) with the corresponding first order kinetics plot (right).

III.14 (*Z*)-11-acetyl-11,12-dihydrodibenzo[c,g][1,2,5]triazocine-3-carbonitrile (23)

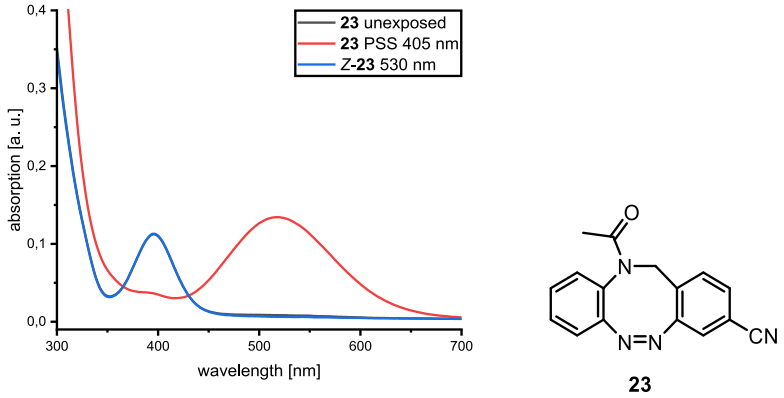

Figure SIII.37: UV-vis spectra of **23** in MeCN at 25 °C. The unexposed sample is plotted in black, the spectra of the PSS between *Z*-**23** and *E*-**23** after irradiation with 405 nm in red and the spectra of *Z*-**23** after irradiation with 530 nm in blue.

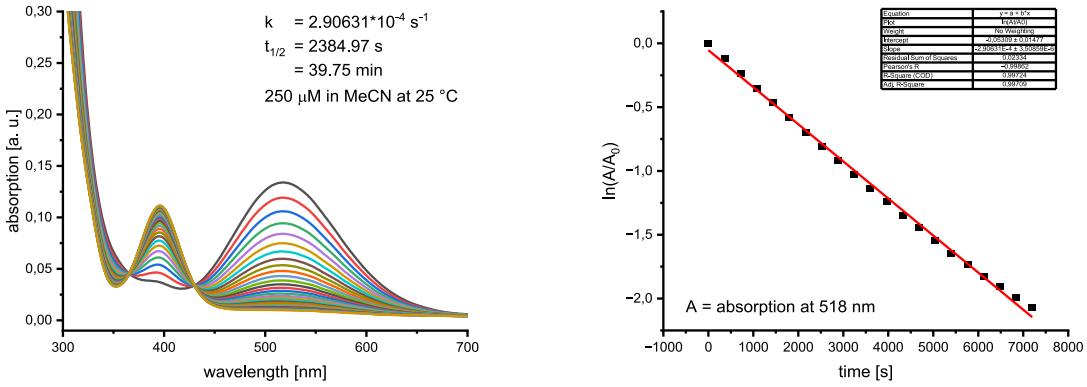

Figure SIII.38: UV-vis spectra of the half-life determination of **23** in MeCN at 25 °C (left) with the corresponding first order kinetics plot (right).

IV. ^{1}H-NMR switching experiments

Photostationary states (PSS) of compounds **4,7-14,17,19-21** and **23** were measured via ^{1}H-NMR by integration of the different species after irradiation with 405 nm, whereby no distinction was made between *E-twist-* and *E-chair*-conformations. The value of the integrals and the extrapolated values are given in Table SIII.1. ^{1}H-NMR spectra were measured at 5 mM concentrations, except pyridine-substituted *N*-acetyl-diazocine **14** (2.55 mM due to low synthesis yield). The following equation (1) was used for extrapolation of the photostationary states:

$$PSS_{extrapol.} = PSS_{measured} \cdot e^{kt} \quad (1)$$

k is the rate constant at 25 °C (see table 6 and 7) and *t* the measuring time (330 s): 120 s preparation (transfer into the spectrometer and shimming after excitation with light) and 210 s measuring time for 32 scans. All spectra were measured at a Bruker AV600 spectrometer.

Table SIV.1: Measured and extrapolated photostationary states of compounds **4,7-14,17,19-21** and **23** in acetonitrile.

	measured PSS %	extrapolated PSS %
4	68	85
7	69	79
8	67	76
9	69	77
10	73	82
11	70	78
12	71	80
13	8	77
14	72	79
17	72	82
19	54	61
20	43	49
21	37	41
23	76	83

Table SIV.2: Measured and extrapolated photostationary states of compounds **13** and **23** in water.

	measured PSS %	extrapolated PSS %
13 pH 7.4	51	53
13 pH 9	46	48
21 pH 7.4	35	37
21 pH 3.5	62	62

IV.1 (Z)-(3,8-dibromodibenzo[c,g][1,2,5]triazocin-11(12H)-yl)ethan-1-one (4)

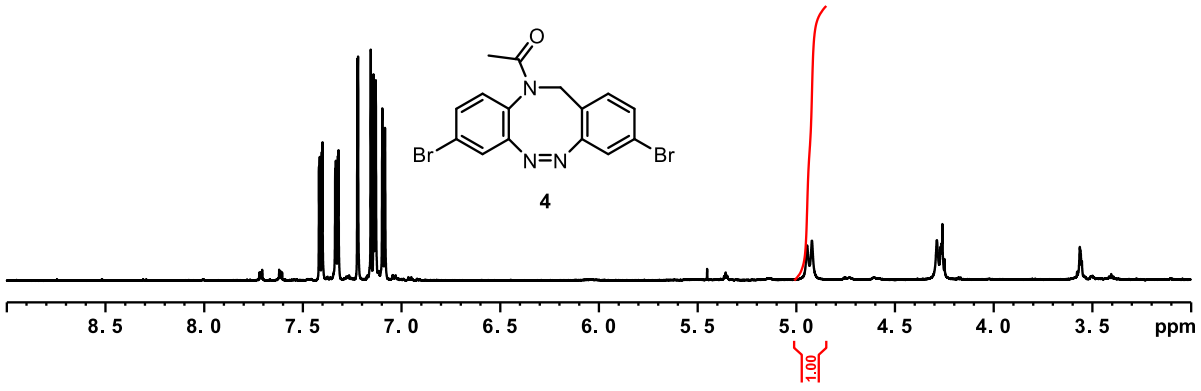

Figure SIV.1: ^{1}H-NMR-spectra of *Z*-**4** in CD_3CN at 298 K.

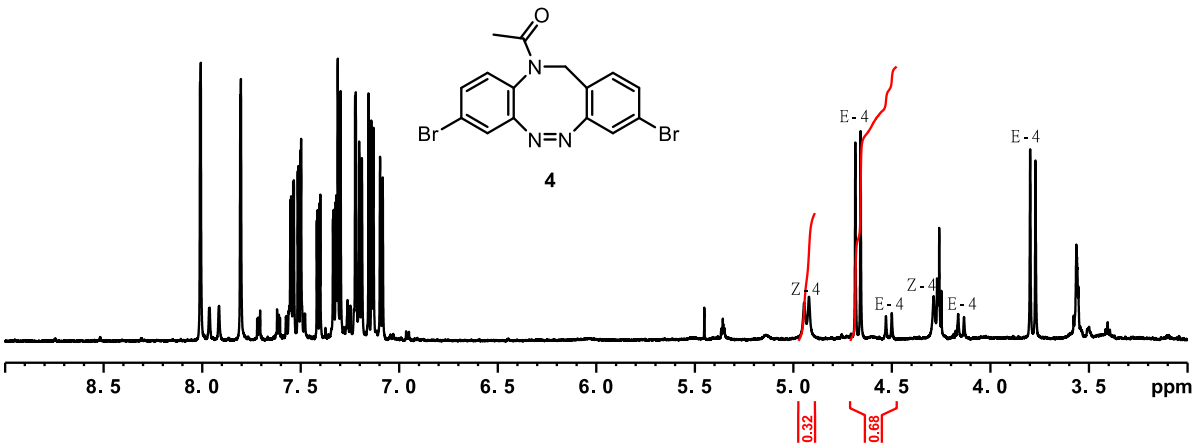

Figure SIV.2: ^{1}H-NMR-spectra of **4** in CD_3CN at 298 K after irradiation with 405 nm.

IV.2 (*Z*)-1-(3-phenyldibenzo[c,g][1,2,5]triazocin-11(12*H*)-yl)ethan-1-one (7)

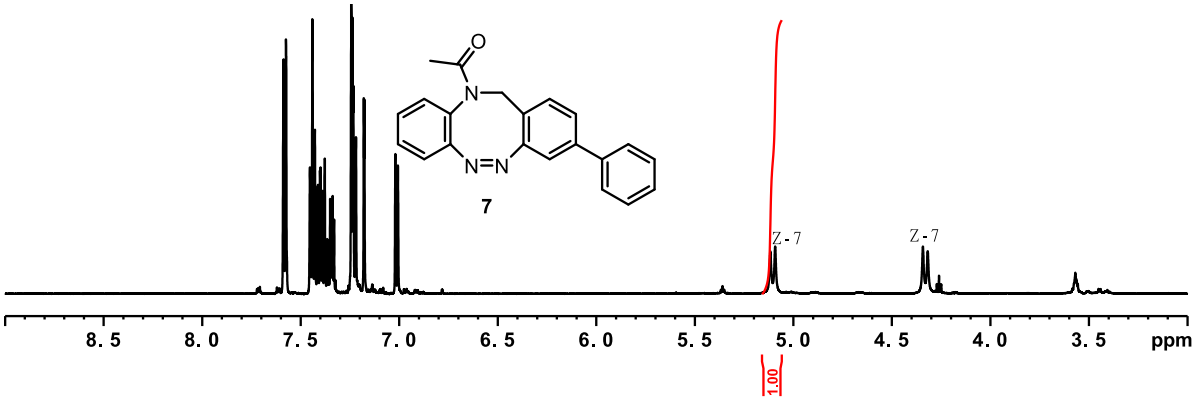

Figure SIV.3: ^{1}H-NMR-spectra of *Z*-**7** in CD_3CN at 298 K.

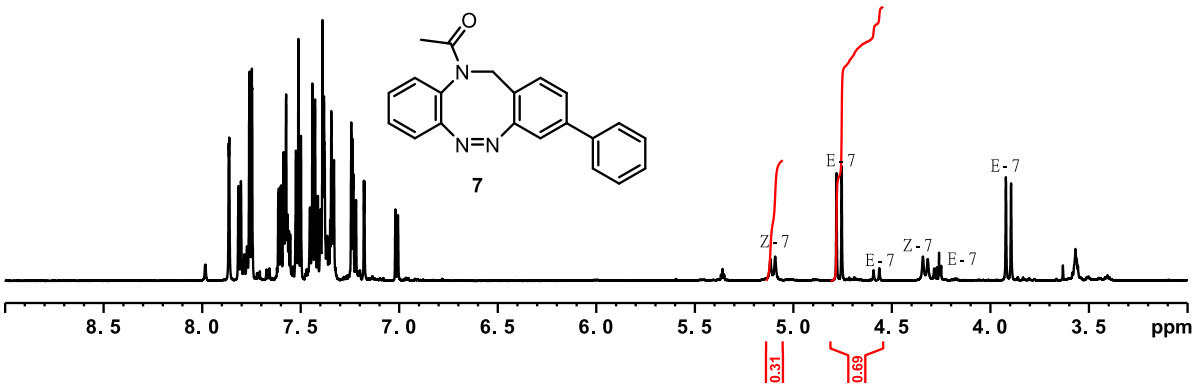

Figure SIV.4: ^{1}H-NMR-spectra of **7** in CD_3CN at 298 K after irradiation with 405 nm.

IV.3 (*Z*)-1-(3-vinyldibenzo[c,g][1,2,5]triazocin-11(12*H*)-yl)ethan-1-one (8)

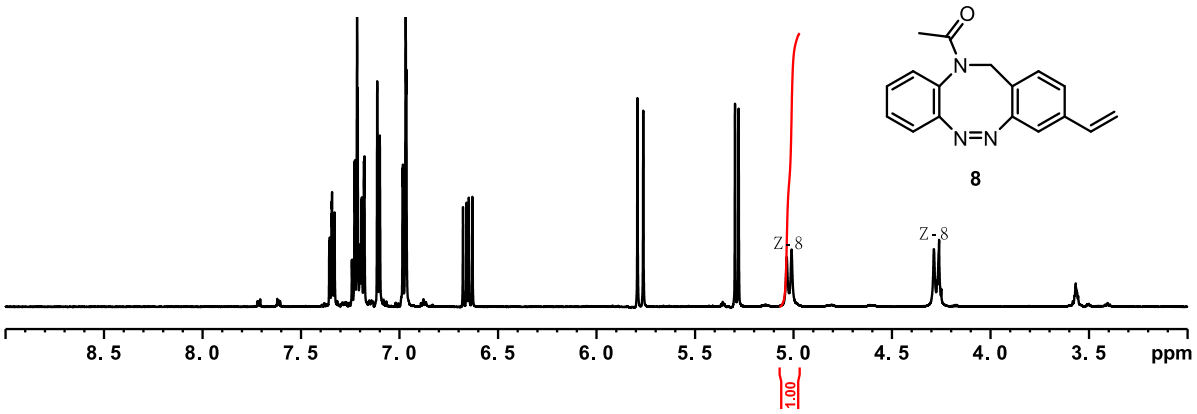

Figure SIV.5: ^{1}H-NMR-spectra of *Z*-**8** in CD_3CN at 298 K.

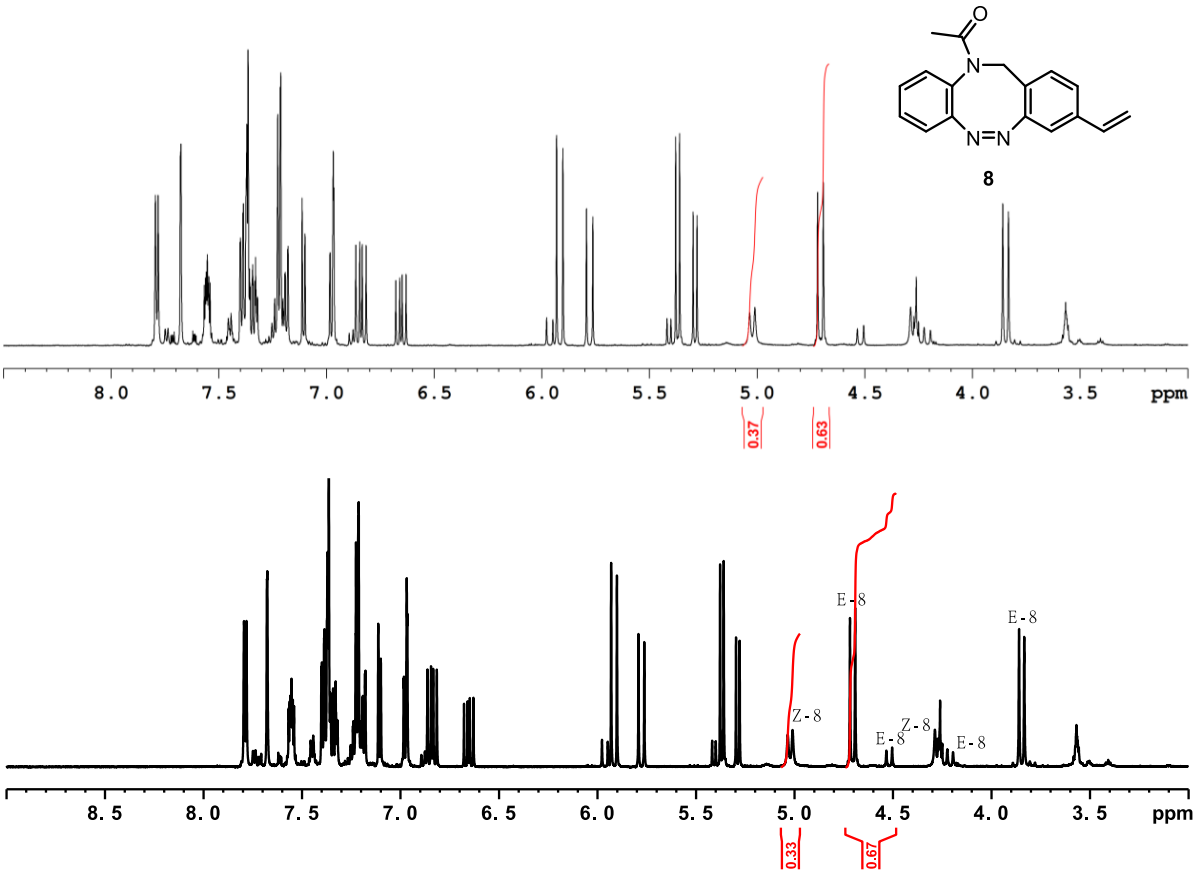

Figure SIV.6: ^{1}H-NMR-spectra of **8** in CD_3CN at 298 K after irradiation with 405 nm.

IV.4 (*Z*)-1-(3-(2,6-dimethylphenyl)dibenzo[c,g][1,2,5]triazocin-11(12*H*)-yl)ethan-1-one (9)

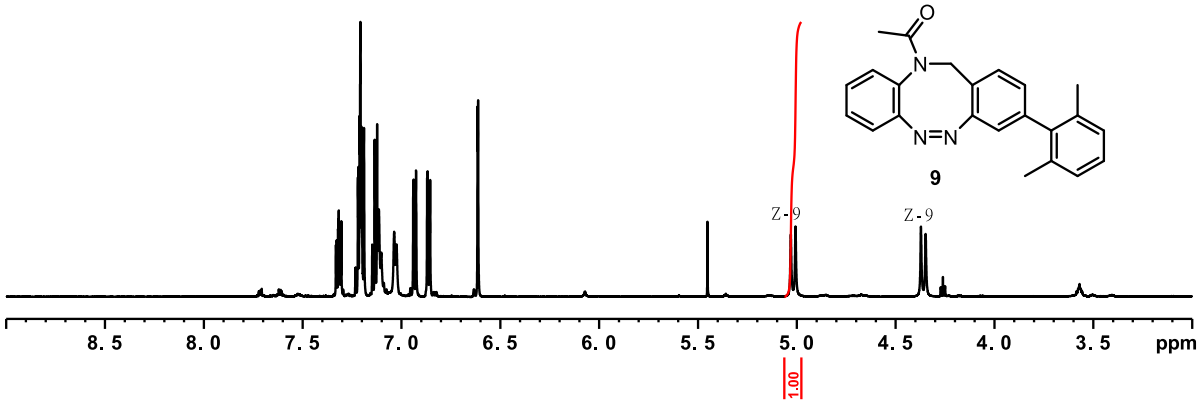

Figure SIV.7: ^{1}H-NMR-spectra of *Z*-**9** in CD_3CN at 298 K.

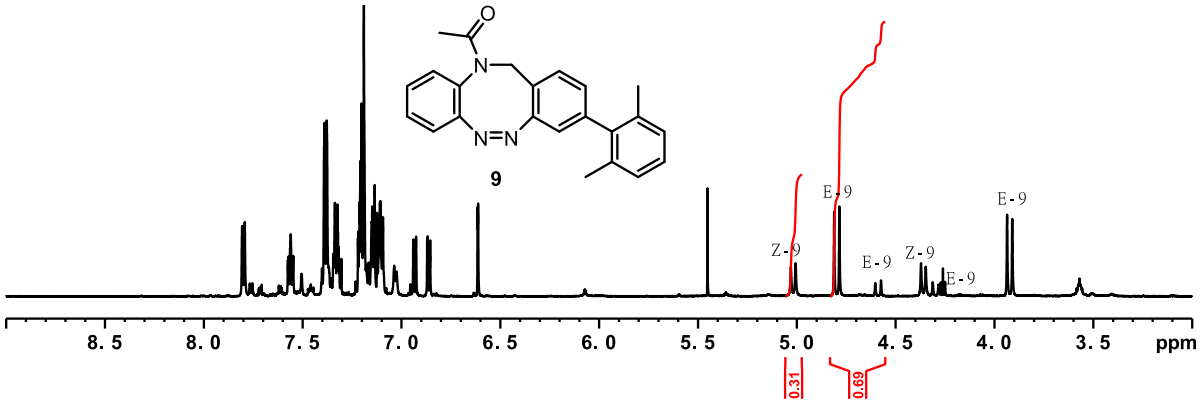

Figure SIV.8: ^{1}H-NMR-spectra of **9** in CD_3CN at 298 K after irradiation with 405 nm.

IV.5 (*Z*)-1-(3-(2-bromophenyl)dibenzo[c,g][1,2,5]triazocin-11(12*H*)-yl)ethan-1-one (10)

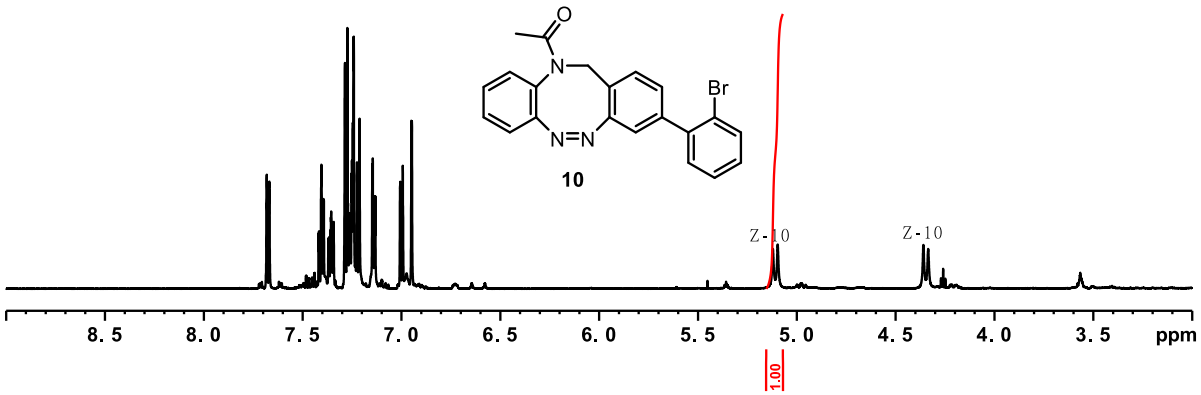

Figure SIV.9: ^{1}H-NMR-spectra of *Z*-**10** in CD_3CN at 298 K.

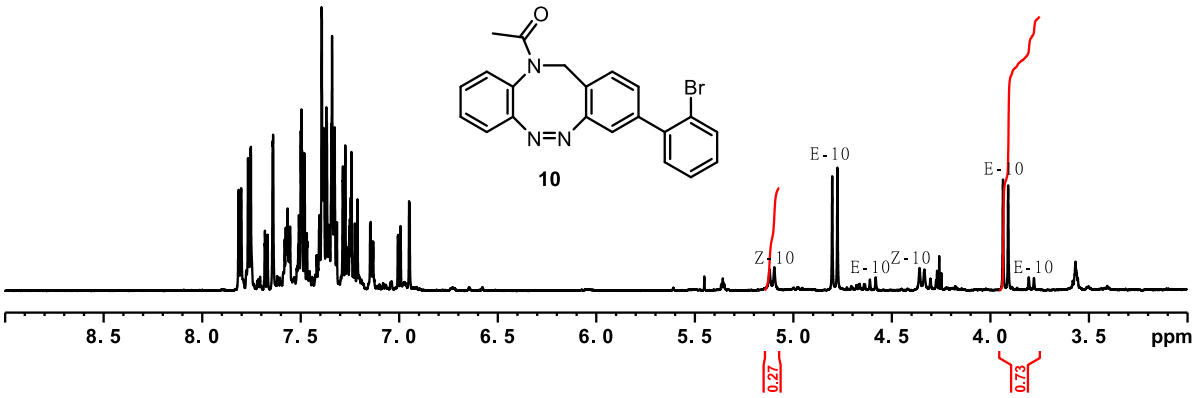

Figure SIV.10: ^{1}H-NMR-spectra of **10** in CD_3CN at 298 K after irradiation with 405 nm.

IV.6 (*Z*)-1-(3-(4-fluorophenyl)dibenzo[c,g][1,2,5]triazocin-11(12*H*)-yl)ethan-1-one (11)

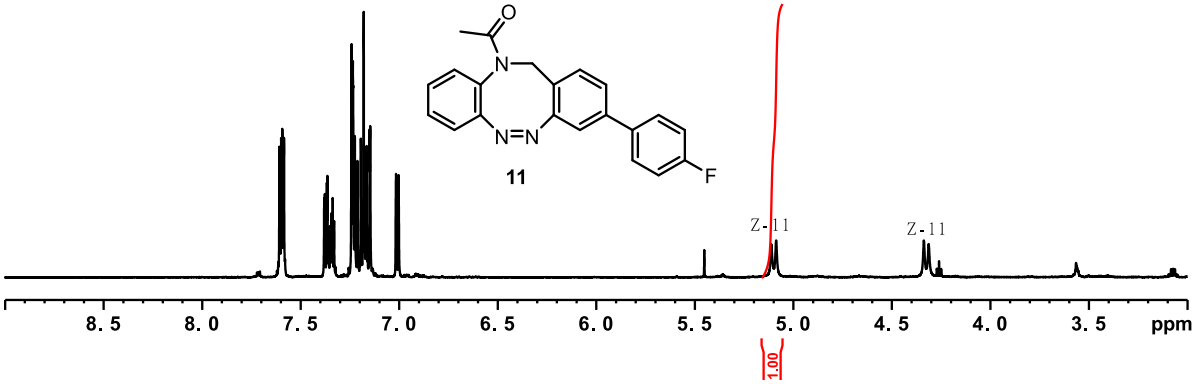

Figure SIV.11: ^{1}H-NMR-spectra of *Z*-**11** in CD_3CN at 298 K.

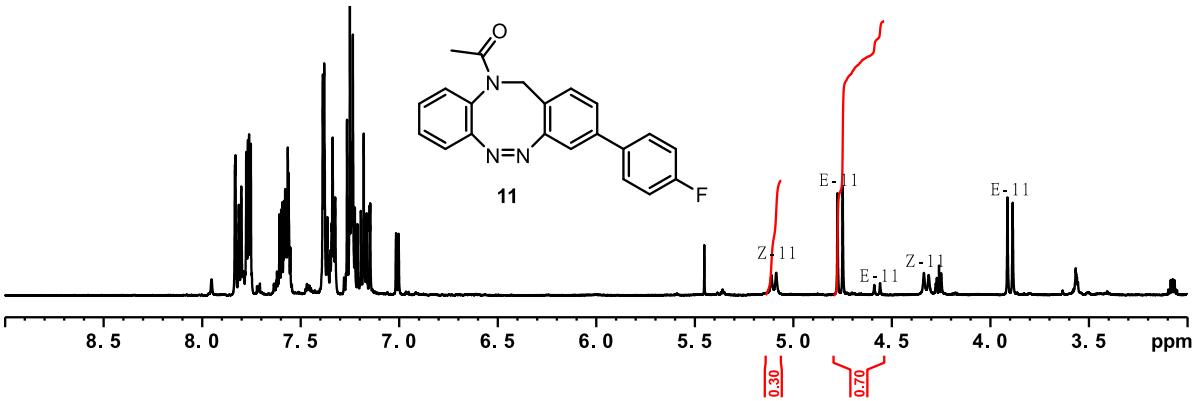

Figure SIV.12: ^{1}H-NMR-spectra of **11** in CD_3CN at 298 K after irradiation with 405 nm.

IV.7 (*Z*)-2-(11-acetyl-11,12-dihydrodibenzo[c,g][1,2,5]triazocin-3-yl)benzaldehyde (12)

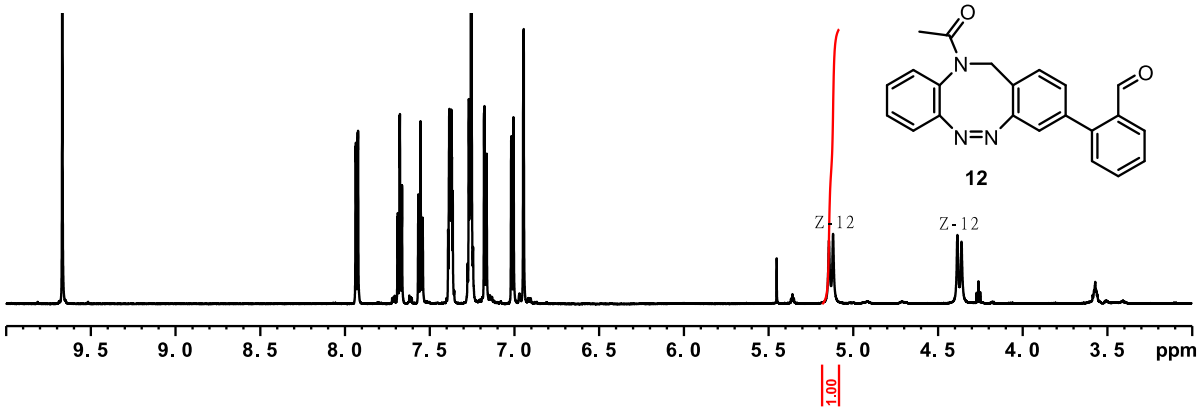

Figure SIV.13: ^{1}H-NMR-spectra of *Z*-**12** in CD_3CN at 298 K.

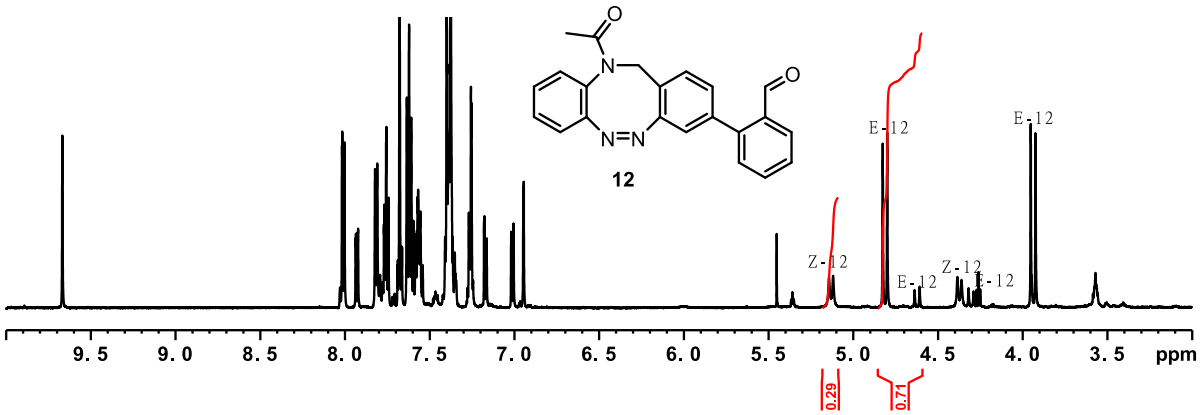

Figure SIV.14: ^{1}H-NMR-spectra of **12** in CD_3CN at 298 K after irradiation with 405 nm.

IV.8 (*Z*)-2-(11-acetyl-11,12-dihydrodibenzo[c,g][1,2,5]triazocin-3-yl)benzoic acid (13)

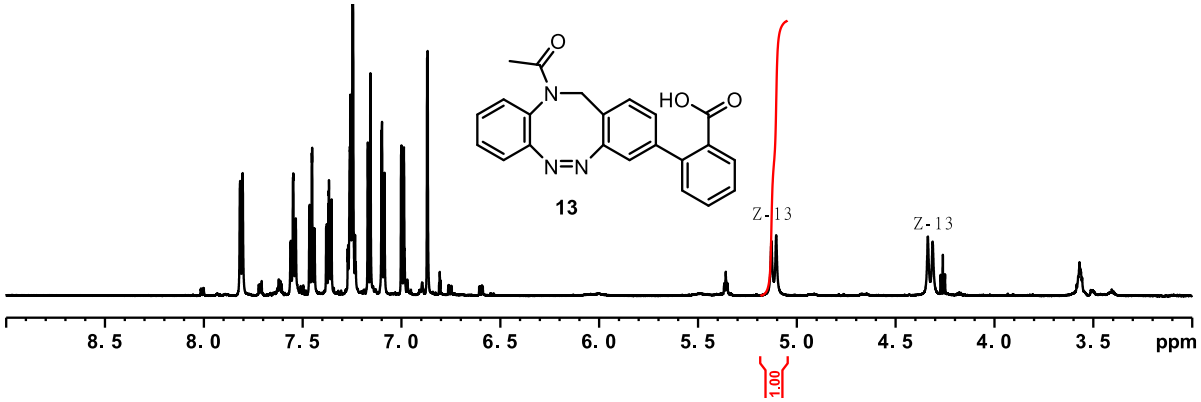

Figure SIV.15: ^{1}H-NMR-spectra of *Z*-**13** in CD_3CN at 298 K.

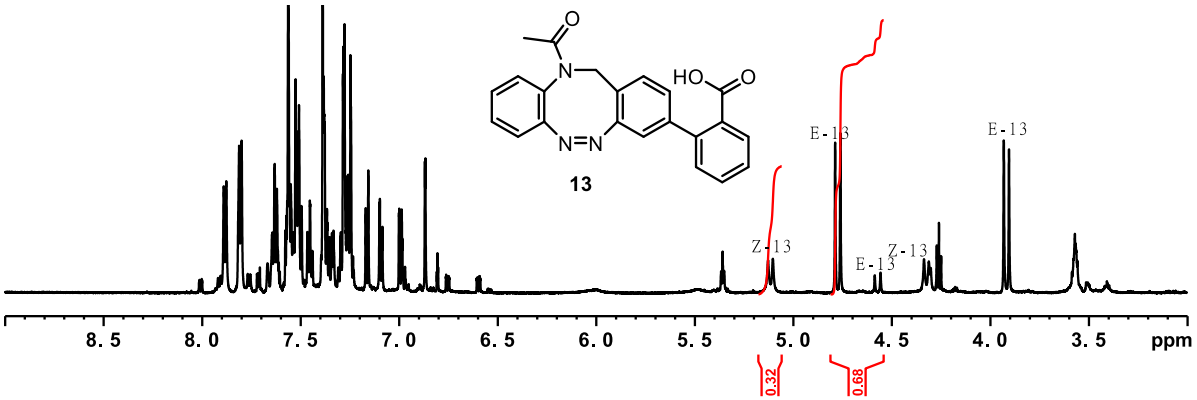

Figure SIV.16: ^{1}H-NMR-spectra of **13** in CD_3CN at 298 K after irradiation with 405 nm.

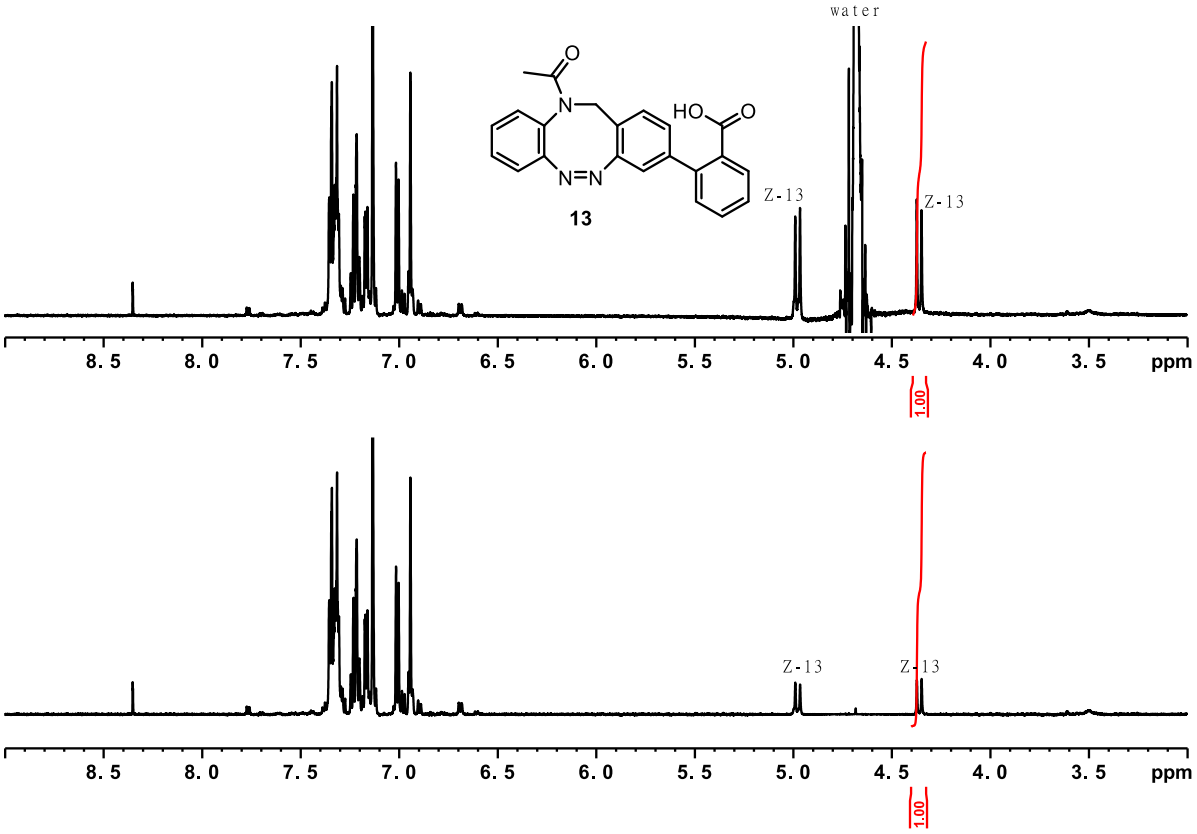

Figure SIV.17: ^{1}H-NMR-spectra of *Z*-**13** in D_2O pH 9 at 298 K (top) and the ^{1}H-NMR-Spektrum of **13** in D_2O pH 9 at 298 K with baseline correction and water suppression performed with MestReNova 14.3.1 NMR analysis Software by Mestrelab (bottom).

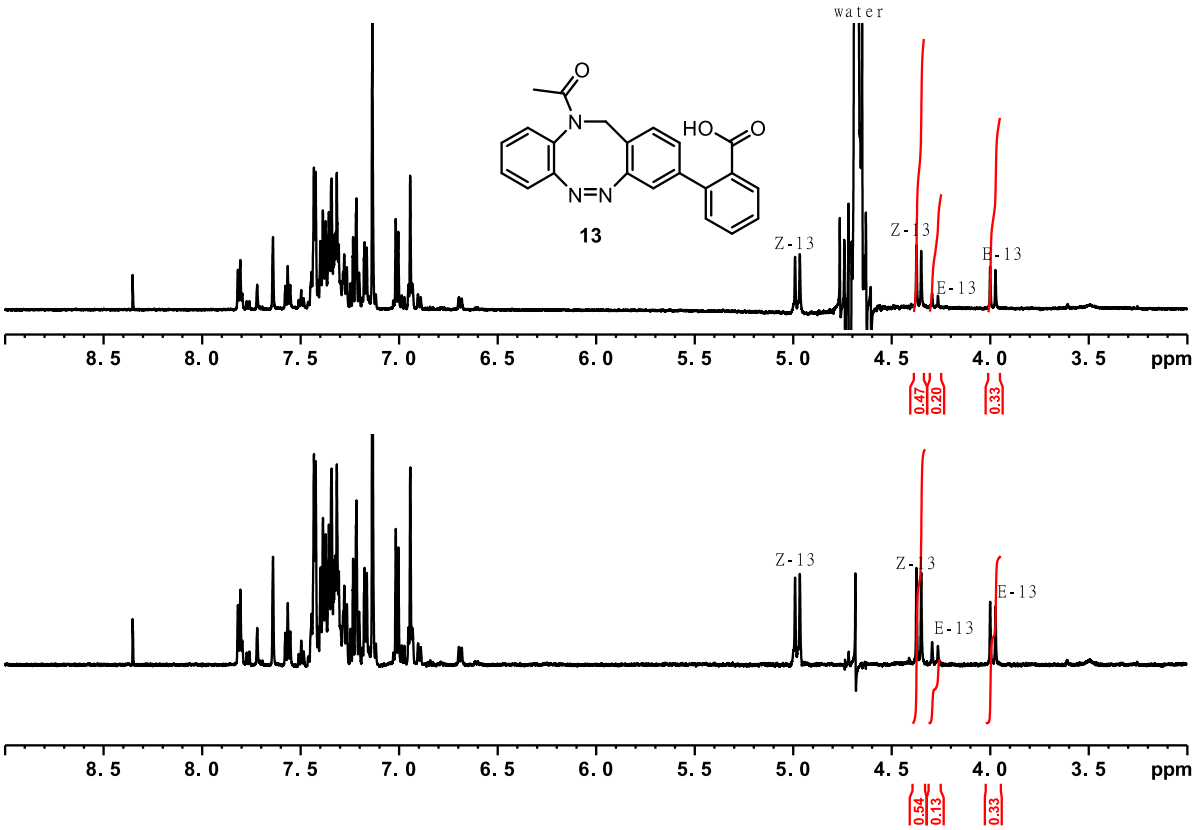

Figure SIV.18: ^{1}H-NMR-spectra of **13** in D_2O pH 9 at 298 K after irradiation with 405 nm (top) and the ^{1}H-NMR-Spektrum of **13** in D_2O pH 9 at 298 K after irradiation with 405 nm with baseline correction and water suppression performed with MestReNova 14.3.1 NMR analysis Software by Mestrelab (bottom)..

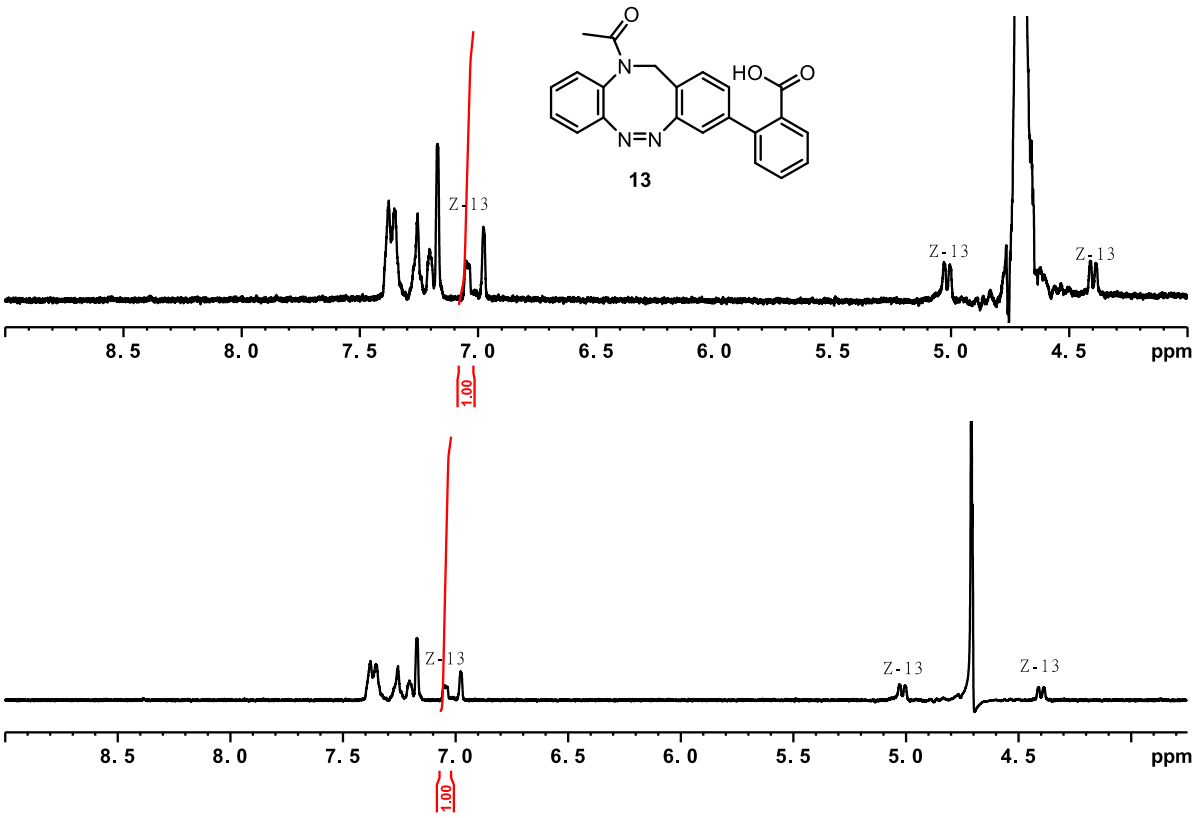

Figure SIV.19: ^{1}H-NMR-spectra of **13** in D_2O PBS buffer solution pH 7.4 at 298 K (top) and the ^{1}H-NMR-Spektrum of **13** in D_2O PBS buffer solution pH 7.4 at 298 K with baseline correction and water suppression performed with MestReNova 14.3.1 NMR analysis Software by Mestrelab (bottom).

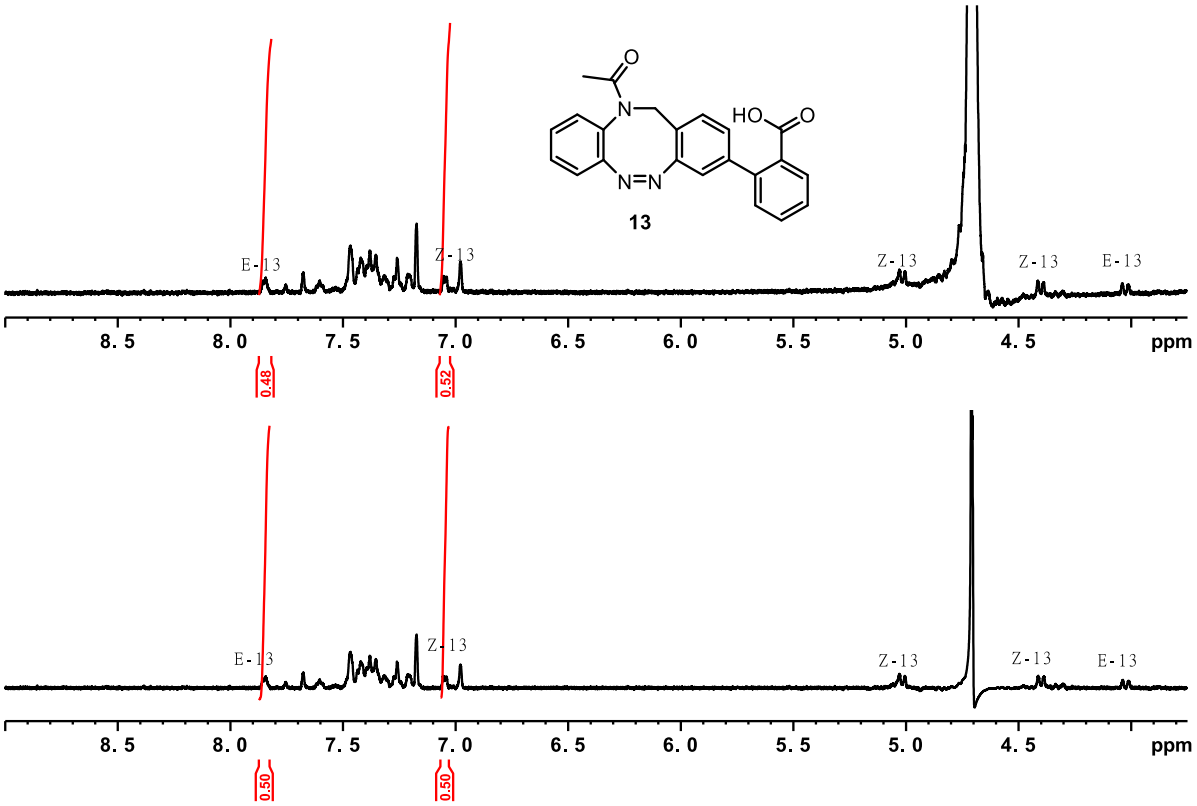

Figure SIV.20: ^{1}H-NMR-spectra of **13** in D_2O PBS buffer solution pH 7.4 at 298 K after irradiation with 405 nm (top) and the ^{1}H-NMR-Spektrum of **13** in D_2O PBS buffer solution pH 7.4 at 298 K after irradiation with 405 nm with

baseline correction and water suppression performed with MestReNova 14.3.1 NMR analysis Software by Mestrelab (bottom).

IV.9 (*Z*)-1-(3-(pyridine-4-yl)dibenzo[c,g][1,2,5]triazocin-11(12*H*)-ethan-1-one (14)

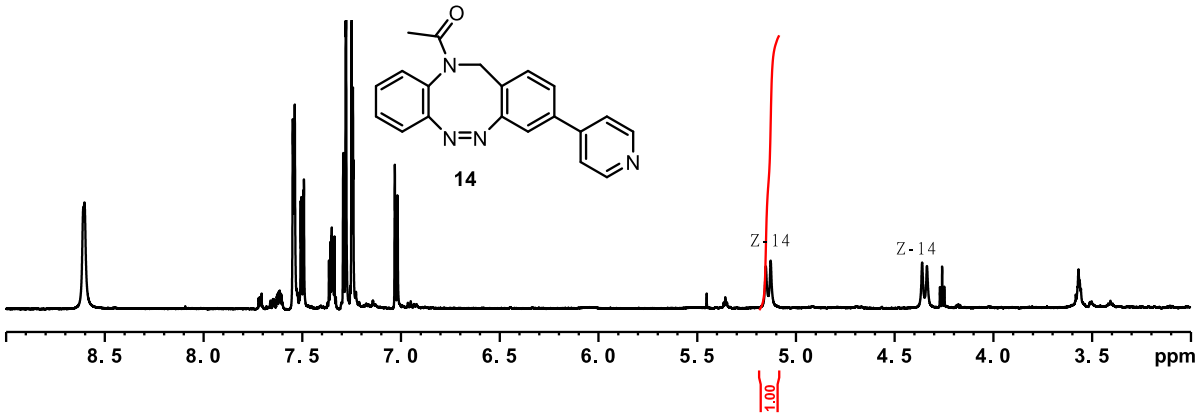

Figure SIV.21: ^{1}H-NMR-spectra of **14** in CD_3CN at 298 K.

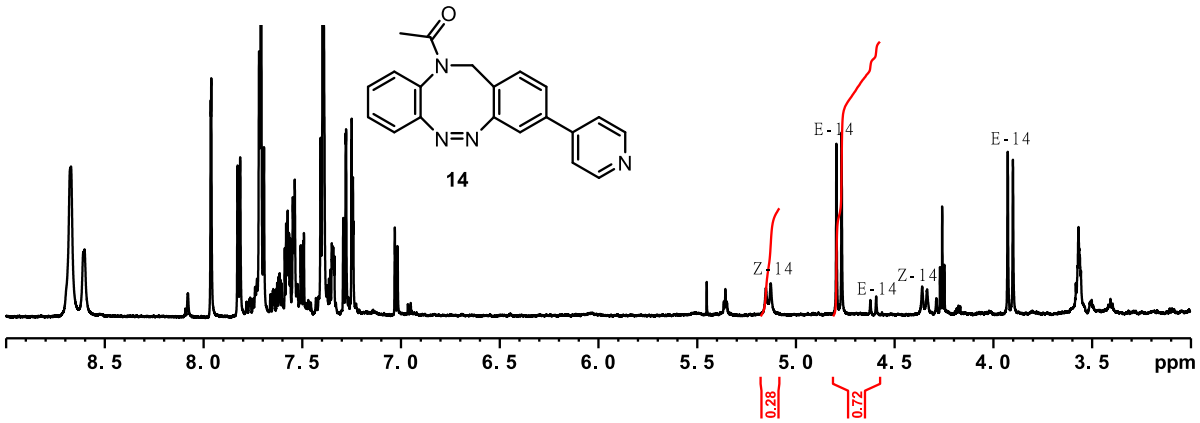

Figure SIV.22: ^{1}H-NMR-spectra of **14** in CD_3CN at 298 K after irradiation with 405 nm.

IV.10 (*Z*)-1-(3-benzyldibenzo[c,g][1,2,5]triazocin-11(12*H*)-ethan-1-one (17)

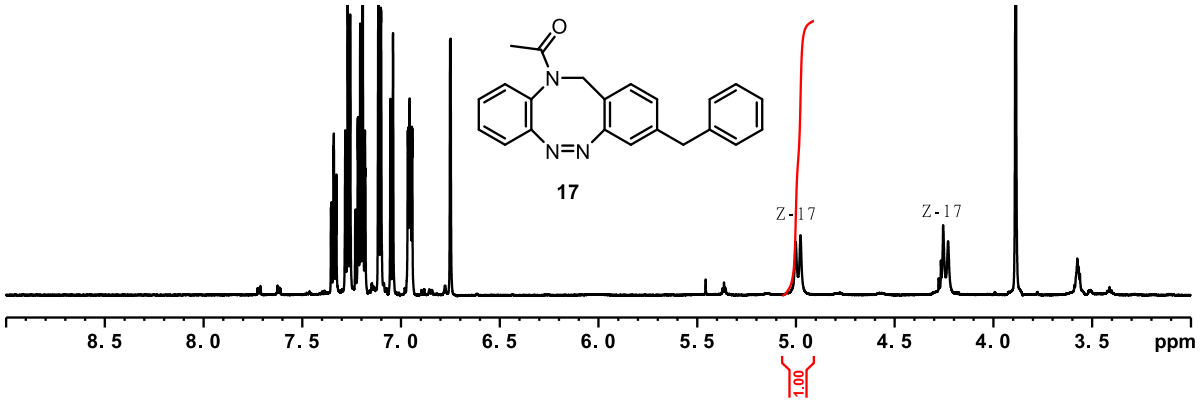

Figure SIV.23: ^{1}H-NMR-spectra of **17** in CD_3CN at 298 K.

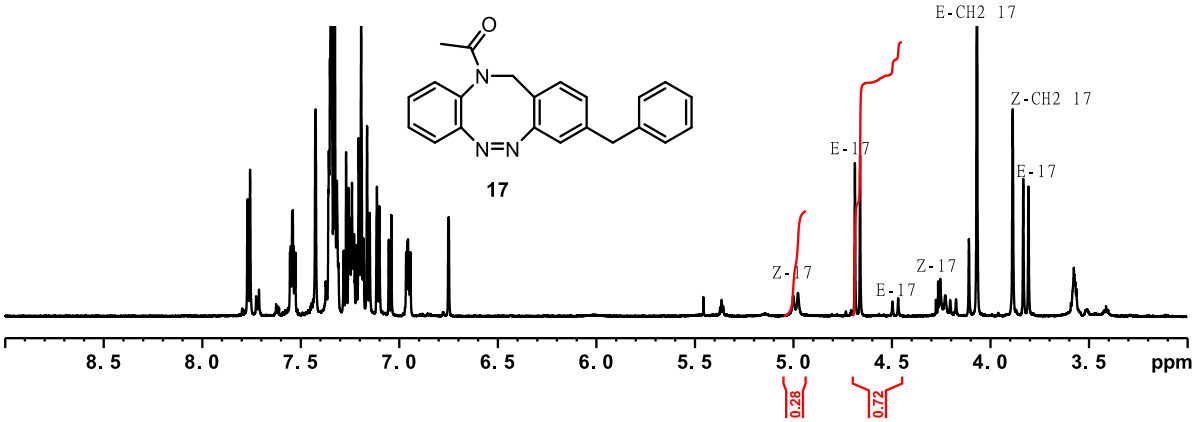

Figure SIV.24: ^{1}H-NMR-spectra of **17** in CD_3CN at 298 K after irradiation with 405 nm.

IV.11 *tert*-butyl-(*Z*)-(11-acetyl-11,12-dihydrodiebenzo[c,g][1,2,5]triazocin-3-yl)carbamate (19)

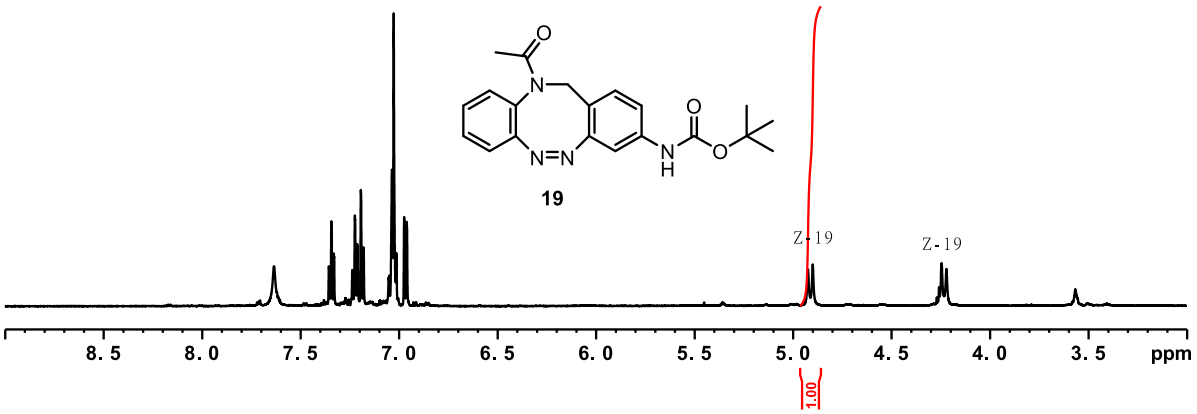

Figure SIV.25: ^{1}H-NMR-spectra of **19** in CD_3CN at 298 K.

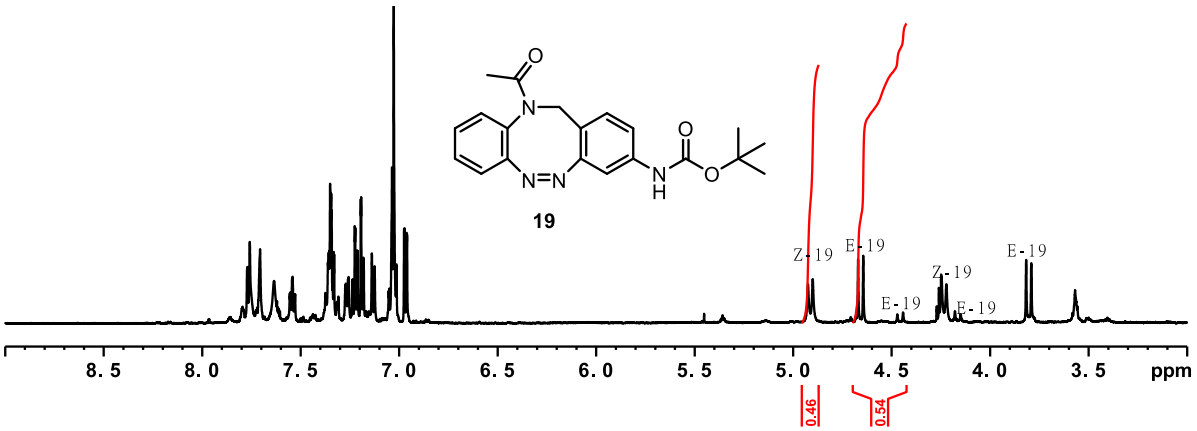

Figure SIV.26: ^{1}H-NMR-spectra of **19** in CD_3CN at 298 K after irradiation with 405 nm.

IV.12 (*Z*)-1-(3-(diphenylamino)dibenzo[c,g][1,2,5]triazocin-11(12*H*)-yl)ethan-1-one (20)

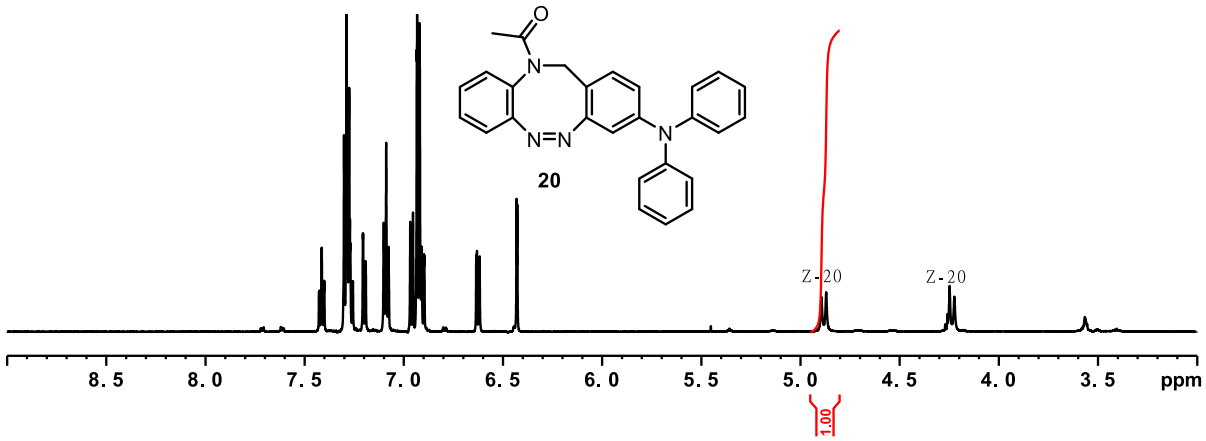

Figure SIV.27: ^{1}H-NMR-spectra of **20** in CD_3CN at 298 K.

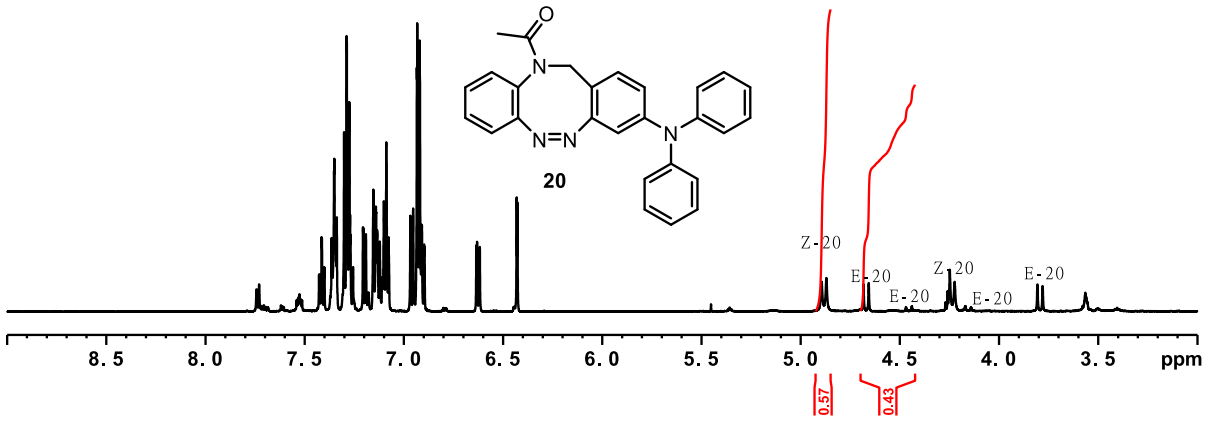

Figure SIV.28: ^{1}H-NMR-spectra of **20** in CD_3CN at 298 K after irradiation with 405 nm.

IV.13 (*Z*)-1-(3-aminodibenzo[c,g][1,2,5]triazocin-11(12*H*)-yl)ethan-1-one (21)

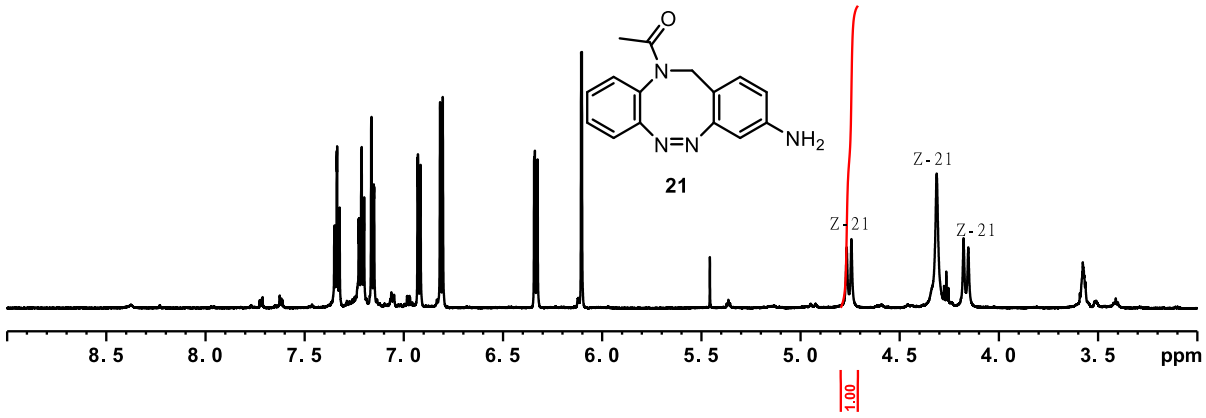

Figure SIV.29: ^{1}H-NMR-spectra of **21** in CD_3CN at 298 K.

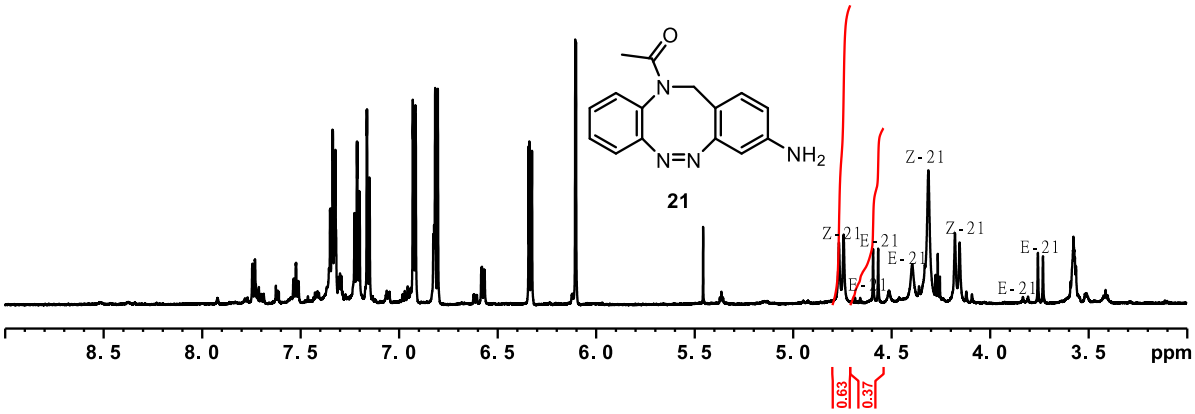

Figure SIV.30: ^{1}H-NMR-spectra of **21** in CD_3CN at 298 K after irradiation with 405 nm.

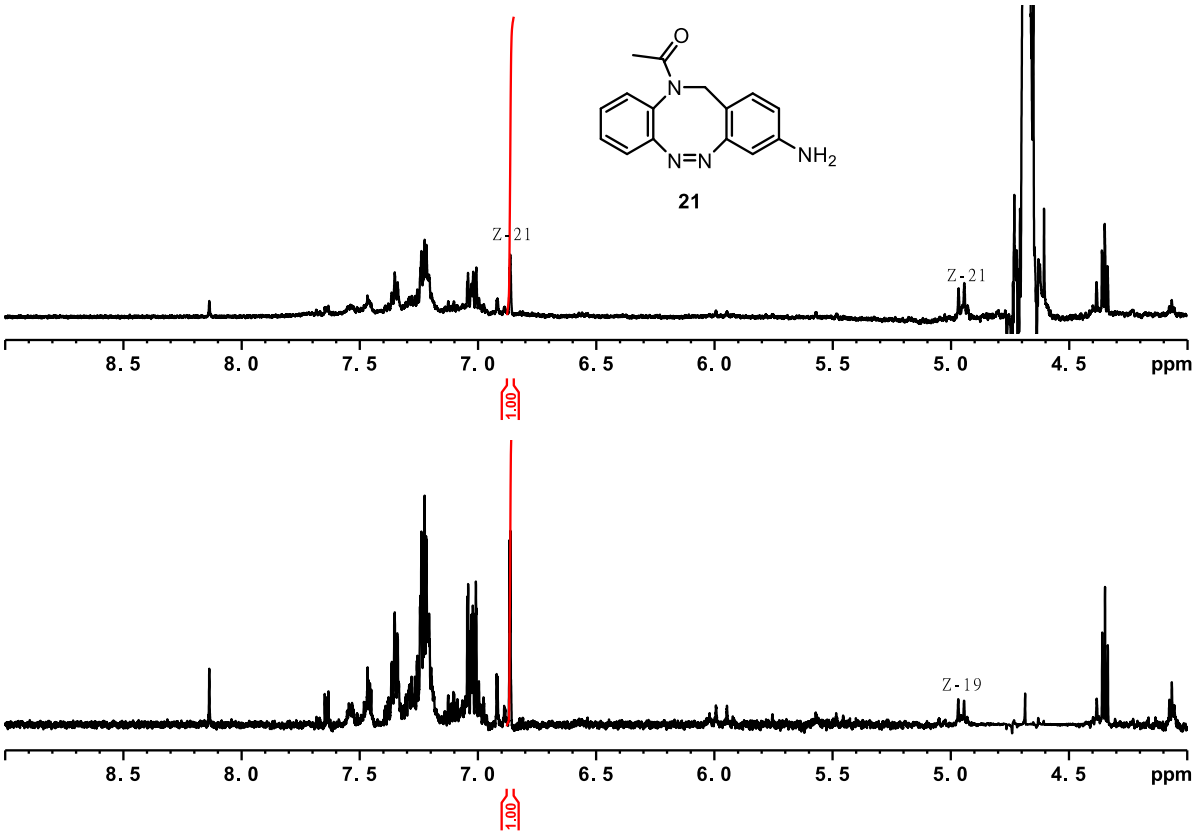

Figure SIV.33: ^{1}H-NMR-spectra of **21** in D_2O pH 3.5 at 298 K (top) and the ^{1}H-NMR-Spektrum of **23** in D_2O pH 3.5 at 298 K with baseline correction and water suppression performed with MestReNova 14.3.1 NMR analysis Software by Mestrelab (bottom).

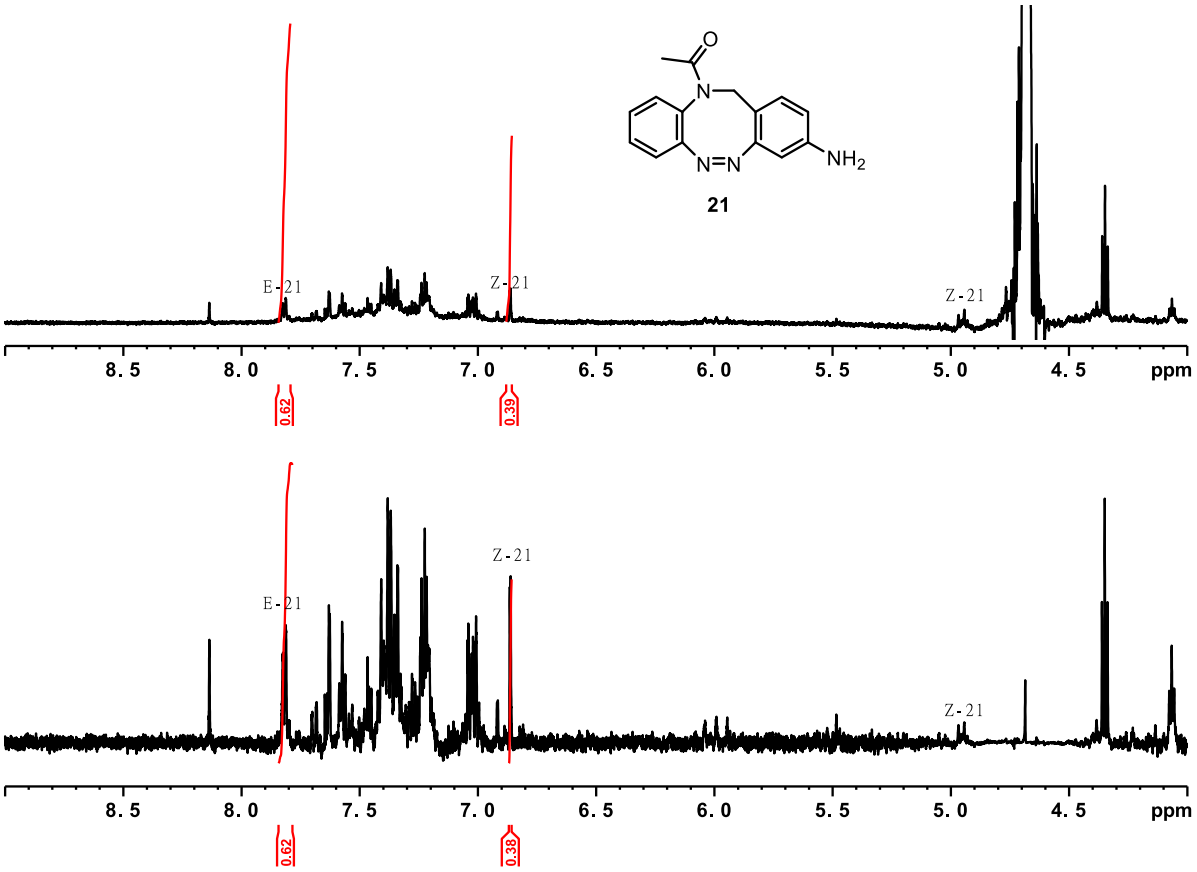

Figure SIV.34: ^{1}H-NMR-spectra of **21** in D_2O pH 3.5 at 298 K after irradiation with 405 nm (top) and the ^{1}H-NMR-Spektrum of **23** in D_2O pH 3.5 at 298 K after irradiation with 405 nm with baseline correction and water suppression performed with MestReNova 14.3.1 NMR analysis Software by Mestrelab (bottom)

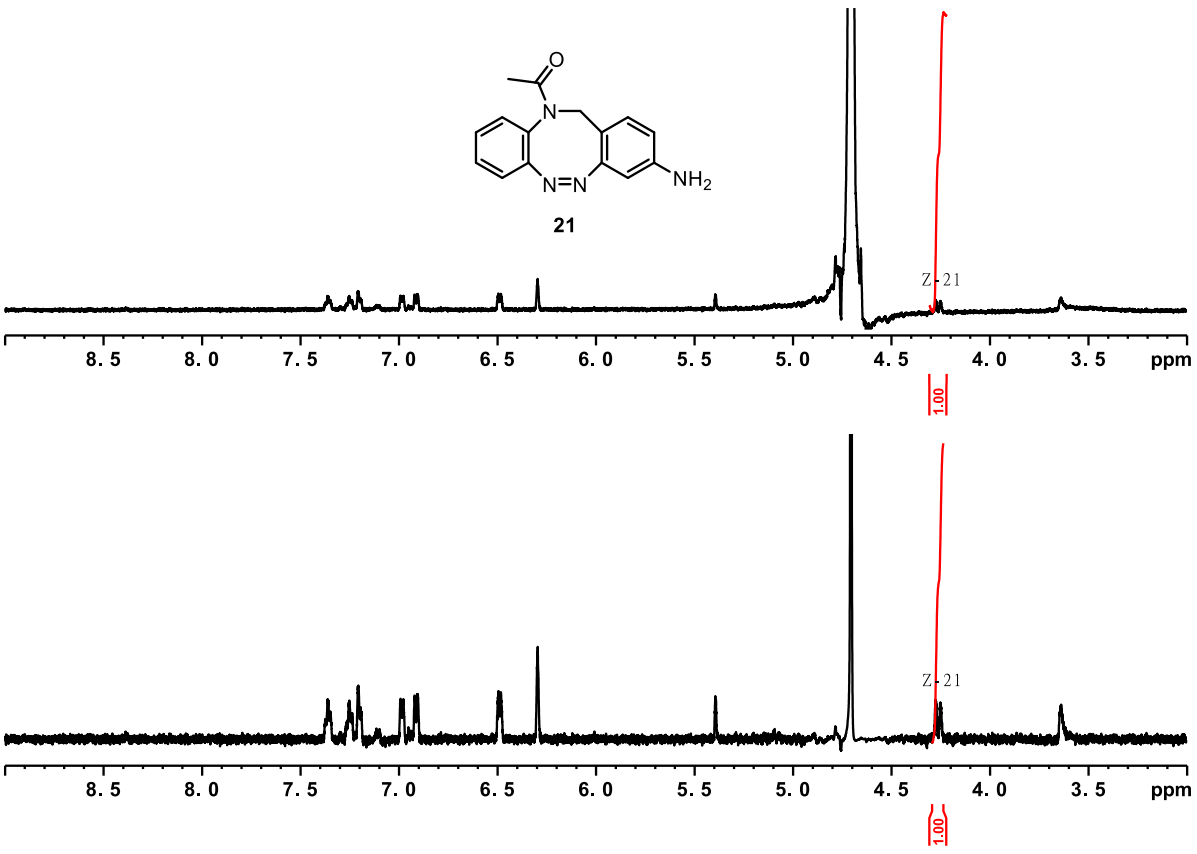

Figure SIV.35: ^{1}H-NMR-spectra of **21** in D_2O PBS buffer solution pH 7.4 at 298 K (top) and the ^{1}H-NMR-Spektrum of **23** in D_2O PBS buffer solution pH 7.4 at 298 K with baseline correction and water suppression performed with MestReNova 14.3.1 NMR analysis Software by Mestrelab (bottom).

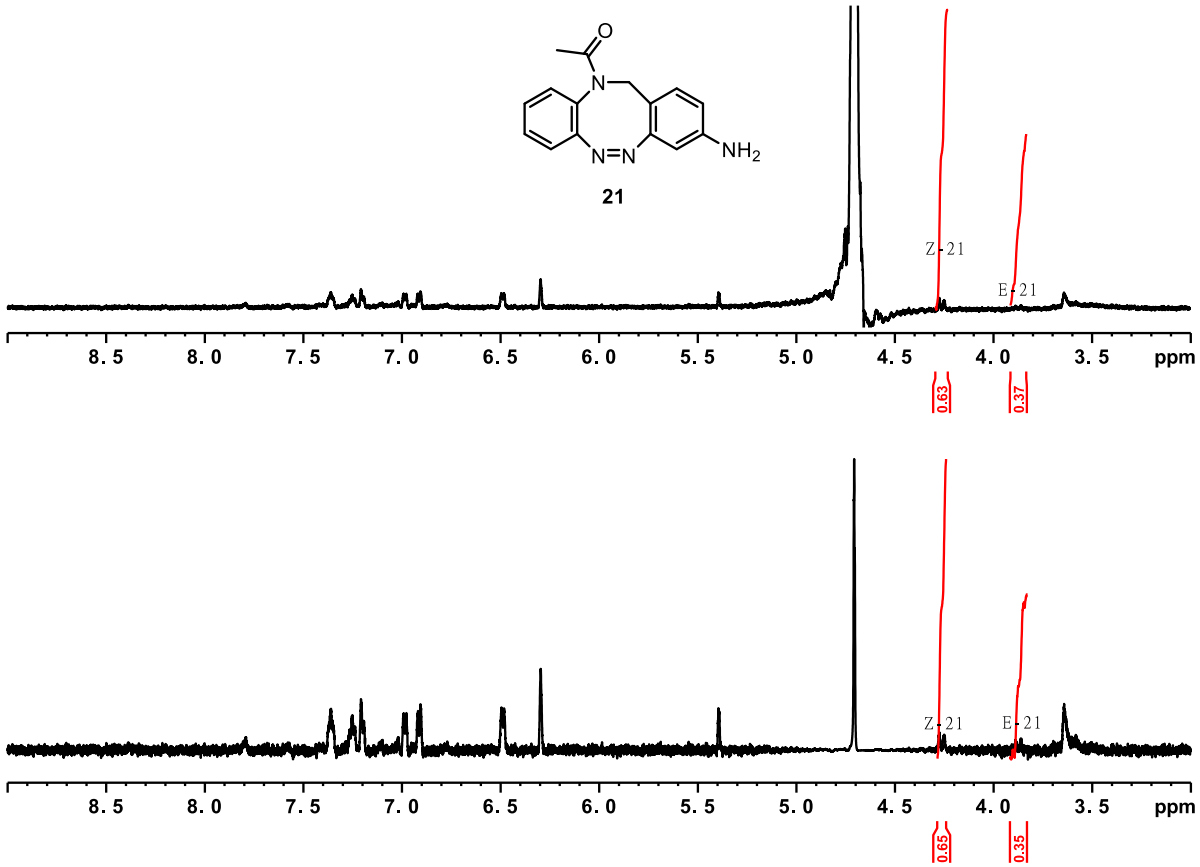

Figure SIV.36: ^{1}H-NMR-spectra of **21** in D_2O PBS buffer solution pH 7.4 at 298 K after irradiation with 405 nm (top) and the ^{1}H-NMR-Spektrum of **23** in D_2O PBS buffer solution pH 7.4 at 298 K after irradiation with 405 nm with baseline correction and water suppression performed with MestReNova 14.3.1 NMR analysis Software by Mestrelab (bottom).

IV.14 (*Z*)-11-acetyl-11,12-dihydrodibenzo[c,g][1,2,5]triazocine-3-carbonitrile (23)

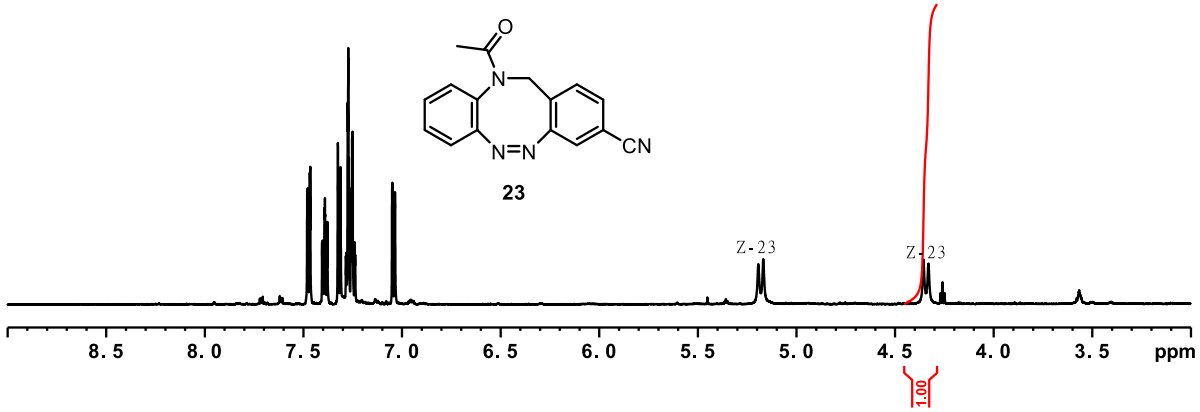

Figure SIV.37: ^{1}H-NMR-spectra of **23** in CD_3CN at 298 K.

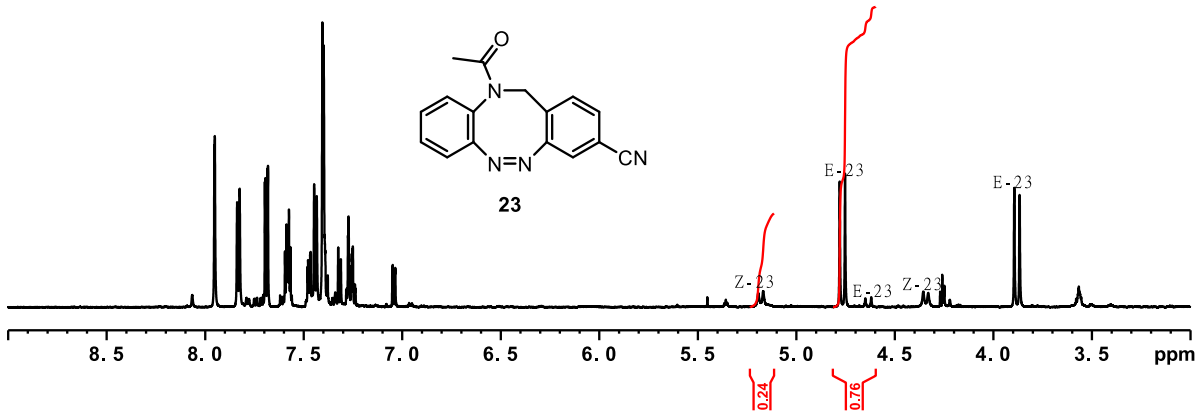

Figure SIV.38: ^{1}H-NMR-spectra of **23** in CD_3CN at 298 K after irradiation with 405 nm.

V. X-ray crystallographic data

Preparation of crystal samples

For crystal growth 10 mg of the given compound were dissolved in 0.2 ml acetone in a small glass vial and a drop of water was added. The vial was closed with a perforated cap and was stored in the dark for 3 weeks for slow evaporation of the solvent. Suitable crystals were selected subsequently.

General

The data collections were performed with a XtaLAB Synergy, Dualflex, HyPix diffractometer with a micro focus tube using Cu-Kα radiation (λ = 1.54184 Å). The structures were solved with SHELXT [1] and refined with SHELXL-2016 [2] using Least Squares minimisation. All non-hydrogen atoms were refined anisotropic. The C-H H atoms were positioned with idealized geometry, methyl H atoms allowed to rotate but not to tip, and were refined isotropic with $U_{iso}(H) = 1.2\ U_{eq}(C)$ (1.5 for methyl H atoms) using a riding model. In compound **1**, the hydrogen atoms of the methyl group are disordered and were refined in two orientations, each rotated by 60 ° (AFIX 127).
ORTEP plots of all compounds can be found in figure SV.1, SV.2 and SV.3.

CCDC-2329263 (**1**), CCDC-2329261 (**2**), and CCDC- 2329262 (**7**) contain the supplementary crystallographic data for this paper. These data can be obtained free charge from the Cambridge Crystallographic Data Centre via http://www.ccdc.cam.ac.uk/data_request/cif.

1. Sheldrick, G.M. (2015). *Acta Cryst*. A71, 3-8.
2. Sheldrick, G.M. (2015). *Acta Cryst*. C71, 3-8.

Table SV.1: Selected crystal data and details of the structure determinations for the diazocine compounds **1**, **2** and **7**.

	1	**2**	**7**
Formula	$C_{15}H_{13}N_3O$	$C_{15}H_{12}BrN_3O$	$C_{21}H_{17}N_3O$
MW /g mol^{-1}	251.28	330.19	327.38
Crystal system	monoclinic	triclinic	monoclinic
Space group	$P2_1/n$	$P\bar{1}$	$P2_1/n$
a /Å	8.7563(1)	7.4471(2)	11.1465(1)
b /Å	8.7647(1)	9.2088(2)	13.0070(1)
c /Å	16.8947(1)	10.8243(2)	11.8469(1)
α /deg	90	84.031(2)	90
β /deg	101.974(1)	77.293(2)	91.709(1)
γ /deg	90	81.905(2)	90
V /Å^3	1268.40(2)	714.87(3)	1716.83(2)
T /K	293	293	293
Z	4	2	4
D_{calcd} /g cm^{-3}	1.316	1.534	1.267
μ /mm^{-1}	0.687	3.911	0.634
2 θ_{max} /deg	159.062	160.064	159.654
Refl. collected	21811	12222	18993
Refl. unique	2704	3001	3685

R_{int}	0.0214	0.0263	0.0188
Refl. [$F_0 > 4\ \sigma(F_0)$]	2592	2885	3440
Parameters	174	182	228
R_1 [$F_0 > 4\ \sigma(F_0)$]	0.0342	0.0381	0.0426
wR_2 (all data)	0.0986	0.1067	0.1230
GOF	1.054	1.035	1.058
$\Delta\rho_{max;\ min}$ /*e* Å^{-3}	0.19; –0.17	0.92; –0.70	0.20; –0.17

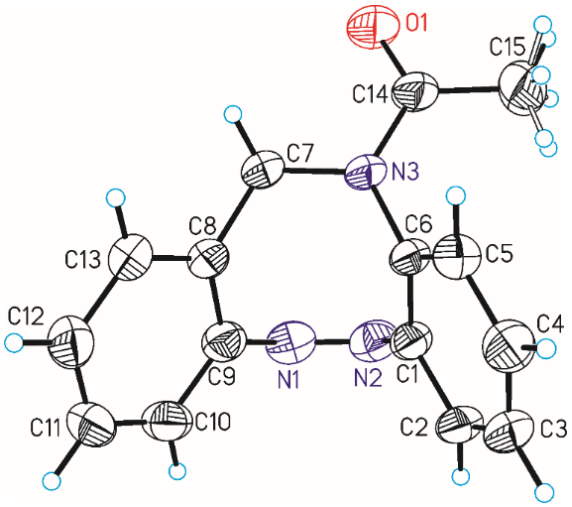

Figure SV.1: Crystal structure of *N*-acetyl diazocine **1** with labeling and displacement ellipsoids drawn at the 50% probability level.

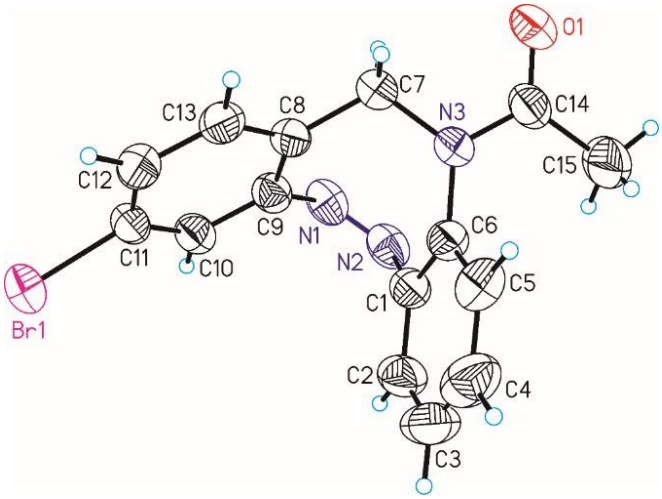

Figure SV.2: Crystal structure of bromo-*N*-acetyl diazocine **2** with labeling and displacement ellipsoids drawn at the 50% probability level.

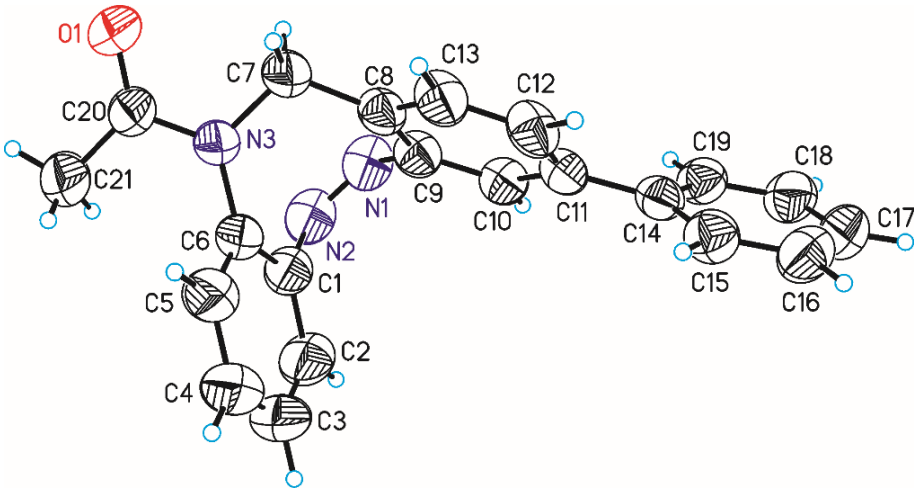

Figure SV.3: Crystal structure of phenyl-*N*-acetyl diazocine **7**.

VI. References

[1] Lentes, P.; Rudtke, J.; Griebenow, T.; Herges, R. Substituted nitrogen-bridged diazocines. *Beilstein J. Org. Chem.* **2021**, *17*, 1503-1508.

[2] Maier, M. S.; Hüll, K.; Reynders, M.; Matsuura, B. S.; Leippe, P.; Ko, T.; Schäffer, L.; Trauner, D. Oxidative Approach Enables Efficient Access to Cyclic Azobenzenes. *J. Am. Chem. Soc.* **2019**, *141*, 17295-17304.

[3] Denmark, S. E.; Butler, C. R.; Vinylation of Aryl Bromides Using an Inexpensive Vinylpolysiloxane. *Org. Lett.* **2006**, *8*, 63-66.

8.2.5 Light-Switchable Diazocines as Potential Inhibitors of Testosterone-Synthesizing 17β-Hydroxysteroid Dehydrogenase 3

Supplementary material to the manuscript

"Light-switchable diazocines as potential inhibitors of testosterone-synthesizing 17β-hydroxysteroid dehydrogenase 3"

Wages F. [1], Brandt T.[2], Martin H.-J.[1], Herges R.[2], Maser E.[1]
[1]Institute of Toxicology and Pharmacology for Natural Scientists, University Medical School Schleswig-Holstein, Campus Kiel, Brunswiker Str. 10, 24105 Kiel, Germany
[2]Otto Diels Institute of Organic Chemistry, Christian-Albrecht University of Kiel, Otto Hahn Platz 4, 24118 Kiel, Germany

Table of contents

Figure S10.2: UV-vis spectra of the half-life determination of pDA in aqueous solution with 2% DMSO at 25 °C with the corresponding first order kinetics plot.

Figure S11.1: UV-vis spectra of 50 µM dmpDA in aqueous solution with 2 % DMSO at 25 °C.

Figure S11.2: UV-vis spectra of the half-life determination of dmpDA in aqueous solution with 2 % DMSO at 25 °C with the corresponding first order kinetics plot.

Figure S12.1: UV-vis spectra of 25 µM fpDA in aqueous solution with 2 % DMSO at 25 °C.

Figure S12.2: UV-vis spectra of the half-life determination of fpDA in aqueous solution with 2 % DMSO at 25 °C with the corresponding first order kinetics plot.

Figure S13.1: UV-vis spectra of 100 µM iDA in aqueous solution with 2 % DMSO at 25 °C.

Figure S13.2: UV-vis spectra of the half-life determination of iDA in aqueous solution with 2 % DMSO at 25 °C with the corresponding first order kinetics plot.

Figure S14.1: UV-vis spectra of 250 µM baDA in aqueous solution with 2 % DMSO at 25 °C.

Figure S14.2: UV-vis spectra of the half-life determination of baDA in aqueous solution with 2 % DMSO at 25 °C with the corresponding first order kinetics plot.

Figure S15.1: UV-vis spectra of 250 µM cnDA in aqueous solution with 2 % DMSO at 25 °C.

Figure S15.2: UV-vis spectra of the half-life determination of cnDA in aqueous solution with 2 % DMSO at 25 °C with the corresponding first order kinetics plot.

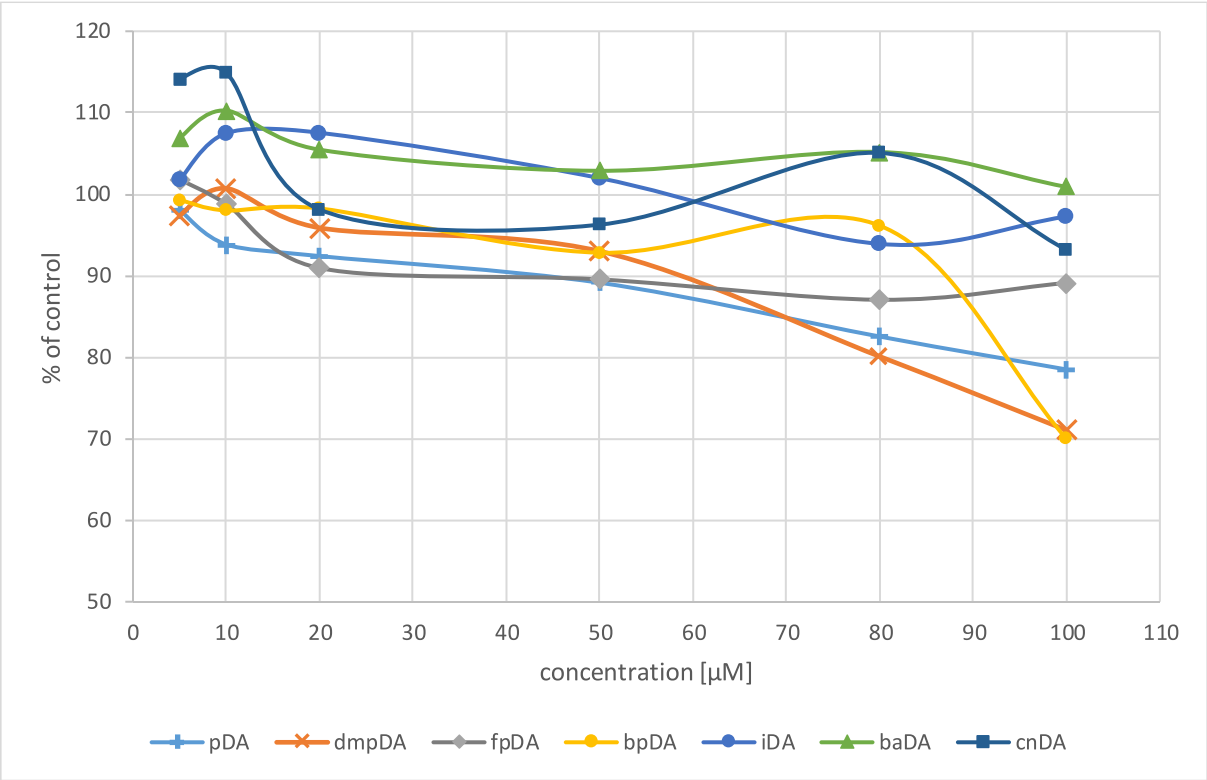

Fig. S1. Results of the 3-hour MTT cytotoxicity assay after treatment with seven different diazocines: phenyl N-acetyl diazocine (pDA), dimethylphenyl N-acetyl diazocine (dmpDA), fluorophenyl N-acetyl diazocine (fpDA), bromophenyl N-acetyl diazocine (bpDA), iodinated N-acetyl diazocine (iDA), benzoic acid N-acetyl diazocine (baDA) and cyano N-acetyl diazocine (cnDA). The colorimetric method is based on the reduction of the yellow tetrazolium dye (MTT = 3-(4,5-dimethylthiazol-2-yl)-2,5-diphenyltetrazolium bromide) by cellular enzymes and allows to assess metabolic activity and thus cell viability. The formation of the purple formazan by living cells was determined by spectrophotometer (595 nm). The different treatment groups are presented in percentage of the untreated control. Data are shown from n ≥ 3 independent experiments for each diazocine.

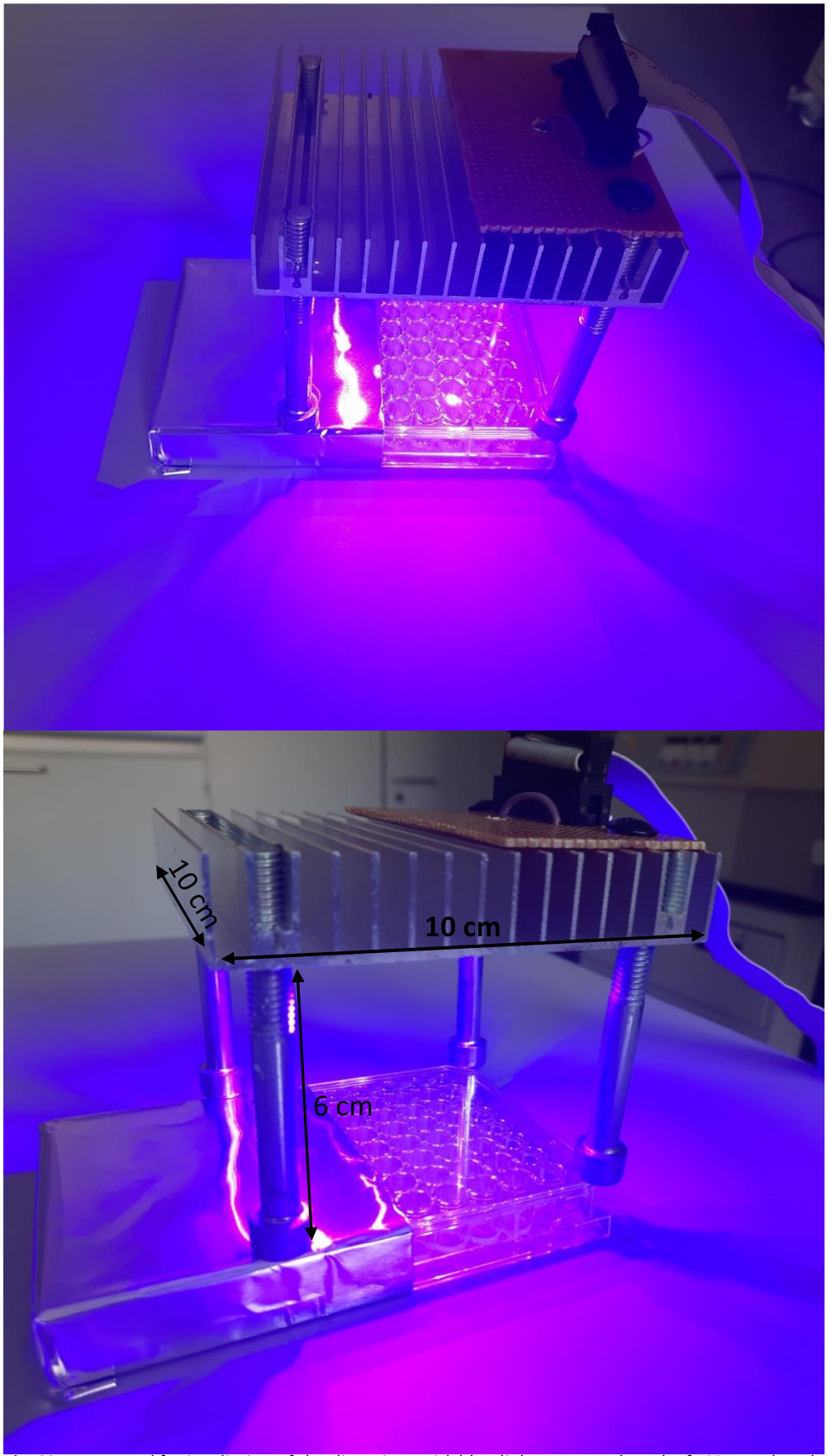

Fig. S2. Lamp used for irradiation of the diazocines with blue light at a wavelength of 400 nm placed on a 96-well plate (half covered with aluminum foil = non-irradiated samples) for microsome inhibition assay. Approximate distance to the light source (five light-emitting diodes (LEDs); 1st test series: VL400-5050, peak wavelenght typ. = 400 nm (Roithner LaserTechnik GmbH, Vienna, Austria); 2nd test series: NCSU275(T), peak wavelenght typ. = 405 nm (Nichia Corporation, Anan, Japan) was 6 cm.

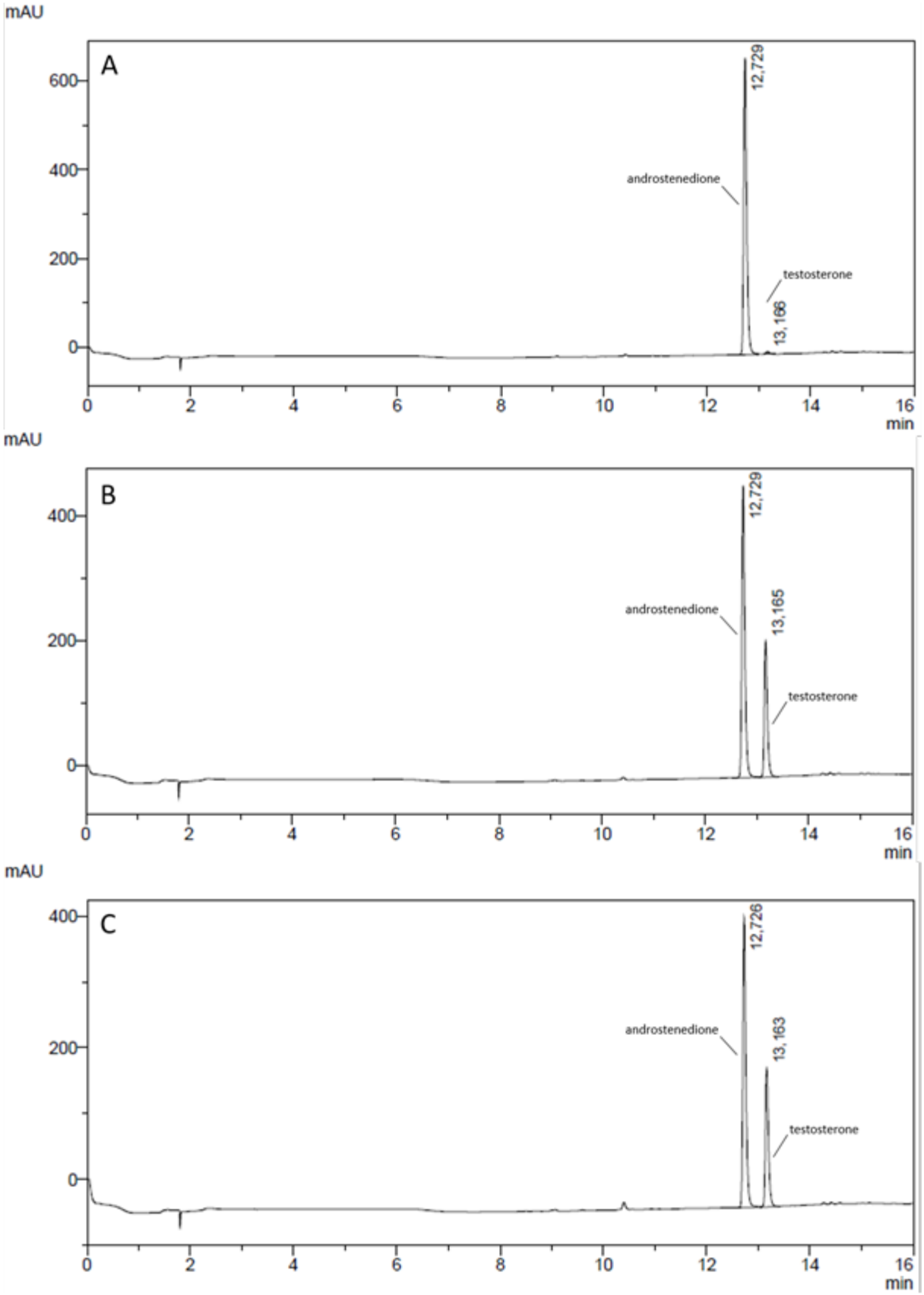

Fig. S3. UHPLC-chromatograms of untransfected (A), 17βHSD3-transfected, non-irradiated (B) and 17βHSD3-transfected, irradiated HEK-293 cells treated with 20 µM androstenedione and incubated for 3 h (retention times 12.7 min androstenedione and 13.2 min testosterone, respectively).

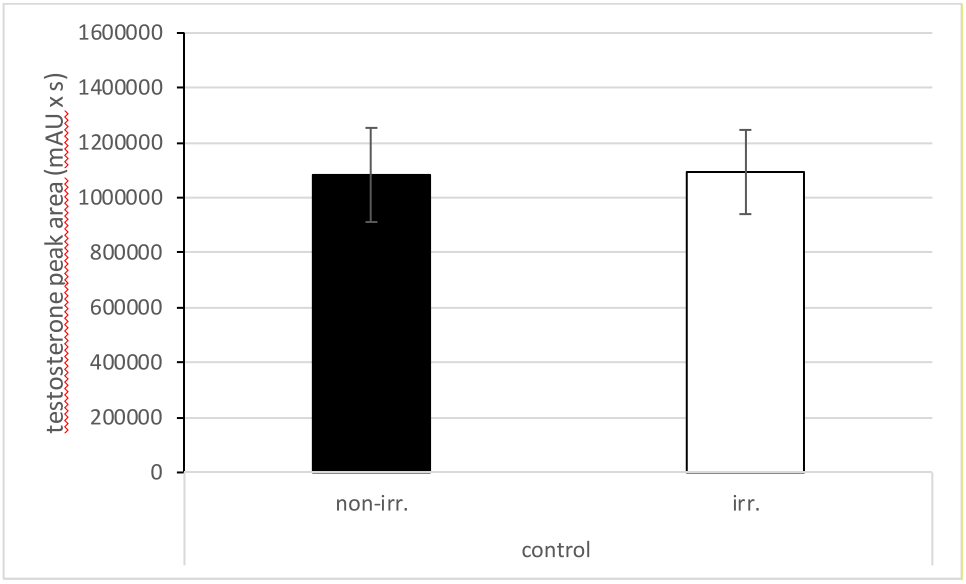

Fig. S4. Produced testosterone in 17βHSD3-transfected HEK-293 cells after 3-hour incubation with 20 µM androstenedione, with (irr.; 3 h at 20 % lamp intensity) and without (non-irr.) irradiation. Data are expressed as peak area of determined testosterone. Values are given as means ± SD of n = 46 biological replicates from 16 independent cell experiments.

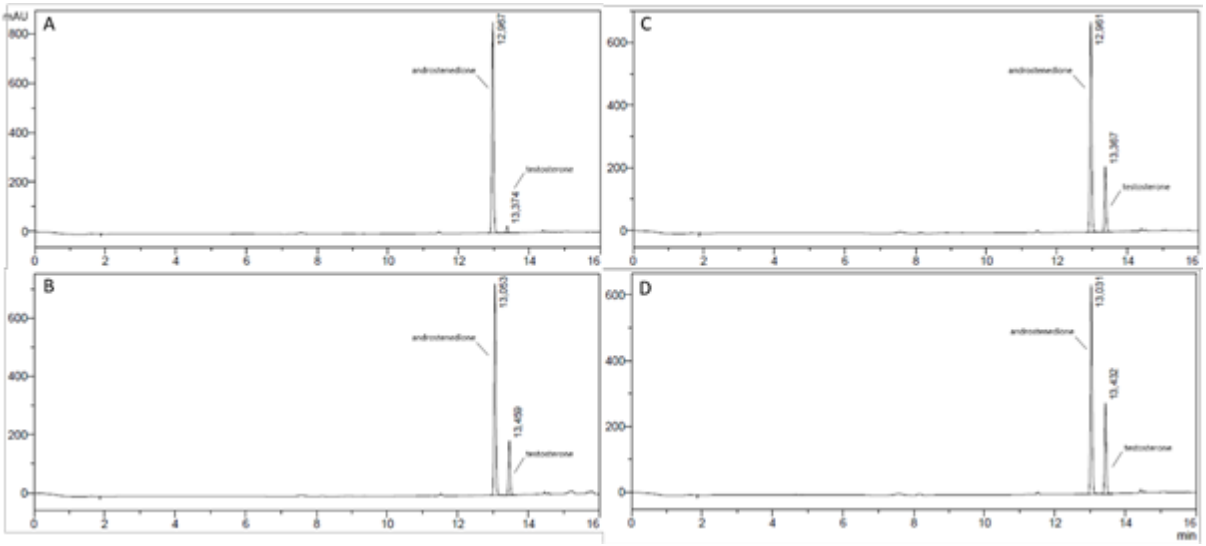

Fig. S5. UHPLC-chromatograms of samples incubated 5 h with 100 µM androstenedione, without microsome (A), with 120 µg microsome (B), with 150 µg microsome (C) and with 200 µg microsome (D) isolated from 17βHSD3-transfected HEK-293 cells (retention times 13.0 min androstenedione and 13.4 min testosterone, respectively). The small testosterone peak in the control without microsome resulted most likely from a substrate impurity (≥98% pure), since it occurred also when androstenedione standard solution was measured.

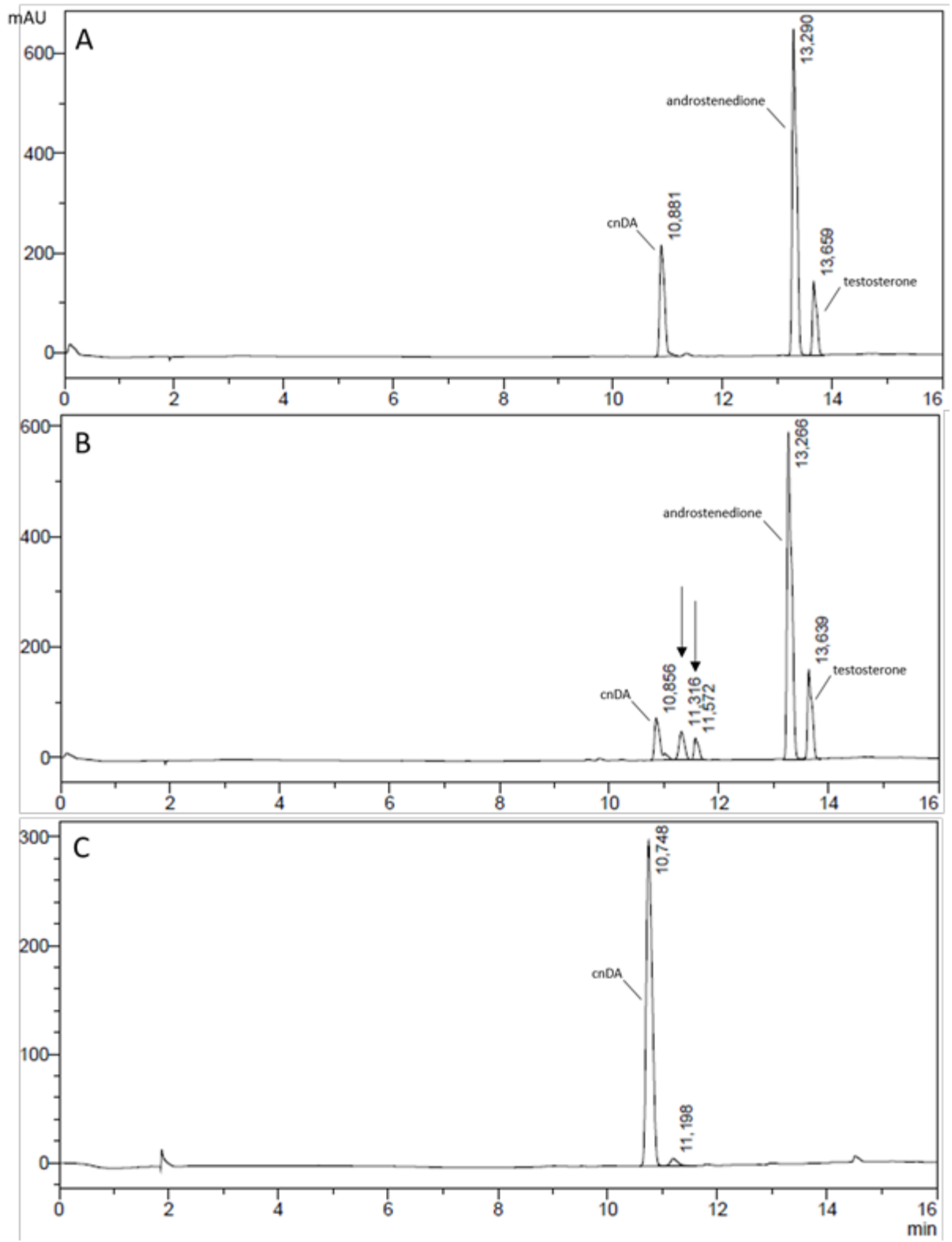

Fig. S6.1. UHPLC-chromatograms of 17βHSD3-transfected HEK-293 cells treated with 20 µM androstenedione and 10 µM cnDA. In the non-irradiated sample (A) only one peak of the test compound was detected (10.9 min); whereas in the irradiated sample (B) two additional peaks (11.3 min and 11.6 min, marked by ↓) emerged and the original peak was smaller (10.9 min). The third chromatogram shows 100 µM cnDA standard in methanol for comparison (C).

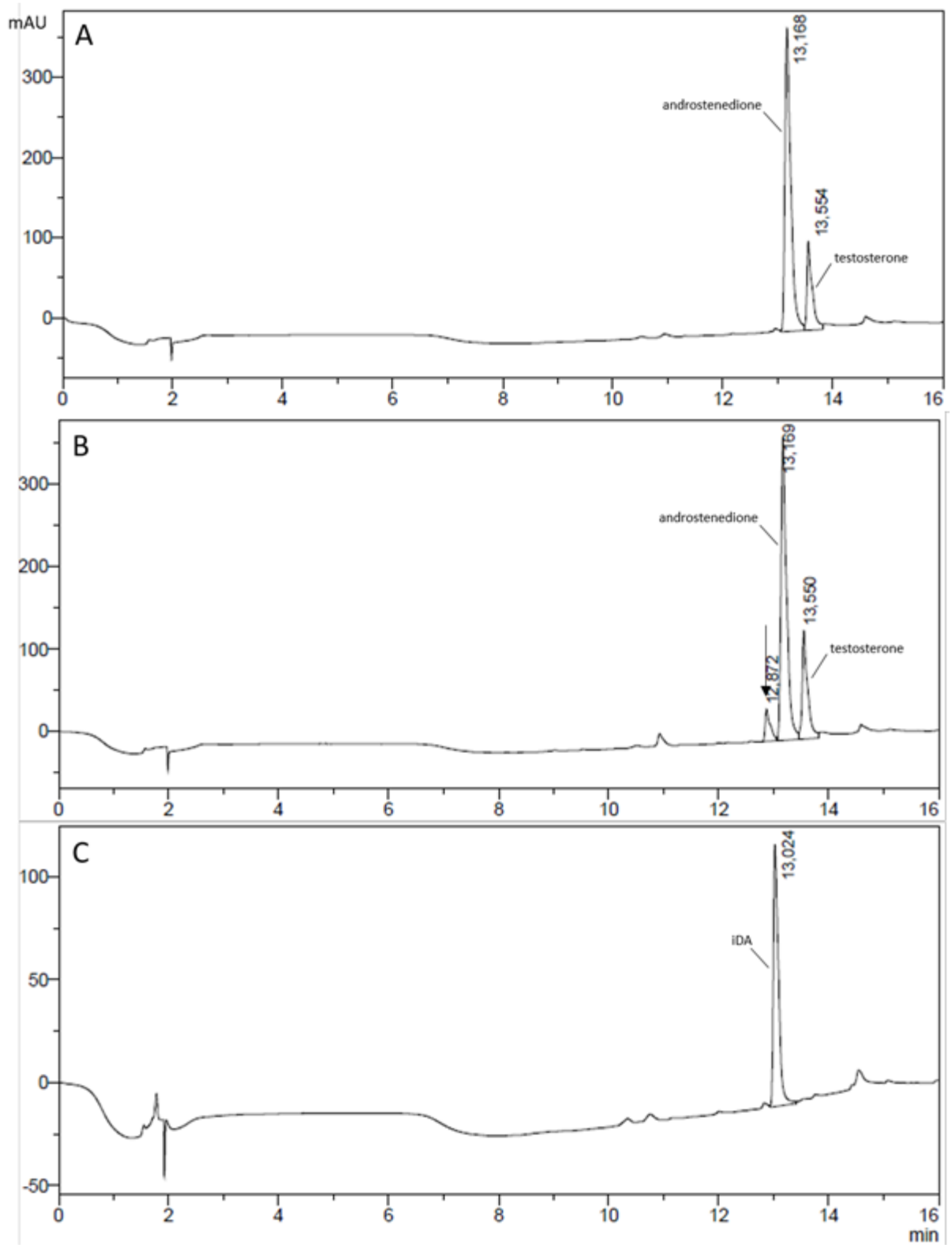

Fig. S6.2. UHPLC-chromatograms of 17βHSD3-transfected HEK-293 cells treated with 20 µM androstenedione and 10 µM iDA. In the non-irradiated sample (A) no iDA peak is seen, because it is hidden behind the androstenedione peak (13.2 min); whereas in the irradiated sample (B) a new peak (12.9 min, marked by ↓) emerged. The third chromatogram shows 100 µM iDA standard in methanol for comparison (C).

Tab. S7. Absorption maxima and thermal half-life of *N*-acetyl diazocine derivatives in aqueous solution with 2 % DMSO at 25 °C. Compounds pDA, dmpDA, fpDA and iDA were measured with lower concentrations due to poor solubility while for bpDA UV-vis absorption was too low to obtain reliable spectra or thermal half-life.

compound	concentration µmol/L	λ_{max} (*Z*) nm	λ_{max} (*E*) nm	$t_{1/2}$ (25 °C) min.
DA	250	392	502	98.20
pDA	25	395	510	45.10
dmpDA	50	391	501	129.04
fpDA	25	397	511	155.10
iDA	100	395	501	258.34
baDA	250	392	502	98.02
cnDA	250	392	505	99.04

UV-vis spectroscopy

UV-vis spectra were measured with a Shimadzu UV-2600i UV-vis spectrometer. Quartz cuvettes of 10 mm optical path length were used.

Light sources

For irradiation different custom-built light sources with a wavelength of 405 nm and 530 nm were used (Sahlmann Photochemistry Solutions & in-house built). Irradiation wavelengths for all (405 nm and 530 nm) LED units were measured via a mobile UV-vis spectrometer (USB4000-UV-VIS, Ocean Optics, Largo, FL, USA). All emission spectra were normalized. Fig. S8 shows the normalized emission spectra of all LED units used.

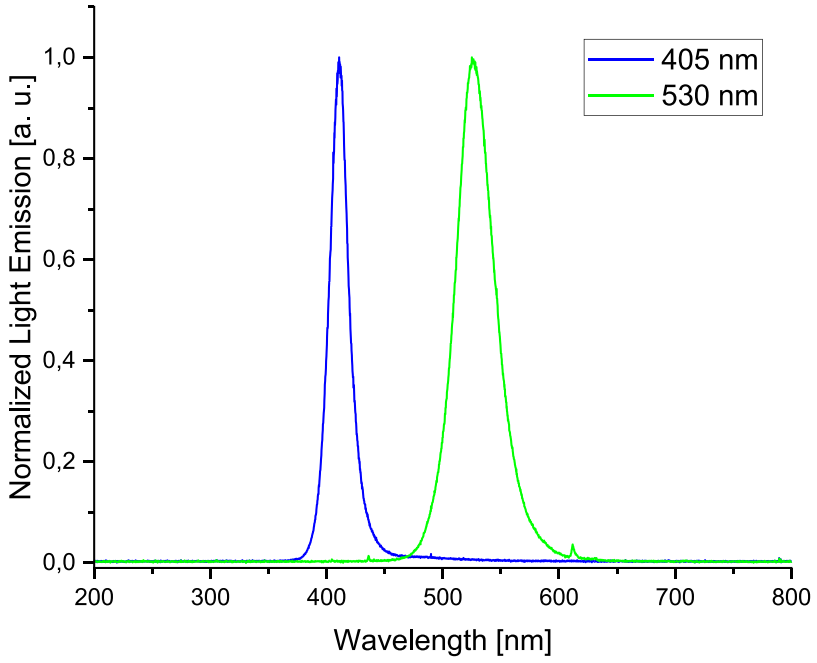

Fig. S8. Emission spectra of all LED units used. For better comparison all datasets were normalized to its maximum.

The full width at half maximum (FWHM) amounts to 19 nm (401-420 nm, maximum at 410 nm) for the 405 nm LED unit and to 38 nm (509-547 nm, maximum at 525 nm) for the 530 nm LED unit.

I. UV-vis switching experiments

All samples were irradiated to the photostationary state (PSS) with 405 nm in aqueous solution containing 2 % of DMSO. The UV-vis spectra were measured with compound concentrations of 250 µM and at 25 °C, except pDA, fpDA (both 25 µM), dmpDA (50 µM) and iDA (100 µM) due to poor solubility. Spectra of bpDA (25 µM) were measured, but poor UV-vis absorption gave no reliable data.

I.1 (*Z*)-11-acetyl-11,12-dihydrodibenzo[c,g][1,2,5]triazocine (DA)

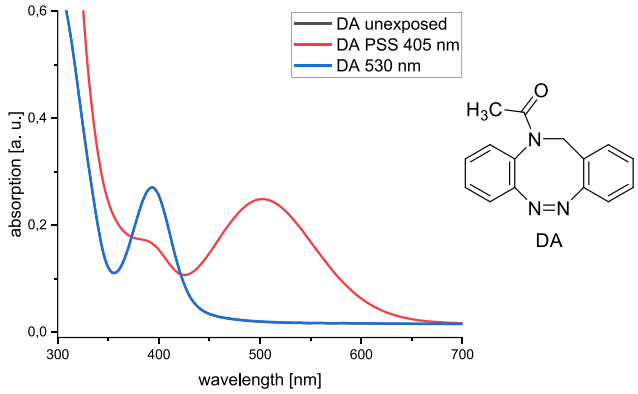

Fig. S9.1. UV-vis spectra of 250 µM DA in aqueous solution with 2 % DMSO at 25 °C. The unexposed sample is plotted in black, the spectra of the PSS between *Z*-DA and *E*-DA after irradiation with 405 nm in red and the spectra of *Z*-DA after irradiation with 530 nm in blue.

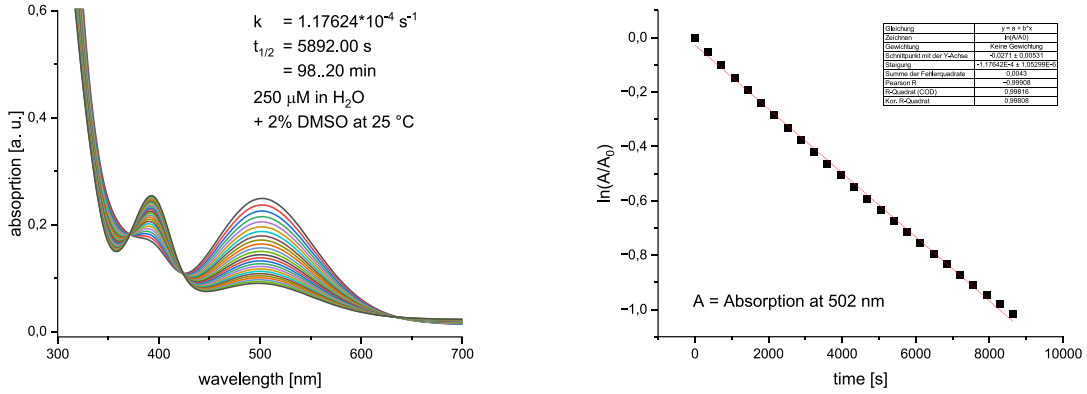

Fig. S9.2. UV-vis spectra of the half-life determination of DA in aqueous solution with 2% DMSO at 25 °C (left) with the corresponding first order kinetics plot (right).

I.2 (*Z*)-1-(3-phenyldibenzo[c,g][1,2,5]triazocin-11(12*H*)-yl)ethan-1-one (pDA)

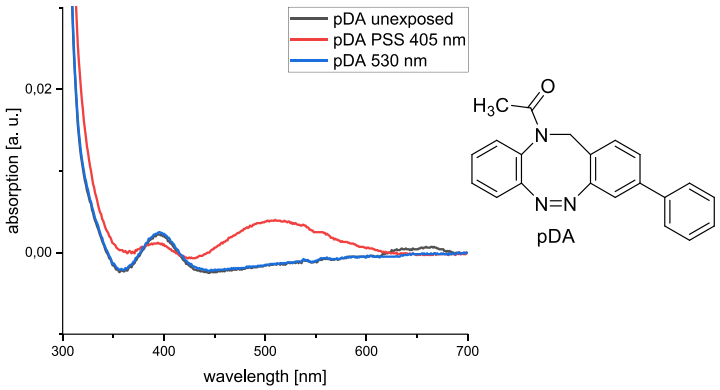

Fig. S10.1. UV-vis spectra of 25 µM pDA in aqueous solution with 2 % DMSO at 25 °C. The unexposed sample is plotted in black, the spectra of the PSS between *Z*-pDA and *E*-pDA after irradiation with 405 nm in red and the spectra of *Z*-pDA after irradiation with 530 nm in blue.

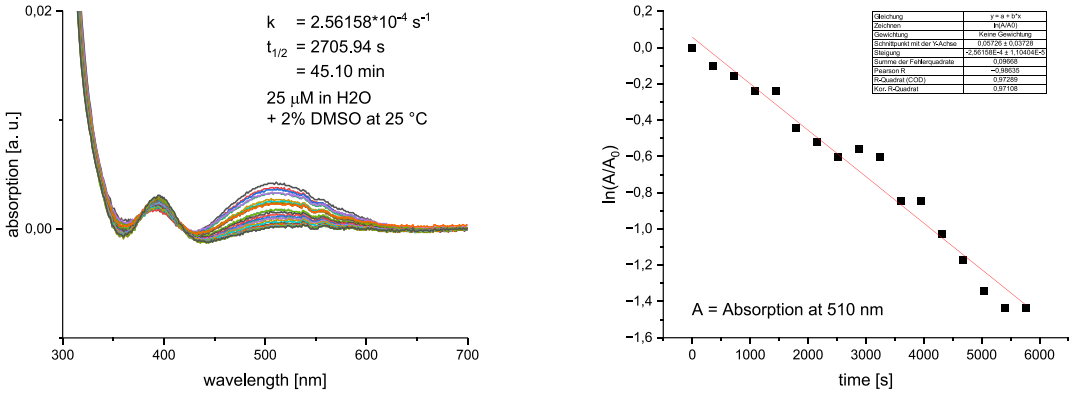

Fig. S10.2. UV-vis spectra of the half-life determination of pDA in aqueous solution with 2 % DMSO at 25 °C (left) with the corresponding first order kinetics plot (right).

I.3 (*Z*)-1-(3-(2,6-dimethylphenyl)dibenzo[c,g][1,2,5]triazocin-11(12*H*)-yl)ethan-1-one (dmpDA)

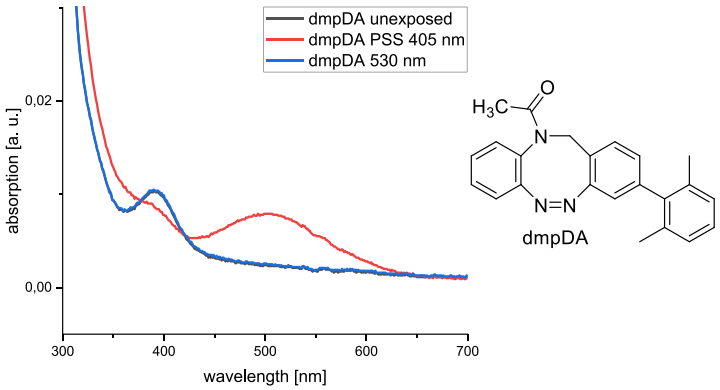

Fig. S11.1. UV-vis spectra of 50 µM dmpDA in aqueous solution with 2 % DMSO at 25 °C. The unexposed sample is plotted in black, the spectra of the PSS between *Z*-dmpDA and *E*-dmpDA after irradiation with 405 nm in red and the spectra of *Z*-dmpDA after irradiation with 530 nm in blue.

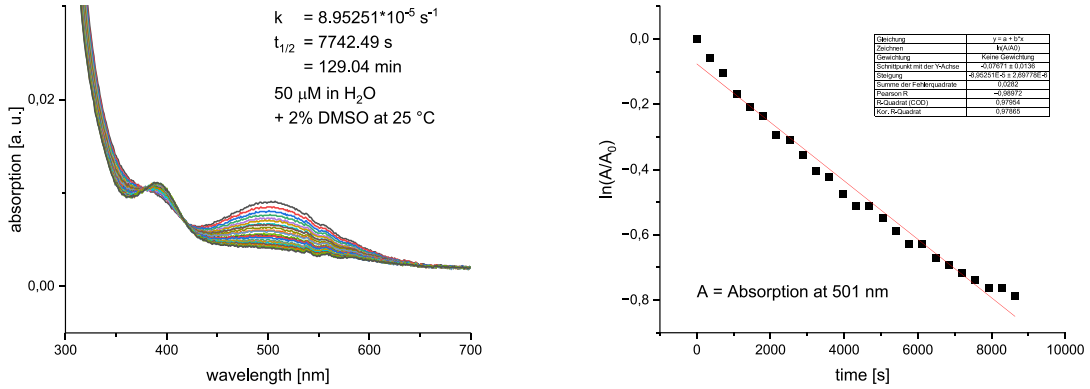

Fig. S11.2. UV-vis spectra of the half-life determination of dmpDA in aqueous solution with 2 % DMSO at 25 °C (left) with the corresponding first order kinetics plot (right).

I.4 (*Z*)-1-(3-(4-fluorophenyl)dibenzo[c,g][1,2,5]triazocin-11(12*H*)-yl)ethan-1-one (fpDA)

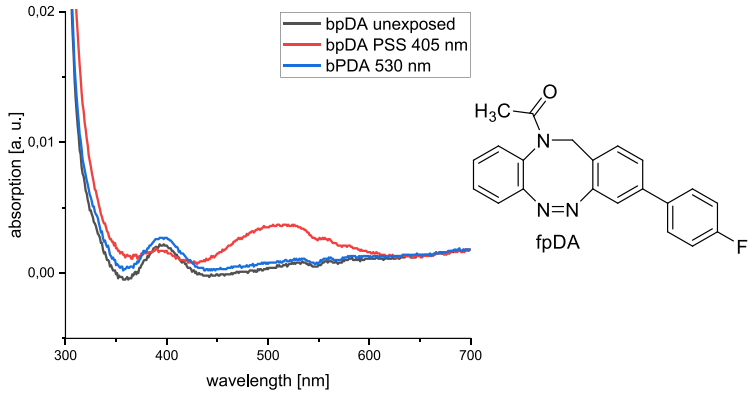

Fig. S12.1. UV-vis spectra of 25 µM fpDA in aqueous solution with 2 % DMSO at 25 °C. The unexposed sample is plotted in black, the spectra of the PSS between *Z*-fpDA and *E*-fpDA after irradiation with 405 nm in red and the spectra of *Z*-fpDA after irradiation with 530 nm in blue.

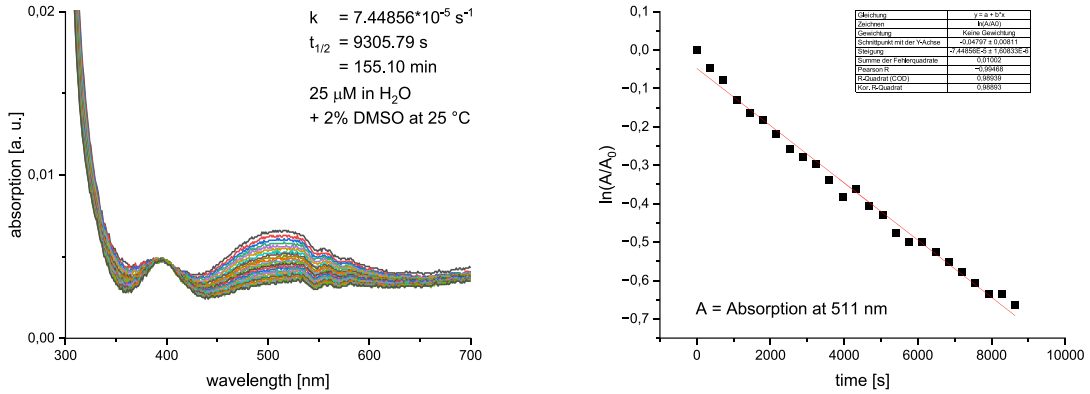

Fig. S12.2. UV-vis spectra of the half-life determination of fpDA in aqueous solution with 2 % DMSO at 25 °C (left) with the corresponding first order kinetics plot (right).

I.5 (Z)-1-(3-iododibenzo[c,g][1,2,5]triazocine-11(12H)-yl)ethan-1-one (iDA)

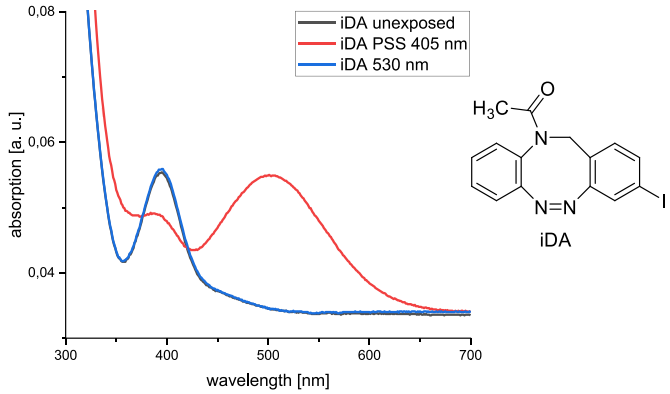

Fig. S13.1. UV-vis spectra of 100 µM iDA in aqueous solution with 2 % DMSO at 25 °C. The unexposed sample is plotted in black, the spectra of the PSS between *Z*-iDA and *E*-iDA after irradiation with 405 nm in red and the spectra of *Z*-iDA after irradiation with 530 nm in blue.

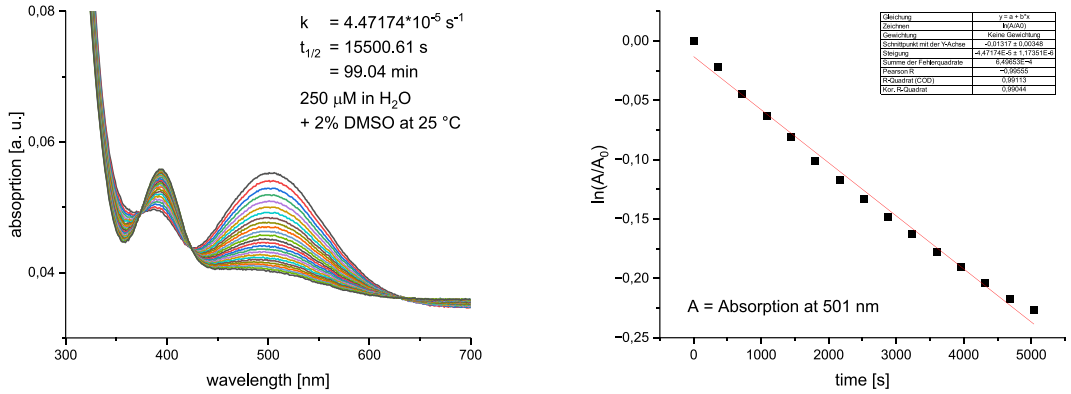

Fig. S13.2. UV-vis spectra of the half-life determination of iDA in aqueous solution with 2 % DMSO at 25 °C (left) with the corresponding first order kinetics plot (right).

I.6 (*Z*)-2-(11-acetyl-11,12-dihydrodibenzo[c,g][1,2,5]triazocin-3-yl)benzoic acid (baDA)

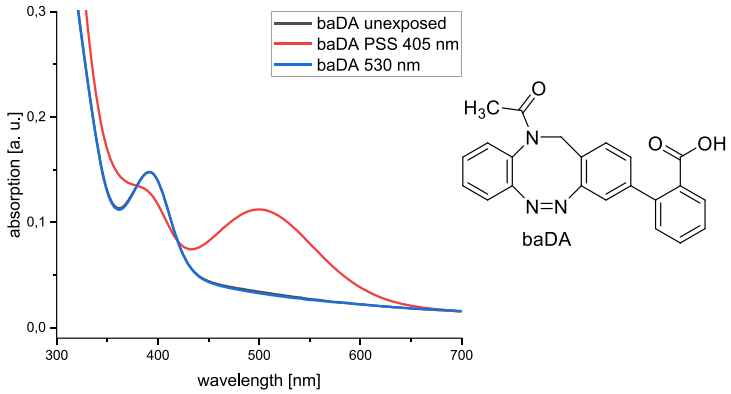

Fig. S14.1. UV-vis spectra of 250 µM baDA in aqueous solution with 2 % DMSO at 25 °C. The unexposed sample is plotted in black, the spectra of the PSS between *Z*-baDA and *E*-baDA after irradiation with 405 nm in red and the spectra of *Z*-baDA after irradiation with 530 nm in blue.

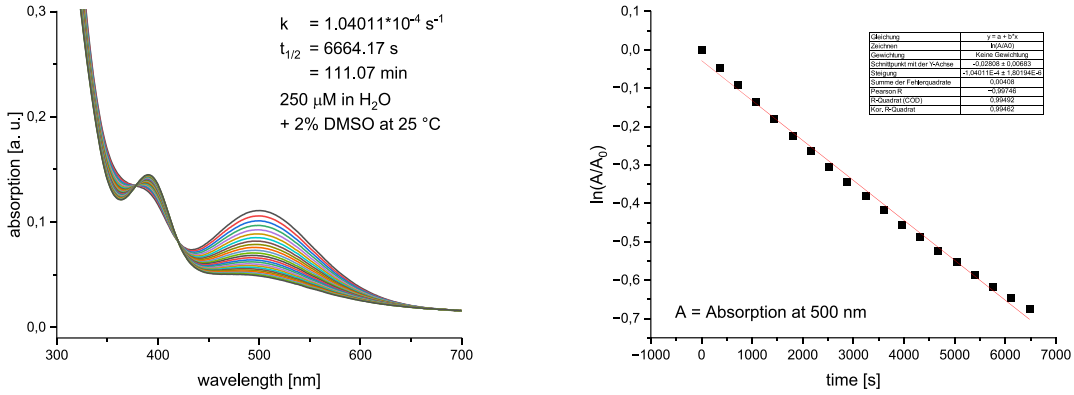

Fig. S14.2. UV-vis spectra of the half-life determination of baDA in aqueous solution with 2 % DMSO at 25 °C (left) with the corresponding first order kinetics plot (right).

I.7 (*Z*)-11-acetyl-11,12-dihydrodibenzo[c,g][1,2,5]triazocine-3-carbonitrile (cnDA)

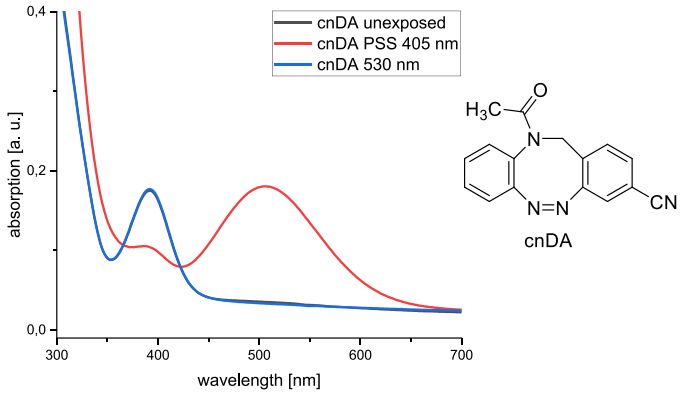

Fig. S15.1. UV-vis spectra of 250 µM cnDA in aqueous solution with 2 % DMSO at 25 °C. The unexposed sample is plotted in black, the spectra of the PSS between *Z*-cnDA and *E*-cnDA after irradiation with 405 nm in red and the spectra of *Z*-cnDA after irradiation with 530 nm in blue.

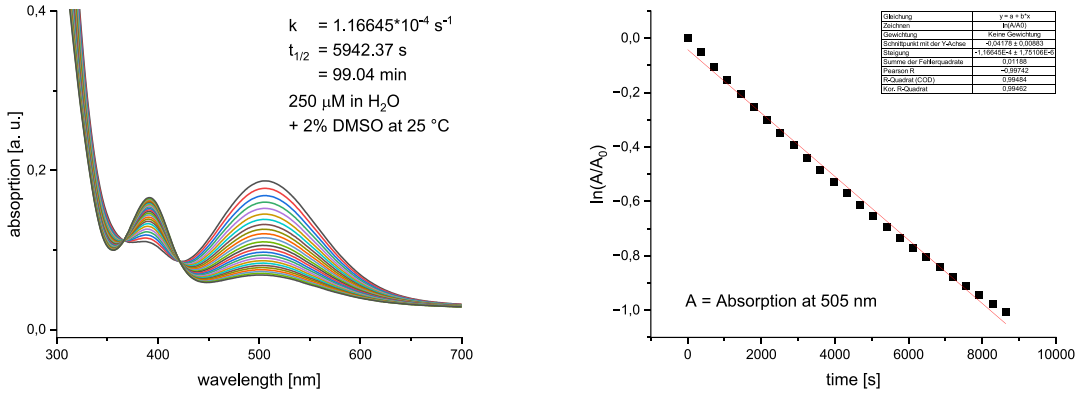

Fig. S15.2. UV-vis spectra of the half-life determination of cnDA in aqueous solution with 2 % DMSO at 25 °C (left) with the corresponding first order kinetics plot (right).

9. References

[1] H. Lodish, A. Berk, S. L. Zipursky, D. Baltimore, P. Matsuidara, J. Darnell, *Molecular cell biology*, 4th Edition, W. H. Freeman and Company, New York **2002**, 437-477.

[2] B. Alberts, R. Heald, A. Johnson, D. Morgan, M. Raff, K. Roberts, P. Walter, *Molecular Biology of the Cell*, 7th Edition, W. W. Norton & Company, New York **2022**, 673-681.

[3] J. L. Spudich, *Trends Microbiol.* **2006**, *14*, 480-487.

[4] B. L. Feringa, W. F. Jager, B. de Lange, *Tetrahedron* **1993**, *49*, 8267-8310.

[5] B. L. Feringa, R. A. van Delden, N. Koumura, E. M. Geertsema, *Chem. Rev.* **2000**, *100*, 1789-1816.

[6] M. Jeong, J. Park, S. Kwon, *Eur. J. Org. Chem.* **2020**, *2020*, 7254-7283.

[7] H. Wang, H. K. Bisoyi, X. Zhang, F. Hassan, Q. Li, *Chem. Eur. J.* **2022**, *28*, e202103906.

[8] E. R. Kay, D. A. Leigh, F. Zerbetto, *Angew. Chem. Int. Ed.* **2007**, *46*, 72-191.

[9] S. Erbas-Cakmak, D. A. Leigh, C. T. McTernan, A. L. Nussbaumer, *Chem. Rev.* **2015**, *115*, 10081-10206.

[10] S. Kassem, T. van Leeuwen, A. S. Lubbe, M. R. Wilson, B. L. Feringa, D. A. Leigh, *Chem. Soc. Rev.* **2017**, *46*, 2592-2621.

[11] R. W. Schoenlein, L. A. Peteanu, R. A. Mathies, C. V. Shank, *Science* **1991**, *254*, 412-415.

[12] J. L. Spudich, C. S. Yang, K. H. Jung, E. N. Spudich, *Annu. Rev. Cell Dev. Biol.* **2000**, *16*, 365-392.

[13] D. Polli, P. Altoè, O. Weingart, K. M. Spillane, C. Manzoni, D. Brida, G. Tomasello, G. Orlandi, P. Kukura, R. A. Mathies, M. Garavelli, G. Cerullo, *Nature* **2010**, *467*, 440-443.

[14] P. D. Kiser, M. Golczak, K. Palczewski, *Chem. Rev.* **2014**, *114*, 194-232.

[15] D. Bléger, S. Hecht, *Angew. Chem. Int. Ed.* **2015**, *54*, 11338-11349.

[16] R. Kroon, M. Lenes, J. C. Hummelen, P. W. M. Blom, B. de Boer, *Polym. Rev.* **2008**, *48*, 531-582.

[17] D. M. Schultz, T. P. Yoon, *Science* **2014**, *343*, 1239176.

[18] K. Hüll, J. Morstein, D. Trauner, *Chem. Rev.* **2018**, *118*, 10710-10747.

[19] W. A. Velema, W. Szymanski, B. L. Feringa, *J. Am. Chem. Soc.* **2014**, *136*, 2178-2191.

[20] M. M. Lerch, M. J. Hansen, G. M. van Dam, W. Szymanski, B. L. Feringa, *Angew. Chem. Int. Ed.* **2016**, *55*, 10978-10999.

[21] R. Klajn, *Chem. Soc. Rev.* **2014**, *43*, 148-184.

[22] G. Mayer, A. Heckel, *Angew. Chem. Int. Ed.* **2006**, *45*, 4900-4921.

[23] J. Boelke, S. Hecht, *Adv. Optical Mater.* **2019**, *7*, 1900404.

[24] Z. L. Pianowski, *Chem. Eur. J.* **2019**, *25*, 5128-5144.

[25] A. Lennartson, A. Roffey, K. Moth-Poulsen, *Tetrahedron Lett*. **2015**, *56*, 1457-1465.

[26] T. Tsuji, H. Takeuchi, T. Egawa, S. Konaka, *J. Am. Chem. Soc.* **2001**, *123*, 6381-6387.

[27] J. Griffiths, *Chem. Soc. Rev.* **1972**, *1*, 481-493.

[28] H. M. D. Bandara, S. C. Burdette, *Chem. Soc. Rev*. **2012**, *41*, 1809-1825.

[29] J. Bao, P. M. Weber, *J. Am. Chem. Soc.* **2011**, *133*, 4164-4167.

[30] G. C. Hampson, J. M. Robertson, *J. Chem. Soc.* **1941**, 409-413.

[31] H. Fliegl, A. Köhn, C. Hättig, R. Ahlrichs, *J. Am. Chem. Soc.* **2003**, *125*, 9821-9827.

[32] Y. Ito, H. Ito, T. Matsuura, *Tetrahedron Lett.* **1988**, *29*, 563-566.

[33]. V. Koch, S. Bräse, *Azobenzenes: The Quest for Visible Light Triggering*, in Z. L. Pianowski, *Molecular Photoswitches: Chemistry, Properties, and Applications Volume 2,* 1st Edition, Wiley-VCH, Weinheim **2022**, 42-64.

[34] V. Ladányi, P. Dvořák, J. Al Anshori, Ľ. Vetráková, J. Wirz, D. Heger, *Photochem. Photobiol. Sci.* **2017**, *16*, 1757-1761.

[35] N. Siampiringue, G. Guyot, S. Monti, P. Bortulus, *J. Photochem.* **1987**, 37, 185-188.

[36] P. Bortolus, S. Monti, *J. Phys. Chem.* **1979**, *83*, 648-652.

[37] P. Bortulus, S. Monti, *J. Phys. Chem.* **1987**, *37*, 648-652.

[38] S. Malkin, E. Fischer, *J. Phys. Chem.* 1962, *62*, 2482-2486.
[39] E. Fischer, *J. Am. Chem. Soc.* 1960, *82*, 3249-3252.
[40] M. L. Tiago, S. Ismail-Beigi, S. G. Louie, *J. Chem. Phys.* 2005, *122*, 94311.
[41] A. K. Schnack-Petersen, M. Pápai, K. B. Møller, *J. Photochem. Photobiol. A* 2022, *428*, 113869.
[42] W. Moormann, T. Tellkamp, E. Stadler, F. Röhricht, C. Näther, R. Puttreddy, K. Rissanen, G. Gescheidt, R. Herges, *Angew. Chem. Int. Ed.* 2020, *59*, 15081-15086.
[43] F. Hamon, F. Djedaini-Pilard, F. Barbot, C. Len, *Tetrahedron* 2009, *65*, 10105-10123.
[44] E. Merino, *Chem. Soc. Rev*. 2011, *40*, 3835-3853.
[45] S. Schultzke, N. Scheuring, P. Puylaert, M. Lehmann, A. Staubitz, *Adv. Sci.* 2023, *10*, e2302692.
[46] Z. Mahimwalla, K. G. Yager, J. Mamiya, A. Shishido, A. Priimagi, C. J. Barrett, *Polym. Bull.* 2012, *69*, 967-1006.
[47] L. Dong, Y. Feng, L. Wang, W. Feng, *Chem. Soc. Rev.* 2018, *47*, 7339-7368.
[48] S. Schultzke, P. Puylaert, H. Wang, I. Schultzke, J. Gerken, A. Staubitz, *Adv. Funct. Mater*. 2024, *34*, 2313268.
[49] M. J. Hansen, M. M. Lerch, W. Szymanski, B. L. Feringa, *Angew. Chem. Int. Ed.* 2016, *55*, 13514-13518.
[50] S. Samanta, A. A. Beharry, O. Sadovski, T. M. McCormick, A. Babalhavaeji, V. Tropepe, G. A. Woolley, *J. Am. Chem. Soc.* 2013, *135*, 9777-9784.
[51] A. A. Beharry, O. Sadovski, G. A. Woolley, *J. Am. Chem. Soc*. 2011, *133*, 19684-19687.
[52] M. A. Kienzler, A. Reiner, E. Trautman, S. Yoo, D. Trauner, E. Y. Isacoff, *J. Am. Chem. Soc.* 2013, *135*, 17683-17686.
[53] M. Dong, A. Babalhavaeji, C. V. Collins, K. Jarrah, O. Sadovski, Q. Dai, G. A. Woolley, *J. Am. Chem. Soc.* 2017, *139*, 13483-13486.
[54] D. Bléger, J. Schwarz, A. M. Brouwer, S. Hecht, *J. Am. Chem. Soc.* 2012, *134*, 20597-20600.
[55] A. Goulet-Hanssens, T. C. Corkery, A. Priimagi, C. J. Barrett, *J. Mater. Chem. C* 2014, *2*, 7505-7512.
[56] S. Fredrich, R. Göstl, M. Herder, L. Grubert, S. Hecht, *Angew. Chem. Int. Ed.* 2016, *55*, 1208-1212.
[57] R. Siewertsen, H. Neumann, B. Buchheim-Stehn, R. Herges, C. Näther, F. Renth, F. Temps, *J. Am. Chem. Soc.* 2009, *131*, 15594-15595.
[58] A. Mukherjee, M. D. Seyfried, B. J. Ravoo, *Angew. Chem. Int. Ed*. 2023, *62*, e202304437.
[59] S. Crespi, N. A. Simeth, B. König, *Nat. Rev. Chem.* 2019, *3*, 133-146.
[60] J. Calbo, C. E. Weston, A. J. P. White, H. S. Rzepa, J. Contreras-García, M. J. Fuchter, *J. Am. Chem. Soc.* 2017, *139*, 1261-1274.
[61] S. A. M. Steinmüller, M. Odaybat, G. Galli, D. Prischich, M. J. Fuchter, M. Decker, *Chem. Sci.* 2024, *15*, 5360-5367.
[62] C. E. Weston, R. D. Richardson, P. R. Haycock, A. J. P. White, M. J. Fuchter, *J. Am. Chem. Soc.* 2014, *136*, 11878-11881.
[63] H. Duval, *Bull. Soc. Chim. Fr.* 1910, *7*, 727-732.
[64] P. Lentes, E. Stadler, F. Röhricht, A. Brahms, J. Gröbner, F. D. Sönnichsen, G. Gescheidt, R. Herges, *J. Am. Chem. Soc.* 2019, *141*, 13592-13600.
[65] M. Hammerich, C. Schütt, C. Stähler, P. Lentes, F. Röhricht, R. Höppner, R. Herges, *J. Am. Chem. Soc.* 2016, *138*, 13111-13114.
[66] M. H. Burk, D. Hagenbusch, C. Arndt, L. Pott, M. Hauck, J. Drewes, S. Rehders, T. Strunskus, T. Hartig, F. Schütt, R. Adelung, R. Herges, C. Selhuber-Unkel F. Faupel, S. Schröder, A freestanding photoswitchable aero-polymer with an incorporated bridged azobenzene: 3D structure, photoinduced motion, biocompatibility and potential application as photomechanical cell scaffold, *ChemRxiv* 2023, 10.26434/chemrxiv-2023-15rbd.
[67] M. H. Burk, D. Langbehn, G. Hernández Rodríguez, W. Reichstein, J. Drewes, S. Schröder, S. Rehders, T. Strunskus, R. Herges, F. Faupel, *ACS Appl. Polym. Mater.* 2021, *3*, 1445-1456.

[68] G. Cabré, A. Garrido-Charles, À. González-Lafont, W. Moormann, D. Langbehn, D. Egea, J. M. Lluch, R. Herges, R. Alibés, F. Busqué, P. Gorostiza, J. Hernando, *Org. Lett.* 2019, *21*, 3780-3784.
[69] J. Ewert, L. Heintze, M. Jordà-Redondo, J.-S. von Glasenapp, S. Nonell, G. Bucher, C. Peifer, R. Herges, *J. Am. Chem. Soc.* 2022, *144*, 15059-15071.
[70] L. Heintze, D. Schmidt, T. Rodat, L. Witt, J. Ewert, M. Kriegs, R. Herges, C. Peifer, *Int. J. Mol. Sci.* 2020, *21*, 8961.
[71] T. Ko, M. M. Oliveira, J. M. Alapin, J. Morstein, E. Klann, D. Trauner, *J. Am. Chem. Soc.* 2022, *144*, 21494-21501.
[72] N. Preußke, W. Moormann, K. Bamberg, M. Lipfert, R. Herges, F. D. Sönnichsen, *Org. Biomol. Chem*. 2020, *18*, 2650-2660.
[73] M. Reynders, A. Chaikuad, B.-T. Berger, K. Bauer, P. Koch, S. Laufer, S. Knapp, D. Trauner, *Angew. Chem. Int. Ed*. 2021, *60*, 20178-20183.
[74] M. Schehr, C. Ianes, J. Weisner, L. Heintze, M. P. Müller, C. Pichlo, J. Charl, E. Brunstein, J. Ewert, M. Lehr, U. Baumann, D. Rauh, U. Knippschild, C. Peifer, R. Herges, *Photochem. Photobiol. Sci.* 2019, *18*, 1398-1407.
[75] W. Moormann, D. Langbehn, R. Herges, *Synthesis* 2017, *49*, 3471-3475.
[76] M. S. Maier, K. Hüll, M. Reynders, B. S. Matsuura, P. Leippe, T. Ko, L. Schäffer, D. Trauner, *J. Am. Chem. Soc*. 2019, *141*, 17295-17304.
[77] S. Li, N. Eleya, A. Staubitz, *Org. Lett.* 2020, *22*, 1624-1627.
[78] Y. Ma, S. Wu, S. Jiang, F. Xiao, G.-J. Deng, *Chin. J. Chem*. 2021, *39*, 3334-3338.
[79] D. K. Joshi, M. J. Mitchell, D. Bruce, A. J. Lough, H. Yan, *Tetrahedron* 2012, *68*, 8670-8676.
[80] J. Wang, J. He, C. Zhi, B. Luo, X. Li, Y. Pan, X. Cao, H. Gu, *RSC Adv*. 2014, *4*, 16607-16611.
[81] F. Eljabu, J. Dhruval, H. Yan, *Bioorg. Med. Chem. Lett*. 2015, *25*, 5594-5596.
[82] N. K. Chaudhuri, T. J. Ball, *J. Label. Compd. Radiopharm*. 1981, *18*, 1189-1196.
[83] W. Moormann, D. Langbehn, R. Herges, *Beilstein J. Org. Chem.* 2019, *15*, 727-732.
[84] D. Langbehn, *Dissertation*, Christian-Albrechts-Universität zu Kiel 2020.
[85] J. B. Trads, K. Hüll, B. S. Matsuura, L. Laprell, T. Fehrentz, N. Görldt, K. A. Kozek, C. D. Weaver, N. Klöcker, D. M. Barber, D. Trauner, *Angew. Chem. Int. Ed*. 2019, *58*, 15421-15428.
[86] Z. Qu, X. Chen, S. Zhong, G.-J. Deng, H. Huang, *Org. Lett*. 2021, *23*, 5349-5353.
[87] C. W. Cheung, X. Hu, *Nat. Commun*. 2016, *7*, 12494.
[88] T. Tellkamp, J. Shen, Y. Okamoto, R. Herges, *Eur. J. Org. Chem.* 2014, *2014*, 5456-5461.
[89] H. Sell, C. Näther, R. Herges, *Beilstein J. Org. Chem.* 2013, *9*, 1-7.
[90] S. Li, G. Han, W. Zhang, *Macromolecules* 2018, *51*, 4290-4297.
[91] W. W. Paudler, A. G. Zeiler, *J. Org. Chem*. 1969, *34*, 3237-3239.
[92] F. Klockmann, C. Fangmann, E. Zender, T. Schanz, C. Catapano, A. Terfort, *ACS Omega* 2021, *6*, 18434-18441.
[93] C. Deo, N. Bogliotti, R. Métivier, P. Retailleau, J. Xie, *Chem. Eur. J.* 2016, *22*, 9092-9096.
[94] S. Samanta, C. Qin, A. J. Lough, G. A. Woolley, *Angew. Chem. Int. Ed*. 2012, *51*, 6452-6455.
[95] S. Li, R. Colaco, A. Staubitz, *ACS Appl. Polym. Mater*. 2022, *4*, 6825-6833.
[96] L. Albert, A. Peñalver, N. Djokovic, L. Werel, M. Hoffarth, D. Ruzic, J. Xu, L.-O. Essen, K. Nikolic, Y. Dou, O. Vázquez, *ChemBioChem* 2019, *20*, 1417-1429.
[97] S. Schultzke, M. Walther, A. Staubitz, *Molecules* 2021, 26, 3916.
[98] M. Walther, W. Kipke, S. Schultzke, S. Ghosh, A. Staubitz, *Synthesis* 2021, *53*, 1213-1228.
[99] M. Walther, W. Kipke, R. Renken, A. Staubitz, *RSC Adv*. 2023, *13*, 15805-15809.
[100] A. Businski, *aktuelle Arbeiten*, Christian-Albechts-Universität zu Kiel 2024.
[101] D. Hugenbusch, M. Lehr, J.-S. von Glasenapp, A. J. McConnell, R. Herges, *Angew. Chem. Int. Ed*. 2023, *62*, e202212571.

[102] H. Lee, J. Tessarolo, D. Langbehn, A. Baksi, R. Herges, G. H. Clever, *J. Am. Chem. Soc*. 2022, *144*, 3099-3105.
[103] D. Bléger, J. Dokić, M. V. Peters, L. Grubert, P. Saalfrank, S. Hecht, *J. Phys. Chem. B* 2011, *115*, 9930-9940.
[104] F. Cisnetti, R. Ballardini, A. Credi, M. T. Gandolfi, S. Masiero, F. Negri, S. Pieraccini, G. P. Spada, *Chem. Eur. J*. 2004, *10*, 2011-2021.
[105] D. Hugenbusch, *Dissertation*, Christian-Albechts-Universität zu Kiel 2024.
[106] W. Fang, Y. Feng, J. Gao, H. Wang, J. Ge, Q. Yang, W. Feng, *Molecules* 2022, 27, 3296.
[107] R. Siewertsen, J. B. Schönborn, B. Hartke, F. Renth, F. Temps, Phys. Chem. Chem. Phys. 2011, *13*, 1054-1063.
[108] V. Pansare, S. Hejazi, W. Faenza, R. K. Prud'homme, *Chem. Mater*. 2012, *24*, 812-827.
[109] A. Alabugin, *Photochem. Photobiol*. 2019, *95*, 722-732.
[110] P. Lentes, P. Frühwirt, H. Freißmuth, W. Moormann, F. Kruse, G. Gescheidt, R. Herges, *J. Org. Chem*. 2021, *86*, 4355-4360.
[111] A. A. Beharry, G. A. Woolley, *Chem. Soc. Rev.* 2011, *40*, 4422-4437.
[112] L. N. Lameijer, S. Budzak, N. A. Simeth, M. J. Hansen, B. L. Feringa, D. Jacquemin, W. Szymanski, *Angew. Chem. Int. Ed*. 2020, *59*, 21663-21670.
[113] M. Schehr, *Dissertation*, Christian-Albechts-Universität zu Kiel 2018.
[114] G. Du, J. Fu, Y. Zheng, F. Hu, X. Shen, B. Li, X. Zhao, Z. Yu, *Org. Biomol. Chem*. 2023, *21*, 1021-1026.
[115] W. Szymański, J. M. Beierle, H. A. V. Kistemaker, W. A. Velema, B. L. Feringa, *Chem. Rev*. 2013, *113*, 6114-6178.
[116] M. Mathews, N. Tamaoki, *J. Am. Chem. Soc*. 2008, *130*, 11409-11416.
[117] M. J. Moran, M. Magrini, D. M. Walba, I. Aprahamian, *J. Am. Chem. Soc*. 2018, *140*, 13623-13627.
[118] R. A. van Delden, T. Mecca, C. Rosini, B. L. Feringa, *Chem. Eur. J.* 2004, *10*, 61-70.
[119] Y. Wang, Q. Li, *Adv. Mater*. 2012, *24*, 1926-1945.
[120] P. Lentes, J. Rudtke, T. Griebenow, R. Herges, *Beilstein J. Org. Chem*. 2021, *17*, 1503-1508.
[121] D. Nasipuri, *Stereochemistry of Organic Compounds: Principles and Applications*, 2nd Edition, New Age International (P) Limited, Publishers, New Delhi 1994, 25-26.
[122] J. Clayden, N. Greeves, S. G. Warren, *Organic Chemistry*, 2nd Edition, Oxford University Press, Oxford 2012, 302-327.
[123] D. Sahoo, R. Benny, N. K. Ks, S. De, *ChemPlusChem* 2022, *87*, e202100322.
[124] J. J. D. de Jong, L. N. Lucas, R. M. Kellogg, J. H. van Esch, B. L. Feringa, *Science* 2004, *304*, 278-281.
[125] L. Zhang, H.-X. Wang, S. Li, M. Liu, *Chem. Soc. Rev*. 2020, *49*, 9095-9120.
[126] H. K. Bisoyi, Q. Li, *Angew. Chem. Int. Ed*. 2016, *55*, 2994-3010.
[127] D. J. Lockhart, E. A. Winzeler, *Nature* 2000, *405*, 827-836.
[128] F. A. Samatey, K. Imada, S. Nagashima, F. Vonderviszt, T. Kumasaka, M. Yamamoto, K. Namba, *Nature* 2001, *410*, 331-337.
[129] J. Kim, J. Lee, W. Y. Kim, H. Kim, S. Lee, H. C. Lee, Y. S. Lee, M. Seo, S. Y. Kim, *Nat. Commun*. 2015, *6*, 6959-.
[130] N. Koumura, R. W. Zijlstra, R. A. van Delden, N. Harada, B. L. Feringa, *Nature* 1999, *401*, 152-155.
[131] D. Pijper, B. L. Feringa, *Angew. Chem. Int. Ed*. 2007, *46*, 3693-3696.
[132] D. Zhao, T. van Leeuwen, J. Cheng, B. L. Feringa, *Nat. Chem*. 2017, *9*, 250-256.
[133] J. Wang, B. L. Feringa, *Science* 2011, *331*, 1429-1432.
[134] M. Mueller, R. Zentel, *Macromolecules* 1994, *27*, 4404-4406.
[135] A. Ueno, K. Takahashi, J. Anzai, T. Osa, *J. Am. Chem. Soc.* 1981, *103*, 6410-6415.
[136] A. Adam, G. Haberhauer, *J. Am. Chem. Soc*. 2017, *139*, 9708-9713.
[137] G. Balavoine, A. Moradpour, H. B. Kagan, *J. Am. Chem. Soc*. 1974, *96*, 5152-5158.
[138] N. P. M. Huck, W. F. Jager, B. de Lange, B. L. Feringa, *Science* 1996, *273*, 1686-1688.

[139] W. L. Noorduin, A. A. C. Bode, M. van der Meijden, H. Meekes, A. F. van Etteger, W. J. P. van Enckevort, P. C. M. Christianen, B. Kaptein, R. M. Kellogg, T. Rasing, E. Vlieg, *Nat. Chem*. 2009, *1*, 729-732.
[140] M. Suarez, G. B. Schuster, *J. Am. Chem. Soc*. 1995, *117*, 6732-6738.
[141] J. Bailey, A. Chrysostomou, J. H. Hough, T. M. Gledhill, A. McCall, S. Clark, F. Ménard, M. Tamura, *Science* 1998, *281*, 672-674.
[142] J. R. Cronin, S. Pizzarello, *Science* 1997, *275*, 951-955.
[143] J. A. Le Bel, *Bull. Soc. Chim. Fr*. 1874, *22*, 337-347.
[144] N. Kobayashi, A. Muranaka, J. Mack, *Circular Dichroism and Magnetic Circular Dichroism Spectroscopy for Organic Chemists*, 1st Edition., Royal Society of Chemistry, Cambridge 2011, 1-41.
[145] M. Chekhova, P. Banzer, *Polarization of Light*, Walter De Gruyter GmbH, Berlin/Boston 2021, 10-23.
[146] B. L. Feringa, R. A. van Delden, *Angew. Chem. Int. Ed*. 1999, *38*, 3418-3438.
[147] Y. Inoue, *Chem. Rev*. 1992, *92*, 741-770.
[148] W. Kuhn, *Trans. Faraday Soc*. 1930, *26*, 293.
[149] J. L. Greenfield, J. Wade, J. R. Brandt, X. Shi, T. J. Penfold, M. J. Fuchter, *Chem. Sci*. 2021, *12*, 8589-8602.
[150] Y. Zhang, G. B. Schuster, *J. Org. Chem*. 1995, *60*, 7192-7197.
[151] P. K. Hashim, R. Thomas, N. Tamaoki, *Chem. Eur. J*. 2011, *17*, 7304-7312.
[152] N. Tamaoki, M. Wada, *J. Am. Chem. Soc*. 2006, *128*, 6284-6285.
[153] W. J. Bernstein, M. Calvin, O. Buchardt, *J. Am. Chem. Soc*. 1972, *94*, 494-498.
[154] W. J. Bernstein, M. Calvin, O. Buchardt, *Tetrahedron Lett*. 1972, *13*, 2195-2198.
[155] W. J. Bernstein, M. Calvin, O. Buchardt, *J. Am. Chem. Soc*. 1973, *95*, 527-532.
[156] H. Kagan, A. Moradpour, J. F. Nicoud, G. Balavoine, R. H. Martin, J. P. Cosyn, *Tetrahedron Lett*. 1971, *12*, 2479-2482.
[157] H. Kagan, A. Moradpour, J. F. Nicoud, G. Balavoine, G. Tsoucaris, *J. Am. Chem. Soc.* 1971, *93*, 2353-2354.
[158] K. Rijeesh, P. K. Hashim, S.-I. Noro, N. Tamaoki, *Chem. Sci*. 2015, *6*, 973-980.
[159] R. Dorel, B. L. Feringa, *Angew. Chem. Int. Ed*. 2020, *59*, 785-789.
[160] J. Barberá, L. Giorgini, F. Paris, E. Salatelli, R. M. Tejedor, L. Angiolini, *Chem. Eur. J*. 2008, *14*, 11209-11221.
[161] T. Brandt, W. Moormann, J. S. von Glasenapp, J. P. Mikosch, C. Näther, R. Herges, *Determination of Enantiomeric Excess by Photoswitching of Chiral Diindanodiazocine Racemic Mixture with Circular Polarized Light*, manuscript prepared for submission 2024.
[162] M. J. Fuchter, *J. Med. Chem*. 2020, *63*, 11436-11447.
[163] I. M. Welleman, M. W. H. Hoorens, B. L. Feringa, H. H. Boersma, W. Szymański, *Chem Sci*. 2020, *11*, 11672-11691.
[164] J. Broichhagen, J. A. Frank, D. Trauner, *Acc. Chem. Res*. 2015, *48*, 1947-1960.
[165] M. W. H. Hoorens, W. Szymanski, *Trends in Biochem. Sci*. 2018, *43*, 567-575.
[166] F. Wages, P. Lentes, T. Griebenow, R. Herges, C. Peifer, E. Maser, *Chem. Biol. Interact*. 2022, *354*, 109822.
[167] W. Mnif, A. I. H. Hassine, A. Bouaziz, A. Bartegi, O. Thomas, B. Roig, *Int. J. Environ. Res. Public Health* 2011, *8*, 2265-2303.
[168] Å. Bergman, J. J. Heindel, S. Jobling, K. A. Kidd, R. T. Zoeller, *State of the Science of Endocrine Disrupting Chemicals—2012*, United Nations Environment Programme and the World Health Organization, 2013.
[169] J. Morstein, M. Awale, J.-L. Reymond, D. Trauner, *ACS Cent. Sci*. 2019, *5*, 607-618.
[170] K. Stach, F. Bickelhaupt, *Monatsh. Chem*. 1962, *93*, 896-904.
[171] F. J. Villani, C. A. Ellis, C. Teichman, C. Bigos, *J. Med. Pharm. Chem*. 1962, *5*, 373-383.

[172] M. Kurokawa, F. Sato, I. Fujiwara, N. Hatano, Y. Honda, T. Yoshida, S. Naruto, J. Mastumoto, H. Uno, *J. Med. Chem*. 1991, *34*, 927-934.
[173] E. E. Lee, H. I. Maibach, *Am. J. Clin. Dermatol.* 2001, *2*, 27-32.
[174] B. E. Fink, A. V. Gavai, J. S. Tokarski, B. Goyal, R. Misra, H.-Y. Xiao, S. D. Kimball, W.-C. Han, D. Norris, T. E. Spires, D. You, M. M. Gottardis, M. V. Lorenzi, G. D. Vite, *Bioorg. Med. Chem. Lett*. 2006, *16*, 1532-1536.
[175] P. Lentes, *aktuelle Arbeiten*, Christian-Albrechts-Universität zu Kiel 2024.
[176] V. Luu-The, Y. Zhang, D. Poirier, F. Labrie, *J. Steroid Biochem. Mol. Biol*. 1995, *55*, 581-587.
[177] J. Li, F. Al-Azzawi, *Maturitas* 2009, *63*, 142-148.
[178] B. Legeza, Z. Balázs, L. G. Nashev, A. Odermatt, *Endocrinology* 2013, *154*, 205-213.
[179] W. M. Geissler, D. L. Davis, L. Wu, K. D. Bradshaw, S. Patel, B. B. Mendonca, K. O. Elliston, J. D. Wilson, D. W. Russell, S. Andersson, *Nat. Genet.* 1994, *7*, 34-39.
[180] E. Koh, T. Noda, J. Kanaya, M. Namiki, *Prostate* 2002, *53*, 154-159.
[181] K. Fujita, N. Nonomura, *World J. Mens Health* 2019, 37, 288-295.
[182] T. E. Spires, B. E. Fink, E. K. Kick, D. You, C. A. Rizzo, I. Takenaka, R. M. Lawrence, Z. Ruan, M. E. Salvati, G. D. Vite, R, Weinmann, R. M. Attar, M. M. Gottardis, M. V. Lorenzi, *Prostate* 2005, *65*, 159-170.
[183] T. Brandt, P. Lentes, J. Rudtke, M. Hösgen, C. Näther, R. Herges, *J. Org. Chem*. 2024, submitted, Manuscript ID: jo-2024-00398n.R2.
[184] M. P. Torrens-Spence, C. M. Glinkerman, J. Günther, J.-K. Weng, *Curr. Opin. Plant Biol*. 2021, *60*, 101999.
[185] R. W. Layer, *Chem. Rev*. 1963, *63*, 489-510.
[186] M. E. Belowich, J. F. Stoddart, *Chem. Soc. Rev*. 2012, *41*, 2003-2024.
[187] Y. Toubi, F. Abrigach, S. Radi, F. Souna, A. Hakkou, A. Alsayari, A. Bin Muhsinah, Y. N. Mabkhot, *Molecules* 2019, 24, 3250.
[188] Jan Peter Mikosch, *aktuelle Arbeiten*, Christian-Albechts-Universität zu Kiel 2024.
[189] K. P. C. Vollhardt, N. E. Schore, *Organic Chemistry: Structure and Function*, 6th Edition, W. H. Freeman and Company, New York 2011, 950-951.
[190] L. García, J. Sendra, N. Miralles, E. Reyes, J. J. Carbó, J. L. Vicario, E. Fernández, *Chem. Eur. J.* 2018, *24*, 14059-14063.
[191] G. Kundu, T. Sperger, K. Rissanen, F. Schoenebeck, *Angew. Chem. Int. Ed*. 2020, *59*, 21930-21934.
[192] Z.-J. Wu, S.-R. Li, H.-C. Xu, *Angew. Chem. Int. Ed*. 2018, *130*, 14266-14270.
[193] A. L. J. Beckwith, G. F. Meijs, *J. Org. Chem*. 1987, *52*, 1922-1930.
[194] J.-J. Dai, C. Fang, B. Xiao, J. Yi, J. Xu, Z.-J. Liu, X. Lu, L. Liu, Y. Fu, *J. Am. Chem. Soc*. 2013, *135*, 8436-8439.
[195] J. A. Murphy, F. Rasheed, S. Gastaldi, T. Ravishanker, N. Lewis, *J. Chem. Soc., Perkin Trans*. *1* 1997, 1549-1558.
[196] Y. Li, Y. Zhu, G. Tu, J. Zhang, Y. Zhao, *RSC Adv*. 2018, *8*, 30374-30378.
[197] Michael Hösgen, *Bachelorarbeit*, Christian-Albechts-Universität zu Kiel 2021.
[198] R. Reuter, N. Hostettler, M. Neuburger, H. A. Wegner, *Eur. J. Org. Chem*. 2009, *2009*, 5647-5652.
[199] G. Wettermark, *Nature* 1962, *194*, 677.
[200] A. P. Pelliccioli, J. Wirz, *Photochem. Photobiol. Sci*. 2002, *1*, 441-458.
[201] P. Wang, *Asian J. Org. Chem*. 2013, *2*, 452-464.
[202] Y. V. Il'ichev, M. A. Schwörer, J. Wirz, *J. Am. Chem. Soc*. 2004, *126*, 4581-4595.
[203] D. Kehrloesser, P. J. Behrendt, N. Hampp, *J. Photochem. Photobiol., A* 2012, *248*, 8-14.
[204] K. Schaper, M. Etinski, T. Fleig, *Photochem. Photobiol*. 2009, *85*, 1075-1081.
[205] P. Xiao, J. Zhang, J. Zhao, M. H. Stenzel, *Prog. Polym. Sci*. 2017, *74*, 1-33.

[206] Y. Yu, T. Ikeda, *Photodeformable Materials and Photomechanical Effects Based on Azobenzene-Containing Polymers and Liquid Crystals*, in Y. Zhao, T. Ikeda, *Smart Light-Responsive Materials: Azobenzene-Containing Polymers and Liquid Crystals*, Wiley, New Jersey 2009, 95-144.
[207] M. E. Alf, A. Asatekin, M. C. Barr, S. H. Baxamusa, H. Chelawat, G. Ozaydin-Ince, C. D. Petruczok, R. Sreenivasan, W. E. Tenhaeff, N. J. Trujillo, S. Vaddiraju, J. Xu, K. K. Gleason, *Adv. Mater.* 2010, *22*, 1993-2027.
[208] M. H. Burk, S. Schröder, W. Moormann, D. Langbehn, T. Strunskus, S. Rehders, R. Herges, F. Faupel, *Macromolecules* 2020, *53*, 1164-1170.
[209] M. Reynders, B. S. Matsuura, M. Bérouti, D. Simoneschi, A. Marzio, M. Pagano, D. Trauner, *Sci. Adv*. 2020, *6*, eaay5064.
[210] C. M. Dobson, *Nature* 2003, *426*, 884-890.
[211] L. Albert, O. Vázquez, *Chem. Commun*. 2019, *55*, 10192-10213.
[212] G. M. Sheldrick, *Acta Cryst*. 2015, 3-8.
[213] G. M. Sheldrick, *Acta Cryst*. 2015, 3-8.